2009

Advanced Diagnostics, Control and Testing of Diesel Low Temperature Combustion

Usman Asad
University of Windsor

Recommended Citation

Asad, Usman, "Advanced Diagnostics, Control and Testing of Diesel Low Temperature Combustion" (2009). *Electronic Theses and Dissertations*. 7985.
https://scholar.uwindsor.ca/etd/7985

ADVANCED DIAGNOSTICS, CONTROL AND TESTING OF DIESEL LOW TEMPERATURE COMBUSTION

by

Usman Asad

A Dissertation
Submitted to the Faculty of Graduate Studies
through Mechanical, Automotive and Materials Engineering
in Partial Fulfilment of the Requirements for
the Degree of Doctor of Philosophy at the
University of Windsor

Windsor, Ontario, Canada

2009

Library and Archives
Canada

Published Heritage
Branch

395 Wellington Street
Ottawa ON K1A 0N4
Canada

Bibliothèque et
Archives Canada

Direction du
Patrimoine de l'édition

395, rue Wellington
Ottawa ON K1A 0N4
Canada

Your file Votre référence
ISBN: 978-0-494-83468-8

Our file Notre référence
ISBN: 978-0-494-83468-8

NOTICE:

The author has granted a non-exclusive license allowing Library and Archives Canada to reproduce, publish, archive, preserve, conserve, communicate to the public by telecommunication or on the Internet, loan, distrbute and sell theses worldwide, for commercial or non-commercial purposes, in microform, paper, electronic and/or any other formats.

The author retains copyright ownership and moral rights in this thesis. Neither the thesis nor substantial extracts from it may be printed or otherwise reproduced without the author's permission.

AVIS:

L'auteur a accordé une licence non exclusive permettant à la Bibliothèque et Archives Canada de reproduire, publier, archiver, sauvegarder, conserver, transmettre au public par télécommunication ou par l'Internet, prêter, distribuer et vendre des thèses partout dans le monde, à des fins commerciales ou autres, sur support microforme, papier, électronique et/ou autres formats.

L'auteur conserve la propriété du droit d'auteur et des droits moraux qui protege cette thèse. Ni la thèse ni des extraits substantiels de celle-ci ne doivent être imprimés ou autrement reproduits sans son autorisation.

In compliance with the Canadian Privacy Act some supporting forms may have been removed from this thesis.

While these forms may be included in the document page count, their removal does not represent any loss of content from the thesis.

Conformément à la loi canadienne sur la protection de la vie privée, quelques formulaires secondaires ont été enlevés de cette thèse.

Bien que ces formulaires aient inclus dans la pagination, il n'y aura aucun contenu manquant.

Canada

AUTHOR'S DECLARATION OF ORIGINALITY

I hereby certify that I am the sole author of this thesis and that the framework and the details of the technical core of the thesis have not been published. The proof of the majority of findings has mostly been refereed and produced to original research publications in journals and professional conferences with I being the first author or the co-author.

I certify that, to the best of my knowledge, my thesis does not infringe upon anyone's copyright nor violate any proprietary rights and that any ideas, techniques, quotations, or any other material from the work of other people included in my thesis, published or otherwise, are fully acknowledged in accordance with the standard referencing practices. Furthermore, to the extent that I have included copyrighted material that surpasses the bounds of fair dealing within the meaning of the Canada Copyright Act, I certify that I have obtained a written permission from the copyright owner(s) to include such material(s) in my thesis and have included copies of such copyright clearances to my appendix.

I declare that this is a true copy of my thesis, including any final revisions, as approved by my thesis committee and the Graduate Studies office, and that this thesis has not been submitted for a higher degree to any other University or Institution.

ABSTRACT

The conventional high temperature diesel combustion is constrained by the classical NOx-soot trade-off, so that any technique to reduce one emission generally increases the other. The simultaneous low NOx and soot can be achieved by lowering the combustion temperature and by preparing a cylinder charge of high homogeneity. However, the lowered combustion temperature may significantly reduce the fuel efficiency of such combustion cycles. Therefore, the overall objective of this work was to conduct a detailed analysis of the diesel LTC cycles that result in simultaneous low NOx and low soot, and to improve the LTC performance through advanced diagnostics and combustion control strategies. The empirical and analytical analyses in this dissertation provide an in-depth understanding of diesel LTC and present an effective strategy for navigating the narrow LTC corridors.

The in-cylinder gas sampling tests culminated with the identification of an LTC NOx mechanism whereby the NOx reduction in the presence of combustibles was quantified on a crank angle-resolved basis. The intake gas treatment through catalytic oxidation and fuel reforming of EGR stabilized the LTC cycles. Novel flow management strategies were applied to improve the thermal response and the energy efficiency of the reforming operation.

Adaptive combustion control techniques were developed to improve the fuel efficiency of the LTC cycles and to enable navigation within the narrow LTC corridors. A computationally efficient 'Pressure Departure Ratio' algorithm for estimating the combustion phasing in real-time was proposed along with a methodology for engine load management within-the-same-cycle, and were shown to improve the LTC operational stability. The detailed EGR analysis helped to develop a systematic LTC control strategy by quantifying the effects of intake charge dilution and boost pressure on the LTC performance metrics.

Based on the empirical and analytical analyses, the load management and efficiency improvements of the LTC cycles were demonstrated with three different fuelling strategies as follows:

- Single-injection LTC with heavy EGR at low loads
- Multi-shot LTC (early HCCI) with moderate EGR for mid-load operation, and
- Split burning LTC for higher engine loads with DPF-tolerant soot.

Keywords: Low temperature combustion, diesel, EGR, in-cylinder diagnostics, adaptive control, systematic control

DEDICATION

This dissertation is dedicated to

my wife, daughter and son,
for their unconditional love and support
throughout the course of this work

my parents
whose love, support and encouragement
have always been a source of strength and inspiration

ACKNOWLEDGEMENTS

I wish to acknowledge the inspiration, guidance and encouragement I have received from my advisor Dr. Ming Zheng. His constant intuitive wisdom and resolute leadership were instrumental in seeing this work to fruition. Dr. Zheng also extended his support in all areas of research, experimentation, diagnostics and control. I would also like to thank my co-advisor Dr. David S-K. Ting for his guidance and continued support throughout this work. I would also like to thank the committee members Dr. Richard Stobart, Dr. Xiaohong Xu, Dr. Graham T. Reader, Dr. Jimi Tjong and Dr. Xiang Chen for their guidance in this research.

The contribution of my colleagues in the Clean Diesel Engine Laboratory cannot go unnoticed. Many thanks to Dr. Meiping Wang, Dr. Raj Kumar, Dr. Clarence Mulenga, Yuyu Tan and Xiaoye Han for their invaluable discussions and assistance. Special thanks to Bruce Durfy and the wonderful people at the Technical Support Centre who helped immensely during the experimental setup. Many thanks to Ms. Rosemary Gignac and Ms. Barbara Tattersall with the myriad paperwork while arranging for my financial support, graduate assistantships and the arrangements for the external examiner.

I am grateful for the support from the University of Windsor, AUTO 21 (a member of the Network of Centres of Excellence of Canada programme). Additionally, the collaborators in the Clean Diesel Engine Laboratory are also thanked; Canada Research Chair Programme, Canada Foundation of Innovation (CFI), Ontario Innovation Trust (OIT), Natural Sciences and Engineering Research Council of Canada (NSERC) and Ford Motors Canada.

Finally, but definitely not the least, I must express my deepest appreciation to my wife Marrium, my daughter Sharmeen and my son Shehryar for their love and endless patience.

Usman Asad
Windsor, Ontario
Canada
April 2009

TABLE OF CONTENTS

CHAPTER I

CHAPTER II

CHAPTER III

CHAPTER IV

RESULTS AND DISCUSSION

CHAPTER V

CHAPTER VI

CHAPTER VII

CHAPTER VIII

CHAPTER IX

LIST OF FIGURES

CHAPTER I

CHAPTER II

CHAPTER III

CHAPTER IV

CHAPTER V

CHAPTER VI

CHAPTER VII

CHAPTER VIII

CHAPTER IX

APPENDICES

LIST OF TABLES

CHAPTER I

CHAPTER II

CHAPTER IV

CHAPTER V

CHAPTER VI

CHAPTER VII

CHAPTER VIII

CHAPTER IX

APPENDICES

NOMENCLATURE

AFR	Air Fuel Ratio	[–]
AHR	Apparent Heat Release	
AI	Analog Input	
AO	Analog Output	
ATDC	After Top Dead Centre	[°CA]
BBDC	Before Bottom Dead Centre	[°CA]
BES	Boost-EGR Control System	
BL	Baseline	
BMEP	Brake Mean Effective Pressure	[bar]
BPV	Back pressure Valve	
BTDC	Before Top Dead Centre	[°CA]
CA	Crank Angle	[°CA]
CA50	Crank Angle of 50% Heat Released	[°CA]
CAI	California Analytical Instruments	
CAN	Controller Area Network	
CDEL	Clean Diesel Engine Laboratory	
CDI	Charge Dilution Index	[–]
CEGR	Catalytic Exhaust Gas Recirculation	
CI	Compression Ignition	
CLD	Chemiluminescence Detection	
CN	Cetane Number	[–]
CO	Carbon Monoxide	
CO_2	Carbon Dioxide	
COV	Coefficient of Variance	[%]
CR	Compression Ratio	[–]
DI	Direct Injection	
DIO	Digital Input Output	
DME	Dimethyl Ether	
DOC	Diesel Oxidation Catalyst	
DPF	Diesel Particulate Filter	
EGR	Exhaust Gas Recirculation	
EOC	End of Combustion	[°CA]
EPA	US Environmental Protection Agency	
EPR	Electro-pneumatic Pressure Regulator	

EVO	Exhaust Valve Open	[°CA]
exh	Exhaust	
FBP	Final Boiling Point	[°C]
FCS	Fuel Injection Control System	
FFE	Fast Feedback Estimator	
FID	Flame Ionization Detector	
FPC	Fired Pressure Coefficient	[bar]
FPGA	Field Programmable Gate Array	
FSN	Filter Smoke Number	
FT	Fisher Tropsch	
FTIR	Fourier Transform Infrared Spectroscopy	
GSV	Gas Sampling Valve	
HCCI	Homogeneous Charge Compression Ignition	
HEGO	Heated Exhaust Gas Oxygen Sensor	
HRR	Heat Release Rate	[J/°CA]
HTC	High Temperature Combustion	
HTR	High Temperature Reactions	
IBP	Initial Boiling Point	[°C]
IMEP	Indicated Mean Effective Pressure	
int	Intake	
IVC	Intake Valve Close	[°CA]
LHV	Lower Heating Value	[MJ/kg]
LTC	Low Temperature Combustion	
LTR	Low Temperature Reactions	
LUT	Lookup Table	
MAF	Mass Air Flow	[g/s]
MFB	Mass Fraction Burnt	[–]
MK	Modulated Kinetics	
MPC	Motored Pressure Coefficient	[bar]
NDIR	Non-Dispersive Infra-Red	
NFE	NOx Feedback Estimator	
NI	National Intruments	
NO	Nitrogen Oxide	
NO_2	Nitrogen Dioxide	
NOx	Oxides of Nitrogen	
P	Pressure	[bar, MPa]

PAC	Parametric Analysis and Correction	
PCI	Premixed Compression Ignition	
PDR	Pressure Departure Ratio	[–]
PID	Proportional Integral Derivative Controller	
PM	Particulate Matter	
ppm	Parts per Million	
PREDIC	Premixed Lean Diesel Combustion	
PW	Pulse Width	[μs]
QR	Quotient Remainder Function	
R_{EGR}	EGR Fraction	[–]
RPM	Revolutions per Minute	
RT	Real-time	
SCR	Selective Catalytic Reduction	
SD	Sampling Duration	[ms]
SFE	Slow Feedback Estimator	
SI	Spark Ignition	
SOC	Start of Combustion	[°CA]
SOI	Start of Injection	[°CA]
SOS	Start of Sampling	[°CA]
SRF	Sample Repetition Frequency	
T	Temperature	[°C, K]
TDC	Top Dead Centre	
THC	Total Hydrocarbons	
TTL	Transistor-Transistor Logic	
TWC	Three-Way Catalytic Converter	
UHC	Un-burnt Hydrocarbons	
ULSD	Ultra Low Sulphur Diesel	
UNIBUS	Uniform Bulky Combustion System	
V	Volume	[m^3, litre]
VCR	Variable Compression Ratio	
VGT	Variable Geometry Turbocharger	
VVT	Variable Valve Timing	
y	Mole Fraction	[–]
[ ]	Molar / Volumetric Concentration	[%]

Greek Symbols

ϕ	Equivalence Ratio	[–]
η	Efficiency	[%]
λ	Fresh Air Lambda	[–]
λ_a	In-cylinder Lambda	[–]
λ_o	Fresh Air Lambda without EGR	[–]
ρ	Density	[kg/m^3]
θ	Crank Angle	[°CA]
τ_{ID}	Ignition Delay	[°CA, ms]

CHAPTER I

1. INTRODUCTION

1.1. The Diesel Engine

The diesel engine has been considered an efficient work horse in a wide range of applications for more than a century. The North American heavy-duty transportation sector has relied primarily on diesel-powered prime movers. Besides the automotive industry, diesel engines are increasingly being used in the marine, agricultural and power industries, to name a few. The success of the diesel engine can be attributed to its high efficiency, excellent torque characteristics, mechanical reliability and robustness compared to the spark-ignition (SI) engine. An often overlooked advantage is the fact that the diesel engines emit significantly lower engine-out (raw) exhaust emissions than a similar sized gasoline-fuelled SI engine. The diesel engine emits extremely low concentrations of carbon monoxide (CO) and unburnt hydrocarbon (UHC) emissions, and the oxides of nitrogen (NOx) emission is also less than that for a typical gasoline engine [1,2]. A comparison of the emissions and exhaust conditions between the SI and compression ignition (CI) engines is presented in Figure 1.1 [3].

The stringent emission regulation set out by the United States Environmental Protection Agency (EPA) and concurrently by Environment Canada for automotive engines have required the engine-out emissions to be drastically reduced over the last 2 decades. The SI engine has benefited immensely from the use of the three-way catalytic converter (TWC) which requires the engine to operate close to stoichiometric conditions – essential for reducing the NOx to nitrogen (N_2) while oxidizing the UHC and CO to carbon dioxide (CO_2) and water. However, the application of the TWC to clean up the exhaust of compression ignition (CI) engines like diesel-fuelled engines is complicated by the following two facts. First, the diesel is essentially a lean-burn engine, that is, there is always an abundance of oxygen in the engine exhaust [4]. Second, the high compression ratios employed in diesel engines imply that the engine is able to extract more energy from the working fluid during the expansion stroke, and therefore, the exhaust temperature for diesels is generally low. Moreover, the diesel exhaust temperature also varies widely with load. The TWC is therefore rendered ineffective in the diesel exhaust systems [2–4].

The diesel engine was considered to be dirty and noisy, among automotive consumers worldwide. In recent years, however, the diesel engine has benefited from tremendous technological advances in all the areas where it was traditionally weak such as combustion noise and smoke while its key advantage of high efficiency has been further improved. Modern turbo-charged diesel engines are quiet, cleaner and offer high fuel economy. Furthermore, the lower fuel consumption offers another intrinsic advantage: the diesel engine generally produces up to 20% less carbon dioxide (CO_2), a greenhouse gas considered responsible for global warming compared to the gasoline engine [1,2]. Although the CO_2 emission is currently not regulated in North America, it is being regulated in Europe. Therefore, the diesel engine has gained interest from parties with environmental concerns because of its potential to comparatively reduce the emissions of CO_2.

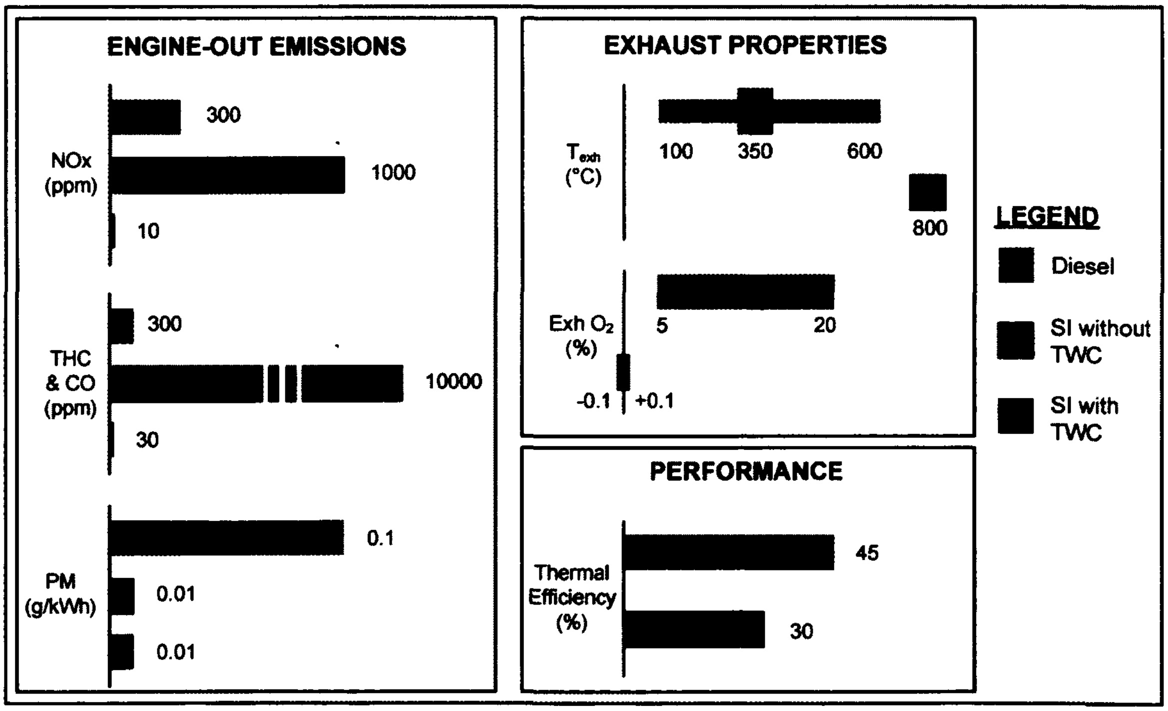

Figure 1.1: Comparison of CI & SI Engine Exhaust Characteristics (Adapted from [3])

1.2. A Review of Available Energy Sources for Automotive Use

Hydrocarbon fuels like diesel and gasoline are an efficient source of energy. They have high volumetric as well as gravimetric energy densities which make them suitable for use in vehicles and other non-stationary applications [5]. Moreover, the internal combustion engines have virtually been the sole source of propulsion in vehicles since they can provide high power-to-weight ratios and have the ability to use energy-dense fuels. However, the burning of hydrocarbon fuels results in the production of harmful pollutants including CO_2, which are believed to be the major cause of global warming, acid rain and other detrimental health effects.

In recent years, the focus has been to shift towards alternate energy sources such as bio-diesel, hydrogen (H_2) or electrical batteries for providing propulsion power in vehicles. However, a comparison of the energy densities of various alternate energy sources including electrical batteries in Figure 1.2 indicates that a number of major hurdles need to be overcome before fuels like hydrogen and electrical batteries can replace the hydrocarbon fuels in mobile applications.

For instance, hydrogen has a very high gravimetric energy density (~120 MJ/kg) but an extremely low volumetric energy density – a major issue in mobile applications. Compressing H_2 to 70 MPa (700 bar) increases the energy density to ~5 MJ/L but it is still considered non-viable for automotive use. There are also safety issues such as gas storage at such high pressures that need to be addressed.

The state-of-the-art electrical batteries also have very low energy densities (~0.8 MJ/kg & ~1.2 MJ/L) compared to the conventional hydrocarbon fuels [6,7]. This has implications on the weight of the battery pack required and the time interval between recharging. Although the production of hybrid-electric vehicles is on the rise, the replacement of conventional hydrocarbon fuels and internal combustion engines with electrical batteries and motors may still take a long time.

Therefore, the current emphasis is to improve the fuel efficiency of the internal combustion engines while making them cleaner and more environmental friendly. The diesel engine, with its high efficiency and lower CO_2 emission as discussed in the previous section, provides an excellent platform for achieving these goals.

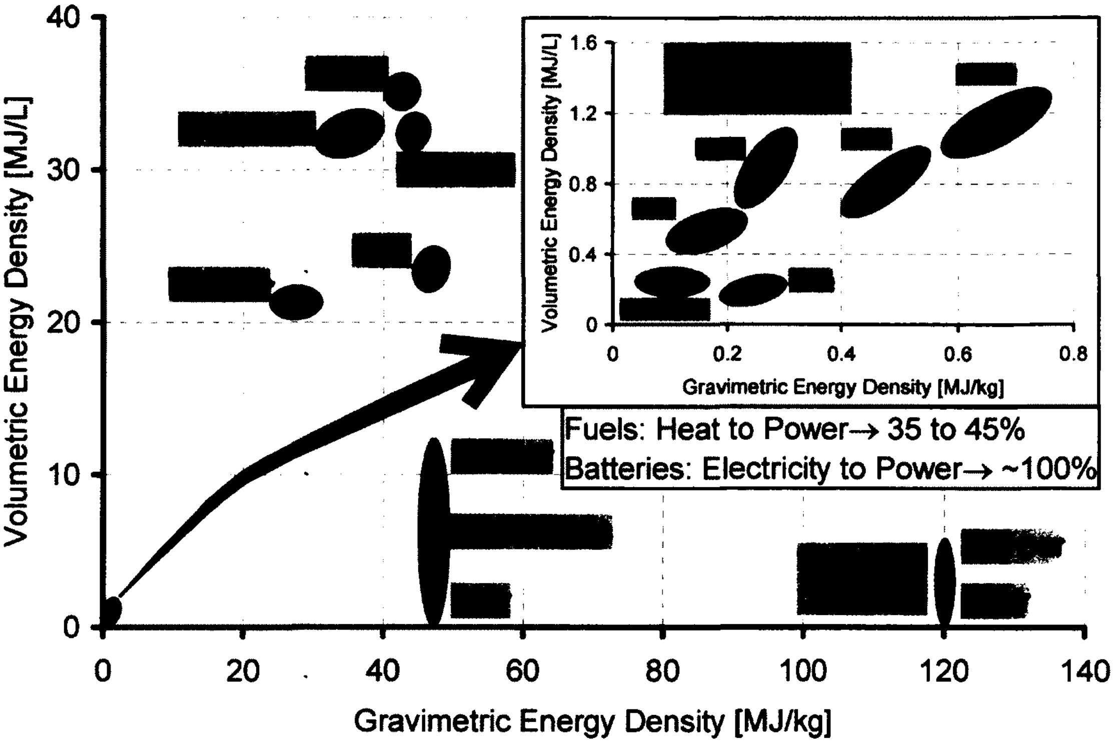

Figure 1.2: Energy Density Comparison between Fuels & Rechargeable Batteries

1.3. Combustion in Diesel Engines

The combustion process in diesel engines is normally described on a heat release rate (HRR) diagram, such as the one shown in Figure 1.3. The heat-release rate is a representation of the rate of release of the chemical energy of the fuel during the combustion process and is estimated from the in-cylinder pressure data. In a conventional diesel engine, the intake air drawn into the cylinders is compressed to high compression ratios which increases its pressure and temperature (typically around 600~900°C). The diesel fuel (commonly at pressures between 30~160 MPa) is injected into this highly compressed and heated air in the liquid state shortly before the end of the compression stroke as the piston approaches the top-dead-centre (TDC). The ensuing diesel combustion process, from the commencement of the fuel injection can be divided into 4 regions as identified on the heat-release rate diagram: ignition delay period (I), premixed combustion phase (II), diffusion combustion phase (III), and the tail of combustion (IV) [4,8–10].

Ignition Delay Period (I): The ignition delay is the time between the start of fuel injection (SOI) and the start of combustion (SOC). The liquid fuel droplets absorb heat from their surroundings and vaporize quickly. The temperature of the thin layer of air in close proximity to the droplet decreases but is raised quickly through heat transfer from the main bulk of air. This process repeats itself at numerous locations in the combustion chamber until auto-ignition take place when the vaporized fuel is mixed with the air to within-flammability limits and the local temperature is above the auto-ignition temperature. The duration of this delay is related to the time needed for atomization, vaporization and mixing of the fuel and air to within-flammability limits (physical delay) and the chemical delay time (pre-ignition chemical reactions to bring the charge to combustible limits).

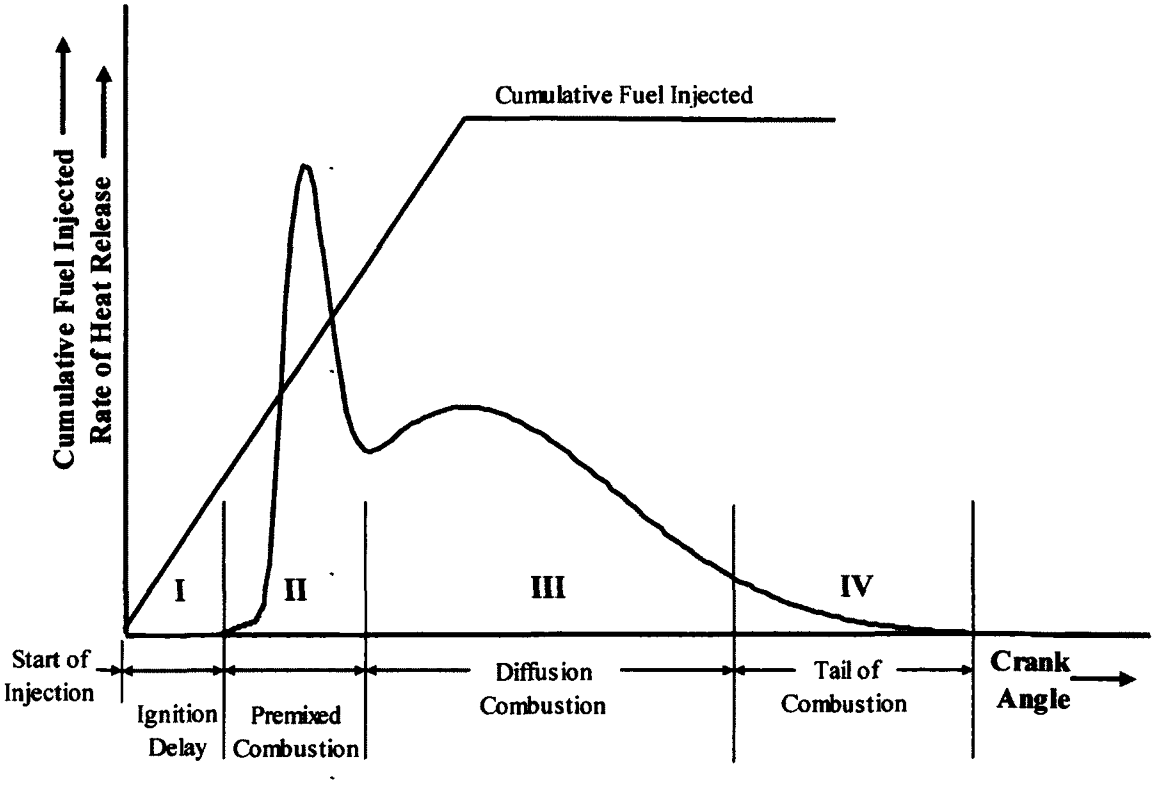

Figure 1.3: Typical Rate of Heat Release Diagram [4,8–10]

Premixed Combustion Phase: This phase is characterized by the rapid burning of the fuel-air mixture prepared during the ignition delay period and is also sometimes referred to as the uncontrolled combustion. The knocking sound of the diesel combustion process is generally attributed to this burning phase because of the increased rate-of-pressure rise (combustion noise). The premixed phase typically lasts for a few crank angle degrees.

Diffusion Combustion Phase: Once the fuel-air mixture prepared during the ignition delay period has been consumed, the rate of combustion or heat release is controlled by the preparation rate of the fuel vapour-air mixture. During this mixing-controlled combustion phase, the ignition delay is much shorter because the cylinder pressure and temperature are much higher as a result of the burning of initial droplets during the premixed phase.

Tail of Combustion: The late combustion phase, also referred to as the tail of combustion, occurs well into the expansion stroke. The rate of combustion is typically low as most of the fuel and oxygen have already been consumed, and depends on the mixing of combustible residuals with the excess oxygen. The energy present in soot and fuel-rich combustion products may also be released during this phase.

The heat release in diesel engines is affected by a number of parameters including engine speed, engine load, exhaust gas recirculation (EGR) rate, fuel scheduling and boost. Figure 1.4 shows the effect of the engine load on the normalized heat release rates from a direct injection (DI) diesel engine with a single fuel injection per combustion cycle at the Clean Diesel Engine laboratory (CDEL), University of Windsor.

At low engine loads, a relatively high fraction of energy is released during the premixed phase of combustion. Consequently, the diffusion combustion phase is small, resulting in a short combustion duration. However as the load increases, the premixed fraction is progressively reduced and the diffusion-controlled combustion becomes predominant. The combustion duration also increases as the combustion progresses well into the expansion stroke.

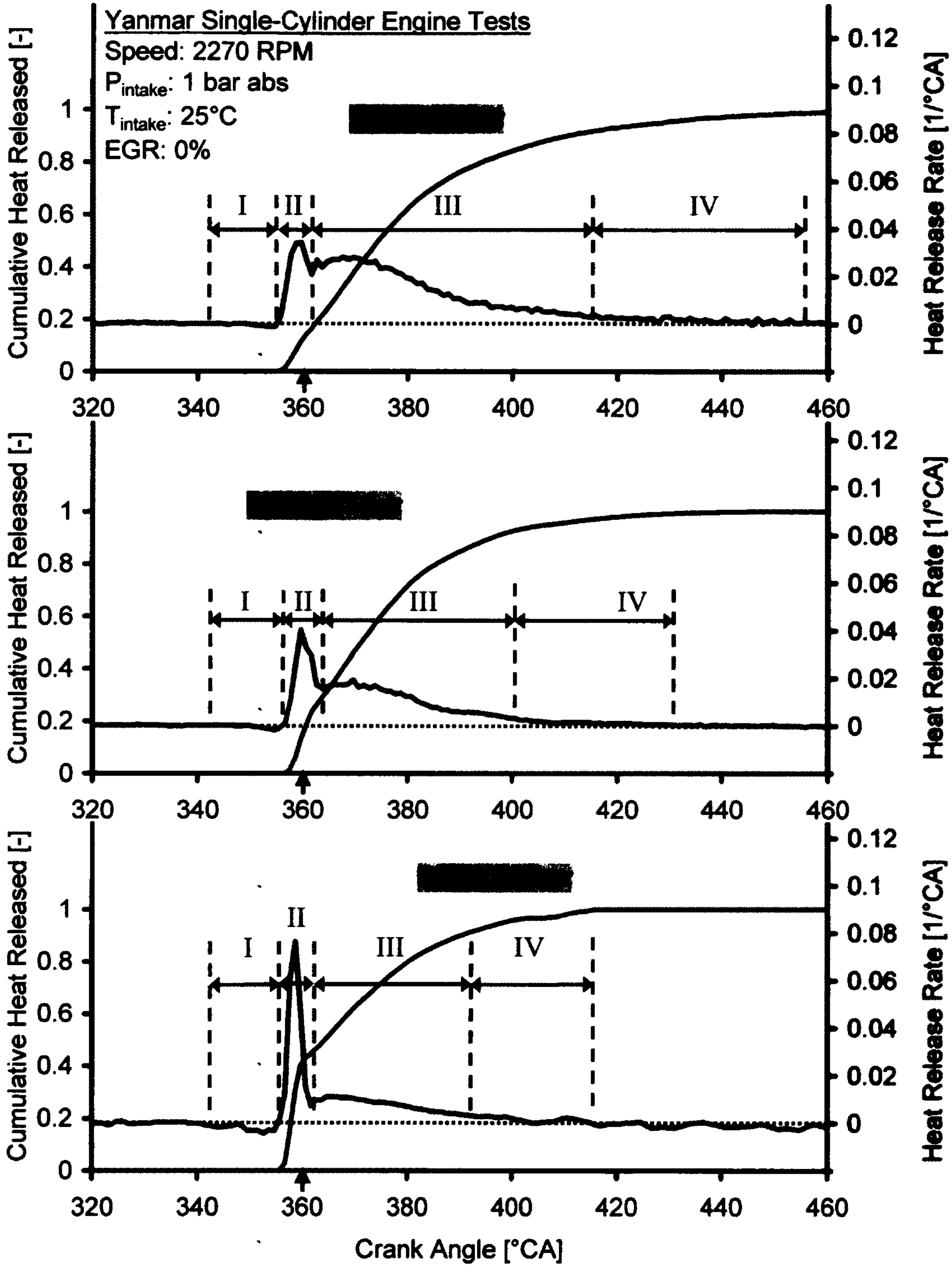

Figure 1.4: Effect of Load on the Heat Release Rate from a Classical Diesel Engine

The duration and magnitude of the premixed and the diffusion combustion phases can have important implications on the engine-out exhaust emissions. The mechanism of pollutant formation inside the combustion chamber has been researched by direct in-cylinder sampling techniques, laser diagnostic procedures and computational fluid dynamics (CFD) studies to provide a better understanding of the time- and space-resolved histories of pollutant formation [9–21]. The results from such studies indicate that the production of pollutant species is dependent on the intensity and duration of the different phases of combustion. For instance, a significant portion of NOx is believed to form during the premixed phase of combustion, which is characterized by locally near-stoichiometric conditions and the resulting high flame temperatures. Soot, on the other hand, is generally thought to reach its maximum production during the mixing-controlled combustion phase.

1.4. Exhaust Emissions from Diesel Engines

The major emissions from conventional diesel engines can be considered to be the oxides of nitrogen and smoke. However, when diesel engines are run under alternate combustion regimes like low temperature combustion (LTC), the lowered combustion temperature usually results in high amounts of unburnt hydrocarbons and carbon monoxide. Therefore, the mechanisms believed to be responsible for the formation of each of the pollutant species are briefly discussed below.

1.4.1. Oxides of Nitrogen (NOx)

The term NOx is used to collectively refer to nitric oxide (NO) and nitrogen dioxide (NO_2) that are produced during the combustion process in diesel engines. Although NO is the dominant species in the conventional diesel exhaust (constituting more than 90% of the total NOx emission [22]), it is quickly oxidized to NO_2 in the atmosphere. NO_2 is believed to be the major precursor for smog formation, acid rain and is known to cause detrimental effects to the human health [9,10,23]. Therefore, the US EPA requires that the exhaust NOx should be regulated on an equivalent NO_2 basis because it is the most prevalent form of NOx in the atmosphere that is generated by human activities [24].

NOx does not have a strong correlation to the fuel structure but depends largely on how the combustion is organized. Therefore, the NOx yield is affected primarily by the prevailing temperature, the oxygen concentration and the residence time during the combustion [9,23]. For the combustion of fuel with very little or no nitrogen, the NOx formation is generally attributed to the thermal NOx mechanism that could be described by the extended Zeldovich mechanism as follows [4,9,23]:

$$O + N_2 \rightleftharpoons NO + N \tag{1.1}$$

$$N + O_2 \rightleftharpoons NO + O \tag{1.2}$$

$$N + OH \rightleftharpoons NO + H \tag{1.3}$$

Using equilibrium assumptions, the rate of NO formation may be approximated by an overall reaction as follows [4,25]:

$$\frac{d[NO]}{dt} = \kappa[O_2]^{1/2}[N_2] \quad \& \quad \kappa = \frac{a}{T^{1/2}} e^{-b/T} \tag{1.4}$$

where κ is an equivalent reaction-rate constant in $(cm^3/mol)^{1/2}/sec$, T is the temperature in Kelvin, [NO], $[O_2]$ and $[N_2]$ are the mole concentrations in mol/cm^3, $a = 6\text{x}10^{16}$ $(K.\ cm^3/mol)^{1/2}/sec$ and $b = 6.91\text{x}10^4$ K. Plotting the equivalent rate constant κ against the temperature as shown in Figure 1.5, it is evident that the prevailing charge temperature is the dominant factor affecting the NOx formation. Therefore, the thermal mechanism is considered responsible for the majority of NOx emissions from conventional diesel engines when the peak combustion temperatures are in excess of 2000K.

Under the prevailing conditions in the diesel engine combustion chamber, the highest temperatures occur at near-stoichiometric conditions in the local diesel flame. Therefore, the thermal NO only appears in significant quantities after the start of the heat-release. The temperature sensitivity of this mechanism also suggests that as the combustion progresses well into the expansion stroke, the in-cylinder temperature decreases and the thermal NO concentrations tend to freeze.

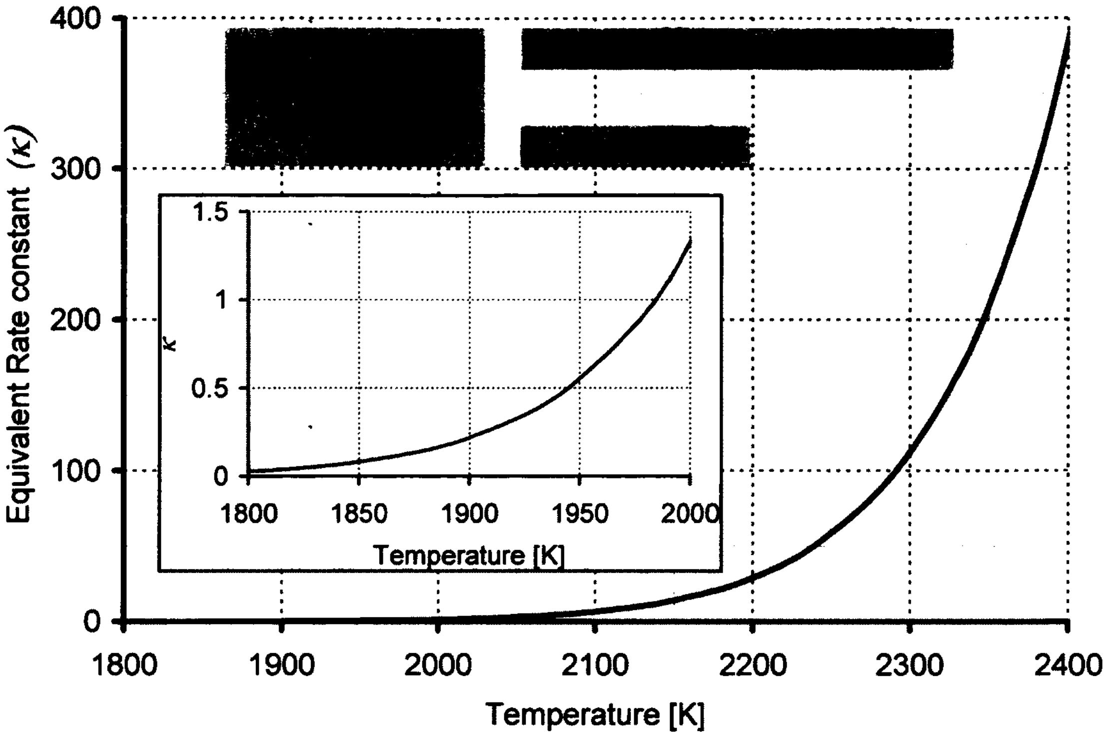

Figure 1.5: Dependence of NOx Formation on Temperature

The N_2O intermediate mechanism is considered important for NO formation during the lean premixed low-temperature combustion process. At sufficiently high pressures, N_2O is formed as a result of the three body reaction [21,23]:

$$O+N_2+M \rightleftharpoons N_2O+M \tag{1.5}$$

where, ' M ' is a third body (molecule) of any compound that is needed to remove energy in order to complete the reaction. NO is then formed through the following reactions:

$$H+N_2O \rightleftharpoons NO+NH \tag{1.6}$$

$$O+N_2O \rightleftharpoons NO+NO \tag{1.7}$$

The Fenimore prompt NO mechanism is another NOx formation pathway, considered significant during the rich combustion process and occurs in the presence of a high concentration of hydrocarbon, O and OH radicals [21,23]. It is believed to contribute a small amount of NO in the diffusion portion of the diesel combustion process [19]. The prompt NO mechanism is initiated by the rapid reaction of hydrocarbon radicals from the fuel with the molecular nitrogen, leading to the formation of amines and cyano compounds that subsequently react to form NO.

1.4.2. Particulate Matter

The EPA defines the particulate matter as: "Particulate-matter (PM) includes dust, dirt, soot, smoke and liquid droplets directly emitted into the air by sources such as factories, power plants, cars, engines, construction activity, fires and natural windblown dust. Particles formed in the atmosphere by condensation or the transformation of emitted gases are also considered particulate matter" [3].

To measure the particulate matter from engines, PM is defined by the EPA as any matter (except unbound water) in the exhaust of an internal combustion engine that can be trapped on a sampling filter medium at a temperature not to exceed 52°C (125°F) [10]. The diesel PM is not considered a well defined physical species but can be broadly divided into three categories as listed in Table 1.1 [26].

Table 1.1: Major Constituents of Particulate Matter

Category	Constituents
Soluble Organic Fraction	Organic materials derived from engine lubricating oil and fuel
Solid Fraction	Soot, ash, trace metals
Sulphate Particulates	Sulphates and sulphuric acid

The primary PM produced in conventional diesel engines is soot [4]. Soot forms on the rich side of the reaction zone during the predominantly diffused-controlled combustion by the pyrolysis of hydrocarbons [8]. However, if the temperature is sufficiently high and oxygen is available, part of the soot will be oxidized. The net soot emission from diesel engines is, therefore, the result of the difference between the soot production and soot oxidation processes [27,28].

1.4.3. Unburnt Hydrocarbons

Unburnt hydrocarbons (UHC) in DI diesel engines are generally the result of over- or under-mixing of the fuel-air mixture and the flame quenching during the combustion process [4]. The injected fuel mixes with the air during the ignition delay period and produces mixture zones with widely varying air/fuel ratios. These can broadly be divided into lean, stoichiometric or rich zones depending upon the relative mixture strength.

At the onset of conventional diesel combustion, the flames tend to initialize in and propagate to regions where the air/fuel ratios are near stoichiometric. The combustion continues till the localized air/fuel ratio decreases rapidly due to over-mixing with the surrounding air or if the flame is quenched at the thermal boundary layer. The over-mixing/quenching can be a source of HC formation. Moreover, the lean mixture zones have to interact with additional evaporated fuel, and the rich zones have to find oxygen to form a flammable mixture to be able to take part in the combustion. However, if the lean mixture fails to find the necessary fuel or the rich mixture fails to find the air before the temperature drops significantly (as the combustion progresses into the expansion stroke), then both these mixtures will have a tendency to produce HC.

1.4.4. Carbon Monoxide (CO)

The combustion of hydrocarbon fuels is believed to include the formation of CO as one of the principal reaction steps [4]. The CO is then oxidized to CO_2 provided two conditions are fulfilled: the availability of oxygen and a high temperature to drive the oxidation reaction. Although the diesel combustion is overall lean, combustion tends to initiate in regions at near-stoichiometric conditions, resulting in high flame temperatures. Therefore, the classical high temperature combustion in diesel engines produces very low quantities of engine-out CO.

When the combustion temperatures are lowered such as with high amounts of EGR or during HCCI type of combustion, the combustion of such lean or EGR-diluted air/fuel mixtures usually produces high amounts of CO, mainly due to the reduction in the oxidation of CO to CO_2. Because of the prolonged ignition delay in LTC systems, over-mixing of the fuel may result in significant portions of the air/fuel mixture with very lean equivalence ratios. Under such conditions, the combustion temperatures can be too low for the oxidation of CO, to be completed on the engine time scales [29].

1.5. Exhaust Emissions Regulation

The exhaust species discussed above are evidently undesirable as they have a harmful effect on the environment and our health. Therefore, the regulatory authorities like the US EPA and Environment Canada have introduced increasingly stringent emission norms to regulate the emission of pollutants from diesel engines in recent years. Figure 1.6 and Figure 1.7 show the compliance roadmap for heavy-duty diesel engines to meet the NOx and soot emission limits in North America over the last two decades.

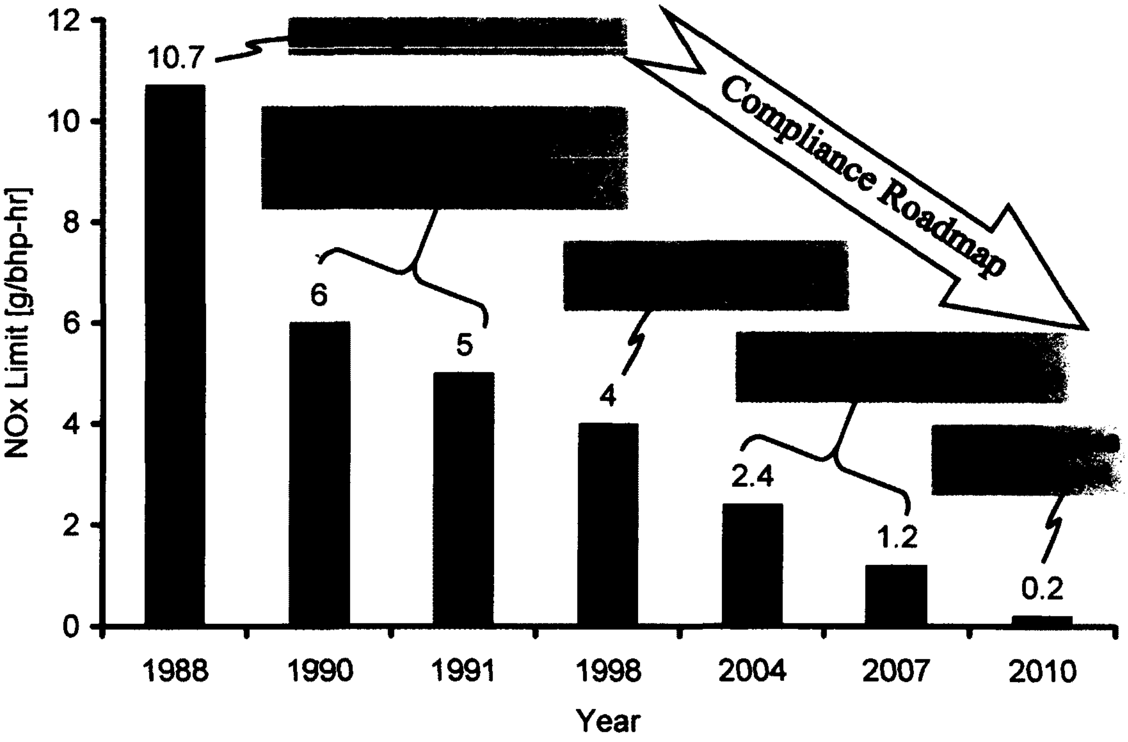

Figure 1.6: Compliance Roadmap for NOx Emission Regulations

It is evident that the emission control features have evolved significantly to keep up with the regulations. The research focus now is on emission reduction strategies that would result in ultra-low emissions of the pollutant species by the year 2010 and beyond. In North America, the EPA 2010 emissions standard is the bench mark for diesel engine applications.

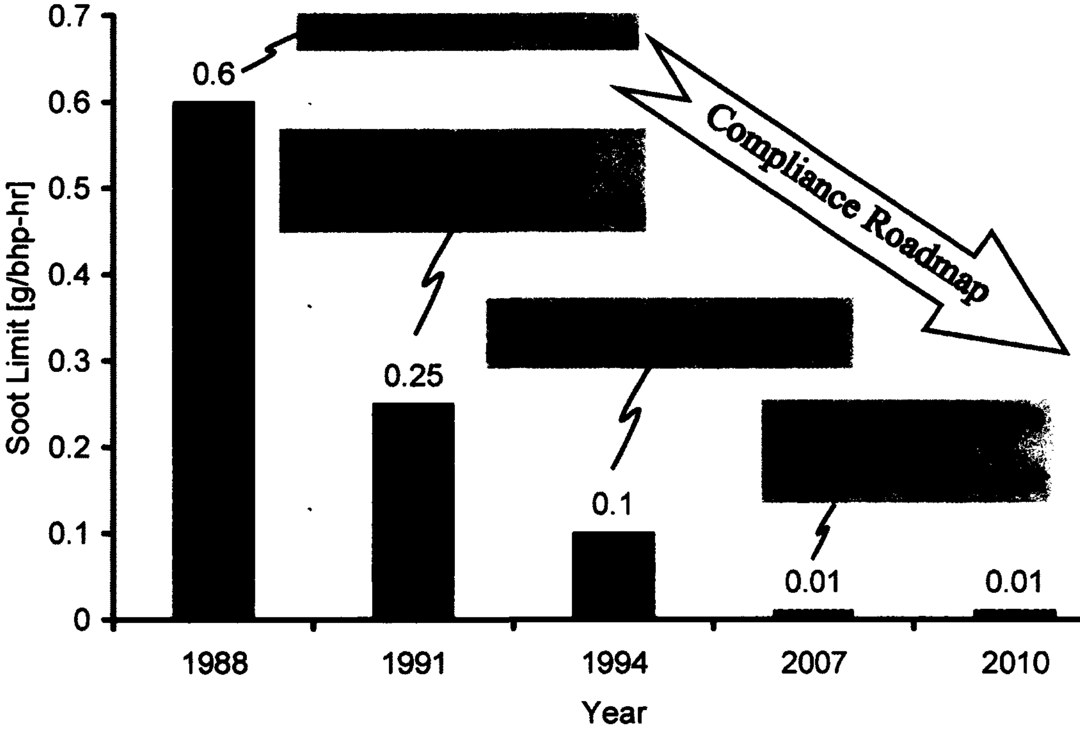

Figure 1.7: Compliance Roadmap for Soot Emission Regulations

1.6. The Classical NOx-Soot Trade-off

Conventional diesel engines are overall lean-burn systems; however, the classical heterogeneous nature of the high-temperature combustion (HTC) presents numerous challenges regarding NOx and PM emissions. In such diesel engines, the flames tend to initialize in and propagate to regions where the air/fuel ratios are near-stoichiometric [11,14,30,31], thus presenting an inherent NOx-PM trade-off. The NOx-PM trade-off is a major obstacle towards the use of in-cylinder emission control measures to meet the emission regulation requirements. The NOx-PM trade-off means that the application of any emission control technique that lowers the NOx, has a tendency to increase the PM or vice-versa.

Figure 1.8 shows the NOx-PM trade-off with the use of EGR for classical low-injection pressure diesel combustion and for diesel engines with modern common-rail high pressure injection systems. The use of EGR is effective to reduce the in-cylinder NOx formation [32] mainly because the thermal, dilution and chemical effects of EGR lower the flame temperature as well as oxygen concentration of the working fluid [30,33-37]. However, the application of EGR usually increases PM formation because of the predominant diffusion-controlled combustion where the lack of oxygen leads to soot formation on the rich side of the reaction zone especially at high load conditions [38].

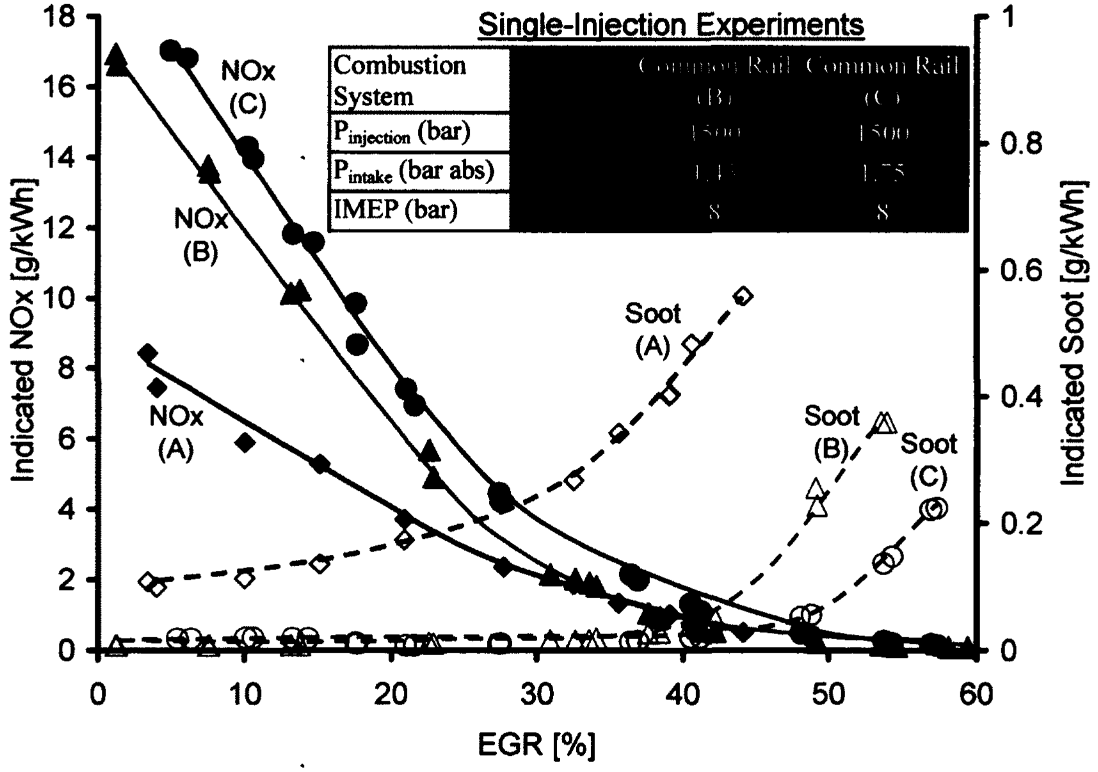

Figure 1.8: Empirical Results highlighting the Classical NOx-Soot Trade-off

Similarly, retarding the injection timing decreases the NOx emission but tends to increase the soot formation that can be attributed to the decreasing temperatures during the expansion stroke [37,39]. When the injection occurs near or after the TDC, the decreased fuel-air mixing time caused by the shorter ignition delay leads to lower combustion temperatures. This reduction in the combustion temperatures tends to inhibit the soot destruction rates, thereby increasing the engine-out soot.

Note that the use of a higher injection pressure in the figure shows a tendency to suppress the soot formation but increases the NOx at a given EGR rate. Therefore, it is considered very challenging to reduce NOx and PM simultaneously to meet the future stringent emission norms, while retaining the power-density levels of the modern diesel engine.

1.7. Scope of Work

The overall objective of this dissertation was to carry out a detailed analysis of the diesel LTC cycles that result in simultaneous low NOx and low soot emissions, and to improve the LTC performance through advanced diagnostics and combustion control strategies. An elaborate and sophisticated experimental program that evolved in a series of phases was developed to accomplish this goal. The focus of each phase was as follows:

Phase 1: The preliminary testing of the diesel LTC cycles highlighted the sensitivity of the LTC cycles to small variations in the engine operating conditions. Therefore, to enable the evaluation of the advantages and the shortcomings of the different LTC strategies, and to successfully implement and evaluate the control strategies, an advanced emission sampling and measurement, data acquisition, and a high performance combustion-control platform was developed during the initial phase of the research.

Phase 2: The objective of the second phase was to perform advanced LTC diagnostics that included in-cylinder direct gas sampling tests to study the survivability of intake NOx in the presence of combustibles and the NOx evolution on a crank angle-resolved basis during combustion. A detailed analysis of the cylinder pressure was performed to ascertain the suitability of pressure-based parameters as feedback for LTC combustion control under a variety of engine operating conditions. Heat release models based on the First Law were compared and a computationally efficient algorithm was proposed for predicting the combustion phasing. An elaborate EGR analysis was performed to quantify the dilution effect of EGR on the LTC cycles. Simplified relationships for estimating the composition differences between the in-cylinder, intake and exhaust conditions were proposed. A two-lambda sensor scheme was developed for implementation of the analysis during the engine tests.

Phase 3: The results of the diagnostics phase provided the essential guidelines for the detailed empirical analyses of the diesel LTC cycles. The HTC and the LTC cycles were investigated under different engine operating conditions. The individual effects of intake gas management (boost pressure and EGR), and fuelling strategies (injection pressure, injection scheduling and number of injections) on the LTC cycles were analyzed and quantified. Detailed emission and efficiency comparisons were made between the different modes of LTC and the limiting conditions for each mode were identified. The effects of the intake gas treatment through catalytic oxidation and fuel reforming of EGR on the LTC cycles were empirically investigated.

Phase 4: The final requirement of this research investigation was to identify the critical control parameters (based on the testing and diagnostics phases) for an effective adaptive LTC control strategy that would enable stable engine operation while reducing the penalty on engine performance and exhaust emissions. An adaptive control strategy was devised to integrate the systematic control of boost and EGR with the combustion control performed on a cycle-by-cycle as well as with the same combustion-cycle basis. Tests were conducted to assess the performance of the control system for enabling and stabilizing the LTC cycles.

1.8. Dissertation Outline

The dissertation outline is schematically shown in Figure 1.9. The diesel combustion is described in Chapter 1 and a brief history of the emission regulations is presented. Thereafter, a brief literature review is presented in Chapter 2 which includes the current solutions for the diesel HTC NOx-Soot trade-off, mechanisms for simultaneous reduction of NOx and soot and a brief description of the diesel LTC. Chapters 3 outlines the research methodology for the research work and Chapter 4 presents the salient features of the experimental setup and the overall system development program in detail.

The combustion diagnostics are reported in Chapter 5. The in-cylinder sampling tests include the LTC NOx reduction mechanism, presented on the crank angle-resolved basis and the crank angle-resolved NOx evolution for Dimethyl Ether fuelled homogeneous combustion. The cylinder pressure analyses for providing a robust feedback for LTC control are then described. The suitability of a number of cylinder pressure based parameters as control feedback is presented. Comparisons are also made between different heat release models, and the effects of combustion phasing and fuelling strategies on the CA50 prediction are analyzed.

Chapter 6 presents the analysis of the exhaust gas recirculation in the context of LTC combustion. The efficacy of EGR under the LTC operating conditions is analyzed and the composition difference between the trapped and intake conditions is characterized with excess air ratios for the in-cylinder and intake conditions. A two-lambda sensor scheme is devised and implemented for the systematic control of the combustion. This is followed by the intake gas treatment through catalytic oxidation and fuel reforming of EGR to generate gaseous fuels. Novel flow management strategies with central heating and central fuelling are devised to improve the energy efficiency of the reformer.

The empirical results highlighting the testing of diesel LTC combustion are presented in Chapter 7. The diesel high temperature combustion is first analyzed and the need for applying LTC regimes is discussed. This is followed by testing of the LTC combustion strategies including single-shot enabled LTC, multi-shot early LTC and split-burning LTC. Efficiency and emission comparisons are made and the individual effects of injection pressure and intake gas treatment (boost and EGR) are analyzed. Based upon the results, a LTC load management strategy is proposed.

The test results for the adaptive and systematic combustion control to stabilize and improve the LTC performance are given in Chapter 8. Both the cycle-by-cycle and within-same-cycle control techniques are developed and implemented. The implementation of the systematic control of boost and EGR with the combustion control is demonstrated with engine tests.

Finally, the most significant findings of the research investigation are summarized, conclusions are drawn and the future work is recommended in Chapter 9.

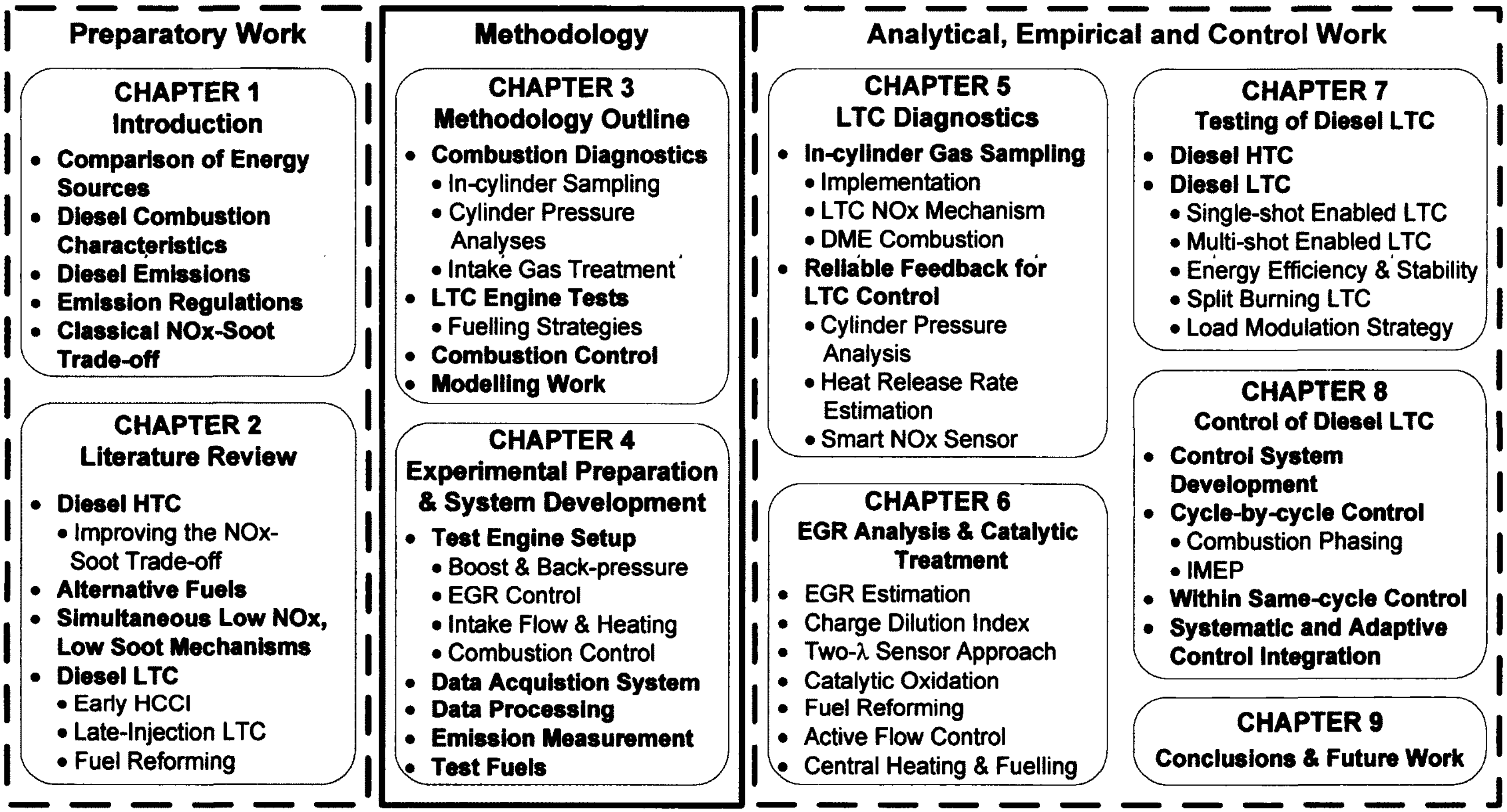

Figure 1.9: Dissertation Outline

CHAPTER II

2. LITERATURE REVIEW

This chapter provides an overview of the previously published work, addressing improvements in the conventional diesel combustion as well as alternate clean diesel-combustion strategies. The first part of the review was to study and gain insight into the various mechanisms used for improving the diesel NOx-soot trade-off. This included the management of combustion parameters like boost, EGR, injection pressure etc as well as the hardware improvements. Modifying the fuel properties is another venue of active research for achieving cleaner combustion in diesel engines. Therefore, a review of the alternative fuels and their performance has also been included. Combustion strategies for simultaneous NOx and soot reduction as reported in the literature were then examined and the salient features and limitations of each strategy were highlighted.

2.1. Improving the Diesel NOx-Soot Trade-off

The improvements in the classical NOx-soot trade-off have been achieved through a combination of hardware changes and combustion system modifications. The underlying objective was to enhance the mixing of the fuel-air charge so that the local strength of the mixture was reduced and a more global distribution of the fuel-air charge was achieved. This resulted in reducing the sooting tendency of diesel combustion while the NOx was suppressed with advanced EGR technologies that resulted in reducing the charge temperature.

The primary hardware changes to shift the NOx-soot trade-off closer to the origin included improvements in the design of the piston bowl (Mexican hat, shallow 'w', re-entrant, double re-entrant profiles) and the injector nozzle (hole size, spray angle and number of holes), chamber swirl enhancement, advanced turbochargers with variable geometry turbines, enhanced EGR coolers, multi-valve cylinder head designs, higher injection pressures with common-rail injection systems and air-path optimization.

The improvements in the combustion included multiple injections to improve the homogeneity of the cylinder charge, post-injection to facilitate soot oxidation during the late combustion phase, higher boost pressures to improve the availability of oxygen for the injected fuel, injection rate shaping, injection timing retard and EGR to prolong the ignition delay, thereby increasing the premixed combustion phase while reducing the combustion temperature. The limitations of the current technologies in meeting the future emission standards with conventional diesel combustion are highlighted in Chapter 7. Some important SAE publications during the last 2 decades that describe the improvements made in the NOx-soot trade-off and the technologies involved are listed in APPENDIX A.

2.2. Alternative Fuels

In recent years, the concern over depleting world reserves of fossil fuels and more stringent emission regulations have led to resolute efforts for renewable alternative fuels and low-emission combustion strategies. Moreover, the fuel properties such as the boiling point and cetane number, among others, can have a significant effect on the LTC performance [40]. These fuel properties can alter the fuel/air mixing characteristics, ignitability and subsequent emissions formation. Therefore, a brief review of some of the commonly used alternative fuels for diesel engines is included.

2.2.1. Fischer-Tropsch Diesel Fuel

Fischer-Tropsch (FT) fuels are synthetic hydrocarbon fuels commonly made by synthesising coal or natural gas using Gas-to-Liquid (GTL) processes [41,42]. This involves the partial oxidation of a hydrocarbon fuel to produce synthesis gas (a mixture of CO and H_2) which is then catalytically converted (usually iron or cobalt based catalyst) into various liquid hydrocarbon fuels. The resulting fuel is composed almost entirely of straight chain hydrocarbons and is free of sulphur and aromatics resulting in a high-cetane distillate. Fischer-Tropsch diesel is similar to conventional diesel fuel with regard to its energy content, density and viscosity and it can be blended with diesel in any proportion without the need for engine or infrastructure modifications [42].

Fischer Tropsch diesel fuels, in neat state or blended with conventional diesels, have been investigated to improve diesel engine exhaust emissions. Previous results have shown that owing to their high cetane number and near zero sulphur and aromatic contents, FT diesel fuels are capable of reducing emissions on a variety of light and heavy-duty engines. The low aromatics content seems to contribute to the lowered particulate matter (PM) production from in-cylinder combustion [43,44].

2.2.2. Biodiesel Fuel

Biodiesel is a non-toxic and biodegradable fuel that is made from vegetable oils, waste cooking oil, animal fats or tall oil (a by-product from pulp and paper processing). Biodiesel is produced from these feedstocks through a process called transesterification, by reacting the oil with an alcohol (usually methanol) and a catalyst (such as sodium hydroxide) [45]. The resulting chemical reaction produces glycerine and an ester called biodiesel. The majority of biodiesel is produced by this method. Biodiesel fuel, derived from agricultural products or recycled fat, is a renewable alternative for petroleum-derived diesel fuels [46–49].

In comparison with conventional diesel fuels, the fuel-borne oxygen in biodiesels, which could be over 10% by mass, is capable of reducing engine-out emissions of PM, CO and UHC in modern four-stroke compression-ignition engines [47,48,51,52]. However, a slight increase in emissions of NOx, which could be partially caused by the fuel property-incurred combustion timing variations, has been observed in the use of oxygenated fuels in general [50].

Biodiesel fuel is being increasingly endorsed by the engine manufacturers to be used in low blend levels (for e.g. B5 i.e. 5% of biodiesel blended with 95% of conventional diesel). However, the impact of higher blends of biodiesel like B20 in modern common-rail injection systems still needs to be identified. Additionally, biodiesel is known to degrade up to four times faster than diesel fuel [51]. The products of biodegrading could have detrimental effects on the injection components especially the high pressure fuel pump.

A new category of biodiesel fuel has emerged recently called the second generation or Fischer Tropsch Biodiesel. FT biodiesel is a synthetic biodiesel fuel that is produced using gasified biomass through the catalytic Fischer-Tropsch process [53]. Compared to the first generation biodiesel, the FT biodiesel is a non-oxygenated fuel, and therefore has higher energy content per unit mass, approaching or exceeding that of the conventional diesel fuel. The FT biodiesel is reported to have good storage stability unlike conventional biodiesel and also has low water solubility [54]. However, the information is scarce on combustion mechanism studies for a FT biodiesel fuel-powered diesel engine. The impact of FT diesels, especially FT biodiesels, on LTC cycles has not been quantified sufficiently.

2.2.3. Dimethyl Ether

Dimethyl ether (DME, chemical structure: $H_3C\text{-}O\text{-}CH_3$) is an oxygenated fuel with ~34% oxygen (O_2) by weight that can be mass-produced by synthesising natural gas or coal. The high fuel-borne oxygen content leads to nearly soot-free combustion in diesel engines while the NOx can also be reduced with EGR without being restricted by the NOx-soot trade-off. DME has a high cetane number and fuel droplets sprayed into the cylinder have been shown to evaporate at a rate about three times that of conventional diesel fuel. The higher evaporation rate reduces the tendency of fuel pyrolysis which promotes soot formation. Therefore, DME is a strong candidate for enabling LTC operation in diesel engines using multiple-injection strategies and a high level of EGR. However, the neat use of DME is hindered by its low lubricity and low viscosity that can shorten the life of the fuel-injection system [25].

Recently, the United States Department of Energy investigated the use of neat DME in a diesel engine operating under LTC cycles [55]. The results showed that the NOx emissions were below the US 2010 emission levels while the soot emission was nearly zero. Therefore, diesel exhaust aftertreatment devices for NOx and soot reduction may not be required with DME-fuelled engines.

Chapman et al. investigated the properties of DME-diesel fuel blends to assess the impact on the fuel-injection systems [56]. Their results showed that a 20% addition of DME into diesel fuel significantly reduced the viscosity of the fuel mixture, below the minimum requirement for the fuel injection system components. Therefore, the long-term equipment durability concerns need to be adequately addressed before widespread use of DME in diesel engines can materialize.

2.3. Mechanism for Simultaneous NOx and Soot Reduction

To attain low levels of NOx and soot simultaneously in diesel engines, a number of experimental and modelling studies have been carried out to understand the mechanisms of soot and NOx formation so that the pathways for simultaneous low NOx and soot combustion could be identified. Aoyagi et al. studied the soot formation process through in-cylinder sampling tests on a diesel engine and observed significant soot formation during the diffusion-controlled combustion when the maximum combustion temperature was between 2100 to 2300K and the maximum equivalence ratio between 1.5 to 3.5 (air-excess ratio, $\lambda \sim 0.67$ to 0.29) [12]. Similarly, Uyehara observed that the temperature range for soot formation was 2000 to 2400K in diffusion flames [20]. Kamimoto et al. studied the soot formation phenomenon in a rapid compression machine. Based on the measured equivalence ratio and flame temperatures, they concluded that the soot was formed in that region of the flame where the average equivalence ratio was rich and the flame temperature was high enough to promote pyrolysis of the evaporated fuel [57]. The effect of temperature and pressure on the soot formation due to fuel pyrolysis was studied in shock tubes by Frenklach et al. and their investigation demonstrated that the soot yield became significant around 1800K, while no soot was formed below 1500K or above 2300K [58].

Kamimoto et al. advanced their previous work with in-cylinder sampling studies on a diesel engine and in combination with their NOx modelling work, produced a local-equivalence-ratio versus local-temperature or the "ϕ-T" diagram that indicated the boundaries of the NOx and soot formation regions [17]. Their work is generally regarded as one of the first attempts to formulate the pathway for simultaneous low-NOx and low-soot. Akihama et al. and Kitamura el al. used CFD modelling to show the variation of soot formation inside the soot region on the ϕ-T map [35,59]. No soot formation was observed below 1500K regardless of the equivalence ratio. Similarly, for an equivalence ratio less than 2, no soot was formed regardless of the temperature. The maximum sooting tendency was around 1800~2000K and at higher temperatures, the sooting tendency was reduced for a given equivalence ratio.

All the above mentioned studies provided insights into the effect of in-cylinder temperature and air-fuel ratio on the formation of NOx and soot, typically shown on a $\phi - T$ diagram such as Figure 2.1.

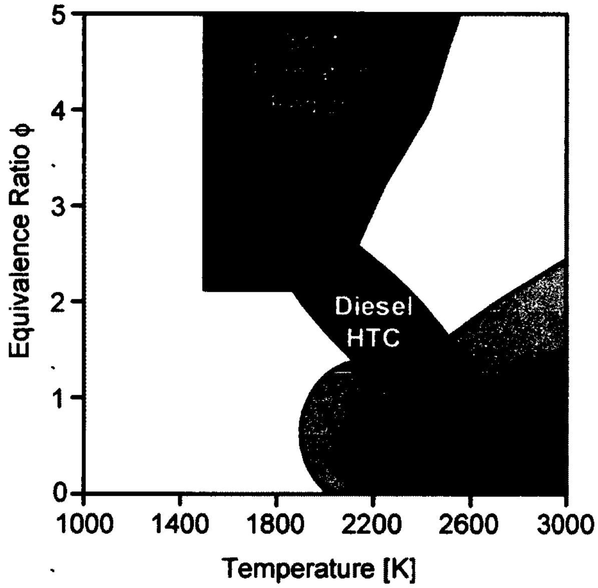

Figure 2.1: φ-T Diagram (Adapted from Kamimoto et al. [17])

The $\phi - T$ correlation is applicable to a homogeneous cylinder charge or the locally homogeneous regions of a heterogeneous charge. For a conventional diesel engine, the non-homogeneity makes the local cylinder charge vary from rich to lean. Zheng et al. noted that the flame is prone to initialize in and propagate towards the locally stoichiometric regions [30]. The stoichiometric burning tends to produce very high flame temperatures that may also ignite the adjacent locally lean or rich mixtures. Thus, simultaneous NOx and soot formation is inevitable in such HTC processes.

Based on the above-mentioned experimental and modelling studies, it was perceived that for a thoroughly-mixed cylinder charge, the tendency for soot formation would be low, largely regardless of the mixture strength. However, to have simultaneous low levels of

NOx, the flame temperature must be kept below the threshold temperature for thermal NOx formation (usually 1800-2000K). Therefore, the preparation of a homogeneous cylinder charge before the initiation of combustion was considered a pre-requisite for achieving low temperature combustion (LTC) that resulted in simultaneous low-NOx and low-soot emissions.

2.4. Low Temperature Combustion

The mechanism discussed in the previous section requires the implementation of the homogeneous LTC either by pre-mixing to very lean equivalence ratios or by reducing the combustion temperatures of homogeneous mixtures with high equivalence ratios. This can be achieved by the heavy use of EGR or the homogeneous charge compression ignition (HCCI)-enabling technologies [60]. Based on experimental and modelling studies conducted at the Clean Diesel Engine Laboratory (CDEL), University of Windsor, the pathways for simultaneous NOx and soot reduction are shown on a $(1/\phi)$-T map in Figure 2.2. To circumvent the NOx and soot formation zones, the combustion temperature must be kept low, regardless of the equivalence ratio. The burning of a diesel fuel in an excessively lean or rich homogeneous cylinder charge tends to release heat less intensively than under stoichiometric burning and thus LTC is prevailing, the representative cases of which are the low-load lean HCCI ($\phi<0.5$) [61] and the fuel rich reforming ($\phi \approx 1.4\sim2$) [62,63]. When the fuel/air ratio is closer to stoichiometric, however, the combustion process tends to render high flame temperatures that need to be lowered with heavy EGR in order to qualify for LTC, the representative cases of which are the high-load HCCI and the smokeless combustion on the lean and rich side of stoichiometry respectively.

For the case of high load HCCI with heavy EGR, the combustion process is constrained to that part of the fuel that has homogenized with the highly diluted intake charge. Any left over fuel that has not vaporized or homogenized is likely to go to the exhaust or cause oil dilution because of the prevailing low temperatures and the high amount of dilution. However, if this portion of the fuel does burn, the combustion is prone to be a highly diluted diffusion process, approaching a high degree of homogeneity.

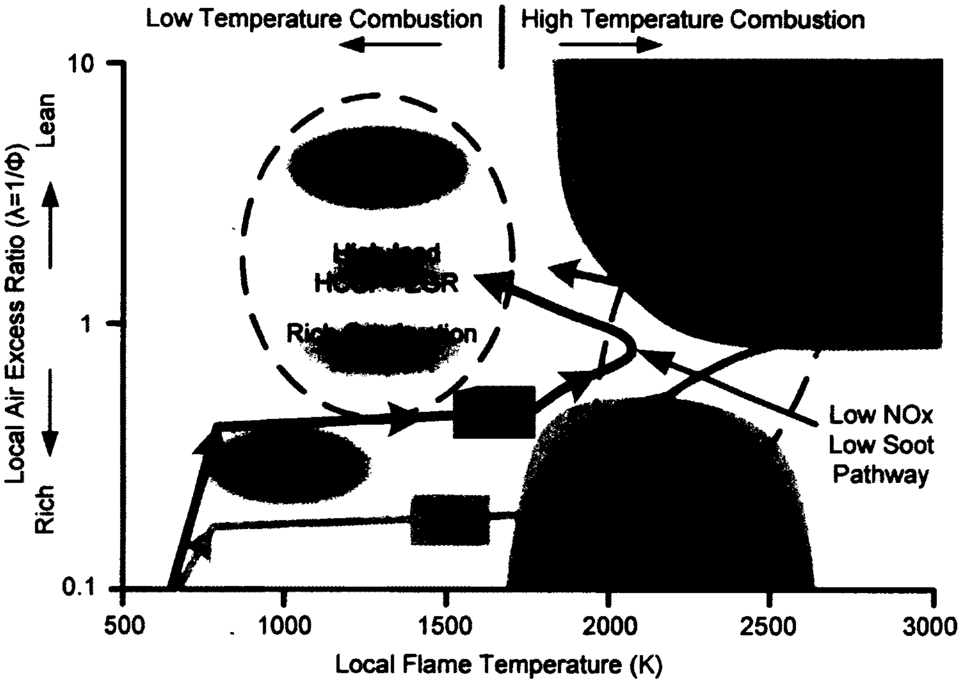

Figure 2.2: Pathways for Simultaneous NOx and Soot Reduction

LTC combustion in diesel engines can be broadly classified into two categories based on the timing of the fuel injection– the 'early-HCCI' where the fuel is injected very early in the compression stroke and the 'late-injection LTC' where a single injection closed to the TDC is employed along with heavy EGR. In the early-HCCI strategy, multiple in-cylinder fuel injections are usually employed to modulate the homogeneity history of diesel-HCCI cycles before the completion of the cylinder compression. Because of the high tendency of auto-ignition of diesel fuels, i.e. the high cetane numbers, EGR is normally employed to withhold the mixture from premature auto-ignition, which also helps with homogenization of the mixture. The late injection approach normally employs a single injection event near or after the end of piston compression, i.e. the TDC, to which high levels of EGR are normally applied concurrently. The effect of temperature reduction in the expansion stroke provides a prolonged ignition delay period thereby facilitating more mixing and resulting in a substantially enhanced premixed burning for such a main combustion event [33].

Stanglmaier and Roberts presented a review of the benefits, challenges and future engine applications of early-HCCI category of LTC [64]. They noted that altering the fuel/air mixture's time-temperature history can provide a means of controlling the ignition timing. The time-temperature history can be altered by modulating the intake temperature, in-cylinder injection timing, variable compression ratio, variable valve timing (VVT) or EGR, among others.

Helmantel and Denbratt studied the HCCI mode in a diesel passenger car using two compression ratios (CR 13.4:1 and CR 11.5:1) with early injection of conventional diesel fuel [65]. Up to 5 early injections were applied during the compression stroke to form a homogeneous fuel/air mixture before the start of combustion. Using high EGR rates coupled with low compression ratio, the combustion phasing was shifted close to the TDC. Both NOx and soot were reduced to near-zero levels; however, the combustion efficiency was compromised due to the high HC and CO emissions by 10~20%.

Kodama et al. [66] used a combination of different CRs, VVT, intake temperatures, a single early injection and appropriate EGR rates to achieve simultaneous low NOx and low soot emissions in a heavy-duty DI diesel engine at different engine loads. With a CR of 16.8:1, they were able to achieve a brake mean effective pressure (BMEP) of 5 bar; CR 13:1 for 8 bar; CR 10:1 + VVT for 18.3 bar (full load). In all the above cases, the CO and THC emissions were very high (>5%). For the full-load HCCI operation, an intake manifold pressure of 4 bar abs was employed and the maximum cylinder pressure and the maximum rate-of-pressure rise were 175 bar and 18 bar/°CA respectively, which are close to the upper limits for most production diesel engines.

The early-HCCI mode has been given various titles such as PREmixed lean DIesel Combustion (PREDIC), UNIform BUlky combustion System (UNIBUS), Premixed Compression Ignition (PCI) combustion while the late-injection LTC has been described as smoke-less rich combustion and Modulated Kinetics (MK) combustion, depending on the methodology employed to improve the homogeneity of the mixture. Figure 2.3 shows the classification of these modes on the basis of the injection timing relative to the timing of the auto-ignition. The fundamental objective of all these combustion modes is the completion of the fuel injection before the initiation of the combustion. It should be noted that the range shown for the injection and ignition timing is a representation of the operational limits and the actual timing would depend on the engine operating conditions. A brief review of these modes is therefore presented hereafter.

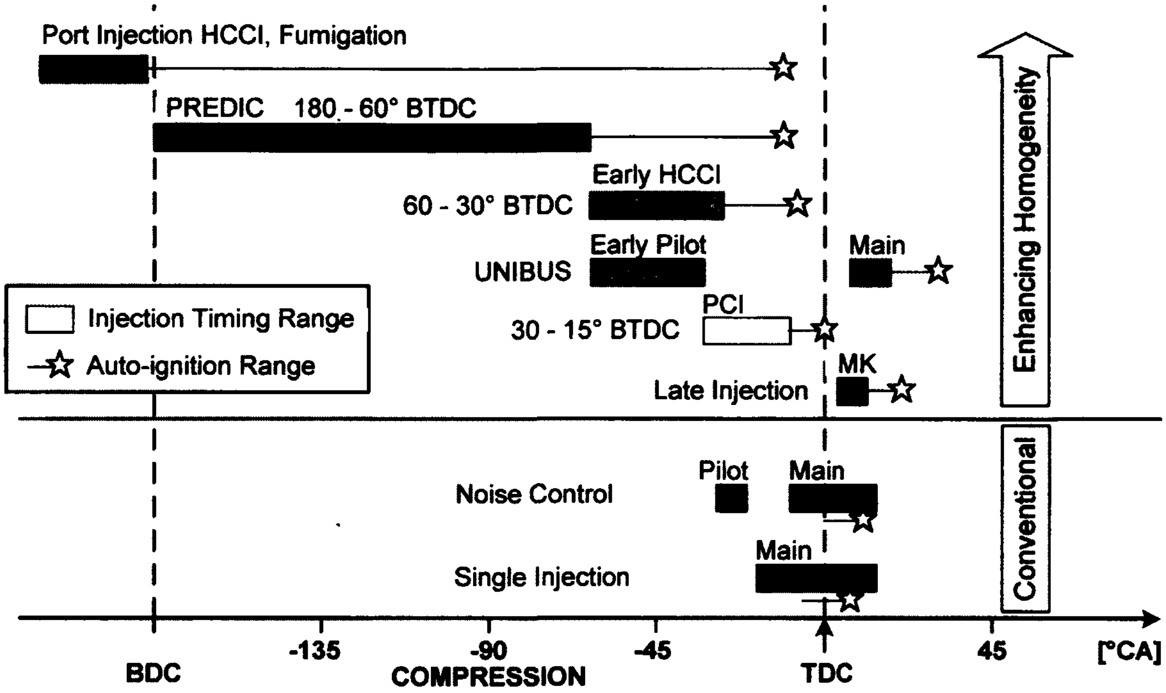

Figure 2.3: Classification of Conventional and LTC Modes based on Injection Scheduling (Adapted from Shimazaki et al. [67])

2.4.1. Early HCCI

The HCCI process utilizes an appropriate lean homogeneous fuel/air mixture which is compressed until combustion occurs as a result of spontaneous auto-ignition at multiple points through the chamber volume. As a result, HCCI combustion has no discernible flame propagation. The fuel-strength of the homogeneous charge has been found critical for stable HCCI combustion. An excessively lean mixture generally results in misfire or elevated hydrocarbon emissions, while a rich or insufficiently lean mixture may result in increased combustion noise (rapid rate of pressure rise) and even detrimental knocking.

A number of fuelling techniques have been used to attain a homogeneous mixture for early-HCCI category and these can be classified as port injection, early in-cylinder (single or multiple injections) and double in-cylinder injection. The port injection HCCI consisted of injecting and pre-mixing the fuel with the air before it entered the cylinder. While this technique worked well with highly volatile and knock-resistance fuels like gasoline, it posed a number of disadvantages for diesel HCCI, the foremost being premature ignition, lack of ignition control and the need for relatively high intake temperatures to prevent oil dilution. Moreover, this technique also resulted in high HC and CO emissions and poor fuel consumption.

The comparison of diesel port injection LTC with conventional diesel operation is shown in Figure 2.4 and Figure 2.5. These tests were run at the University of Windsor on a conventional diesel engine. It can be seen that for similar load levels, port injection HCCI had lower NOx and soot compared to the conventional diesel combustion but suffered from advanced combustion phasing and a high rate of pressure rise. Moreover, the CO and HC emissions were significantly higher compared to the conventional diesel combustion. The dilution of engine-oil with fuel was another significant drawback noticed during the port-injection experiments [68].

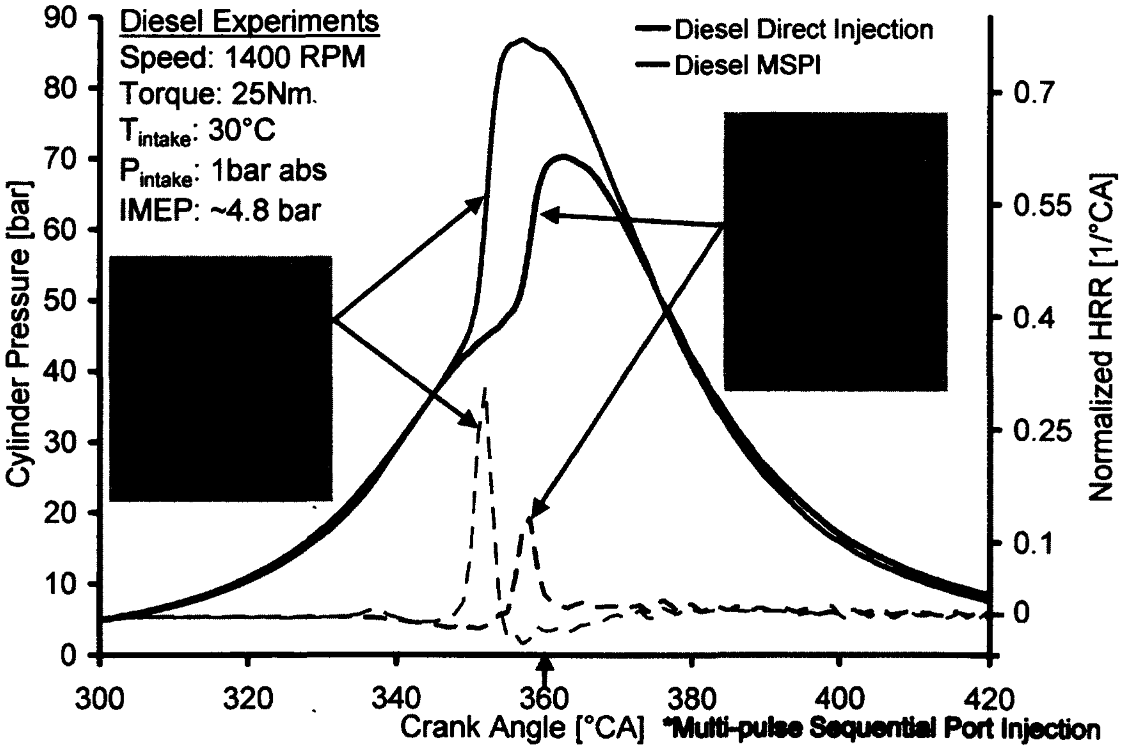

Figure 2.4: Diesel Port Injection Experiments at the University of Windsor

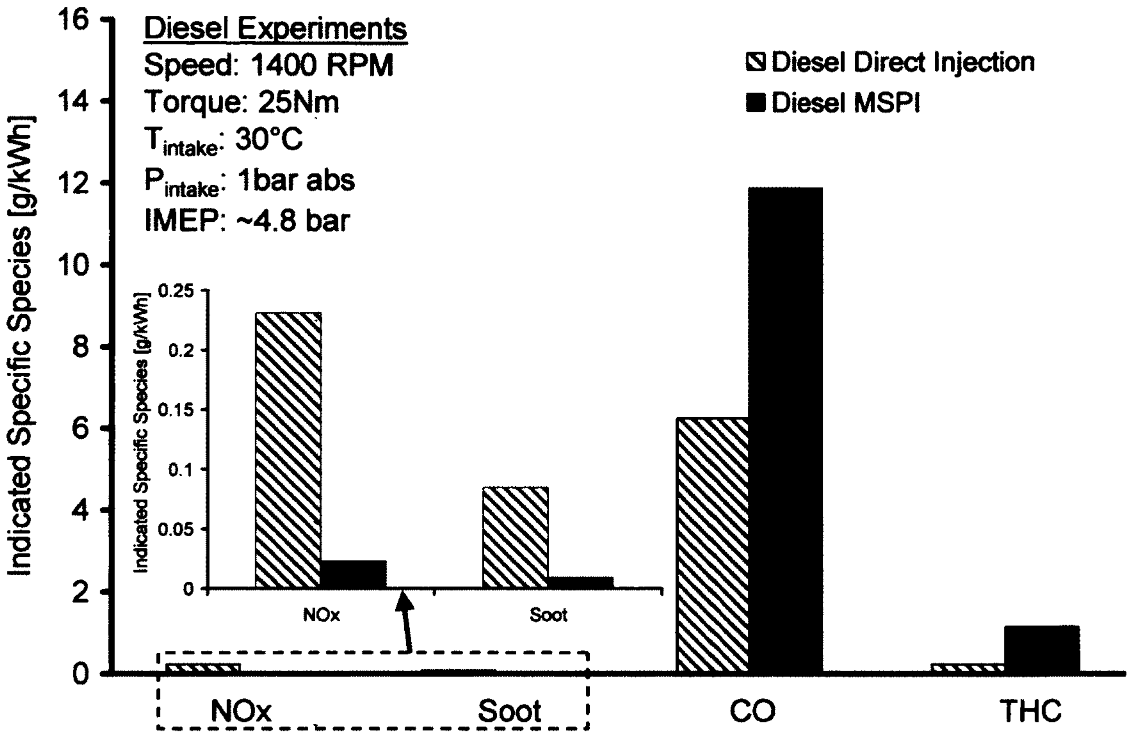

Figure 2.5: Emission Comparison for the Port Injection Experiments

2.4.1.1. PREDIC

In PREDIC mode, the fuel is injected extremely early (60~180°BTDC) into the cylinder, providing sufficient time for the preparation of a lean homogeneous charge necessary for simultaneous low-NOx and low-soot. Results at part load conditions ($\lambda > 2.5$) showed that the NOx concentration could be remarkably reduced to less than 1/10 of typical HTC values [69]. However, the formation of a premixed lean mixture is difficult as the quantity of fuel increases at higher loads. Moreover, fuel impingement on the cylinder walls is a major concern with this technique because of the very low cylinder charge densities at the time of the fuel injection [70,71].

2.4.1.2. UNIBUS

In the UNIBUS combustion concept, the first stage of combustion corresponds to the premixed lean combustion, and the second stage of combustion corresponds to diffusion combustion under high temperature and low oxygen conditions. A double injection is utilized for implementing this technique. The pilot injection is timed early in the compression stroke (40 – 60°BDTC). Injection timing and quantity, intake gas temperature and boost pressure are controlled precisely so that high temperature reaction does not appear before the main injection which takes place close to or after the TDC. The pilot-injected fuel undergoes low temperature reactions to break up the fuel to lower hydrocarbons and the main injection serves as an ignition trigger for the combustion of all the injected fuel [72]. The reported results for the UNIBUS combustion indicated a non-luminous flame with multiple ignition points in the bulk of the cylinder charge and low levels of NOx and soot emissions [73].

2.4.1.3. PCI

In PCI combustion, the fuel is injected into the combustion chamber in the vicinity of the TDC (15~30°BTDC) to prevent fuel from wetting the cylinder walls, while the mixing of the fuel-air charged is enhanced by increasing turbulence in the fuel–air charge (piston bowl shape, high swirl ratio) and also by introducing a large amount of cooled EGR which tends to increase the ignition delay [37]. A decrease in the over-rich regions of the mixture during combustion with EGR-assisted pre-mixing reduces soot emissions, and at the same time lowers the combustion temperature to reduce NOx emissions.

2.4.2. Late-Injection LTC

The late-injection LTC category employs a single injection close to or after the TDC which enables combustion phasing to be controlled by the timing of the injection event, similar to conventional diesel combustion and provides an advantage over port-injection and early-DI HCCI techniques. Since a relatively short ignition delay normally precludes thorough pre-mixing of the fuel-air mixture, high levels of cooled EGR, coupled with injection timing adjustment are commonly employed to prolong the ignition delay and to lower the flame temperature. The increased ignition delay allows more time for the fuel-air mixing and therefore improves the homogeneity of the cylinder charge. LTC tests run by the author (Figure 2.6) confirmed that an increase in the ignition delay over 50% of the baseline value (without EGR) was repeatedly seen to push the combustion into the LTC regime, at different engine operating conditions. Two variations of this LTC mode have been reported in the literature and are briefly discussed below.

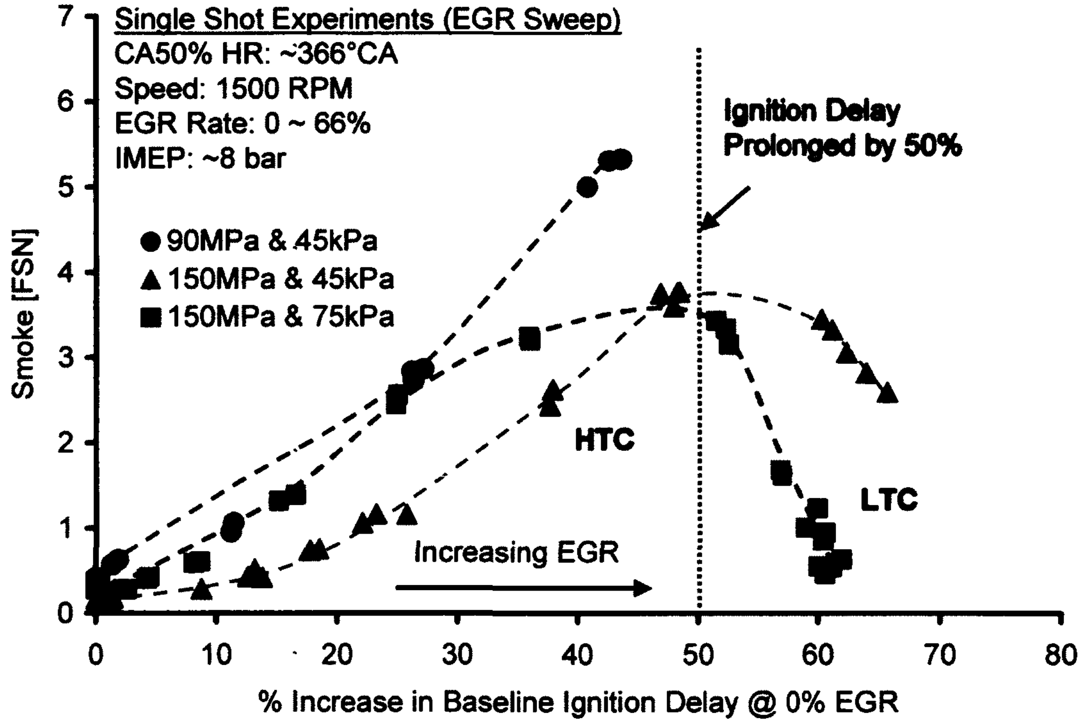

Figure 2.6: Prolonging the Ignition Delay to Enable LTC

2.4.2.1. Modulated Kinetics Combustion

The MK concept can be essentially characterized as a low-temperature, premixed combustion that is aimed at simultaneously reducing NOx and soot emissions. The lowered combustion temperature is accomplished by applying heavy EGR while smoke reduction is achieved by increasing the premixed combustion phase. The mixing time is increased by prolonging the ignition delay and dispersion of the injected fuel is promoted by increasing turbulence in the fuel–air charge (piston bowl shape, high swirl ratio, high injection pressure) to promote premixed combustion. The generation of turbulence also helps to lower the HC emissions [74–76].

2.4.2.2. Smokeless Rich Combustion

The smokeless rich combustion avoids the soot formation regions on the ϕ-T map by reducing the combustion temperature below the critical temperature for soot formation (approximately 1650 K) [35]. This can be realized by using large amounts of cooled EGR and the air-fuel ratio approaching near-stoichiometric or rich operating conditions instead of the lean-premixed conditions. However, the engine operation is characterized with high cycle-to-cycle variations, high HC and CO emissions and resultantly, a lower thermal efficiency. The same has been observed during experimental investigations carried out by the author and a typical result for an IMEP of 4.2 bar is shown in Figure 2.7 [77]. As the combustion transitions into the LTC cycles, the HC emission tends to rise sharply. Moreover, a significant drop in the IMEP is observed, which results in a significant penalty on the thermal efficiency.

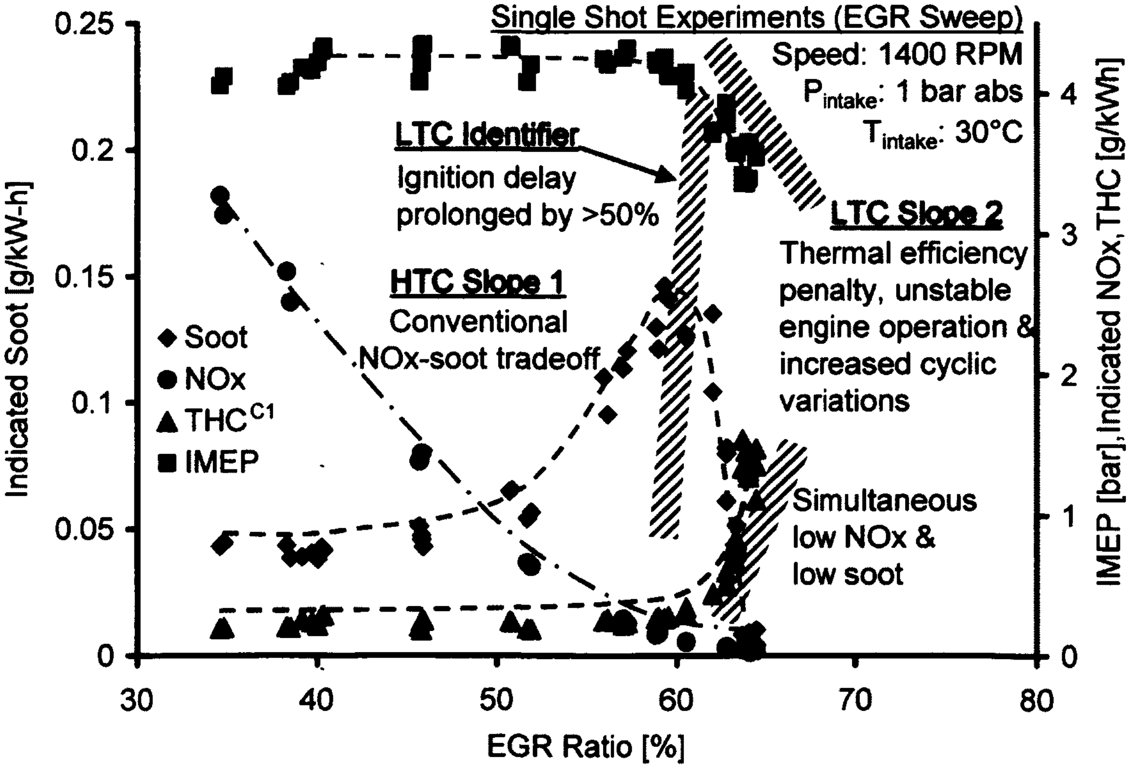

Figure 2.7: Fuel Efficiency Penalty associated with the Late-Injection LTC Mode

The smokeless rich combustion can also be realized using early-HCCI strategy, coupled with heavy EGR as shown by the test results generated at the Clean Diesel Engine Lab (CDEL). This allows moderate engine loads to be achieved compared to the single-injection LTC while maintaining low levels of NOx and soot emissions.

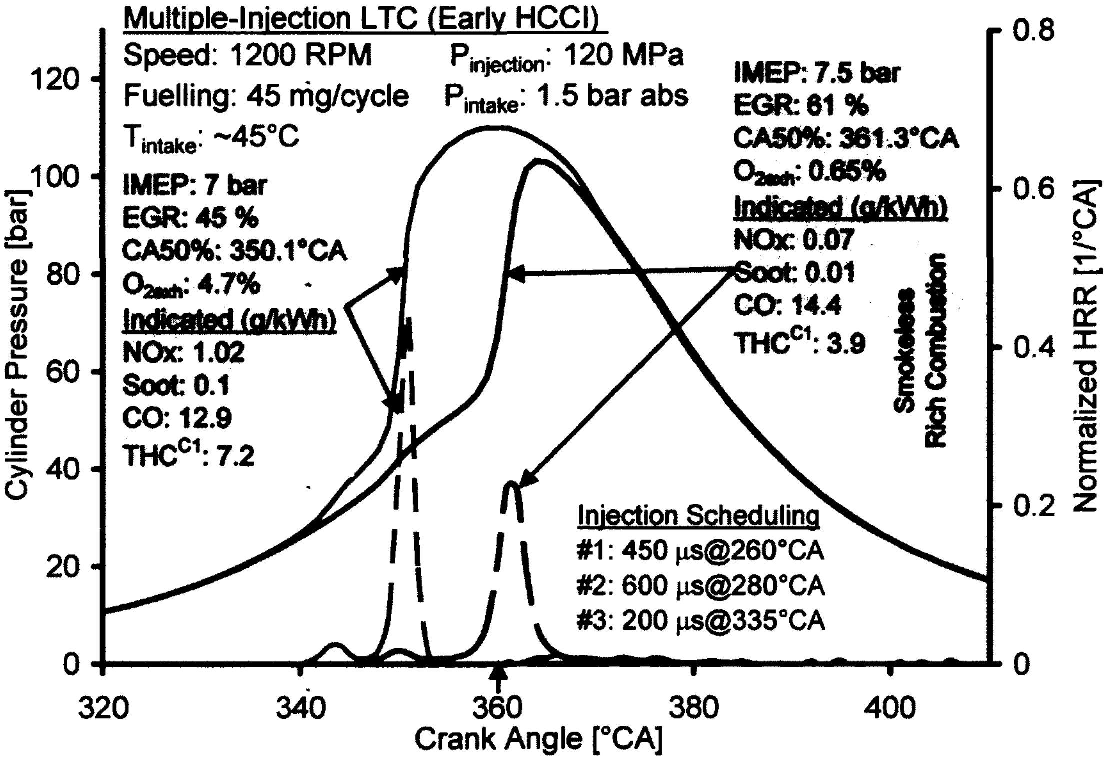

Figure 2.8: Smokeless Rich Combustion with Multiple-Injection LTC [78]

2.4.3. Diesel Fuel Reforming

Another mechanism for enhancing the premixed combustion during LTC operation is the generation of gaseous fuels like hydrogen (H_2) and CO, outside the engine cylinder. The participation of a gaseous fuel that increases premixed combustion may significantly alleviate problems with soot formation and may help to reduce the cyclic variations. Diesel exhaust normally contains significant amounts of surplus oxygen and has a temperature close to the level required for fuel reforming. Thus, it is reasonable to use the exhaust to catalytically reform some of the diesel fuel because the oxygen and heat of the exhaust can be utilized simultaneously.

The author has extensively investigated the diesel reforming process in the EGR loop of a conventional diesel engine and a detailed description and analysis of the EGR reforming is given in Chapter 6.

2.4.4. LTC Load Range

The maximum engine loads attained at different compression ratios as reported in the literature are shown in Figure 2.9. The results show that the load range of the LTC operation is significantly dependent on the compression ratio (CR) of the diesel engines since a higher compression ratio translates into a higher compression-end cylinder temperature. For diesel fuel injected in the intake port or very early in the compression stroke, the propensity of the cylinder charge to auto-ignite early in the compression stroke is therefore increased. As the quantity of the injected fuel is increased to enhance the engine load, it is difficult to withhold the cylinder charge from auto-igniting since the ignition delay is adversely affected by

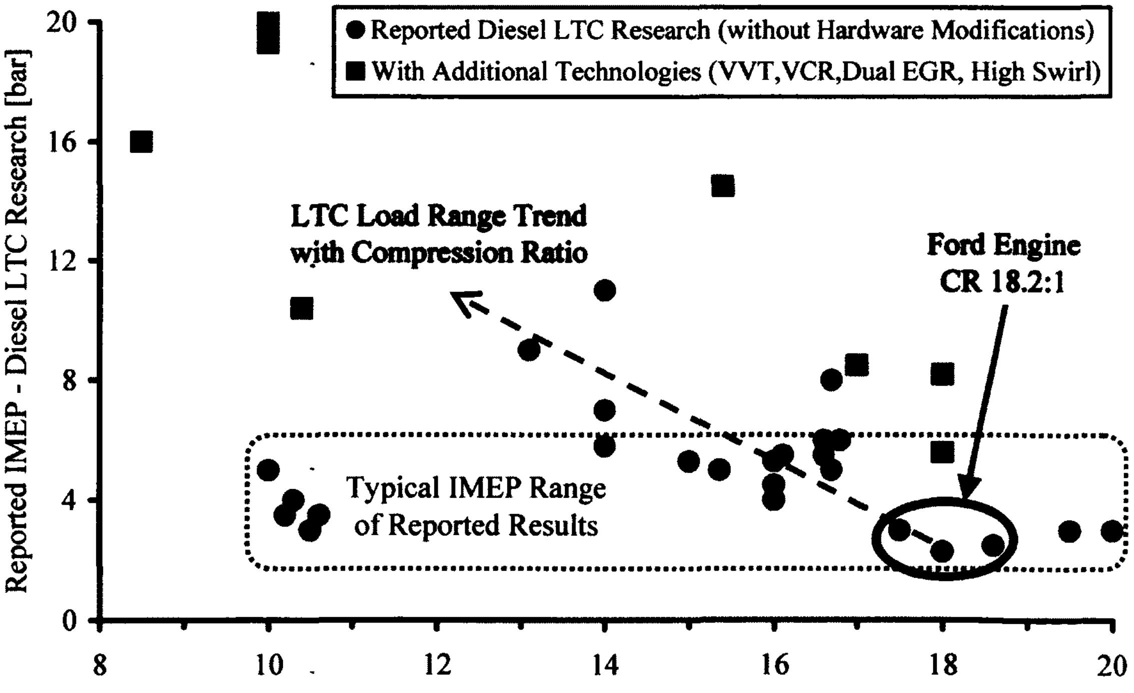

Figure 2.9: Reported IMEP for LTC Cycles in the Literature

the temperature and the fuel strength of the cylinder charge (equivalence ratio). The combustion process tends to produce very high rates of cylinder pressure rise $(dp/d\theta)_{max} > 20$ bar/°CA). Furthermore, the use of a higher boost pressure to reduce the equivalence ratio is restricted by the peak cylinder pressures of the early LTC which tend to increase above 160 bar, the nominal P_{max} threshold for production diesel engines.

Therefore, at compression ratios around 18:1 such as for the Ford test engine used in this research (details in Chapter 4), the maximum reported load is less than 4 bar IMEP for LTC operation.

2.5. Summary

Based on the literature review and the extensive testing of the diesel LTC cycles by the author and colleagues at the CDEL, the diesel LTC enabling technologies are summarized in Figure 2.10. The LTC enabling technologies are those techniques that assist in the transition from the conventional heterogeneous cylinder charge to a more homogeneous charge before the onset of combustion. If an early injection strategy is applied (port injection or early in-cylinder injections), then a sufficiently long time is available for mixture preparation, and a lean- or weak-homogeneous (EGR diluted) mixture can be prepared before the start of combustion. Similarly, a late-injection close to the TDC is afforded a long ignition delay with heavy EGR to enhance the charge homogeneity. The combustion of a lean- and/or EGR-diluted homogeneous mixture has the potential to produce a low combustion temperature that can simultaneously yield low-NOx and low-soot levels.

The current status of the LTC implementation in high compression ratio diesel engines is summarized in Table 2.1. The major limitations of the LTC operation include the high CO and HC penalty, low engine loads and unstable engine operation.

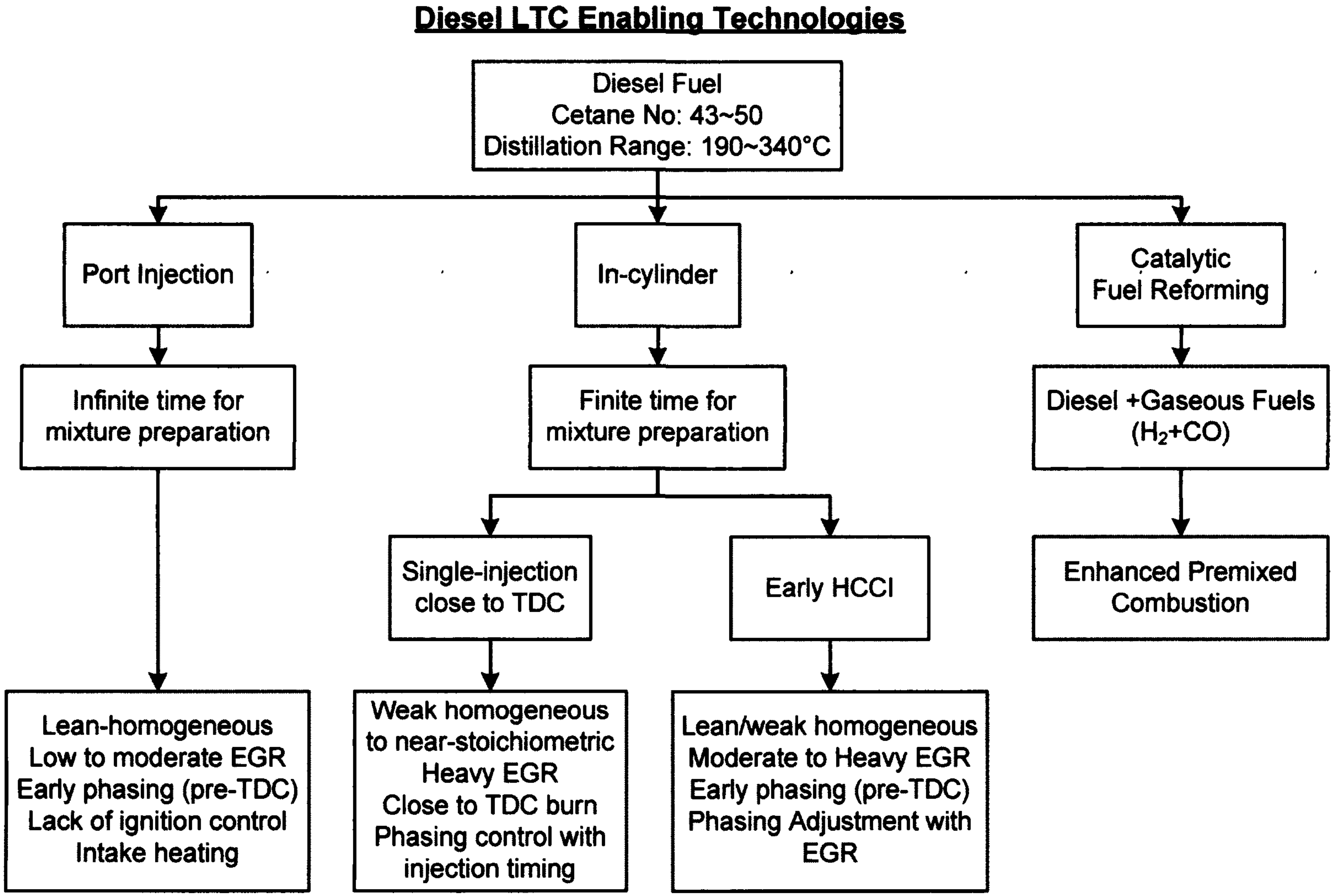

Figure 2.10: Diesel LTC Enabling Technologies

Table 2.1: Summary of High Compression Ratio Diesel LTC Operation

LTC	Status
Enabling Requirement	Separation of the fuel injection events from the combustion process
Combustion Characteristics	High cylinder charge homogeneity Low combustion temperatures Lean/EGR diluted
Thermal Efficiency	10 ~ 20 % Penalty
Emissions	Simultaneous low NOx and low soot achievable Moderate to very high HC and CO (>5%)
Load Range	Low (< 4 bar IMEP) Limited by P_{max}, $(dp/d\theta)_{max}$
Stability	Close to flame-out limits Higher cyclic variability
Fuelling Strategy	
Port Injection	High CO & HC Significant oil dilution (low volatility of Diesel) Lack of ignition control Intake heating Requirement
Early HCCI	Lack of ignition control P_{max}, $(dp/d\theta)_{max}$ restriction Moderate CO & HC
Late-injection	High CO & HC Unstable operation leading to mis-fire

CHAPTER III

3. METHODOLOGY OUTLINE

The literature review provided the motivation and the framework for formulating the objectives of this research. An overview of the research plan is shown in Figure 3.1. The current limitations of the LTC operation in high compression ratio diesel engines were translated into the main objectives of the research that include improvement in the LTC fuel efficiency and stability, extension of the LTC load range and enabling transition between the HTC and LTC combustion modes.

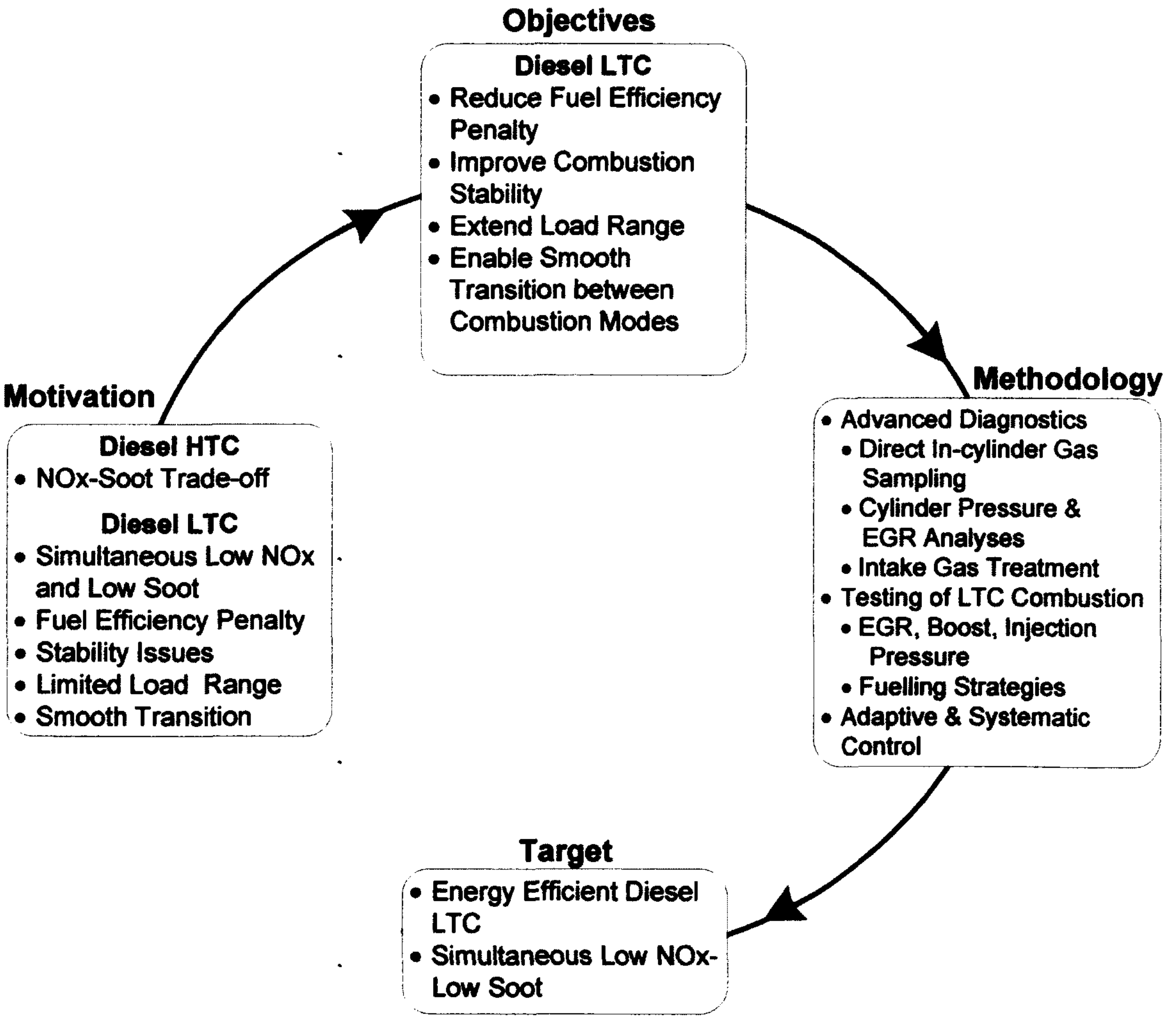

Figure 3.1: Overview of the Research Work

Figure 3.2 presents a summary of the research methodology employed in this work. The improvements of the diesel LTC cycles were primarily based on experimental investigations and observations. Therefore, the empirical work undertaken during the course of the research entailed an elaborate and sophisticated experimental setup, described in Chapter 4. Theoretical analyses were performed to understand the empirical results and to develop the boundary condition for the tests, and the details of the modelling tools used for the analysis have therefore been provided.

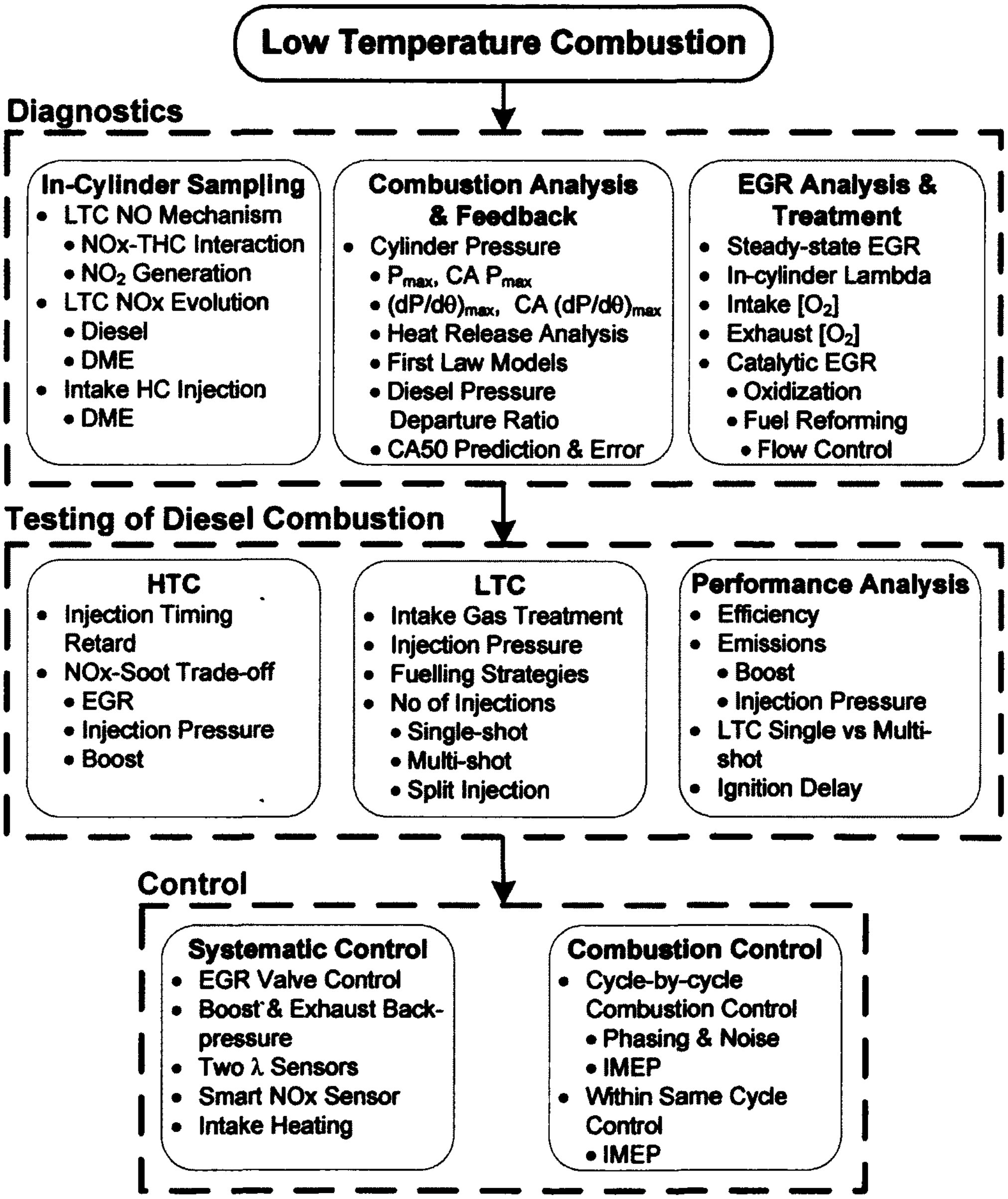

Figure 3.2: Schematic of the Research Methodology

3.1. LTC Diagnostics

The formulation of the diesel LTC testing phase and the development of an effective control strategy in this research were supported with in-cylinder combustion diagnostics, cylinder pressure analyses and intake gas treatment studies. A brief description of each is provided below.

3.1.1. In-cylinder Direct Gas Sampling

The pollutant formation processes during the high temperature combustion in a conventional diesel engine have been investigated extensively through in-cylinder sampling studies, laser diagnostic procedures and high-speed imagery and high-speed exhaust gas analysis [11–20]. As a result, several mathematical models of various complexities have been reported in the literature to accurately simulate the diesel combustion and the resulting exhaust pollutants [21,26,31,80]. Some optical studies for diesel LTC have been recently reported in the literature but a quantitative picture of the in-cylinder LTC mechanism that results in simultaneous low NOx and low soot is generally not available.

Therefore, to provide an insight into the combustion and pollutant formation processes during LTC mode and to help improve the methodology for LTC research, an elaborate in-cylinder sampling system was implemented. Engine tests were conducted to study the LTC NOx mechanism in the presence of high amounts of unburnt hydrocarbons on a crank angle-resolved basis. The in-cylinder NOx evolution was studied for the DME-fuelled combustion. DME, a fuel with cetane number and combustion characteristics similar to diesel, also has high oxygen contents which offer the intrinsic advantage of nearly soot-free combustion. The use of DME was primarily done to prevent damage to the in-cylinder gas sampling valve which would otherwise be clogged with the soot generated during the combustion of conventional diesel fuel.

3.1.2. Combustion Analysis & Feedback

The cylinder pressure was analyzed in the context of providing a robust feedback for LTC control. The suitability of a number of cylinder pressure based parameters as control feedback was examined. Comparisons were also made between different heat release models, and the effects of combustion phasing and fuelling strategies on the CA50 prediction were quantified. A computationally efficient algorithm was proposed for predicting the combustion phasing with sufficient accuracy for a wide range of diesel combustion regimes.

3.1.3. EGR Analysis & Catalytic Treatment

An elaborate EGR analysis was performed to develop simplified relationships for estimating the composition differences between the in-cylinder, intake and exhaust conditions. The efficacy of EGR for LTC mode was quantified in terms of the intake gas composition and the load level.

The composition and properties of the intake gas have been reported to significantly influence the performance of the LTC cycles [27,60,79]. Therefore, the test program was to investigate and quantify the effects of the major intake gas parameters including pressure and composition on the LTC operation as indicated in Figure 3.3. The catalytic treatment of EGR was also studied in detail as a means to reduce the fluctuations in the intake gas composition, pressure and temperature, and to reduce the detrimental effects of EGR.

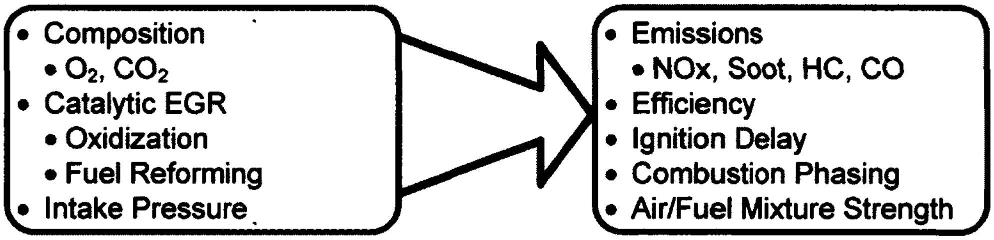

Figure 3.3: Intake Gas Treatment

3.2. Testing of Diesel LTC

The testing phase of the diesel LTC included a detailed analysis of the LTC performance metrics through engine tests. Emission, stability and efficiency comparisons were made between the different modes of LTC and the limiting conditions for each mode were identified. The individual effects of injection pressure and intake gas treatment (boost, composition) on enabling the LTC cycles was also analyzed.

3.2.1. LTC Fuelling Strategies

A number of in-cylinder fuelling strategies to enable LTC combustion in diesel engines were investigated as shown in Figure 3.4. The late-injection approach normally employs a single injection event near or after the end of piston compression, i.e. the TDC, to which high levels of EGR are normally applied concurrently. The effect of temperature reduction by piston expansion stroke provides a prolonged ignition delay thereby facilitating more mixing, resulting in substantially enhanced premixed-burning in such a main combustion event.

In the early-injection strategy, multiple in-cylinder fuel injections are usually employed to modulate the homogeneity history of diesel HCCI cycles before the completion of the cylinder compression. Because of the high tendency of auto-ignition of diesel fuels, i.e. the high Cetane numbers, EGR is normally employed to withhold the mixture from premature auto-ignition, which also helps with homogenization of the mixture.

To extend the load level of the LTC operation, a split-injection strategy was also investigated where a part of the fuel was delivered early with multiple injection events while the load enhancement was achieved with post-TDC fuelling. The post-TDC combustion can also benefit from the virtual EGR generated by the combustion of the early-injections.

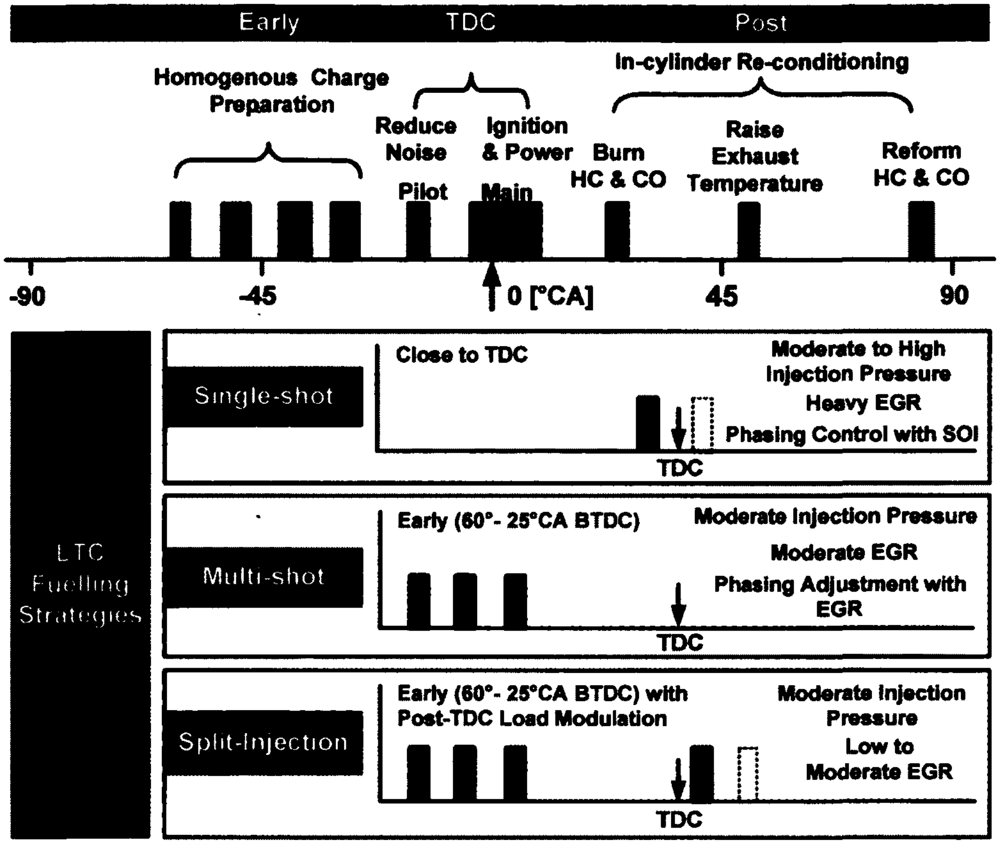

Figure 3.4: In-cylinder LTC Fuelling Strategies

3.3. LTC Control Methodology

Based upon the experimental findings and the diagnostics results of the LTC cycles, there was a need to devise an adaptive LTC control strategy that would enable stable engine operation while reducing the penalty on engine performance and exhaust emissions. A composite strategy was formulated by developing systematic control of boost and EGR and integrating it with an adaptive combustion control technique performed on a cycle-by-cycle as well as within-same-cycle basis. Confirmation tests were conducted to verify the improvement in the LTC operation with the proposed control system.

3.4. Modelling Work

The high complexity of the processes occurring in an internal combustion engine makes it difficult to develop mathematical models that can accurately predict the engine performance as observed with empirical investigations under a wide range of operating conditions. The scope of application of these modelling tools is narrow mainly due to the complexity of the processes involved. This is also the reason why the field of internal combustion engine research is dominated by sophisticated experimental techniques. However, the use of modelling tools, primarily in the form of computer codes, is still widespread as it is less resource intensive and far less time consuming compared to conducting actual engine tests. The models after proper calibration and validation with experimental data can provide useful insights into some of the fundamental mechanisms governing the combustion.

In this work, 0-D engine-cycle simulations were performed to perform a parametric evaluation of the diesel combustion. Engine-cycle simulation packages including Ricardo WAVE and Synthetic Atmosphere Engine-cycle Simulation (SAES) [81] were used to analyze the cylinder pressure and heat release characteristics. A 0-D EGR simulation program was developed to analyze the intake gas treatment of LTC operation and to facilitate the development of the control feedback. The liquid spray penetration for diesel sprays under the engine compression process was simulated by integrating a spray penetration model with a 0-D diesel engine cycle simulation program. The effect of injection pressure, boost pressure and the injection timing was analyzed to improve the selection criterion for the early injection HCCI cycles. Chemical kinetic simulations using CHEMKIN software were also performed to improve the understanding of the LTC regimes and to help explain the in-cylinder diagnostics results.

CHAPTER IV

4. EXPERIMENTAL PREPARATION AND SYSTEM DEVELOPMENT

In this chapter, the details of the hardware preparation work carried out including the baseline engine setup, engine sub-system development, fast-response emission analyzer repair, data acquisition, control system setup and fuel system are described. The modifications carried out on the engines for in-cylinder gas-sampling system installation, EGR reforming tests are explained in the subsequent chapters. The post-processing techniques employed for analyzing the test results are also briefly covered and include the quantitative and qualitative analysis of the engine performance and emissions of NOx, soot, THC and CO.

4.1. Test Engines

The engine tests have been carried out on two DI diesel engines. The first is a naturally-aspirated, four-stroke, single-cylinder Yanmar NFD170 engine, coupled to a DC motoring dynamometer. The second is a modern common-rail Ford Duratorq DI diesel engine, coupled to an eddy current dynamometer.

4.1.1. Yanmar Single Cylinder DI Diesel Engine

The Yanmar NFD170 is a horizontal type, single cylinder DI diesel engine with the specifications given in Table 4.1. The original engine configuration was modified to include independent control of EGR, sequential intake port injection, intake air pre-heating and throttling. The resulting baseline configuration is shown in Figure 4.1.

The EGR flow rate was controlled through a combination of EGR valve opening and intake air throttling to achieve the desired levels of EGR. Conversely, an exhaust back-pressure control system could also be utilized for enabling EGR as was done for the Ford engine. The baseline engine setup was extensively modified for the in-cylinder gas sampling, EGR oxidation and fuel reforming tests. The details of the modifications are given in detail in the subsequent chapters.

Table 4.1: Geometric Specifications of the Yanmar Engine

Displacement [Litre]	857 cm^3
Bore [mm]	102 mm
Stroke [mm]	105 mm
Connecting Rod Length [mm]	165
Compression Ratio	17.8:1
Deck Clearance [mm]	1.13
Intake Valve Closing (IVC)	-135°ATDC
Exhaust Valve Opening (EVO)	45°BBDC
Combustion System	Direct Injection
Injection System	Inline Pump with Mechanical Governor
Injection Timing	Single Injection @ -17°ATDC
Nozzle Opening Pressure	204 bar

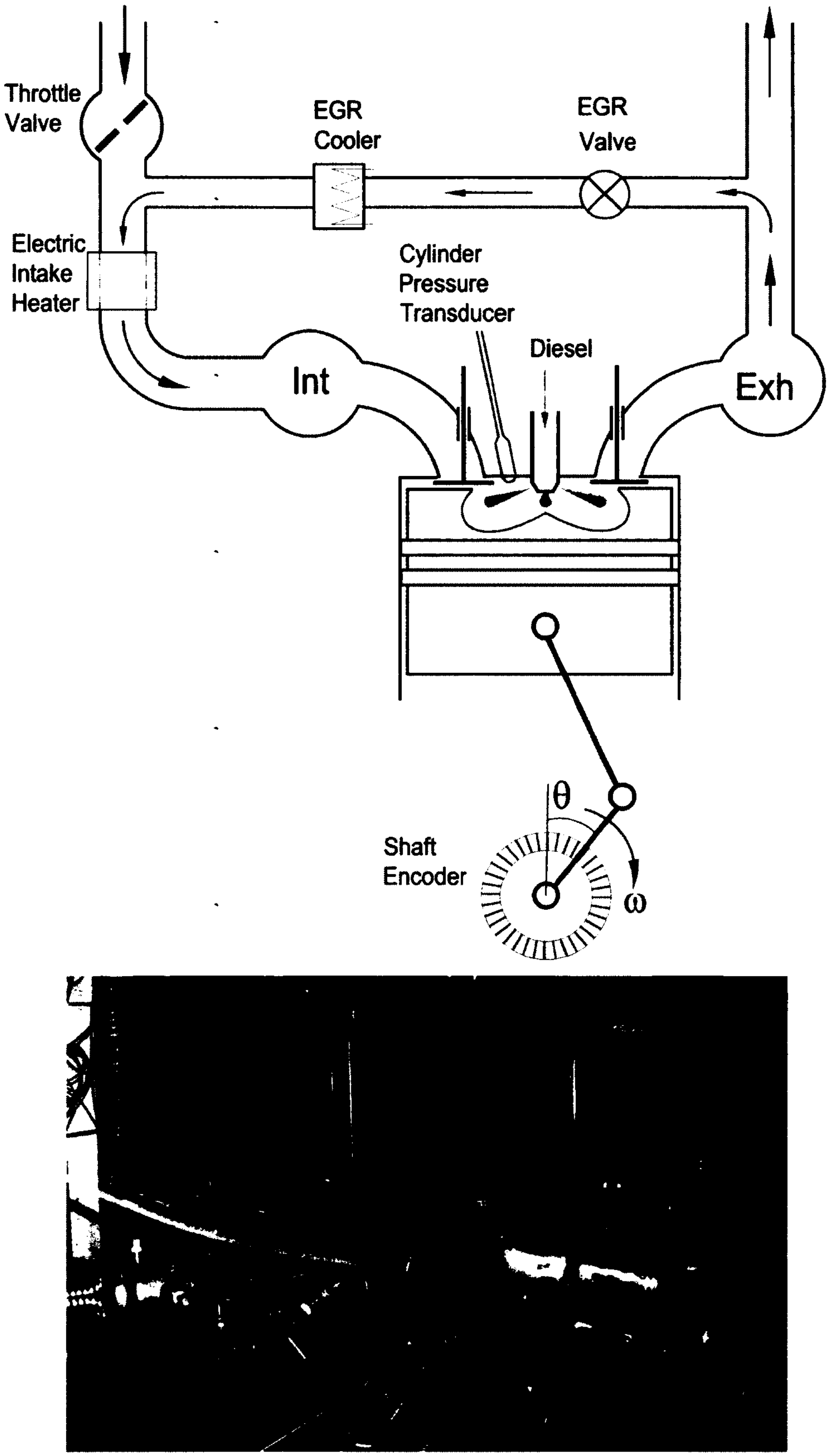

Figure 4.1: Baseline Setup of the Yanmar DI Diesel Engine

4.1.2. Ford Common Rail DI Diesel Engine

The Ford ZSD-420 Duratorq is a 2.0L, 4-cylinder, common-rail DI diesel engine commonly known as "Ford Puma", with the specifications as given in Table 4.2.

Table 4.2: Geometric Specifications of the Ford Engine

Displacement [Litre]	1988 cm^3
Bore [mm]	86 mm
Stroke [mm]	86 mm
Compression Ratio	18.2:1
Combustion System	Direct Injection
Swirl Ratio	1.7
Injection System	DELPHI Common-rail (Rail pressure up to ~ 1600bar)

The original engine configuration consisted of a single-stage variable geometry turbocharger (VGT) that provided the required levels of boost and EGR by adjusting the vane position and the opening of the EGR valve. The coupling of the boost pressure and the EGR in this manner limited the simultaneous availability of high boost pressure and high EGR required for investigating the alternate combustion regimes. Moreover, since the engine was coupled to an eddy current dynamometer, operating the engine at high cycle-to-cycle variation conditions which are inherent with the use of heavy EGR was not possible.

The original Ford engine configuration was therefore modified by separating Cylinder #1 from the other three cylinders to run in a single-cylinder mode as shown in Figure 4.2. The 3 cylinders–to–1 cylinder configuration enabled the investigation of unstable combustion regimes with a non-motoring dynamometer [82]. The 3 cylinders were operated in the conventional HTC mode at low load for stable engine operation. The combustion in Cylinder #1 was then pushed into the LTC cycles by independently controlling the EGR, boost, exhaust back-pressure and the fuel injection scheduling. An alternate to this strategy could be the use of a motoring dynamometer with the 3 cylinders operating under motoring conditions while the first cylinder is fired during the tests.

The single-cylinder mode required the intake and the exhaust systems of Cylinder # 1 to be separated from the other three cylinders. A new intake manifold was constructed with the provision of running Cylinder #1 with either an independent intake system or using the same intake as the rest of the cylinders. The exhaust stream of Cylinder #1 was also separated from the rest of the cylinders because the exhaust gas from the single cylinder was required for measuring the emissions. Tests were carried out to ensure that there was no cylinder-to-cylinder cross-contamination during the emission measurements [82].

The engine coolant condition was monitored and controlled closely with an external conditioning system to minimize the discrepancies of the testing results. For all the tests described in this thesis, the coolant temperature was set at 80°C.

To run the engine in the modified configuration, the original engine control unit (ECU) could not be used. Therefore, independent control of fuel injection scheduling and the common-rail fuel-injection pump was implemented using real-time (RT) controllers embedded with field programmable gate array (FPGA) devices. The details of the control hardware are given later in this chapter.

4.2. Fuel System

The fuel system for both the engines is schematically shown in Figure 4.3. The Yanmar engine could be supplied fuel either from the internal fuel tank, the external fuel system or from two glass bulbs having volumes of 37 ml and 57 ml. This provided flexibility in measuring and verifying the fuel consumption at different engine operating conditions. The fuel supply to the Ford engine consisted of a low-pressure supply circuit. Two volumetric fuel-flow detectors were used to provide an accurate measurement of the fuel consumption. Heat exchangers were installed in the fuel return lines to minimize the variations in the fuel supply temperature.

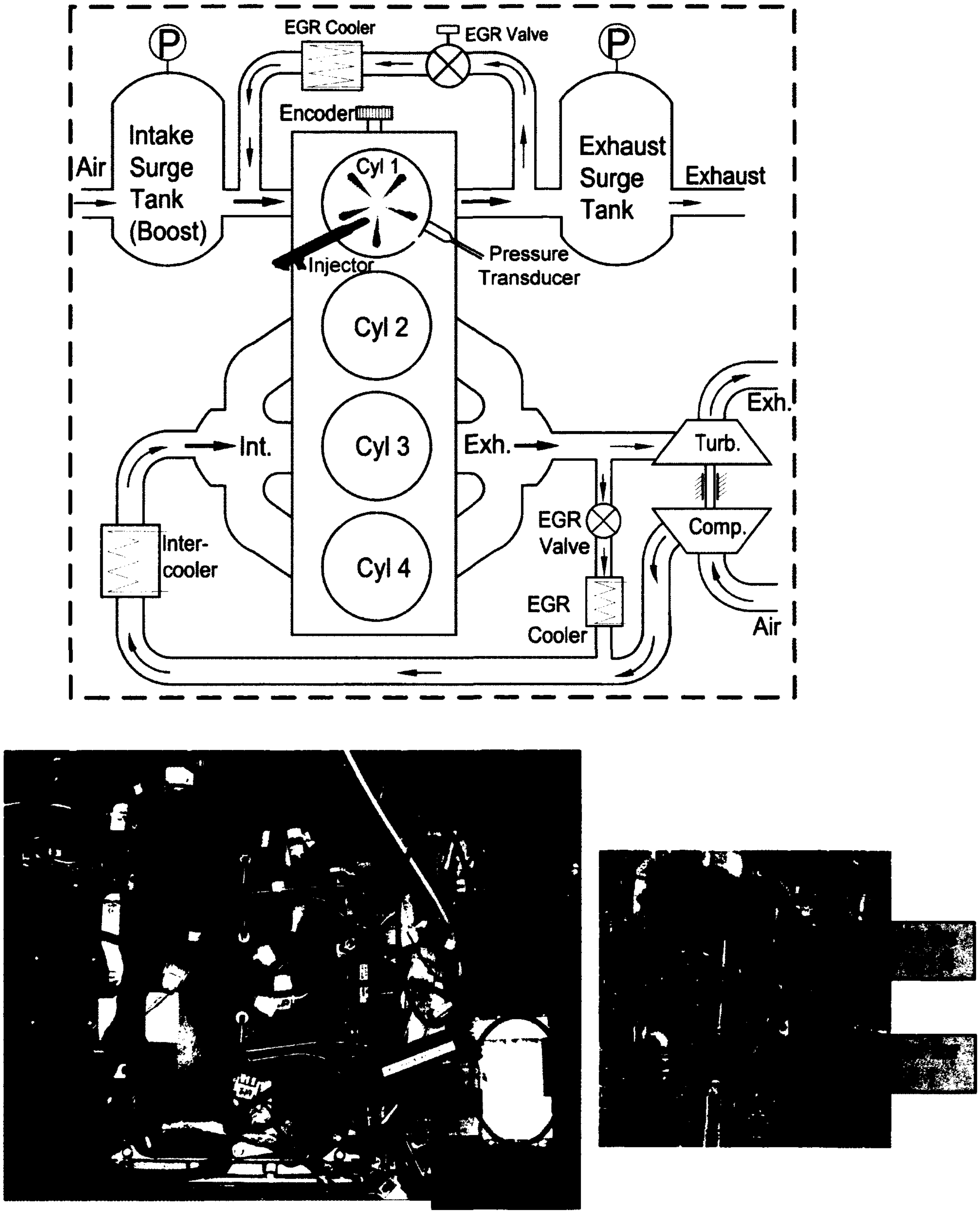

Figure 4.2: Modified Ford Engine Setup

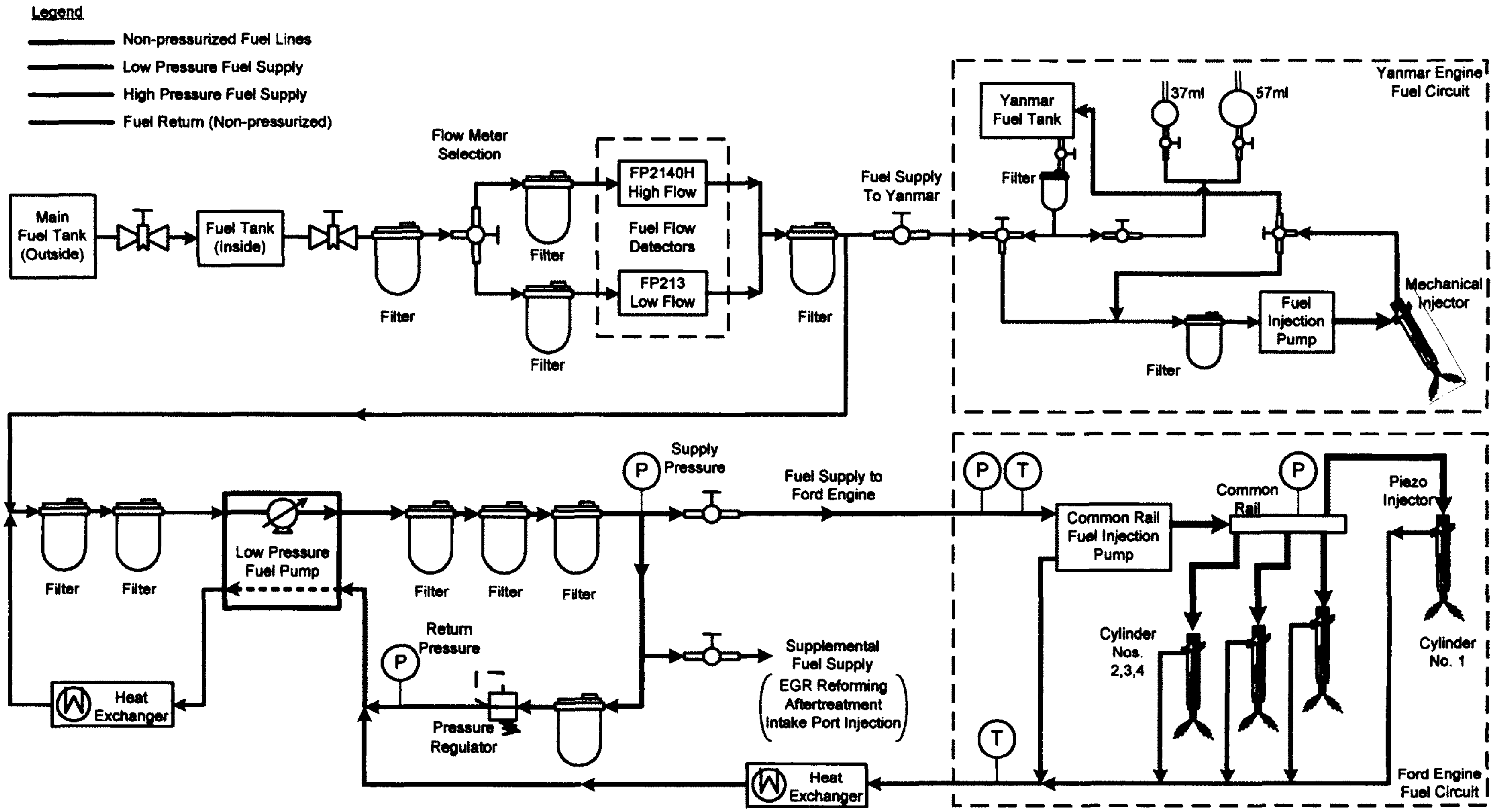

Figure 4.3: Fuel System Schematic for the Test Engines

4.3. Intake Boost and Exhaust Back-Pressure System

To simulate the effect of turbocharging on the test engines, the intake air was supplied from an oil-free dry air compressor. An electro-pneumatic pressure regulator was installed in the intake system to maintain the desired intake boost pressure. To regulate the exhaust pressure, an exhaust back-pressure valve was installed in the exhaust stream. The position of the back-pressure valve was pneumatically controlled through another electro-pneumatic pressure regulator.

An automatic closed-loop feedback control system was setup as a part of this research work to actively control the intake boost and exhaust back-pressure. The control system is schematically shown in Figure 4.4.

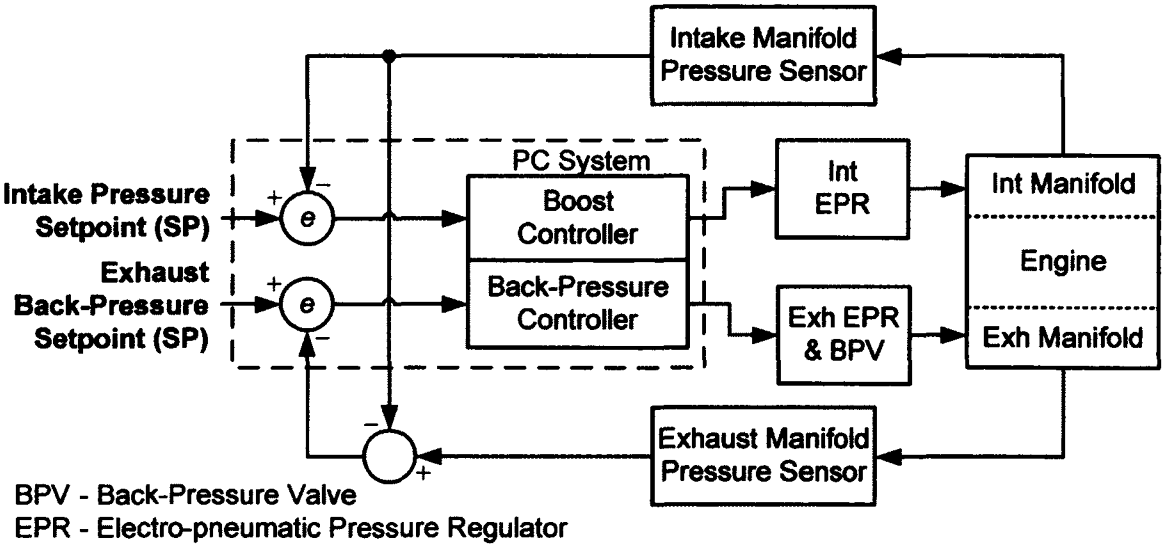

Figure 4.4: Boost & Exhaust Back-Pressure Control Scheme

The LabVIEW programming platform was utilized for the system implementation [84]. Both the boost and the back-pressure controllers are the proportional-gain type. An option of overriding the automatic control with manual control is also incorporated in the system. The exhaust back-pressure is primarily affected by the engine speed, engine load and the EGR valve opening while the intake pressure varies with the engine speed and the exhaust back-pressure. The closed-loop control system maintains the intake pressure and the exhaust back-pressure within prescribed limits around the desired setpoints.

4.4. Intake Flow Measurement

The precise measurement of the engine intake flow rate is critical for the accurate analysis and estimation of the combustion characteristics such as the in-cylinder charge strength, the specific emissions and the EGR rate. The conventional mass air flow (MAF) sensors used in the production vehicles are based on the hot-wire anemometry principle. A major disadvantage of such meters is their inability to withstand high intake pressures and are therefore required to be installed upstream of the compressor (turbocharger). In case of using simulated boost using an air compressor such as in a research laboratory environment, conventional MAF meters cannot be used.

For the current test setup, a Dresser ROOTS meter was installed in the intake system. The ROOTS meter is a positive displacement, rotary-type gas meter with a maximum operating pressure of 12 bar (175 psig). The meter was fitted with a 'counter with electronic transmitter' device (ICEX) that provided a non-compensated, high frequency pulse output. Each pulse of the ICEX indicated a volumetric flow rate of 0.0002621931 m^3 (0.2621931 L). The acquisition of the pulse output through the data-acquisition hardware presented a problem since the ICEX pulse output was not Transistor-Transistor Logic (TTL) compatible and therefore, the pulses could not be acquired with a digital/counter input.

This issue was resolved by the author as a part of the system setup and development. The ICEX pulse output signal was first acquired as an analog voltage signal at a very high sampling rate. The signal was analyzed online to extract the pulse data (width of each pulse, number of pulses) and a digital signal which was a TTL-compatible replica of the original ICEX pulse output was generated and output from a digital channel. A counter channel was then used to count the number of pulses in the generated digital signal within a small time step and the data was converted into the instantaneous volumetric flow rate.

To convert the volumetric flow rate to the mass flow rate, the pressure and the temperature of the air stream were measured and using the ideal gas law, the mass flow rate of the fresh air intake was obtained.

4.5. Intake Heating System

A 1500W inline electric heater, operated with 120VAC was installed in the intake system of the Ford engine as part of this research. The heater design incorporated a heating element which was electrically isolated from the flow stream. The heater was placed before the intake surge tank with a large thermal mass to maintain a stable intake charge temperature at different engine operating conditions. The heater was coupled with a proportional-integral-derivative (PID) controller that allowed the temperature to be closely monitored and controlled at the required temperature setpoint.

Another electric heater was installed in the intake system of the Yanmar engine. The heater consisted of heat tapes made up of electrically insulated resistance wires, sewn between two layers of fibreglass cloth. The heater tape was wrapped around the stainless steel intake pipe to heat up the intake flow. This allowed injection of fuel through the intake system which would not have been possible if an inline heater was used. This heater was also coupled with a PID controller for monitoring and controlling the intake temperature.

4.6. Exhaust Gas Recirculation Estimation and Control

To precisely regulate the amount of EGR, the amount of EGR was regulated with a combination of the EGR valve opening and the exhaust backpressure was used, independent of the engine operating conditions. The control of the EGR valve was programmed using National Instruments' Controller Area Network (CAN) hardware and LabVIEW programming interface as a part of this research work. The CAN network utilizes a 'Bus' topology, meaning all the communication between the devices on the network is handled by only two wires that form the back bone of the communication link. The CAN Bus allows a multi-master architecture in which all the sensors (or nodes) connect to this central bus and send or receive messages using the bus. The CAN Bus incorporates non-destructive bitwise arbitration between the messages sent by the different nodes and allows data transfer speeds up to 1 Mbit/s (mega bits per second).

The amount of EGR can be estimated from Equation (4.1), where $\dot{m}_{EGR}$ is the mass flow rate of the recycled gases, $\dot{m}_a$ is the mass flow rate of the fresh air and $\dot{m}_f$, the mass flow rate of the fuel.

$$\text{EGR Fraction} = \frac{\dot{m}_{EGR}}{\dot{m}_a + \dot{m}_f + \dot{m}_{EGR}} \tag{4.1}$$

Empirically, the amount of EGR could be evaluated with sufficient accuracy by measuring the carbon dioxide (CO_2) concentration in the intake and exhaust [3,4,9,30,83]. Alternatively, under steady operating conditions, the EGR rate could be evaluated from Equation (4.2) where $MAF_{current}$ and $MAF_{initial(w/o\ EGR)}$ are the intake mass air flow rates with and without EGR application, respectively:

$$\text{EGR Fraction} = 1 - \frac{MAF_{current}}{MAF_{initial(w/o\ EGR)}} \approx \frac{\text{Intake } CO_2}{\text{Exhaust } CO_2} \tag{4.2}$$

In this work, the EGR was calculated based on the intake and exhaust CO_2 concentrations. This was done because the mass-based definition required the estimation of the total intake flow rate (EGR+ fresh air). This estimation is in turn dependent on the engine volumetric efficiency which is a function of the intake temperature, the intake pressure and the engine speed. During engine tests at different intake pressures and during the transient LTC tests with intake pressure and engine speed variation, the assumption of a constant volumetric efficiency does not hold true. Secondly, during the catalytic fuel reforming tests with EGR, the mass flow rate of EGR was not changed but the CO_2 generated during the reforming process significantly increased the intake charge dilution. Since the mass-based definition of EGR did not account for this aspect, therefore, the CO_2-based definition was used throughout the empirical work.

4.7. Combustion Control System Setup

The hardware setup to run the modified Ford engine in the 3 cylinders–to–1 cylinder configuration is shown in Figure 4.5. The RT-FPGA hardware provides a deterministic platform for fast data acquisition with a large computational capacity and reliable control at loop speeds up to 40 MHz. The RT-FPGA platform can perform thousands of complex numerical operations during short time intervals, thereby providing immense capacity and flexibility for deterministic execution of control algorithms.

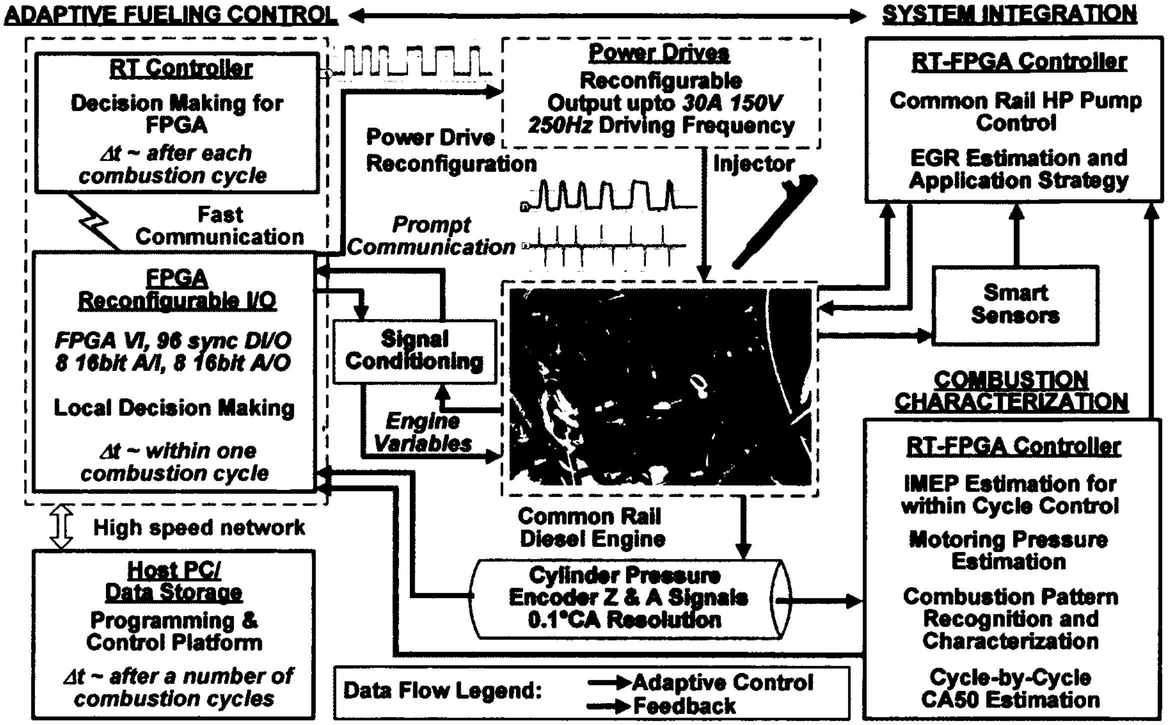

Figure 4.5: Combustion Control Platform [78]

The precise fuel injection scheduling was implemented using a RT-FPGA system. The FPGA device generated the desired TTL compatible pulse patterns corresponding to the on-the-fly updated injection schedule. The timing of the commanded injection pulses was crank-angle resolved at 0.1 °CA intervals and the duration of the injection was time-resolved in microseconds deterministically. This TTL output signal was amplified using the injector power drivers, which were programmed to drive the injectors with the suitable voltage and current profiles. The multi-pulse injection strategies were implemented for Cylinder No. 1 while for the Cylinder Nos. 2, 3 and 4, a single-shot injection strategy was implemented. The FPGA device was additionally used to perform cylinder pressure data-acquisition and to implement cylinder-pressure based control strategies. All the programming required for configuring the FPGA logic gates was done using the LabVIEW programming environment. The FPGA device was accommodated in a 'Peripheral Component Interconnect Extension for Instrumentation' (PXI) chassis that also included the RT controller used for floating point calculations. Another RT-FPGA system was set-up for the fuel-rail pressure control.

4.8. In-Cylinder Gas Sampling and Analysis System

The in-cylinder gas sampling system consisted of the direct gas sampling valve (GSV), fast-response NOx and THC emission analyzers and a Fourier Transform Infrared Spectroscopy (FTIR) MultiGas Analyzer. Their operation is briefly described below.

4.8.1. Direct Gas Sampling System

The GSV-System manufactured by SMETEC GmbH consists of a gas sampling valve (GSV) and an electronic controller. The valve is electromagnetically actuated and does not require any hydraulic or pneumatic assistance for actuation. The gas tubes inside the GSV are heated to prevent the sampling gases from condensing. The system is capable of variable sampling lengths (< 1ms up to 3ms) and provides the option of setting the start of the sampling at any crank angle within the engine cycle (0 to 720°CA in 1°CA steps). The sampling frequency (the repetition of the valve stroke after a specified number of engine cycles) is user selectable and can be as low as 8. The controller requires a clock signal with 1°CA resolution (Index A) and a trigger signal (Index Z) once every 720°CA (one engine cycle) to synchronize the controller operation with the engine operation. The GSV needs to be supplied with pure Nitrogen (inert transportation gas) at a specified mass flow rate and the sampled gases + nitrogen mixture can then be fed to the analyzing systems. Mass flow meters are therefore required to be installed on both the inlet and the outlet of the GSV to accurately measure the mass flow rate of the sampled gases. The details of the GSV installation and system integration are provided in Chapter 5.

4.8.2. Fast-Response Emission Analyzers

A non-functional set of Cambustion HC and NOx fast-response emission analyzers was received from external sources. The fault tracing and rectification was undertaken as a part of this research work by the author and both analyzer systems were made operational.

4.8.2.1. Cambustion HFR500 Fast FID System

The HFR500 is a Flame Ionisation Detector (FID) used for measuring total hydrocarbon (THC) concentration in a sample gas with a very fast response time. The system consists of two remote sampling heads which house the FID detector flame and are located close to the sample point. The sample heads operate at sub-atmospheric pressure; a vacuum pump induces the sample to flow through heated sample probes and into the detector with a typical $T_{10\text{-}90\%}$ response time (time taken by the system output to reach 90% value of a step change at the source) of 1.3 milliseconds and a typical transit time (how long it takes a sample entering the sampling system to produce an electrical response) of 4-5 milliseconds. A standard PC is used to provide a user interface to the control unit [85].

4.8.2.2. Cambustion *f*NOx400 Fast CLD System

The *f*NOx400 is designed to measure the NO concentrations with a typical $T_{10\text{-}90\%}$ time response of around 4ms and a typical transit time of around 10 milliseconds. The system uses the standard principle of chemiluminescence detection (CLD) in which a sample containing the NO to be measured is mixed with ozone, which results in a spontaneous light emission, the level of which is very nearly proportional to the NO concentration in the sample [86].

4.8.3. Fourier Transform Infrared Spectroscopy (FTIR) MultiGas Analyzer

All compounds except for elemental diatomic gases such as N_2, H_2 and O_2, have infrared spectra and most components present in the exhaust gas can be analysed by their characteristic infrared absorption. An infrared spectrum represents a fingerprint of a sample with absorption peaks that correspond to the frequencies of vibrations between the bonds of the atoms making up the compound. Because each compound is a unique combination of atoms, no two compounds produce the exact same infrared spectrum. Therefore, infrared spectroscopy can provide positive identification (qualitative analysis) of different kind of compounds. In addition, the size of the peaks is a direct indication of the quantity of the compound.

An MKS 2030 MultiGas FTIR Analyzer was used to analyze the species in the exhaust gas for the LTC combustion fuelled with DME. The MultiGas 2030 can perform analysis in gas streams that contain up to 30% water, and can simultaneously analyze and display more than 30 gases.

4.9. Data Acquisition System

A set of 14 personal computers (PCs) were used to acquire and record the data during the engine tests (Table 4.3). The programs was developed in-house using the LabVIEW programming environment to acquire, analyze and record the data on each computer. The PC designations marked with an asterisk (*) were developed by the author.

Table 4.3: Overview of the CDEL Data Acquisition System

PC Designation	DAQ Model	Details	Applicable Engine
TEMPERATURE*	NI SCXI 1102	96 Thermocouple	Yanmar, Ford
	NI PCI-6023E	16 AI, 8 DIO	
EMISSION*	NI PCI-6229	32 AI, 4 AO, 48 DIO	Yanmar, Ford
MAF/FUEL*	NI PCI-6221	16 AI, 2 AO, 24 DIO	Yanmar, Ford
PRESSURE*	NI PCI-6024E	16 AI, 2AO, 8 DIO	Yanmar, Ford
ONLINE HEAT RELEASE*	NI 6070E	16AI, 2 AO, 8 DIO	Yanmar, Ford
SIMULTANEOUS	NI PCI-6122	4 AI (Simultaneous), 8 DIO	Yanmar, Ford
MAF BOSCH*	NI PCI-6023E	16 AI, 8 DIO	Yanmar, Ford
BOOST*	NI PCI-6024E	16 AI, 2AO, 8 DIO	Yanmar, Ford
SYNC MANAGER*	–	DataSocket Server	Yanmar, Ford
SUPPLEMENTAL FUELLING	NI PCI-6602	8 Counters/Timers, 32 DIO	Yanmar
EGR*	NI USB-8473	High Speed CAN	Ford
RAIL PRESSURE	–	Host computer for Real-time Controller	Ford
FUEL INJECTION	–	Host computer for RT	Ford
COMBUSTION ANALYSIS*	–	Host computer for RT	Ford

NI: National Instruments DIO: Digital Input/Output
AI: Analog Input AO: Analog Output
* Developed as a part of this work

4.10. Cylinder Pressure Acquisition & Processing

The cylinder pressure data was logged for 200 consecutive cycles at each operating condition. The number of consecutive cycles to be used for averaging was found by considering the variability inherent in the data and the accuracy required. To ensure the confidence level of 99.9% so that the sample mean was within 3% of the population mean, the sample average was based on 200 cycles [87].

The hardware used for acquiring the cylinder pressure is given in Table 4.4. The membrane of the pressure transducers was flush-mounted to minimize any resonance effect in the pressure data.

Table 4.4: Instrumentation for Cylinder Pressure Acquisition

Hardware	Model	Details	Applicable Engine
Piezo-electric Cylinder Pressure Transducer	Kistler 6043A60	Direct mounted, water cooled	Yanmar
	AVL GU13P	Glow-plug mounted, un-cooled	Ford
Kistler Charge Amplifier	5010B	Output: ±10 volts	Yanmar, Ford
Gurley Rotary Incremental Encoder	9125S-03600H-5L01-C18SQ-06EN	Index A: 3600 ticks Index Z: Aligned with physical TDC	Yanmar, Ford

For phasing the measured pressure data with the cylinder volume, the data acquisition was externally triggered at the TDC by the 'Index Z' generated by the encoder. The encoder 'Index A' with a crank angle resolution of 0.1°CA (3600 pulses per revolution) was used as an external clock to provide a Phase Locked Loop (PLL) signal that indicated when a certain amount of engine rotation has occurred [14]. The block diagram for the data-acquisition of the cylinder pressure is shown in Figure 4.6. The cylinder pressure data was processed both during the tests (on-line) and afterwards to provide information about the combustion process.

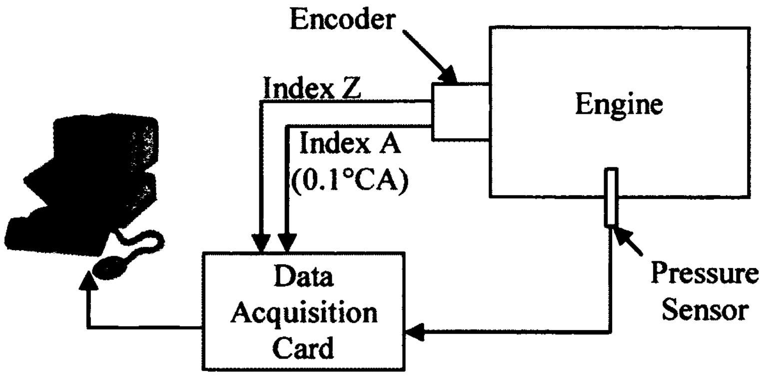

Figure 4.6: System Layout for Cylinder Pressure Data Acquisition

4.10.1. On-line Heat Release Analysis

The LabVIEW programming environment was utilized for on-line processing of the acquired cylinder pressure data for each engine cycle as part of this research. The data acquisition and processing were programmed for parallel execution using a producer-consumer model to ensure cycle-by-cycle acquisition and analysis. The data was processed to calculate and display the following parameters during the on-line monitoring of the combustion process:

- Heat Release Rate (J/°CA) & Crank Angle of 50% Heat Released (CA50- °CA)
- Start of Combustion (SOC -°CA) & End of Combustion (EOC - °CA)
- Crank Angle of the Peak of Heat Release Rate (°ATDC)
- Rate of Change of Pressure (bar/°CA) & the Indicated Mean Effective Pressure (IMEP - bar)

The last 200-cycle data (to ensure the confidence level of 99.9% so that the sample mean was within 3% of the population mean) was also continuously processed to report the following averaged values:

- Maximum Cylinder Pressure (P_{max} - bar)
- Maximum Rate of Pressure Rise ($(dp/d\theta)_{max}$ - bar/°CA)

- CA50 (°CA) & IMEP (bar)

The heat-release rate at each crank angle was evaluated based on the First Law of Thermodynamics. A detailed description of the heat release analysis is given in Chapter 5.

4.10.2. Off-line Post-Processing of Pressure Data

The post-processing of the pressure data was also done using LabVIEW. A comprehensive code was written by the author to process the 200-cycle, 0.1°CA resolution pressure recorded for each data point as follows:

- The pressure data was initially referenced to the intake pressure at the IVC. The pressure referencing was then checked and corrected by analyzing the polytropic index of the compression stroke against a fixed value of 1.37.

- The IMEP was calculated for each cycle with 0.1°CA resolution.

- The cycle-to-cycle variation analysis was performed with either 0.1°CA or 1°CA resolution. The cycle-by-cycle values of $P_{max,}$ crank angle of P_{max}, $(dp/d\theta)_{max}$, crank angle of $(dp/d\theta)_{max}$ and IMEP were calculated. The mean value, standard deviation and the coefficient of variance (COV) of these parameters were also evaluated.

- The heat release analysis was performed using pressure data with 1°CA resolution for each cycle as well as for the 200-cycle averaged pressure data. The heat release rate at each crank angle as well as the normalized cumulative heat released trace were calculated and the SOC, EOC, CA50 were reported. The mean value, standard deviation and COV of CA50 were also calculated.

- The 200-cycle averaged pressure data, the cycle-by-cycle evaluated parameters and the heat release analysis were saved as separate MS Excel files.

4.11. Automatic Data Synchronization & Processing System

The sampling rate for the test data acquired and recorded on each computer was different and depended on the type of sensors and their response characteristics. The temperature and the emission data were acquired at a sampling frequency of 2 Hz. The cylinder pressure data was acquired at a variable sampling rate which depended on the engine speed. The mass flow rates, the intake and the exhaust pressures were sampled at frequencies of several kHz.

The unification and management of the data from the individual computers presented a multifaceted problem. The problem was addressed as a part of this research work and a data synchronization program was developed in LabVIEW. The salient features of the 'Data Sync Manager' include:

- Acquisition and synchronization of data from all computers
- Absolute and relative time-stamping of the data
- On-line processing of raw data including calculation of specific emissions, specific fuel consumption, efficiencies etc.
- Graphical & tabulated plotting with threshold value detection
- Summarized test report generation in Microsoft Word format
- Synchronized data logging continuously at 2 Hz in a tab-delimited text file.
- Synchronized data recording at discrete points in a tab-delimited text file.
- Network communication status and fault indication

An overview of the 'Data Sync Manager' is shown in Figure 4.7. The DataSocket communication protocol built into LabVIEW was utilized to establish a communication network over the local area network. The DataSocket technology allows publishing of data on the network and subscribing of the data from multiple computers.

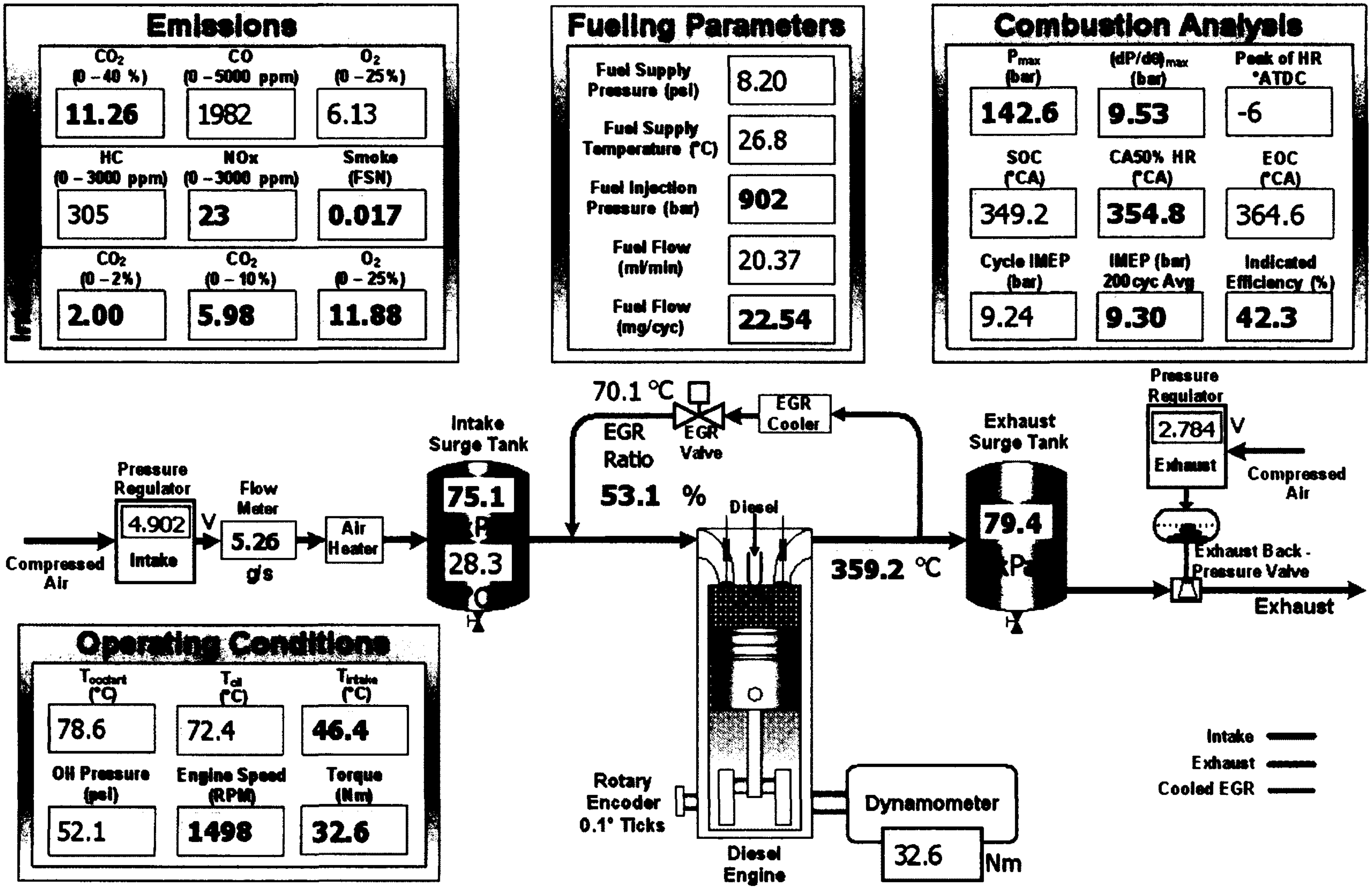

Figure 4.7: Engine Test Data Synchronization and Processing

4.12. Emission Analyzers

A dual-bank emission analyzer system, one for the exhaust emissions and the other for the intake gas concentrations was instrumented for the tests. Two sample conditioning units consisting of heated sampling lines, water-removal chiller units, heated pumps and filters condition the exhaust and the intake gases to provide clear and dry samples to the analyzer benches. One analyzer bank measured the concentrations of NOx, HC, CO, CO_2, O_2, in the exhaust while only the O_2 and CO_2 concentrations were monitored at the engine intake. The HC analyzer measured the total concentration of hydrocarbons within a gaseous sample on a C1 basis. Table 4.5 summarizes the types and working principles of the emission analyzers used in the laboratory for the present research. The detailed specifications of the hardware are given in APPENDIX H.

Table 4.5: Details of Dual-Bank Emission Analyzer System

Species	Working Principle	Range	Manufacturer & Model
Intake			
CO_2	Non-Dispersive Infra-Red (NDIR)	0–2 % 0–10 %	CAI 602P
O_2	Paramagnetic	0–25 %	
Exhaust			
NOx	Chemiluminescence	0–3000 ppm	CAI 600 HCLD
THC	Heated Flame Ionization Detector	0–3000 ppm	CAI 300M-HFID
CO	NDIR	0–2000 ppm 0–5000 ppm	CAI 300
O_2	Paramagnetic	0–25 %	
CO_2	NDIR	0–8 % 0–40 %	CAI 200
Smoke / Dry Soot	Variable Sampling Smoke Meter	0–10 FSN (0–32) g/m^3	AVL 415S

ppm:	parts per million
THC:	total hydrocarbons
FSN:	filter smoke number
CAI:	California Analytical Instruments, Inc.
AVL:	AVL List GmbH

4.13. The Test Fuels

The empirical work was primarily performed using a certified diesel fuel. Additionally, two gaseous fuels, propane and DME were also used during the in-cylinder sampling experiments.

4.13.1. Diesel

A 2007 certification ultra low sulphur diesel (ULSD) was used during the engine experiment. This ensured consistency in the results by avoiding variations in the fuel properties that may occur when fuels from different sources are used. The properties of the ULSD fuel are given in Table 4.6.

Table 4.6: Diesel Fuel Specifications

Fuel Parameter		Reported Value
Type		ULSD, Certified
Specific Gravity [-]		0.846
Viscosity 40°C [cSt]		2.5
Distillation [°C]	IBP	188
	50%	256
	100%	341
Sulphur [ppm]		14
LHV [MJ/kg]		43.1
Carbon [wt %]		86.4
Hydrogen [wt %]		13.6
Hydrogen-to-Carbon Ratio [-]		1.88
Cetane Number		46.5
Stoichiometric Air/fuel Ratio		14.5

4.13.2. DME

A separate fuel injection system was set up for the port injection of DME. The properties of the DME used during the tests are given in Table 4.7. DME has a hydrogen-to-carbon ratio of 3 and its energy contents are approximately 35% lower than those for the diesel fuel. The high oxygen contents of DME result in a stoichiometric air/fuel ratio of ~9:1, much lower than 14.6, the typical stoichiometric air/fuel ratio of diesel. However, as a diesel fuel-substitute, the DME fuelling rate has to be nearly 1.5 times that for the diesel fuel under the same engine operating conditions. Therefore, the actual air requirement by mass for 1 kg of DME is ~13.4 kg.

Table 4.7: Physical and Chemical Properties of DME

Fuel Parameter	Reported Value
Chemical Formula	$H_3C{-}O{-}CH_3$
Molecular Weight [kg/kmol]	46.07
Carbon [wt %]	52.2
Hydrogen [wt %]	13
Fuel Oxygen [wt %]	34.8
Hydrogen-to-Carbon Ratio [-]	3
Boiling Temperature [°C]	-24.9
Vapour Pressure @ 20°C [bar]	5.1
Ignition Temperature [°C]	235
LHV [MJ/kg]	28.4
Stoichiometric Air/fuel Ratio [kg/kg]	8.95
Cetane Number [-]	55-60
Sulphur [ppm]	< 1

4.13.3. Propane

To study the low temperature NOx LTC mechanism, propane fuel was used as the source for the hydrocarbon dosing in the intake stream. Propane has a very low cetane number and has a higher auto-ignition temperature (~540°C) than methane (~450°C). Since the tests were planned to be done without combustion, the use of propane was suitable for this purpose. The composition of the propane was analyzed with the FTIR, and is given in Table 4.8 along with some important properties of propane.

Table 4.8: Composition and Properties of Propane

Fuel Parameter	Value
Composition [Vol %]	
Propane (C_3H_8)	96.58
Methane (CH_4)	0.3
Ethane (C_2H_6)	2.7
Formaldehyde	0.15
HNCO	0.27
Physical & Chemical Properties	
Molecular Weight [kg/kmol]	44.1
Carbon [wt %]	81.8
Hydrogen [wt %]	18.2
Hydrogen-to-Carbon Ratio [-]	2.67
Vapour Pressure @ 20°C [bar]	8.7
Ignition Temperature [°C]	540
LHV [MJ/kg]	46.2
Stoichiometric Air/fuel Ratio [kg/kg]	15.6
Cetane Number [-]	5-10

CHAPTER V

5. LTC DIAGNOSTICS

This chapter presents the experimental setup, the hardware modifications and the results for the direct in-cylinder sampling investigations on the Yanmar engine. The in-cylinder sampling system was used to investigate the LTC-NOx mechanism under engine motoring conditions and to study the NOx generation with DME-fuelled combustion. The later part of this chapter includes a detailed analysis of the cylinder pressure for producing a reliable feedback for LTC control.

5.1. Challenges for In-cylinder Gas Sampling Implementation

The task of direct in-cylinder gas sampling involves numerous challenges that must be realized and overcome for a successful implementation. The Valve is exposed to very harsh conditions that exist in the combustion chamber. Therefore, the valve must have a fast actuation, remain open for a short duration (1~2 ms) and be able to close quickly. This is critical to ensure that the combustion process is not adversely affected so as to change its characteristics. This results in extremely high mechanical and thermal stresses on the valve.

The installation requires modifications to the cylinder head to gain access to the combustion chamber. The mounting of the valve is another critical issue that must be properly addressed. The combustion chamber sealing must be ensured to prevent damage to both the valve and the engine. For the GSV to function properly, the TDC position must be supplied to the controller as well as the position of the crank shaft (in terms of crank angle degrees).

The operation of the GSV requires the integration of a number of systems. The transportation mechanism for the sampled gases involves the use of an inert gas like nitrogen to be supplied. The flow into and out of the GSV must be accurately determined since the measurement of the species concentration would require an accurate estimate of the dilution factor. Therefore, mass flow meters, pressure and temperature sensors need to be integrated into the system. Fast response emission analyzers are also required so that the sample composition is as close as possible to the cylinder-charge composition.

5.2. Experimental Setup & Verification

The setting up of the GSV system required extensive hardware modifications and integration of the various components. A brief description of each aspect is provided below.

5.2.1. Engine Modifications & Installation

A new cylinder head of the Yanmar engine was modified to provide direct access to the combustion chamber. The engine modifications were validated through accurate three-dimensional parametric drawings shown in Figure 5.1 and the actual machining work was subsequently done. An adapter sleeve was fabricated to mount the GSV. The sleeve provides sealing between the combustion chamber and the coolant jackets, and also between the coolant jackets and the outside. The valve itself is inserted with a Teflon ring between the sleeve and the valve. The Teflon seal serves three purposes: first, it prevents leakage of the combustion gases through the central passage of the sleeve; second, it provides shock protection to the GSV; and third, it allows the valve depth (protrusion) inside the combustion chamber to be adjusted by changing the thickness of the Teflon ring. The GSV is held in place using a stainless steel (SS) plate and SS rods which also press the ring surface of the valve against the sleeve. An o-ring groove was machined into the cylinder head to provide a leak-tight seal between the adapter sleeve and the cooling water jackets. A hole in the cylinder head was also machined to accommodate a cylinder pressure transducer.

The actual installation on the cylinder head and the combustion chamber surface of the head are shown in Figure 5.2. It can be seen that the sleeve is nearly flush mounted.

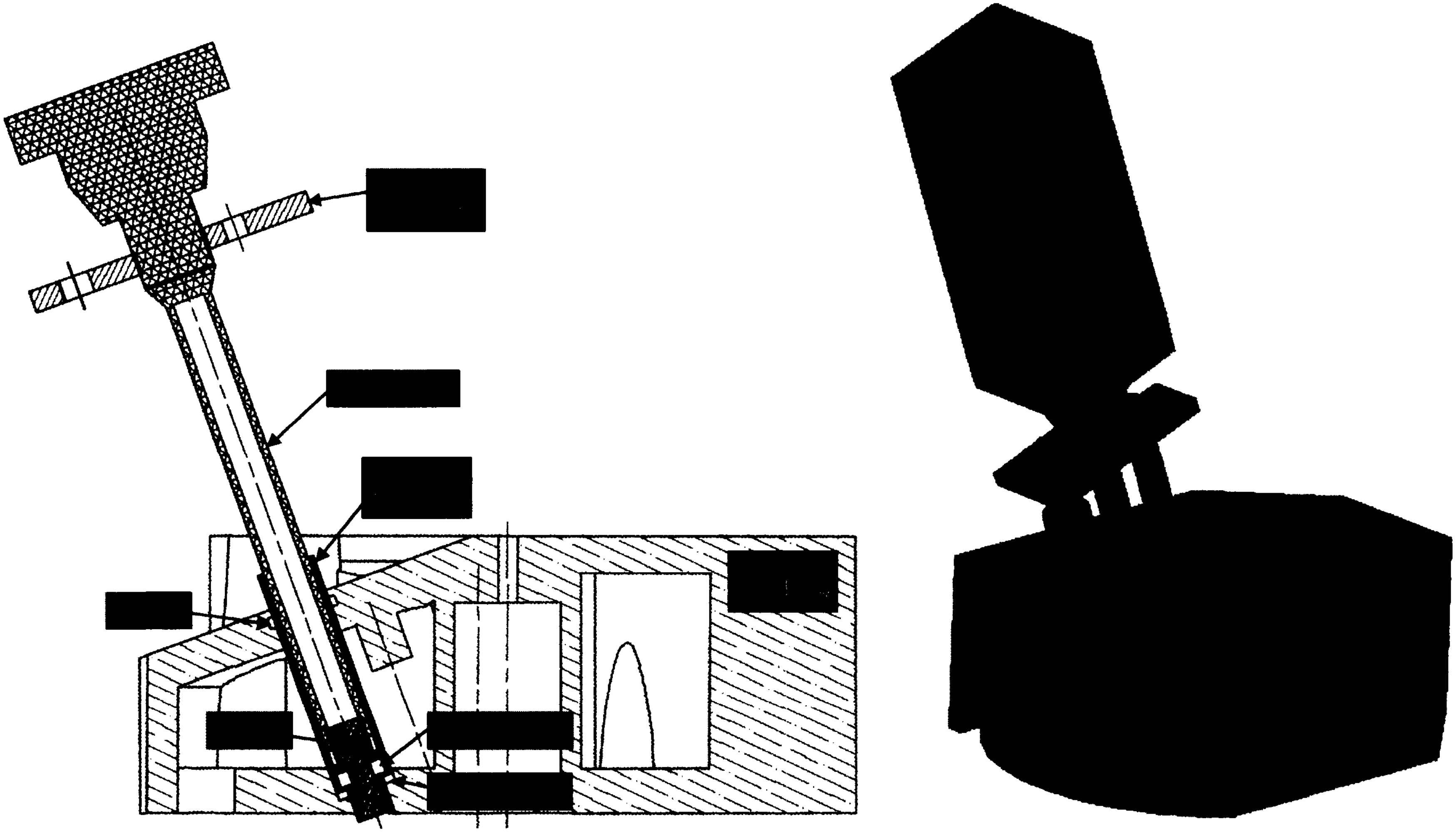

Figure 5.1: Cross-sectional View of the GSV Installation – Design Validation

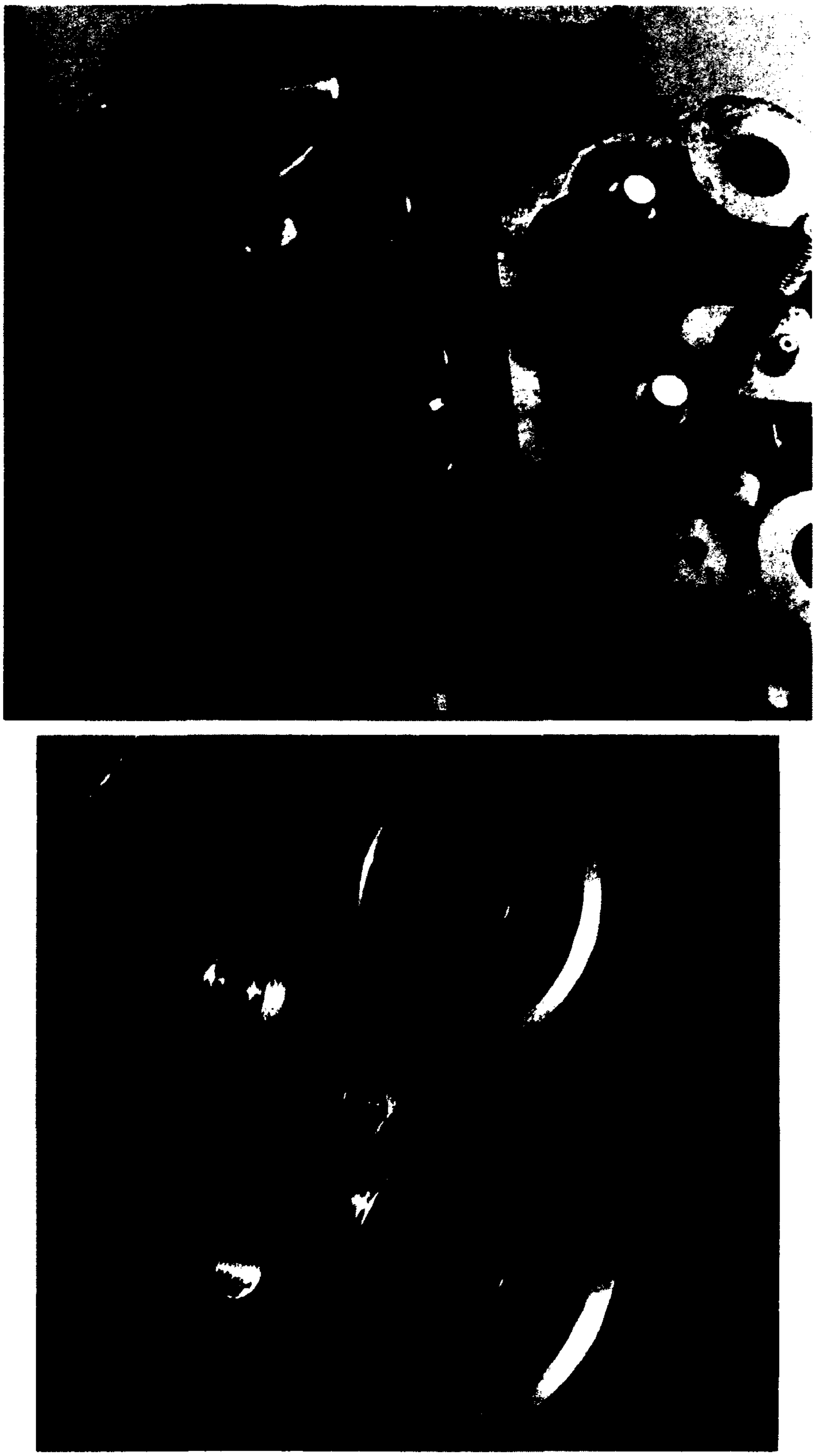

Figure 5.2: Actual Installation & Flush Mounting of the GSV Adapter Sleeve

5.2.2. GSV Encoder Signals

The GSV controller requires a TTL signal for every 1°CA of engine rotation (Index A) and one trigger pulse (Index Z) per combustion cycle (720°CA). The encoder installed on the Yanmar engine had a resolution of 0.1°CA and provided a trigger pulse (aligned with the TDC) every revolution (360°CA) of the crankshaft. To resolve this issue, the encoder Index Z (2 per combustion cycle) and Index A (7200 per combustion cycle) were acquired through an RT-FPGA system and using the LabVIEW programming interface, a modified Index Z (Index Z^*) was generated once every combustion cycle. The Index A was also mathematically treated so that one modified Index A (Index A^*) would be generated after every 10th Index A of the encoder (720 pulses per combustion cycle). The program also identified the compression TDC based on the cylinder pressure to provide an absolute reference for the GSV System. The original and the modified pulse trains are shown in Figure 5.3.

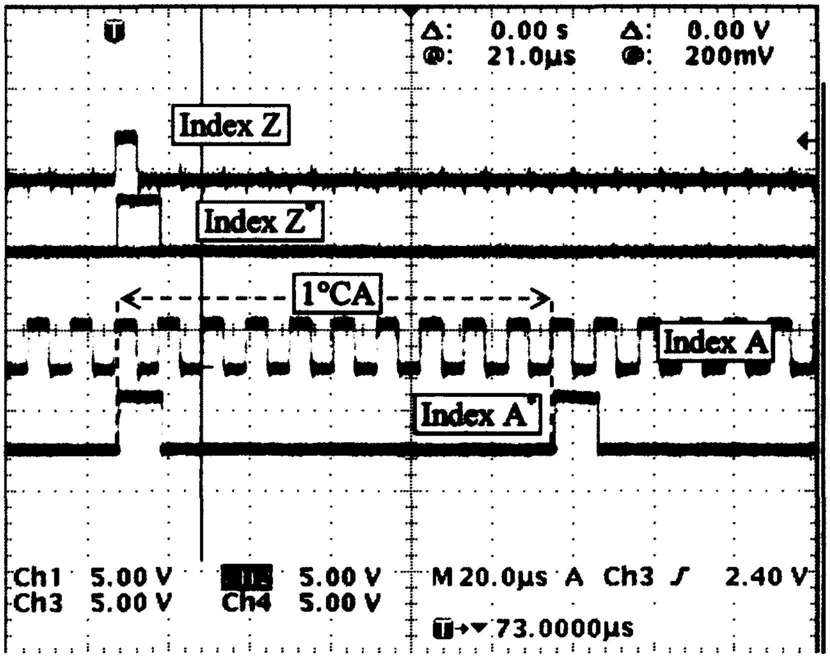

Figure 5.3: Conversion of Encoder Signal to Conform to GSV Requirements

5.2.3. Fast HC & NOx Analyzer Setup

The fast HC and the fast NOx analyzers were setup to provide sampling capability in both the intake system (Figure 5.4) as well as the gases being sampled out through the GSV.

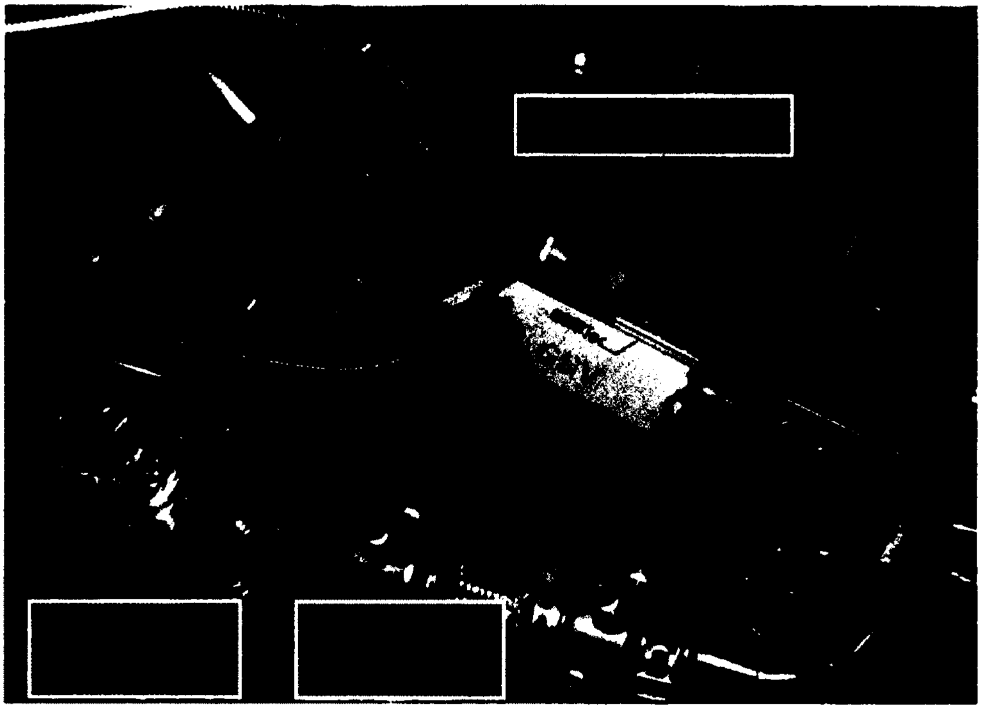

Figure 5.4: Fast Response HC/NOx Sampling Probes in the Intake System

5.3. System Integration

A schematic representation of the in-cylinder sampling system setup is shown in Figure 5.5. Dry nitrogen gas was used as the transportation medium for the sampled gases. Two mass flow meters were installed to measure the flow into and out of the GSV, the difference being the sampled gas flow rate. An accurate measurement of the flows was essential since the dilution factor was required to be determined to ascertain the actual concentration of the species in the sample. The pressure and temperature were therefore closely monitored to ensure accuracy in the calculations. A LabVIEW program that acquired and processed the data from the GSV, the fast response analyzers as well as the flow meters, was written to synchronize and record the data.

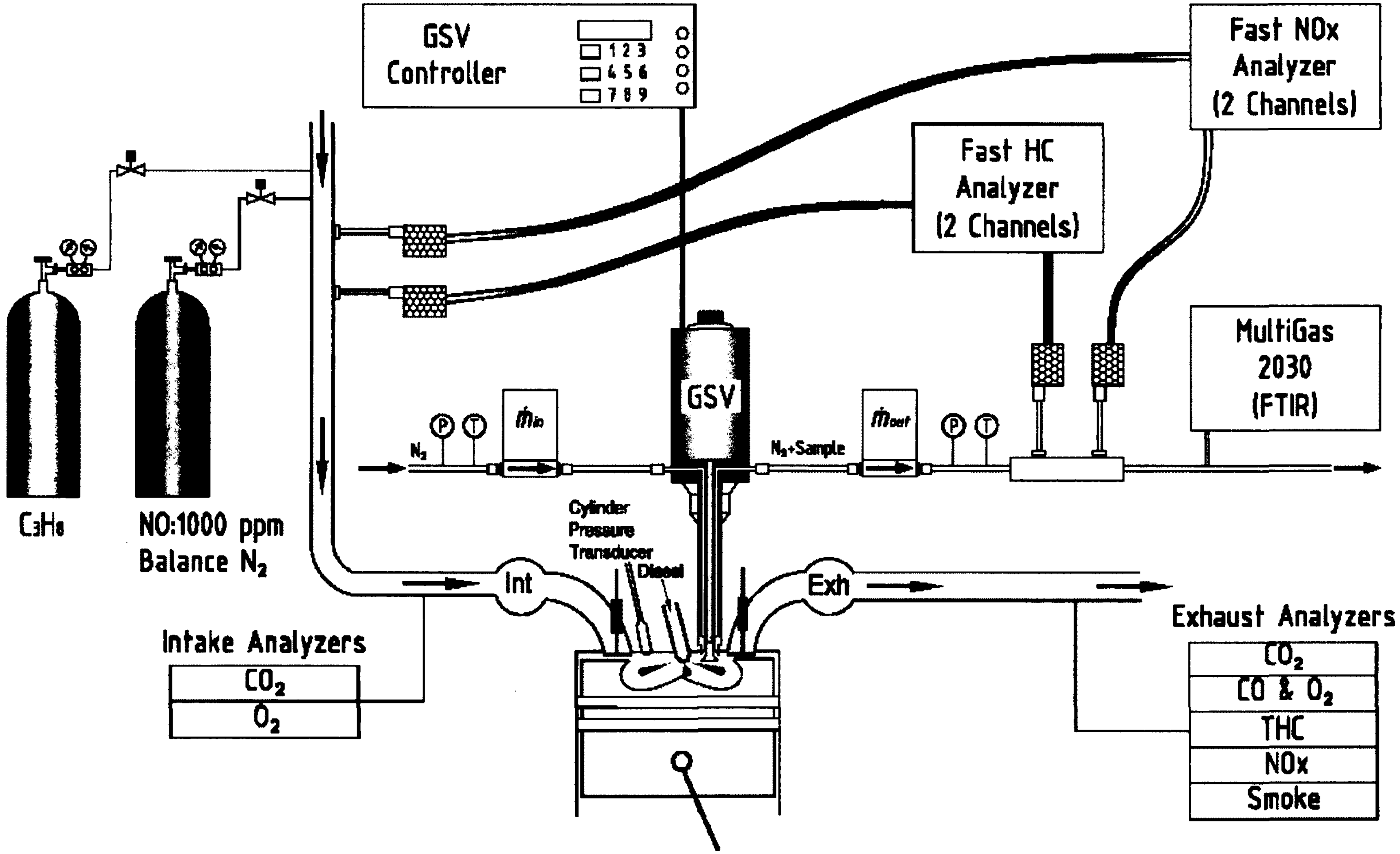

Figure 5.5: Schematic of the In-cylinder Sampling System Setup

5.3.1. System Calibration

The quantity of the in-cylinder gases sampled at every opening of the valve depends on the length of the sampling time and the in-cylinder conditions (pressure and temperature). The quantity of the sampled gases should be adjusted so as not to significantly affect the combustion process. Therefore, the determination of the sampling time duration is critical for accurate in-cylinder measurements. The results of the sampling time calibration are shown in Figure 5.6. The valve stroke was adjusted by turning a knob on the GSV. The GSV controller translated the stroke length into a pulse signal, the width of the pulse being the sampling duration.

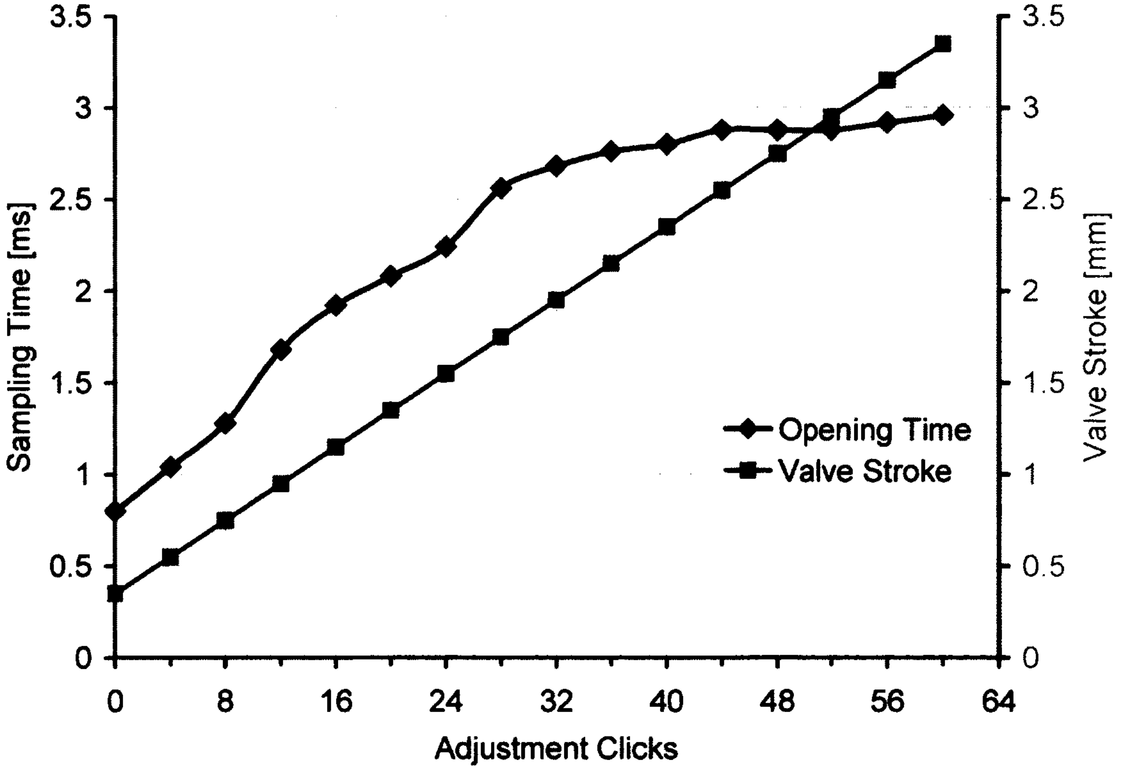

Figure 5.6: GSV Sampling Time Calibration

5.4. LTC NOx Mechanism

The ultra low levels of NOx achieved during LTC cycles are commonly attributed to the lowered combustion temperature and the high dilution due to the heavy use of EGR.

However, during LTC experiments conducted at the University of Windsor, it was observed that reduction in NOx would mostly coincide with the increase in the HC emissions. Moreover, a higher proportion of NO_2 relative to the NO concentration was seen in the LTC exhaust. To confirm if the LTC NOx mechanism was affected by the high levels of HC, dosing tests were carried out by introducing a known concentration of NO and propane in the intake, and observing the interaction of NO-C_3H_8, if any with the in-cylinder sampling system. During the tests, the engine was motored at a fixed speed.

5.4.1. Experimental Results

The initial testing to check the system integration was done by introducing ~100ppm of NO in the engine intake system. The start of sampling (SOS) was chosen as 380°CA and the sample repetition frequency (SRF) was 10 cycles (a sample was drawn after every 10 engine cycles). The sampling duration (SD) was 3ms. The results are shown in Figure 5.7. The steady-state value of NO calculated from the sampling gas matched the dosing NO concentration. This test confirmed the correctness of the dilution factor calculation and the system integrity.

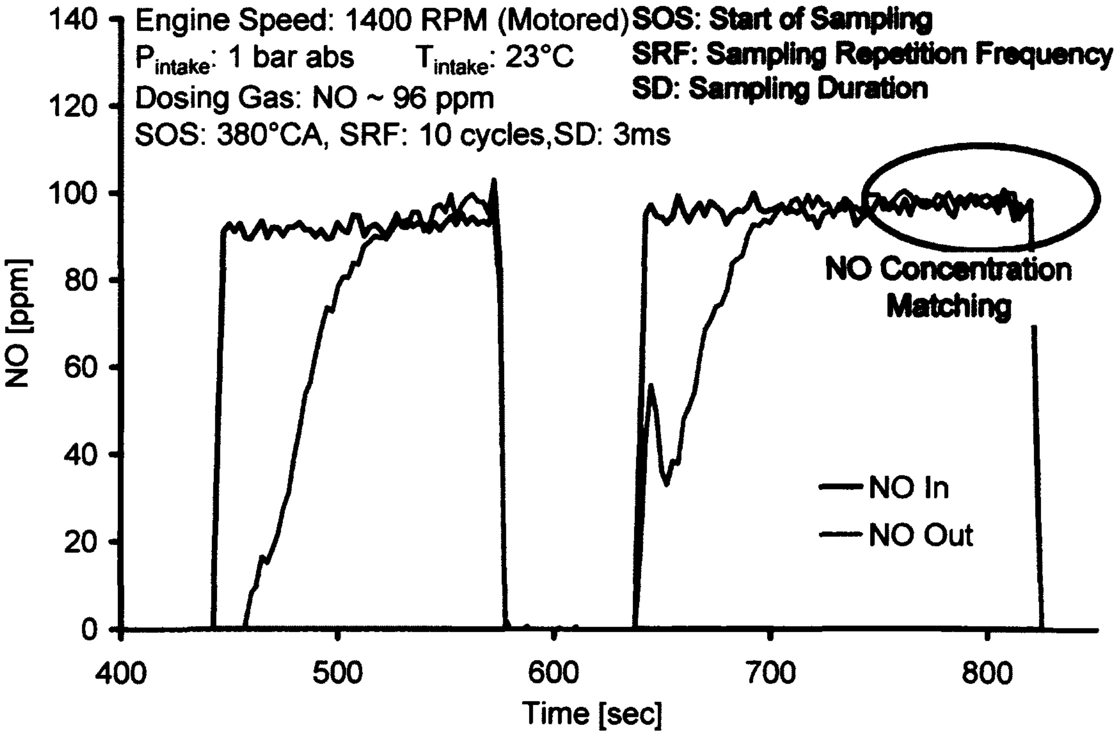

Figure 5.7: System Integration Test

The test was repeated by introducing propane gas in the intake along with NO. The GSV was operated with SOS at 390°CA, a SRF of 10 cycles and a SD of 3 ms. The results are shown in Figure 5.8. The introduction of ~6000 ppm^{C1} of propane resulted in a reduction of about 80% NO concentration in the sampled gas. The test was repeated with a reduced propane concentration of ~2800 ppm^{C1} and a similar reduction in the NO concentration of the sampled gas was observed.

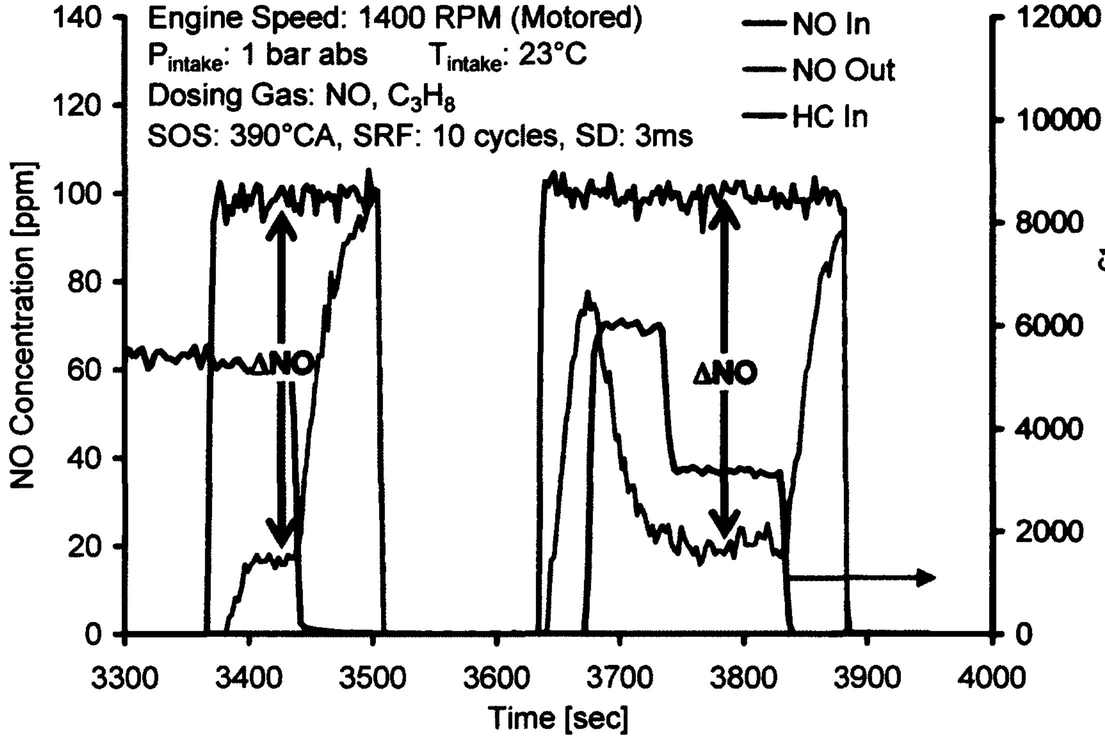

Figure 5.8: NO-C_3H_8 Interaction with SOS @ 390°CA

To confirm the above mentioned observations, the steady-state CO concentration in the engine exhaust has been plotted in Figure 5.9. The departure of the CO from zero to about 16 ppm indicated the occurrence of some reaction of the propane gas. The concentration of NO in Figure 5.10 also agreed with the levels observed with the in-cylinder sampling. However, the presence of 42 ppm of NO_2 in the exhaust suggested that the NO was being converted to NO_2 in the presence of propane. The overall NOx level of 58 ppm also indicated that about 40% of the NO was being destroyed or converted into some other compound.

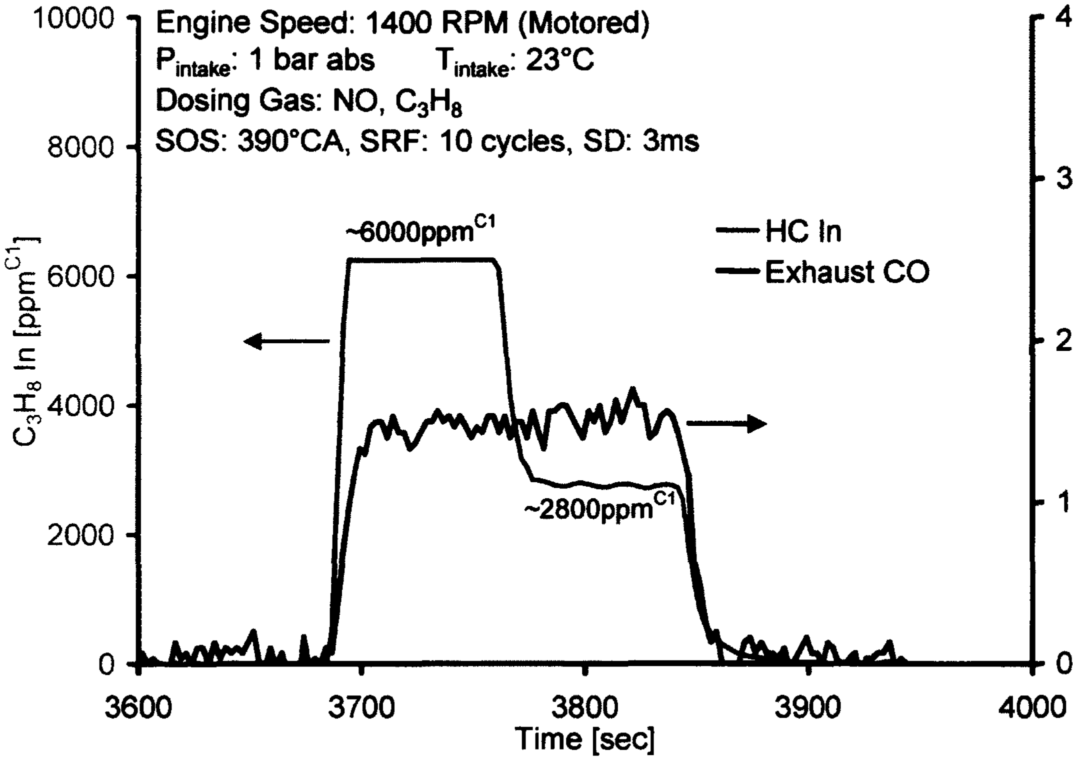

Figure 5.9: Steady-state Exhaust Emissions for the Results of Figure 5.8

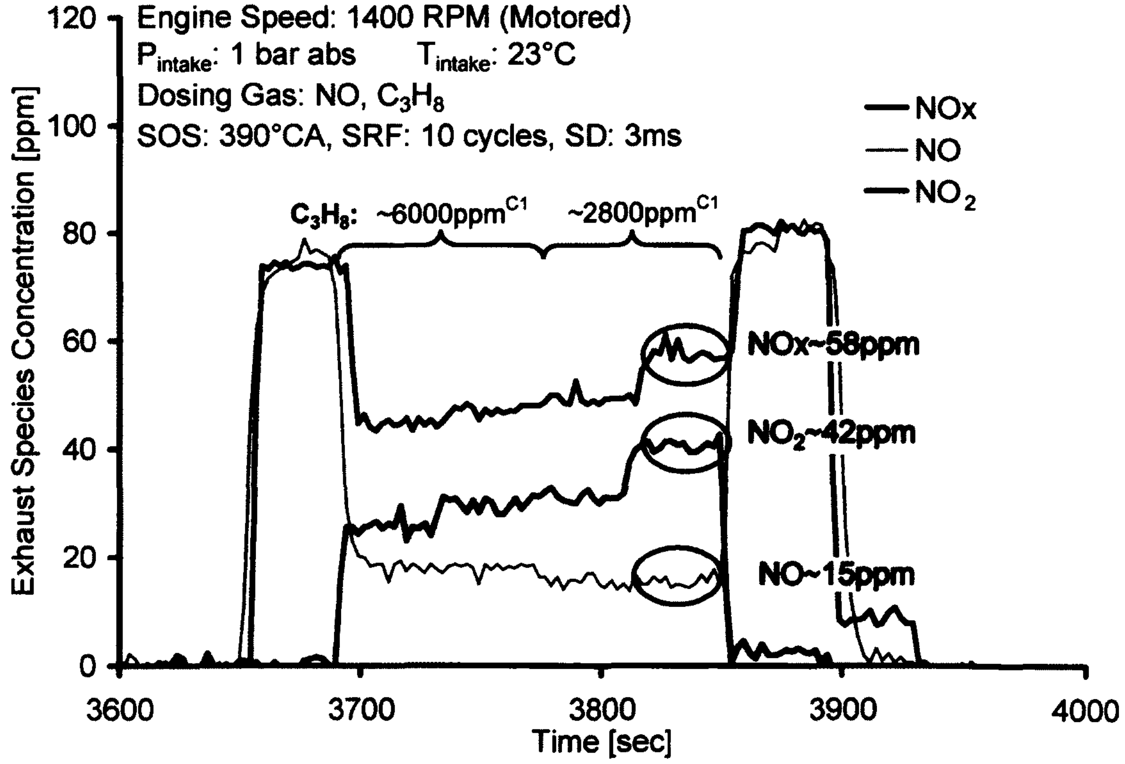

Figure 5.10: Break Down of NOx in terms of NO & NO_2

A detailed test was then conducted by performing a crank angle sweep from 300 to 390°CA at different HC dosing concentrations for a fixed NO dosing of ~100 ppm and the results are shown in Figure 5.11. It can be seen that there is no change in the NO concentration with SOS@300°CA, irrespective of the HC concentration. The mean cylinder temperature calculated from the cylinder pressure for the Yanmar engine came to about 490K which is much lower than 750K, the auto-ignition temperature of propane. However, the change in the NO concentration was observed after SOS@330°CA, where the mean cylinder temperature was estimated as ~700K. A rapid increase in the NO destruction was then observed for higher HC concentrations. A steady-state value of NO was approached with the SOS@360°CA.

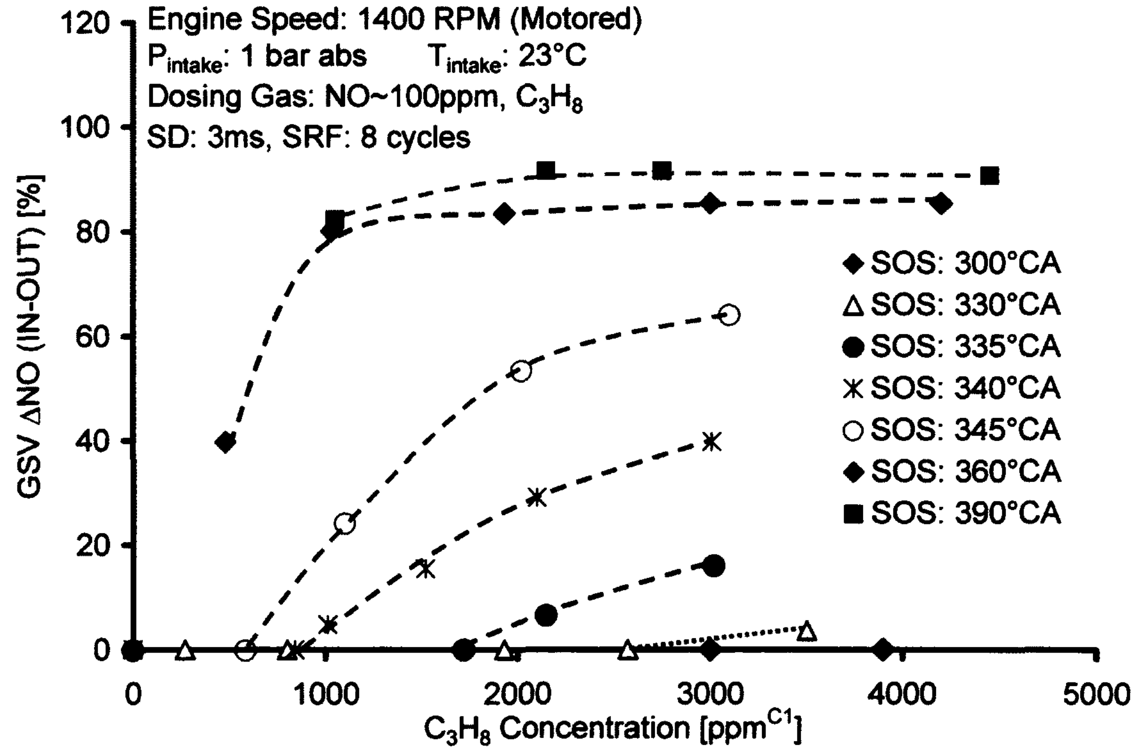

Figure 5.11: Crank Angle Resolved NO Concentration in the Combustion Chamber

The corresponding steady-state exhaust emissions are shown in Figure 5.12. The effect of HC concentration on the NO and NO_2 concentrations was significant up to 1000~1500 ppm^{C1}. Above this, the NO and the NO_2 concentrations did not change.

About 50 ppm of the NO was converted into NO_2 while the NOx reading indicated the destruction of approximately 40 ppm of NO.

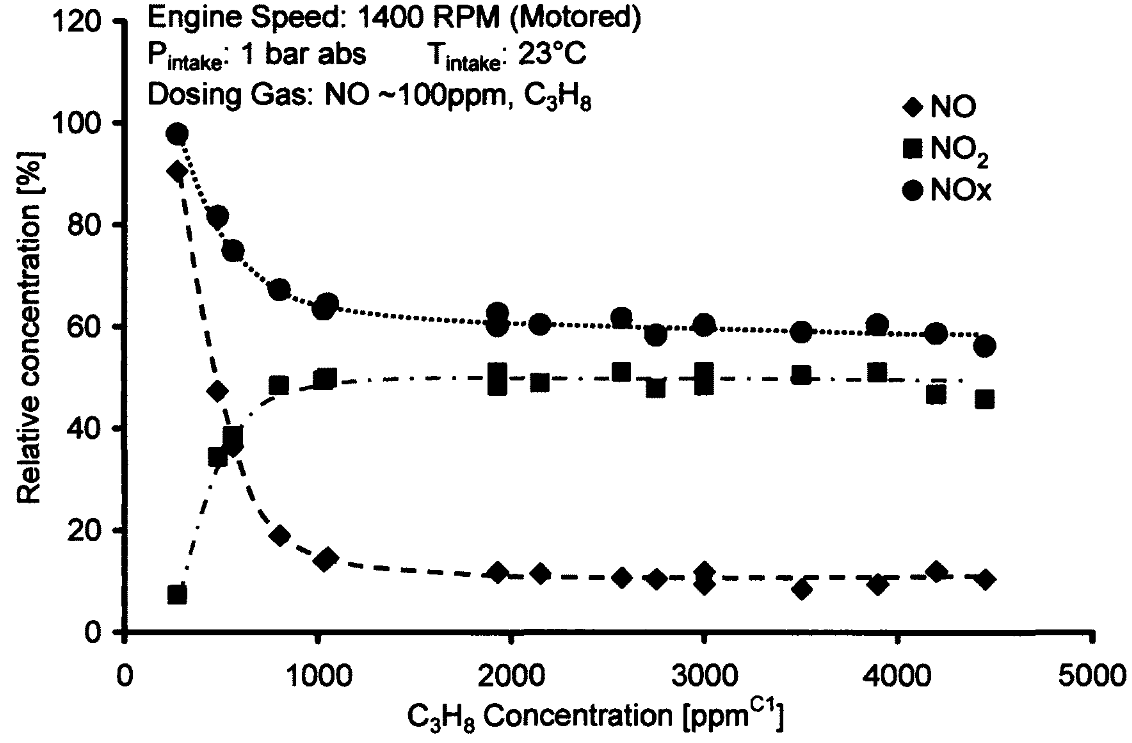

Figure 5.12: Steady State Exhaust Emissions for the Results of Figure 5.11

The effect of the HC concentration on ΔNO at different crank angles is shown in Figure 5.13. From 335 to 345°CA, a higher HC concentration resulted in a higher change in the NO concentration but the effect was reduced for HC concentrations above 1500 ppm^{C1}. However, at 360°CA, the ΔNO values converged for all the HC concentration, suggesting that the higher compression temperature prevailing around TDC accelerated the reaction.

Having observed that the HC concentration effect was not significant when the HC to NO ratio was roughly greater than 15, another test was run with lower concentrations of HC and the results are shown in Figure 5.14. A 1.2 ms sampling duration which translates into a 10°CA window at 1400 RPM was used. With 1160 ppm^{C1} of propane, over 60% reduction in the NO concentration was seen.

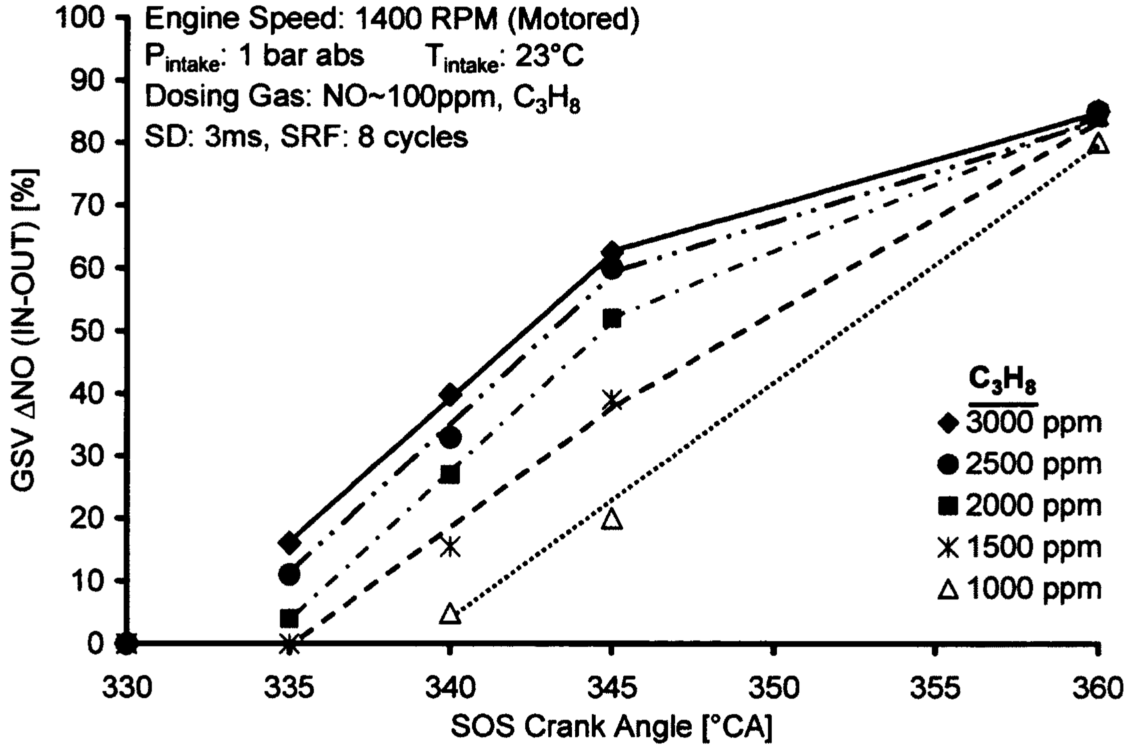

Figure 5.13: Effect of HC Concentration on ΔNO at Different Crank Angles

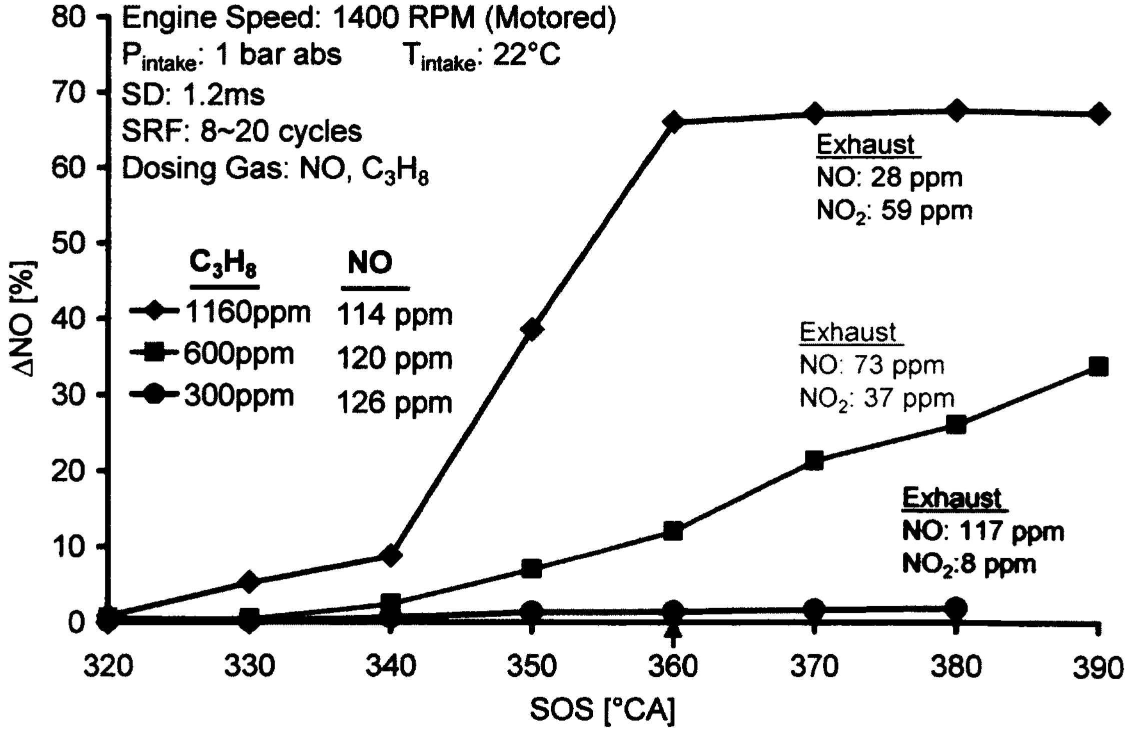

Figure 5.14: Effect of Low HC Concentrations on the ΔNO Value

However, reducing the propane concentration by half reduced the NO reduction to slightly above 30%. The NO reduction was negligible with 300 ppm^{C1} of propane.

All of the results discussed above suggested the existence of a critical ratio between the HC and NO concentrations. With a HC/NO ratio lower than a certain threshold value, the NO conversion was strongly inhibited. To confirm this observation, the NO concentration was varied from 50~300 ppm at three different HC values. The results are shown in Figure 5.15. With 100 ppm^{C1} of HC, a sharp fall in the ΔNO was observed as the dosing NO concentration increased above 80-100 ppm. A similar trend was seen for the HC concentration of 2000 ppm^{C1} where the ΔNO value reduced rapidly for NO concentrations above 200 ppm.

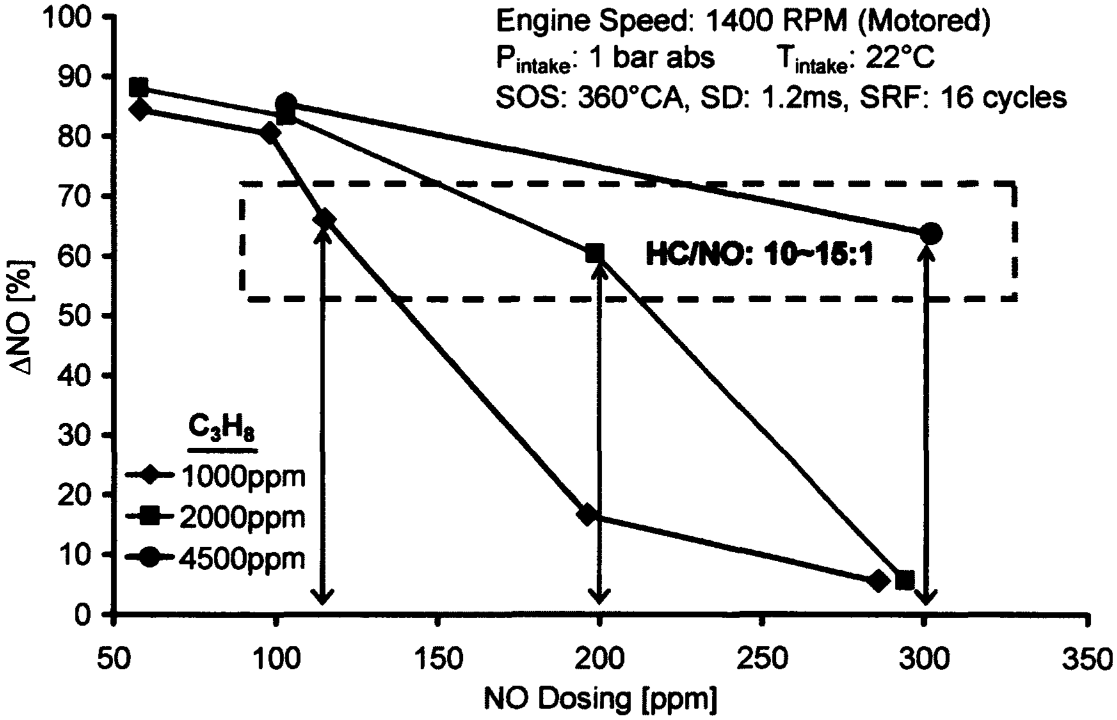

Figure 5.15: Investigating the Critical HC to NO Ratio

Based on these results, a critical HC/NO ratio of 10~15:1 was found to exist that resulted in a significant conversion and/or destruction of NO. A lower ratio considerably decreased the NO conversion while a high ratio indicated an insignificant or a small increase in the conversion.

5.4.2. Chemical Kinetics Simulations

Chemical kinetics simulations were run in CHEMKIN Software to provide an understanding of the underlying mechanisms affecting the NO to NO_2 conversion in the presence of propane. The chemical kinetics mechanism used for this study was obtained from the Lawrence Livermore National Laboratory, USA. The mechanism pertains to the effect of hydrocarbons (C_1 to C_3) on the NO–NO_2 conversion. It consists of 126 species and 639 reversible reactions. The details of the mechanism validation can be found in [88].

The simulation was setup using the 0-D internal combustion engine model in CHEMKIN that includes only the compression and the expansion processes. The model simulates the time evolution of a homogeneous reacting gas mixture under auto-ignition conditions. The Yanmar geometry was used in the simulation setup. The simulation was first calibrated to match the motoring pressure trace of the Yanmar engine as shown in Figure 5.16. The input parameters obtained from this calibration process were then used for the rest of the simulation work.

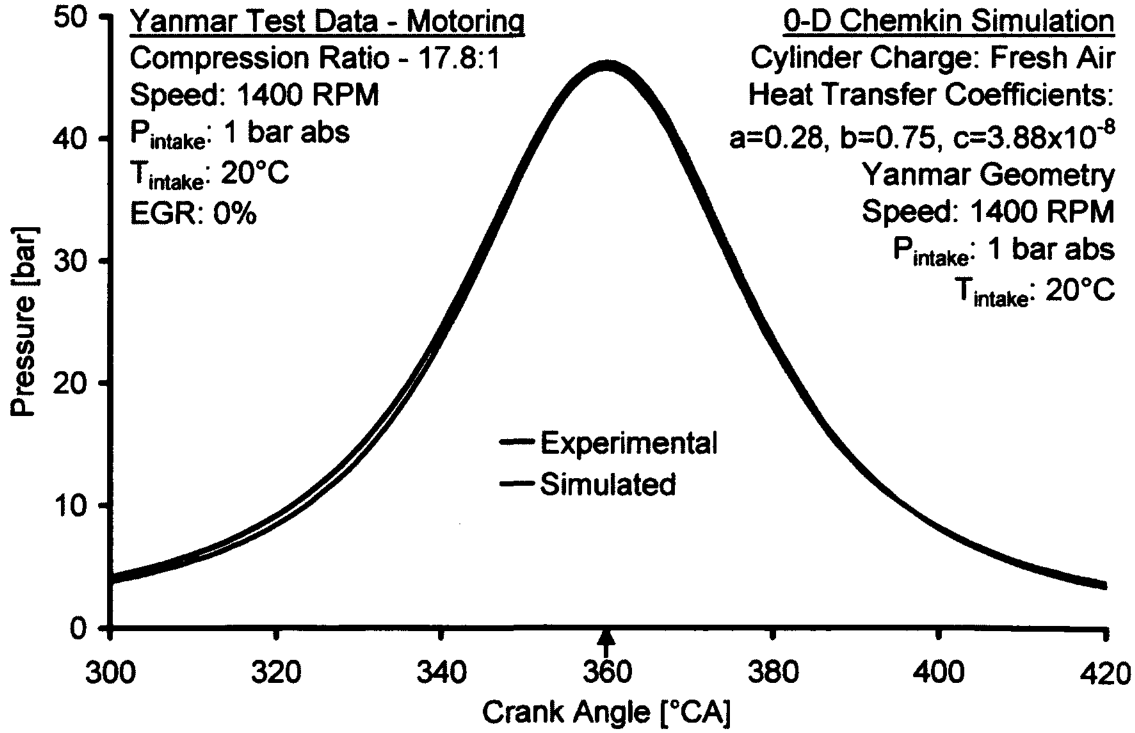

Figure 5.16: Motoring Pressure Matching between Experimental & Simulation Results

The composition of the propane gas determined with the FTIR (Table 4.8) was used as the input and the simulation was run with 100 ppm of NO and 1000 ppm of C_3H_8. The results shown in Figure 5.17 indicated a reduction in the NO concentration and an increase in the NO_2 concentration. Moreover, about 15 ppm of CO was also produced similar to the empirical results (Figure 5.9). The reduction in the propane concentration indicated that some of the propane was consumed during the NO to NO_2 conversion process.

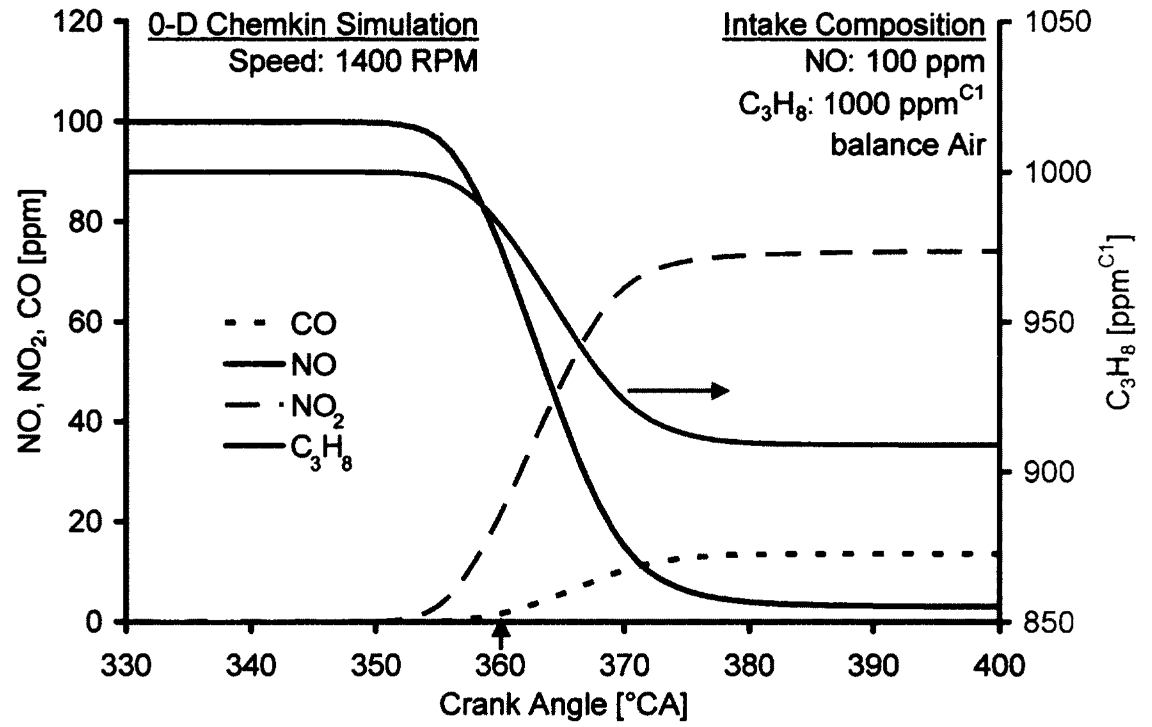

Figure 5.17: Simulation Results showing the NO to NO_2 Conversion with Propane

The simulations were rerun at different HC concentrations and the results are shown in Figure 5.18. With 250 ppm of HC in the cylinder charge, only 5 ppm of NO was converted into NO_2. However, as the HC concentration was progressively increased to 1000 ppm, the NO to NO_2 conversion increased significantly. Moreover, it can be observed that all the NO was not converted into NO_2. For example, with 1000 ppm of HC, only 3 ppm of NO remained at the end of the simulation. Out of the 97 ppm of NO that under went some chemical reaction, only

75 ppm were converted to NO_2 and therefore, 22 ppm of NO remained unaccounted for.

The simulation results indicated the initiation of the conversion process after 350°CA. This is slightly later than the empirical results which showed the process beginning around 340 °CA. For the empirical results (Figure 5.14), an important point to remember is that the SOS represented the crank angle for the start of the sampling process and the valve opening duration was 1.2 ms (10°CA at 1400 RPM). Therefore, the value shown at 340°CA actually represented the average concentration over a crank angle window from 340°CA to 350°CA.

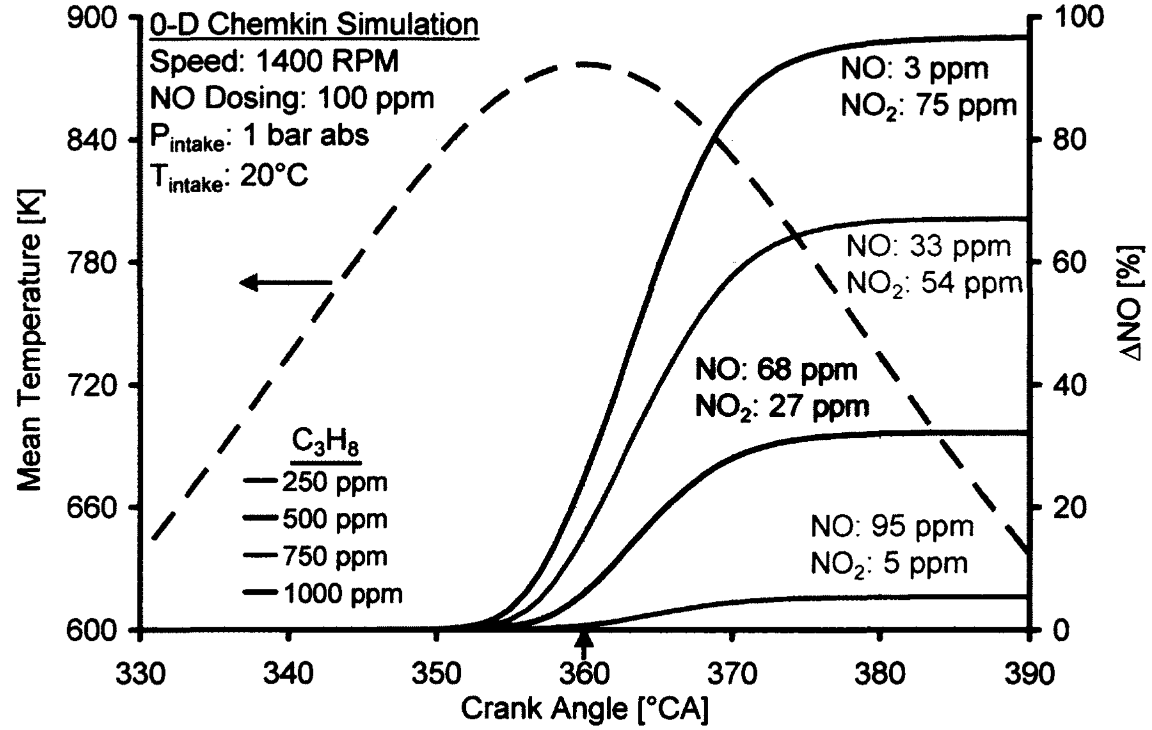

Figure 5.18: Simulated NO-C_3H_8 Interaction (100 ppm NO)

Another aspect of interest was the effect of the HC concentration on the change in the NO concentration at different crank angles. The simulations were run from 500 ppm to 4000 ppm of HC and the ΔNO profiles at different crank angles were plotted in Figure 5.19. The resulted showed that the conversion process reached steady values by 370°CA. Moreover, for HC concentration above 1000 ppm, the conversion efficiency was largely insensitive to the HC concentration. These results were in general agreement with the empirical results of Figure 5.11.

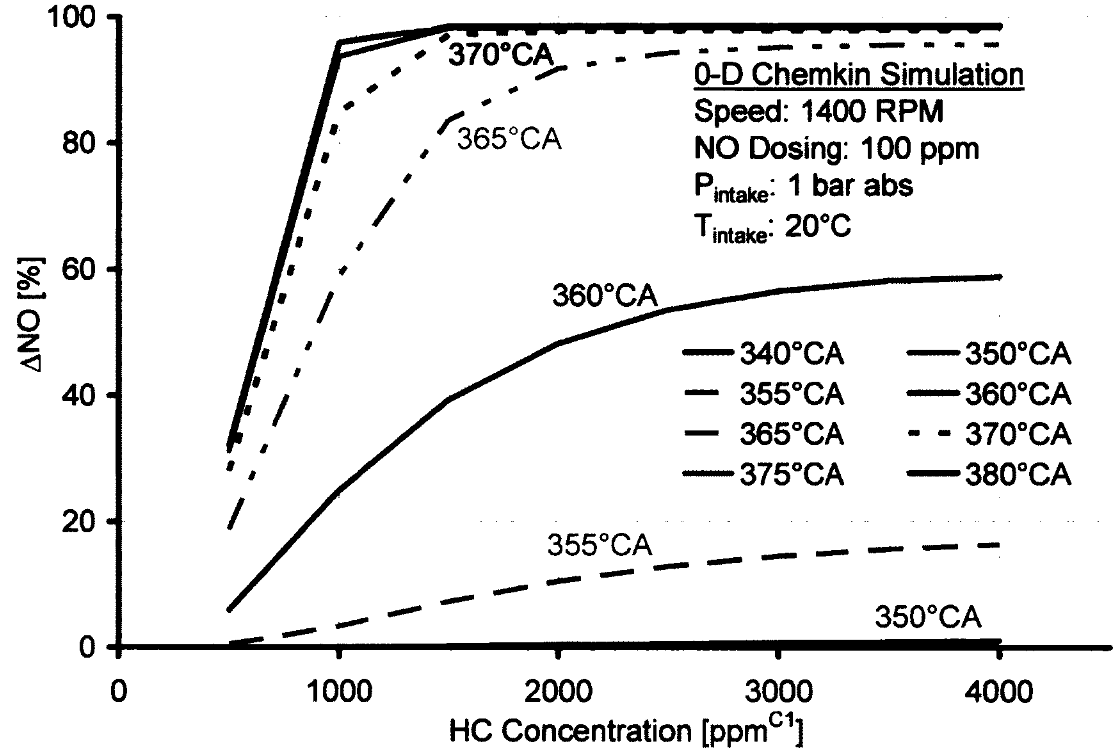

Figure 5.19: Simulated Results of Crank Angle Resolved NO Concentration

An analysis of the product concentrations from the simulations indicated that the 'disappeared' NO (as observed in both the empirical and the simulation results) was converted mostly into nitromethane (CH_3NO_2) and to a much lesser extent into nitrous acid (HONO) as shown in Figure 5.20. Therefore, the NO_2 formed as a result of the NO oxidation further reacted to form these two chemical compounds. The general reaction for the combustion of nitromethane (commonly called 'Nitro' in the racing industry) is given by:

$$\begin{array}{ll} \text{With Oxygen:} & 4CH_3NO_2 + 3O_2 \rightarrow 4CO_2 + 6H_2O + 2N_2 \\ \text{Without Oxygen:} & 4CH_3NO_2 \rightarrow 4CO + 4H_2O + 2H_2 + 2N_2 \end{array} \tag{4.3}$$

Therefore, the conversion of the NO into nitromethane can be assumed as the destruction of NO.

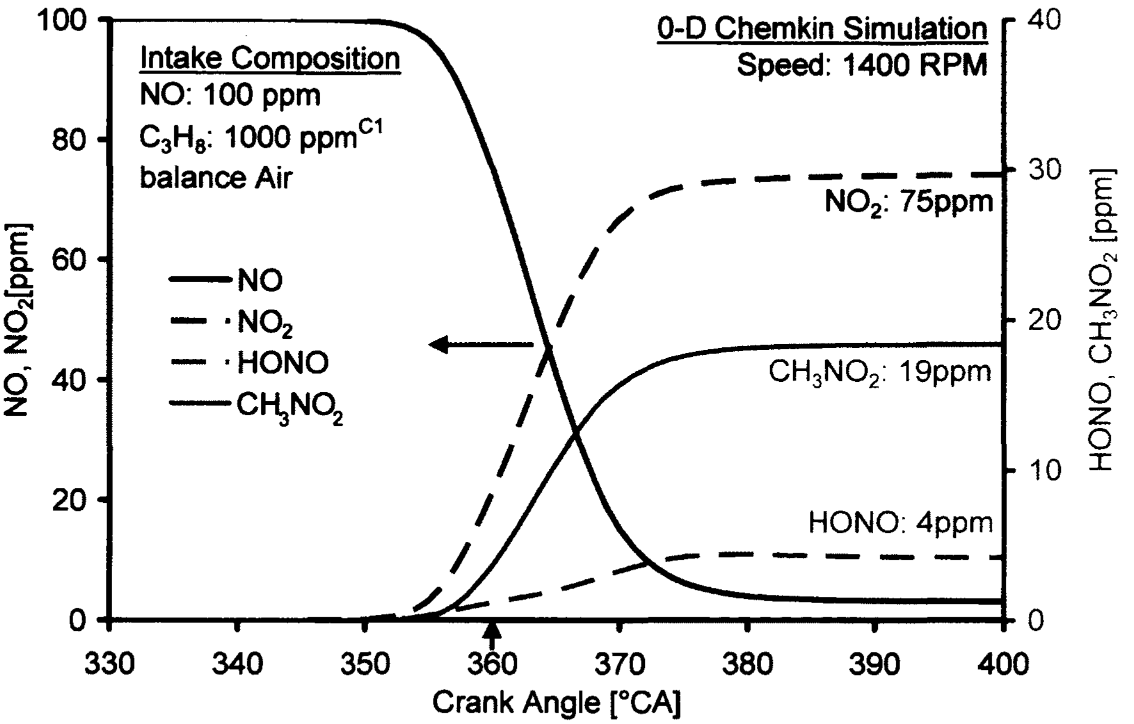

Figure 5.20: Accounting for the Disappeared NO (Simulated Results)

The oxidation of NO to NO_2 has been reported to occur predominantly through the following reaction [88] in the presence of C_2 to C_3 hydrocarbons from 600 to 1100 K:

$$NO + HO_2 \rightleftharpoons NO_2 + OH \tag{4.4}$$

In the referred study [88], the effectiveness of the hydrocarbon type towards NO to NO_2 conversion was suggested to depend on the hydrocarbon's propensity to produce reactive radicals like OH to sustain fuel oxidation while simultaneously producing the hydroperoxyl (HO_2) radicals for subsequent NO to NO_2 conversion. Propane and ethylene were shown to effectively oxidize NO to NO_2 while the use of methane or ethane resulted in insignificant conversion rates. This was primarily attributed to the slow nature of methane oxidation that produced a limited amount of HO_2 radicals and in case of ethane, to the destruction of the reactive radicals like ethyl (C_2H_5) that promote the production of the HO_2 radical.

It is pertinent to mention here that methane was initially used as a dosing gas in this work but no conversion of NO was observed for the motored engine operation. Thereafter, it was decided to use propane as the dosing gas.

To observe if the existence of a critical ratio between the HC and NO concentrations was also predicted with the simulations, the NO concentration was varied from 100 to 400 ppm at three different HC levels as shown in Figure 5.21. The results for 1000 ppm of HC indicated a trend similar to that obtained during the experiments. An increased concentration of HC resulted in a moderate increase in the conversion of NO to NO_2, for NO levels above 100 ppm. However, the conversion was lower than that observed during the experimental investigations (Figure 5.15). It was noted that the chemical kinetic mechanism used in this study was produced with a HC/NO mixture containing 20 ppm of NO. Therefore, it was suspected that the application of the mechanism may have been limited to low concentrations of NO (up to 100 ppm).

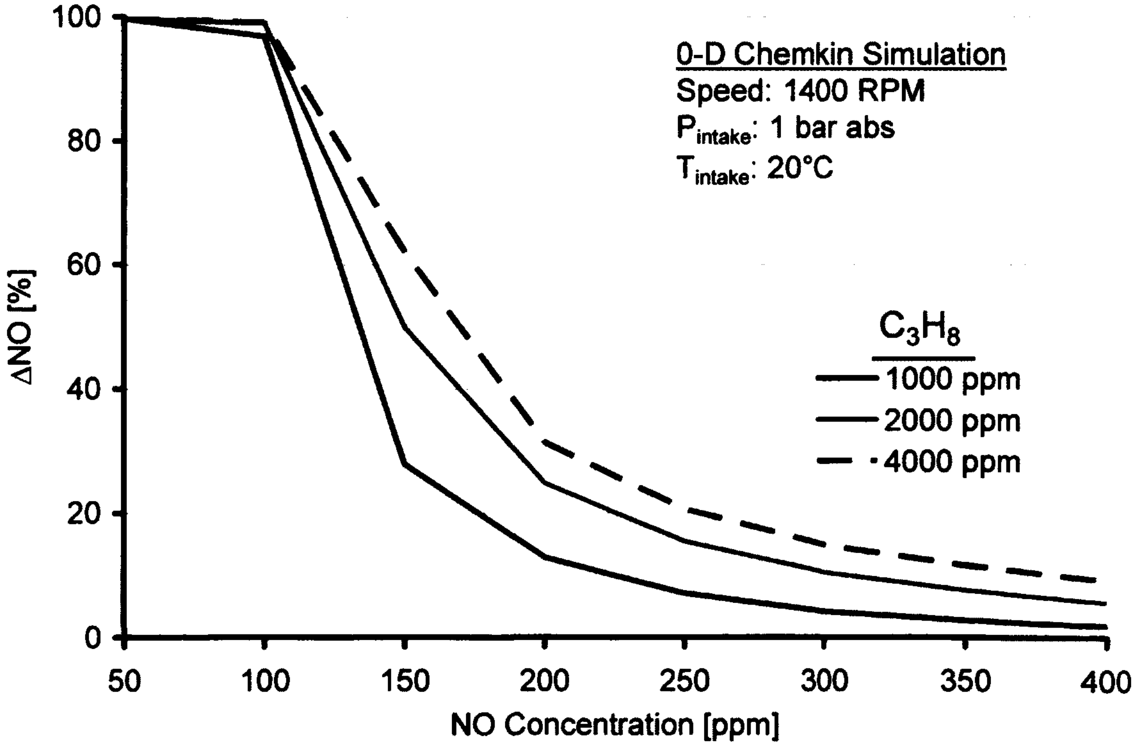

Figure 5.21: Simulation Results highlighting the existence of the Critical HC to NO Ratio

During engine operation in the LTC regime, the NOx levels commonly observed are very low (as low as a few ppm) and therefore, the trends obtained with the experimental results and the simulation studies validate the existence of a critical HC to NO ratio for achieving ultra low emissions of NOx.

5.5. LTC Combustion Analysis

The second portion of the in-cylinder sampling study included the investigation of temporal evolution of NOx under actual engine operating conditions. The exhaust composition was also analyzed to characterize the HC speciation under LTC cycles. These tests were performed with Dimethyl Ether (DME) as the surrogate fuel for diesel. DME has a high cetane number, similar to diesel fuels but has high oxygen contents (32~34%). This results in ultra low levels of soot that enable the gas sampling valve to operate without getting clogged for extended periods. Moreover, DME vaporizes easily at room temperature and is therefore, suitable for port injection.

A typical heat release rate for the DME port injection tests is shown in Figure 5.22. The DME combustion is characterized by two distinct heat release phases: a low temperature reaction (LTR) regime which signifies the cool-flame reactions and a high temperature reaction (HTR) regime which comprises of the main combustion event. Because of the high compression ratio of the Yanmar engine (17.8:1) and the high cetane number of DME, the phasing of the LTR regime was very early in the compression stroke. The HTR regime also occurred at ~10°CA BTDC. Increasing the quantity of the DME fuel resulted in engine knock. This placed a severe limit on the level of load that could be achieved. To investigate the effect of varying the air-fuel ratio, the intake of the engine was therefore throttled to vary the flow rate and in turn, modulate the fuel strength of the mixture.

The test matrix for the DME port injection experiments is given in Table 5.1. The first five tests were run without EGR at various throttled intake conditions. For the EGR tests, the engine was throttled to maintain an intake flowrate of 8.7 g/s. Three different levels of EGR (33, 55 & 74%) were then applied and the effects on the combustion and the in-cylinder NO history were investigated.

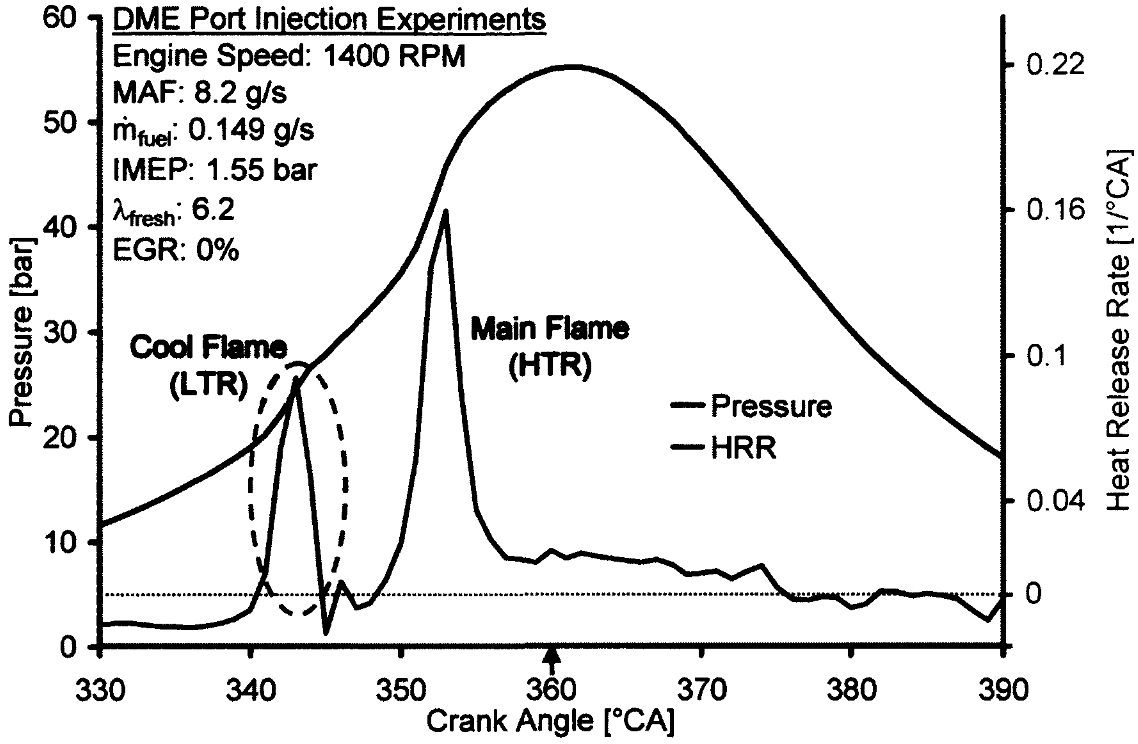

Figure 5.22: Typical Heat Release Rate for DME Combustion (CR = 17.8:1)

Table 5.1: DME Port Injection Test Matrix (CR- 17.8:1)

MAF [g/s]	DME [g/s]	EGR [g/s]	A/F Ratio [-]	Fresh Air Lambda
8.2	0.149	0	55:1	6.2
8.6	0.141	0	60:1	6.8
8.94	0.138	0	65:1	7.3
9.35	0.137	0	68:1	7.7
10.6	0.164	0	62:1	7.2
5.86	0.128	2.84	46:1	5.1
3.89	0.128	4.81	30:1	3.4
2.29	0.128	6.41	18:1	2

The in-cylinder NOx evolution for the test with λ_{fresh} of 6.8 is shown in Figure 5.23. The in-cylinder gases were sampled with a sampling duration of 1.2 ms (10°CA) during these tests. The NOx values have been plotted at the centre point of the sampling window

(335°CA in case of SOS @ 330°CA) so that the trends can be related with the heat release rates. It was observed that around 20 ppm of NO formed during the first part of the heat release, i.e. the LTR regime. However, during the main combustion or the HTR regime, the NO reduced progressively. Looking at the engine-out emissions, it was seen that HC emission was nearly 1100 ppm which resulted in a HC to NO ratio of ~50. Although NOx was generated during the combustion process, the presence of the unburnt hydrocarbons in sufficient amount presumably reduced the engine out NOx to 2 ppm.

A similar trend was observed with the engine operating at λ_{fresh} of 7.7 as shown in Figure 5.24. With a leaner cylinder charge, the peak NO concentration during the combustion was slightly lower which may be attributed to the lowered combustion temperature during the burning of the homogeneous cylinder charge.

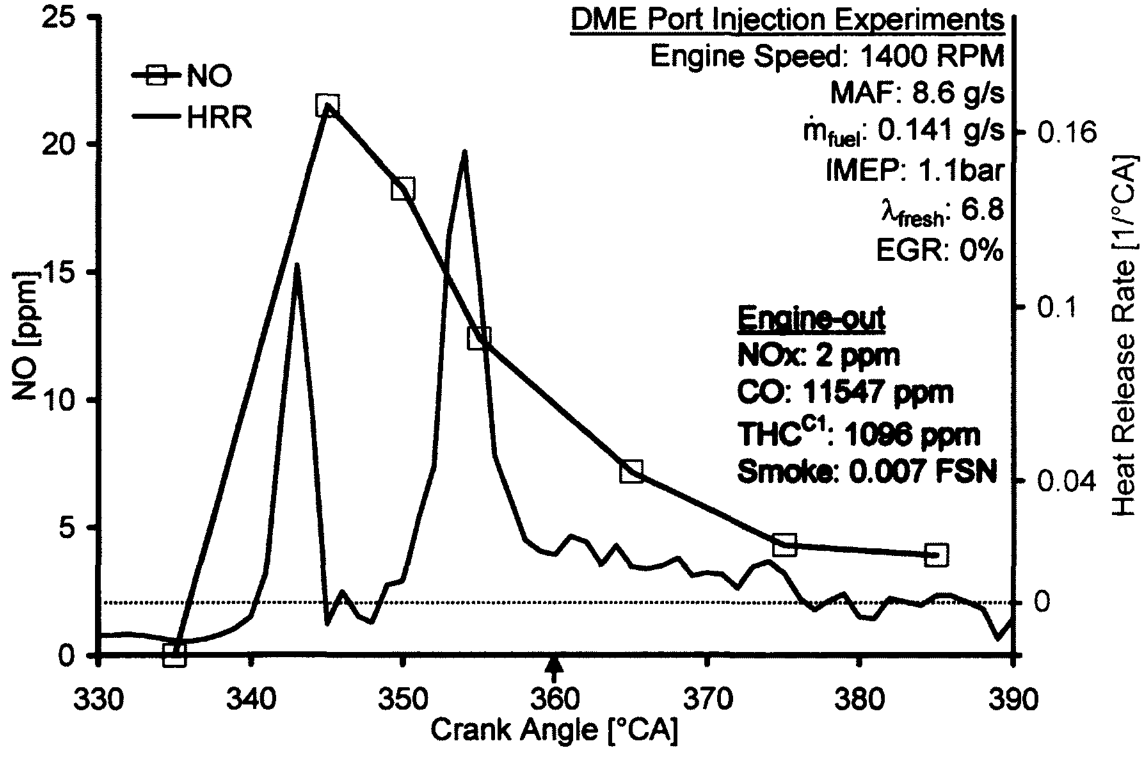

Figure 5.23: In-cylinder NO Evolution (λ_{fresh}= 6.8, CR = 17.8:1)

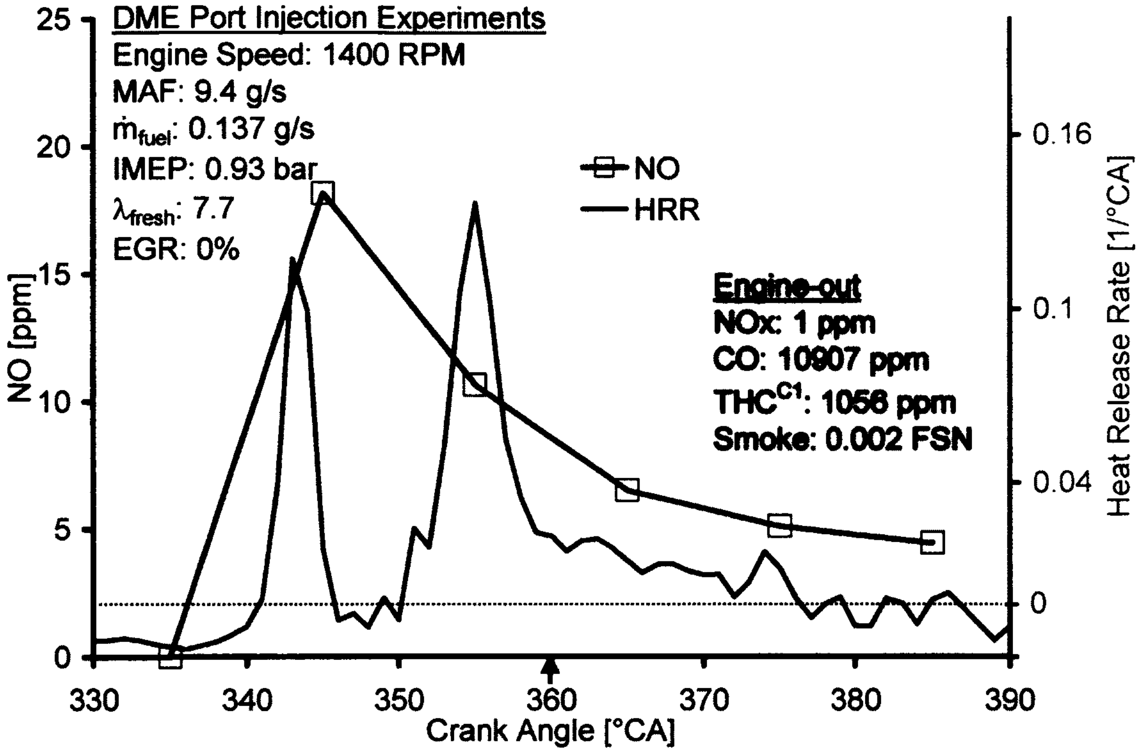

Figure 5.24: In-cylinder NO Evolution (λ_{fresh}= 7.7, CR = 17.8:1)

The cylinder pressure and the heat release rates for the two cases presented above are shown in Figure 5.25. Since the engine intake was throttled to modify the strength of the cylinder charge, therefore, the pressure for the case with λ_{fresh} of 7.7 (less throttling) is higher than that for the case with λ_{fresh} of 6.8 (more throttling). However, two differences were seen between the heat release rates. First, the heat release rate of the main combustion event was lower for the leaner combustion (λ_{fresh}= 7.7) and second, the phasing of the main combustion was also slightly retarded towards TDC as compared to the heat release rate with λ_{fresh} of 6.8.

A comparison of the in-cylinder NO concentration and the cumulative heat release traces is shown in Figure 5.26. It was observed that although the LTR accounted for only ~20% of the total heat release, the NO concentration peaked during this period. The reduction in the NO thereafter indicated that the LTR phase also generated the lower chain hydrocarbons (C_1~C_3) that are essential for the oxidation of NO to NO_2. The low engine-out NOx further indicated the conversion of NO_2 into other species as shown earlier.

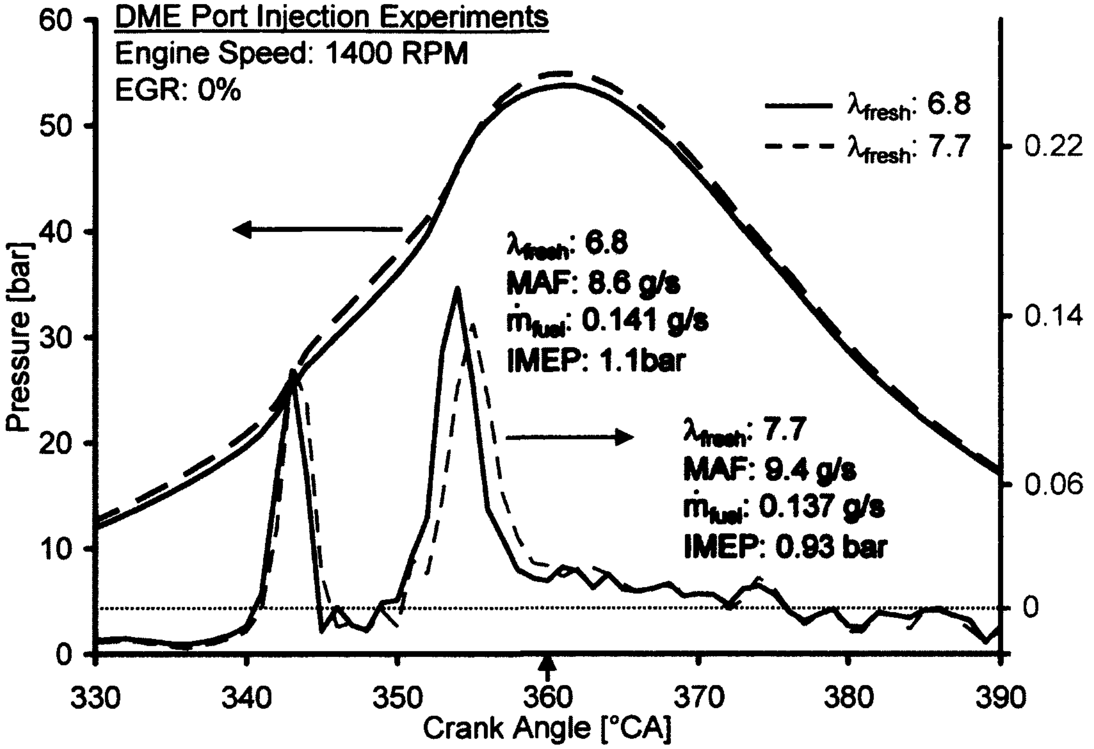

Figure 5.25: Cylinder Pressure & Heat Release Comparison (CR = 17.8:1)

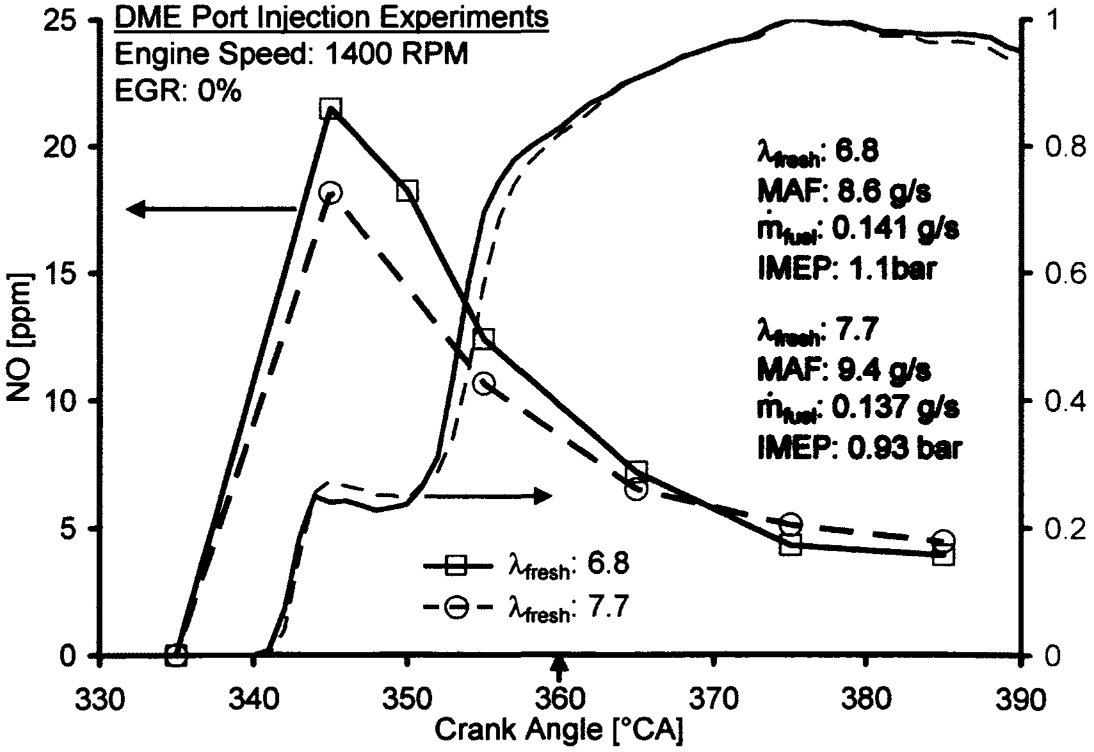

Figure 5.26: In-cylinder NOx Evolution Comparison (CR = 17.8:1)

The summary of the crank angle-resolved in-cylinder NO concentration is shown in Figure 5.27. Although the λ_{fresh} was varied from 6.8 to 7.7, the NO was generated within the LTR regime for all the cases. The destruction of the NO was also observed to be similar for all the cases.

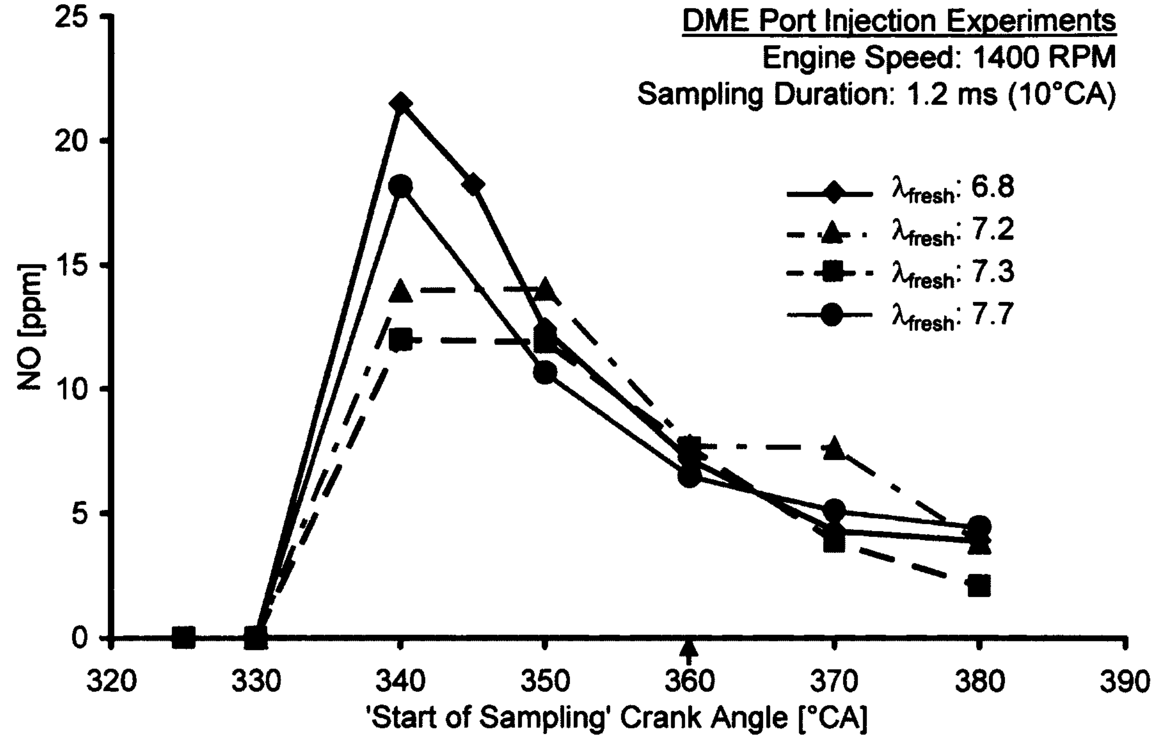

Figure 5.27: Summary of Crank Angle-resolved In-cylinder NO (CR = 17.8:1)

The summary of the tests without EGR is given in Table 5.2. The indicated thermal efficiency was quite low which can be attributed to the low engine loads, and the high HC and CO emissions. The engine out NOx was 1 to 2 ppm and there was virtually no smoke in the exhaust stream (FSN<0.008).

Tests were then carried out with EGR to improve the phasing of the combustion. The cylinder pressure traces and the heat release rates for the tests with EGR are shown in Figure 5.28. As the EGR was increased, the off-phasing of the combustion from the TDC was reduced. However, the improvement in the phasing of the LTR was less than that observed for the main combustion event. Furthermore, the rate of heat release was considerably lower for the main combustion event as the main combustion can benefit from the virtual EGR produced during the LTR regime. It was noted that the peak of the LTR portion was also suppressed with higher levels of EGR. Another consequence of the EGR was a reduction in the peak cylinder pressure.

Table 5.2: Performance Summary for DME Experiments (No EGR; CR = 17.8:1)

MAF [g/s]	Fresh Air Lambda	IMEP [bar]	Indicated η_{th} [%]	Engine-out Emissions		
				NOx [ppm]	CO [ppm]	THC^{C1} [ppm]
8.2	6.2	1.55	29.9	2	8308	1106
8.6	6.8	1.1	26.7	2	11547	1096
8.94	7.3	0.97	24.3	2	11302	1080
9.35	7.7	0.93	23.9	1	10907	1056
10.4	7.2	0.87	24.4	2	9840	883

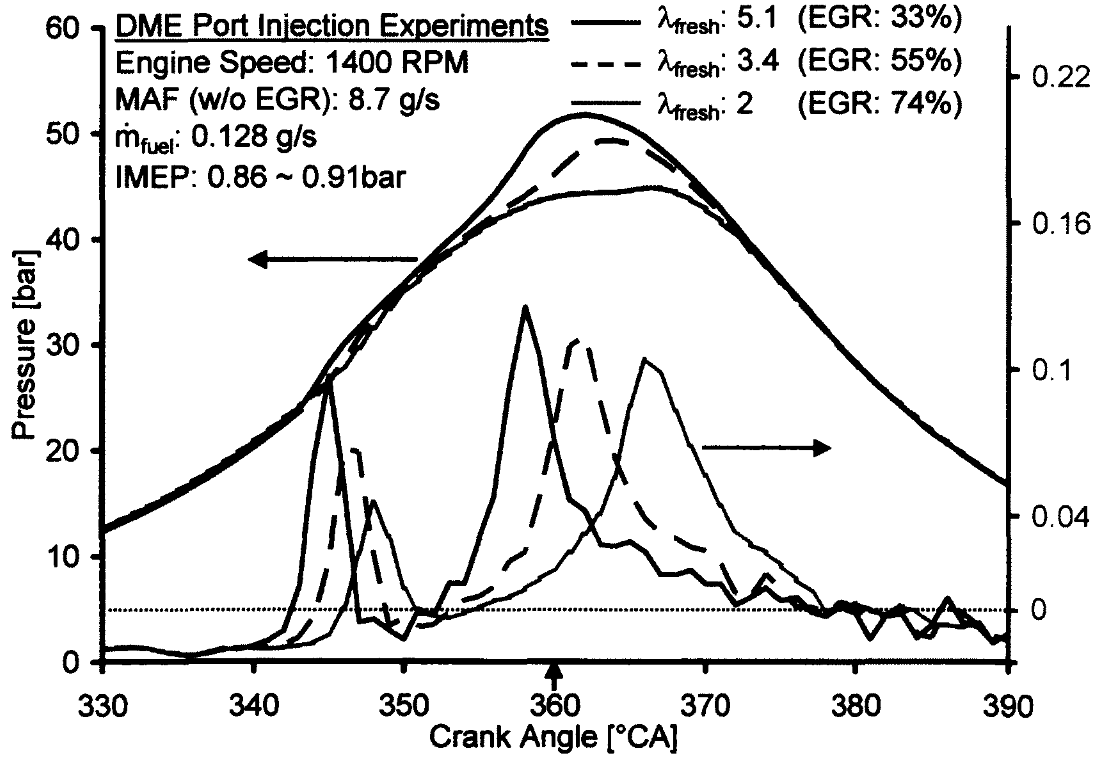

Figure 5.28: Cylinder Pressure & Heat Release Rates with EGR (CR = 17.8:1)

The in-cylinder NO concentrations and the cumulative heat release traces are shown in Figure 5.29. The peak NO concentration was observed to decrease with increasing EGR as a result of the lowered combustion temperatures and the high dilution of the intake charge. Moreover, with 75% EGR, the phasing of the NO curve was also retarded in conjunction with the combustion phasing. The cumulative heat release traces for the three EGR levels indicate that the heat release during the LTR was reduced by half, from about 20% to 10% of the total fraction.

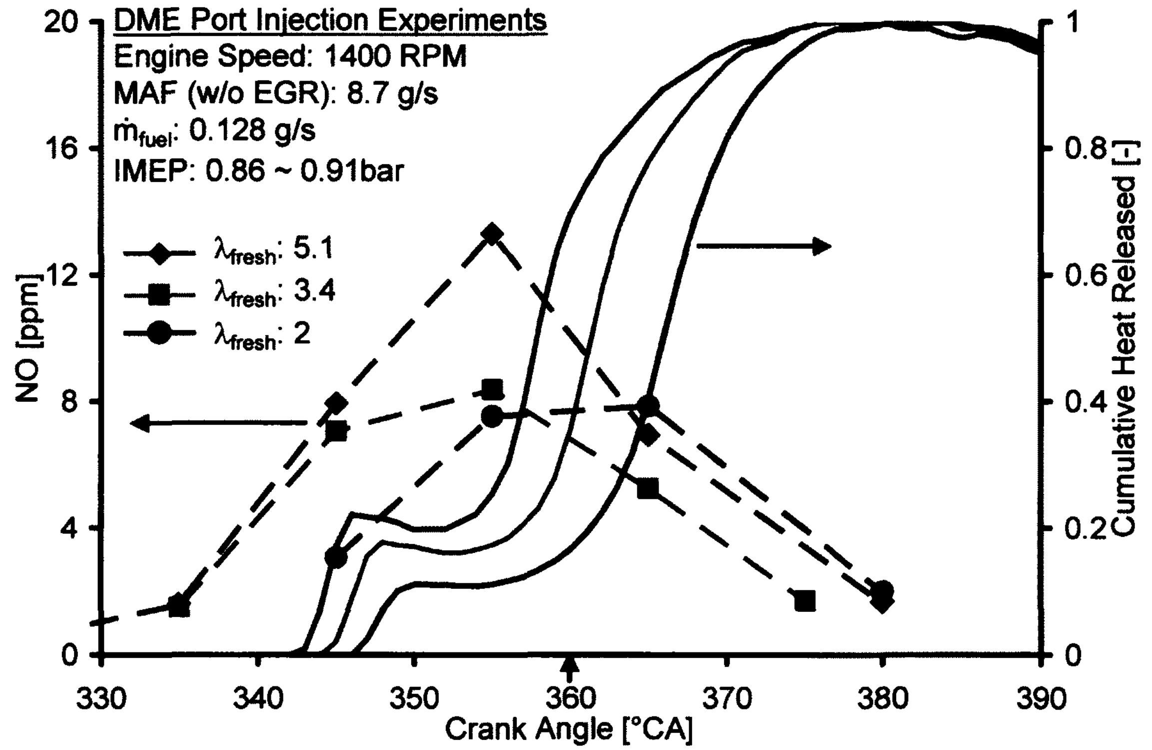

Figure 5.29: Crank Angle-resolved NO Concentration with EGR (CR = 17.8:1)

The summary of the tests with EGR is given in Table 5.3. It was seen that a slight increase in the engine load was observed up to 55% EGR that could be attributed to the improvement in the combustion phasing. However, operation with 74% EGR resulted in a significant deterioration in the fuel efficiency caused by the very high engine-out HC and CO emissions. The NOx and smoke emissions were nearly zero during these tests.

Table 5.3: Performance Summary for DME Experiments with EGR (CR = 17.8:1)

MAF [g/s]	Fresh Air Lambda	EGR [g/s]	EGR [%]	IMEP [bar]	Indicated η_{th} [%]	Engine-out Emissions		
						NOx [ppm]	CO [ppm]	THC^{CT} [ppm]
5.86	5.1	2.84	33	0.89	24.7	1	13756	1365
3.89	3.4	4.81	55	0.91	25.2	1	16874	1936
2.29	2	6.41	74	0.59	16.3	1	22710	>3194*

5.5.1. Exhaust HC Speciation

The engine-out exhaust was analyzed with the FTIR in an effort to identify the major species comprising the HC emission and to understand the effect of the lowered combustion temperature (with the application of EGR) on the HC composition from the homogeneous DME combustion. A simplified overview of the DME combustion processes indicating the important species and the dominant reaction paths is presented in Figure 5.30 [89].

The by-products of the combustion process can be broadly grouped into four major categories as follows:

- Hydrocarbons with no O: These include methane (CH_4), ethane (C_2H_6), ethylene (C_2H_4) and acetylene (C_2H_2)
- One O-containing species: These include alcohols, ether, epoxides such as methanol (CH_3OH), iso-butanol ($C_5H_{11}OH$) and ethylene oxide (C_2H_4O).
- Carbonyl Group: CO-containing species such as aldehydes, acetates, ketones. These are the precursors or the intermediate products in the generation of CO and CO_2, and include formaldehyde (H_2CO), benzaldehyde (C_7H_7O), iso-butyl acetate (C_4H_9-COO-C_2H_5), ethyl acetate ($C_2H_5COOC_2H_5$), acetone (CH_3COCH_3) and methyl iso-butyl ketone ($C_4H_9COCH_3$).
- Aromatics: These are hydrocarbons containing a benzene ring and include benzaldehyde (C_7H_7O), o-xylene (C_8H_{10}) and ethyl-benzene (C_8H_{10}).

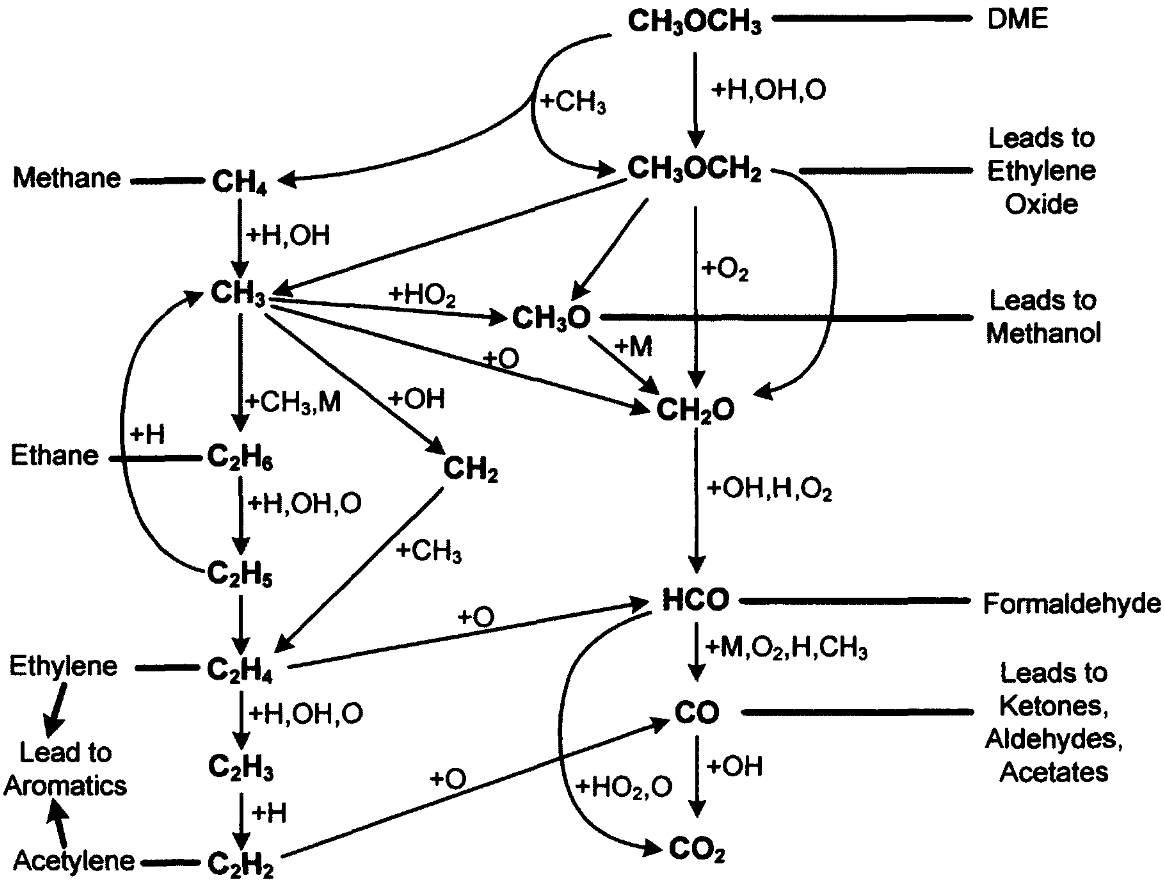

Figure 5.30: Overview of DME Combustion Processes

The data from the FTIR was analyzed and the species were grouped into the above defined four categories. The results are presented in Figure 5.31. It was observed that the concentration of the hydrocarbon group with no oxygen was very small while the carbonyl group displayed the highest concentration. For the tests without EGR, the effect of the air/fuel ratio variation (done by throttling the intake) was minor for all the four groups. Except the HC group, the concentrations increased slightly as the fuel strength of the cylinder charge was progressively increased. The application of EGR was found to increase the emissions for all the four groups compared to the values without EGR.

A comparison of the relative fraction of each group in the exhaust HC for the test conditions is shown in Figure 5.32. It was observed that with EGR, the relative fraction of the O-containing group increased while that of the carbonyl groups decreased in the exhaust HC. The aromatics and the HC group did not show any appreciable change.

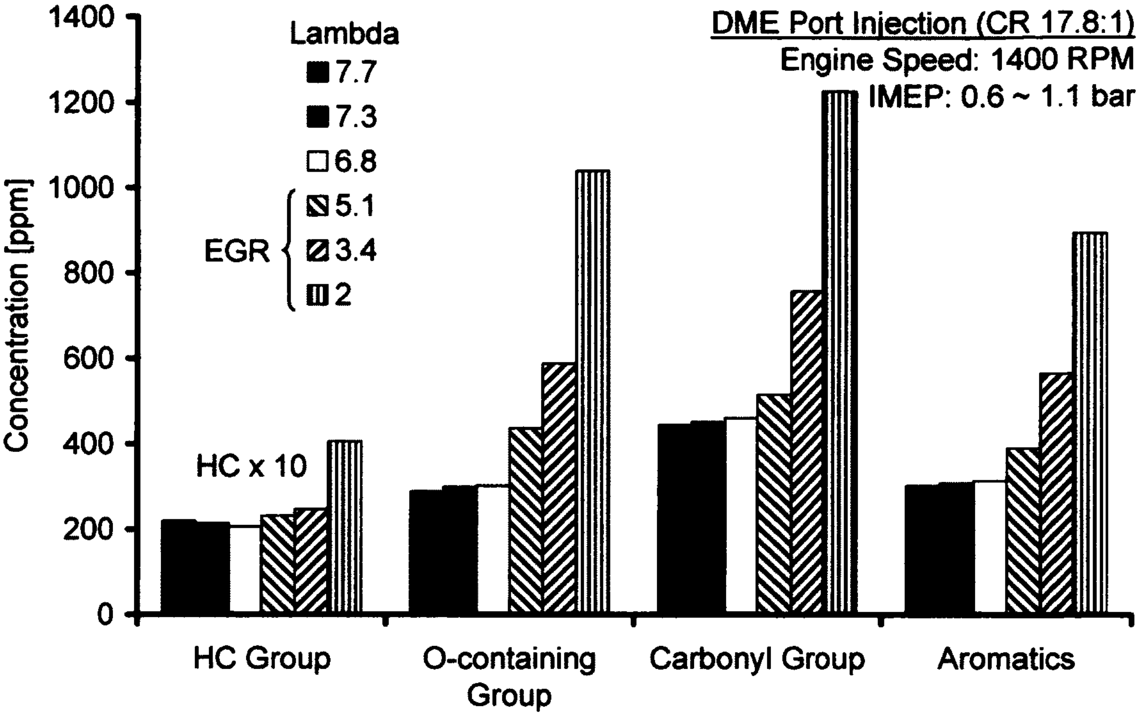

Figure 5.31: Exhaust HC Speciation for DME Combustion (CR = 17.8:1)

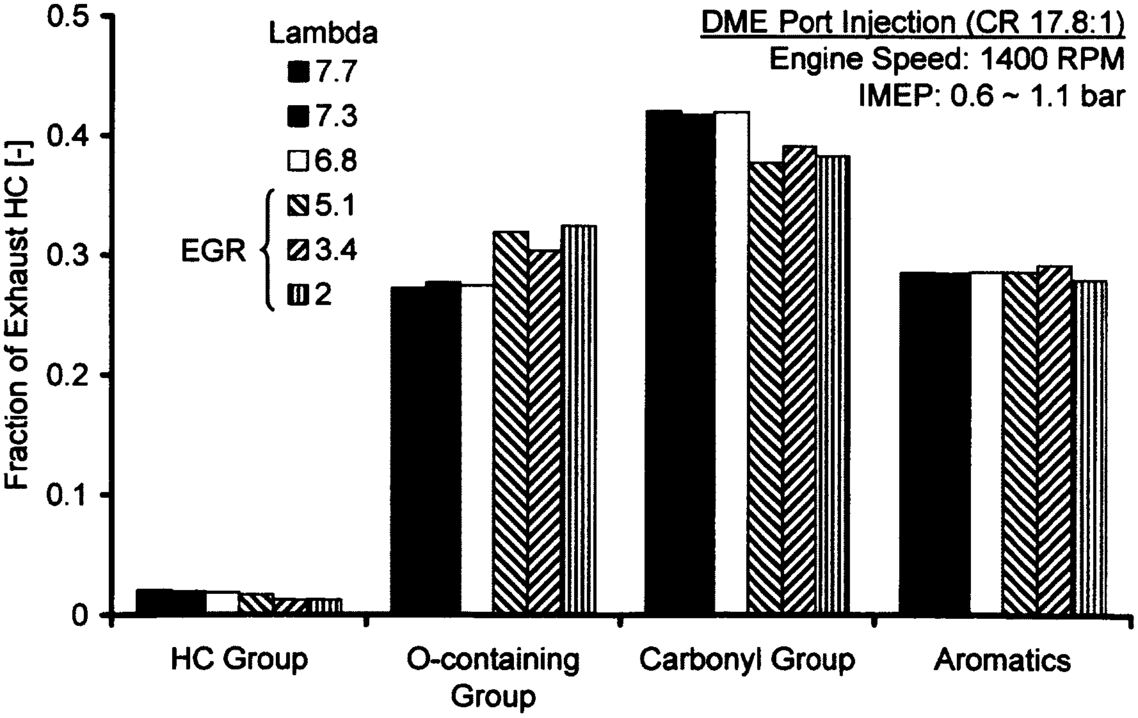

Figure 5.32: Relative Fraction of each Group in Exhaust HC (CR = 17.8:1)

5.6. Engine Compression Ratio Modification

A review of the literature pertaining to DME combustion indicated that the compression ratio of 17.8 was too high for port injection DME. The reported compression ratio is between 9 to 12:1 for port injection homogeneous combustion [90,91]. However, at such low compression ratios, the conventional diesel operation was not possible. Therefore, it was decided to reduce the compression ratio of the Yanmar engine such that the engine could be operated with both the conventional diesel and DME.

The existing piston bowl geometry and the combustion chamber cross-section are shown in Figure 5.33. The piston had a Mexican-hat shaped bowl. To reduce the compression ratio, a nominal compression ratio of 13:1 was chosen as a compromise between the diesel DI and DME port-injection performance. To reduce the propensity for HC emissions with a gaseous fuel, the crevices and the boundary layer need to be reduced. Therefore, a shallow piston bowl was designed as shown in Figure 5.34. The actual compression ratio after machining the piston was estimated to be 13.1:1.

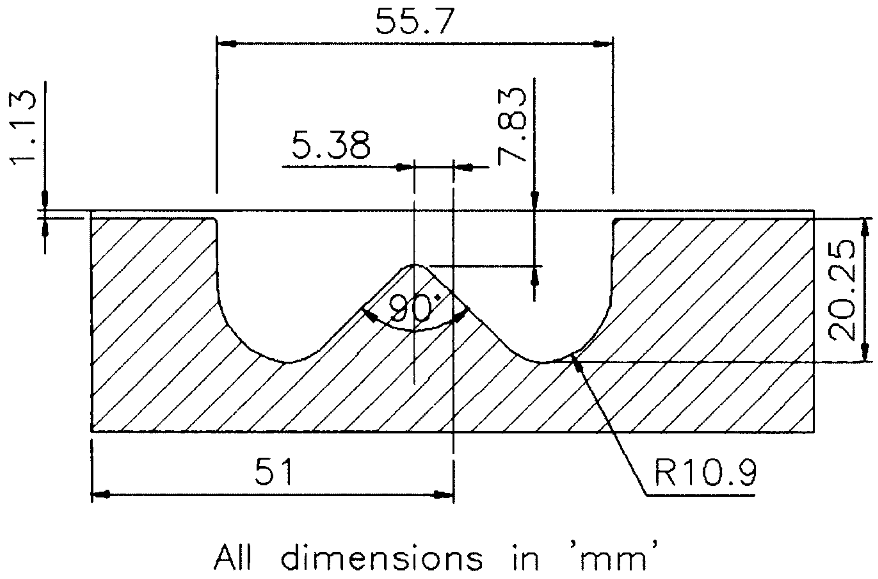

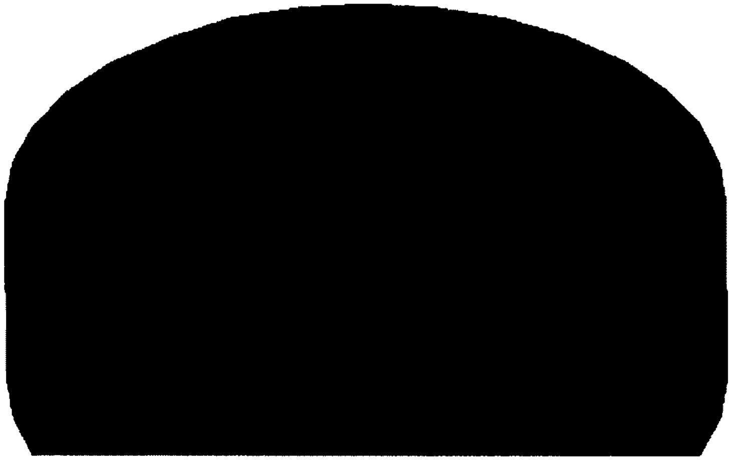

Parameter	Value
Compression Ratio	17.8
Swept Volume	857 cm^3
Combustion Chamber Volume	51.01 cm^3
Piston Bowl Volume (measured)	41.46 cm^3
Clearance Volume (calculated)	9.55 cm^3
Piston Crown to Cylinder Head Gap at TDC (calculated)	1.13 mm

Figure 5.33: Original Combustion Chamber & Piston Details (Compression Ratio – 17.8:1)

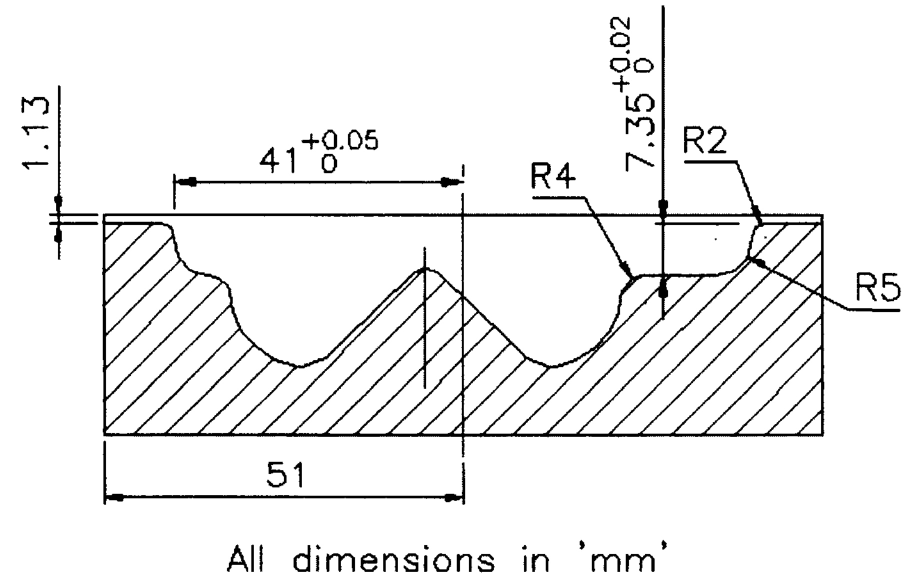

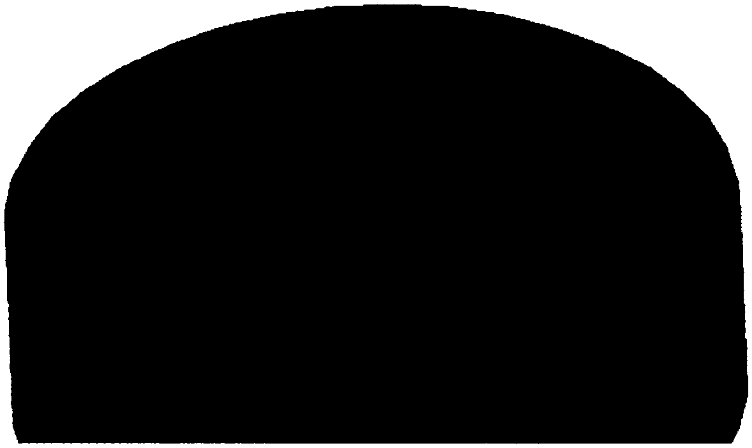

Parameter	Value
Compression Ratio	13.1
Swept Volume	857 cm³
Combustion Chamber Volume	70.98 cm³
Piston Bowl Volume (measured)	61.43 cm³
Clearance Volume (calculated)	9.55 cm³
Piston Crown to Cylinder Head Gap at TDC (calculated)	1.13 mm

Figure 5.34: Modified Combustion Chamber & Piston Details (Compression Ratio – 13.1:1)

5.7. DME Port Injection Tests- 13.1:1 Compression Ratio

The effect of the lowered compression ratio on the cylinder pressure and heat release rates was compared with the pressure and heat release traces for the original compression ratio of 17.8:1 as shown in Figure 5.35. The MAF was similar in both the tests. The IMEP was 0.87 bar in case of CR 17.8:1 and was limited by the onset of knocking. The IMEP was 2.1 bar for CR 13.1:1. It was seen that even with a higher engine load, the peak cylinder pressure was significantly lower. The phasing of the LTR heat release was retarded by about 3°CA while the phasing of the HTR heat release was retarded or improved by about 2°CA.

The mean cylinder temperatures were calculated for the motored pressure traces (not shown) and the reduction in the mean cylinder temperature was estimated to be ~81K (maximum T_{mean}: 865K for CR 17.8:1 and 784K for CR 13.1:1). The reduced in-cylinder temperature during the compression stroke delays the onset of auto-ignition and therefore results in an improved phasing of the combustion.

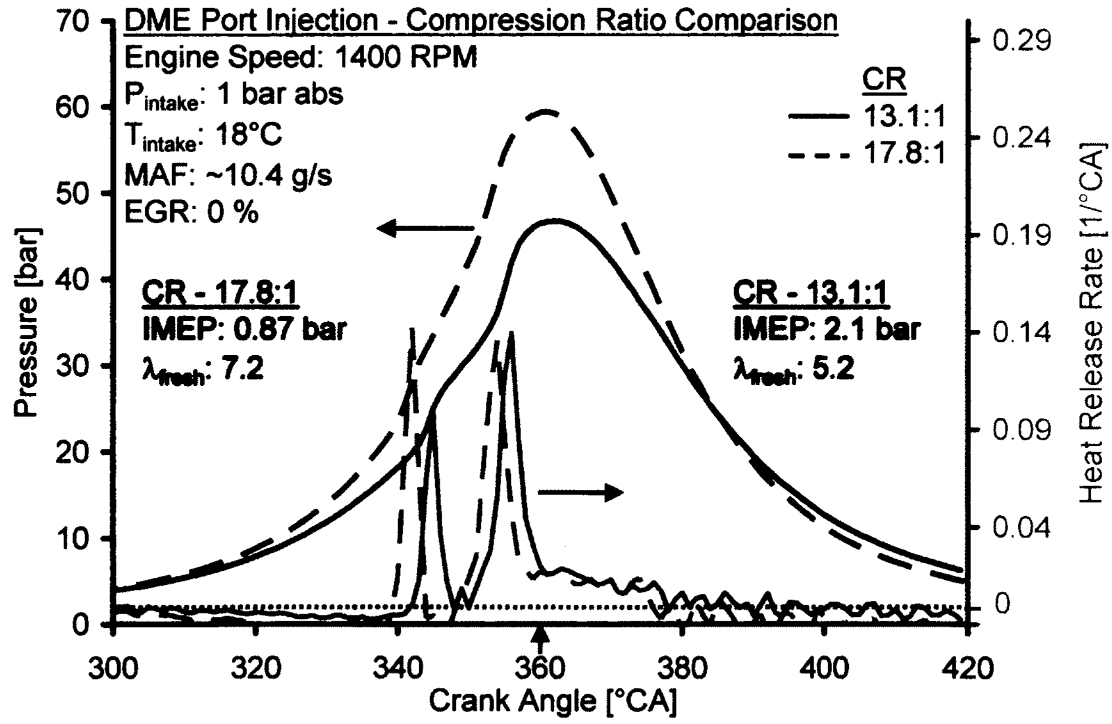

Figure 5.35: Effect of Compression Ratio on the Cylinder Pressure & Heat Release Rates

Another consequence of the reduced compression ratio was noted to be a reduction in the compression work as highlighted on the Log (p) vs. Log (V) plot in Figure 5.36. The reduced compression work and the improved phasing resulted in an increase in the net useful work output.

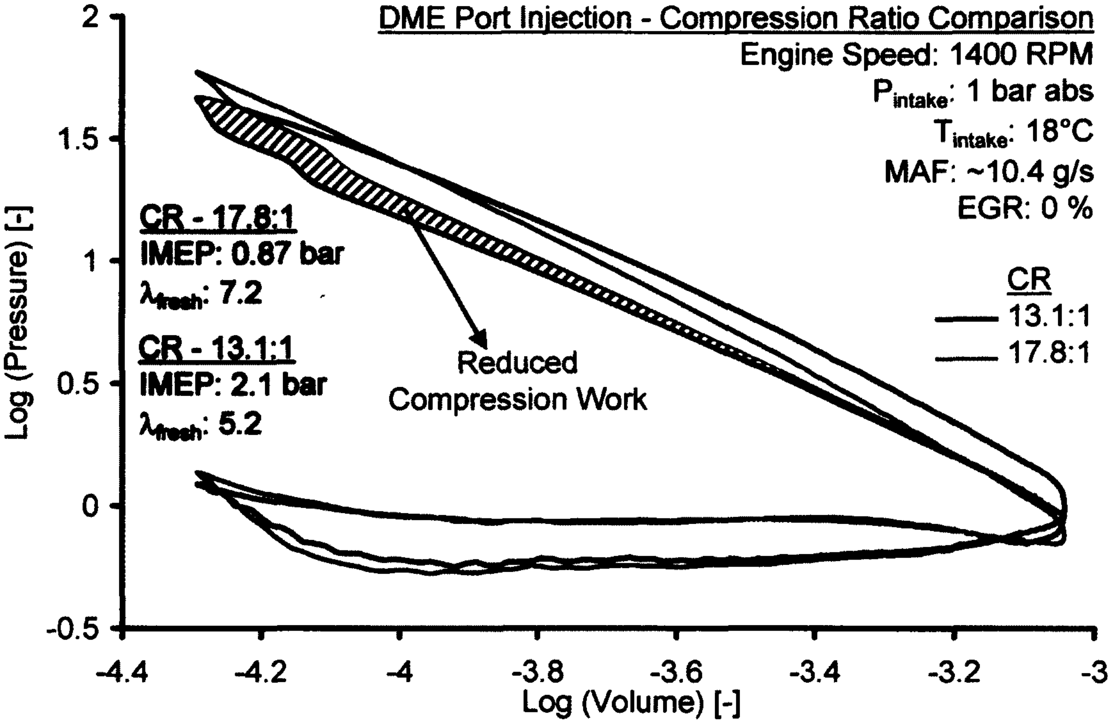

Figure 5.36: Log (p) vs. Log (V) Traces for the two Compression Ratios

The test matrix for the DME port injection tests with CR 13.1:1 is given in Table 5.4. The first run with MAF 10.4 g/s was an unthrottled operation at an IMEP of 2.2 bar. The engine intake was then throttled to 8.8 g/s and the engine load was increased to ~2.5 bar IMEP. This served as the baseline condition (λ_{fresh}= 3.9) for the following two tests with EGR. Two levels of EGR, 8% (low) and 30% (moderate) were applied to investigate the effects on the in-cylinder NOx history as well as the phasing of the combustion.

Since the load (2.5 bar IMEP) was low, the 8% EGR case did not show any difference from the 0% EGR test results. At low loads and low EGR rates, the recycled gases contain very little carbon dioxide and contain mostly oxygen. Therefore, the results presented henceforth compare the operation at 10.4 g/s (λ_{fresh}= 4.6), 8.8 g/s (λ_{fresh}= 3.9 & 0 % EGR), and 6.2 g/s (λ_{fresh}= 3 & 30% EGR).

Table 5.4: DME Port Injection Test Matrix (CR- 13.1:1)

MAF [g/s]	DME [g/s]	EGR [g/s]	A/F Ratio [-]	Fresh Air Lambda
10.4	0.251	0	41.4:1	4.6
8.8	0.254	0	34.6:1	3.9
8.1	0.256	0.7	31.6:1	3.5
6.2	0.234	2.6	26.5:1	3

The cylinder pressure and heat release rates for the 3 cases highlighted above are shown in Figure 5.37. The apparent location of the heat release peaks (LTR & HTR) was similar for both the unthrottled (10.4 g/s) and the throttled (8.8 g/s) operation without EGR. However, the fraction of the LTR heat release reduced as the fuel strength of the cylinder increased with the lower MAF as indicated in Figure 5.38. Therefore, the phasing of the combustion process, represented by the crank angle of 50% heat released (CA50) was improved slightly (357°CA versus 355°CA), although the location of the heat release peaks did not change.

With the application of EGR, both the LTR and the HTR heat release phases were postponed, with a larger delay of the main combustion (HTR) event as the effect of EGR was enhanced by the virtual EGR produced during the LTR regime. As a result, the CA50 was shifted to ~360°CA. The fraction of the LTR heat release remained ~20%, similar to that seen without EGR (8.8 g/s). However, the fraction of heat released till TDC was reduced significantly from about 70% (8.8g/s) to 52%. This implied a significant reduction in the compression work and therefore, the fuelling had to be slightly reduced during the test to maintain the same IMEP.

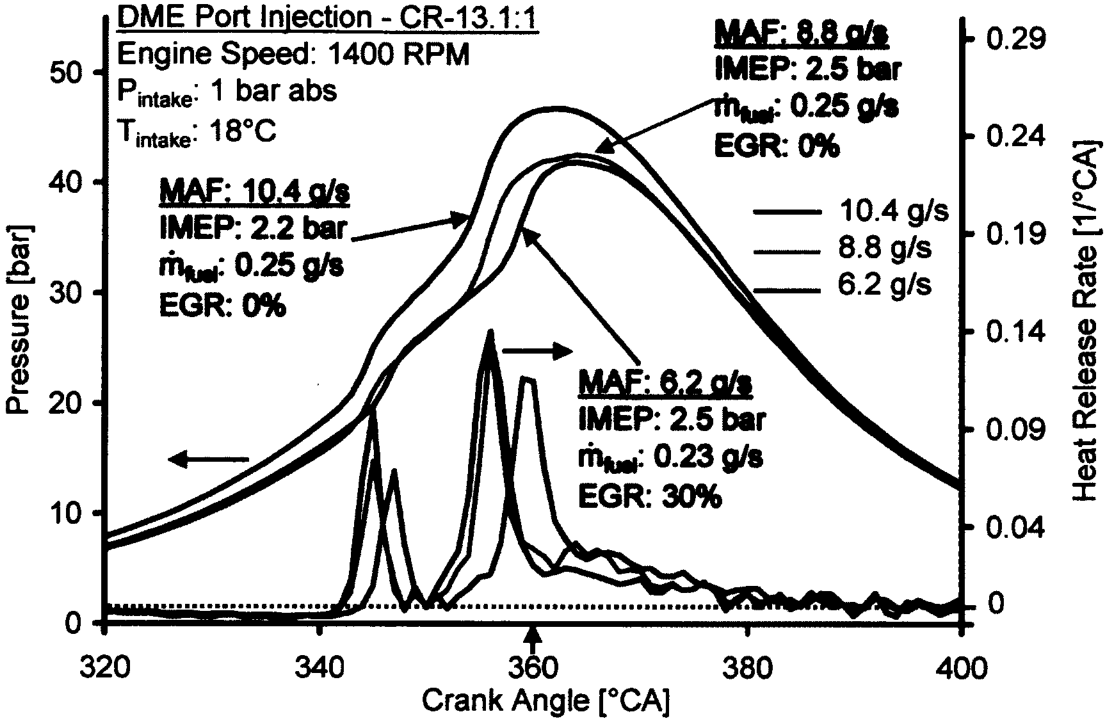

Figure 5.37: Comparison of Cylinder Pressure & Heat Release Rates (CR = 13.1:1)

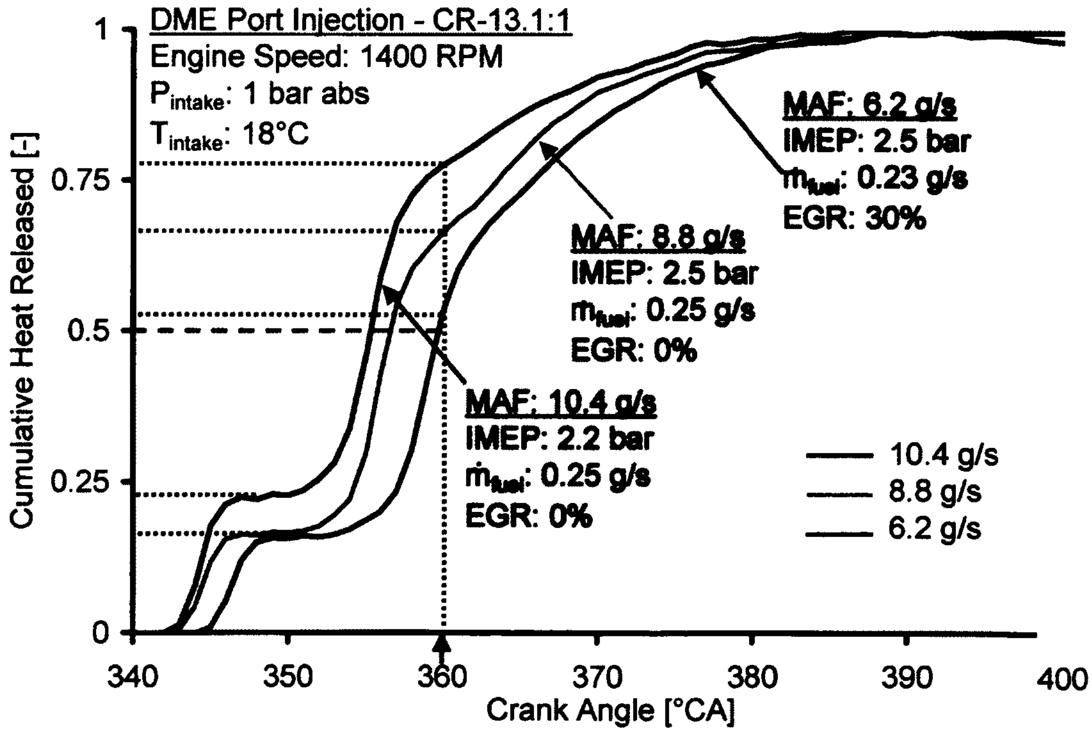

Figure 5.38: Cumulative Heat Release Traces (CR = 13.1:1)

The crank angle-resolved histories of the in-cylinder NO for the three tests are shown from Figure 5.39 to Figure 5.41. The sampling duration was kept constant and equal to 1.2 ms (10°CA) during these tests. The results have been plotted at the centre point of the sampling window to improve the correlation with the heat release rates.

For the test with unthrottled operation (10.4 g/s), the sampling was done after every 2°CA within the combustion regime to provide a better estimate of the in-cylinder NO history. As shown in Figure 5.39, the start of NO production coincided with the LTR heat release but the concentration decreased during the dwell time between the two heat release events. This can be attributed to the generation of lower chain hydrocarbons as a result of the dissociation of DME during the LTR phase. A small peak in the NO concentration was observed in the HTR phase but the NO concentration reduced steadily thereafter. The maximum in-cylinder NO concentration was ~10 ppm.

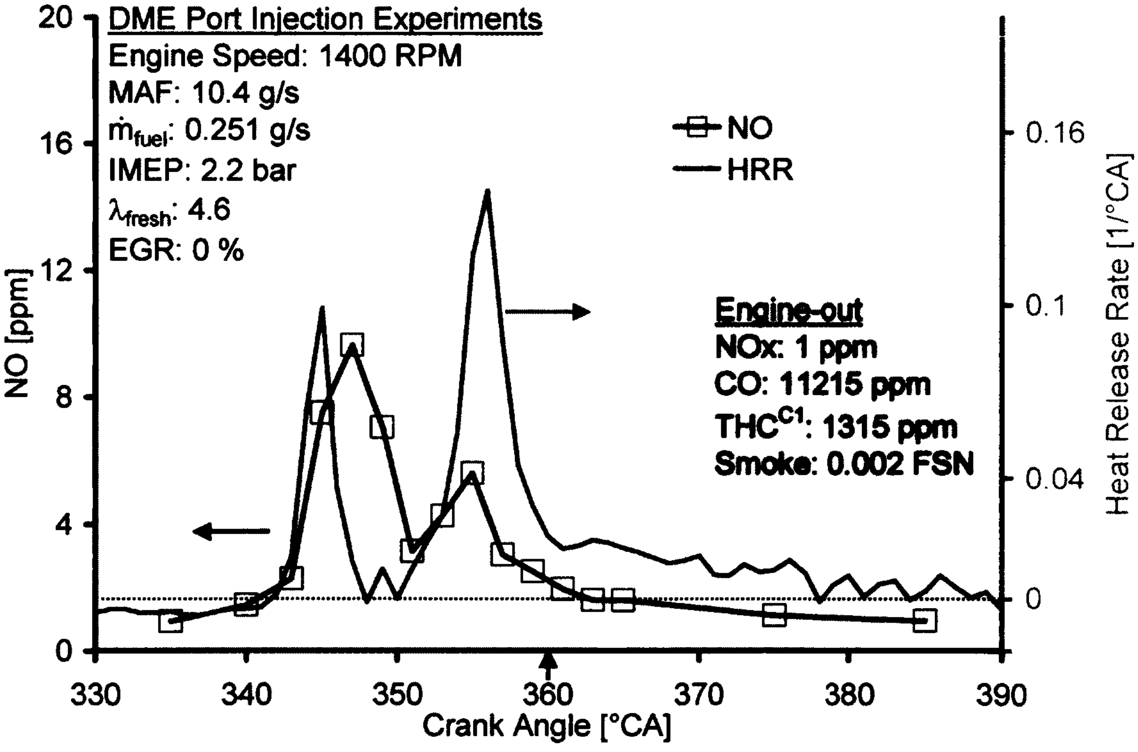

Figure 5.39: In-cylinder NO Evolution (λ_{fresh}= 4.6, CR = 13.1:1)

The results of the in-cylinder sampling with throttled operation (8.8 g/s & 0% EGR) are shown in Figure 5.40. The sampling was done after every 5°CA in this case and therefore, the NOx history is not as detailed. However, the trend was observed to be similar, with the NO generated during the LTR phase and the oxidation of the NO occurring during the main combustion event.

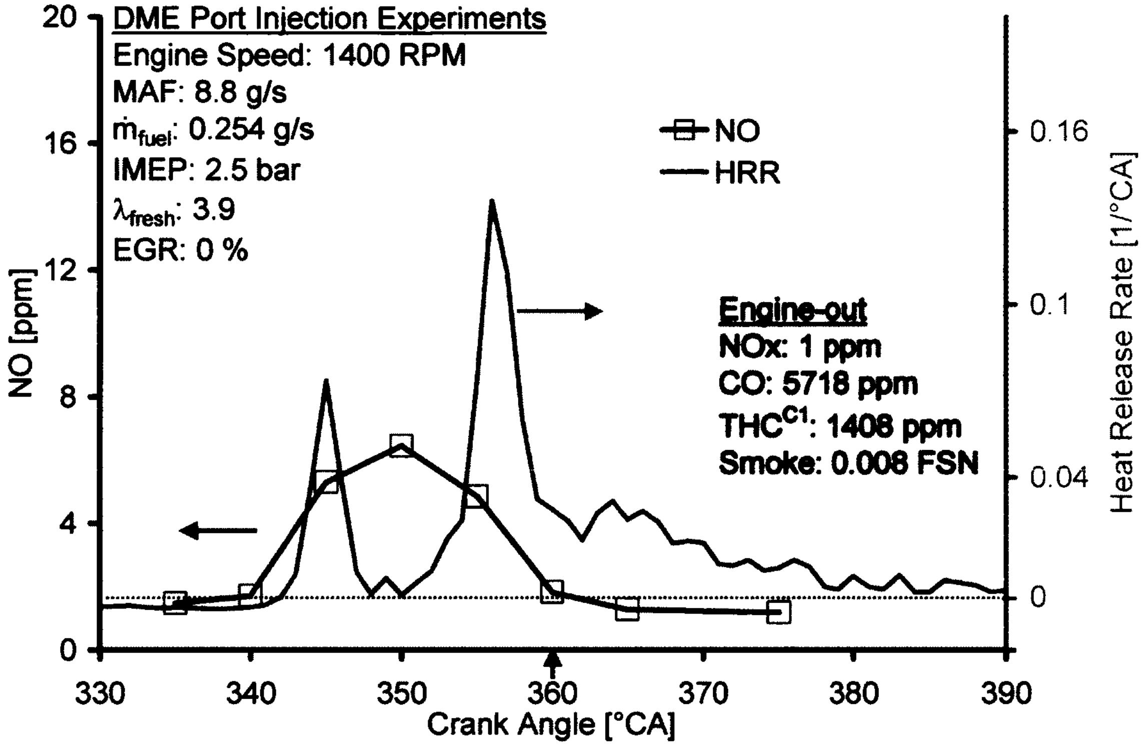

Figure 5.40: In-cylinder NO Evolution (λ_{fresh}= 3.9, CR = 13.1:1)

When 30% EGR was applied, the peak of the NO concentration was observed to shift towards the second heat release peak (HTR zone) as shown in Figure 5.41. The higher heat capacity and the reduced oxygen concentration of the cylinder charge with EGR may be responsible for reducing the rate of oxidation of the NO. However, the NO was rapidly oxidized during the main combustion event, similar to the trends observed previously.

The summary of the tests without EGR is given in Table 5.5. The indicated thermal efficiency was higher compared to the test results with CR 17.8:1. This is a consequence of the reduced compression work as shown earlier. Moreover, the efficiency was observed to improve with the application of EGR. There exists a trade-off between the off-phasing of the combustion, and the engine-out HC and CO emissions (quantitatively described in Chapter 7). It can be seen that the HC emissions did not change considerably with the application of EGR but a significant improvement in the combustion phasing was achieved (Figure 5.38). Therefore, the improvement in the efficiency can be attributed to the improved combustion phasing.

The engine-out NOx was only 1 ppm and there was virtually no smoke in the exhaust stream (FSN<0.008). The HC emission was comparable to the values seen during tests with CR 17.8:1 (Table 5.2 and Table 5.3) even though the loads were different. However, the CO emission was significantly less at 2.5 bar IMEP compared to the 2.1 bar IMEP (CR= 13.1:1) and 1 bar IMEP (CR= 17.8:1) results. The burning of a lean or EGR-diluted air/fuel mixture is believed to produce high amounts of CO, mainly due to the reduction in the oxidation of CO to CO_2 because of the low combustion temperatures.

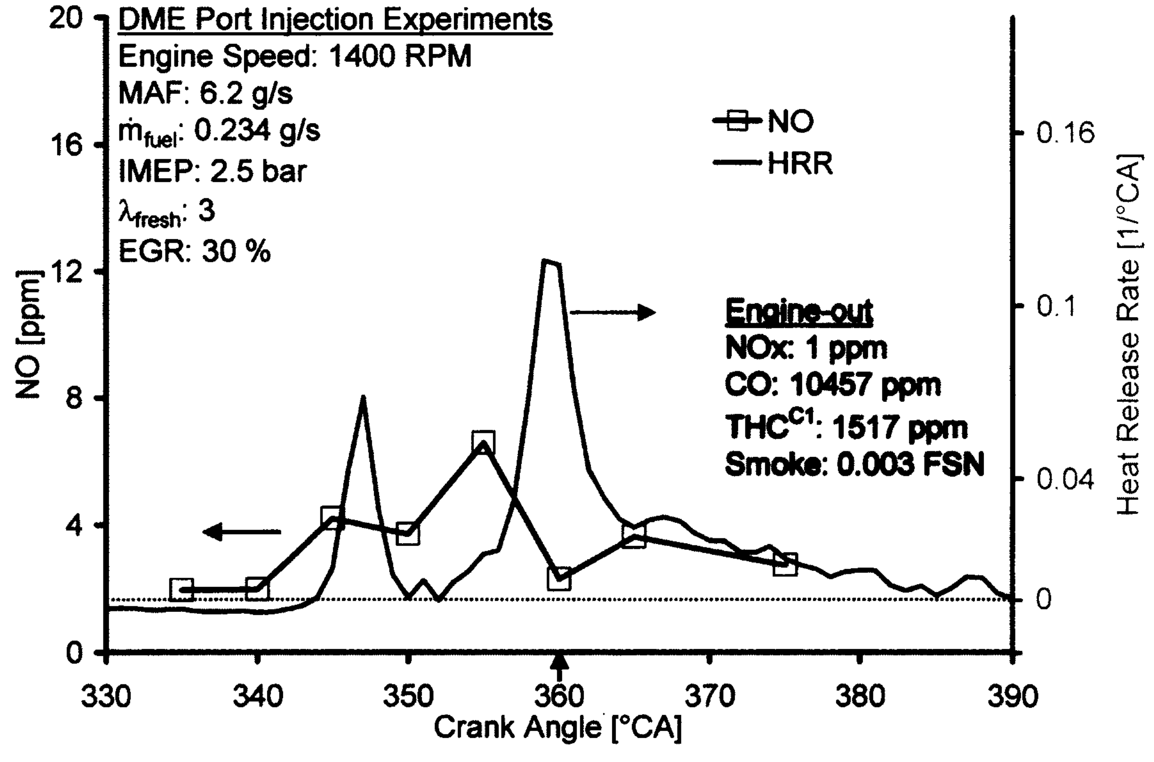

Figure 5.41: In-cylinder NO Evolution (λ_{fresh}= 3, CR = 13.1:1)

Table 5.5: Performance Summary of the DME Port Injection Tests (CR = 13.1:1)

MAF [g/s]	Fresh Air Lambda	EGR [%]	IMEP [bar]	Indicated η_{th} [%]	Engine-out Emissions		
					NOx [ppm]	CO [ppm]	THC^{C1} [ppm]
10.4	4.6	0	2.2	30.5	1	11215	1315
8.8	3.9	0	2.53	35.1	1	5718	1408
8.1	3.5	8	2.59	35.6	1	5380	1383
6.2	3	30	2.56	38.5	1	10457	1517

5.7.1. Exhaust HC Speciation

The results for the test with CR=13.1:1 are shown in Figure 5.42. The trends between the four groups were found to be similar to those obtained during the CR=17.8:1 tests. The concentration of the hydrocarbon group with no oxygen was very small while the carbonyl group displayed the highest concentration. For the tests without EGR, as the engine was throttled to decrease the air/fuel ratio, the concentrations increased slightly for all the groups except the HC group, for which it slightly decreased. The application of 8% EGR did not have any noticeable effect on the emission levels. With 30% EGR, the emissions increased for all the groups except the carbonyl group. The O-containing group showed the highest increase while a slight decrease was observed in the carbonyl group.

A comparison of the relative fraction of each group in the exhaust HC for the test conditions is shown in Figure 5.43. It was observed that with 30% EGR, the relative fraction of the O-containing group increased by about 5% while that of the carbonyl group decreased by the same amount in the exhaust HC. The aromatics and the HC group did not show any appreciable change. This trend was the same as observed during the low load tests with CR=17.8:1.

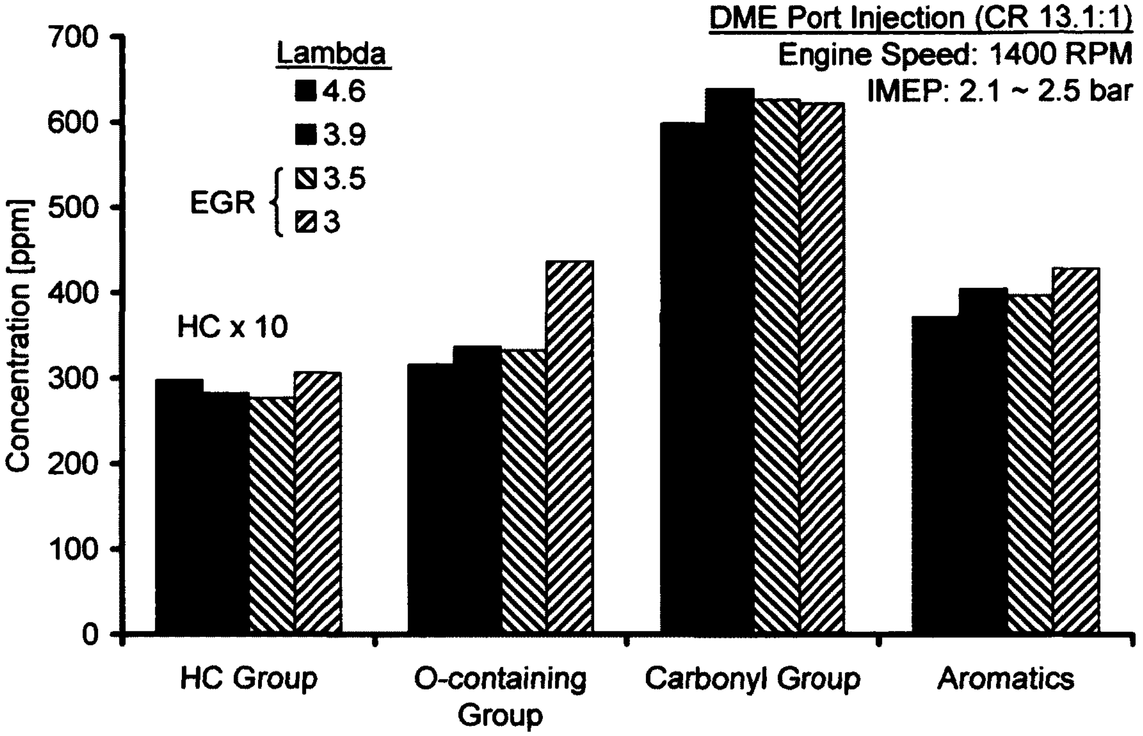

Figure 5.42: Exhaust HC Speciation for DME Combustion (CR = 13.1:1)

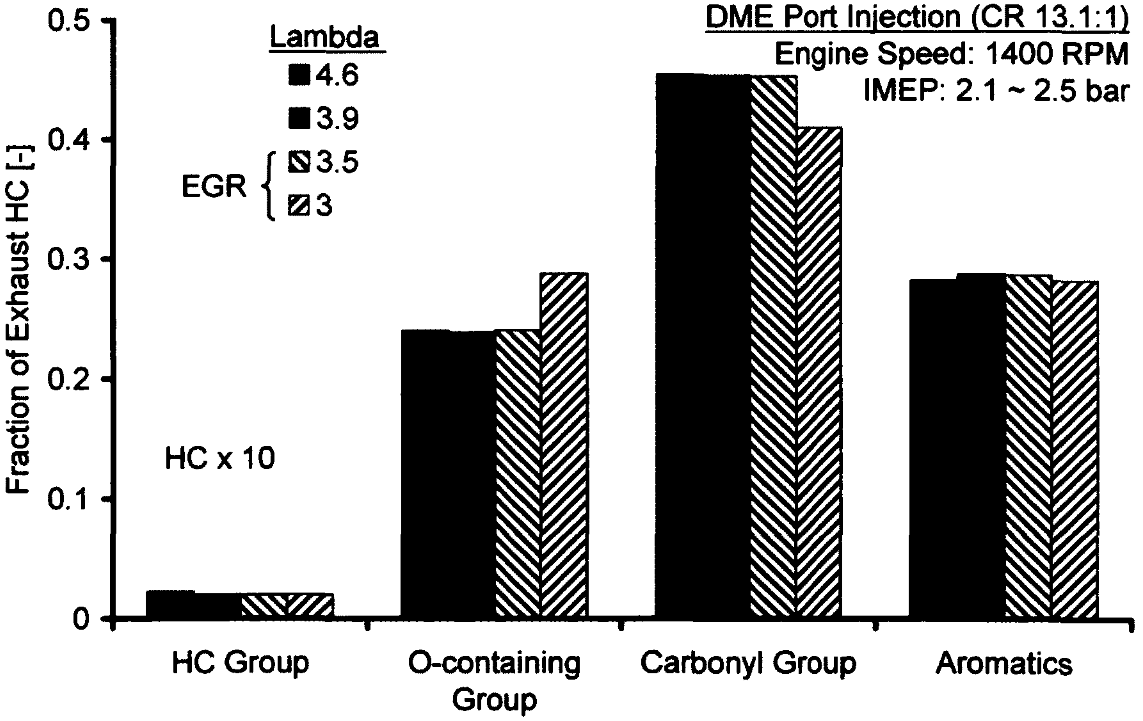

Figure 5.43: Relative Fraction of each Group in Exhaust HC (CR = 13.1:1)

5.8. Producing Reliable Feedback for LTC Control

The process of heat release can largely reflect the performance and emission characteristics of a diesel engine, when certain additional information is available such as the exhaust oxygen concentration, engine load level or ignition delay [92]. The mid heat release of conventional diesel engines has traditionally been phased close to the end of the compression stroke i.e. the top dead centre (TDC) and commonly with a profile of single hump or double humps for light and heavy load operations respectively. A number of phenomenological models for the steady-state heat release analysis can be found in the literature [93–98]. Such models are normally capable of calculating the heat release characteristics of the conventional diesel combustion with sufficient accuracy [4,98–100]. However, the modern diesel engines utilize a multitude of advanced combustion strategies to enable compliance with the diesel emission norms as presented in Chapter 2. The current trend has been to split the heat release into multi-events or even to shift the heat release away from the TDC in order to lower the combustion temperature when low emissions of oxides of nitrogen (NOx) or low combustion noise are targeted [101–104].

The phasing could be early (before TDC) or late (after TDC), for example, to accommodate high boost pressure and heavy exhaust gas recirculation (EGR) under high engine loads. Figure 5.44 shows the experimental heat release rates for a number of fuelling strategies and alternate combustion modes, obtained from tests run on the Ford Puma engine during light-duty diesel research. It can be seen that the phasing and the duration of the heat release can vary extensively depending upon the mode of operation. For example, the noise control may be achieved with split injection events while a delayed phasing is necessary with high boost pressure to reduce the maximum cylinder pressure. Post flame control may also be employed for torque modulation or the destruction of soot in certain cases [105]. Since the previous heat release analysis techniques were developed for the conventional cases where the phasing is close to the best fuel efficiency timing, the impact of the combustion off-phasing and splitting on the heat release analysis was required to be evaluated.

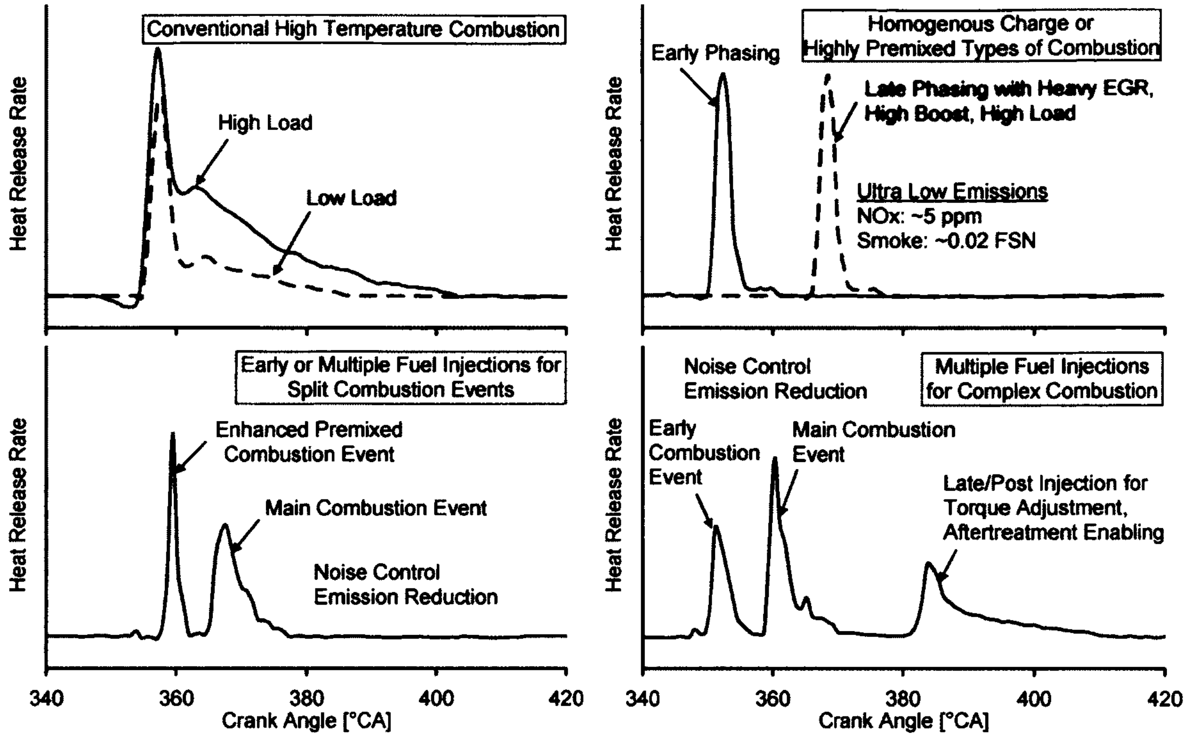

Figure 5.44: Heat Release Rates for Modern Diesel Engines

The combustion examples presented in Figure 5.44 include a significant premixed combustion part. This is typical of light-duty operation with high injection pressures so that the injection event is separated from the combustion and the longer ignition delay results in a large premixed part. With alternate fuels like biodiesel, the higher cetane number reduces the ignition delay and the premixed phase is low compared to the diffusive part. The same is true for heavy-duty, high load operation where the combustion can be purely diffusive.

As discussed in Chapter 2, the lowered combustion temperature prevalent during alternate combustion modes like HCCI and low temperature combustion (LTC) may reduce the combustion efficiency that is manifested by the increase in the emissions of carbon monoxide (CO) and unburnt hydrocarbons (HC) under extreme conditions. Lubricating oil dilution can also be another significant attribute of the combustion inefficiency. The empirical results for such an operating regime are given in Figure 5.45, which shows the consecutive 200 pressure traces and the 200 cycle-averaged heat release rate for neat bio-diesel experiments [106]. The off-phasing of the heat release from the

TDC and the use of multi-event combustion imply that the heat release may be significantly affected by the extended change in the cylinder volume (increased surface area for heat transfer), and the high CO and HC emissions. With the simplified heat release algorithms (constant specific heat ratio and neglecting the cylinder charge-to-wall heat transfer), the general shape of the heat release curve may still be attained but the magnitudes of the heat release rates are generally incorrect [4,97]. While normalizing the cumulative heat release (Cum. HR) with the total apparent energy release simplifies the analysis by not considering the effects of the combustion inefficiency, nevertheless, the uncertainty in the calculated combustion phasing and hence the estimation of the crank angle of 50% heat released which is of paramount importance for control purposes may be increased.

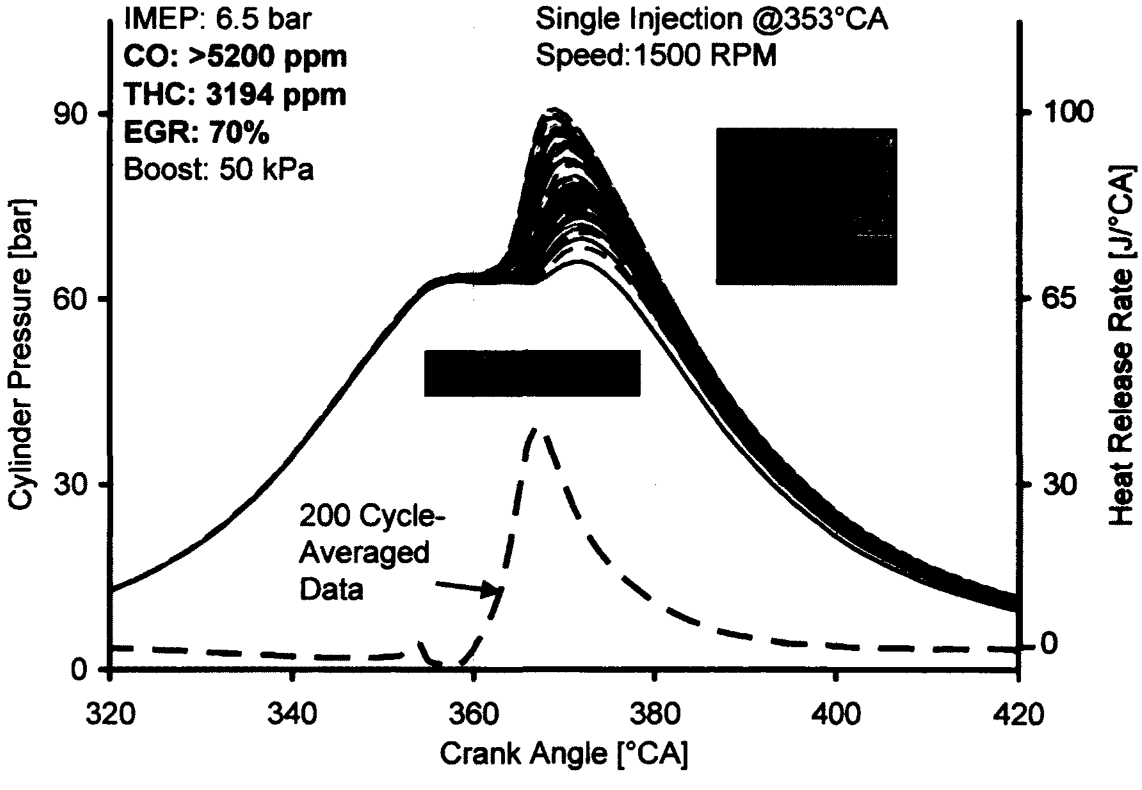

Figure 5.45: Unstable Combustion due to Lowered Flame Temperature with Heavy EGR

Moreover, the implementation of such combustion modes is challenging due to the higher cycle-to-cycle variation of heavy EGR operation and the narrower operating corridors.

While the transition from the high temperature combustion (HTC) to the LTC regime is relatively easier to control, maintaining stable engine operation in the LTC mode is generally not possible. Therefore, it is preferable to apply adaptive control to lock the phasing of the combustion process in a desired crank angle window to alleviate the problems associated with cyclic dispersion and to stabilize the combustion process. Adaptive diesel combustion control strategies have the potential to navigate through the narrow operating corridors for achieving low emissions of NOx and soot while maintaining stable engine operation as will be demonstrated in Chapter 8 [103,107,108]. To enable adaptive control, the fast heat release calculation should be able to capture the transient nature of the combustion and provide the necessary feedback for control. However, the cycle-by-cycle calculation in real-time of the heat release characteristics in the above perspective is quite a challenging task. While the existing heat release models typically work well for general laboratory data analysis, their use in combustion control applications requiring on-the-fly calculation of the heat release is difficult because of the numerical complexity and computational time-constraints.

The control problem is compounded by the complexities of the modern diesel combustion systems, as outlined below:

- Increased technological sophistication (common rail high pressure injection systems with multiple fuel injections per cycle, variable geometry turbines, advanced EGR handling techniques).
- A wide variety of combustion modes including LTC, HCCI, and enhanced premixed combustion.
- Combustion phasing adjustment to address a number of issues including limiting the peak cylinder pressure, reduction of combustion noise/emissions and aftertreatment control.

The cycle-by-cycle adaptive control of the diesel combustion process requires a robust and fast feedback that can effectively identify the heat release characteristics. The heat release phasing is often used as the main feedback signal since it can be directly correlated to the combustion efficiency, emissions or power production capability [109,110]. Therefore, experimental and analytical comparisons were performed to estimate the characteristics of heat release from the cylinder pressure histories. A number of heat release models such as apparent heat release model, Rassweiler-Withrow model, and Diesel Pressure Departure Ratio model were investigated under the various cycle conditions. The emphasis of this research was on the fast and accurate estimation of the heat release phasing over a wide range of engine operating conditions on a cycle-by-cycle basis, and therefore, the key issues addressed in this section are as follows:

- Analysis of a number of cylinder-pressure derived parameters for representing the heat release phasing
- Implementation of a new computationally-efficient algorithm for estimating the heat release characteristics and its performance comparison with other models
- Demonstration of the efficacy of the new algorithm against selected cases of boost, engine load and exhaust gas recirculation on the Ford engine.

5.9. Heat Release Phasing Feedback

The selection of the feedback parameters can strongly influence the dynamics of the closed-loop adaptive control system. The selection is constrained by the speed and capacity of an engine control unit and the numerical complexity of the control algorithms. Requirements for a practical feedback for the cycle-by-cycle control of combustion phasing are that the feedback should be accurate, stable and feasible for real-time control. Therefore, a comparison of the following parameters was made on the basis of numerical complexity, applicability to different fuelling strategies, shape of the heat release curve and the relative accuracy.

- Crank angle of maximum cylinder pressure, $CA\ P_{\max}$
- Crank angle of the maximum rate of pressure rise, $CA(dP/d\theta)_{\max}$
- Crank angle of 50% heat released, $CA50$

5.9.1. Crank Angle of Maximum Cylinder Pressure

This is the simplest of the parameters as it requires minimum computational resources. The use of $CA\ P_{\max}$ as a rough estimation of the heat release phasing is only valid when a global maximum pressure due to combustion occurs such as in case of HCCI/LTC combustion or with single-shot conventional high temperature combustion. With early or late combustion, or multiple injection events per cycle, $CA\ P_{\max}$ is a poor representation of the heat release phasing since it is closely coupled to the combustion volume. The accuracy of the $CA\ P_{\max}$ can be somewhat improved by subtracting the motored pressure from the fired pressure. The new pressure curve, thus obtained, represents the change in the cylinder pressure due to combustion and would provide a better estimate for late combustion phasing of conventional diesel combustion as shown in Figure 5.46.

5.9.2. Crank Angle of Maximum Rate of Pressure Rise

The $CA\left(dP/d\theta\right)_{\max}$ is generally able to identify retarded combustion events (since it is the derivative of the pressure) as shown in Figure 5.46 that are otherwise not detectable using the $CA\ P_{\max}$ as far as providing an estimate for the heat release phasing is concerned. However, there are a few aspects that need to be mentioned. First, it requires more than double the computational resources required for the calculation of $CA\ P_{\max}$. Second, for late combustion timing, the accuracy can be improved by subtracting the motoring $dP/d\theta$ trace from the fired $dP/d\theta$, to obtain the combustion $dP/d\theta$ only. However, if for example, oscillations exist in the pressure signal (unstable combustion) or the pressure transducer is not flush-mounted in the cylinder head, the fluctuations in the pressure signal are amplified during the calculation of the $\left(dP/d\theta\right)_{\max}$, resulting in large errors (up to 20°CA) in the estimation of the heat release phasing. Therefore, filtering or smoothing of the pressure signals becomes necessary.

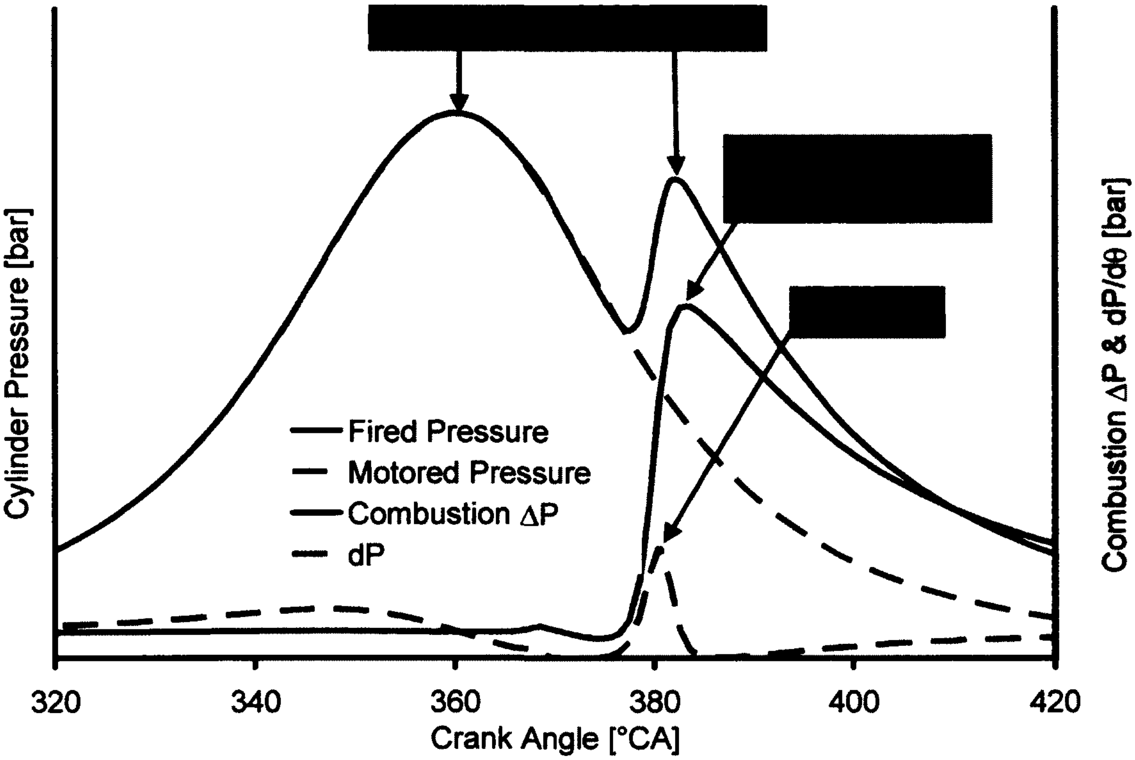

Figure 5.46: $CA\ P_{\max}$ & $CA(dP/d\theta)_{\max}$ as the Feedback Parameters

5.9.3. Crank Angle of 50% Heat Released

Although diesel engines are overall lean-burn systems, the combustion is predominantly and locally stoichiometric burn, because the flames tend to initialize and propagate to approximately stoichiometric regions. Therefore, the heat release slope is generally steep and the $CA50$ represents a stable and robust measure of the phasing of combustion, compared to $CA\ P_{\max}$ and $CA(dP/d\theta)_{\max}$, as shown in Figure 5.47. However, the calculation of the $CA50$ is computationally quite intensive and therefore, simplifications to the heat release analysis are generally made to reduce the numerical complexity while maintaining sufficient accuracy of the calculation. Therefore, three heat release models for estimating the $CA50$ with varying degrees of complexity and accuracy were considered in the following section.

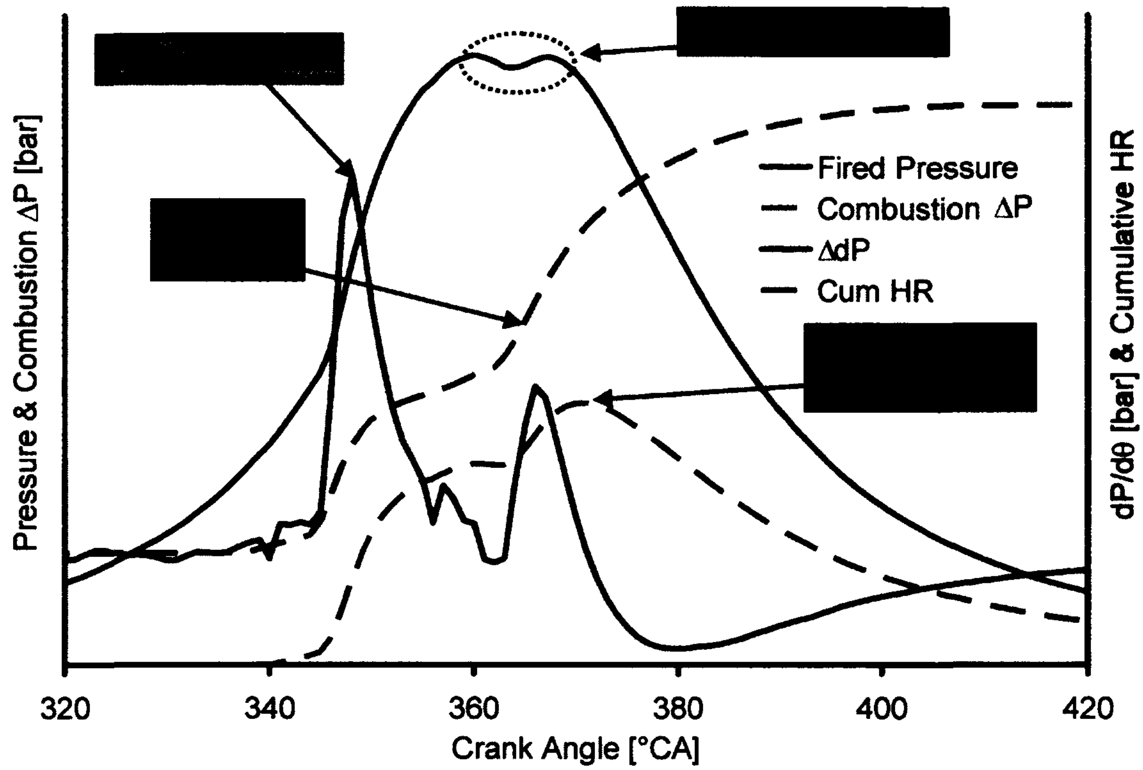

Figure 5.47: Comparison of the Feedback Parameters for a Split Heat Release Pattern

5.10. Heat Release Modelling

The basis for the modelling of the heat release is the first law of thermodynamics for an open system. Assuming the cylinder charge as a single zone and using the ideal gas law, the heat release during combustion, dQ_{gr} on a crank angle basis is given by:

$$\frac{dQ_{gr}}{d\theta}=\frac{1}{\gamma-1}\left[\gamma p\frac{dV}{d\theta}+V\frac{dp}{d\theta}+\left(u-c_vT\right)\frac{dm_c}{d\theta}\right]-\sum h_i\frac{dm_i}{d\theta}+\frac{dQ_{ht}}{d\theta} \tag{5.1}$$

where m_c is the mass of the cylinder charge, c_v is the specific heat at constant volume, u is the specific internal energy, T is the mean charge temperature, p is the cylinder pressure, V is the cylinder volume, γ (gamma) is the ratio of the specific heats, dQ_{ht} is the charge-to-wall heat transfer and $\sum h_i m_i$ represents the enthalpy flux across the system boundary.

Equation (5.1) gives the gross heat release rate during the period from intake valve closure (IVC) to exhaust valve opening (EVO) for the crank angle interval, $d\theta$. It also forms the basis for three different heat release models of reduced levels of complexity that have been analyzed in this work. APPENDIX B gives detailed information on the First Law equation derivation, the implicit assumptions made, the nomenclature used, and the empirical correlations to estimate the in-cylinder heat transfer and the temperature dependence of the specific heat ratio.

5.10.1. Apparent Heat Release Model

By neglecting the heat transfer, crevice volume, blow-by and the fuel injection effects in Equation (1), the resulting heat release rate is termed as the apparent or net heat release rate, dQ_{app} [4–8]. Substituting $dQ_{app} = dQ_{gr} - dQ_{ht}$ and $dm_c = dm_i = 0$, Equation (5.1) gives the apparent heat release rate (AHRR) as follows:

$$AHRR = \frac{dQ_{app}}{d\theta} = \frac{dQ_{gr}}{d\theta} - \frac{dQ_{ht}}{d\theta} = \frac{1}{\gamma - 1}\left[\gamma p \frac{dV}{d\theta} + V\frac{dp}{d\theta}\right] \tag{5.2}$$

The cumulative apparent heat release (Cum. AHR) is obtained by summing the incremental values from Equation (5.2) over the combustion period. Apparent heat release values are typically 15% lower than those obtained on a gross heat release basis [4,97]. Apparent heat release values are very often used in preference to gross heat release values because this reduces the amount of computation and avoids the need for heat transfer parameters to be specified.

Equation (5.2) can be used to calculate the apparent heat release rate and the normalized cumulative fraction of heat released either by using a temperature dependent specific heat ratio or a fixed value of the specific heat ratio (1.32~1.37). The apparent heat release rate calculated with a constant gamma value of 1.37 for the conventional diesel combustion phased close to the TDC with the start of combustion (SOC) @ -10°ATDC, is shown in Figure 5.48. The baseline (BL) heat release rate was calculated using Ricardo Wave software and Synthetic

Atmosphere Engine Simulation (SAES) software. The SAES uses a comprehensive validated model for heat release calculations and includes the effect of heat transfer, crevice volume, charge composition etc. on the heat release rate.

It can be seen that the AHRR curve was in good agreement with the baseline heat release rate curve. Although the apparent heat release analysis generally provides reasonable accuracy for heat release phased close to the TDC, however, under certain operating conditions, the use of a fixed value of the specific heat ratio and neglecting the cylinder charge-to-wall heat transfer can lead to errors in the calculated results as shown in Figure 5.49.

For the case with SOC @ -30°ATDC, a considerable difference in the magnitudes of the heat release rates and a large deviation in the end of combustion (EOC) were observed between the baseline curve and the AHRR curve computed with a constant gamma value of 1.37. Since the calculation of the $CA50$ with the apparent heat release approach requires an accurate estimation of the EOC crank angle, a large error was observed in the calculation of the $CA50$.

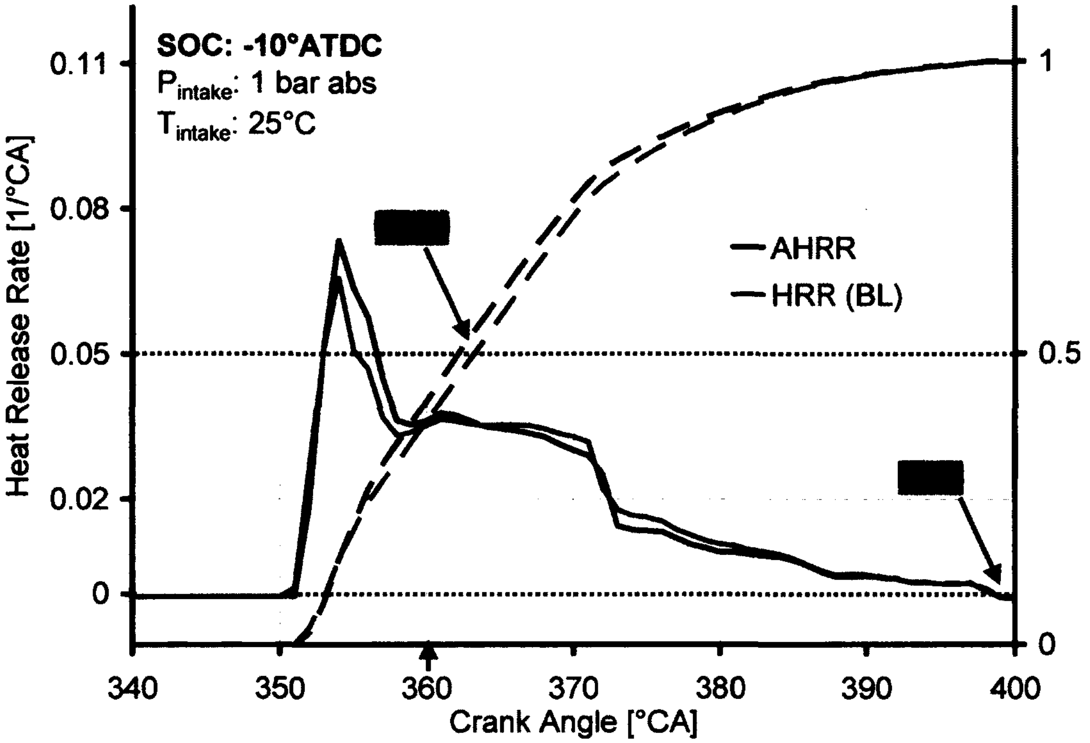

Figure 5.48: Apparent Heat Release Analysis with SOC @ -10°ATDC

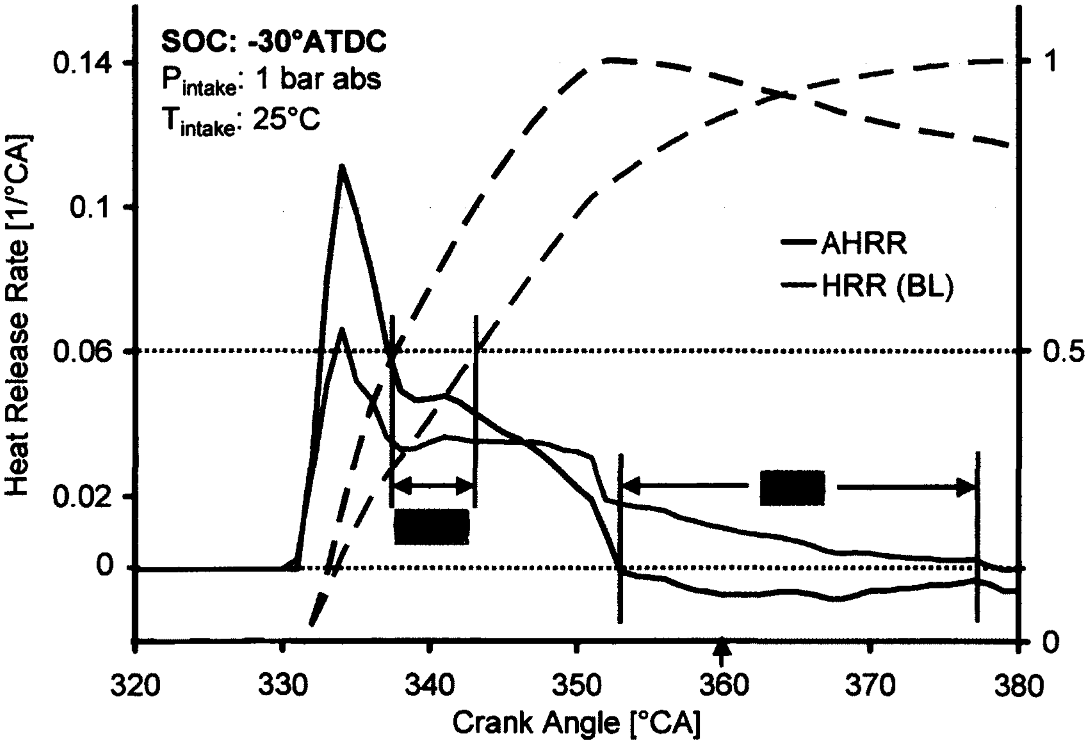

Figure 5.49: Apparent Heat Release Analysis with SOC @ -30° ATDC

The specific heat ratio varies primarily with the temperature inside the combustion chamber and may also be affected by the charge composition. The variation of the specific heat ratio with the mean cylinder temperature is shown in Figure 5.50. It is a common practice to use the value of the specific heat ratio based on the mean cylinder temperature for the calculation of the AHRR.

The AHRR for the case of SOC@-30°ATDC (Figure 5.49: Lower) was plotted again in Figure 5.51 by using the temperature dependent specific heat ratio and also including the charge-to-wall heat transfer. The inclusion of the temperature dependent specific heat ratio caused a change in the magnitudes of the burn rates and the error in the EOC was slightly reduced. Consequently, the prediction of the *CA*50 also showed a slight improvement. However, the inclusion of the charge-to-wall heat transfer estimation into the analysis caused the calculated HRR and the *CA*50 to nearly match with the baseline results.

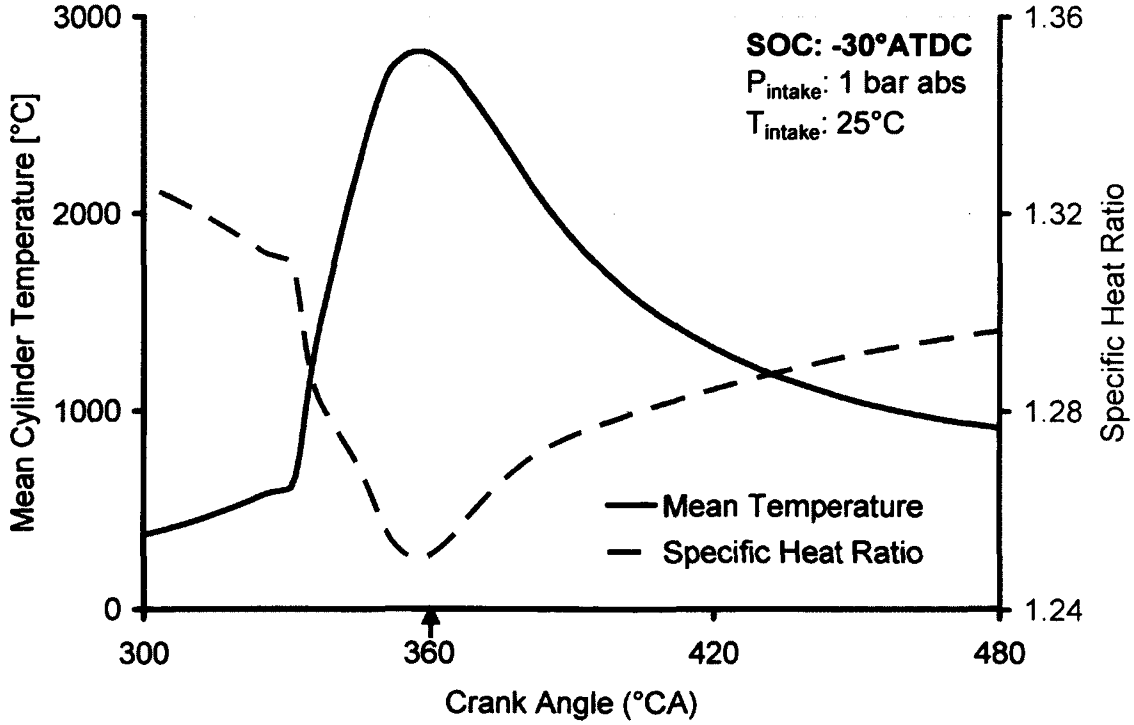

Figure 5.50: Variation of the Specific Heat Ratio with the Mean Cylinder Temperature

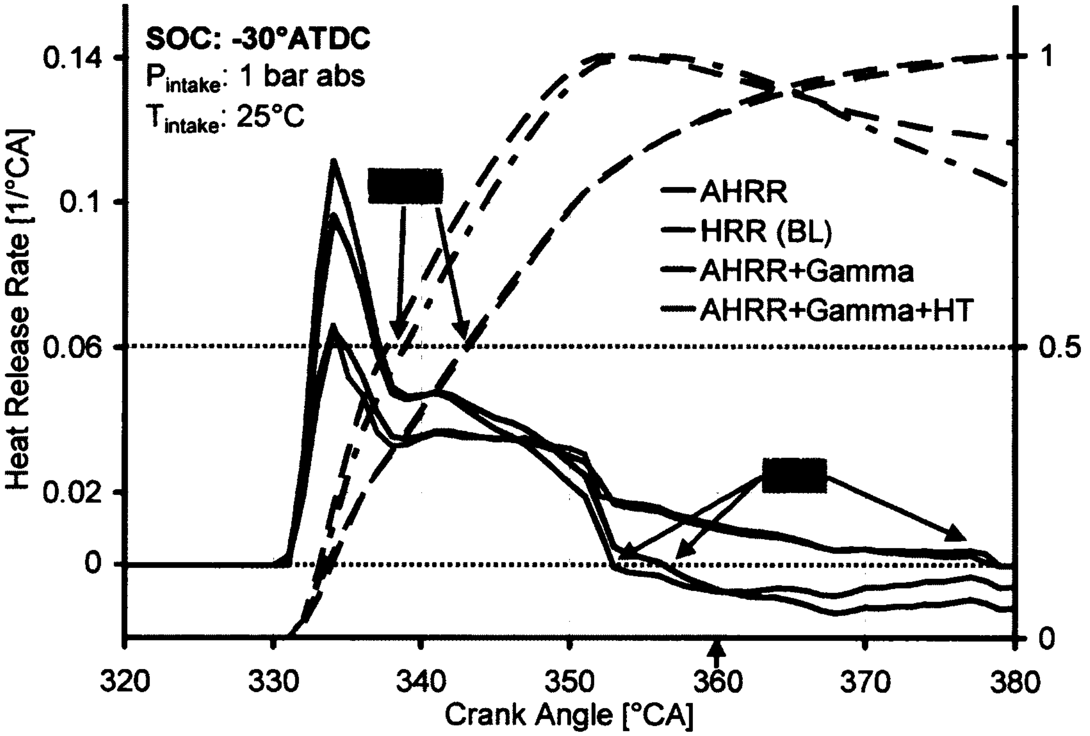

Figure 5.51: Inclusion of Specific Heat Ratio Variation and Heat Transfer in the Heat Release Analysis

5.10.2. Rassweiler-Withrow Model

The Rassweiler-Withrow model (referred to as RW Model) is commonly used to estimate the mass fraction burnt (MFB) and can be taken as a normalized version of the cumulative heat released [111–113]. It is based on the assumption that the change in pressure due to the piston motion and charge-to-wall heat transfer can be represented by polytropic processes. In this method, the pressure change during any crank angle interval is assumed to be made up of a pressure rise due to combustion Δp_{comb} and a pressure rise due to the volume change Δp_{vol}. Therefore, by assuming that the pressure rise due to combustion is proportional to the mass of the fuel that burns, the MFB at the end of the $i'th$ interval can be approximated by

$$MFB_{RW}(\theta)=\sum_{i=0}^{\theta}\Delta p_{comb}(i)\bigg/\sum_{i=0}^{K}\Delta p_{comb}(i) \tag{5.3}$$

where K is the total combustion duration.

The detailed information on the RW Model derivation is given in References [97,111,112].

5.10.3. Diesel Pressure Departure Ratio Model

The Diesel Pressure Departure Ratio algorithm (referred to as *PDR* algorithm hereafter) is a new approach proposed by the author for fast and reliable estimation of the mass fraction burnt for diesel combustion. It is based on the principle of RW Model which states that the fractional pressure rise due to combustion can provide an estimate of the MFB. The PDR algorithm utilizes the fired and the motoring traces for cycle-by-cycle estimation of the *CA*50 and the calculated MFB closely matches the normalized cumulative heat release trace.

It is pertinent to mention here that a somewhat similar approach was applied for spark-ignition engines by Sellnau [114] and Matekunas [115], and is called the Pressure-Ratio Management (PRM). PRM involves the calculation of the ratio between the fired pressure and the corresponding motored cylinder pressure at every crank angle. The ratio is then normalized by its maximum value (also called the final pressure ratio) which typically occurs around 55°CA ATDC for spark-ignition engines. The resulting trace is a close approximation of the MFB trace at every crank angle and published results indicate that the technique works well for spark ignition engines.

The direct application of the PRM to diesel engine pressure data results in a MFB curve that may differ from the actual cumulative heat release trace because of a number of reasons. First, the much higher compression ratios of the diesel cause the maximum pressure ratio to occur towards exhaust valve opening. Second, unlike the spark ignition engines where the combustion typically occurs as a single event, the diesel combustion process can consist of discrete heat release events with a multitude of fuel injection scheduling strategies (split injections, post injection etc.). Therefore, the PRM estimation departs from the actual diesel combustion characteristics even for the conventional high temperature diesel combustion with a single fuel injection as shown in Figure 5.52.

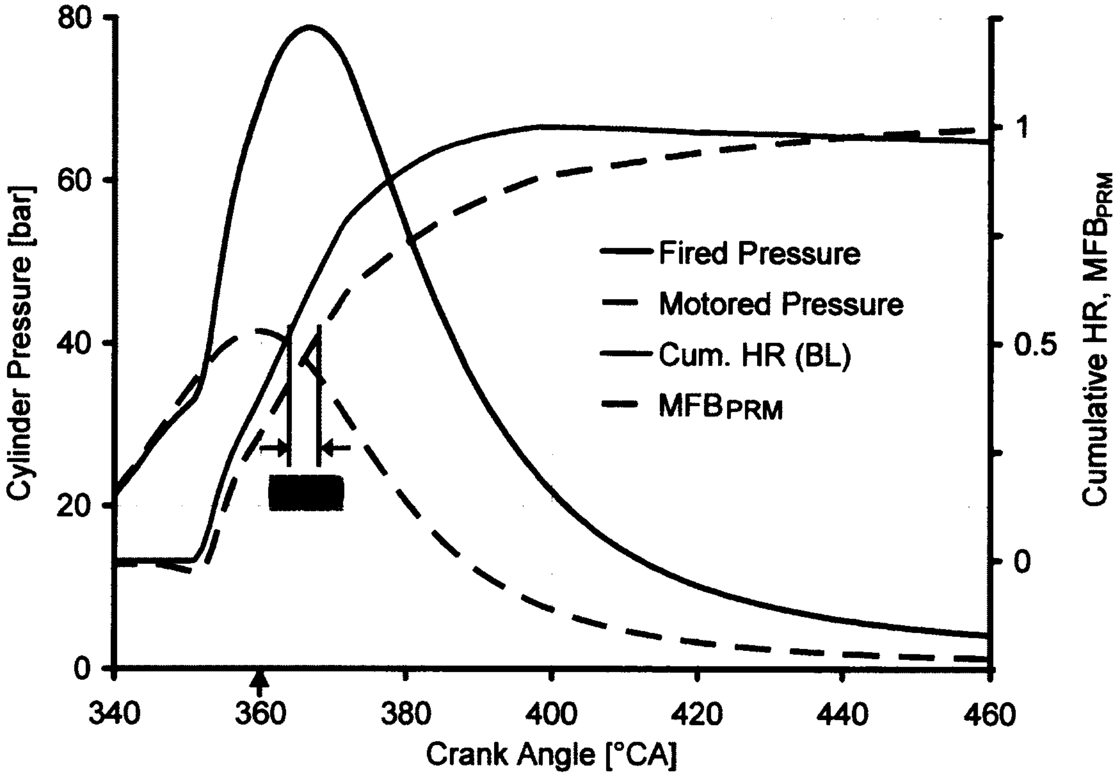

Figure 5.52: Demonstration of MFB_{PRM} for typical Diesel Combustion

To identify the diesel combustion characteristics, a Diesel Pressure Departure Ratio (PDR) is proposed that is expressed at any crank angle, θ as:

$$PDR(\theta) = f\{p(\theta), p_{mot}(\theta), V(\theta), n, C_1, C_2\} \tag{5.4}$$

where $p(\theta)$ is the fired cylinder pressure data, $p_{mot}(\theta)$ is the motored cylinder pressure data, $V(\theta)$ is the cylinder volume, n is the polytropic index and C_1, C_2 are constants.

The basis of the PDR algorithm is the fact that the cylinder pressure and the volume data during the compression and the expansion processes can be described by the polytropic relation $pV^n = Constant$. The exponent n is comparable to the average value of γ during the compression phase, prior to combustion, but the increased heat transfer to the cylinder walls during combustion and the expansion process makes the exponent n greater than the corresponding γ [4].

To determine the polytropic relationship from Equation (5.1), the following assumptions are made:

- The effects of crevice volume and piston ring blowby are neglected, i.e., $dm_c = dm_i = 0$
- Cylinder charge-to-wall transfer is not explicitly accounted for, i.e., $dQ_{ht} = 0$ and therefore, $dQ = dQ_{gr} - dQ_{ht}$
- The constant polytropic index, n, accounts for the specific heat ratio of the charge
- There is no release of chemical energy before and after combustion, and therefore $dQ = 0$.

For the period before and after combustion, this reduces Equation (5.1) to yield

$$dp = \left(-{np}/{V}\right) dV \qquad (5.5)$$

and for the combustion duration

$$dp = \frac{n-1}{V} dQ - \frac{np}{V} dV = dp_{comb} + dp_{vol} \qquad (5.6)$$

where dp_{comb} is the pressure change due to combustion and dp_{vol} is the pressure change due to volume change. In the *PDR* method, the actual pressure change, $\Delta p = p_i - p_{i-1}$, during any crank angle interval $\Delta\theta = \Delta\theta_i - \Delta\theta_{i-1}$ is assumed to be made up of a pressure rise due to combustion Δp_{comb} and a pressure rise due to the volume change Δp_{vol}. Therefore,

$$\Delta p = \Delta p_{comb} + \Delta p_{vol} \tag{5.7}$$

where Δp_{vol} and Δp_{comb} can be approximated using the polytropic relationship as

$$\Delta p_{vol}(i) = -p_{i-1}\left(V_{i-1}/V_i\right)^n \;\&\; \Delta p_{comb}(i) = p_i - p_{i-1}\left(V_{i-1}/V_i\right)^n \tag{5.8}$$

The incremental heat release rate can then be estimated from Equation (5.6) as follows:

$$\Delta Q(i) = \frac{V_{avg}(i)}{n-1}\Delta p_c(i) \tag{5.9}$$

where $V_{avg}(i) = \frac{\left(V_i + V_{i-1}\right)}{2}$ is the average volume over the interval $\Delta\theta$.

The total heat released up to any crank angle can then be calculated as follows:

$$\sum_{i=SOC}^{\theta} \Delta Q(i) = Q(i) = \frac{1}{n-1}\sum_{i=SOC}^{\theta} V_{avg}(i)\cdot\Delta p_{comb}(i) \tag{5.10}$$

The heat release traces calculated using Equations (5.9) and (5.10) are compared with the baseline heat release for the pressure data of Figure 5.52 and the comparison is shown in Figure 5.53. It is evident that the estimation of the heat release rate shows good agreement with the baseline results.

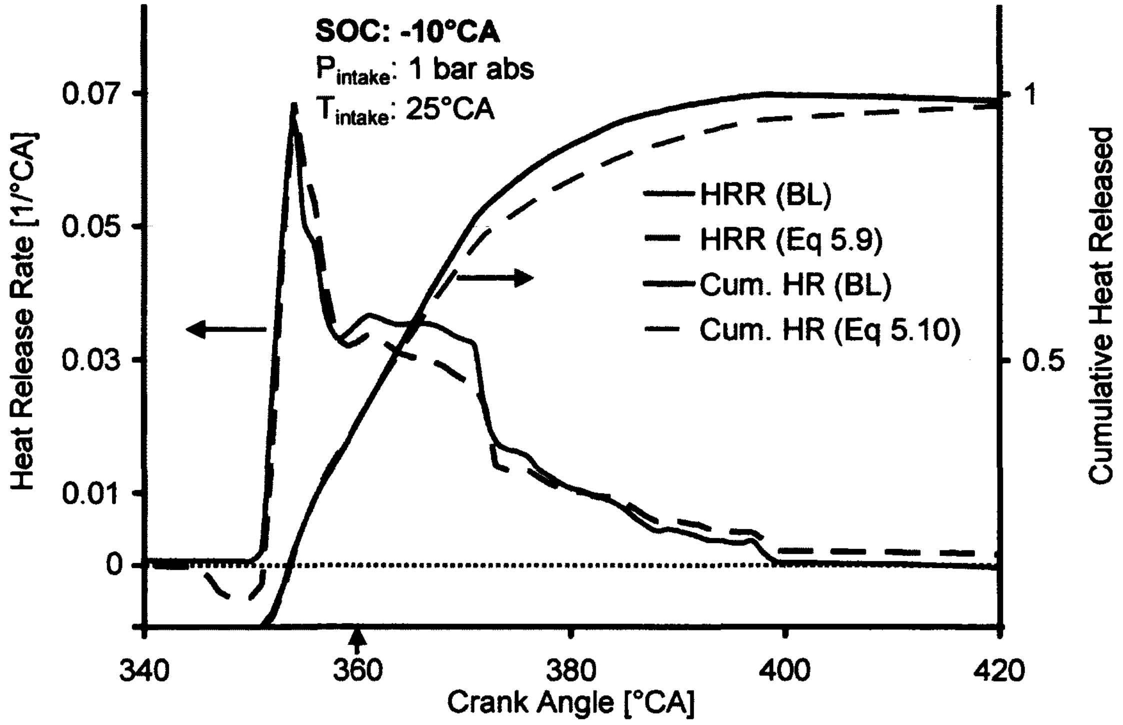

Figure 5.53: Comparison of HR Results from Equations (5.9) & (5.10) with Baseline Results (Figure 5.52)

A comparison of Equations (5.2) and (5.9) indicates that both equations involve the calculation of the derivative of pressure. During fast signal processing applications such as those required for fast estimation of the diesel combustion characterization, the process of differentiating a measured signal may result in the amplification of the electrical noise which make the estimation susceptible to errors.

Moreover, the implementation of Equations (5.2) and (5.9) involve the same number of steps, that is, the calculation of the heat release rate, followed by the cumulative heat released and its normalization by the maximum value of cumulative heat released, Q_{max} before the combustion parameters like *CA*50 can be obtained from Equations (5.2) & (5.9).

For fast feedback of the combustion process, it is necessary to reduce the number of calculation steps and the numerical complexity involved. Also, the desired objective of the analysis is the estimation of the mass fraction burnt within the interval $\{0,1\}$ and not the actual heat release rate. Therefore, a numerically reduced form of Equation (5.9) that is computationally efficient was devised as follows:

The value of the cylinder volume is very small compared to the pressure change due to combustion over the crank angle interval $\Delta\theta$. Therefore, if a constant value of the cylinder volume is used in Equation (5.9), the equation can be rewritten as

$$\Delta Q(i) \approx \frac{V}{n-1} \Delta p_c(i) \tag{5.11}$$

and similarly, Equation (5.10) becomes

$$Q(i) \approx \frac{V}{n-1} \sum_{i=SOC}^{\theta} \Delta p_c(i) \tag{5.12}$$

Using the volume at TDC, the approximate heat release rate is shown in Figure 5.54. It can be seen that the general shape of the trace remains similar to the actual heat release rate traces.

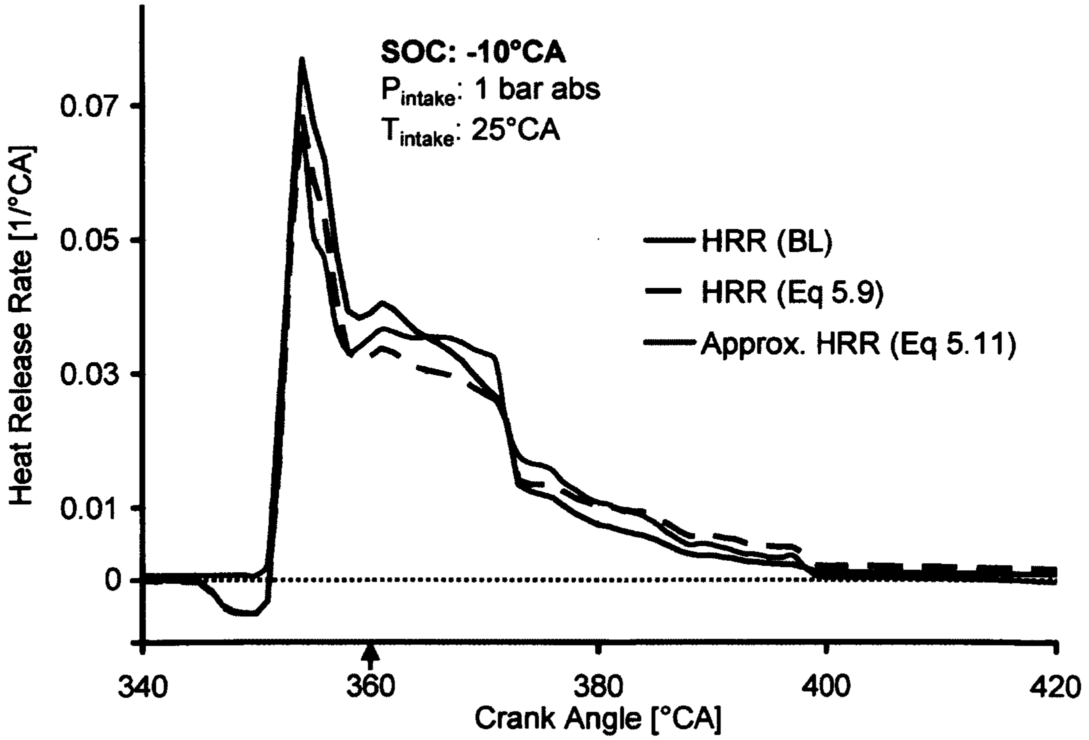

Figure 5.54: Approximate Heat Release using Equation (5.11)

To further reduce the numerical complexity of Equation (5.12), at the end of the $i'th$ interval immediately after the start of combustion, the pressure can be represented as $p(i)=\Delta p_{comb}(i)+p_{mot}(i)$

Similarly,

$$\begin{aligned}
&p(i+1)=\Delta p_{comb}(i+1)+\Delta p_{comb}(i)+p_{mot}(i+1)\\
&p(\theta)=\Delta p_{comb}(\theta)+\cdots+\Delta p_{comb}(i+1)+\Delta p_{comb}(i)+p_{mot}(\theta)\\
&p(\theta)=p_{mot}(\theta)-\sum_{i=SOC}^{\theta}\Delta p_{comb}(i)
\end{aligned}$$

Therefore, the pressure change due to combustion can be rewritten in terms of the fired and the motored pressure values as

$$\sum_{i=SOC}^{\theta}\Delta p_{comb}(i)=p(\theta)-p_{mot}(\theta) \tag{5.13}$$

Substituting Equation (5.13) into Equation (5.12), we get

$$\begin{aligned}
Q(\theta) &\propto \frac{V}{n-1}\left[p(\theta)-p_{mot}(\theta)\right]\\
&\propto \frac{1}{\left(\frac{n-1}{V}\right)}\left[p(\theta)-p_{mot}(\theta)\right]
\end{aligned} \tag{5.14}$$

The proportionality has been introduced in Equation (5.14) because of the underlying assumption that at the end of crank angle interval $\Delta\theta$, the pressure change due to the change in volume during the fired cycle $\Delta p_{vol,fired}(\theta)$ will be equal to the pressure change due to the change in volume, $\Delta p_{vol,mot}(\theta)$ if the engine was motored (no combustion), that is,

$$\begin{aligned}
&\text{Fired Cycle}: p(\theta)=\Delta p_{comb}(\theta)+\Delta p_{vol,fired}(\theta)+p_{mot}(\theta-1)\\
&\text{Motored Cycle}: p_{mot}(\theta)=\Delta p_{vol,mot}(\theta)+p_{mot}(\theta-1)\\
&\text{Assumption: }\Delta p_{vol,fired}(\theta)=\Delta p_{vol,mot}(\theta)
\end{aligned}$$

However, $\Delta p_{vol,fired}(\theta) \neq \Delta p_{vol,mot}(\theta)$ because of the different in-cylinder conditions (primarily in-cylinder temperature and charge composition) prevailing during the motoring and the fired cycles, which would significantly affect the ratio of the specific heats and the cylinder charge-to-wall heat transfer.

For a given engine configuration, the cylinder volume versus crank angle relationship is fixed and the term $\left(\frac{n-1}{V}\right)$ can be related to the motoring pressure, since the motoring pressure is a consequence of the changing cylinder volume ($pV^n = Constant$). Plotting $\left(\frac{n-1}{V}\right)$ and p_{mot} as a function of the crank angle in Figure 5.55, it can be seen that

$$\left(\frac{n-1}{V}\right) \propto p_{mot} \tag{5.15}$$

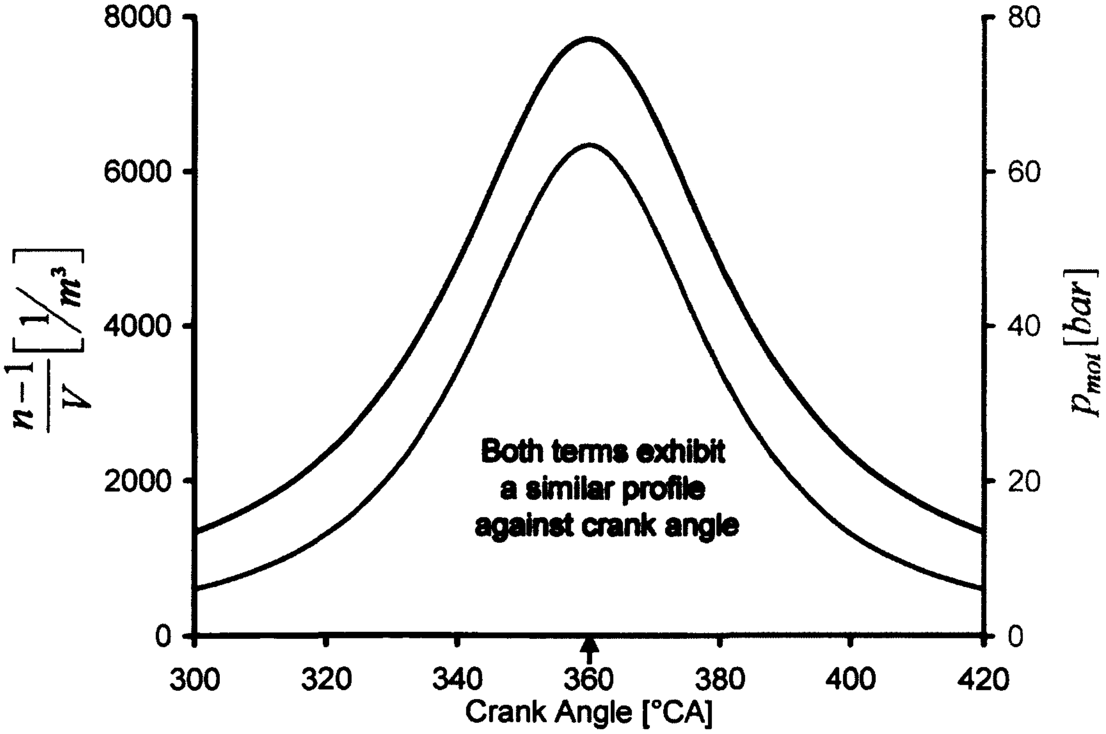

Figure 5.55: Profiles for Reciprocal of Cylinder Volume & Motoring Pressure

At this time, re-introducing the variation of volume and therefore, the motoring pressure with the crank angle, and substituting Equation (5.15) in Equation (5.14),

$$Q(\theta) \propto \frac{p(\theta) - p_{mot}(\theta)}{p_{mot}(\theta)} \tag{5.16}$$

Equation (5.16) is the representation of the cumulative heat released up to any crank angle based on the departure of the fired pressure from the motoring pressure, and therefore, can be rewritten as

$$PDR(\theta) \propto \frac{p(\theta) - p_{mot}(\theta)}{p_{mot}(\theta)} \tag{5.17}$$

To remove the proportionality constant, two constants have been introduced such that

$$PDR(\theta) = \frac{p(\theta) + FPC}{p_{mot}(\theta) + MPC} - 1 \tag{5.18}$$

where *FPC* is the 'fired pressure characterization' coefficient, and *MPC* is the 'motored pressure characterization' coefficient. The *MPC* is a correction for the polytropic relationship between the volume and the motoring pressure while the *FPC* is a correction for the difference between the Δp_{vol} of the fired and the motored cycles as explained earlier. The coefficients, *FPC* and *MPC* are constants for a given engine configuration and are largely not affected by the boost pressure, EGR etc. as is shown later. The *PDR* has a nearly zero value before combustion and rises to maximum value which corresponds to the end of combustion (EOC).

An estimate of the mass fraction burnt is then obtained by normalizing the *PDR* from Equation (5.18) with its maximum value $PDR_{\max}$ as follows:

$$MFB_{PDR}(\theta) = \frac{PDR(\theta)}{PDR_{\max}} \tag{5.19}$$

To illustrate the *PDR* algorithm, the calculated *PDR* and the MFB_{PDR} are shown in Figure 5.56 for the data shown in Figure 5.52. It can be seen that the *PDR* reaches a maximum value close to the crank angle where the combustion ends. Also the MFB_{PDR} is in good agreement with the baseline normalized cumulative heat release trace which includes the effects of charge-to-wall heat transfer and the temperature dependence of the specific heat ratio.

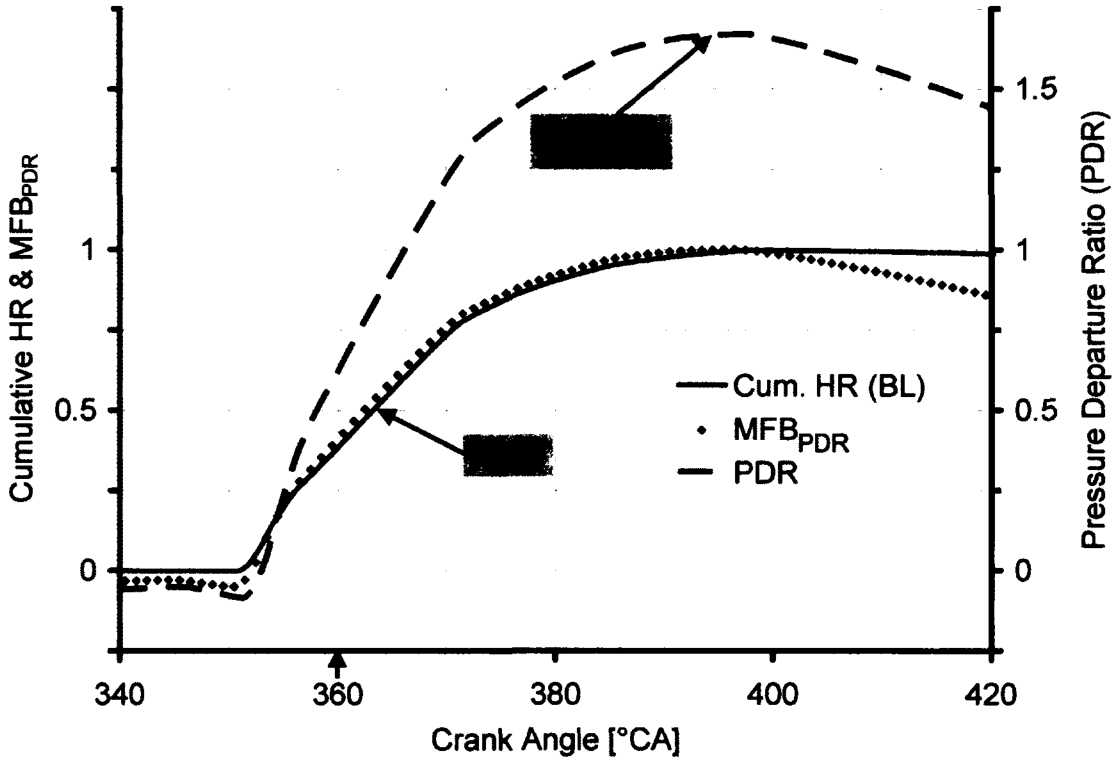

Figure 5.56: MFB_{PDR} for the data of Figure 5.52

The empirical model constants (FPC and MPC) are calibrated by first adjusting the MPC value so that the MFB_{PDR} approximately matches the baseline heat release trace as shown in Figure 5.57. Small changes in the MPC value cause the curve to pivot about a point. The FPC is then adjusted to shift the pivotal point so that the predicted $CA50$ is as close as possible to the actual $CA50$ as shown in Figure 5.58. This also ensures that small deviations on the extreme ends of the curve will have minimal effect on the prediction of the $CA50$. The calibrated values of the constants are then checked against few traces representing early/late phasing and different fuelling strategies. Once this trial and error process is completed, the constants have been calibrated for the engine under consideration and are not required to be adjusted. Using the procedure outlined above, the calibrated values of *MPC* and *FPC* were 4.8 and 4.0 respectively for the Ford engine used in the experimental investigation.

The calibration of the *PDR*

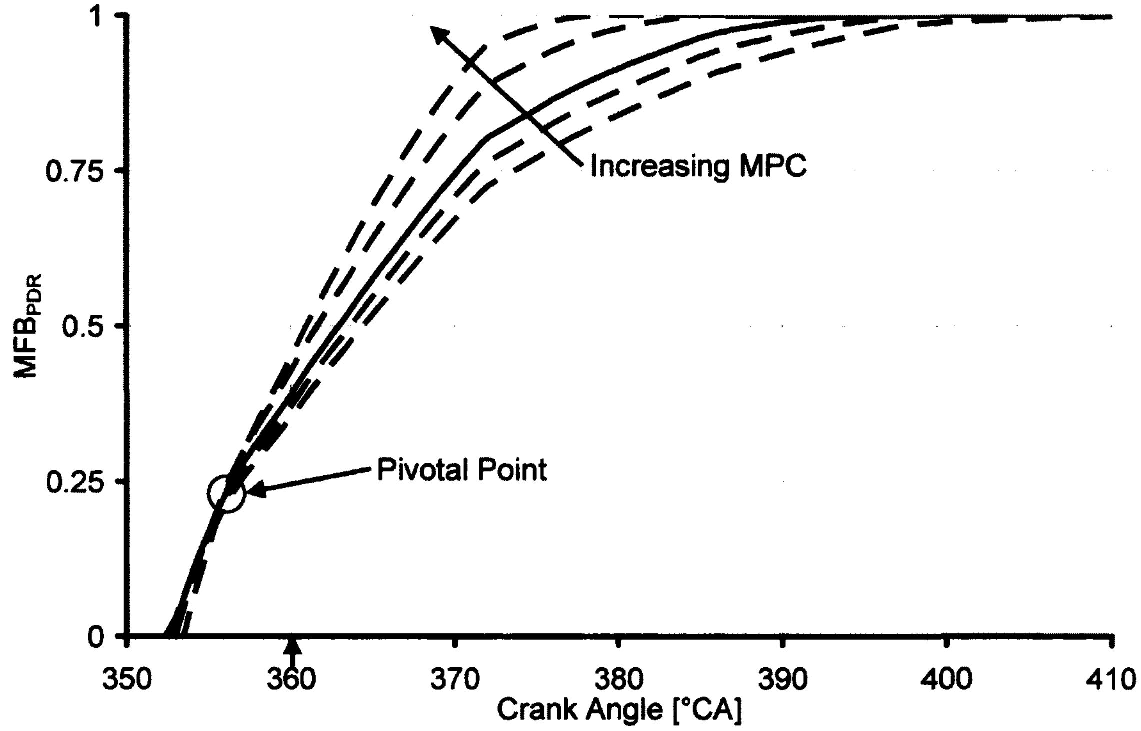

Figure 5.57: Effect of *MPC* on the MFB_{PDR}

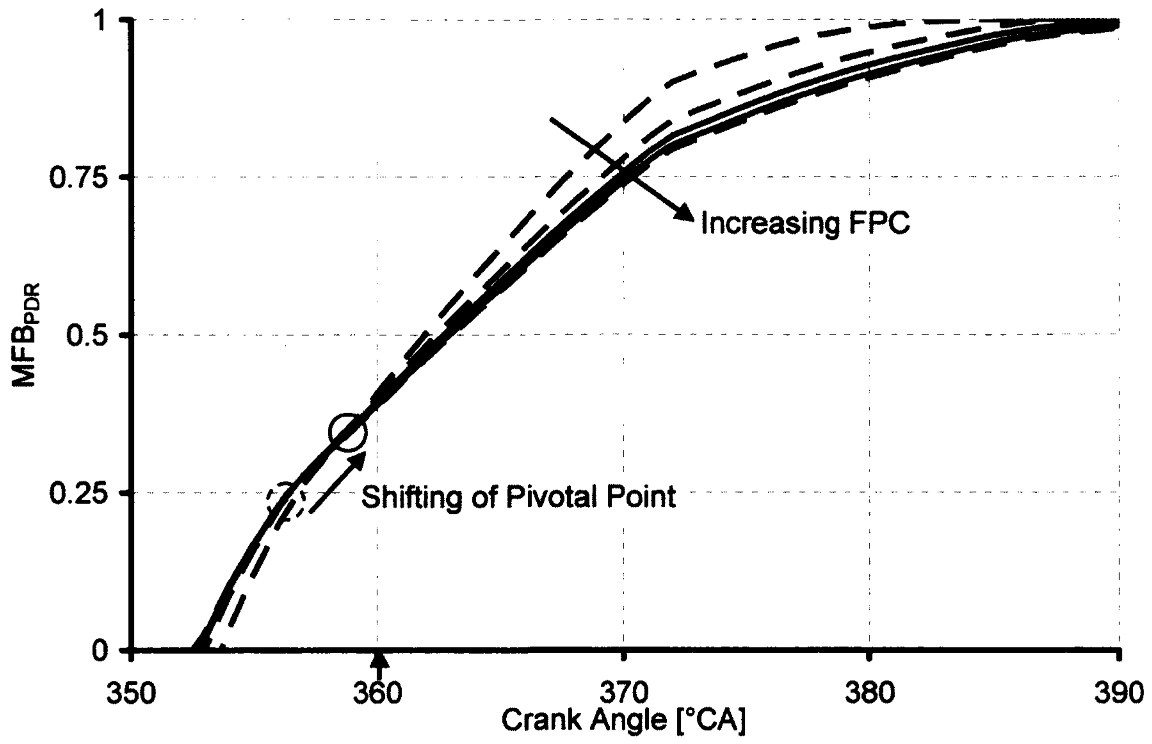

Figure 5.58: Effect of *FPC* on the MFB_{PDR}

5.11. Experimental Apparatus and Procedures

A number of researchers have previously carried out an analysis of the apparent heat release model for errors in the gross heat released (in joules) due to constant specific heat ratio, heat transfer and pressure data errors [97,98,116–119]. However, the pressure data used was typical of the conventional high temperature combustion regime for both low-load and high-load diesel operation. The modern diesel engines utilize multiple injections per cycle and unconventional combustion modes like HCCI, LTC. Moreover, for control applications, the phasing of the heat release (given by $CA50$) is of far more importance than the absolute value of the heat released. Therefore, the prediction of the apparent heat release model was required to be critically analyzed in this new perspective. Moreover, for feedback-control purposes, a compromise must be made between the required accuracy and the system resource constraints such that the simplest algorithm with the minimum required accuracy can be implemented for real-time control.

The methodology for evaluation of the errors with the assumption of a constant specific heat ratio value and neglecting the heat transfer was investigated for four different fuel burn rate patterns as shown in Figure 5.59. These burn rates were adapted from empirical data and comprehensively summarize the modern diesel combustion operating regimes.

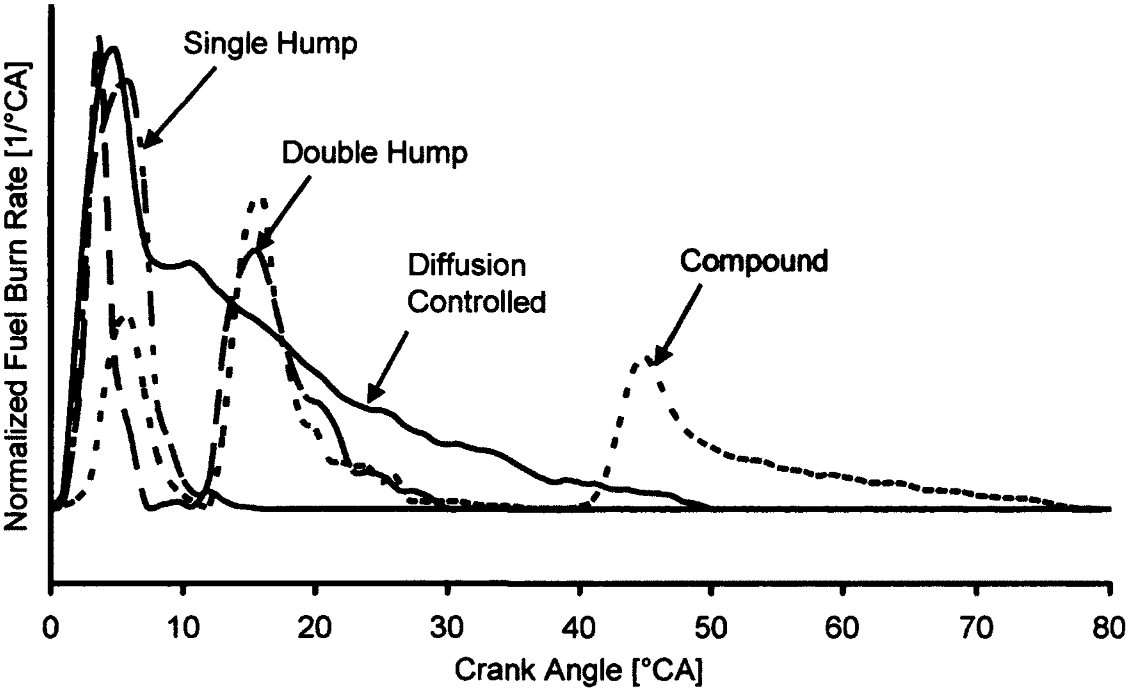

Figure 5.59: Fuel Burn Rate Patterns

These fuel burn rate patterns were categorized as follows:

- Diffusion Controlled mode (DIFF) – corresponding to conventional high temperature diesel combustion
- Single hump (SH) – representing homogeneous charge or highly premixed types of combustion modes
- Double hump (DH) – representing split combustion events by fuel injection strategies including early or multiple injections
- Compound (CMPD) – representing complex combustion by split injections along with late/post injections for enabling aftertreatment or soot destruction

The evaluation of the errors was carried out using both simulated and experimental pressure data. The fuel burn profiles of Figure 5.59 were entered as the user-defined fuel burn rate input to generate the simulated pressures using Ricardo WAVE and SAES softwares. The calculated gross heat release from the softwares and the resulting *CA*50 was taken as the baseline reference against which all errors have been evaluated. A timing sweep was performed for each of the four burn rates by varying the start of combustion (SOC) from -30°CA ATDC to 30°CA ATDC. The motored pressure used during the analysis was calculated by starting with a baseline experimental motoring pressure trace for naturally aspirated conditions at zero EGR and corrected for boost and EGR using the fired pressure trace. The effect of charge-to-wall heat transfer, trapped residual mass, etc. was therefore accounted for. The details of this technique are explained later in the RT-FPGA programming section. The engine tests were run on the Ford Puma Diesel Engine and the same specifications were used in the simulations. The assumed engine operating conditions are given in Table 5.6.

Table 5.6: Engine Operating Conditions

Engine Speed	1200 RPM
Intake Pressure	1 bar abs
Intake Temperature	298 K
Injection Timing	-35°CA ATDC → 25°CA ATDC (10° Increment)
Ignition Delay	5°CA
Burn Duration	10° → 80°CA
Residual Fraction	0.08
Combustion Efficiency	100%

5.11.1. *PDR* Algorithm Application

The *PDR* algorithm was programmed on a National Instruments' Real-time (RT) embedded controller with a field programmable gate array (FPGA) device that conditioned the cylinder pressure signal, processed/analyzed the data and provided the necessary feedback to the fuel-injection controller.

A reliable feedback that is robust and minimally affected by external disturbances is essential for acceptable performance of the model-based algorithms. The computation of the feedback should be fast enough to capture the characteristics of each combustion cycle and the algorithm for the feedback estimation should be able to capture the effect of changes in the engine operating conditions. Therefore, the experimental results presented investigate the robustness of the *PDR* algorithm against variation in a number of engine variables.

5.11.2. RT-FPGA Programming

The FPGA code [103,107,108] acquires the cylinder pressure (16 bit resolution) with a crank angle resolution of 0.1°CA and performs a number of operations including detection and filtering of the pressure data, and the estimation of the motoring cylinder pressure trace. The calculation of the MFB_{PDR} and $CA50$ is then carried out on a cycle-to-cycle basis and the value is passed on to the adaptive fuel injection control algorithms, to enable control of the next combustion cycle.

The baseline condition, i.e., the motoring pressure for naturally aspirated conditions without EGR is programmed into the FPGA memory (4 kB block size with 16 bit resolution) at the start of the tests. The code execution occurs every time the external clock signal (Index A) from the engine-mounted encoder is detected. The key sequence of the calculation includes the following:

- The fired pressure is referenced at -60°CA ATDC (no combustion) to automatically adjust the motoring trace for the current operating conditions (boost, intake temperature, EGR etc).

- A correction to the estimated motoring trace is made by referencing the actual pressure at -30°CA ATDC (no combustion). This enables the effect of EGR to be approximated in the motoring trace.
- The PDR trace is calculated for the crank angle window from -30°CA ATDC to 100°CA ATDC.
- The maximum value of the PDR is used to get the MFB_{PDR} trace.
- The crank angle corresponding to the 50% heat released is then identified and provided as feedback for control purposes.
- The calculation is then repeated for the next cycle.

A problem encountered during programming of the FPGA was the inability to perform floating point calculations in the FPGA. The FPGA can only perform integer arithmetic operations and therefore, division in the FPGA is limited to a quotient and remainder (QR) function. The QR function works by repeatedly subtracting the divisor from the dividend in a while loop until the difference becomes less than the divisor. The difference is reported as the remainder value and the while loop number is the quotient. The execution of this operation is diagrammatically shown in Figure 5.60.

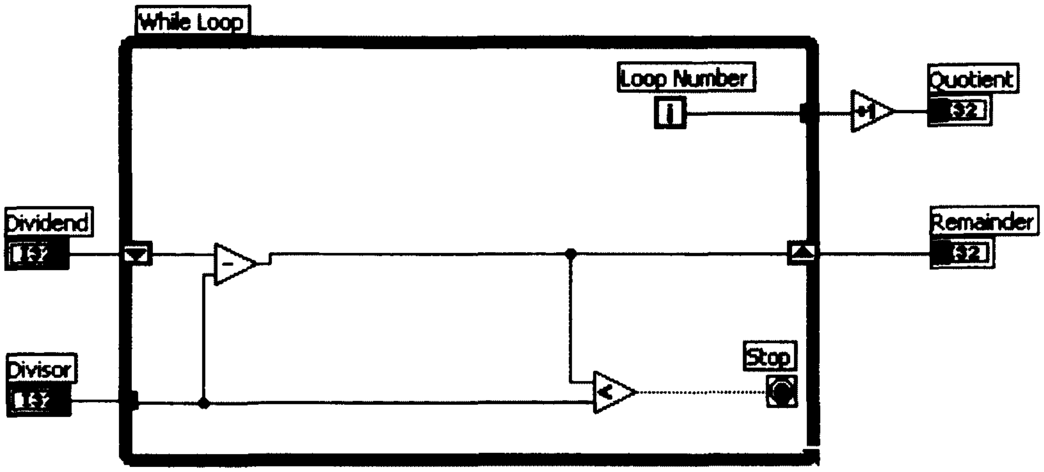

Figure 5.60: Implementation of Division Function in the FPGA

The QR function is useful if the dividend is much larger than the divisor so that the use of the quotient only (and ignoring the remainder) still yields an acceptable solution. However, to scale the baseline motoring pressure to match the actual pressure, the actual pressure needs to be divided by the baseline motoring pressure at the referencing crank angle to generate a multiplication factor that will be used for the scaling operation. This multiplication factor is commonly in the range of 0.9 to 2. Therefore, for the implementation of the *PDR* algorithm, the use of the QR function was not suitable since the division of the actual cylinder pressure by the baseline motoring pressure would normally result in a quotient of one and the difference between the actual and the baseline pressures simply becoming the remainder.

Another method for division in the FPGA involves a scaling technique with bit-level manipulation to obtain the approximate floating-point division. This technique is useful if the divisor does not change. Since the value of motoring pressure varies at each crank angle, therefore, this method also does not provide a viable solution to the problem at hand.

To address this issue, an algorithm to enable floating-point division in the FPGA was devised as shown in Figure 5.61. At the referencing crank angle, that is, -60°CA ATDC, the actual (or fired) pressure is divided by the baseline motoring pressure. If the remainder is a non-zero number, then the following operations are performed:

- The fired and the motoring pressure are multiplied by a constant value of 1000.
- The 1000 x fired pressure value is then divided by the remainder to obtain the scaling multiplier.
- The 1000 x baseline motoring pressure value is also divided by the remainder to obtain the scaling divisor.
- The scaling multiplier and the scaling divisor are then stored in memory for the duration of the engine cycle and are used to adapt the baseline motoring trace at each crank angle to the current operating conditions.

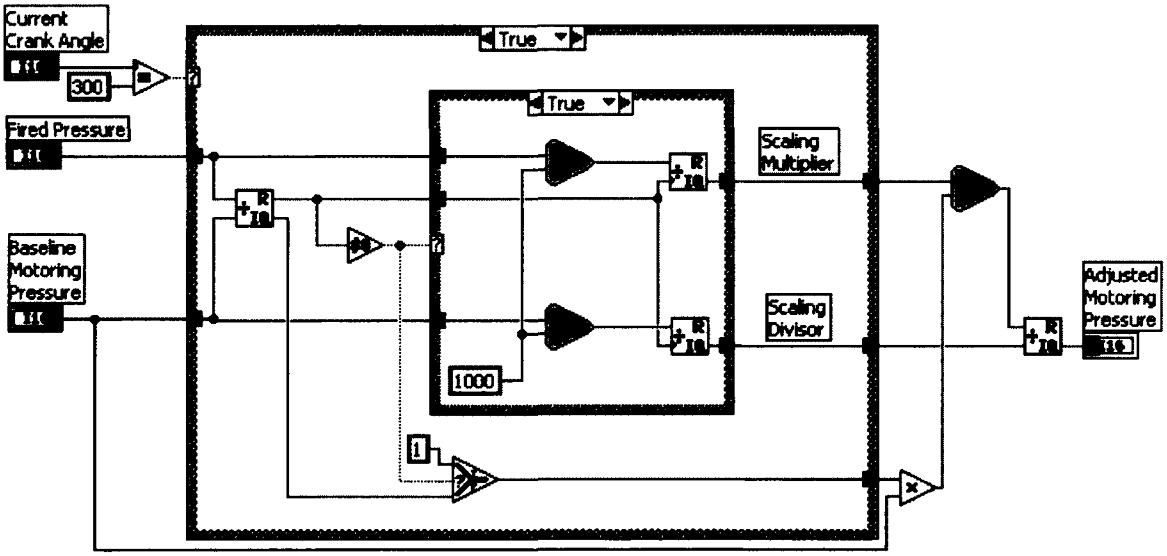

Figure 5.61: Algorithm for Floating-point Division in the FPGA

A few sample conversions using the algorithm are given in Table 5.7. It can be seen that the algorithm provided a high level of accuracy for use in estimating the actual motoring pressure trace.

Table 5.7: Examples of the Floating-point Division in the FPGA

Actual Pressure		Baseline Motoring Pressure		Scaling Multiplier	Scaling Divisor	Scaled Motoring Pressure	
bar	FPGA Integer Value	bar	FPGA Integer Value			FPGA Integer Value	bar
30.20	4948	31.9	5226	1000	1056	4948	30.20
37.60	6160	22.8	3736	2541	1541	6160	37.60
48.30	7913	27.5	4505	2321	1321	7915	48.31
61.70	10109	31.4	5145	2036	1036	10111	61.71
95.40	15630	28.1	4604	8597	2532	15632	95.41

5.12. Evaluation of Errors

Selected results for each of the four fuel burn rate patterns for the injection timing sweep from -35°CA ATDC to 25°CA ATDC (SOC from -30°CA ATDC to 30°CA ATDC) for the heat release models under investigation are given below. The error in the *CA*50 was considered to be negative if the model prediction was earlier than the baseline value. An error of ±1°CA or less was considered as acceptable in this study and is indicated on the figures.

5.12.1. Apparent Heat Release Model Analysis

The apparent heat release rate (AHRR) computed with a constant gamma value of 1.37, was compared against the baseline (BL) results to compute the difference in the prediction of the *CA*50. The timing sweep result such as the one shown in Figure 5.62 for the DIFF mode was repeated for all the fuel burn rate patterns and the resulting error analysis is summarized in Figure 5.63. In Figure 5.62, once the cumulative heat release curves reached a value of one, the curves was assigned a constant value of one to improve the figure readability.

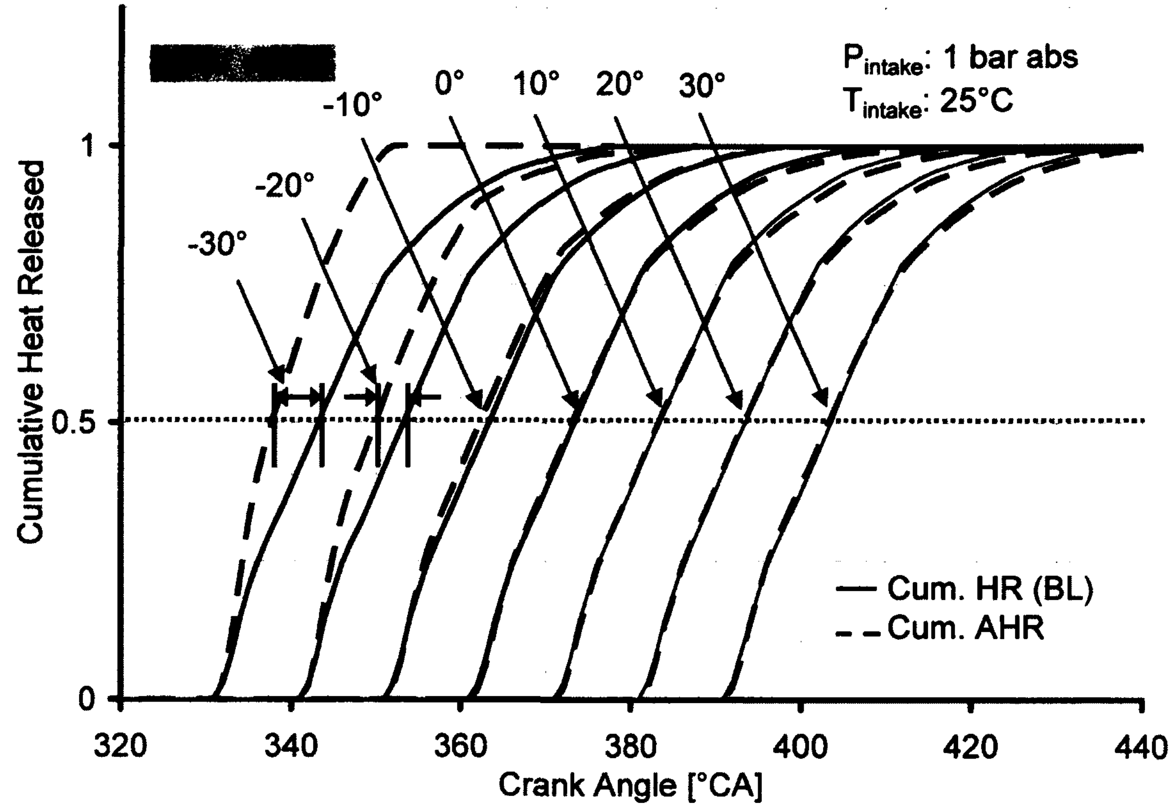

Figure 5.62: Comparison of the Cumulative Heat Released Traces for DIFF Mode

5.12.1.1. Diffusion Controlled Mode

The error in the prediction of the *CA*50 was large for the cases with the *CA*50 before the TDC. However, for combustion phasing at and after TDC, the prediction of the AHR model matched the baseline results. This can be attributed to the higher heat transfer rates for the early combustion because of the larger combustion chamber surface area and the sustained high temperatures due to the longer combustion duration (50°CA) and the ongoing compression process.

5.12.1.2. Single Hump Mode

A short combustion duration of about 10°CA and low-load operation is typical of homogeneous charge or highly premixed types of combustion modes. Since the combustion is quite rapid, the AHR analysis was able to

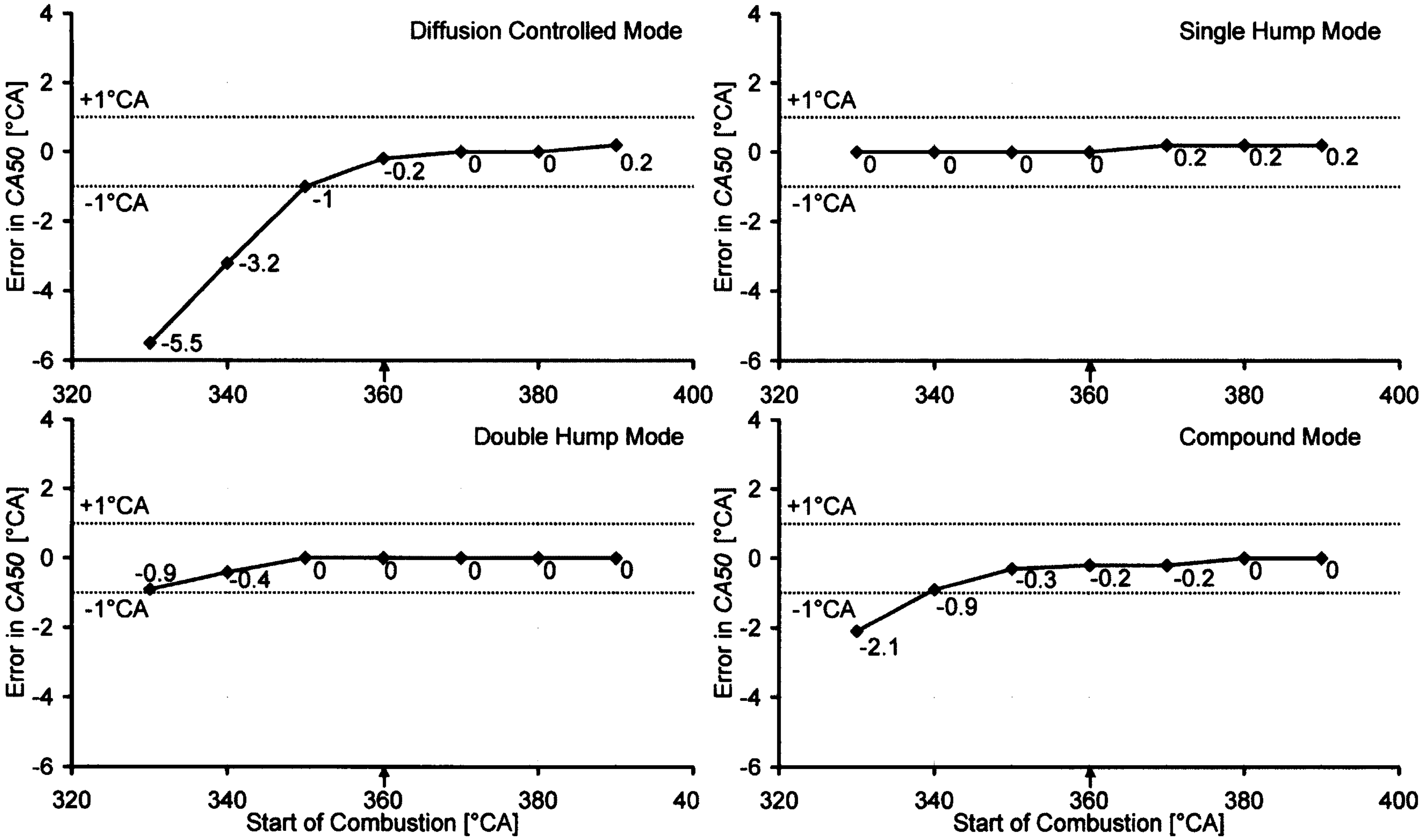

Figure 5.63: Summary of the AHR Error Analysis

effectively capture the combustion phasing. Therefore, the cumulative AHR traces matched the baseline results for all the timing sweep cases.

5.12.1.3. Double Hump Mode

The results shown are for a typical split injection strategy, with a ratio of the pilot injection to the main injection quantity equal to 0.7, and a dwell of 15°CA between the two injections. The cumulative AHR error in the early phased cases did not affect the calculated *CA*50 significantly as the less quantity of the pilot injection confined the error below the *CA*50 level. However, if a ratio greater than 0.8 is employed, significant errors may result in the *CA*50 calculations for the early phased cases.

5.12.1.4. Compound Mode

The use of a post or late injection for enabling aftertreatment or destruction of soot was categorized under the compound fuel-burn pattern. The simulated combustion duration was quite long, about 80°CA in this case. However, as long as the pilot and main injections represented the majority of the fuel injected, the error in the calculated values was small.

The largest error in the heat release calculation is most likely incurred by ignoring the charge-to-wall heat transfer. However, it can be seen that the AHR analysis provided a reasonable estimate of the *CA*50 for all the four fuel burn patterns considered, for most of the timing sweep.

5.12.2. Rassweiler-Withrow Model Analysis

The error analysis was repeated with the RW model for the SOC timing sweep from -30°CA ATDC to 30°CA ATDC. The results for the four fuel burn patterns with the SOC at -10°CA ATDC are shown in Figure 5.64. The MFB traces have been staggered on the x-axis (crank angle) for the same SOC to make the comparison easier to understand. The MFB traces showed very good agreement for the first three fuel burn patterns. However, for the compound mode of combustion, the MFB_{RW} showed a deviation from the cumulative HR trace. Analysis of similar traces for different SOC revealed that for early combustion phasing, the error was similar to that observed with the AHR model. However, for the compound mode of combustion, a significant error was observed for all cases of the combustion phasing sweep.

For the compound mode, the combustion duration was 80°CA so that the combustion progressed well into the expansion stroke. At this stage, the change in pressure due to the volume change becomes significantly higher than that due to combustion, especially so because of the higher compression ratio of the diesel engines. Therefore, the assumption of a fixed polytropic index caused the MFB_{RW} to deviate significantly. Care should be taken in using the MFB_{RW} for delayed combustion phasing or for combustion modes with late injection events.

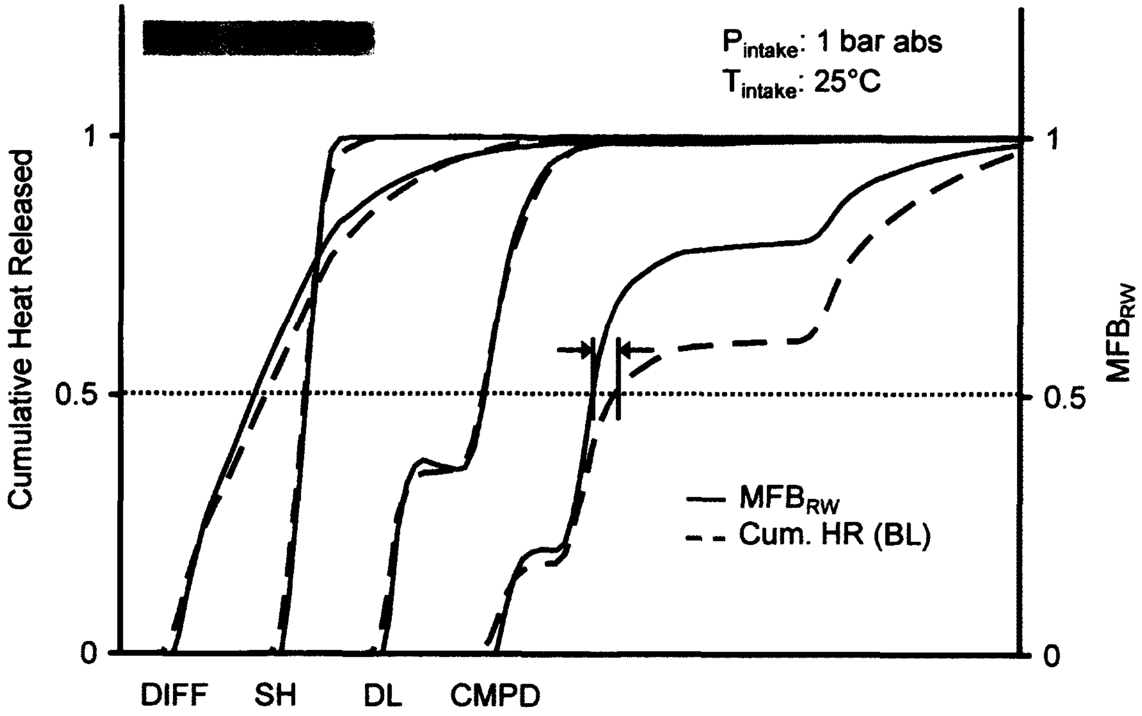

Figure 5.64: Comparison of *CA*50 Prediction between MFB_{RW} and Cum. HR

5.12.3. Diesel Pressure Departure Ratio Model Analysis

The estimation of the *CA*50 using the MFB_{PDR} is presented for all the four modes of combustion in Figure 5.65. The FPC and MPC were determined initially and

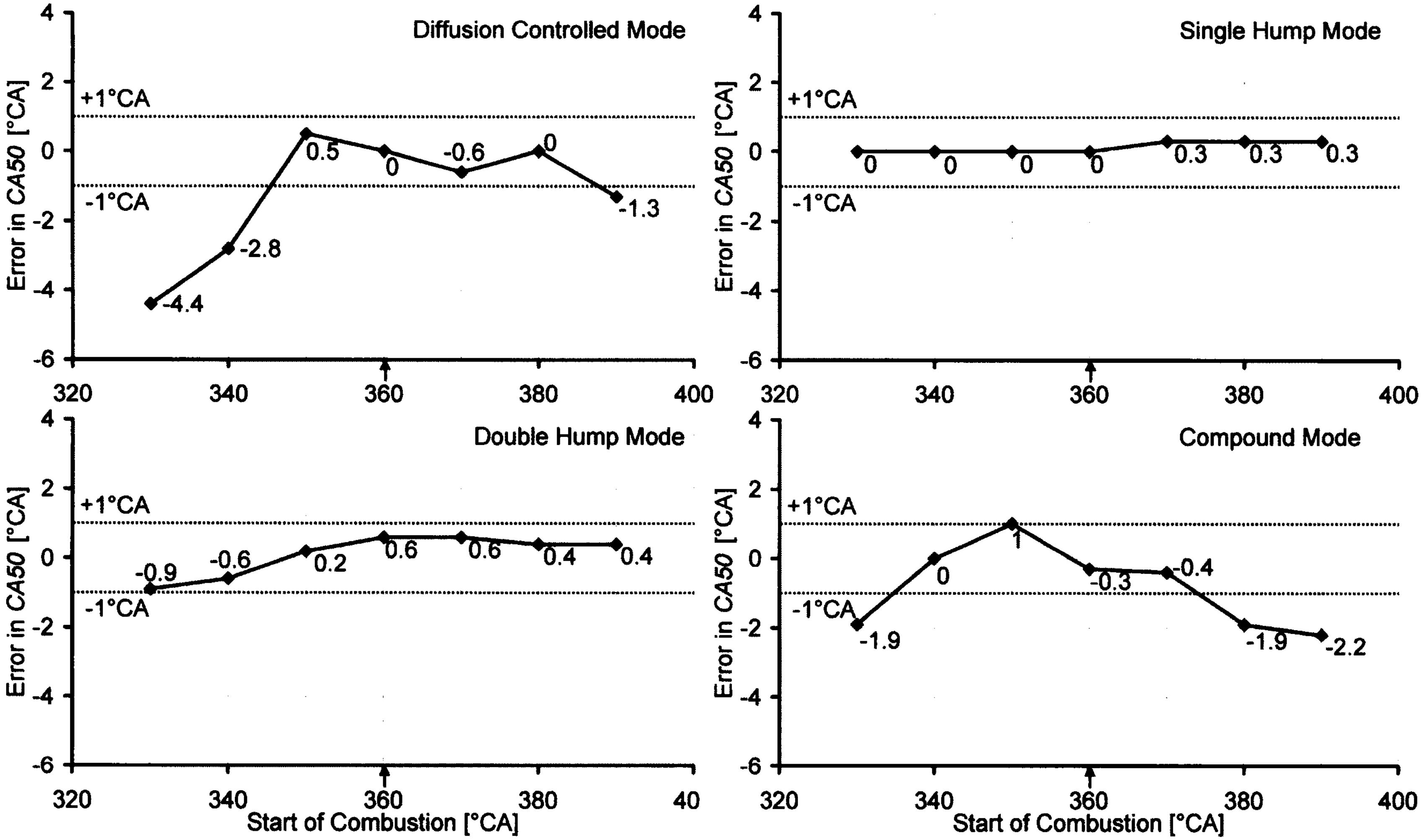

Figure 5.65: Summary of the MFB_{PDR} Error Analysis

kept constant through out the analysis. For the DIFF mode, the MFB_{PDR} showed large errors in the $CA50$ for the early SOC cases. For combustion starting around TDC, the results were similar to those obtained with the AHR analysis, and the MFB_{PDR} generally followed the baseline results except for the late SOC cases where a small deviation was observed. When the combustion duration was short (SH mode), the performance of both the AHR and the PDR models matched the baseline cumulative HR traces. As already discussed for the AHR model in the SH mode, the combustion phasing has negligible effect on the calculations of the simplified algorithms for the SH mode.

For the DH Mode, although deviations from the baseline results were observed similar to the AHR predicted traces, the estimation of the $CA50$ was not affected. The reasons for this were highlighted during the error analysis of the AHR model. For the compound mode, the MFB_{PDR} traces for the early phasing were similar to those from the AHR model. Unlike the results from the RW model, the MFB_{PDR} was able to capture the heat release characteristics for combustion phased around the TDC. However, for late combustion phasing with the $CA50$ occurring after 380°CA, the MFB_{PDR} traces deviated from the baseline results. Although such late phasing might be considered impractical for engine applications, nevertheless, the results indicated a limitation of the PDR model for compound type of heat release patterns with late phasing.

The PDR analysis provided a reasonable estimate of the $CA50$ for all the four fuel burn patterns considered, for most of the timing sweep. It can be seen that the results were quite similar to those obtained with the AHR model.

A comparison of the three models for the compound mode with SOC at -10°CA ATDC is shown in Figure 5.66. Although being the simplest of the three models, the MFB_{PDR} was able to capture the $CA50$ with reasonable accuracy while the error with the RW model was significant. It is pertinent to add here that a situation may arise where the MFB value between the two combustion events (from 370 to 390°CA) may be 0.5. Although the HR algorithms would predict 370°CA as the *CA*50 (the first crank angle at which the trace reaches the 0.5 value), the *CA*50 determination in such cases would be imprecise. This also highlights the limitations of the *CA*50 as a measure of the combustion phasing under such combustion modes.

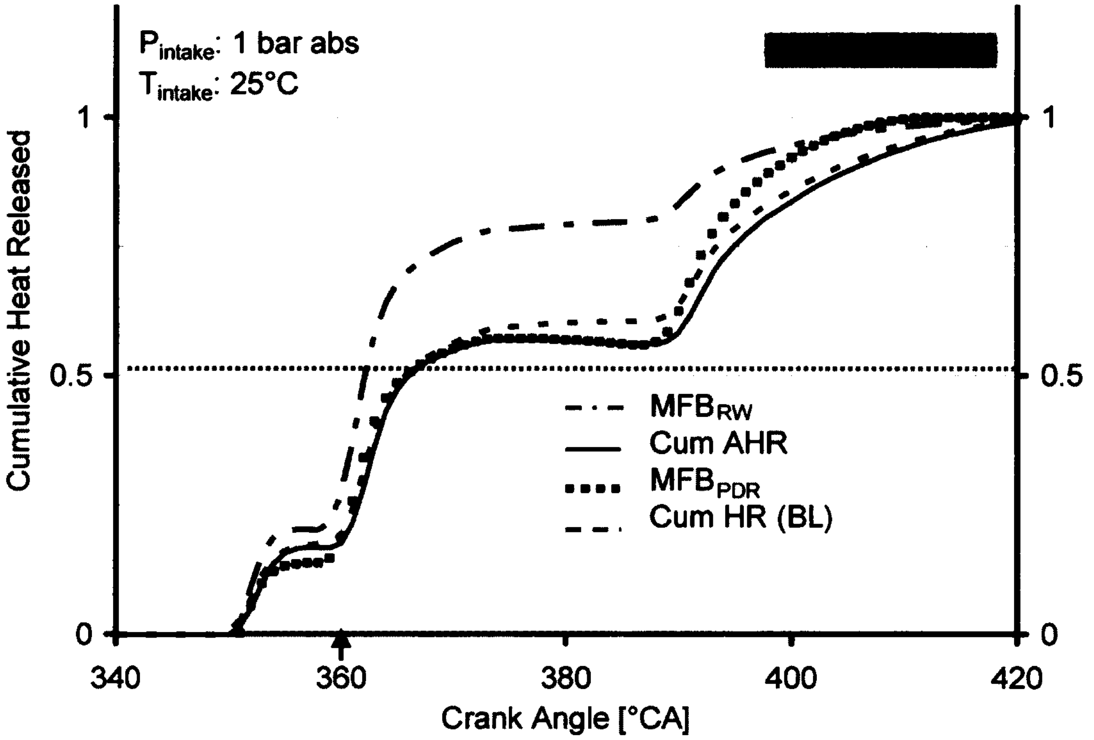

Figure 5.66: Comparison between MFB_{PDR}, MFB_{RW} and AHR Models (CMPD Mode)

5.13. Quality of Pressure Data

The quality of the pressure data can affect the prediction and thereby the robustness of the heat release models. The AHR model is more susceptible to disturbances in the pressure signal as it includes the derivative of the pressure which amplifies any disturbance present in the signal. This is clearly shown in Figure 5.67 and has significant implications on the calculation of the cumulative heat released since it requires the EOC to be identified with reasonable accuracy. Therefore, heavy smoothing or filtering of the pressure data needs to be performed before any reasonable estimate of the *CA*50 can be made, which significantly increases the computational overheads. On the other hand, the *PDR* model was able to predict the *CA*50 with sufficient accuracy without any treatment applied to the pressure data. This makes the model more robust and suitable for real-time applications than the apparent HR model.

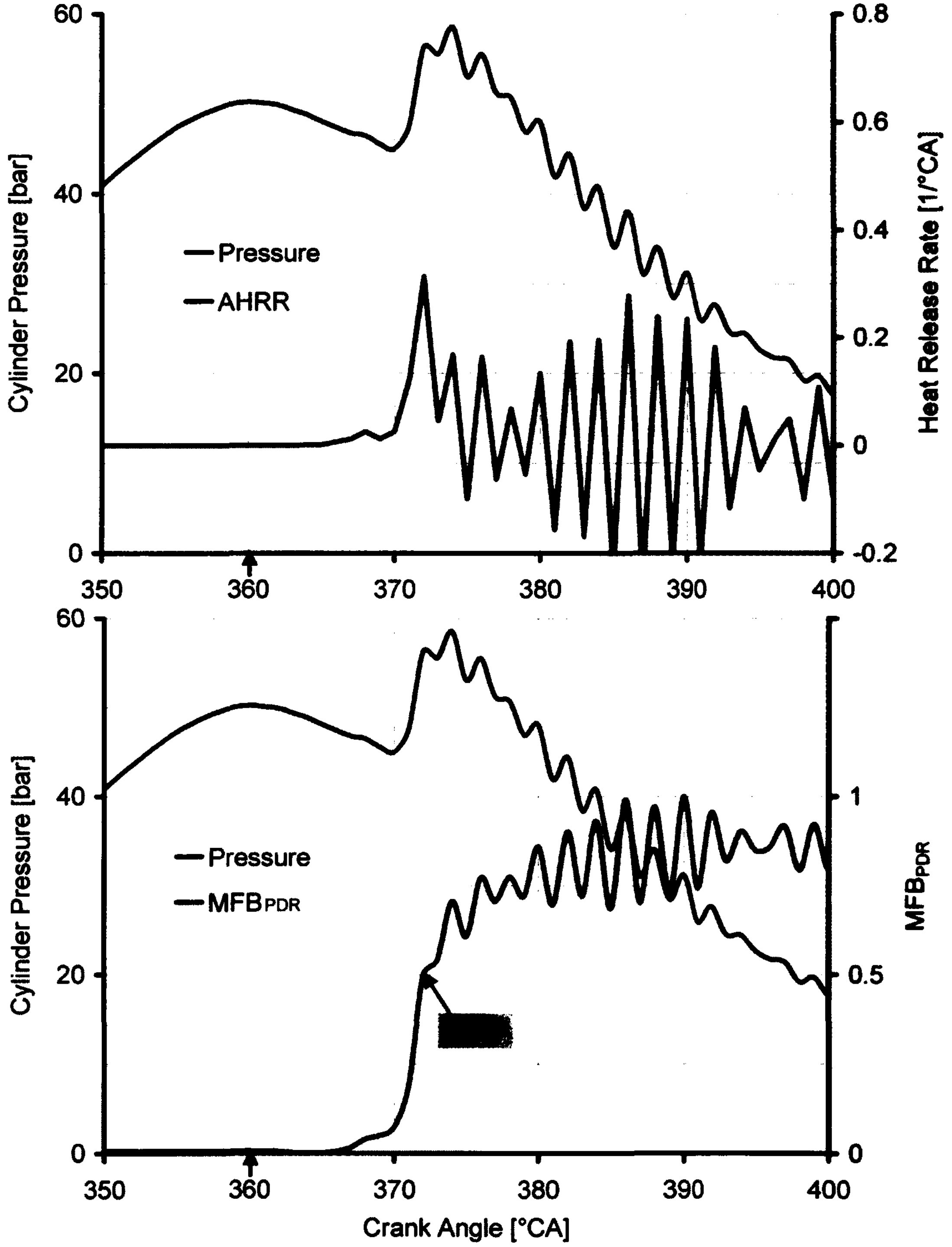

Figure 5.67: Model Comparison for a Noisy Pressure Trace; Upper: AHRR; Lower: MFB_{PDR}

5.14. *PDR* Algorithm Performance Tests

Additional experiments were performed to demonstrate the *PDR* algorithm performance for selected cases with variation in boost, EGR, engine load, and fuel injection strategies. The baseline cumulative heat release was calculated using both the AHR model and the comprehensive model including the heat transfer estimation and specific heat ratio variation with temperature. If a difference existed between these two models, then the baseline value shown in the figures represents the value from comprehensive HR model. High values of EGR are presented in these results to test the performance of the algorithm at the extreme conditions of EGR with high cycle-to-cycle variation and increased emissions of CO and HC so that the limitations of the model may be better identified.

The estimation of the motoring pressure trace can have a significant effect on the *PDR* model performance. The predicted motoring traces for different levels of EGR are shown in Figure 5.68. High levels of EGR cause a reduction in the cylinder pressure during the compression stroke. The RT-FPGA code was able to track this trend and modify the motoring traces as the amount of EGR was changed. This also implies that the algorithm can to some extent, account for changes in the composition, the specific heat ratio and the charge-to-wall heat transfer.

The effects of EGR variation with a single injection per cycle on the MFB_{PDR} are shown in Figure 5.69. As the amount of EGR was increased from zero to 56%, the start of combustion was progressively delayed. It can be seen that the *PDR* model was able to accurately predict the retarded combustion phasing.

The effects of changing the boost pressure and the fuel injection strategy are shown in Figure 5.70. With multiple injections per cycle (3 early injections and one main injection), the heat release curve takes the shape of the double hump pattern. The *PDR* model was able to reasonable predict the *CA*50 within the prescribed limits of accuracy, that is, ±1°CA.

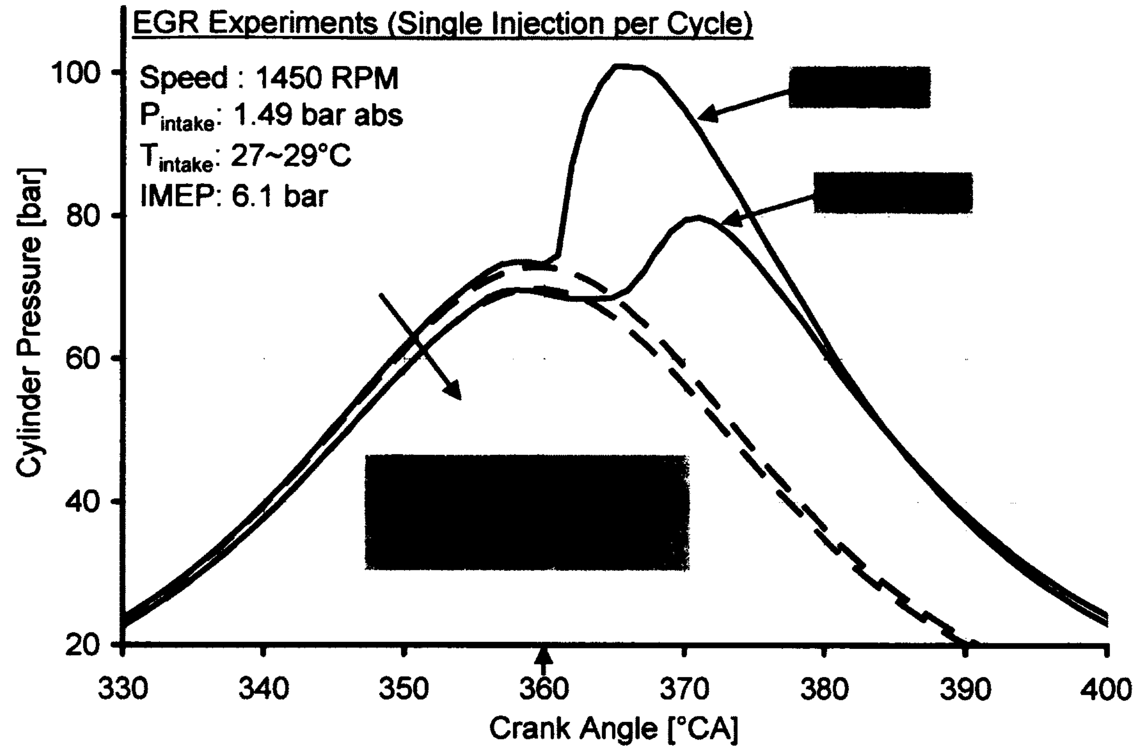

Figure 5.68: Estimation of Motoring Pressure

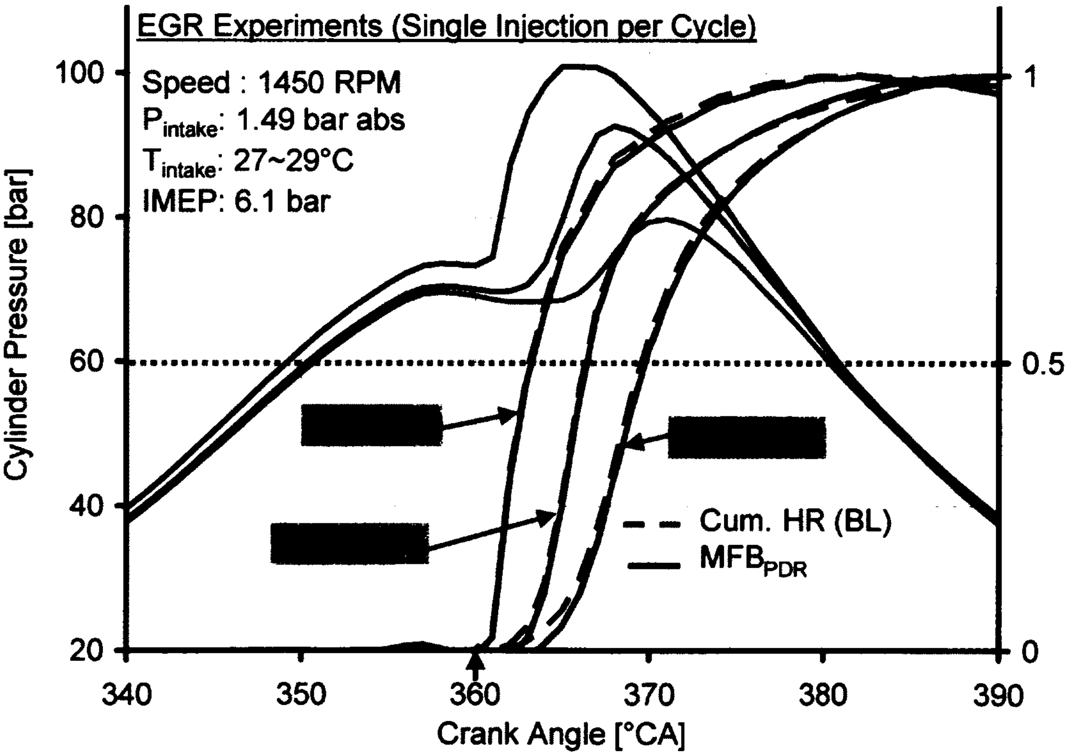

Figure 5.69: EGR Sweep Experiments

The variation of the engine load while the boost pressure was held constant is shown in Figure 5.71. The low indicated mean effective pressure (IMEP) case represents the single hump type of combustion, while the higher load case falls in the double hump category. The *PDR* algorithm in these cases was also able to fairly predict the occurrence of the *CA*50.

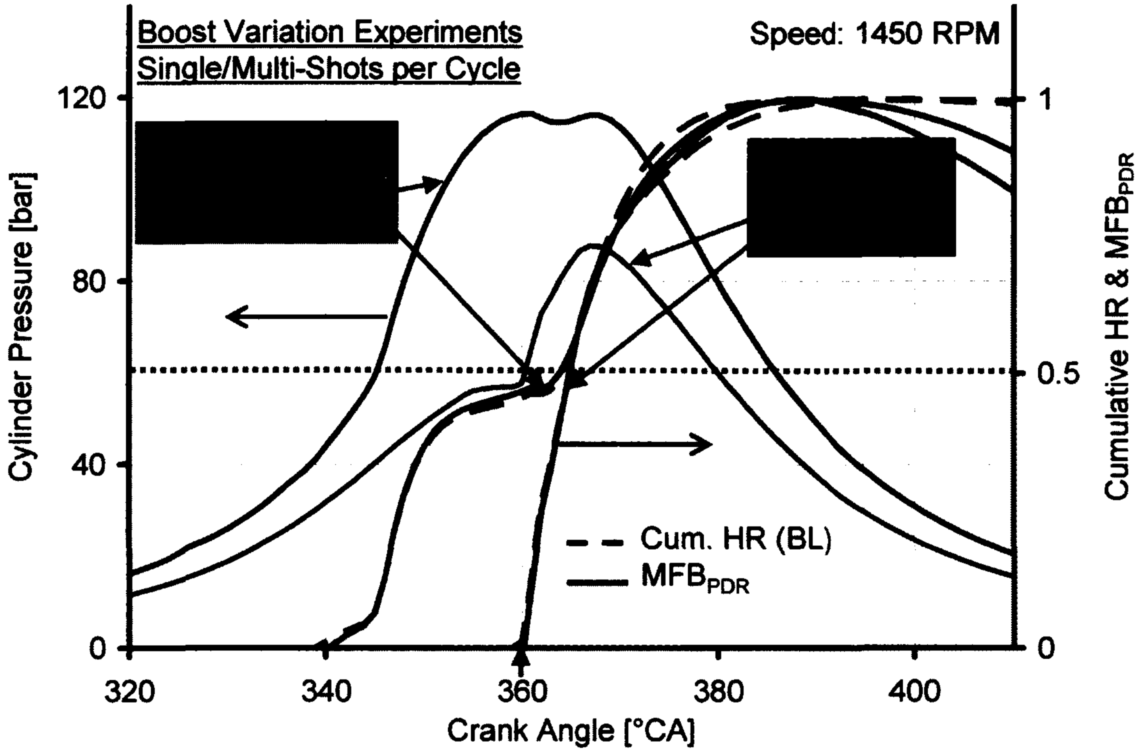

Figure 5.70: Variation of Boost & Fuel Injection Strategy

The application of the *PDR* algorithm for various combustion modes and fuel injection strategies showed that the estimation of the heat release characteristics using the *PDR* algorithm was least affected by the combustion off-phasing and split combustion events. Moreover, the numerically simplified form of the *PDR* algorithm given in Equation (5.19) provided the normalized heat release comparable to the baseline and apparent heat release data by using significantly less computational resources.

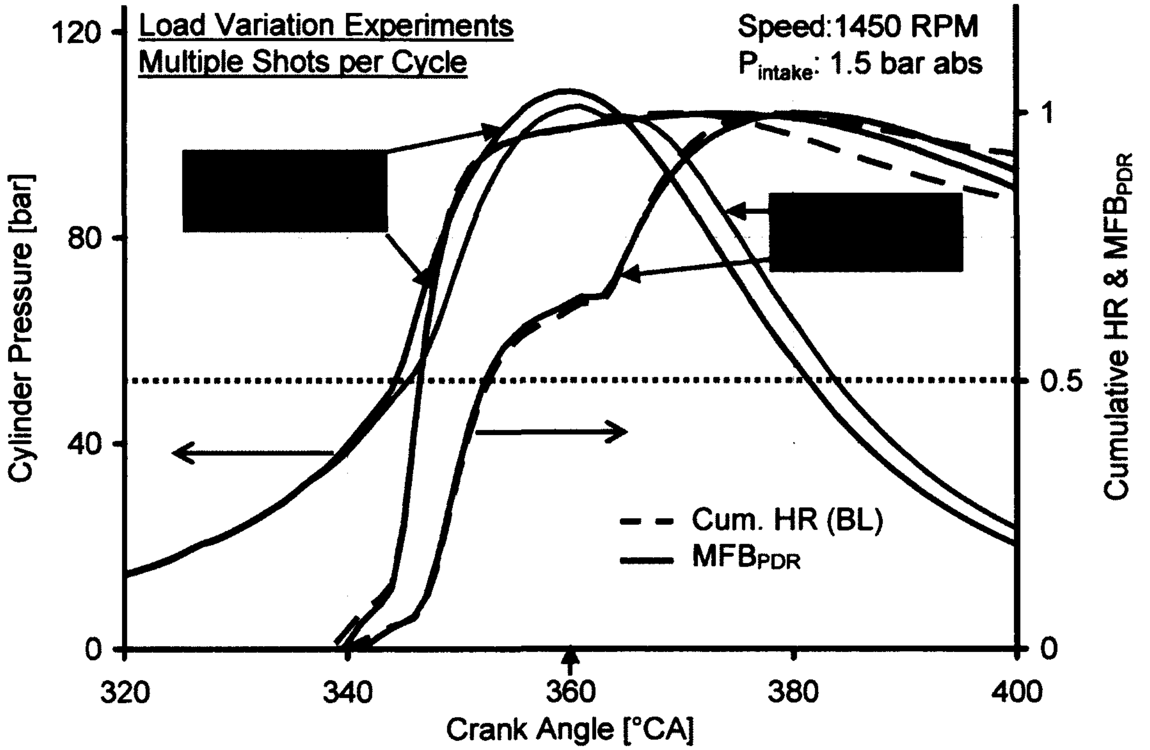

Figure 5.71: Load Variation Experiments

5.15. Smart NOx Sensor

The aim of developing a control strategy for the LTC cycles is to improve their stability while maintaining low emissions of NOx and soot. Therefore, feedback on these emissions is necessary for the control system to guarantee efficient operation. To provide such a feedback, a smart NOx sensor was installed in the exhaust of the cylinder # 1 of the Ford engine.

The sensors uses the CAN bus communication protocol which was implemented with LabVIEW software as a part of this work. The sensor can measure ultra low levels of NOx with sufficient accuracy and also provides feedback on the excess air ratio (λ). The specifications of the NOx sensor are given in Table 5.8.

Table 5.8: Specification of the Smart NOx Sensor

Type	Zirconia (ZrO_2)-based multilayer sensor with 3 oxygen pumps
Measuring Range	NOx: 0–1650 ppm λ: 0.75 to Air
Accuracy	NOx: ±10 ppm at 0 ppm ±10 % ppm at 1500 ppm λ: ±0.06 at λ=1
Response Time (T_{66})	NOx: 750 ms λ: 550 ms
Control	Built in Controller for internal heater & communication
Communication Interface	CAN Bus Standard 500 kbaud, 11 bit Data Update Rate: 10 ms

Initial testing of the sensor showed that the sensor response was susceptible to the exhaust pressure and especially, to the flow rate fluctuations. In case of a single cylinder configuration, the flow fluctuations are more distinct compared to a multi-cylinder configuration and therefore, the sensor output was not usable. To overcome this problem, a bleed line was installed upstream of the exhaust surge tank and the exhaust backpressure valve (Figure 4.7). The sensor was installed in the bleed line and the other end of the bleed line was connected downstream of the backpressure valve. A throttling valve was also installed to adjust the flow. This allowed a steady flow to be maintained over the sensor while providing a fast response time as well.

The sensor was tested over a wide range of engine operating conditions and the results for λ and NOx are shown in Figure 5.72 and Figure 5.73 respectively. The results for the λ output were compared with the reference values (λ_{ref}) calculated using the carbon balance method. Since the data presented involved transient engine operation that included load transients as well, the fuel flow rate reading was not accurate to calculate the λ. The carbon balance method (APPENDIX C) provides a fairly accurate estimate of the air/fuel ratio based on the exhaust concentrations, and the intake fresh air mass flow rate (MAF). The results showed that the sensor accurately captured the changing trends and provided a reasonable estimate of the air excess ratio.

The NOx output of the sensor was compared with the NOx readings (obtained from the exhaust NOx emission analyzer marked as NOx_{ref} in the figure). The results indicated that the sensor was able to provide a fairly accurate estimate of the engine-out NOx, especially at low levels of NOx seen during LTC operation. The actual response time was the sum of the digital delay (the sensor response) and the physical delay (a consequence of the sensor location, delay in the exhaust system as dictated by the flow characteristics), and was observed to be a few seconds (typically 1 to 2 seconds).

The feedback from the smart NOx sensor was used to ensure the emission level conformity while navigating the narrow LTC operating corridors as part of the systematic combustion control system (Chapter 8).

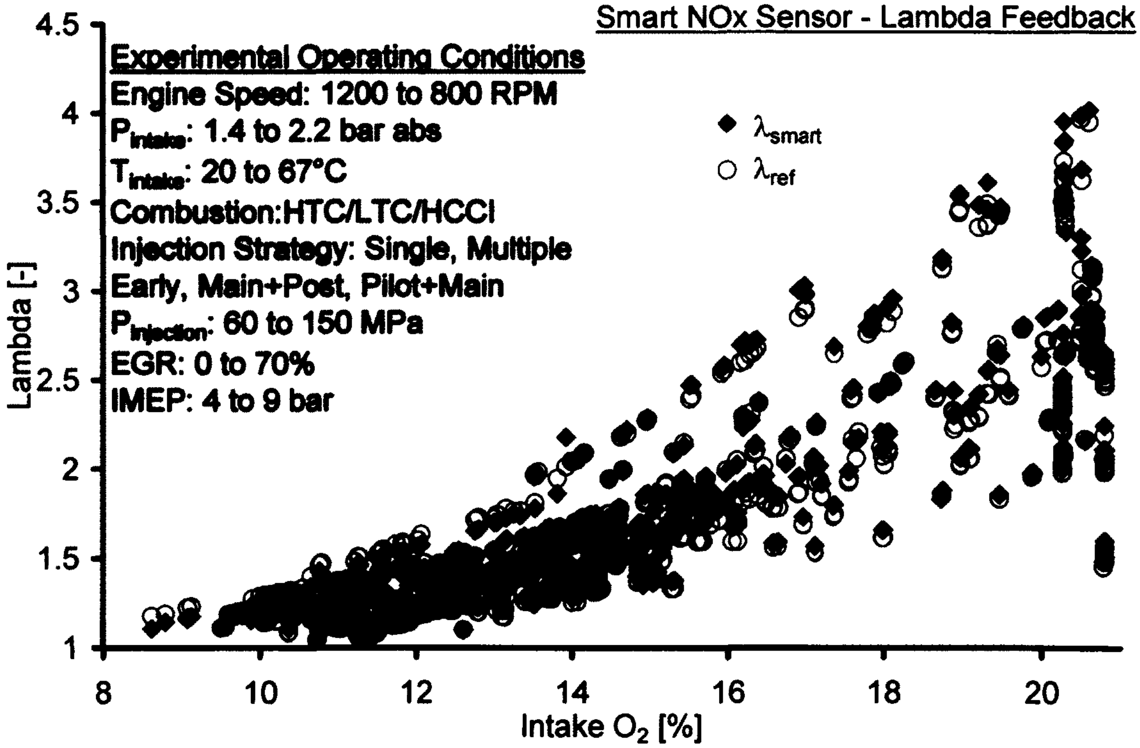

Figure 5.72: Air Excess Ratio estimated by the Smart NOx Sensor

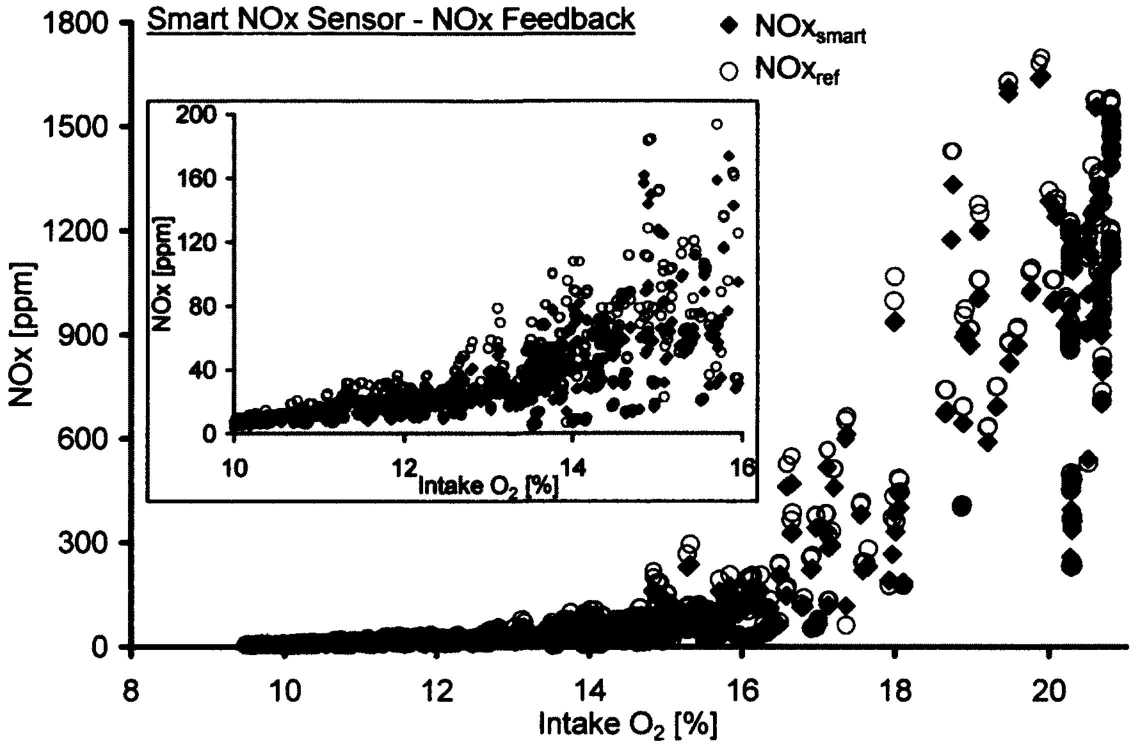

Figure 5.73: NOx Emission estimated by the Smart NOx Sensor

5.16. Conclusions

The work presented in this chapter can be summarized as follows:

- An LTC NOx reduction mechanism was identified through direct in-cylinder sampling experiments. The low NOx levels in the exhaust were confirmed to be the result of the NO-HC interaction.

- A critical HC/NO ratio of 10~15:1 was found to exist that resulted in a significant conversion and/or destruction of NO. A lower ratio considerably decreased the NO conversion while a high ratio indicated an insignificant or a small increase in the conversion.

- In-cylinder sampling studies for lean homogeneous charge combustion fuelled with DME confirmed the production and subsequent oxidation/destruction of NO within the combustion regime. The engine-out NOx was 1~2 ppm for all the testing conditions.

- To enable closed-loop control of the diesel combustion, a number of cylinder pressure based parameters were analyzed for their numerical complexity accuracy and robustness under different diesel combustion modes. The crank angle of 50% heat released (CA50) was found to provide a stable and robust feedback on the phasing of the combustion process.

- A computationally efficient 'Diesel Pressure Departure Ratio' algorithm for estimating the combustion phasing for a multitude of combustion strategies was proposed, implemented and validated with engine tests. The algorithm performance was empirically compared against the conventional heat release algorithms and was found to provide accurate feedback within ±1 °CA.

CHAPTER VI

6. EGR ANALYSIS AND CATALYTIC TREATMENT

The heavy use of EGR was considered unnecessary during conventional diesel combustion as a low rate of EGR in combination with injection timing retard and low boost pressure was sufficient to enable compliance with the emission regulations. However, the introduction of stringent emission standards has resulted in alternate combustion regimes to be applied to the diesel engines. The use of heavy EGR is an important enabler for LTC cycles as will be shown in Chapter 7. Moreover, the stability of the LTC operation is very sensitive to the EGR rates as shown in Figure 6.1.

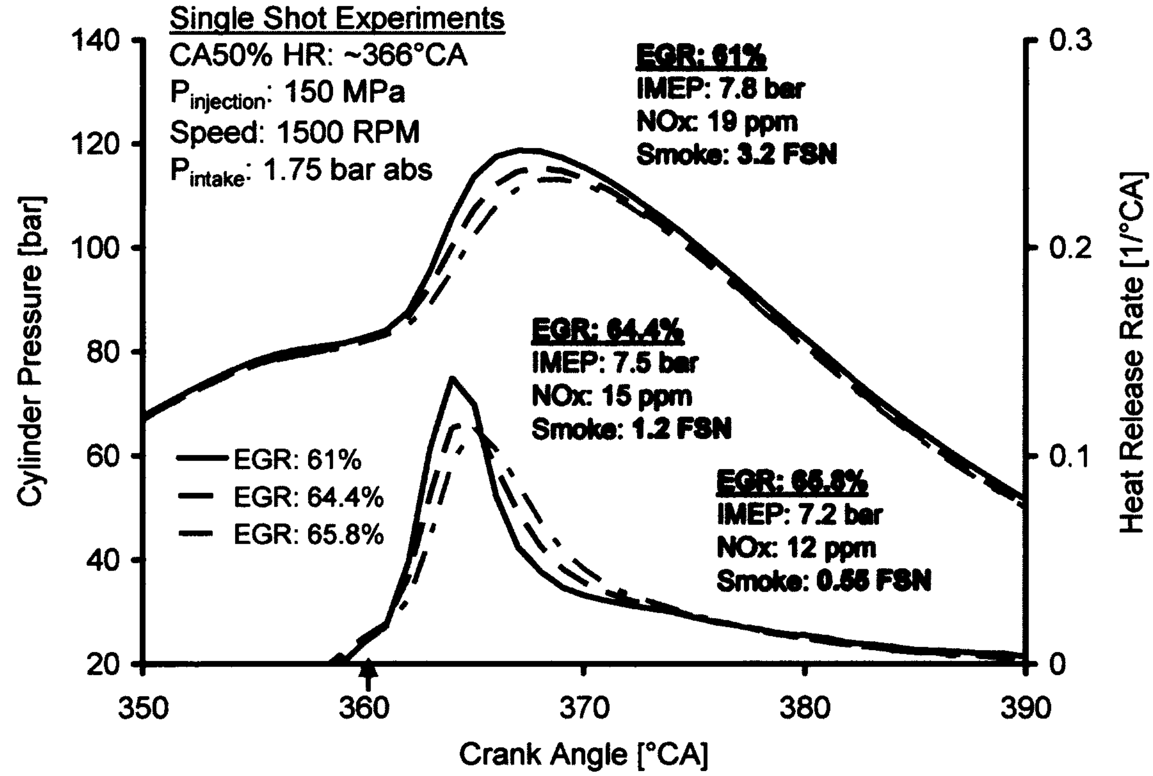

Figure 6.1: Sensitivity of LTC Cycles to EGR

The use of higher boost pressures changes the fuel-strength of the cylinder charge and in turn has a significant effect on the quality and effectiveness of the EGR. Therefore, a detailed analysis of the EGR was decided to be carried out to characterize the efficacy of EGR for LTC operation as well as to develop suitable parameters that can provide feedback for the LTC control. Moreover, an extensive study was carried out by reforming a small quantity of diesel fuel in the EGR loop to generate gaseous fuels on demand. The participation of these gaseous fuels in the combustion enhanced the premixed combustion and reduced the soot emission while maintaining low levels of engine out-NOx. Novel flow-management strategies were also applied to improve the efficiency of the reforming process.

6.1. Defining EGR

To quantify the amount of the recirculated exhaust gas, a number of mathematical definitions have been adopted in the literature [83]. As such, there is no standard definition of EGR to quantify the amount of recirculation. However, two basics formulae have been most commonly used to define the amount or rate of EGR.

6.1.1. Mass Based EGR

The definition of EGR on a mass basis is schematically shown in Figure 6.2.

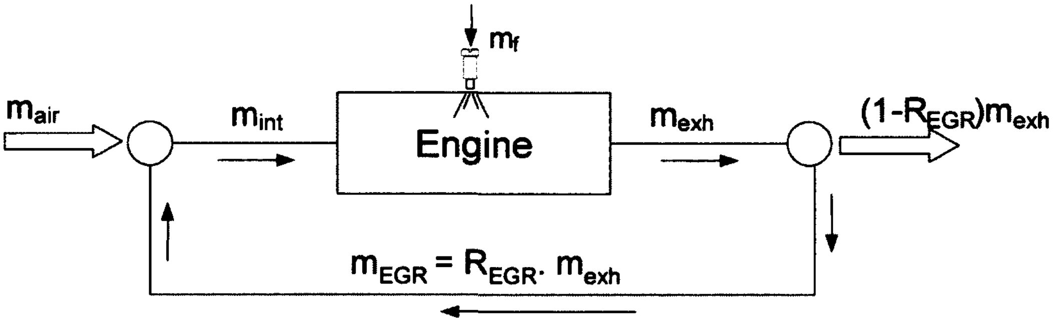

Figure 6.2: Defining EGR on a Mass Basis

Mathematically, it can be expressed as follows:

$$R_{EGR} = \frac{\dot{m}_{EGR}}{\dot{m}_{air} + \dot{m}_f + \dot{m}_{EGR}} \tag{6.1}$$

where

$\dot{m}_{EGR}$ = mass flow rate of recirculated exhaust gas

$\dot{m}_{air}$ = mass flow rate of fresh air

$\dot{m}_f$ = mass flow rate of the injected fuel

R_{EGR} = mass fraction of the recirculated exhaust gas

A simplified form of this equation is usually used:

$$R_{EGR} = \frac{\dot{m}_{EGR}}{\dot{m}_{intake}} \tag{6.2}$$

where

$\dot{m}_{intake}$ = total intake charge mass flow rate with EGR ($\dot{m}_{intake} = \dot{m}_{air} + \dot{m}_{EGR}$)

Alternatively, under steady operating conditions, the EGR rate can be evaluated from Equation (2) where $\mathrm{MAF}_{\mathrm{current}}$ and $\mathrm{MAF}_{\mathrm{initial}}$(w/o EGR) are the fresh air mass flow rates with and without EGR application, respectively.

$$R_{EGR} = 1 - \frac{\mathrm{MAF}_{\mathrm{current}}}{\mathrm{MAF}_{\mathrm{initial(w/o\ EGR)}}} \tag{6.3}$$

6.1.2. Carbon Dioxide Concentration Based EGR

$$R_{EGR} = \frac{CO_{2(int)} - CO_{2(amb)}}{CO_{2(exh)} - CO_{2(amb)}} \approx \frac{CO_{2(int)}}{CO_{2(exh)}} \tag{6.4}$$

where

int = CO_2 concentration in the intake (by volume)

exh = CO_2 concentration in the exhaust (by volume)

amb = CO_2 concentration in the ambient air (by volume)

These definitions do not provide exactly the same results for a given engine operating condition but the trends have been found to be consistent over a wide range of engine operating conditions including engine load and boost. However, from the point of view of estimating the EGR for control feedback purposes, as long as the same definition of EGR is used, the repeatability of the results takes precedence over the absolute accuracy of the results.

6.2. EGR Analysis

A molar-based analysis can provide helpful insight into the applicability of the EGR and its effect on the composition of the intake charge. For combustion without EGR, the global combustion reaction for the complete combustion of any hydrocarbon fuel with fresh air can be written as

$$\begin{gathered} C_\alpha H_\beta O_\gamma + \lambda_o\left(\alpha+\frac{\beta}{4}-\frac{\gamma}{2}\right)(O_2+3.76N_2)\rightarrow \\ \alpha CO_2+\frac{\beta}{2}H_2O+\lambda_o\left(\alpha+\frac{\beta}{4}-\frac{\gamma}{2}\right)3.76N_2+(\lambda_o-1)\left(\alpha+\frac{\beta}{4}-\frac{\gamma}{2}\right)O_2 \end{gathered} \tag{6.5}$$

where

λ_o = air excess ratio without EGR

With the application of EGR, the reaction is modified as follows:

$$\begin{gathered} C_\alpha H_\beta O_\gamma + (1-R_{EGR})\lambda_o\left(\alpha+\frac{\beta}{4}-\frac{\gamma}{2}\right)(O_2+3.76N_2) \\ +R_{EGR}\left[\alpha CO_2+\frac{\beta}{2}H_2O+\lambda_o\left(\alpha+\frac{\beta}{4}-\frac{\gamma}{2}\right)3.76N_2+(\lambda_o-1)\left(\alpha+\frac{\beta}{4}-\frac{\gamma}{2}\right)O_2\right]\rightarrow \\ (1+R_{EGR})\left(\alpha CO_2+\frac{\beta}{2}H_2O\right)+\lambda_o\left(\alpha+\frac{\beta}{4}-\frac{\gamma}{2}\right)3.76N_2+(\lambda_o-1-R_{EGR})\left(\alpha+\frac{\beta}{4}-\frac{\gamma}{2}\right)O_2 \end{gathered} \tag{6.6}$$

The application of EGR is commonly represented by Equation (6.6) in the literature. However, if Equation (6.6) is used to estimate the intake and exhaust concentrations at any EGR level (R_{EGR}), the results would be grossly incorrect. The recirculation of some of the exhaust CO_2 to the intake results in a higher level of CO_2 in the exhaust during the next engine cycle. This translates into a higher CO_2 concentration in the intake system as well. The process continues until equilibrium is reached between the intake and the exhaust concentrations. Therefore, the steady state EGR levels observed during engine operation are the result of an iterative process that results in the convergence of the EGR value over a number of engine cycles.

To express this phenomenon mathematically so that the steady-state concentrations could be easily estimated at any engine load and EGR level, an expression was derived as detailed in the following section.

6.2.1. Estimation of Steady-State EGR

Equation (6.6) represents the calculation of the concentrations for the first engine cycle after EGR is applied. The process was repeated for a number of engine cycles and a single equation has been proposed that can be used for determining the intake and the exhaust concentrations for any cycle. Using Equation (6.6) as the starting point, the reactant and the products for the 2nd cycle, after the recycling of the exhaust products from the 1st cycle can be expressed as

$$\begin{aligned}
&C_\alpha H_\beta O_\gamma + (1 - R_{EGR})\lambda_o\left(\alpha + \frac{\beta}{4} - \frac{\gamma}{2}\right)(O_2 + 3.76N_2)\\
&+R_{EGR}\begin{bmatrix}(1+R_{EGR})\left(\alpha CO_2 + \frac{\beta}{2}H_2O\right) + \lambda_o\left(\alpha + \frac{\beta}{4} - \frac{\gamma}{2}\right)3.76N_2\\ +(\lambda_o - 1 - R_{EGR})\left(\alpha + \frac{\beta}{4} - \frac{\gamma}{2}\right)O_2 \end{bmatrix} \rightarrow\\
&\left(1 + R_{EGR} + R_{EGR}^2\right)\left(\alpha CO_2 + \frac{\beta}{2}H_2O\right) + \lambda_o\left(\alpha + \frac{\beta}{4} - \frac{\gamma}{2}\right)3.76N_2\\
&+(\lambda_o - 1 - R_{EGR} - R_{EGR}^2)\left(\alpha + \frac{\beta}{4} - \frac{\gamma}{2}\right)O_2
\end{aligned}$$

For the n^{th} cycle, the general equation for the reactants and the products becomes:

$$\begin{aligned}
&C_\alpha H_\beta O_\gamma + (1 - R_{EGR})\lambda_o\left(\alpha + \frac{\beta}{4} - \frac{\gamma}{2}\right)(O_2 + 3.76N_2)\\
&+R_{EGR}\begin{bmatrix}\left(1 + R_{EGR} + R_{EGR}^2 + \cdots + R_{EGR}^{n-1}\right)\left(\alpha CO_2 + \frac{\beta}{2}H_2O\right) + \lambda_o\left(\alpha + \frac{\beta}{4} - \frac{\gamma}{2}\right)3.76N_2\\ +\left(\lambda_o - 1 - R_{EGR} - R_{EGR}^2 - \cdots - R_{EGR}^{n-1}\right)\left(\alpha + \frac{\beta}{4} - \frac{\gamma}{2}\right)O_2 \end{bmatrix} \rightarrow \qquad (6.7)\\
&\left(1 + R_{EGR} + R_{EGR}^2 + \cdots + R_{EGR}^{n}\right)\left(\alpha CO_2 + \frac{\beta}{2}H_2O\right) + \lambda_o\left(\alpha + \frac{\beta}{4} - \frac{\gamma}{2}\right)3.76N_2\\
&+\left(\lambda_o - 1 - R_{EGR} - R_{EGR}^2 - \cdots - R_{EGR}^{n}\right)\left(\alpha + \frac{\beta}{4} - \frac{\gamma}{2}\right)O_2
\end{aligned}$$

Combining the fresh air and the recycled concentrations and simplifying, Equation ((6.7) can be written as

$$\begin{aligned}
&C_\alpha H_\beta O_\gamma + \lambda_o\left(\alpha+\frac{\beta}{4}-\frac{\gamma}{2}\right)3.76N_2 + \left(R_{EGR}+R_{EGR}^2+\cdots+R_{EGR}^n\right)\left(\alpha CO_2+\frac{\beta}{2}H_2O\right)\\
&+\left[\lambda_o - R_{EGR}\left(1+R_{EGR}+R_{EGR}^2+\cdots+R_{EGR}^{n-1}\right)\right]\left(\alpha+\frac{\beta}{4}-\frac{\gamma}{2}\right)O_2 \rightarrow\\
&\left(1+R_{EGR}+R_{EGR}^2+\cdots+R_{EGR}^n\right)\left(\alpha CO_2+\frac{\beta}{2}H_2O\right)+\lambda_o\left(\alpha+\frac{\beta}{4}-\frac{\gamma}{2}\right)3.76N_2\\
&+\left[\lambda_o-\left(1+R_{EGR}+R_{EGR}^2+\cdots+R_{EGR}^n\right)\right]\left(\alpha+\frac{\beta}{4}-\frac{\gamma}{2}\right)O_2
\end{aligned} \tag{6.8}$$

The term $1+R_{EGR}+R_{EGR}^2+\cdots+R_{EGR}^n$ can be expressed as a geometric series $\sum_{k=0}^{n} ar^k = ar^0+ar^1+ar^2+\cdots+ar^n$, with the common ratio $r = R_{EGR} \neq 1$ and a scale factor of $a = 1$. Therefore, Equation (6.8) can be expressed as:

$$\begin{aligned}
&C_\alpha H_\beta O_\gamma + \lambda_o\left(\alpha+\frac{\beta}{4}-\frac{\gamma}{2}\right)3.76N_2 + R_{EGR}\left(\frac{1-R_{EGR}{}^n}{1-R_{EGR}}\right)\left(\alpha CO_2+\frac{\beta}{2}H_2O\right)\\
&+\left(\alpha+\frac{\beta}{4}-\frac{\gamma}{2}\right)\left\{\lambda_o - R_{EGR}\left(\frac{1-R_{EGR}{}^n}{1-R_{EGR}}\right)\right\}O_2 \rightarrow\\
&\left(\frac{1-R_{EGR}{}^{n+1}}{1-R_{EGR}}\right)\left(\alpha CO_2+\frac{\beta}{2}H_2O\right)+\lambda_o\left(\alpha+\frac{\beta}{4}-\frac{\gamma}{2}\right)3.76N_2\\
&+\left(\alpha+\frac{\beta}{4}-\frac{\gamma}{2}\right)\left\{\lambda_o-\left(\frac{1-R_{EGR}{}^{n+1}}{1-R_{EGR}}\right)\right\}O_2
\end{aligned} \tag{6.9}$$

Equation (6.9) can be used to track the cycle-by-cycle effect of EGR on the intake and the exhaust species concentrations. Moreover, for steady state concentrations, selecting an n value greater than or equal to 20 was found to provide satisfactory results over a wide range of EGR and λ_o values.

From Equation (6.9), the molar concentrations of the intake species are determined by the following equations:

$$y_{CO_2(\text{int})} = \frac{\alpha R_{EGR}\left(\frac{1-R_{EGR}{}^{n}}{1-R_{EGR}}\right)}{R_{EGR}\left(\alpha+\frac{\beta}{2}\right)\left(\frac{1-R_{EGR}{}^{n}}{1-R_{EGR}}\right)+\left(\alpha+\frac{\beta}{4}-\frac{\gamma}{2}\right)\left\{4.76\lambda_o - R_{EGR}\left(\frac{1-R_{EGR}{}^{n}}{1-R_{EGR}}\right)\right\}} \tag{6.10}$$

$$y_{O_2(\text{int})} = \frac{\left(\alpha+\frac{\beta}{4}-\frac{\gamma}{2}\right)\left\{\lambda_o - R_{EGR}\left(\frac{1-R_{EGR}{}^{n}}{1-R_{EGR}}\right)\right\}}{R_{EGR}\left(\alpha+\frac{\beta}{2}\right)\left(\frac{1-R_{EGR}{}^{n}}{1-R_{EGR}}\right)+\left(\alpha+\frac{\beta}{4}-\frac{\gamma}{2}\right)\left\{4.76\lambda_o - R_{EGR}\left(\frac{1-R_{EGR}{}^{n}}{1-R_{EGR}}\right)\right\}} \tag{6.11}$$

$$y_{H_2O(\text{int})} = \frac{\frac{\beta}{2} R_{EGR}\left(\frac{1-R_{EGR}{}^{n}}{1-R_{EGR}}\right)}{R_{EGR}\left(\alpha+\frac{\beta}{2}\right)\left(\frac{1-R_{EGR}{}^{n}}{1-R_{EGR}}\right)+\left(\alpha+\frac{\beta}{4}-\frac{\gamma}{2}\right)\left\{4.76\lambda_o - R_{EGR}\left(\frac{1-R_{EGR}{}^{n}}{1-R_{EGR}}\right)\right\}} \tag{6.12}$$

$$y_{N_2(\text{int})} = \frac{3.76\lambda_o\left(\alpha+\frac{\beta}{4}-\frac{\gamma}{2}\right)}{R_{EGR}\left(\alpha+\frac{\beta}{2}\right)\left(\frac{1-R_{EGR}{}^{n}}{1-R_{EGR}}\right)+\left(\alpha+\frac{\beta}{4}-\frac{\gamma}{2}\right)\left\{4.76\lambda_o - R_{EGR}\left(\frac{1-R_{EGR}{}^{n}}{1-R_{EGR}}\right)\right\}} \tag{6.13}$$

Similarly, the molar concentrations of the exhaust species are:

$$y_{CO_2(\text{exh})} = \frac{\alpha\left(\frac{1-R_{EGR}{}^{n+1}}{1-R_{EGR}}\right)}{\left(\frac{1-R_{EGR}{}^{n+1}}{1-R_{EGR}}\right)\left(\alpha+\frac{\beta}{2}\right)+\left(\alpha+\frac{\beta}{4}-\frac{\gamma}{2}\right)\left\{4.76\lambda_o - \left(\frac{1-R_{EGR}{}^{n+1}}{1-R_{EGR}}\right)\right\}} \tag{6.14}$$

$$y_{O_2(\text{exh})} = \frac{\left(\alpha+\frac{\beta}{4}-\frac{\gamma}{2}\right)\left\{\lambda_o - \left(\frac{1-R_{EGR}{}^{n+1}}{1-R_{EGR}}\right)\right\}}{\left(\frac{1-R_{EGR}{}^{n+1}}{1-R_{EGR}}\right)\left(\alpha+\frac{\beta}{2}\right)+\left(\alpha+\frac{\beta}{4}-\frac{\gamma}{2}\right)\left\{4.76\lambda_o - \left(\frac{1-R_{EGR}{}^{n+1}}{1-R_{EGR}}\right)\right\}} \tag{6.15}$$

$$y_{H_2O(\text{exh})} = \frac{\dfrac{\beta}{2}\left(\dfrac{1-R_{EGR}{}^{n+1}}{1-R_{EGR}}\right)}{\left(\dfrac{1-R_{EGR}{}^{n+1}}{1-R_{EGR}}\right)\left(\alpha+\dfrac{\beta}{2}\right)+\left(\alpha+\dfrac{\beta}{4}-\dfrac{\gamma}{2}\right)\left\{4.76\lambda_o-\left(\dfrac{1-R_{EGR}{}^{n+1}}{1-R_{EGR}}\right)\right\}} \tag{6.16}$$

$$y_{H_2O(\text{exh})} = \frac{3.76\lambda_o\left(\alpha+\dfrac{\beta}{4}-\dfrac{\gamma}{2}\right)}{\left(\dfrac{1-R_{EGR}{}^{n+1}}{1-R_{EGR}}\right)\left(\alpha+\dfrac{\beta}{2}\right)+\left(\alpha+\dfrac{\beta}{4}-\dfrac{\gamma}{2}\right)\left\{4.76\lambda_o-\left(\dfrac{1-R_{EGR}{}^{n+1}}{1-R_{EGR}}\right)\right\}} \tag{6.17}$$

The results for a calculation using Equations (6.9) to (6.17) for the intake and exhaust concentrations are shown in Figure 6.3 and Figure 6.4. Cycle # 0 represents the concentrations obtained without the application of EGR. When EGR is applied and the exhaust gases are recycled back into the intake, the concentrations obtained at the end of Cycle # 1 are CO_2: 2.2%, O_2: 17.5%, H_2O: 1.9%, N_2: 78.3% for the intake, and CO_2: 5.1%, O_2: 13.2%, H_2O: 4.4%, N_2: 77.4% for the exhaust. It should be noted that these are not the steady state concentrations because of the application of EGR. The recycling of the exhaust gases after each cycle results in the concentrations reaching a steady state value by Cycle # 19 in this case; the concentrations being CO_2: 9.7%, O_2: 6.2%, H_2O: 8.4%, N_2: 75.8% for the intake, and CO_2: 12.4%, O_2: 2%, H_2O: 10.7%, N_2: 74.9% for the exhaust. A summary of the results for O_2 and CO_2 concentrations at different cycles is provided in Table 6.1.

Table 6.1: Comparison of O_2 & CO_2 Concentrations After EGR Application

Cycle #	Intake O_2 [%]	Intake CO_2 [%]	Exhaust O_2 [%]	Exhaust CO_2 [%]
0	20.9	0	16.5	2.9
1	17.5	2.2	13.2	5.1
5	10.1	7.1	5.9	9.9
20	6.14	9.69	1.96	12.43
30	6.07	9.73	1.89	12.48

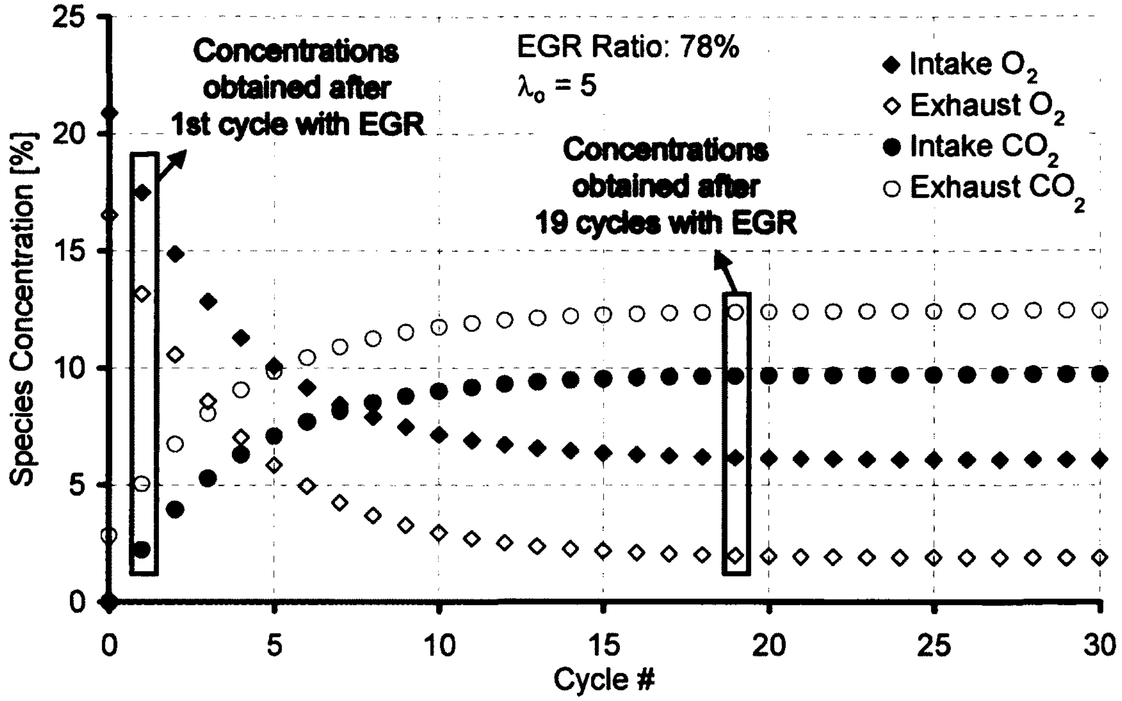

Figure 6.3: History of O_2 & CO_2 Concentrations in the Intake & Exhaust after EGR Application

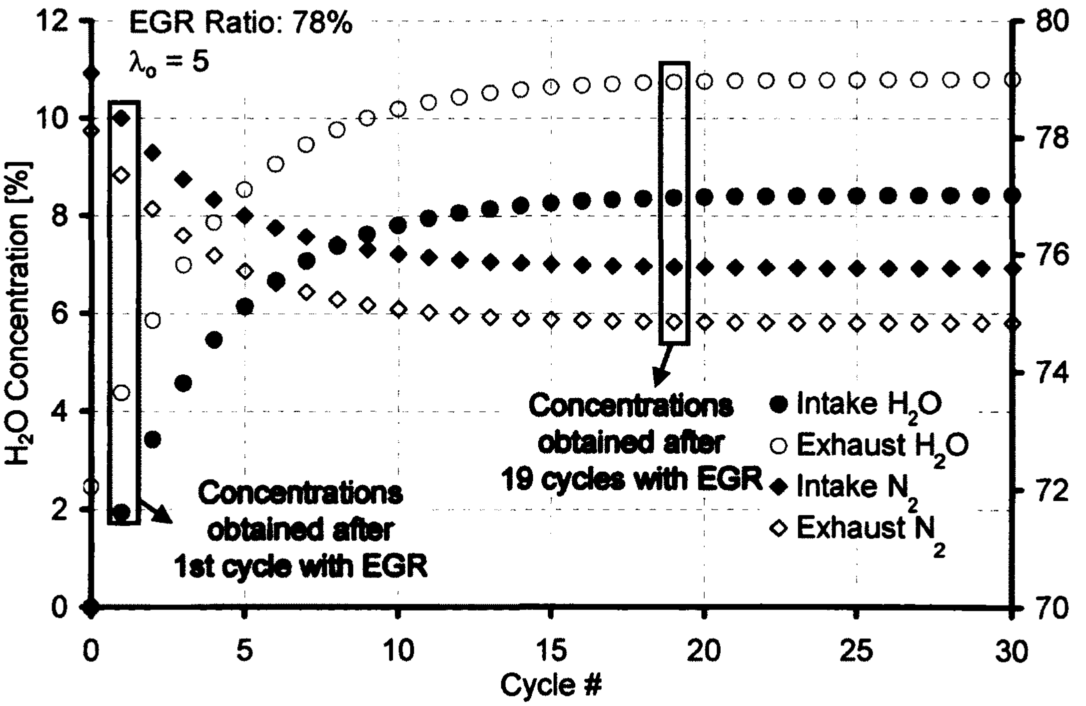

Figure 6.4: History of H_2O & N_2 Concentrations in the Intake & Exhaust after EGR Application

EGR is an effective technique to lower the combustion temperatures because of its thermal, dilution and chemical effects [4,23], and is one of the key enablers for LTC cycles. The thermal effect of EGR is attributed to the increased heat capacity of the cylinder charge because of the higher specific heat capacity of recirculated CO_2 and H_2O compared with O_2 and N_2. This results in lowered in-cylinder peak compression and thus, lower combustion temperatures.

The dilution effect describes the reduction in the intake O_2 concentration whose main consequence is the deceleration of the mixing between O_2 and fuel. This results in the extension of the flame region and therefore the gas quantity that absorbs the released heat is increased, subsequently leading to a lower flame temperature. It is noted that since the oxygen is replaced with inert gases, one consequence of the charge dilution is the reduction of local temperatures which can also be considered as a local thermal effect. Furthermore, the dilution effect contributes to the reduction of the oxygen partial pressure and thus effects the kinetics of the elementary NO formation reactions.

The recirculated H_2O and CO_2 are dissociated during combustion. The dissociation of H_2O and CO_2, constituting the chemical effect, is believed to affect the combustion process and the NOx formation. In particular, the endothermic dissociation of H_2O results in a decrease of the flame temperature.

To identify the effect of EGR on the air/fuel ratios, two different types of air excess ratios have been defined as shown in Figure 6.5. At any given EGR level, the fresh air lambda (λ) represents the air/fuel ratio based upon the amount of fresh air entering the engine cylinder. If EGR is changed, the fresh air in the intake reduces and so the values of λ also decreases (towards 1). However, since the diesel engines are inherently lean-burn systems, thus the re-circulated gases will also contain some oxygen. As such, λ is not a true representation of the in-cylinder conditions but is commonly used because of the availability of the MAF sensors in almost all production diesel engines. The in-cylinder lambda (λ_a) represents the actual air/fuel ratio existing inside the cylinder and accounts for the exhaust oxygen that has been added to the intake stream through the EGR. A special case of λ is also defined as λ_o which represents the fresh air/fuel ratio without EGR.

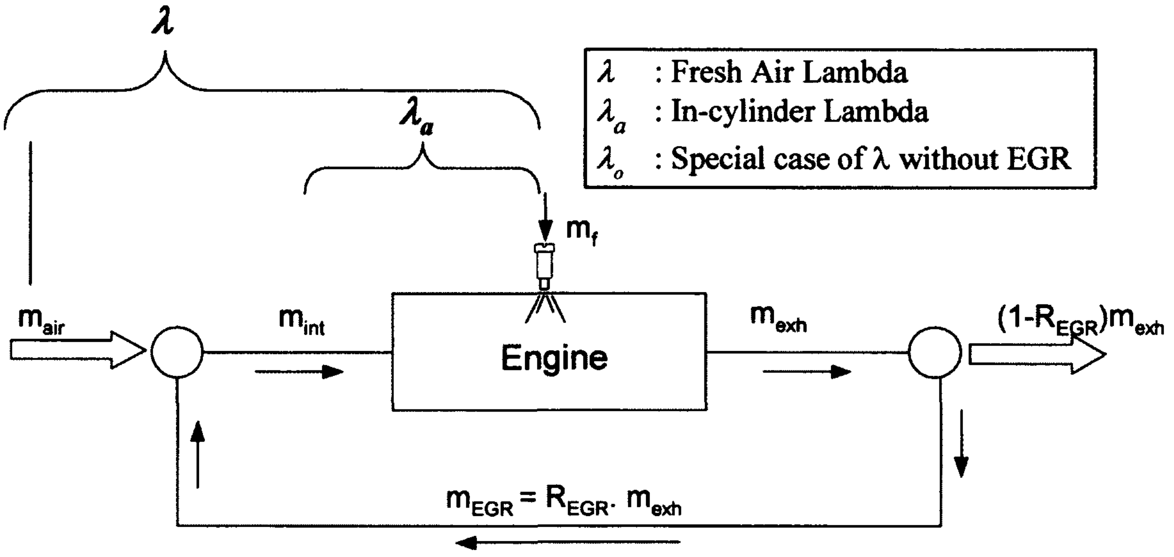

Figure 6.5: Defining the Air Excess Ratios with EGR

Based on the above description, some important correlations can be developed from the molar analysis. Although these correlations are approximate, yet these provide a simple method of estimating the operating conditions of the engine at any EGR level.

Without EGR, the air excess ratios λ and λ_a should be the same and equal to λ_o. As EGR is applied, the fresh air lambda λ would decrease linearly with the EGR rate. From Equation (6.7), it can be seen that the fresh air part of the intake, i.e., the oxygen decreases by the amount $(1-R_{EGR})$ at any given EGR level. Therefore, the fresh air lambda λ can be expressed as:

$$\lambda = \lambda_o(1-R_{EGR}) \tag{6.18}$$

In case of the in-cylinder lambda λ_a, the oxygen contained in the EGR will result in comparatively more oxygen available in the cylinder and as such, the in-cylinder lambda would be leaner than the fresh air lambda at any given EGR level. It should also be noted that when λ_a attains stoichiometric condition, there would be no oxygen in the exhaust to recirculate. Accordingly, $\lambda_a = \lambda = 1$ at stoichiometric conditions.

From Equation (6.7), it can be seen that the λ_a can be expressed by the contribution of both the fresh air and the EGR streams such that:

$$\lambda_a = \underbrace{\lambda_o\left(1 - R_{EGR}\right)}_{\text{Fresh Air}} + \underbrace{R_{EGR}\left(\lambda_o - 1 - R_{EGR} - R_{EGR}^2 - \cdots - R_{EGR}^{n-1}\right)}_{\text{EGR}}$$

Simplifying, the final equation for λ_a can be written as:

$$\lambda_a = \lambda_o - R_{EGR}\left(\frac{1 - R_{EGR}{}^n}{1 - R_{EGR}}\right) \tag{6.19}$$

which is essentially the same as the coefficient of the intake oxygen term in Equation (6.9).

6.2.2. Formulation of the EGR Analysis Technique

To develop a deeper understanding of the efficacy of EGR and to look at ways for formulating a control strategy, a zero-dimensional EGR simulation program was written so that the intake and exhaust concentration could be calculated based on the mass basis. The residual mass fraction was also included so that the effect of increased residuals because of higher exhaust back-pressure could be analyzed.

The flowchart for implementation of zero-dimensional EGR simulations is shown in Figure 6.6. The implementation of the EGR simulation was done in the 'C' programming environment. The assumptions for the calculation are as follows:

- The moles of the in-cylinder charge are fixed, based on the initial conditions that include the intake pressure and temperature, the engine geometric constraints, volumetric efficiency η_{vol}, and the engine speed.

- The EGR stream is assumed to be fully cooled and at the same temperature as the fresh air part of the intake charge.

- The EGR ratio is taken as the mass fraction of the exhaust. Therefore, the quantity of the recycled gases is calculated by multiplying the EGR ratio with the mass of the exhaust (mass of intake charge + mass of injected fuel).

- The compositions of the intake and the residual portions of the cylinder charge are updated at each iteration until a stable exhaust composition is attained.

- The air-excess ratios (λ_a, λ) are obtained by first calculating the air/fuel ratio on a mass basis and then dividing it with the mass-based stoichiometric air/fuel ratio for the diesel fuel.

- The output is written as a tab-separated text file at the termination of the simulation.

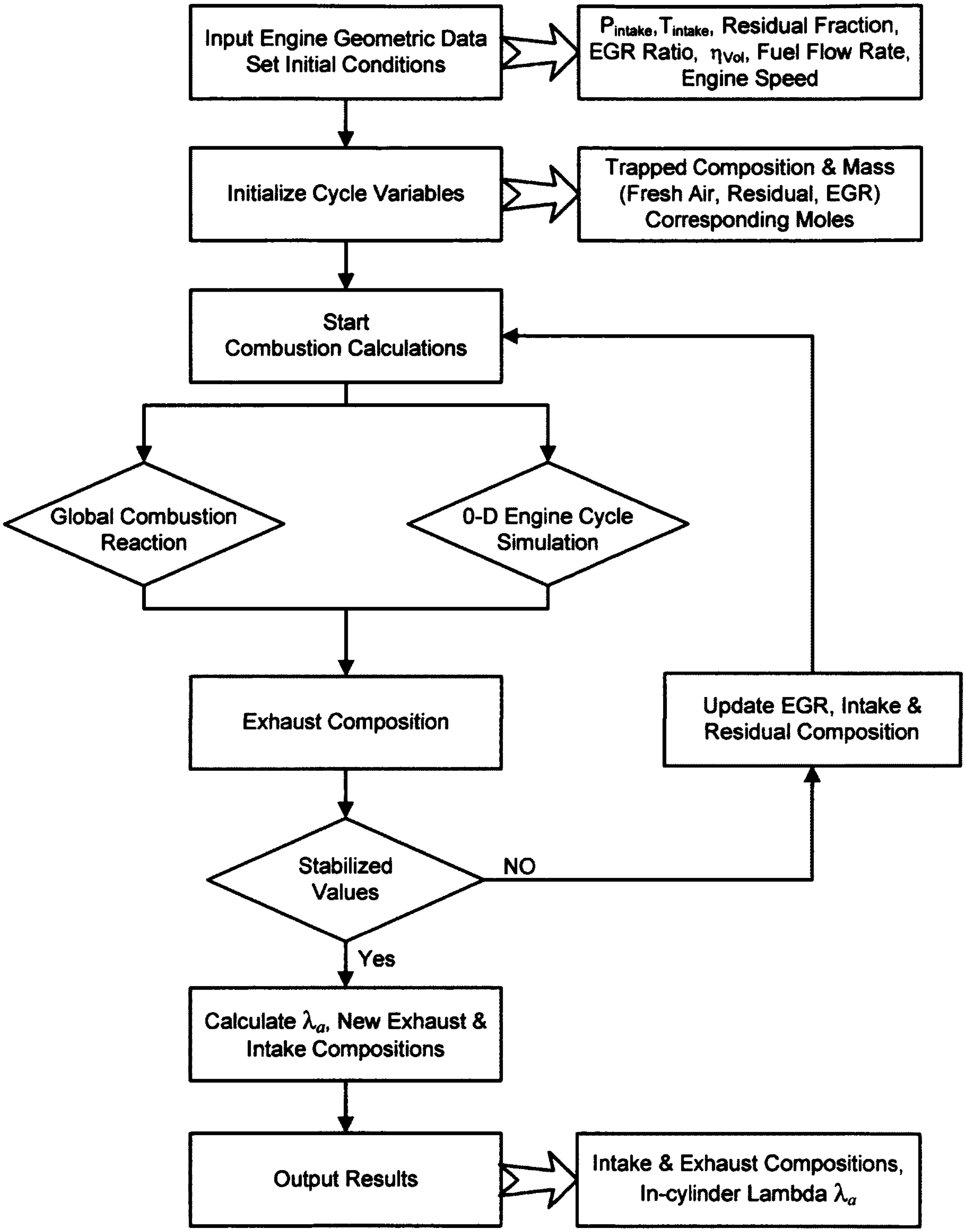

Figure 6.6: Flowchart for the Implementation of Zero-Dimensional EGR Simulation

The difference between the two definitions of lambda, i.e. λ_a and λ calculated with the 0-D simulation is highlighted in Figure 6.7. At low loads, the EGR contains a significant amount of oxygen. Therefore, the difference between the in-cylinder lambda and the fresh-air lambda is significant. As the engine load increases, the difference between the two values reduces. It can be seen that as the exhaust oxygen tends to approach a very low value, the contribution of the EGR-borne oxygen to the intake is diminished and the two lambda values tend to converge as the EGR pushes the in-cylinder charge towards stoichiometric operation.

Figure 6.7 also shows similar trends obtained from the experimental investigations with diesel fuel using the MAF-based EGR rate up to 55%. The results were in good agreement with the analysis. Because the combustion inefficiency in diesel HTC mode is normally <2% [4], the assumption that the diesel engine exhaust gas is composed of N_2, CO_2, H_2O and O_2 only is thermodynamically reasonable.

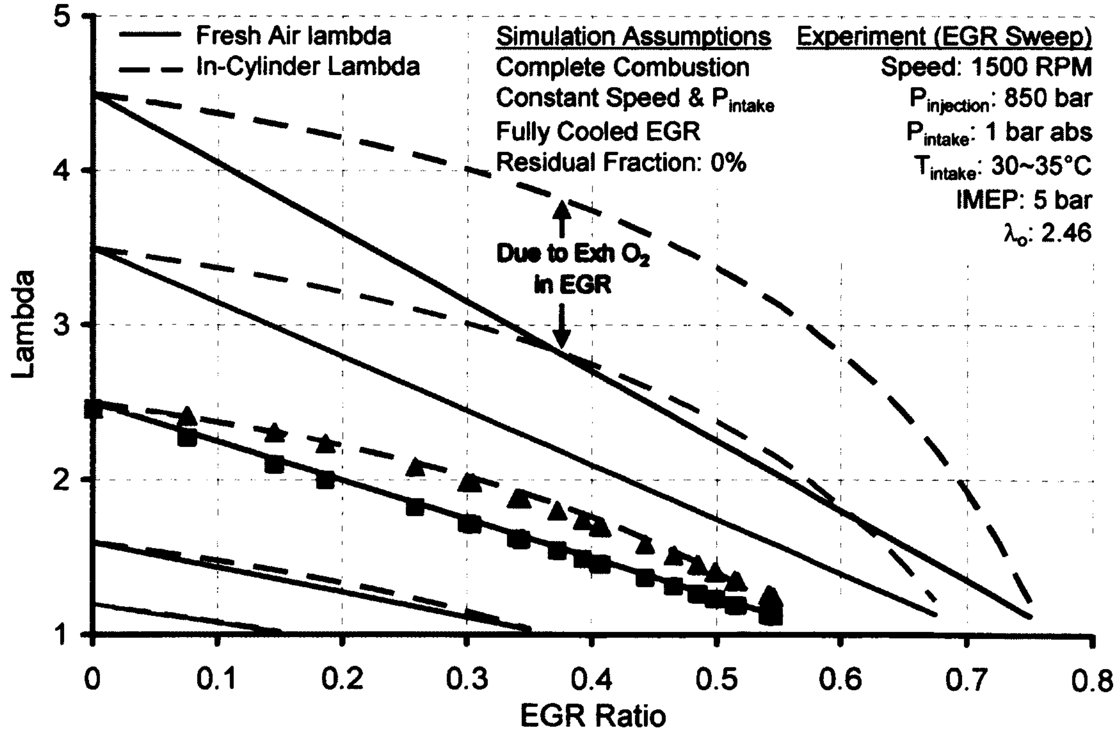

Figure 6.7: Effect of EGR on the Air Excess Ratios

A comparison of the molar analysis and the 0-D EGR simulation at two different λ_o is shown in Figure 6.8. The residual fraction was set equal to zero to make a fair comparison. It was observed that the general trend of the λ_a variation with EGR was captured by the molar analysis. However, the magnitudes were predicted to be slightly higher compared to the 0-D simulation results. This is because with molar analysis, the intake moles are not constant at each iteration and increase slightly during the calculation at each cycle repetition.

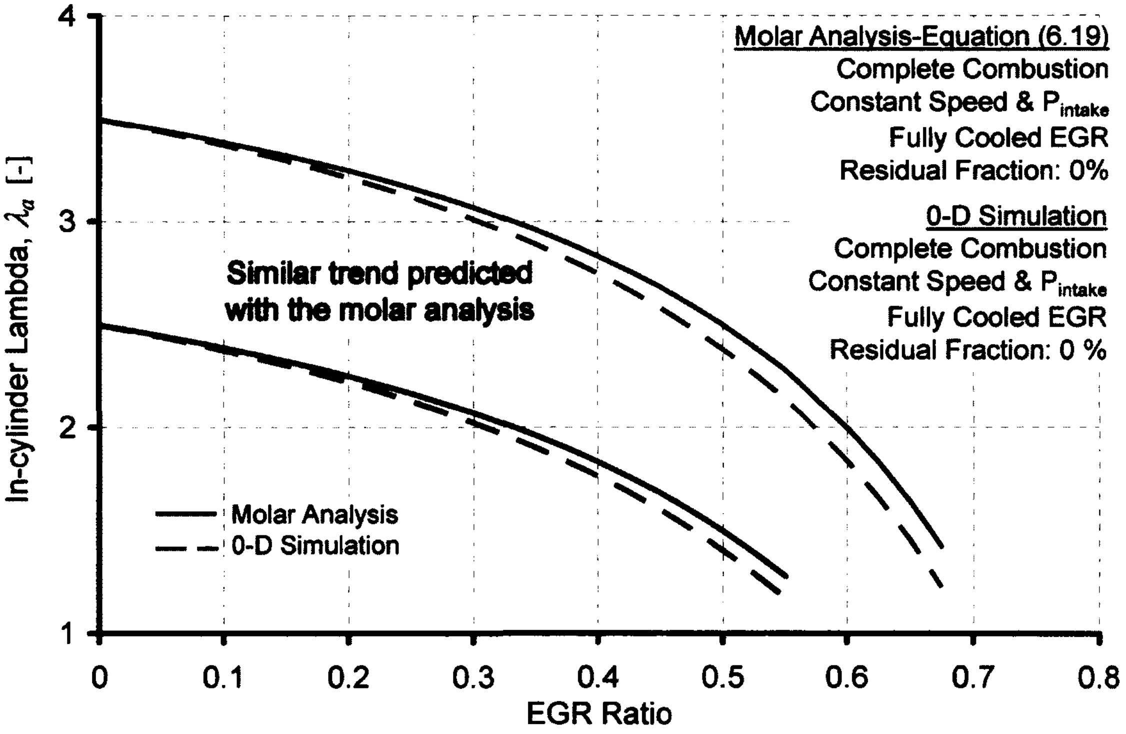

Figure 6.8: Comparison of the Molar Analysis & 0-D EGR Simulation

A higher exhaust backpressure should increase the amount of residuals that remain in the cylinder at the end of the exhaust stroke. This in turn reduces the amount of the fresh intake charge entering the cylinder. The effect of increasing the exhaust back pressure was analyzed with the 0-D simulation by changing the residual fraction at two different intake pressure levels as shown in Figure 6.9. As the proportion of the fresh intake is reduced, the fuel strength of the cylinder charge increases (become slightly rich) for the same fuelling. Therefore, the effective in-cylinder air excess ratio is reduced across the EGR range.

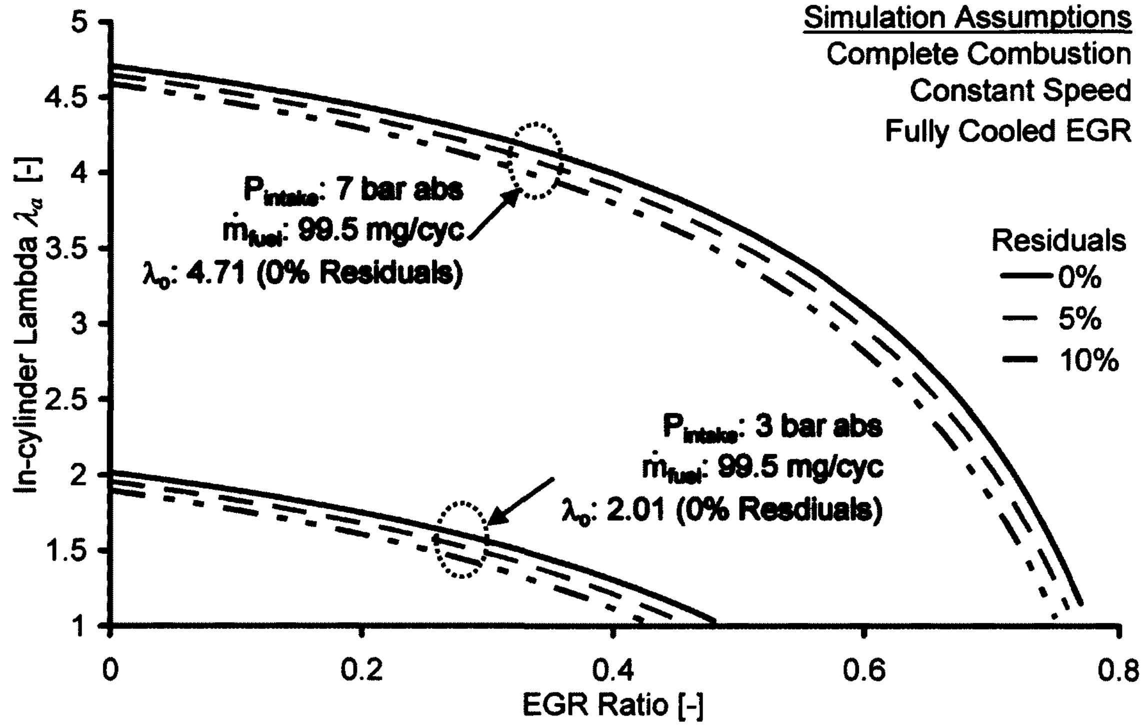

Figure 6.9: Effect of Residuals on the In-cylinder Lambda

6.2.3. Effect of Engine Load

The dilution and the heat capacity enhancement are strongly affected by the engine load. As EGR is increased, the strength of the in-cylinder charge increases but the relationship is not linear. As shown in Figure 6.10, the application of 60% EGR at low loads ($\lambda_o = 5$) changes the in-cylinder lambda from 5 to about 3.4. However, further increasing the EGR from 60 to 80% only, results in the in-cylinder lambda reducing by about '2' units (from 3.4 to 1.4). At higher engine loads without EGR, the exhaust already contains less oxygen. The application of a low EGR level is also sufficient to push the exhaust oxygen towards zero, thus limiting the application of EGR at high load conditions.

Therefore, the efficacy of EGR needs to be quantified or standardized so that the load dependency of EGR can be adequately integrated in the control system.

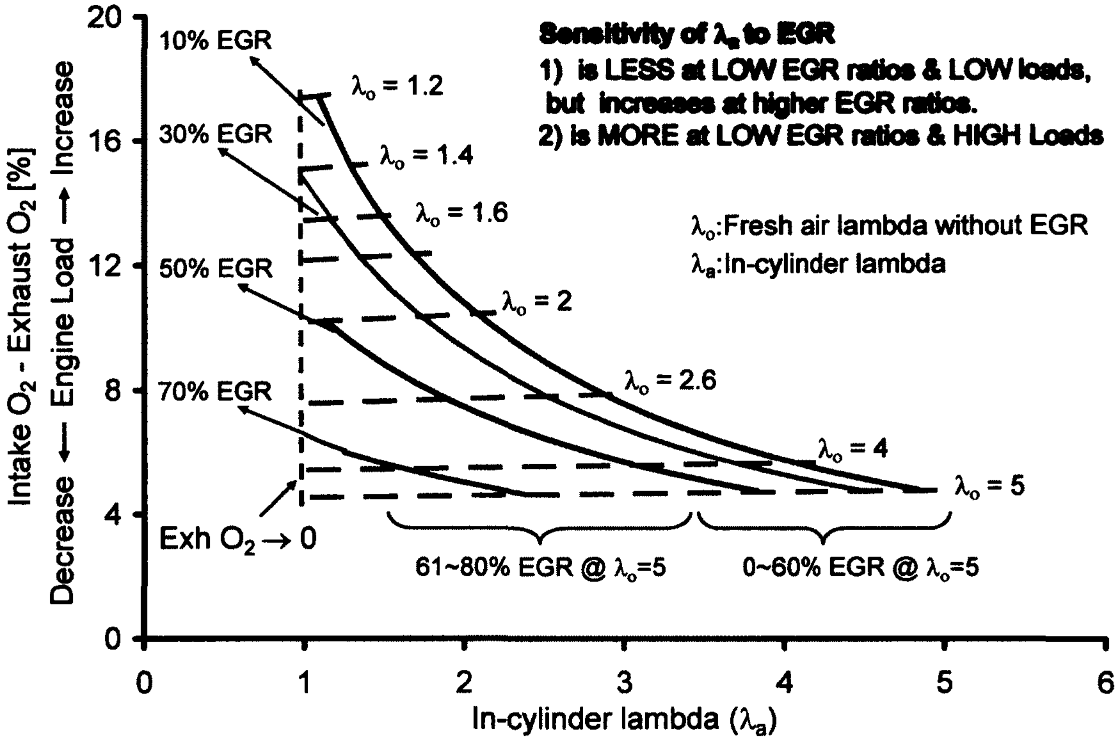

Figure 6.10: Effect of Engine Load on Efficacy of EGR

6.2.4. Effect of Boost Pressure

Increasing the boost pressure at a given engine load (constant fuelling) has a direct effect on the efficacy of the EGR. To understand the interaction between the boost and EGR, the simulations were run with an initial air/fuel ratio of 30:1 without EGR at 3 bar abs intake pressure. The effects of increasing the EGR and boost pressure were then studied while keeping the fuelling constant. The results in terms of the in-cylinder lambda λ_a and the fresh lambda λ are shown in Figure 6.11 and Figure 6.12 respectively. The solid lines represent lines of constant EGR while the broken lines indicate a constant intake pressure.

If the EGR is held constant while the boost pressure is increased, the cylinder charge becomes leaner as more fresh air is forced into the cylinder for the same injected fuel. This increases the intake oxygen concentration and therefore, reduces the effectiveness of the EGR as marked in the figures as Path (1). Additionally, the higher O_2 concentration with the increased boost allows higher levels of EGR to be employed, therefore extending the EGR application range. Conversely, to attain the same intake O_2 concentration with higher boost, higher levels of EGR need to be employed as indicated the Path (2).

The results in these figures again highlight the difference between basing the calculations on the actual in-cylinder conditions or on the fresh-air contribution to the intake charge only. The fresh-air air/fuel ratio indicates a comparatively richer operation than the actual in-cylinder conditions. It is noted that the fresh-air based metrics are generally used because of the availability of the mass-air-flow (MAF) sensors in nearly all production vehicles.

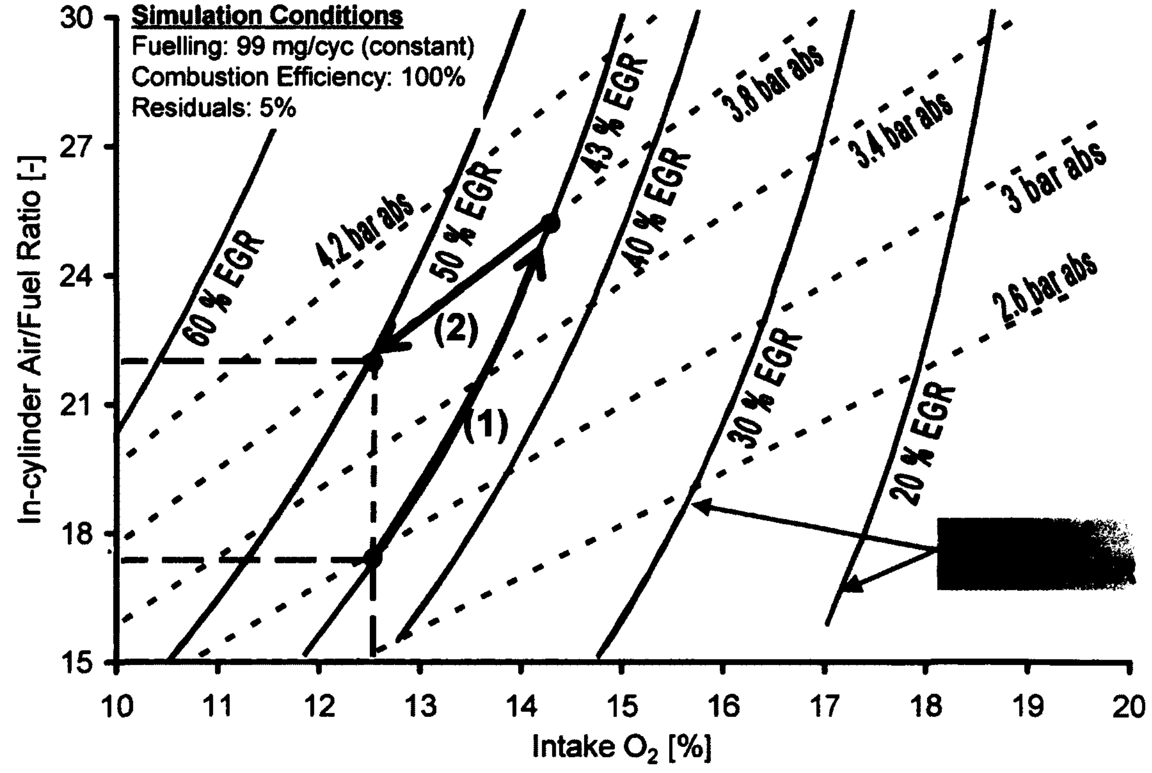

Figure 6.11: Understanding the Boost-EGR Interaction (In-cylinder Lambda)

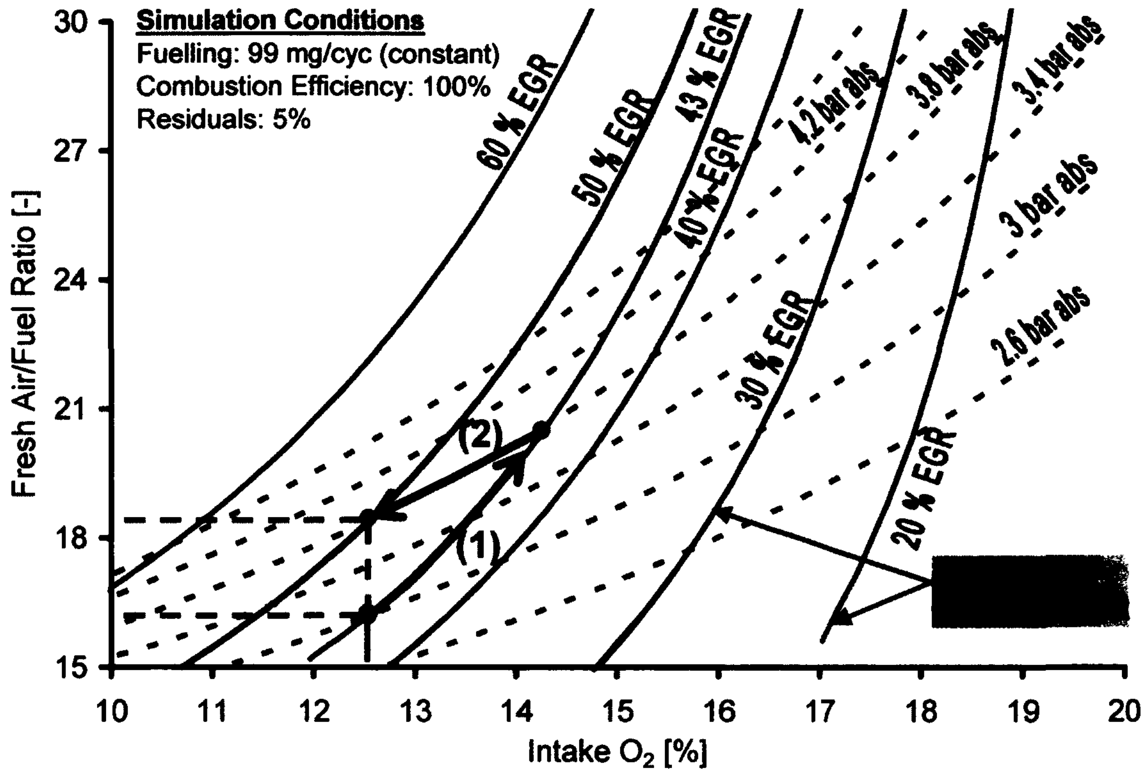

Figure 6.12: Understanding the Boost-EGR Interaction (Fresh-air Lambda)

6.2.5. Intake Oxygen Concentration

Based upon the discussion in the previous section, intake O_2 is an effective indicator of the intake charge dilution with EGR. Therefore, while analyzing the effect of variations in the boost pressure, it is beneficial to plot all the results against the intake O_2 concentration so that a fair comparison can be made between the results.

The LTC results shown in Chapter 7 indicate that the combustion enters the LTC cycles once the intake O_2 concentration is reduced to approximately 10~14%, over a wide range of engine operating conditions. Therefore, using intake oxygen as a representation of the EGR level, the effect of boost and load on the in-cylinder lambda was incorporated into a single map as shown in Figure 6.13. A similar map for the fresh air lambda is given in Figure 6.14 .

The effect of increased boost is to make the cylinder charge leaner at any given fuelling and to increase the intake O_2. Therefore, the effect can be visualized on the map as an increase in the lambda value, indicated by the path (1). The increase in the intake O_2 can then be readjusted by increasing the EGR, indicated by the path (2). From a control point of view, this approach is not feasible for LTC cycles since the increase in the boost pressure can cause the combustion to move out of the LTC regime. The desired path during LTC cycles is indicated by the path marked with an asterisk (*) which would require the boost and EGR to be adjusted simultaneously to maintain a constant level of O_2 in the intake.

From the figures, it is evident that the fuel strength of the cylinder charge (λ_a or λ) retains a higher value (leaner) even after the intake O_2 is adjusted back to its original value with higher EGR. Thus, the effect of boost is not only to extend the EGR range but also to move the combustion to leaner operating conditions. An implication of the leaner charge is the possibility of increasing the fuelling to make use of the available oxygen in the intake charge.

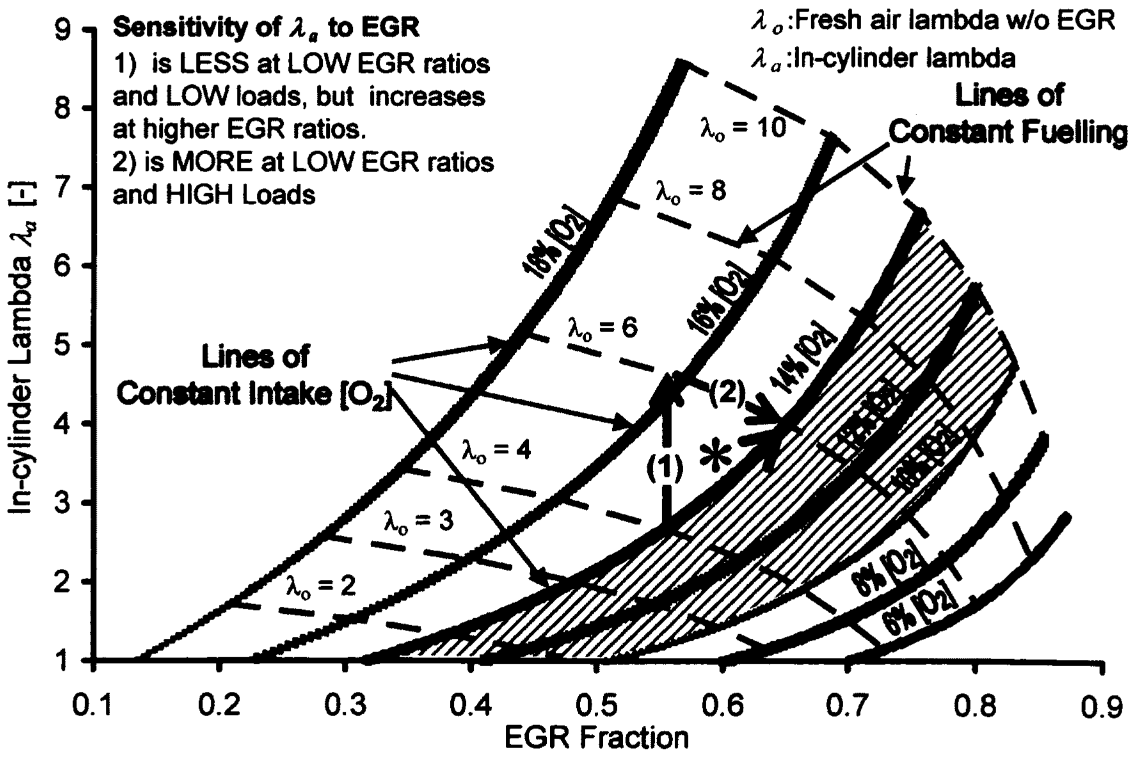

Figure 6.13: Theoretical Operating Map for LTC Cycles based on λ_a

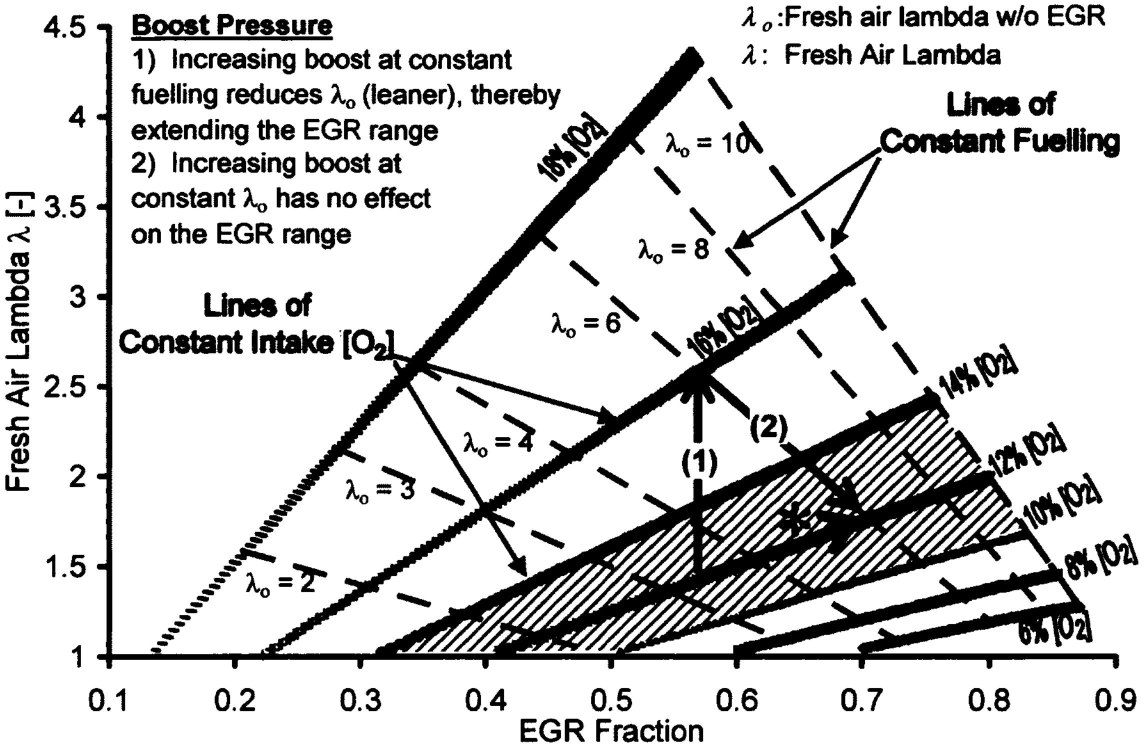

Figure 6.14: Theoretical Operating Map for LTC Cycles based on λ

6.3. EGR Characterization

The analyses presented so far indicate the effectiveness as well as the complexity of EGR. EGR is one of the key techniques for enabling the LTC cycles. However, the use of heavy EGR during LTC cycles escalates the consecutive cyclic variations of the cylinder charge in terms of temperature, pressure and composition. This problem is further compounded by the fact that the burning of a homogeneous charge that is lean and/or EGR-diluted is inherently close to the flame-out limits. Therefore, the LTC cycles for diesel engines are bounded within narrow operating pathways and a small disturbance in the operating conditions normally results in a sharp deterioration in exhaust emissions, fuel efficiency, combustion noise, and operational stability (presented in detail in Chapter 7). Therefore, a robust feedback on the EGR and the quantification of the EGR effects on the LTC combustion are deemed essential.

To develop such a feedback for the control of the LTC combustion, a number of parameters were defined based on the oxygen concentrations in the intake and exhaust systems (Figure 6.15).

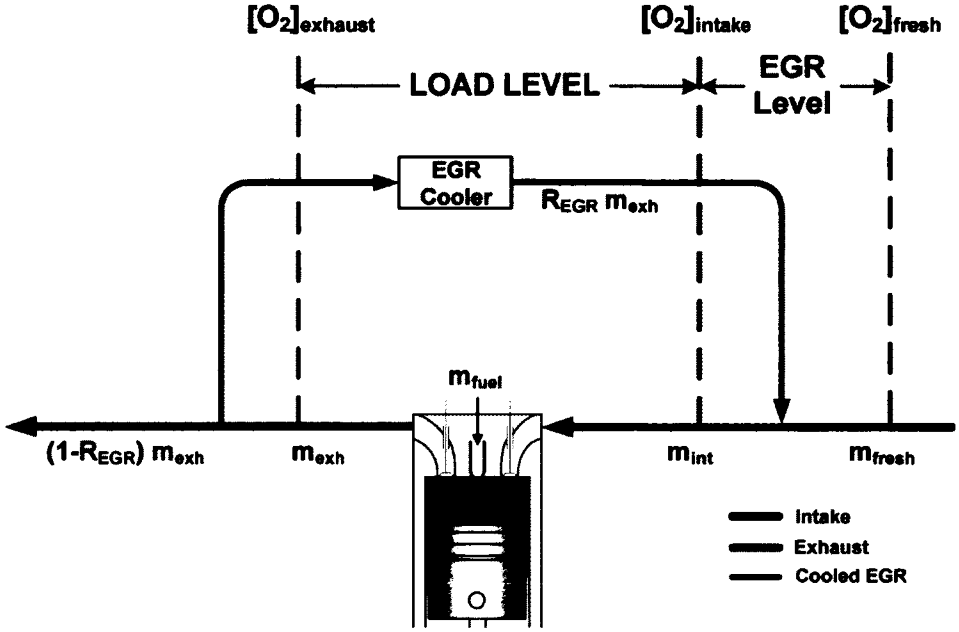

Figure 6.15: Defining New Parameters for EGR Feedback

One of the main consequence of the EGR is the departure of the intake oxygen concentration from that of the fresh air (~20.9%). Therefore, an 'EGR level' to account for the intake concentration deviation from that of the fresh air was defined as:

$$\text{EGR Level} = [O_2]_{fresh} - [O_2]_{intake} \tag{6.20}$$

Furthermore, the departure of the intake oxygen concentration from that of the fresh air at any EGR level is dependent on the engine load. At low loads, the difference between the intake and the exhaust oxygen concentrations is less, and the difference progressively increases as the fuelling and thus the load is increased. Therefore, the engine 'load level' was defined in terms of the oxygen consumption during the combustion process as:

$$\text{Load Level} = [O_2]_{intake} - [O_2]_{exhaust} \tag{6.21}$$

Since the effectiveness of EGR at any given level is also dependent on the engine load, a new 'Charge Dilution Index' (CDI) was created to normalize the effect of the engine load so that the CDI at any EGR level should be the same across the load range. Therefore, CDI was defined as:

$$\text{Charge Dilution Index} = \frac{\text{EGR Level}}{\text{Load Level}} = \frac{[O_2]_{fresh} - [O_2]_{intake}}{[O_2]_{intake} - [O_2]_{exhaust}} \tag{6.22}$$

Simulation were run to map the CDI for a wide range of engine operating conditions (P_{intake}: 1 to 5 bar abs, λ_o :1.1 to 10, EGR: 0 to 77%) and the results were plotted against the EGR as shown in Figure 6.16. The CDI is a representation of the EGR independent of the engine load and the boost pressure and its value ranges from 0 to 3.5 for 0 to 77% EGR. Empirical data from a vast array of engine operating conditions was used to calculate the CDI and showed a good agreement with the simulated CDI.

The CDI could therefore be used to estimate the EGR at any engine operating condition. The simulated data was curve-fitted to obtain the following two correlations:

$$\begin{gathered} EGR\ Fraction = 0.456CDI^2 + 0.891CDI + 0.00433 \\ for\ \ 0 < CDI < 0.67 \end{gathered} \tag{6.23}$$

$$\begin{gathered} EGR\ Fraction = 0.0159CDI^3 - 0.142CDI^2 + 0.486CDI + 0.138 \\ for\ 0.67 \le CDI < 3.5 \end{gathered} \tag{6.24}$$

In a research laboratory environment, a single polynomial of order 5 or 6 can also have been used since the available computational resources are significantly more as compared to those available in production vehicles. However, a lower order polynomial requiring less computational resources is generally preferred by the automotive industry because the computational resources of the production engine control units are usually limited (cost being the main factor). A lower order algorithm can readily be applied by the industry without major hardware modifications. Therefore, throughout this research work, the effort was to minimize the computational complexity of the proposed control algorithms while maintaining a sufficient level of accuracy.

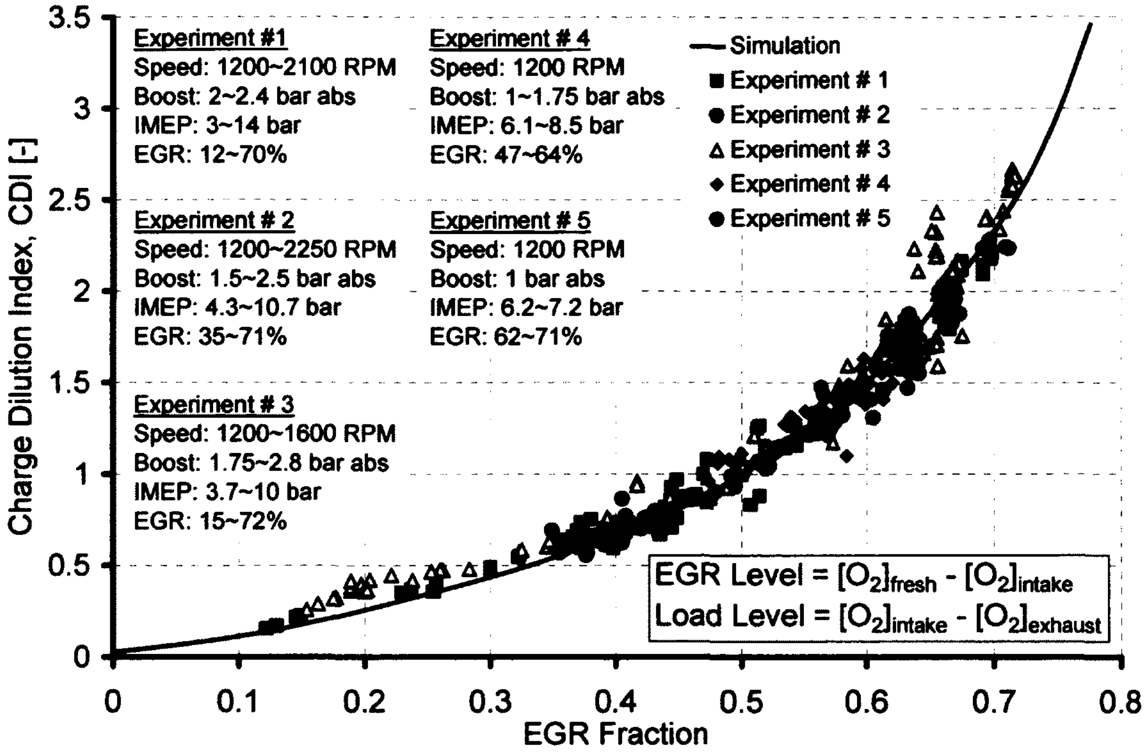

Figure 6.16: Defining the Charge Dilution Index

The oxygen concentration in the intake can be assumed to represent the total oxygen utilization potential available during the combustion process. The exhaust oxygen concentration can then be taken as a measure of the potential that has been wasted or not utilized for a given intake oxygen concentration. A low exhaust oxygen concentration therefore signifies a high utilization of the available potential. Since the oxygen utilization is also a representation of the load level, the 'oxygen utilization' was quantified in terms of the load level, and defined using the exhaust and intake oxygen concentrations as:

$$\text{Oxygen Utilization} = 1 - \frac{[O_2]_{exhaust}}{[O_2]_{intake}} = \frac{Load\ Level}{[O_2]_{intake}} \tag{6.25}$$

The simulated 'oxygen utilization' was plotted against the in-cylinder lambda as shown in Figure 6.17. The simulation showed that the calculated oxygen utilization for different operating conditions collapsed into a single curve. Therefore, the oxygen utilization can be used to provide a direct estimate of the in-cylinder lambda λ_a. The empirical data plotted over the simulation result showed reasonable agreement with the simulated results. The dispersion seen in the empirical data can be partly due to the transient operation data where the fuel flow measurement is not accurate; which in turn affects the in-cylinder lambda calculation.

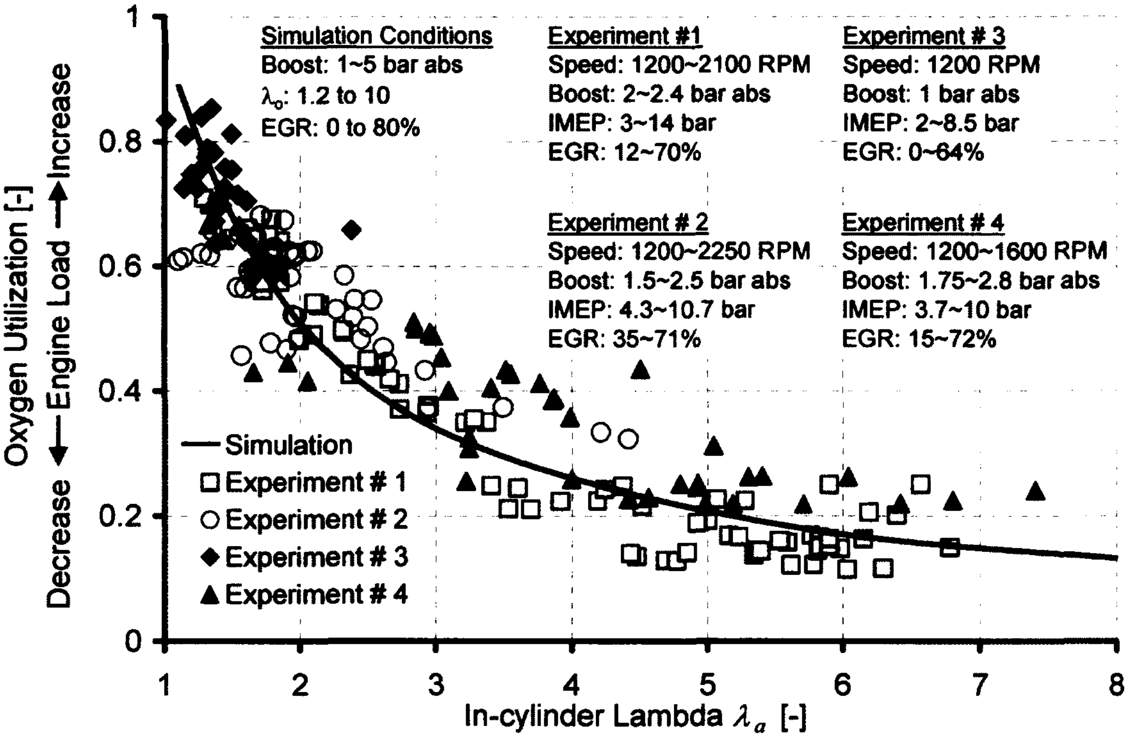

Figure 6.17: Oxygen Utilization as a function of In-cylinder Lambda

To estimate the fresh air lambda λ, it was found that the exhaust oxygen concentration alone was sufficient to quantify the fresh air lambda independent of the engine load or boost pressure as shown in Figure 6.18. Since the amount of fresh air reduces linearly with the increasing EGR, which in turn modifies the exhaust oxygen, the change in the fresh air lambda follows the trend observed in the exhaust oxygen. The mathematical expression for the λ-exhaust O_2 relationship is included in the next section.

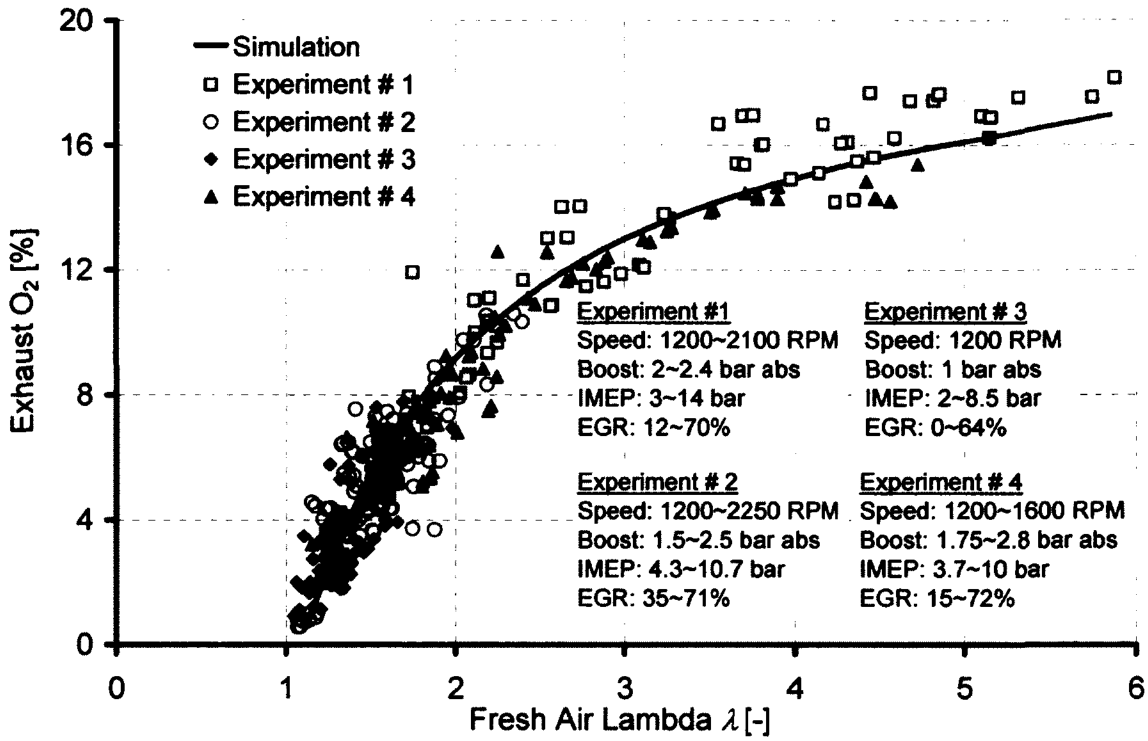

Figure 6.18: Exhaust Oxygen as a function of the Fresh Air Lambda

All the above figures showed that the experimental data from a large pool of tests done at different operating conditions was in good agreement with the simulated data. Therefore, by using the parameters as defined above, it should be possible to estimate the engine operating conditions such as the in-cylinder lambda, the intake and exhaust oxygen concentrations, and the EGR at any engine load or boost pressure.

6.4. Two-Lambda Sensor Approach

For the implementation of the EGR analysis, a two-lambda sensor approach was devised, with one sensor installed in the intake and the other in the exhaust. The lambda sensors were the heated wide-band type made by Bosch (model no: LSU 4.9) that enabled the air excess ratio to be determined from near-stoichiometric to ∞. These sensors also required a special controller for operation. The main specifications of the sensors are given in Table 6.2 [120].

Table 6.2: Wide-band Lambda Sensor Specifications

Type	Zirconia (ZrO_2)-based sensor with current-limiting dual-oxygen pump cells and an integrated heater
Measuring Range	λ: 0.65 to Air
Accuracy	±0.1 at λ>1
Response Time	~500 ms
Operating Pressure	Continuous Operation: < 2.5 bar abs Transient Operation: < 4 bar abs
Control	Tech Edge 3H1 Dual-channel programmable controller with analog signal outputs

The typical output of the lambda sensor is in terms of the fresh air lambda λ and is related to the exhaust oxygen concentration as shown in Figure 6.19. The correlation given by Bosch for the λ-to-Exhaust O_2 conversion is also displayed in the figure. This expression is for a hydrogen-to-carbon $\left(H/C\right)$ mass ratio of 2.

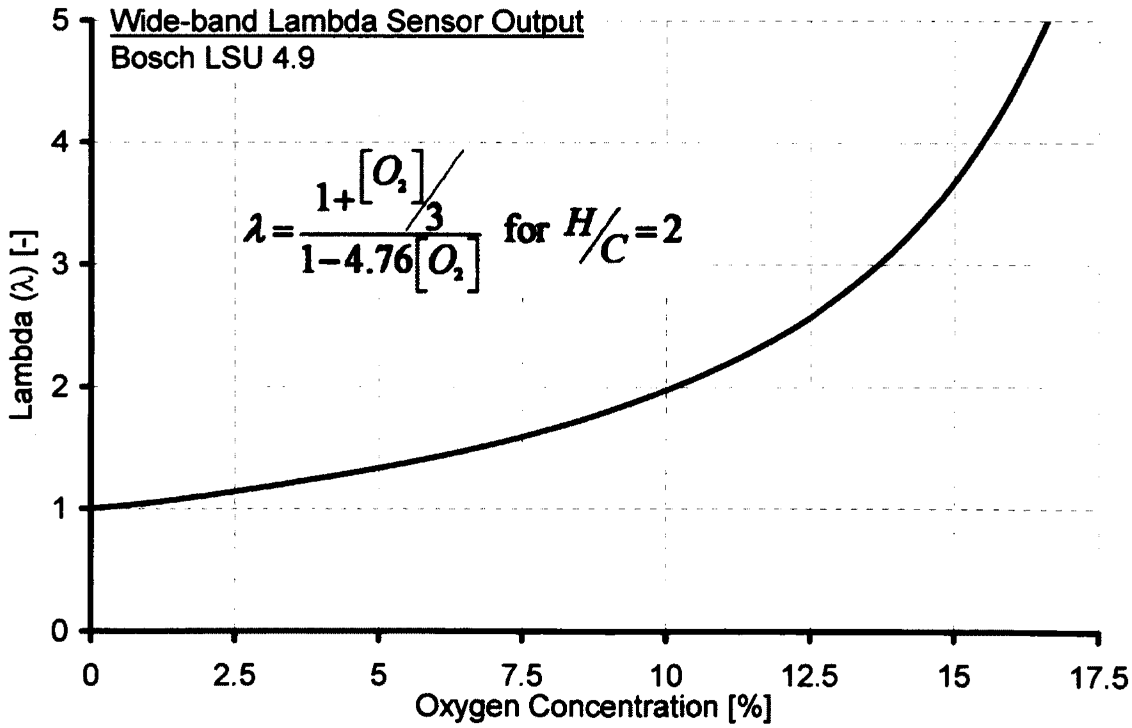

Figure 6.19: Typical Wide-band Lambda Sensor Output at 1 bar Absolute Pressure

The fuel used throughout this research had a $\left({}^{H}\!/\!_{C}\right)$ ratio of 1.88 (Table 4.6). Therefore, the relationship between lambda and the O_2 concentration was corrected as follows:

From Equation (6.5), the oxygen concentration in the exhaust on a dry basis can be written as

$$y_{O_2} = \frac{(\lambda-1)\left(\alpha+\frac{\beta}{4}-\frac{\gamma}{2}\right)}{\alpha+\lambda\left(\alpha+\frac{\beta}{4}-\frac{\gamma}{2}\right)3.76+(\lambda-1)\left(\alpha+\frac{\beta}{4}-\frac{\gamma}{2}\right)} \tag{6.26}$$

Solving for lambda, we get

$$\lambda = \frac{\left(\alpha+\frac{\beta}{4}-\frac{\gamma}{2}\right)+\left(\frac{\beta}{4}-\frac{\gamma}{2}\right)y_{O_2}}{\left(\alpha+\frac{\beta}{4}-\frac{\gamma}{2}\right)\left(1-4.76y_{O_2}\right)}$$

or

$$\lambda = \frac{1+\dfrac{\left(\frac{\beta}{4}-\frac{\gamma}{2}\right)y_{O_2}}{\left(\alpha+\frac{\beta}{4}-\frac{\gamma}{2}\right)}}{1-4.76y_{O_2}} \tag{6.27}$$

For a diesel fuel with a $\left({}^{H}\!/\!_{C}\right)$ ratio of 2 $(\alpha=1,\beta=2,\gamma=0)$, the equation reduces to

$$\lambda = \frac{1+\frac{y_{O_2}}{3}}{1-4.76y_{O_2}}$$

which is exactly the same equation as given by Bosch [120].

Substituting the values of $(\alpha = 1, \beta = 1.88, \gamma = 0)$ for the laboratory diesel fuel in Equation (6.27) yields

$$\lambda = \frac{1 + \frac{y_{O_2}}{3.13}}{1 - 4.76 y_{O_2}} \tag{6.28}$$

The results shown in the following sections use Equation (6.28), for converting the output of the wide-band lambda sensors into the corresponding oxygen concentrations.

The Bosch LSU 4.9 sensor maintains a constant temperature (~780°C) of the pump cell with the built-in heater and operates by pumping more or less current (I_P) to maintain the mixture in the pump cell at stoichiometric conditions. The pump cell current is related to the oxygen concentration of the working fluid (normally the exhaust gas). For the Bosch sensor, the pump cell current characteristics are shown in Figure 6.20. The curve-fit equation for the sensor characteristics is also shown in the figure.

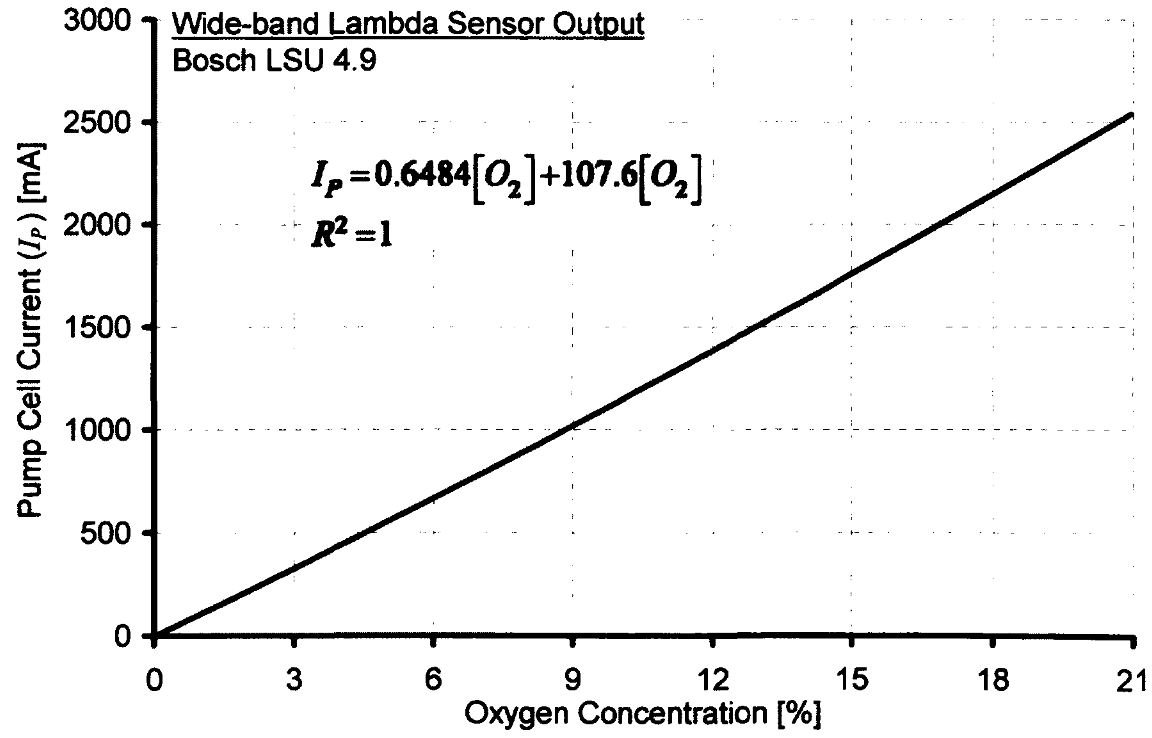

Figure 6.20: Bosch Wide-band Lambda Sensor Characteristics

6.4.1. Pressure Dependency of the Sensor Signal

The use of the wide-band lambda sensors in pressurized environment is complicated because a change of the intake/exhaust gas pressure leads to a deviation of the sensor signal, which can be approximately described as shown in Figure 6.21.

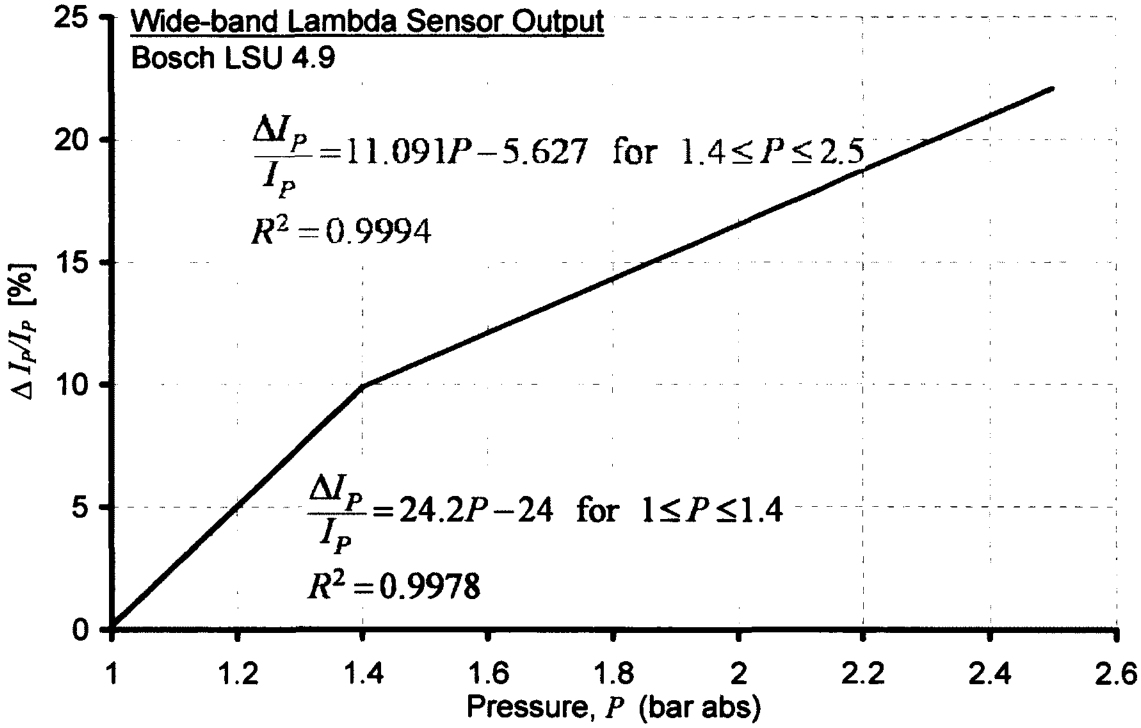

Figure 6.21: Pressure Dependency of the Bosch Wide-band Lambda Sensor

The procedure adopted for correcting the output of the wide-band lambda sensor for the intake/exhaust pressure, is as follows:

- The output of the sensor in terms of lambda values is first converted into the equivalent oxygen concentration using Equation (6.28).

- The current of the pump cell (I_P) is then calculated from the oxygen concentration using the relationship shown in Figure 6.20.

- Next, the influence of the intake or exhaust pressure on I_P is determined. The measured pressure is used to find the deviation (ΔI_P) from the relationships shown in Figure 6.21.
- The new I_P (corrected for the deviation) is then used as the input to estimate the correct oxygen concentration and the lambda values.

6.4.2. Testing of the Two-Lambda Sensor Technique

An extensive test matrix was setup to ascertain the accuracy of the two-lambda sensor approach over a wide range of engine operating conditions. One result for an EGR sweep is presented in Figure 6.22. The engine was naturally aspirated so that the sensor signal was not required to be corrected for the pressure. The exhaust lambda sensor was programmed to measure the λ values from 1 to 50, while the intake lambda sensor's measurable range was programmed for λ from 1 to 100.

The EGR was varied from a low value up to ~55% and the lambda value output of the sensors was recorded. The lambda value was then converted into the intake and the exhaust oxygen concentrations, based on the conversion expression described previously. These concentrations were then compared with the oxygen concentrations recorded with the laboratory emission analyzers as shown in Figure 6.23. It can be seen that the general trend of the concentrations in the intake and the exhaust is quite similar. The exhaust oxygen values calculated from the lambda sensor were in better agreement with the reference values compared to those from the intake sensor.

The deviation of the intake sensor output can be primarily attributed to two factors. First, the intake oxygen concentration span (~21% for fresh air to approximately zero) is large compared to that for the exhaust. This reduces the resolution of the output signal since the maximum output voltage span is fixed (~8V for the 3H1 controller). This is evident by the fluctuations seen in the intake lambda values in

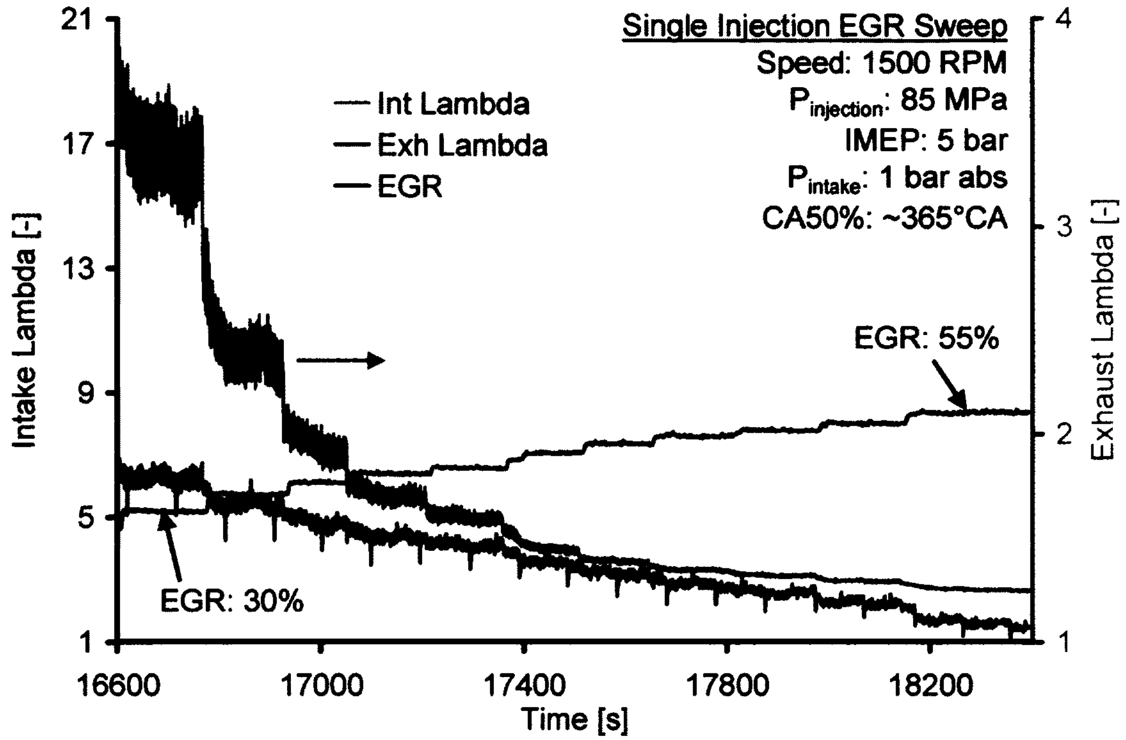

Figure 6.22: Two-Lambda Sensor Response to EGR Sweep

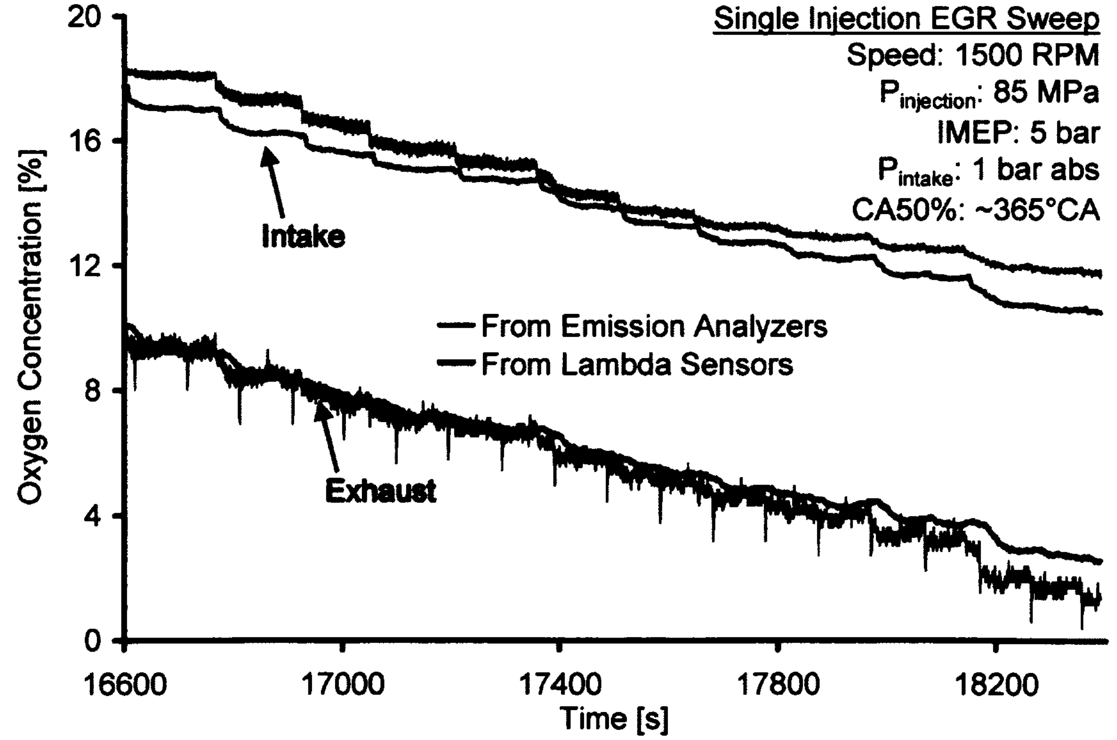

Figure 6.23: Comparison of the Oxygen Concentrations

Figure 6.22. Second, the flow in the manifolds of a single cylinder engine is highly periodic. Compared to the exhaust system, the intake temperature is very low. Since the sensor temperature must be maintained at ~780°C for the sensor output to be accurate, the fluctuating flow combined with the low temperatures is presumed to make it difficult for the controller to efficiently maintain the sensor temperature within close limits.

The EGR ratio was calculated using Equations (6.23) and (6.24), and compared with the EGR ratio based on the measured CO_2 concentrations from the emission analyzers. The result is shown in Figure 6.24. The EGR estimation from the two-lambda sensor approach was generally in agreement with the CO_2 concentration based value except at the lower and higher ends. The deviation at the extremes was the result of the inaccuracy of the intake lambda sensor output as discussed above.

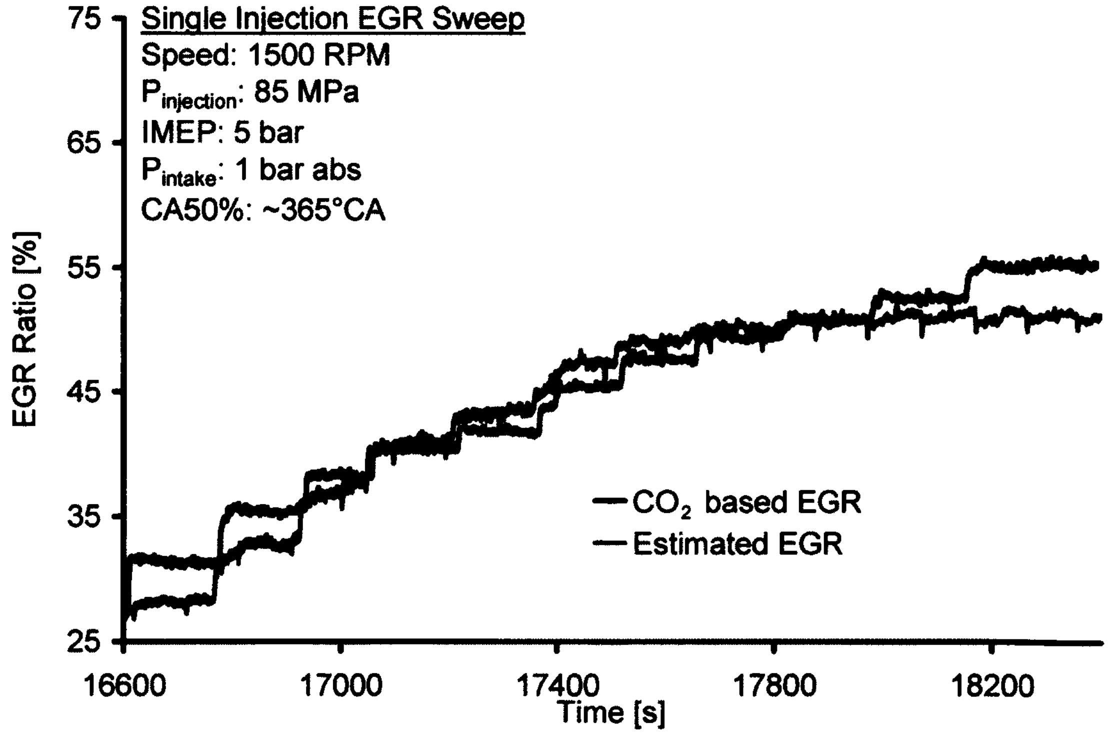

Figure 6.24: EGR Estimation from the Two-Lambda Sensor Approach

The two-lambda sensor approach was then tested under a wide range of both steady state and transient engine operations. Three different cases are presented below.

The results for the first dataset are shown in Figure 6.25 and Figure 6.26 for the exhaust sensor and the intake sensor respectively. Without applying the correction for the exhaust pressure, the raw signal deviated from the reference exhaust concentration. The application of the pressure correction as outlined earlier improved the sensor accuracy and the results were in close agreement with the reference values for most of the testing conditions.

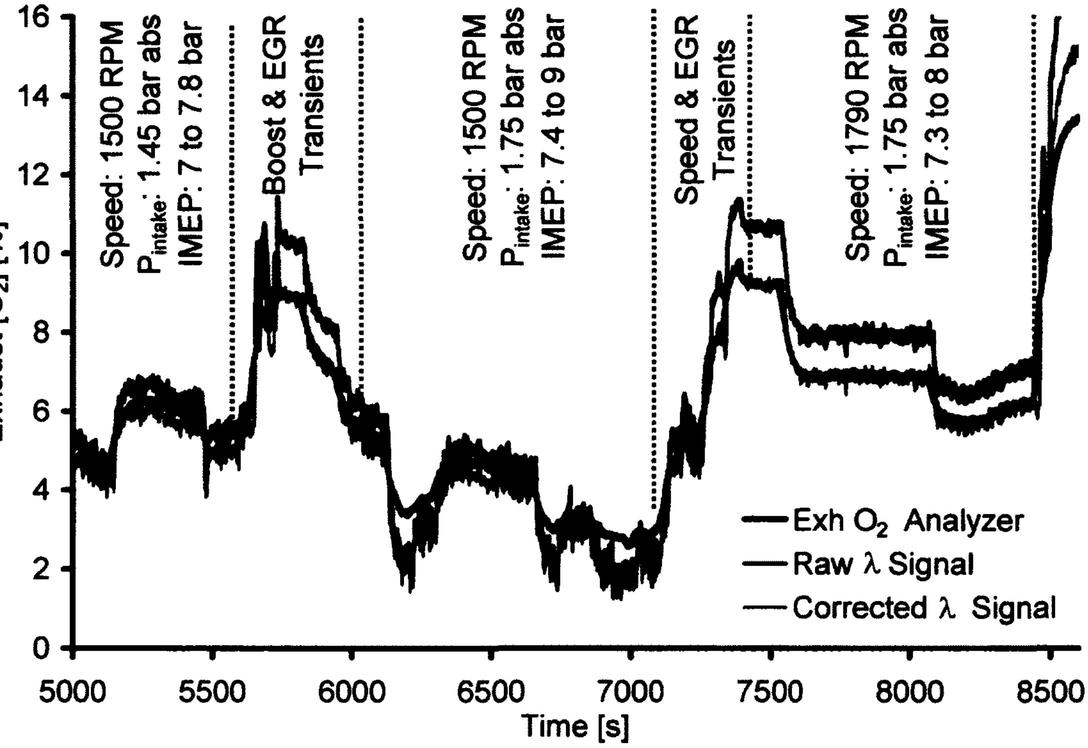

Figure 6.25: Pressure Dependency Correction of the Exhaust Sensor Output (Dataset #1)

For the intake sensor, the error in the raw signal was significantly higher compared to that for the exhaust. The application of the pressure correction improved the sensor accuracy but significant errors were still observed for intake oxygen concentration greater than ~14%.

Since the intake oxygen concentrations for LTC operation are generally below 14%, it was decided to modify the upper limit of the intake lambda sensor measurement range from $\lambda=100$ to $\lambda=50$.

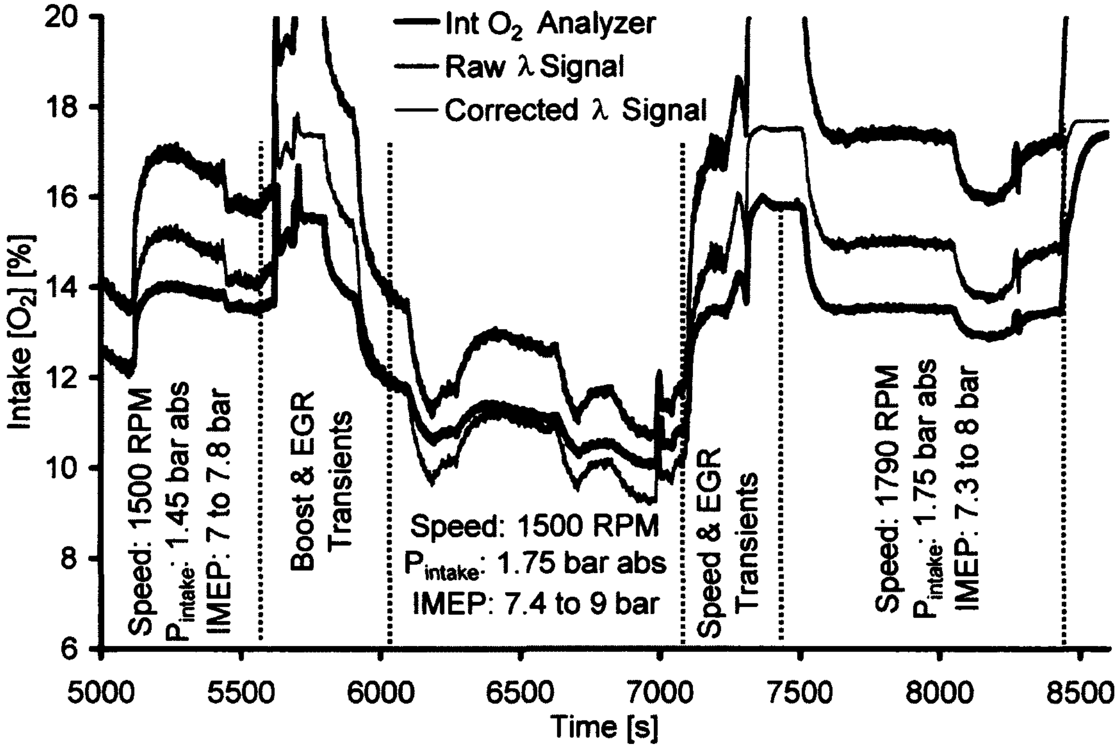

Figure 6.26: Pressure Dependency Correction of the Intake Sensor Output (Dataset #1)

The results for the second dataset are presented in Figure 6.27 and Figure 6.28 for the exhaust sensor and the intake sensor respectively. The exhaust oxygen concentration was in good agreement for values below 12%. For the intake oxygen, a reasonable agreement was generally seen for oxygen concentration below 14%. The intake oxygen concentration range generally observed for the LTC cycles has also been marked on the figure. The results for the dataset # 3 are presented in Figure 6.29 and Figure 6.30 for the exhaust sensor and the intake sensor respectively. The exhaust oxygen concentration was again in good agreement for values below 12%. For the intake oxygen, a reasonable agreement was also seen for oxygen concentration below 14%.

To provide feedback for the LTC control, the values of the intake concentration are not as critical as detecting a change in the concentration itself, because of a change in the operating conditions. Based on the above results, the two lambda sensor technique was seen to provide an adequate response for both the intake and the exhaust oxygen concentrations.

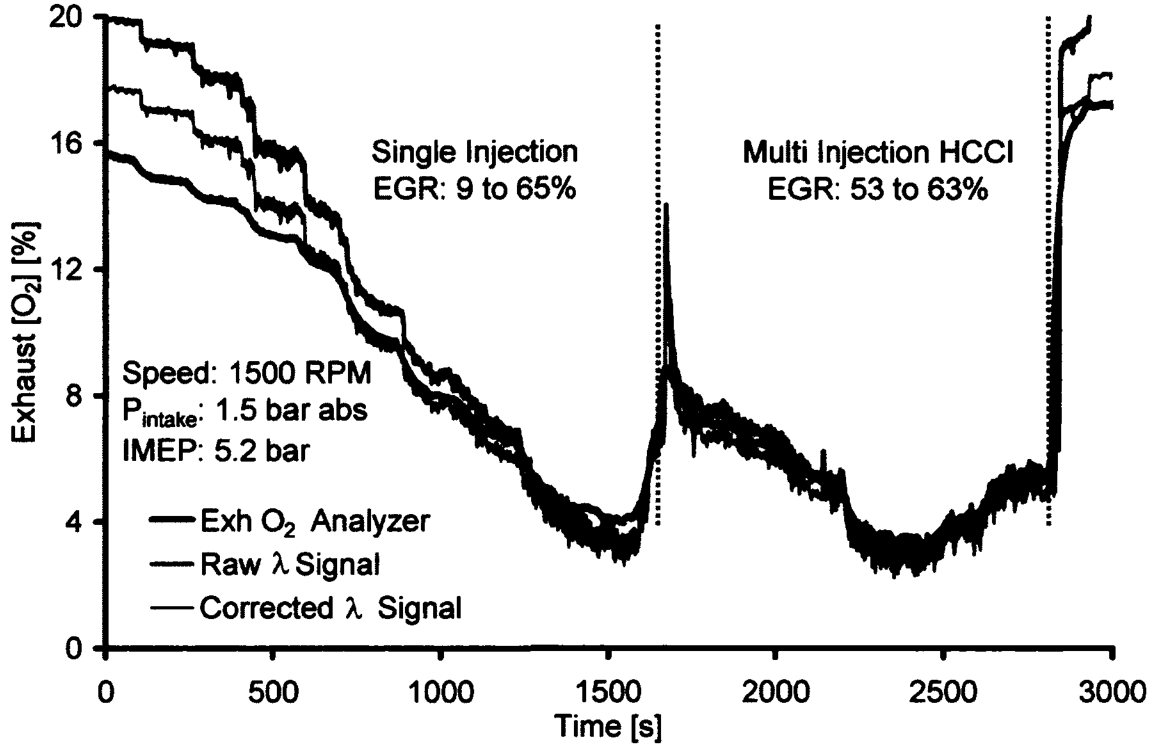

Figure 6.27: Pressure Dependency Correction of the Exhaust Sensor Output (Dataset #2)

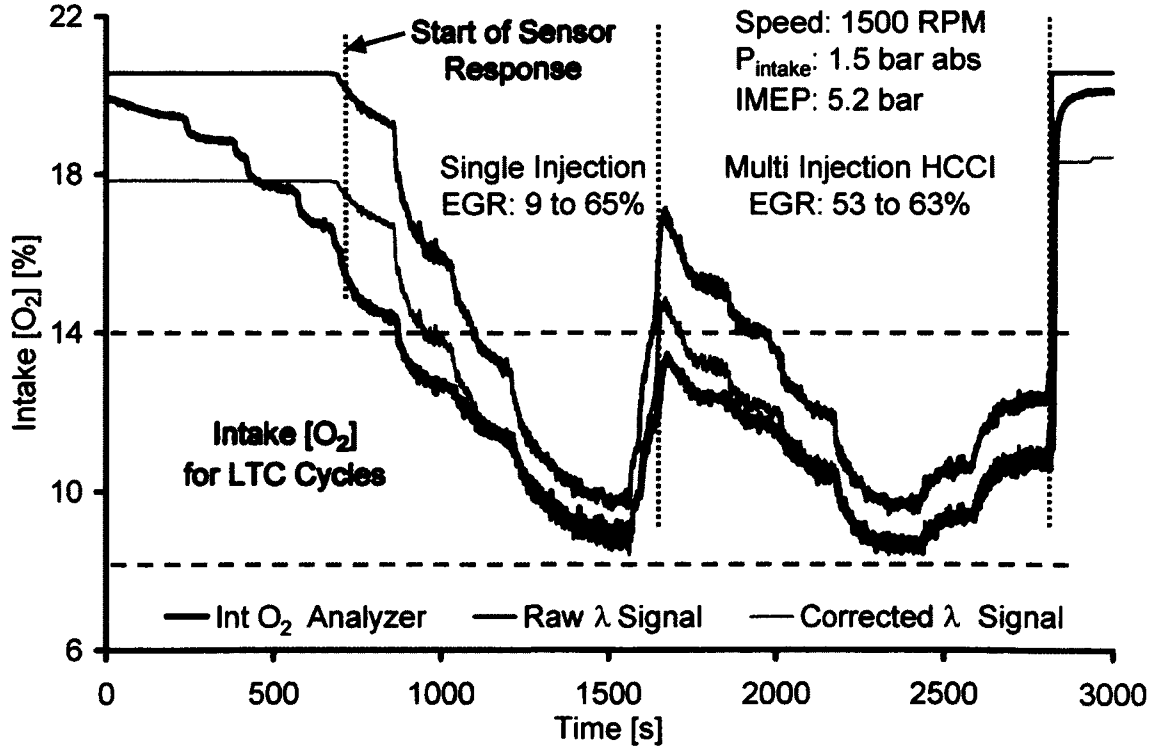

Figure 6.28: Pressure Dependency Correction of the Intake Sensor Output (Dataset #2)

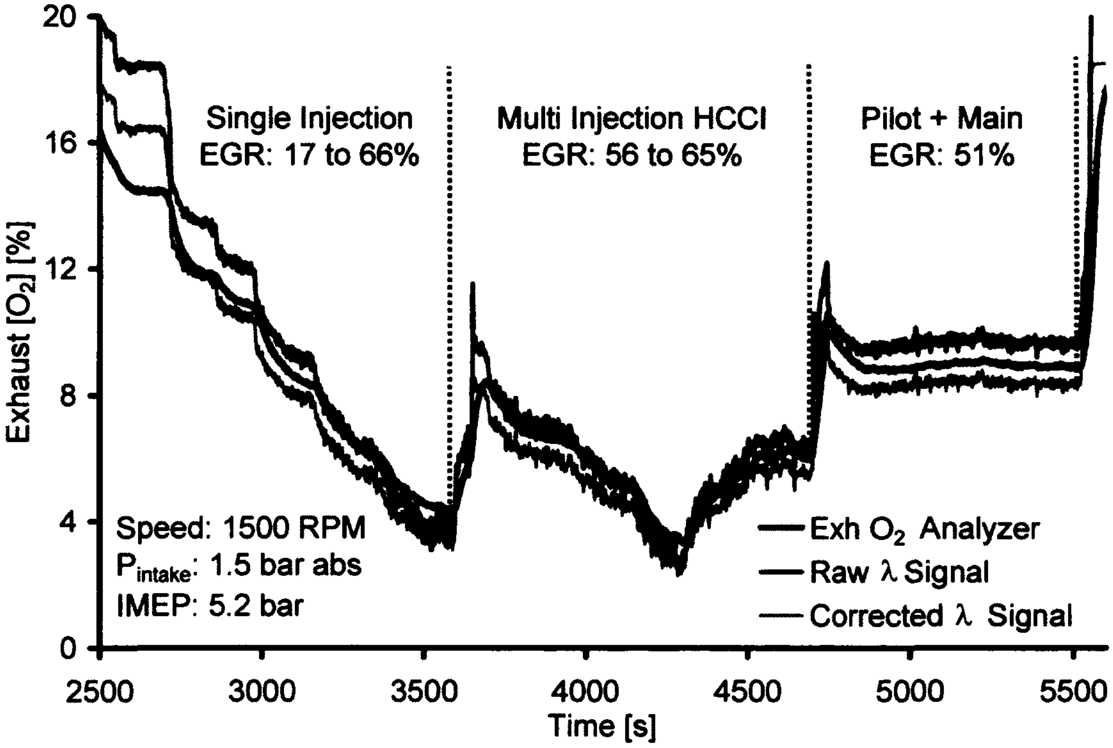

Figure 6.29: Pressure Dependency Correction of the Exhaust Sensor Output (Dataset #3)

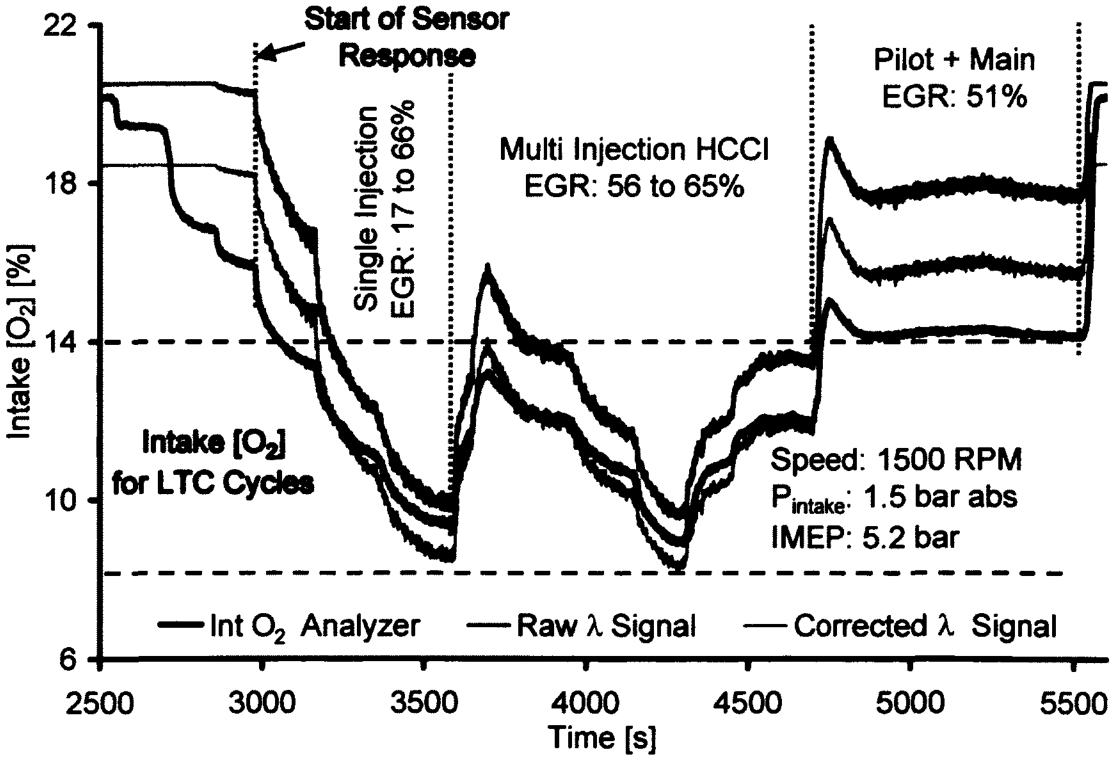

Figure 6.30: Pressure Dependency Correction of the Intake Sensor Output (Dataset #3)

6.5. Catalytic EGR Treatment and Fuel Reforming

EGR is effective in reducing the NOx emission because it lowers the flame temperatures due to the dilution and increased heat capacity of the recirculated gases. However, excessive soot formation occurs as EGR is progressively increased during the HTC regime. Moreover, the excessive use of EGR pushes the combustion into the LTC cycles that may result in the engine operation reaching zones of high instabilities (increased cycle-to-cycle variation) and even power loss.

EGR induced cyclic variations are largely associated with the prolonged ignition delay caused by increased CO_2 and decreased O_2 in the intake. An increased ignition delay deteriorates combustion efficiency that, in turn, causes fluctuations in the combustion products. These variations escalate the consecutive cyclic variations of the cylinder charge in terms of temperature, pressure and composition. However, to alleviate problems associated with the excessive use of EGR, the participation of a gaseous fuel that increases premixed combustion may result in the simultaneous reduction of both NOx and soot emissions and may help to reduce the cyclic variations [77,121,122]. When a gaseous fuel forms a homogeneous charge in the engine cylinders, the combustion process tends to use oxygen more efficiently.

To enhance the premixed combustion, gaseous fuels such as hydrogen can be generated by catalytically reforming diesel fuel in the EGR stream. Since the diesel exhaust normally contains significant amounts of surplus oxygen, therefore, it is reasonable to use the exhaust to catalytically reform some of the diesel fuel because the oxygen and heat of the exhaust can be utilized simultaneously.

In this work, tests were conducted to improve the use of EGR on the Yanmar engine with different EGR stream treatment techniques. The effect of treated EGR on the engine operational stabilities and pollutant emission was investigated at different loads and EGR rates. The research was aimed at stabilizing and expanding the limits of heavy EGR during steady and transient operations so that the individual limiting conditions of EGR could be better identified.

6.6. Concept of Catalytic EGR System

The EGR catalytic fuel reforming is a departure from conventional EGR operations. Conventional or raw EGR (Figure 6.31a) circulates untreated raw exhaust to the engine intake, while the CEGR modifies the exhaust contents before recirculation. The CEGR can have two modes of operation- an oxidization mode (Figure 6.31b), where the incomplete products of combustion are oxidized on a palladium/platinum based catalyst to reduce the instabilities introduced with the application of EGR, and a reforming mode (Figure 6.31c), where a small amount of diesel fuel is injected in the EGR stream and catalytically reformed on the catalyst in the rich combustor to generate gaseous fuels like hydrogen which can improve the overall combustion efficiency [123].

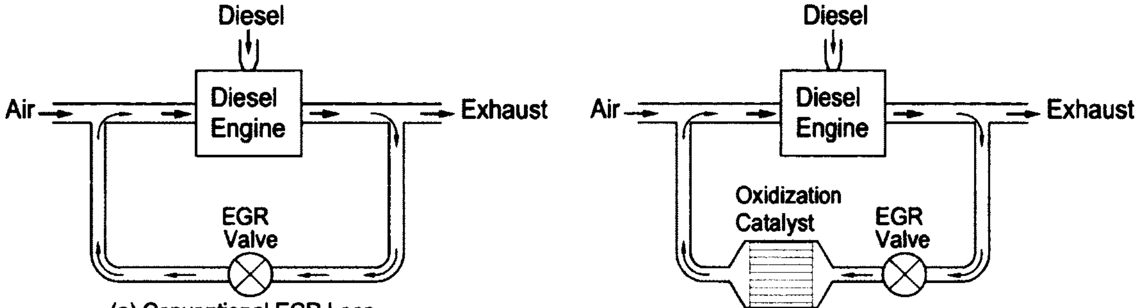

(a) Conventional EGR Loop (EGR bypass)

(b) CEGR-Oxidization Mode

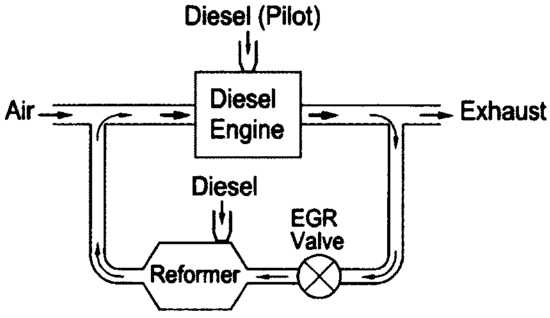

(c) CEGR-Reforming Mode

Figure 6.31: Conventional vs. Catalytic EGR

To conduct fuel reforming, liquid diesel fuel supplied to the EGR fuel reformer is vaporized and brought in contact with hot exhaust in the presence of catalysts. Through partial oxidation and water-gas shift mechanisms, the resulting gas mixture can contain significant amount of hydrogen, carbon monoxide, nitrogen, carbon dioxide, water and traces of partial oxidization radicals. The sequence of catalytic EGR operation characterizes temporally and spatially discrete rich-quench-lean combustion processes. Rich combustion occurs in the EGR combustor followed by quench processes downstream of the combustor and in the EGR cooler. Lean burn combustion then occurs in the engine combustion chamber.

The potential benefits of the reformed gases include:

- Increasing the EGR application limits
- Generating synthetic EGR at low-load conditions
- Simultaneous reduction of engine-out emissions of NOx and soot
- Stabilization of the combustion process in unconventional combustion modes
- Improve the transient performance of exhaust aftertreatment devices.

The EGR reforming process can also have advantages over conventional engine intake or engine cylinder fuel-reforming systems [124], from considerations such as thermal energy regeneration, oxygen content usage, and partial bypass-flow control.

6.7. EGR Treatment Strategies

The EGR treatment techniques explored in this work were based on a flow-through DOC installed in the EGR loop of the Yanmar engine. A number of flow strategies were investigated to improve the thermal response as well as the energy efficiency of the CEGR reformer. The effect of electric heating and supplemental fuelling at two different locations in the CEGR loop were studied and some work was done to observe the effect of water injection on the reformer output. The EGR techniques are summarized in Figure 6.32.

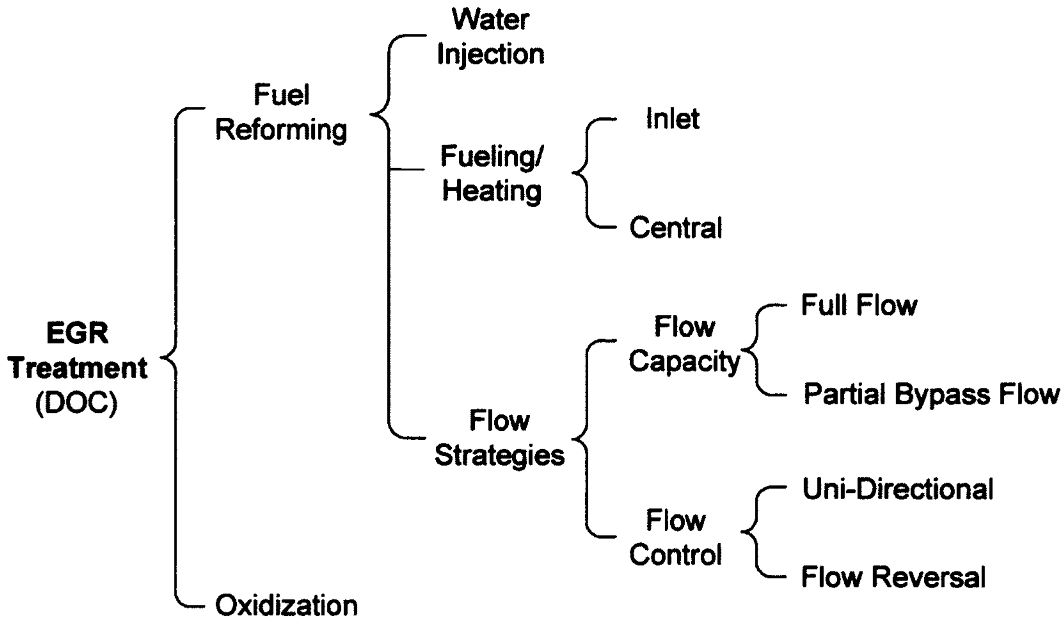

Figure 6.32: EGR Treatment Strategies based on a Flow-through DOC

6.8. Unidirectional Flow Experimental Setup

The modified Yanmar engine setup is schematically shown in Figure 6.33. The setup was based on the conceptual usage of EGR reformer, proposed by Zheng et al. as a technique to increase EGR application limits and reduce soot in modern diesel engines [30]. The EGR system consisted of two loops in parallel – a conventional EGR loop (called an EGR bypass loop hereafter) and a CEGR loop with a rich combustor incorporated into the system so that gaseous fuels could be generated on demand. The CEGR loop also included an electric heater with a variable DC power supply to heat up the exhaust gas when needed. A measured quantity of diesel fuel was vaporized through atomization and by mixing with the hot exhaust gas to generate a homogeneous rich mixture, upstream of the CEGR combustor. The mixing zone constituted a leading section of the combustor. A water injection system was also added upstream of the CEGR combustor. An advanced EGR cooler was installed downstream of the CEGR combustor to quench the reformed gases to the desired temperature before the gases mixed with the intake air stream.

A number of thermocouples and pressure sensors were placed at several locations in the system for monitoring the system operation. A Heated Exhaust Gas Oxygen Sensor

(HEGO) and a wide-range lambda sensor placed down stream of the rich combustor provided the necessary feedback for the CEGR fuel injection calibration and control.

The properties of the flow-through diesel oxidation catalyst (DOC) used in the CEGR are given in Table 6.3. All the components including the CEGR combustor, electric heater etc. were fabricated as a part of this project. The electric heater could provide up to 0.8kW of heating power using a 0-40V, 25A variable DC power supply. The actual setup of the dual-EGR loop system on the Yanmar engine is shown in Figure 6.34.

Table 6.3: Diesel Oxidation Catalyst Properties

Type	Palladium/Platinum
Catalyst Loading	150 g/ft^3
Diameter x Length	60 mm x 140 mm
Cell Density	200 cpsi
Substrate Material	Cordierite

cpsi – cells per square inch

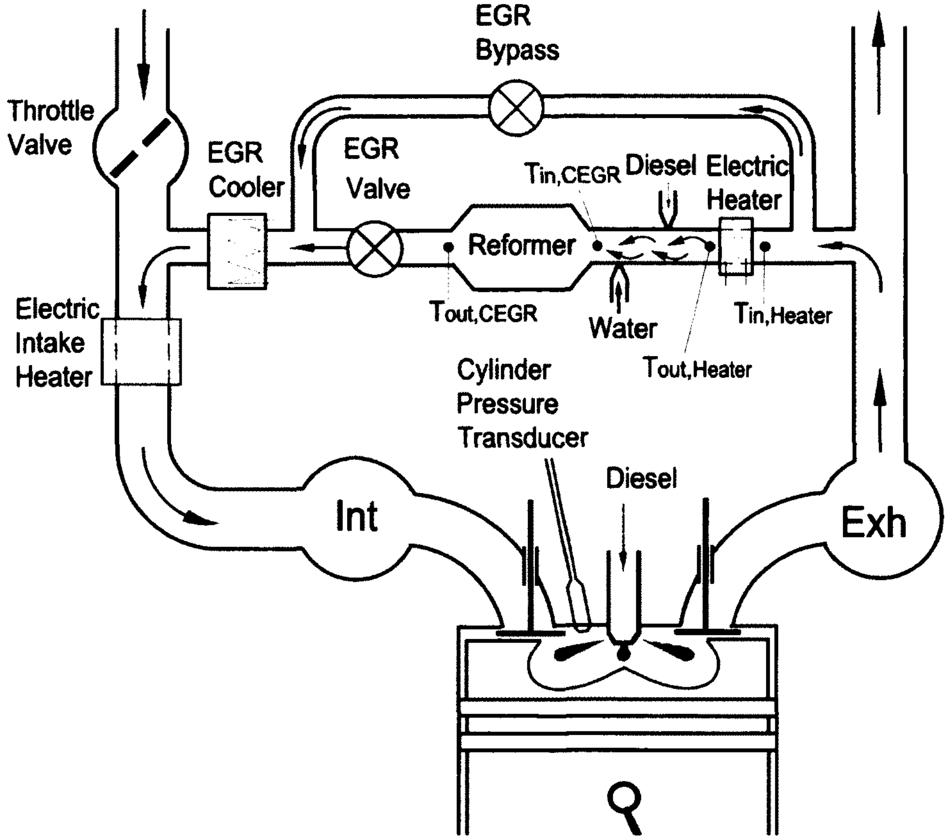

Figure 6.33: Schematic Representation of the Test Setup

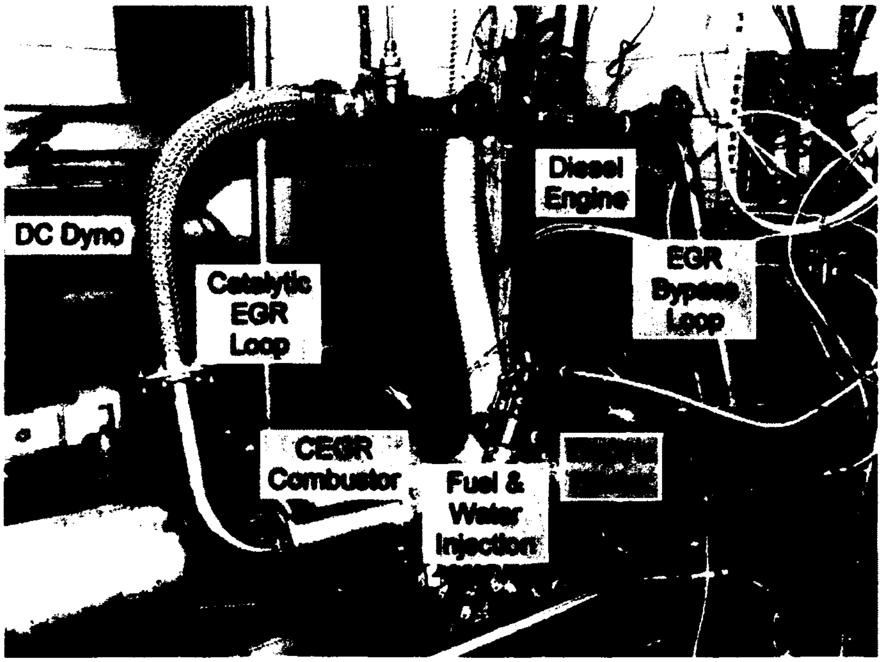

Figure 6.34: Experimental Setup of the EGR Fuel Reformer

6.9. CEGR in Oxidization Mode

If the combustion process can be stabilized at high EGR rates commonly employed for LTC cycles, it may help to improve the combustion efficiency so that the benefits of simultaneous low emissions of NOx and soot can be exploited.

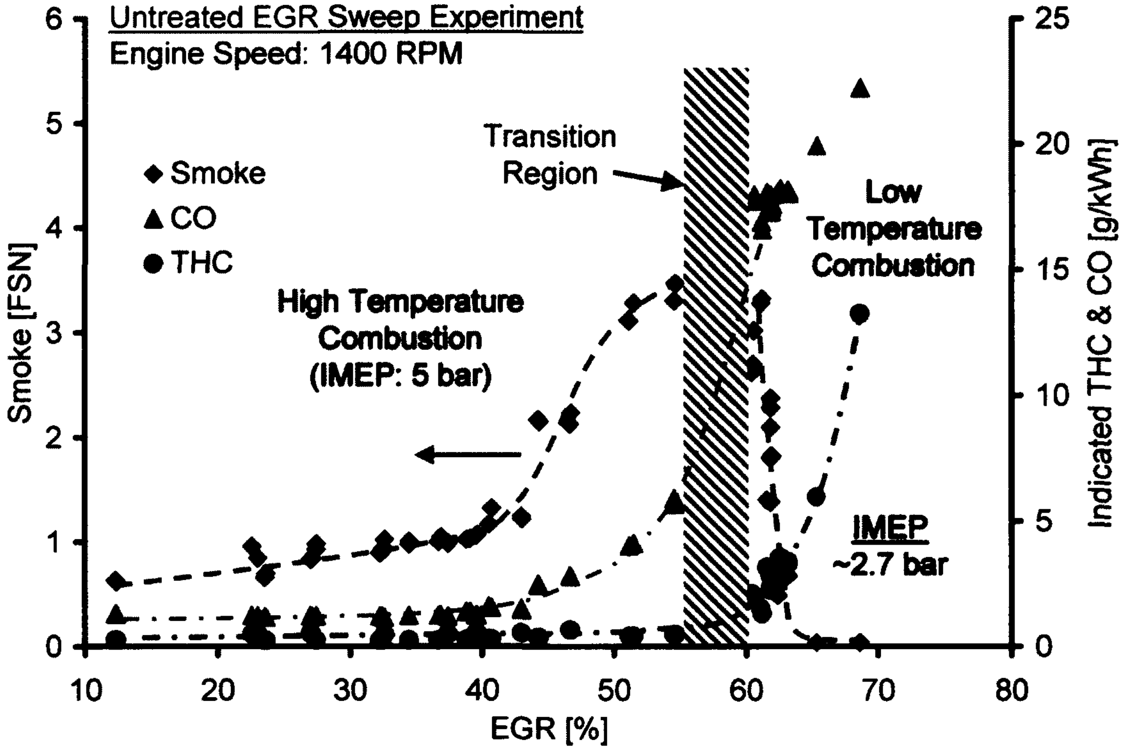

Figure 6.35: Effects of Excessive EGR on Engine-out THC & CO

To verify if the application of CEGR would enable the engine to be run continuously in the otherwise unstable regions with high cycle-to-cycle variations (using raw or untreated EGR), the effect of treated EGR on the engine operational stability in the LTC regime was investigated by replacing the raw EGR with CEGR (oxidization mode) at two different engine loads. The EGR was switched between the untreated and treated EGR, keeping the EGR mass flow rate and other engine operating conditions as constant.

6.9.1. Oxidization Tests – 3.3 bar IMEP

The analysis of 1000 consecutive pressure traces for the engine load of 3.3 bar IMEP is shown in Figure 6.36. The operation with untreated EGR displayed significant variations in the IMEP. In fact, the flame progressively weakens and continuous operation can lead to higher engine operational instabilities resulting in 'mis-fire'. CEGR, on the other hand, reduced the fluctuations in IMEP, enabling continuous operation. The corresponding crank angle of 50% heat released (CA50) is shown in Figure 6.37. A similar trend (like IMEP) was observed for the CA50. It is pertinent to mention here that some of the engine cycles 'mis-fired' (Figure 6.38), so that the actual scatter in the CA50 was more than that seen in the figure.

The continuous cylinder pressure traces for engine operation with untreated EGR are shown in Figure 6.38. The results show a high variation in the peak combustion pressure (to differentiate from the peak cylinder pressure which for a number of cycles was the compression pressure). From the pressure traces for the treated EGR shown in Figure 6.39, it can be seen that by oxidizing the combustibles in the EGR stream, the cycle-to-cycle variations are reduced and the combustion process tends to be relatively stable. Raw EGR caused cyclic variations are largely associated with the prolonged ignition delay which deteriorates the combustion efficiency that, in turn, causes fluctuations in the combustion products.

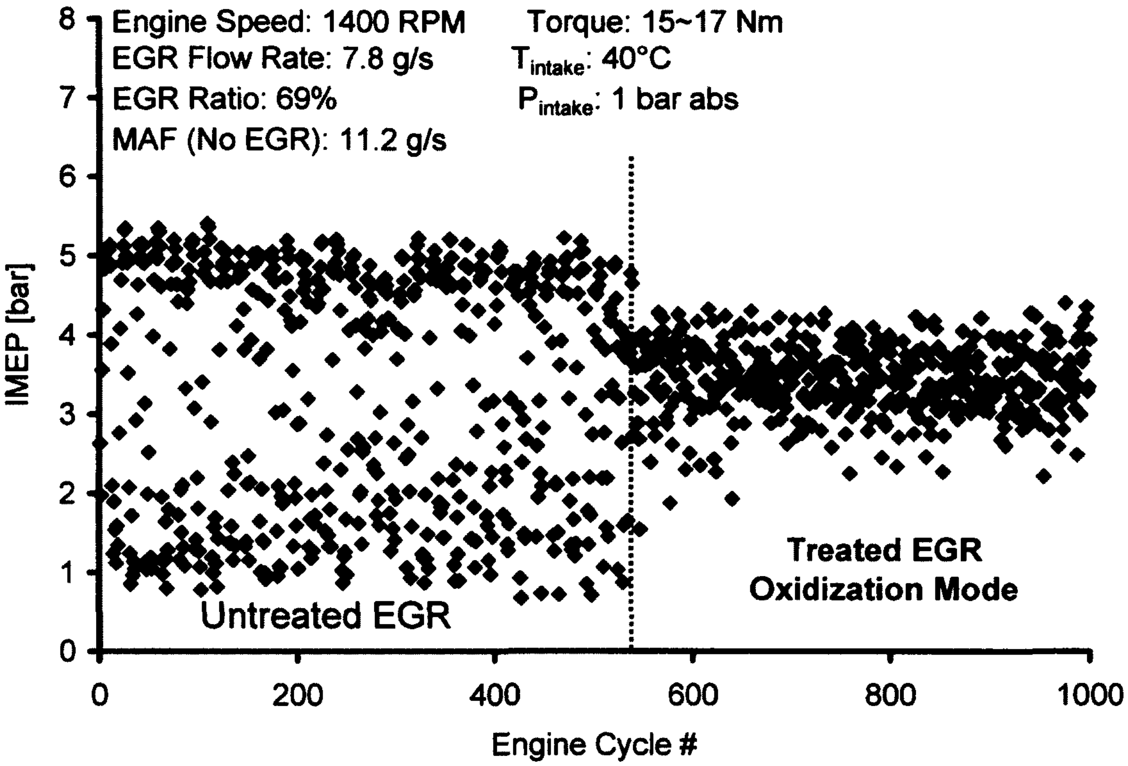

Figure 6.36: IMEP Comparison between Untreated EGR & Treated EGR (Oxidization)

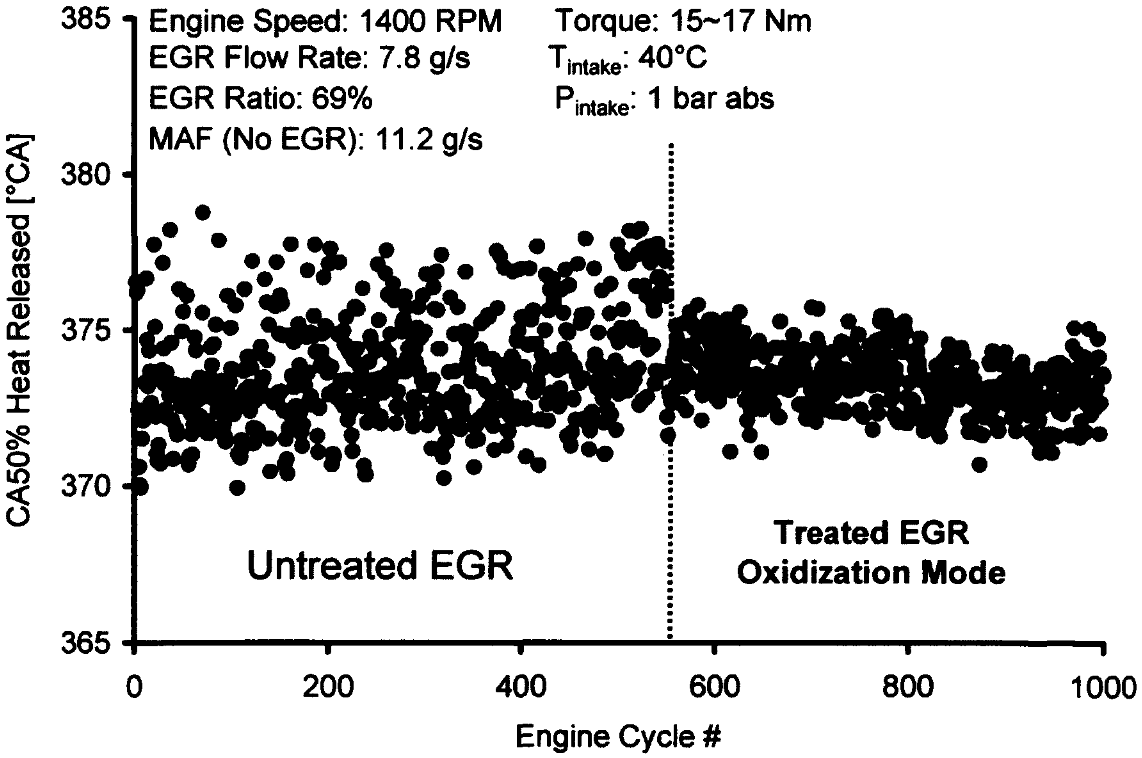

Figure 6.37: CA50 Comparison between Untreated EGR & Treated EGR (Oxidization)

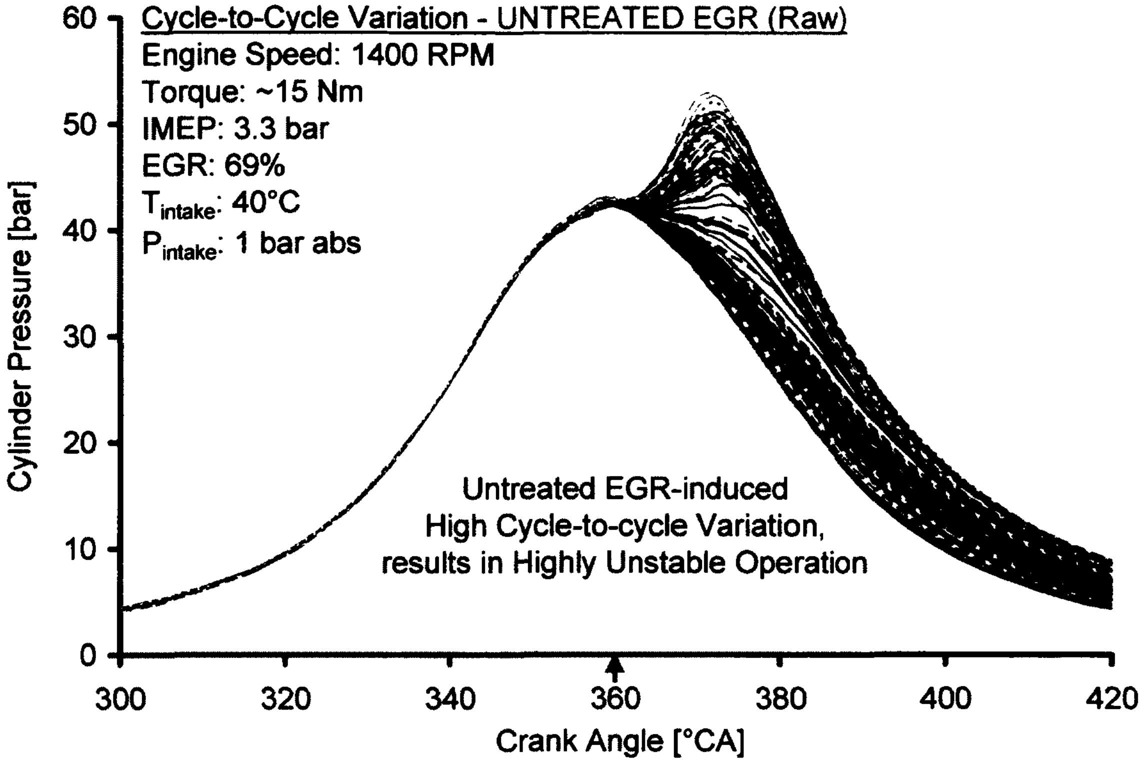

Figure 6.38: Cycle-to-cycle Variation with Untreated Heavy EGR

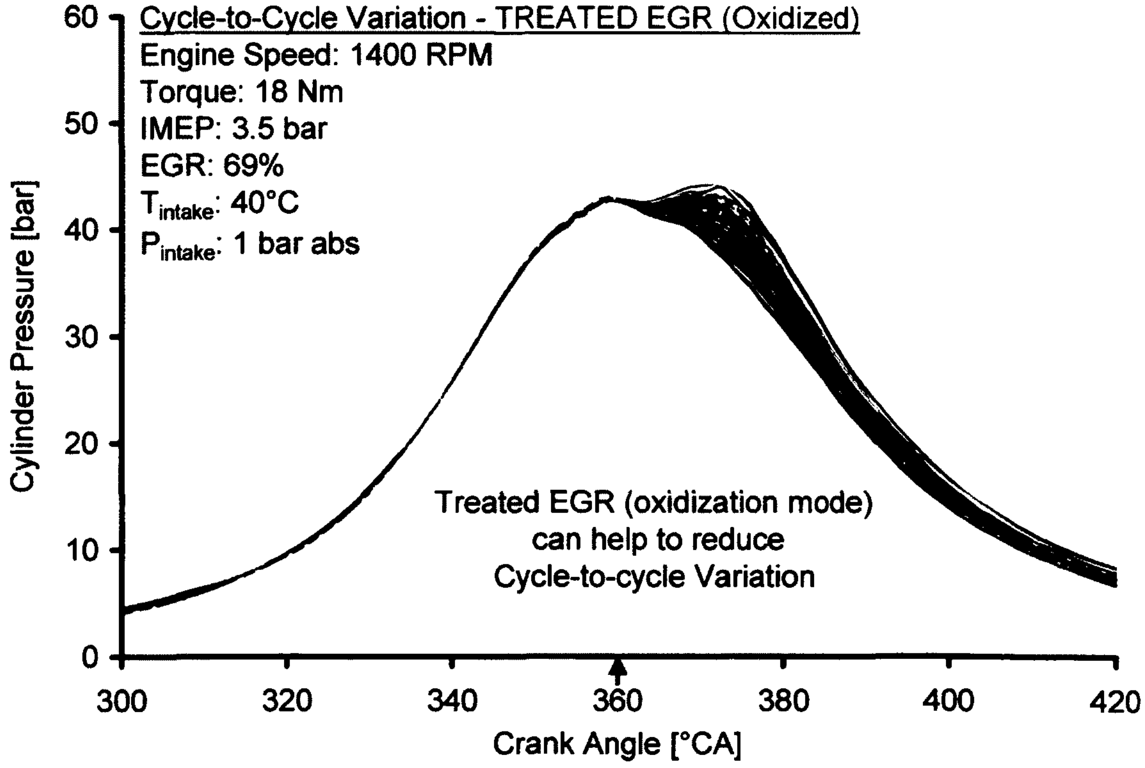

Figure 6.39: Cycle-to-cycle Variation with Treated Heavy EGR (Oxidization Mode)

During LTC, the combustion efficiency drops with high CO & THC emissions. These variations escalate the consecutive cyclic variations of the cylinder charge in terms of temperature, pressure and composition. CEGR oxidizes a significant amount of these combustibles, lowering the cyclic fluctuations of the cylinder charge and thus, helps to stabilize the combustion process. The efficacy of the treated EGR is also evident from a comparison of the engine-out emissions. Table 6.4 summarizes the results for the cycle-to-cycle variation analysis and the engine-out emissions for both the untreated and treated EGR cases.

Table 6.4: Summary of the Oxidization Test Results at 3.3 bar IMEP

		Untreated EGR	Treated EGR (Oxidization)
IMEP (bar)	Mean	3.3	3.5
	Standard Deviation	1.52	0.44
	COV (%)	46	12.6
CA50 (%)	Mean	373.8	373.4
	Standard Deviation	1.84	0.96
	COV (%)	0.5	0.26
EGR Ratio (%)		69	
Indicated Thermal Efficiency (%)		35.3	37
NOx (ppm)		9	9
Indicated NOx (g/kWh)		0.05	0.05
Soot (FSN)		0.5	0.03
Indicated Soot (g/kWh)		0.02	0.001
CO (ppm)		>5000*	>5000*
Indicated CO (g/kWh)		>17	>17
THC (ppm^{C1})		>3200*	1848
Indicated THC (g/kWh)		>6	3.5

*Limited by the upper range of the CO/THC Emission Analyzers

6.9.2. Oxidization Tests – 4.2 bar IMEP

The EGR stream may need to be heated up to enable catalytic reactions if the EGR stream temperature is low. The catalyst light-off temperature depends on the type of the catalyst, the characteristics of the fuel and the catalyst aging. The engine tests at 3.3 bar IMEP were done using a fresh catalyst which generally did not require any heating at EGR stream temperatures above 250°C. Moreover, the exhaust pipe and the EGR loop up till the CEGR combustor were heavily insulated to reduce the heat loss and to minimize the requirements of electrical heating.

For the tests at 4.2 bar IMEP, the insulation was removed and an aged catalyst was used to study the impact on the performance of the CEGR system. The EGR stream was heated up with the electric heater (set at 0.75 kW) to enable catalytic reactions. The combustion was pushed into the LTC regime as shown in Figure 6.40. At high EGR levels, the standard deviation of IMEP was considerably lower than that with raw EGR while maintaining low levels of soot emission.

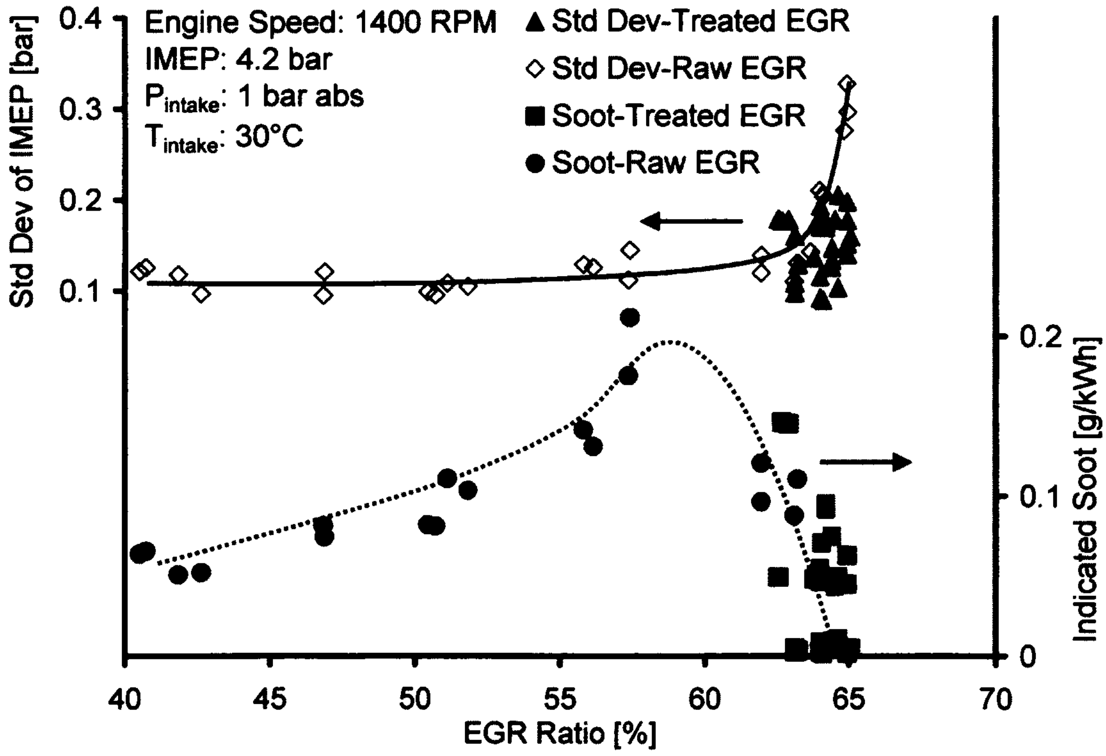

Figure 6.40: Effect of Treated EGR (Oxidization Mode) on Engine Stability (4.2 bar IMEP)

To verify if the application of CEGR would enable the engine to be run continuously in the otherwise unstable regions with high cycle-to-cycle variations (using raw EGR), the analysis of 600 consecutive pressure traces is shown in Figure 6.41. The operation with raw EGR displayed significant variations in both the IMEP and the CA50. In fact, the engine operation could not be sustained with raw EGR as 'mis-fire' occurred.

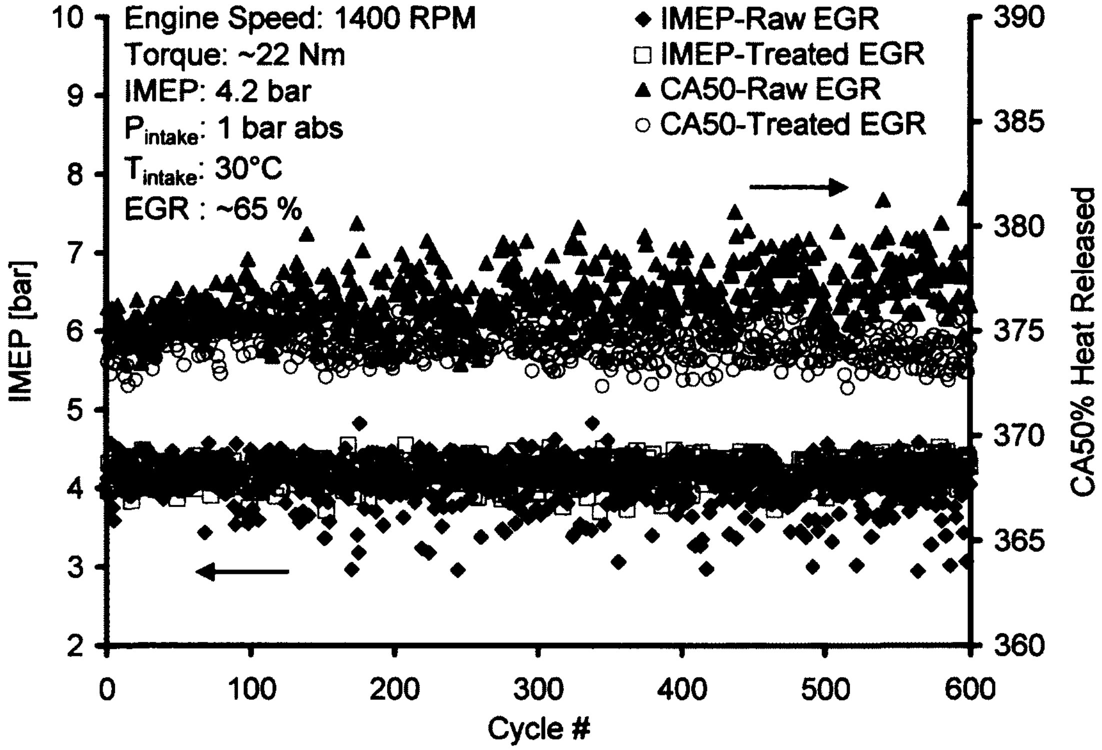

Figure 6.41: Engine Operation Comparison between Raw & Treated EGR (4.2bar IMEP)

The 200 cycles-averaged heat release rates for the 600 cycles in Figure 6.41 are shown in Figure 6.42. The results show a higher variation in the heat release rates with raw EGR. Treating the EGR helped to reduce the cyclic variations, thereby stabilizing the combustion and improving the engine operation.

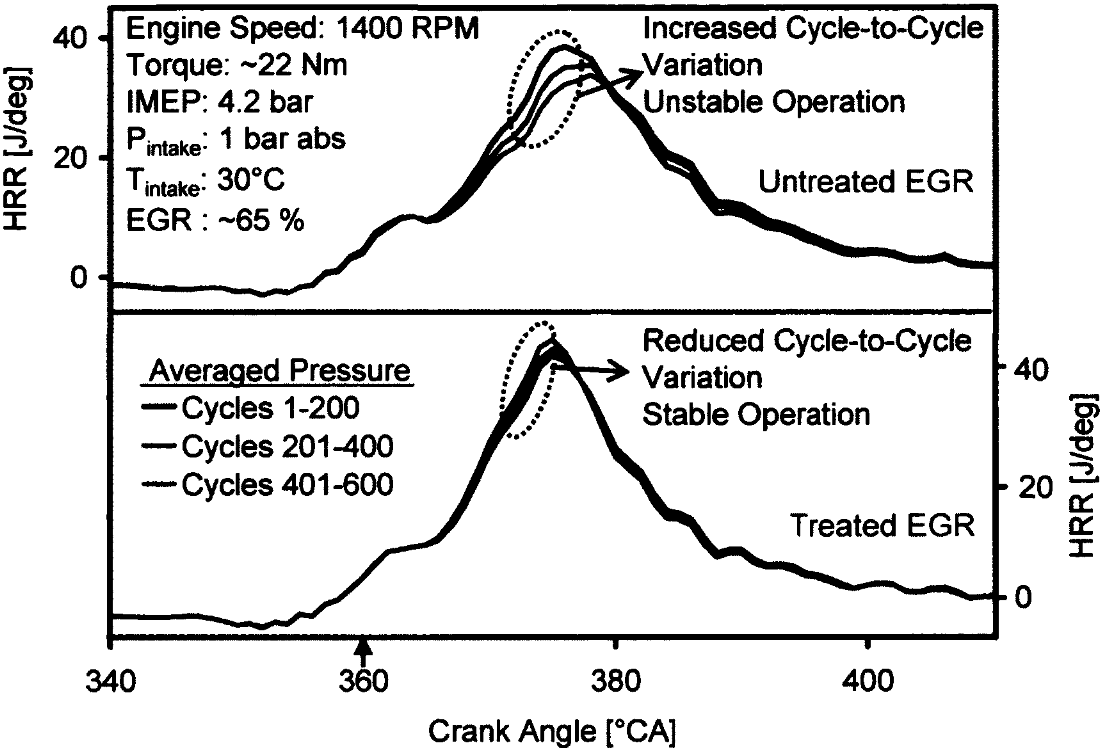

Figure 6.42: Heat Release Rate Comparison between for Raw & Treated EGR

The summary of the 4.2 bar IMEP tests is given in Table 6.5. The heater power of 0.75kW was included in the efficiency calculations. It can be seen that the indicated thermal efficiency dropped considerably below that obtained with raw EGR. If the heater power was excluded from the calculations, the resulting indicated thermal efficiency was 35.2%. It is considered that the heater power can be reduced significantly with a compact design of the CEGR system and proper thermal insulation.

The improvement in the cycle-to-cycle variations was significant as the catalytically treated EGR reduced the fluctuations in the composition of the EGR stream while maintaining ultra-low emissions of NOx and soot. The longer path provided by the CEGR loop may also help to reduce the consecutive cyclic variations of the cylinder charge in terms of temperature and pressure.

Table 6.5: Summary of the Oxidization Test Results at 4.2 bar IMEP

		Untreated EGR	Treated EGR (Oxidization)
IMEP (bar)	Mean	4.1	4.2
	Standard Deviation	0.31	0.15
	COV (%)	7.5	3.6
CA50 (%)	Mean	376.6	374.5
	Standard Deviation	1.37	0.86
	COV (%)	0.36	0.23
EGR Ratio (%)		65	
Indicated Thermal Efficiency (%)		34.9	32.5†
NOx (ppm)		5	4
Indicated NOx (g/kWh)		0.022	0.02
Soot (FSN)		0.17	0.16
Indicated Soot (g/kWh)		0.004	0.004
CO (ppm)		>5000*	>5000*
Indicated CO (g/kWh)		>16.6	>16.6
THC (ppm^{C1})		2622	2170
Indicated THC (g/kWh)		4.6	4.1

†Including electrical heater power of 0.75kW

*Limited by the upper range of the CO Emission Analyzer

6.10. Unidirectional CEGR in Reforming Mode

In the CEGR reforming operation, there are two streams of diesel fuel supplied to the engine – one stream to the CEGR combustor and the other to the engine cylinders. The fuel quantity directly injected in the engine cylinder (called the pilot fuel hereafter) is used for both ignition control and power production while the fuel supplied to the rich combustor is converted to gaseous fuels that subsequently burn in-cylinder to produce power. Therefore, the total energy for power production comes from the combination of the gaseous fuel and the pilot fuel.

The fuel reforming process in the EGR loop can be carried out using either the full-flow or the partial flow modes. Since CEGR operation generates gaseous fuel on demand, power requirements largely determine the total fuel supplied to the engine cylinders and therefore affect the gaseous fuel generation rate. If the entire EGR stream is used for fuel reforming particularly at low engine-loads, conflicts exist between the NOx control and the fuel reforming processes. During low torque operations, the engine exhaust contains high concentrations of oxygen and low concentrations of CO_2. A high EGR rate is required to achieve significant NOx reduction. However, a low EGR rate is required for a low rate of reformer fuel injection. Therefore, a partial or reduced EGR flow is needed for gaseous fuel reforming during low torque operation, which requires implementing a scheme for by-passing EGR around the reformer.

Partial bypass-flow control was enabled by dividing the EGR stream between the bypass loop and the CEGR loop so that only the desired flow passed through the CEGR while the remaining flow, required for NOx control followed the bypass loop.

6.10.1. CEGR Reformer Fuel Calibration

The reformer fuel injection quantity was calibrated at the start of the research work. With the EGR flow rate held constant, the injected quantity was changed to identify the fuel quantity that results in a stoichiometric mixture in the rich combustor. The results of one such calibration test are shown in Figure 6.43. When the mixture is rich, the mixture undergoes partial oxidization and water gas-shift reactions. The overall reaction is normally endothermic and the gas temperature at the reformer outlet decreases (compared to stoichiometric/lean operation). The HEGO sensor output in this instance was high (> 1 volt). As the mixture was brought to stoichiometric proportions, the gas temperature rose due to the complete oxidization of the mixture.

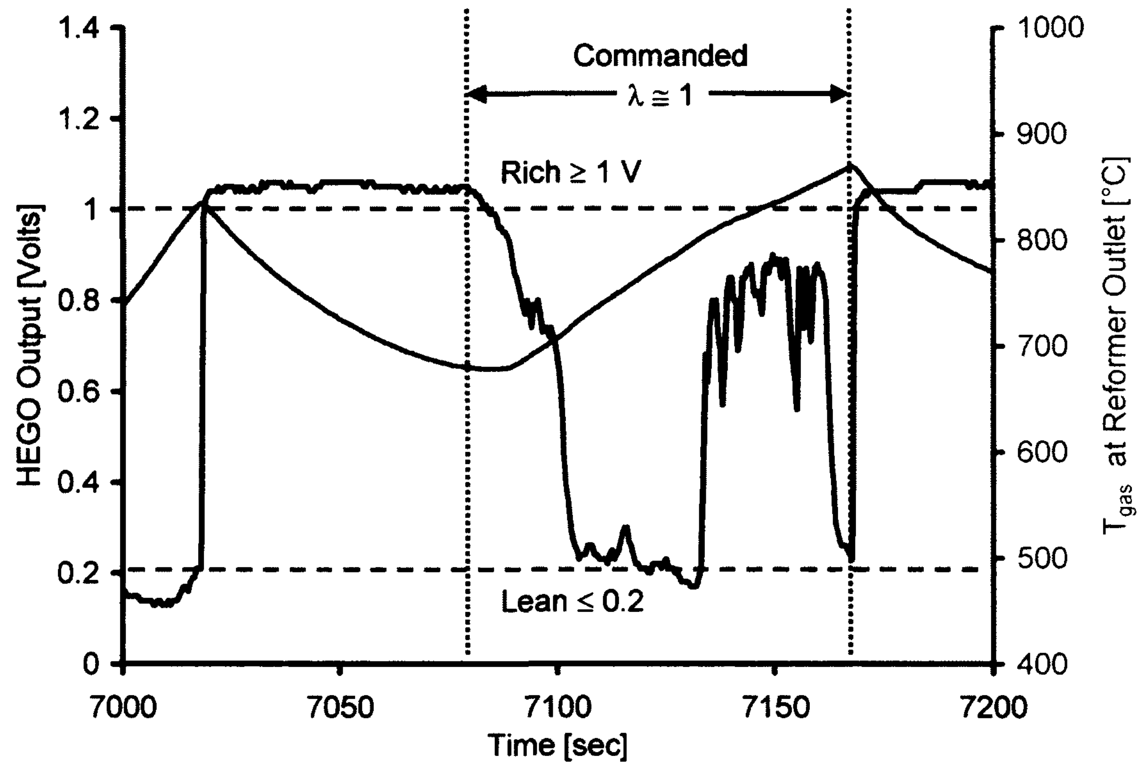

Figure 6.43: CEGR Reformer Fuel Calibration Tests

The fluctuations in the HEGO sensor output can be due to several reasons. Fuel slip through the catalytic reformer due to non-homogeneities in the fuel-EGR mixture, will create local rich pockets in the mixture. Secondly, some of the fuel can deposit on the pipe walls in the mixing zone during rich operation and this deposit evaporation will transiently and sporadically enrich the stoichiometric mixture. Another parameter affecting the mixture strength can be the fluctuating nature of the EGR stream.

6.10.2. CEGR Full Flow Operation

Tests were conducted by holding one of the fuel streams constant and varying the other to identify the individual limiting conditions of CEGR. In the first set of experiments, the reformer fuel injection was kept constant and the pilot injection quantity was changed. The EGR was kept at 32%. The results are shown in Figure 6.44. The engine baseline conditions in the figures represent the engine operation without CEGR operation and all comparisons for emission and power production have been referenced against the baseline. Moreover, the pilot quantity was varied by changing the engine speed through the dynamometer (the mechanical governor adjusts the fuelling). The EGR stream was heated up with the electric heater (set at 0.75 kW).

As the pilot fuel was progressively reduced, the oxygen contents in the exhaust gas increased. This reduced the strength of the rich mixture which resulted in an increase in the oxygen excess ratio of the CEGR Reformer. The contribution of the gaseous fuel (from CEGR) to power production also increased. The soot emission reduced due to the progressively enhanced premixed combustion phase. This, however, did not increase the NOx emission as the overall flame temperature was thought to be lower due to decreased intake oxygen contents and the overall lean mixture inside the cylinder.

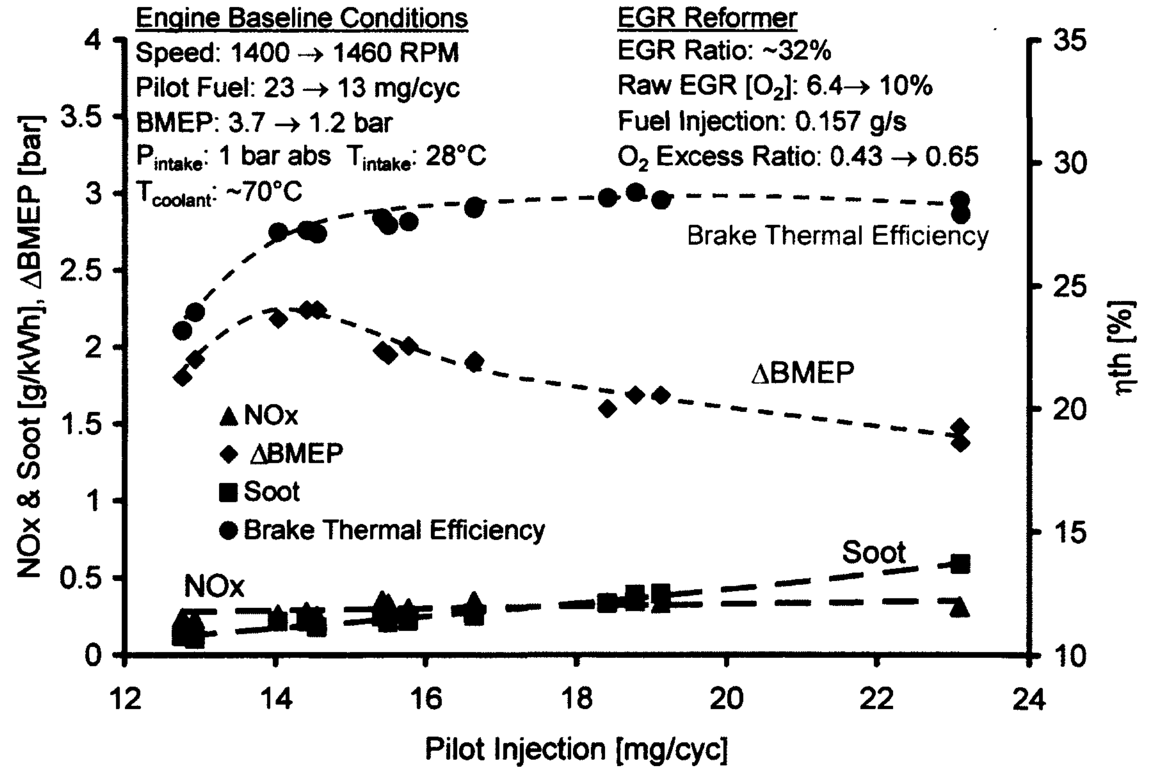

Figure 6.44: Full-Flow EGR Reforming – Pilot Injection Quantity Variation (32% EGR)

The experiments were repeated at a lower EGR level of 20%. As the EGR was reduced, the oxygen concentration in the exhaust increased. However, the flow through the CEGR also reduced. Thus when using the same CEGR fuel injection quantity as with moderate EGR, the strength of the fuel rich mixture increased, which reduced the oxygen excess ratio. The heating requirement with the electric heater also reduced to 0.4 kW. The results are shown in Figure 6.45. The thermal efficiency was higher as compared to the 32% EGR case since the gaseous fuel quantity was increased (ΔBMEP is higher). NOx decreased as the pilot diesel was reduced (the combustion became leaner). The soot emission remained low at this EGR level.

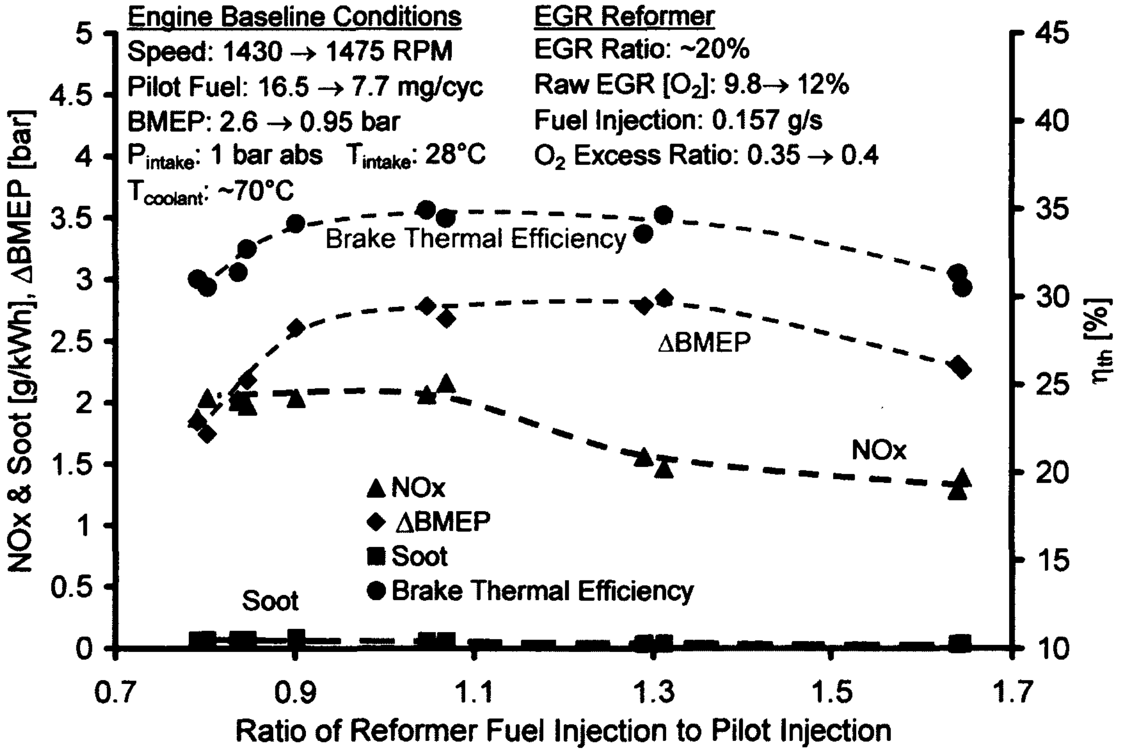

Figure 6.45: Full Flow EGR Reforming – Pilot Injection Quantity Variation (20% EGR)

The procedure was repeated by varying the reformer fuel injection quantity (thereby changing the CEGR oxygen excess ratio) while keeping a fixed pilot quantity of 23.1 mg/cyc (EGR: 20%). The contribution of gaseous fuel was therefore referenced against the baseline BMEP at the fixed pilot injection quantity. The results are shown in Figure 6.46. With the full-flow operation, an increase in the hydrogen production was observed around oxygen excess ratio greater than 0.65. Moreover, the maximum increase in the BMEP was around 2 bar. However, no substantial gains in the BMEP were observed by further increasing the reformer fuel injection quantity and therefore a decrease in the overall system efficiency occurred.

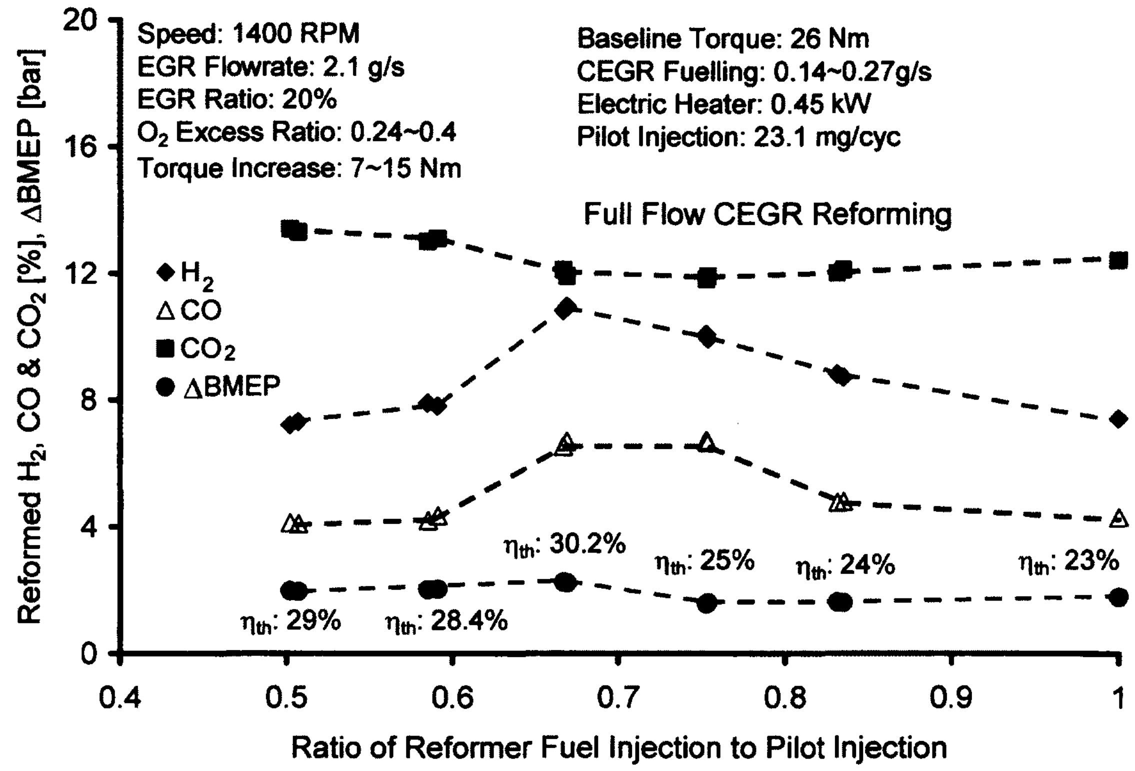

Figure 6.46: Full-Flow EGR Reforming (20% EGR) – Reformer Fuel Quantity Variation

To observe the effect of varying the reformer injection quantity at a lower quantity of pilot fuel, tests were conducted with a fixed low pilot injection quantity and 16% EGR and the results are shown in Figure 6.47. As the reformer fuel injection quantity was increased, it resulted in an increase in the gaseous fuel production which was evident by the increase in ΔBMEP and the brake thermal efficiency.

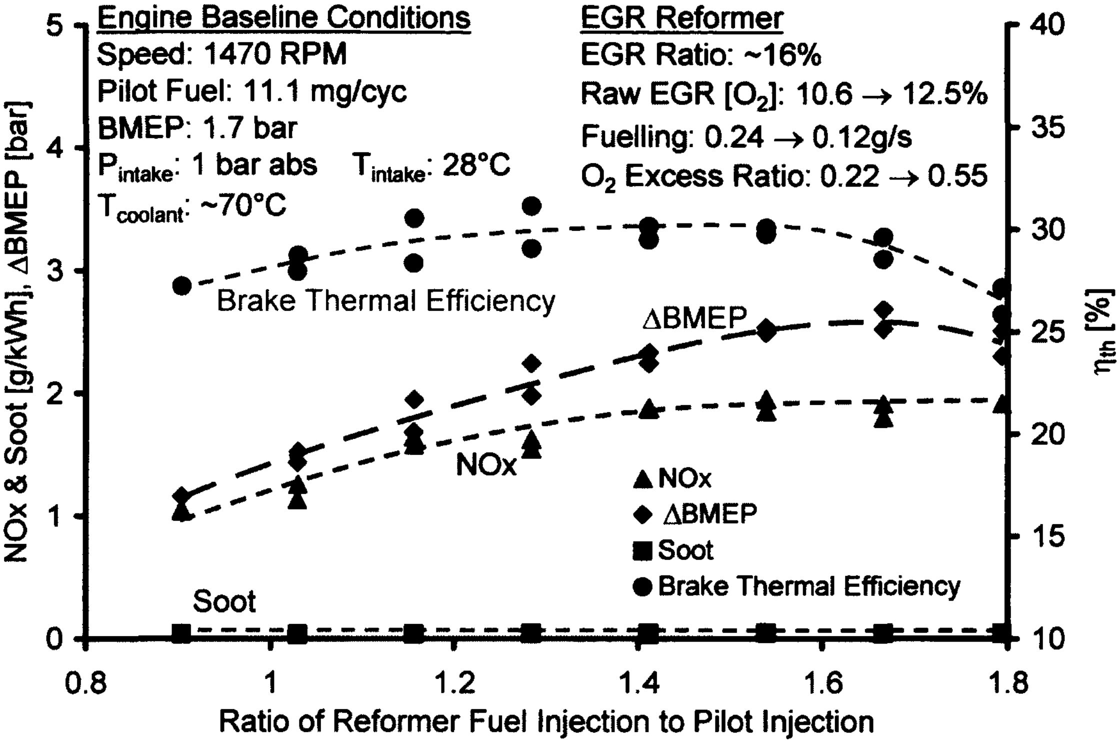

Figure 6.47: Full Flow EGR Reforming – Pilot Injection Quantity Variation (16% EGR)

The reformed gas composition is shown in Figure 6.48. As the ratio of the reformer fuel injection to the pilot fuel was increased, the HC emission and the CO_2 quantity started to increase. However, a reduction in the CO concentration was observed as the hydrogen production started together with an increase in the BMEP (Figure 6.47). Since the oxygen excess ratio indicated a significantly rich operation, it is believed that a substantial amount of hydrogen was generated under these conditions via partial oxidation mechanisms and water gas-shift reactions. Previous research [123,125,126] also suggests that under rich conditions, hydrogen is generated from the partial oxidation of the fuel vapour. It was also observed that the contribution of the reformed gases to the engine power was at a maximum when the CO concentration was nearly half of the hydrogen concentration. However, beyond a certain limit, the efficiency started to drop possibly due to reduction in the production of the gaseous fuels.

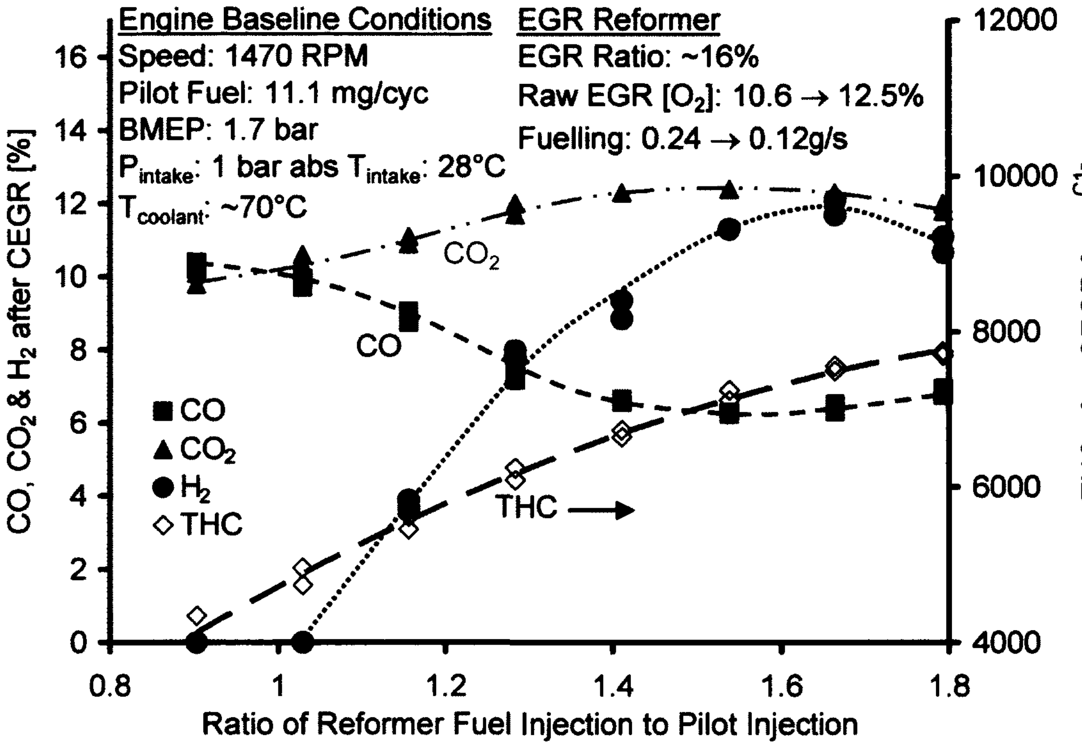

Figure 6.48: Reformed Gas Composition – Full Flow (16% EGR & Low Fixed Pilot)

A comparison of the NOx and soot emissions with CEGR, to the baseline emissions with raw EGR is given in Table 6.6. The NOx emission was found to be significantly lower with CEGR due to the overall lean combustion. The soot emission also reduced, indicating the possible enhancement of the premixed part of the combustion.

Table 6.6: Exhaust Emission Comparison for Full Flow CEGR

EGR		NOx (g/kW-h)	Soot (g/kW-h)
32%	Untreated	1.3	0.21
	Treated (Reforming)	0.25	0.17
20%	Untreated	4.1	0.11
	Treated (Reforming)	2	0.06

6.10.3. CEGR Partial Bypass-Flow Operation

The CEGR partial bypass-flow operation was first investigated at different CEGR injection quantities with a fixed pilot quantity. The results shown in Figure 6.49 indicated that the brake thermal efficiency was not significantly affected since the low EGR flow through the reformer required less fuel for rich operation. Thus the contribution to power production can be relatively higher as compared to the full flow operation at the same CEGR fuelling rate.

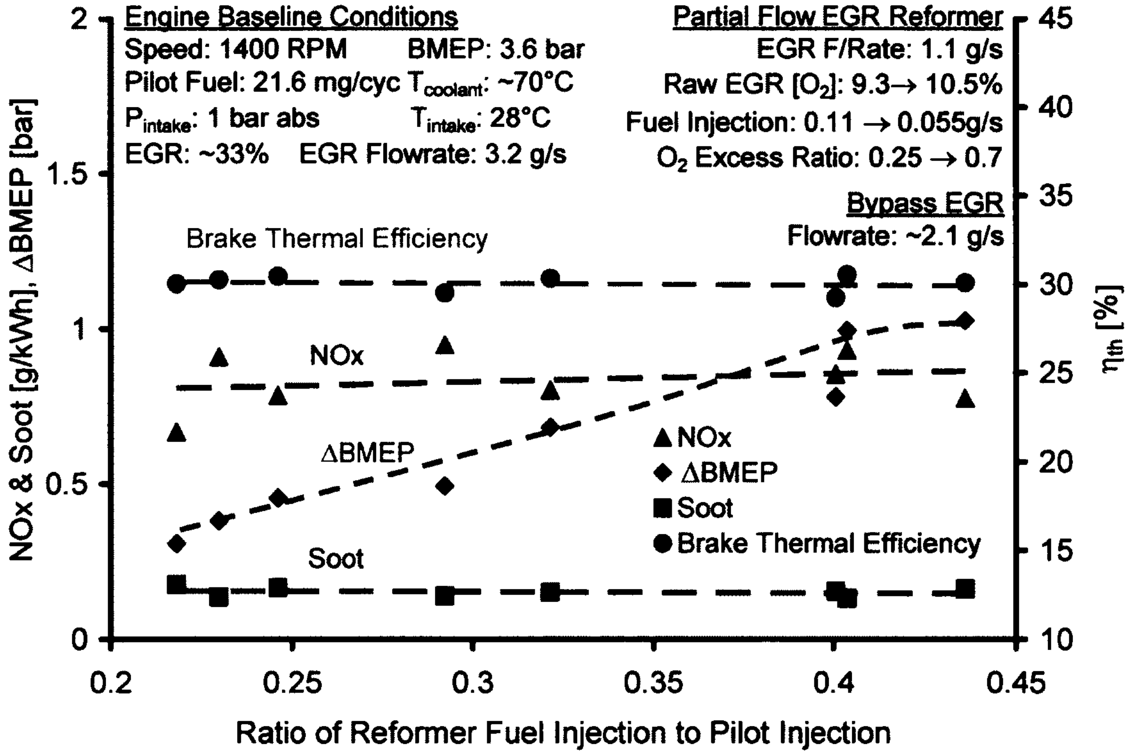

Figure 6.49: Partial Flow EGR Reformer with Fixed Pilot- Ratio of the Two Fuel Injections

The partial-flow operation was repeated at a lower EGR (20%). At low load operation, the production of hydrogen was around 10~12% over a wider oxygen excess ratio range as shown in Figure 6.50. The increase in the BMEP was less as the partial exhaust stream limited the quantity of gaseous fuel that could be generated during the reforming process. Since the reformer fuelling in this case was nearly the same as for the full flow operation of Figure 6.46, the thermal efficiency during partial-flow operation was also lower. This can be attributed to the inability of the fuel to mix thoroughly with the slower exhaust stream, resulting in fuel-slip through the reformer, and locally very rich and lean monolith channels which do not contribute to gaseous fuel production.

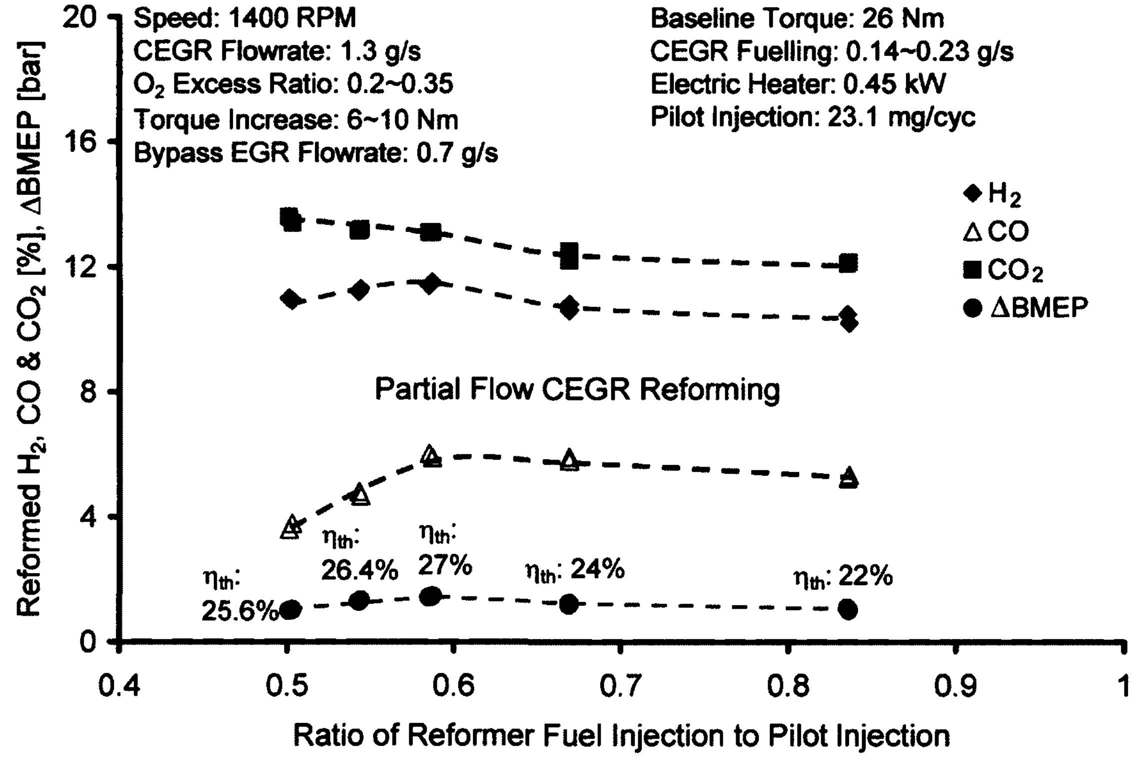

Figure 6.50: Partial-Flow EGR Reforming with Fixed Pilot – Reformer Fuel Quantity Variation

The exhaust emission comparison between the full-flow and the partial flow for the same baseline condition is given in Table 6.7. The partial flow CEGR operation helped to reduce the NOx but the reduction was less than that with full flow CEGR operation. However, the soot emission was similar to that with the full-flow operation and indicated that a small increase in the premixed combustion can be quite effective to reduce the soot emission.

Table 6.7: Exhaust Emission Comparison (Full vs. Partial Flow)

EGR		NOx (g/kWh)	Soot (g/kWh)
32%	Untreated	1.3	0.21
	Full Flow (Treated)	0.25	0.17
	Partial Flow (Treated)	0.8	0.15
20%	Untreated	4.1	0.11
	Full Flow (Treated)	2	0.06
	Partial Flow (Treated)	2.7	0.07

During both the CEGR partial-flow and the full-flow modes, the hydrogen content of the reformed gases was typically around 10~12% which was similar to values reported in the literature [122,125,126]. The CO content was approximately half of the corresponding hydrogen content and was almost produced entirely in the reformer since the engine-out CO concentration was very low.

6.10.4. Effect of Reformed Gases on Engine Power

For the results shown in Figure 6.46, the pressure-time history and the heat release rate for the EGR reforming were compared against those for the baseline operation with untreated EGR in Figure 6.51. The pressure trace deviated significantly from the baseline pressure, indicating an increase in the power output. A maximum increase of 2.2 bar in the BMEP was obtained over the baseline BMEP of 3.8 bar for a reformer-to-pilot fuel ratio around 0.65. Moreover, the premixed combustion in the heat release was observed to increase, because of the addition of the reformed gases to the cylinder charge.

Taking into account the electric power for the heating, there was a slight decrease of about 1~2% in the brake thermal efficiency. However, no substantial gains in the BMEP were observed by further increasing the reformer fuel injection quantity and therefore a decrease in the overall system efficiency occurred.

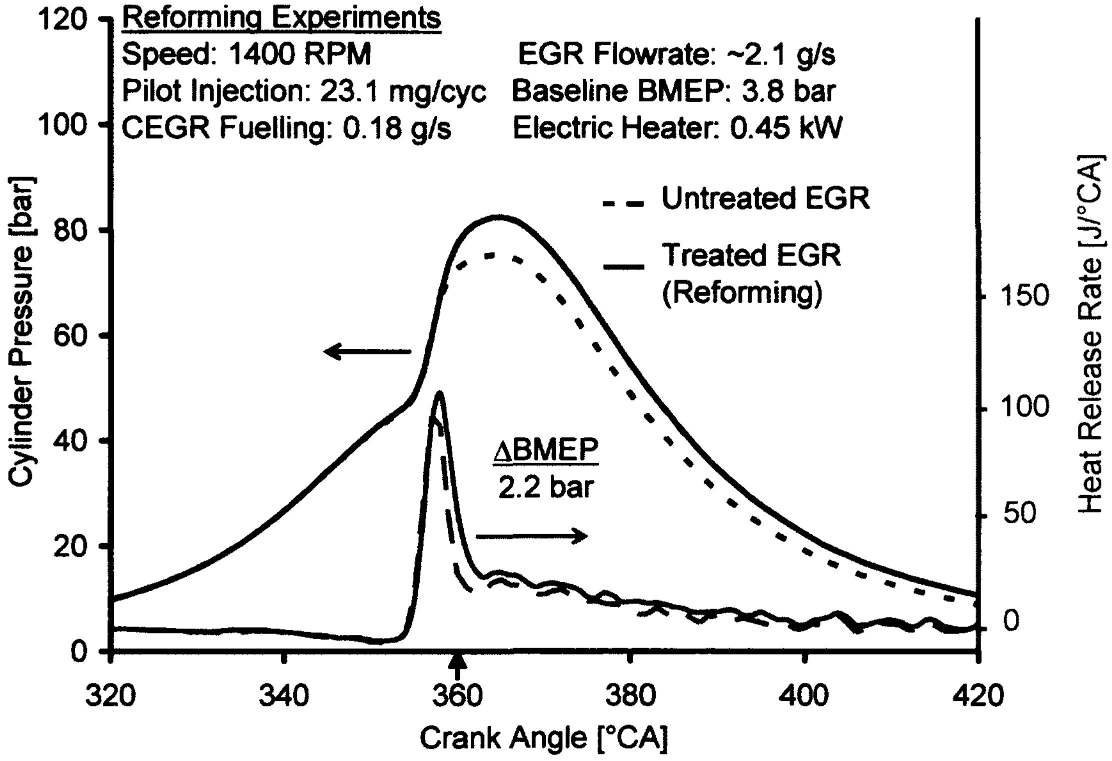

Figure 6.51: Pressure-time History and Heat Release Rate for CEGR Reforming Operation

The results presented above indicated that an optimal ratio exists between the CEGR fuel injection quantity and the pilot fuel quantity. The total energy for power production comes from the combination of gaseous fuel and pilot diesel. These two quantities are largely related to each other for a given power demand. With the baseline condition set at 1400 RPM (BMEP = 3.8 bar) during the experiments, the contribution of the two fuel streams to power production was investigated at different flow rates and fuelling of the CEGR, and the result for one set of operating condition is shown in Figure 6.52.

Since the Yanmar engine had a mechanical fuel injection pump fitted with a governor, the pilot injection at a fixed fuel rack position was reduced by increasing the engine speed through the dynamometer controller (the governor cuts the fuels at a fixed fuel rack position).

The CEGR operation was started with a fixed injection quantity while reducing the pilot injection quantity from the baseline quantity of 23 mg/cyc. It was observed that the CEGR increased the BMEP above the baseline value (at 1440 RPM). By progressively reducing the pilot injection, the BMEP matched the baseline value at 1450 RPM with a pilot injection of 14.4 mg/cycle. The penalty in the BMEP and therefore the thermal efficiency started to increase once the pilot quantity was reduced further.

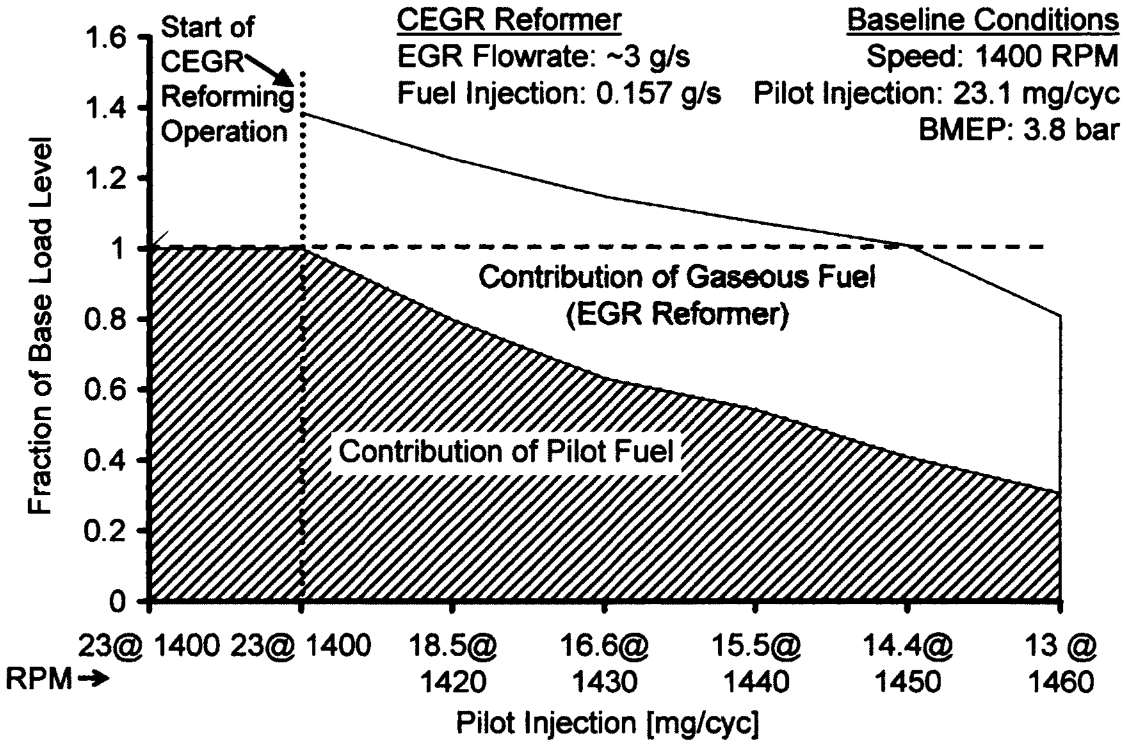

Figure 6.52: CEGR Fuel Injection &and Pilot Fuel Injection Matching for a Given Power Demand

The emissions corresponding to the data shown in Figure 6.52 are given in Table 6.8. The baseline emissions at 1400 RPM were 0.71 and 0.24 g/kWh for NOx and soot respectively. As the reforming operation was started, the NOx reduced by half but the soot increased since the engine load was also increased. At 1450 RPM when the load matched the baseline load, the NOx emission was 0.27g/kWh while the soot emission was 0.21g/kWh. Thus, the two fuel quantities or their ratio can be matched for the best fuel efficiency or reduced exhaust emissions.

Table 6.8: NOx & Soot Emissions for Figure 6.52

Speed (RPM)	1400	1400	1420	1430	1440	1450	1460
NOx (g/kWh)	0.71	0.32	0.34	0.34	0.33	0.27	0.24
Soot (g/kWh)	0.24	0.6	0.39	0.26	0.22	0.21	0.12

The gain in the BMEP was higher for the full-flow mode as shown in Figure 6.53. This is because the whole of the EGR stream was used during the reforming process, resulting in a higher yield of gaseous fuels. However, the partial-flow operation was more energy efficient (η_{th}: ~30% vs η_{th}: ~27% for full flow) during low torque and high EGR operation, as the engine exhaust contained high concentrations of oxygen and low concentrations of CO_2.

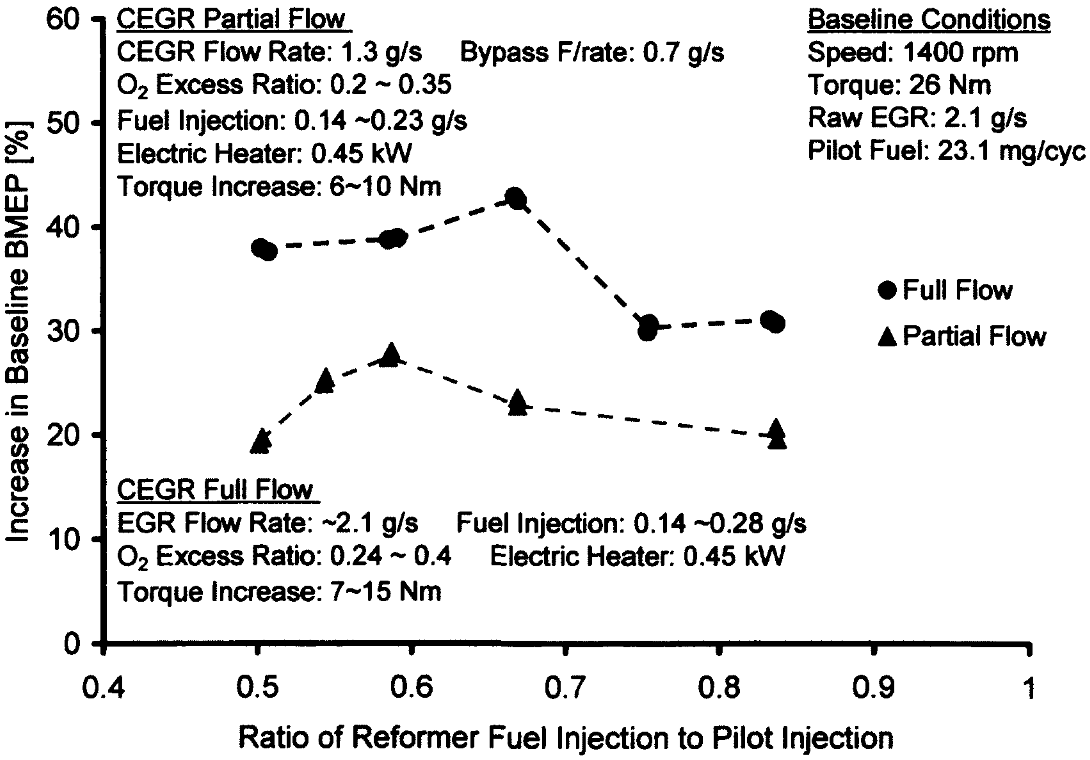

Figure 6.53: Percentage Increase in Baseline BMEP with CEGR Reforming

6.10.5. Effects of Water Addition on Reformer Operation

Application tests were conducted to ascertain the effects of water injection on the reformed gas production and the in-cylinder combustion. The pressure-time history and the heat release rate for EGR reforming operation with water addition were compared against those for the baseline operation with raw untreated EGR in Figure 6.54. It was observed that the pressure trace deviated from the baseline pressure, indicating a small increase in the power output (ΔBMEP=0.6 bar). Moreover, the premixed combustion in the heat release was increased slightly, indicating a possible enhancement of the charge homogeneity with the addition of the reformed gases to the cylinder charge.

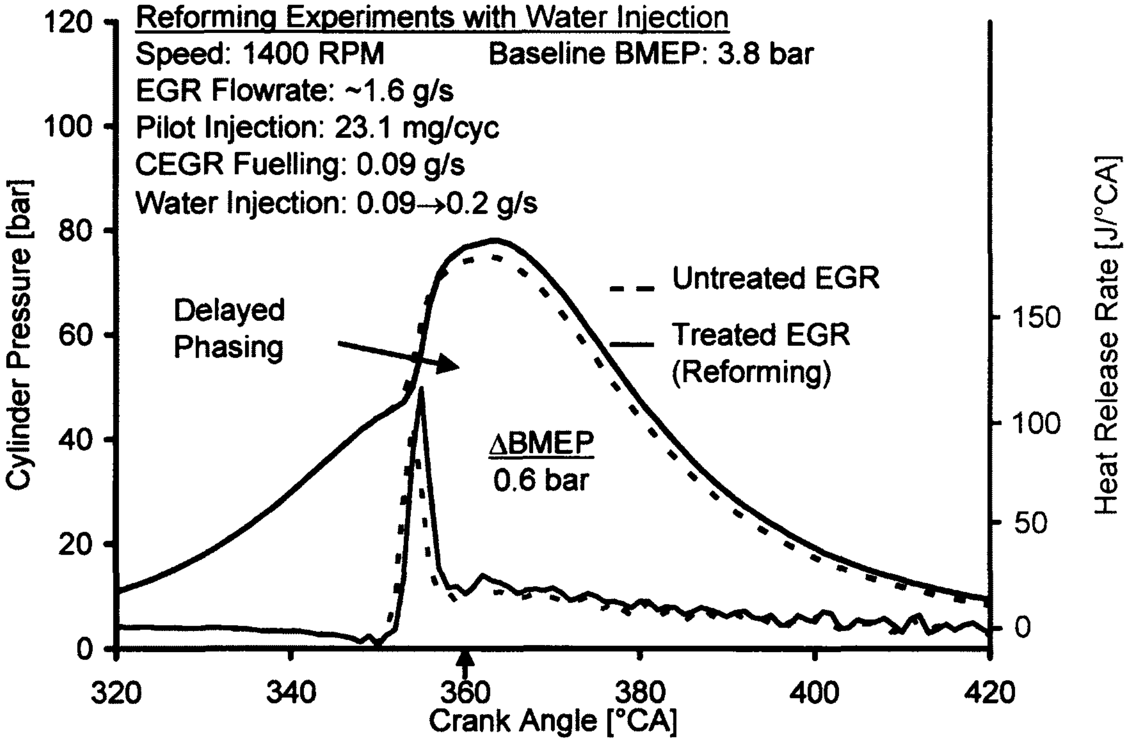

Figure 6.54: Pressure-time History and Heat Release Rate for CEGR Reforming Operation with Water Injection

The change in the engine torque as the reformed gases were recycled to the engine intake is shown in Figure 6.55. The engine torque started to increase immediately as the fuel was injected into the reformer. The increase in the torque stabilized as the reformer temperature reached steady state conditions. A constant amount of fuel (0.09 g/s) was injected into the EGR stream during these experiments.

A significant advantage of the EGR reforming process (with or without water addition) is the potential to generate higher levels of EGR (CO_2), especially at low load conditions. The generation of the synthetic EGR is due to the high CO_2 concentration (12~14%) in the reformed gas because a part of the injected fuel undergoes partial or complete oxidation while the rest of the fuel is used in the endothermic reforming process [63].

For the results shown in Figure 6.55, the EGR rate was about 15% once calculated on the mass flow rate basis. The EGR rate based on the CO_2 concentrations in the intake and the exhaust gases was also close to 14% before the start of the reforming process. However, it is evident that the synthetic EGR enhanced the effective EGR rate to about 25% during the reforming process. This can have significant implications on the engine-out emissions as is discussed later.

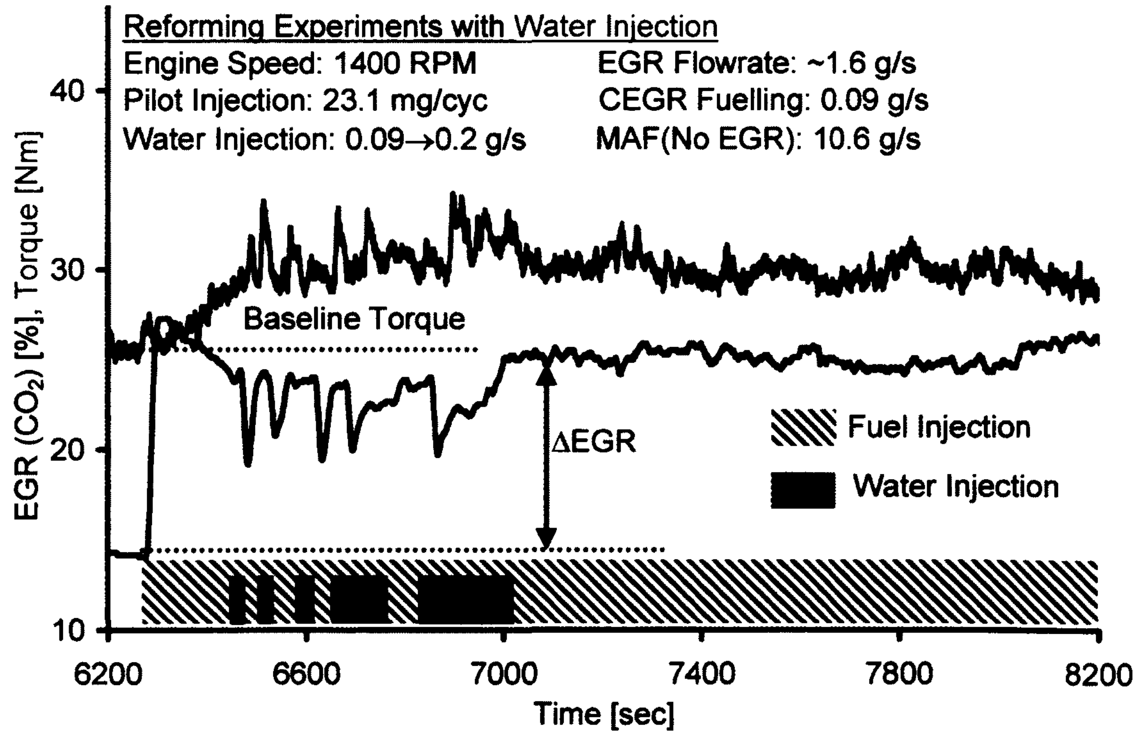

Figure 6.55: Synthetic EGR Generation with CEGR Reforming with Water Injection

The effect of water injection on the power increase is also indicated in Figure 6.55. It was observed that a surge in the torque was seen corresponding to each water injection event. Moreover, the increase in the torque was momentary and was not sustained during the entire duration of the water injection. To verify this phenomenon, the cycle-by-cycle IMEP was calculated from continuously recorded pressure traces and is presented in Figure 6.56.

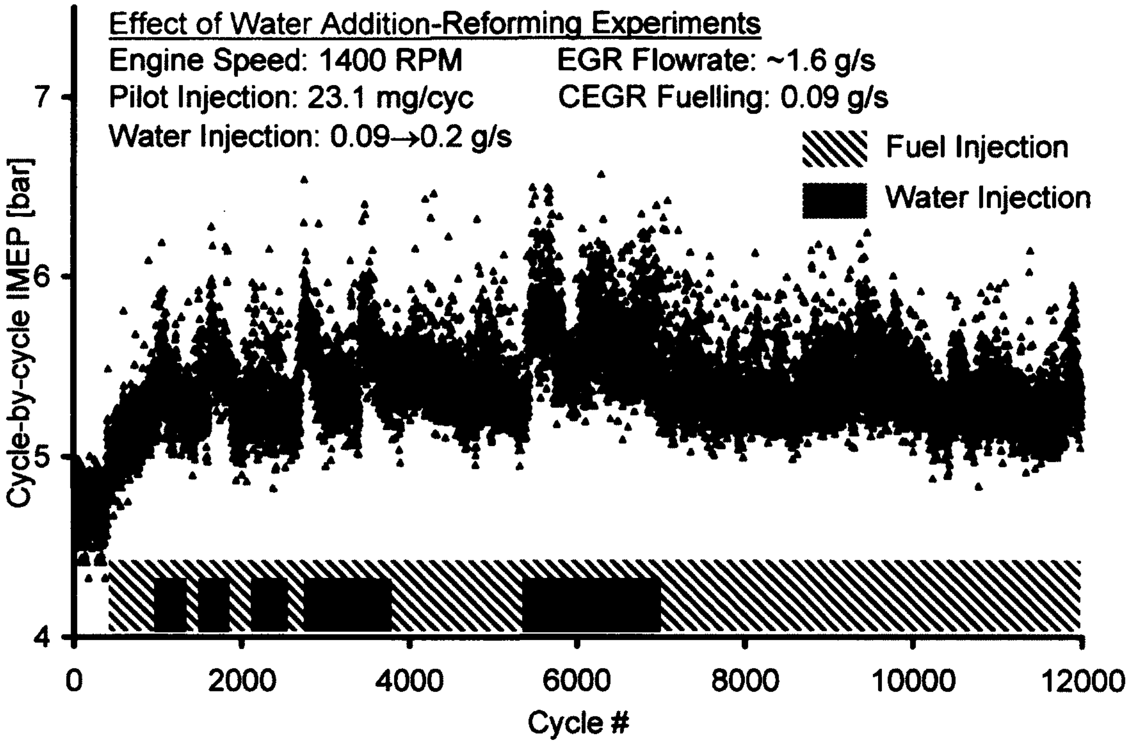

Figure 6.56: Cycle-by-cycle IMEP Calculation – Effect of Water Injection

The cycle-by-cycle IMEP clearly showed the transient effect of the water injection on the engine power output. First, a surge in the power output was accompanied by a decrease in the CO_2 concentration in the EGR loop (CO_2 based EGR- Figure 6.55). A brief explanation for this phenomenon is presented here. The decrease in CO_2 may have initiated the dry reforming process of hydrocarbon fuels where a part of the fuel and carbon dioxide may react to produce more hydrogen at elevated temperatures. This highlighted the importance of closely monitoring the reformer substrate temperature to see if any localized high temperature regions developed during the reforming process. Second, the catalytic substrate in the reformer consisted of two portions with a gap of about 13 mm. This was done to facilitate mixing so that any mal-distribution of the fuel-gas-water mixture at the reformer inlet may be corrected by allowing the mixing and redistribution of any rich channel streams with the lean channel streams. It is thought that some of the hydrogen produced may have been destroyed during this redistribution as any interaction with oxygen (from lean channels) at such high temperatures would certainly result in hydrogen reacting with the oxygen.

A comparison of the emissions and other performance parameters is given in Table 6.9. It can be seen that NOx was reduced considerably without an increase in the soot emission. The emissions of CO and THC were slightly higher but these can easily be dealt with diesel oxidation catalysts in the exhaust system.

Table 6.9: Performance Comparison of Untreated & Treated EGR (Water Addition)

	Raw EGR (Baseline)	Treated EGR (Reforming with Water)
Pilot Injection [g/s]	0.27	0.27
Reformer Injection [g/s]	-	0.09
Torque [Nm]	26	33
BMEP [bar]	3.8	4.4
IMEP [bar]	4.9	5.5
Indicated Thermal Efficiency [%]	42.3	36
NOx [g/kWh]	7.4	4.9
Soot [g/kWh]	0.13	0.1
CO [g/kWh]	1.6	6.8
THC^{C1} [g/kWh]	0.23	0.55

6.11. Flow Reversal CEGR Reformer

The active management of the exhaust flow through periodic flow reversal, flow stagnation and parallel flow was first proposed and implemented in the exhaust system of a diesel engine by Zheng et al. [127,129,130]. Periodic flow reversal operation is, in essence, a heat energy trap that performs active heat recovery in addition to the heat retention capability of the monolith structure. By cyclically alternating the direction of exhaust flow, a thermal wave is produced along the catalyst at the frequency of flow reversal, so that the central catalyst temperature is elevated above the reformer inlet/engine exhaust temperature. Thus, the averaged temperature level of the catalytic monolith is raised substantially independent of the inflow gas temperature from the engine exhaust, while an ordinary flow-through catalyst reformer would lose light off (unable to sustain catalytic reactions) following similar operations with low exhaust temperatures.

The flow–reversal catalytic reformer can have three modes of operation: forward flow where the exhaust gas flows as in a conventional unidirectional reformer; reverse flow where the inlet and the outlet are switched to reverse the flow direction through the catalytic monolith and bypass flow where the catalytic monolith is bypassed and the exhaust gas flows directly from the inlet to the outlet.

6.12. Flow Reversal Experimental Setup

The test setup for the flow reversal reformer with central heating/fuelling is schematically shown in Figure 6.57 and the actual test setup is shown in Figure 6.58. The flow reversal setup is a novel departure from the unidirectional reforming setup. For the flow-reversal setup, the CEGR loop includes the flow-reversal reformer with an electric heater, a fuel dispenser, a water dispenser and a mixer at the central portion of the catalyst. A measured quantity of diesel fuel is vaporized through atomization and by mixing with the localized hot exhaust gas in the central portion to generate a homogeneous rich mixture.

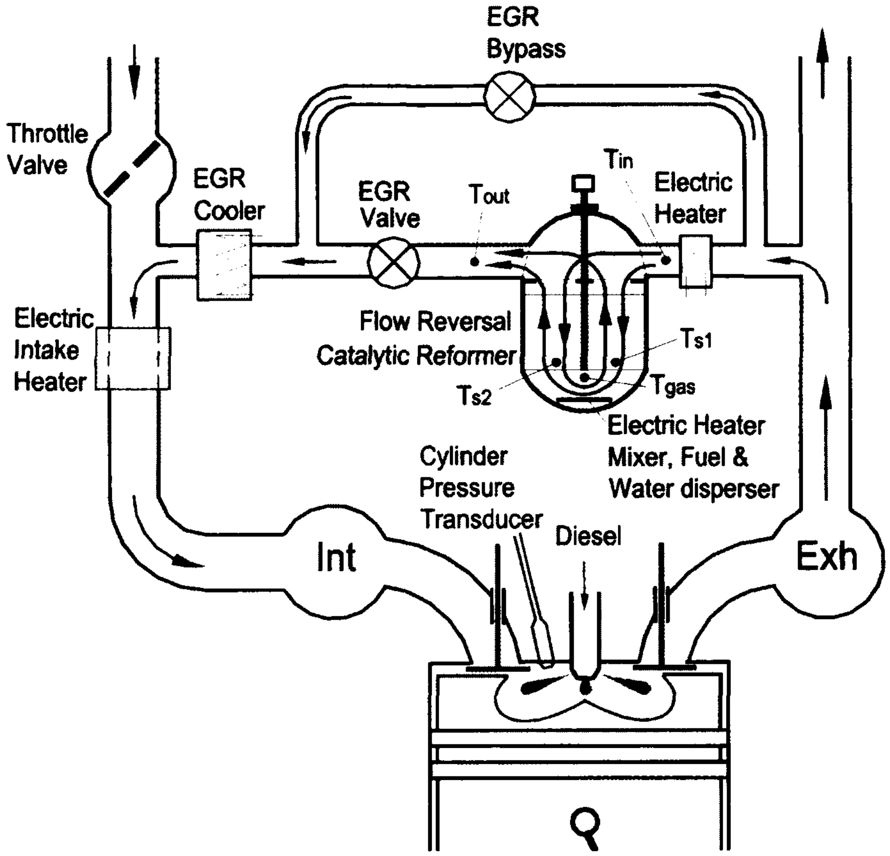

Figure 6.57: Schematic Representation of the Experimental Setup – Flow Reversal

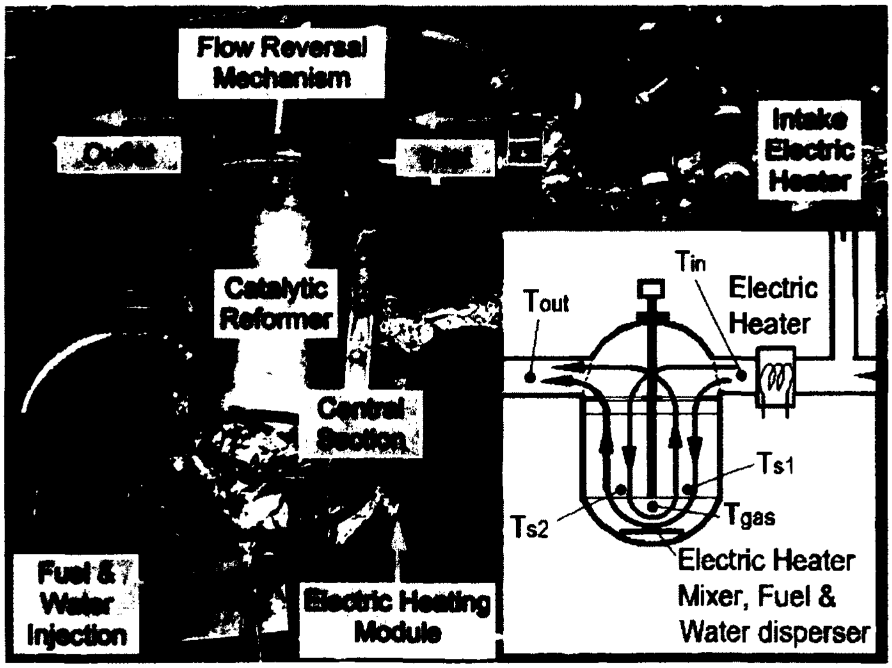

Figure 6.58: EGR Fuel Reformer in a Flow Reversal Central Fuelling Embedment

6.13. Flow Reversal CEGR in Reforming Mode

The potential of the flow reversal CEGR for gaseous fuel generation was investigated by keeping the ΔBMEP approximately constant while changing the pilot and the reformer fuel quantities. The results, shown in Figure 6.59 indicate that the contribution of the reformed gaseous fuel towards power production can be optimized for each pilot fuel injection quantity. The maximum hydrogen production during this test was about 10%. It should be noted here that the baseline BMEP and IMEP reduced as the pilot injection was progressively decreased. However, the increase in the reformer fuel injection was used to maintain the same ΔBMEP. The percentage increase in the baseline IMEP signified the relative contribution of the reformed gases towards power production.

The effective of the reforming operation was similar to that observed with the uni-directional flow. However, the lower heating requirements (the heater was switched off once the reformer operation started in the flow reversal tests) resulted in recovering a part of the fuel efficiency penalty (1 to 2%).

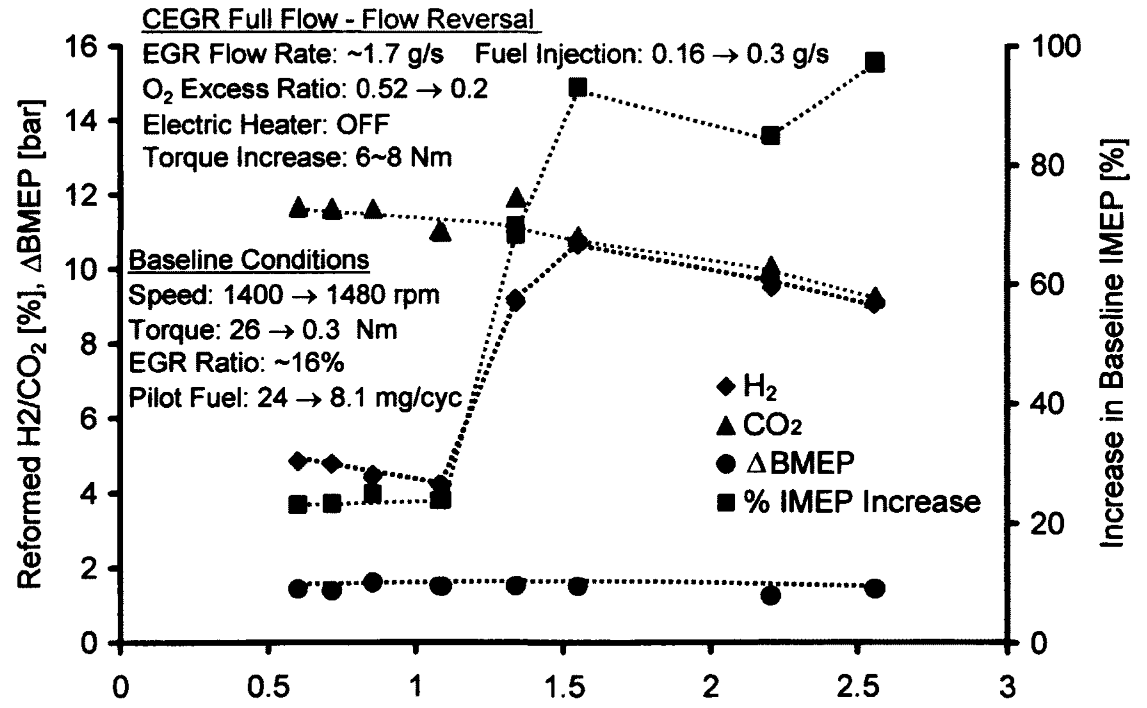

Figure 6.59: Flow Reversal CEGR for Constant ΔBMEP

6.13.1. Heat Retention Capability

The biggest advantage of the flow reversal operation is the excellent heat retention capability. Periodic flow reversal operation is, in essence, a heat energy trap that performs active heat recovery in addition to the heat retention capability of the monolith structure. By cyclically alternating the direction of exhaust flow, a thermal wave is produced along the catalyst at the frequency of flow reversal, so that the central catalyst temperature is elevated above the reformer inlet/engine exhaust temperature. Thus, the averaged temperature level of the catalytic monolith is raised substantially independent of the inflow gas temperature from the engine exhaust, while an ordinary flow-through catalyst reformer would lose light off (unable to sustain catalytic reactions) following similar operations with low exhaust temperatures because the thermal energy stored in the monolith will quickly migrate out of the reformer with the EGR flow. Therefore, in case of the unidirectional flow reformer, a large amount of supplemental heating is generally required to sustain catalytic reactions.

The efficiency of the flow reversal setup in retaining a high temperature at the centre of the substrate with significantly less external energy compared to the unidirectional flow setup in the exhaust system has been extensively demonstrated, both empirically and theoretically previously [127,129,130]. A typical result is shown in Figure 6.60. It can be seen that the flow reversal is able to maintain nearly 40% of the reformer substrate over 500°C with 300 W of external heating. However, even a smaller sized unidirectional reformer ($1\!/_3\,rd$ of the flow reversal reformer in terms of the monolith volume) with inlet heating will require approximately 1 kW of external heating to maintain a temperature above 500°C.

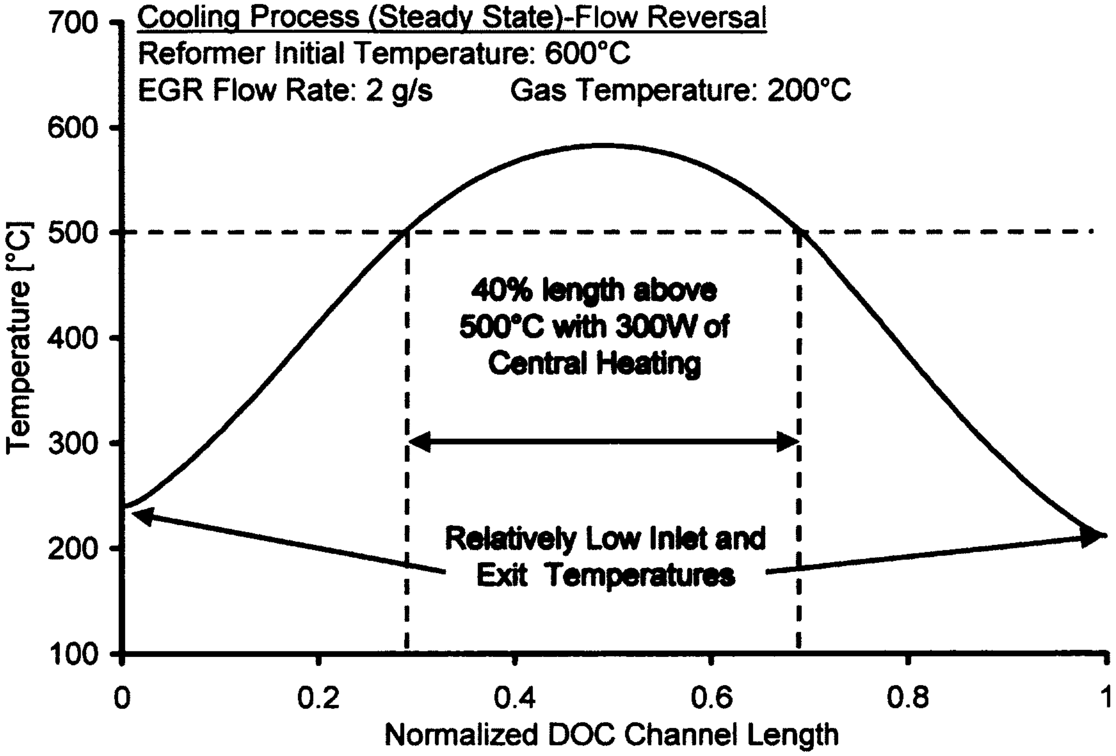

Figure 6.60: Temperature Profile (FR Cycle @ 30 sec) - Simulated Result

It is pertinent to mention here that the triangular temperature profile (high central temperature with lower inlet and exit temperatures) is also effective with inlet fuelling once gaseous fuels like methane are used. Since methane has reduced reactivity at temperatures lower than 500°C, the gaseous fuel effectively combusts in the high-temperature central region of the substrate and is in effect, equivalent to the central heating approach as demonstrated by Zheng et al. [127]. However, with highly reactive fuels like diesel, the inlet fuelling approach will result in heat release reactions occurring closer to the ends (inlet/exit) so that with flow reversal, the thermal wave will be pushed out of the monolith. Therefore, the central fuelling approach is more effective when using reactive fuels like diesel fuel.

6.14. Comparison Between Unidirectional and Flow Reversal CEGR

Compared to the unidirectional EGR reformer with inlet fuelling and heating, the localized central heating/fuelling with flow-reversal has the potential to effectively reduce the heating/fuelling energy requirements by an order of magnitude because of the prevalent high temperatures in the localized central zone of the reformer.

6.14.1. Inlet Heating vs. Central Heating

To enable fuel reforming in the EGR loop, the catalyst monolith must be heated up to temperatures generally above 300°C. The exhaust temperature from modern diesel engines, especially in an EGR loop, is commonly insufficient to enable and/or sustain a high yield of reforming. Supplemental heating is therefore required to raise the exhaust gas temperature to a level that is sufficient to maintain the reformer monolith temperature above the catalyst light-off temperature and to enable the vaporization of the diesel fuel injected into the EGR stream.

The boiling range for the common automotive fuels is given in Figure 6.61 [128]. Compared to gasoline, diesel fuel has a much higher boiling range and requires a temperature above 300°C to vaporize most of the injected fuel. In case of biodiesels, the boiling range is quite narrow and a higher temperature is required for the fuel vaporization. This has important implications for the supplemental heating requirements in the EGR loop.

The experimental results for the unidirectional EGR reformer with inlet heating are shown in Figure 6.62. The exhaust gas temperature in the EGR loop at the heater inlet was about 230°C. With supplemental electrical heating of 560 W, a temperature close to 350°C was attained at the heater outlet. However, due to heat loss from the mixer, the temperature of the exhaust gas was only 245°C at the reformer inlet. When fuel (or water) was injected in the mixing section (Figure 6.33), the temperature dropped further as the fuel vaporized. Therefore, in order to maintain the temperature of the EGR stream around 300°C at the reformer inlet, experiments indicated that a supplemental heating of about 1 kW was required.

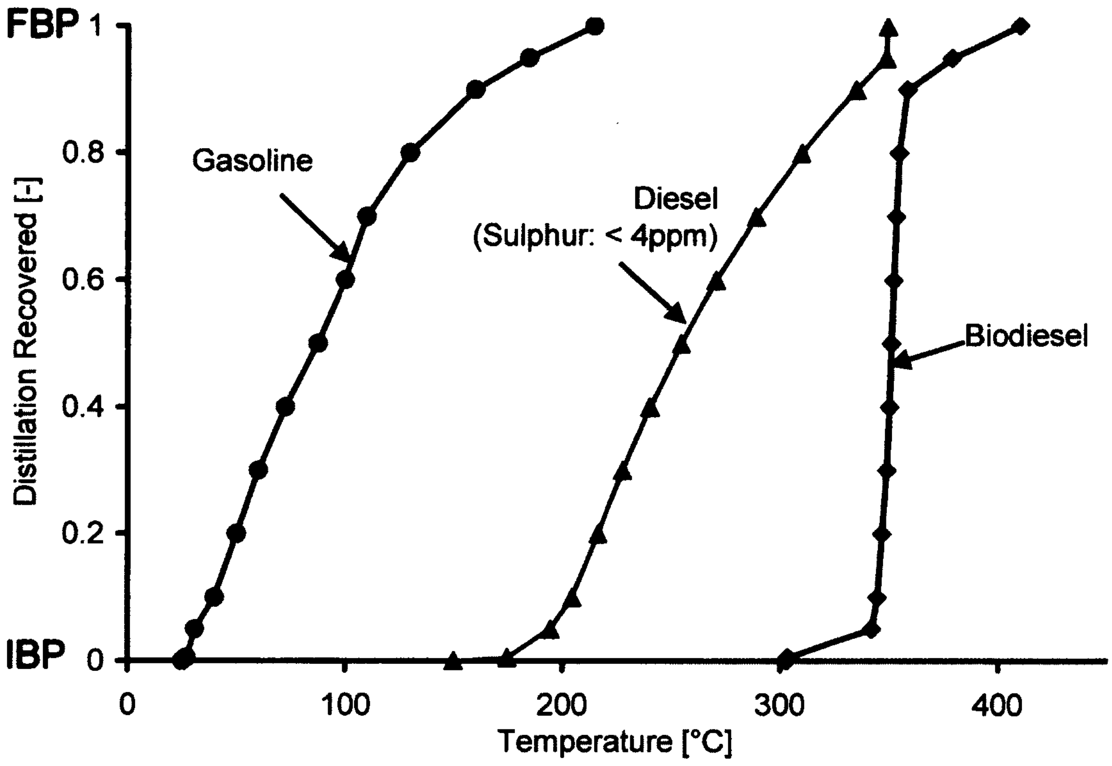

Figure 6.61: Boiling Range for Automotive Fuels

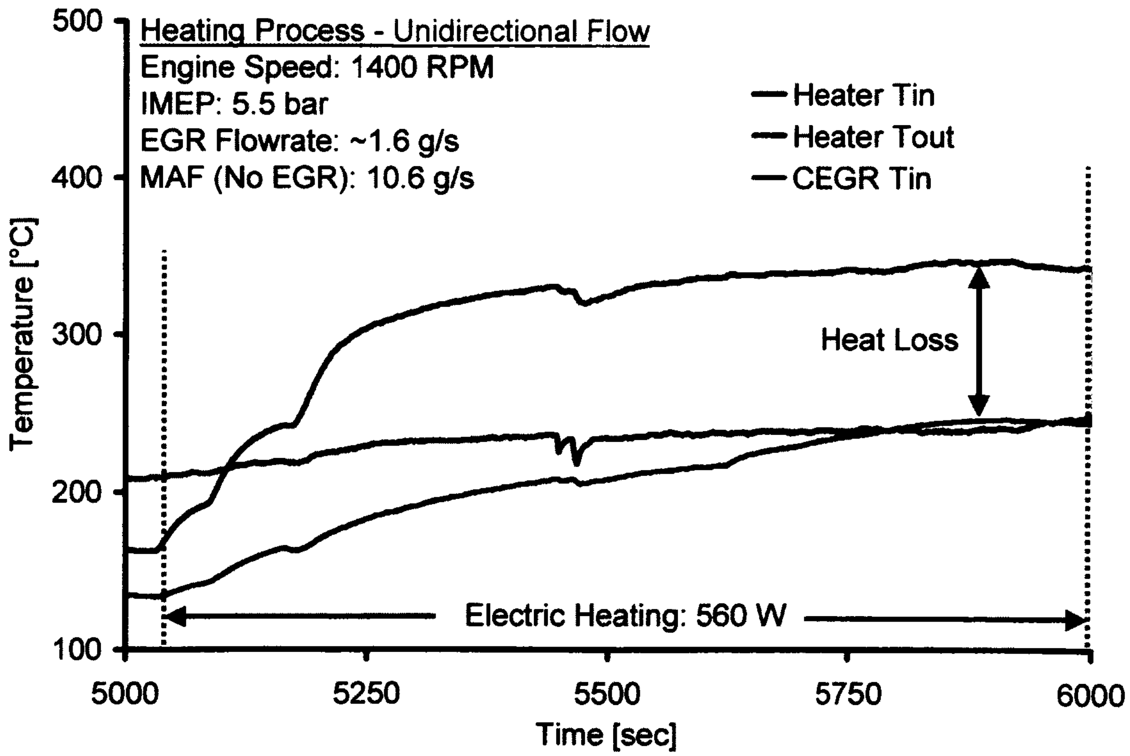

Figure 6.62: Unidirectional Reformer with Inlet Heating

Compared to the unidirectional EGR reformer with inlet heating, the results for the heating process with the flow reversal reformer and central fuelling are shown in Figure 6.63. The engine was motored in this case so that the temperature at the reformer inlet was 25°C. The EGR flow rate was maintained at 2 g/s with a flow reversal interval of 10 to 20 sec. It can be seen that the gas temperature at the centre rose sharply with a similar trend for the two solid temperatures Ts_1 & Ts_2 (see Figure 6.57 for thermocouple locations). However, the reformer inlet and outlet temperatures were negligibly affected by the heating process since the flow reversal operation was able to effectively lock-in the heat at the central section only. With 420 W of supplemental heating, the gas temperature at the central region was increased by about 300°C. This was in sharp contrast to the temperature rise of only 120°C with inlet heating of 560 W for the unidirectional flow. The temperature of the substrate also followed closely because of the reduced heat loss and the superior thermal energy retention with the flow reversal strategy.

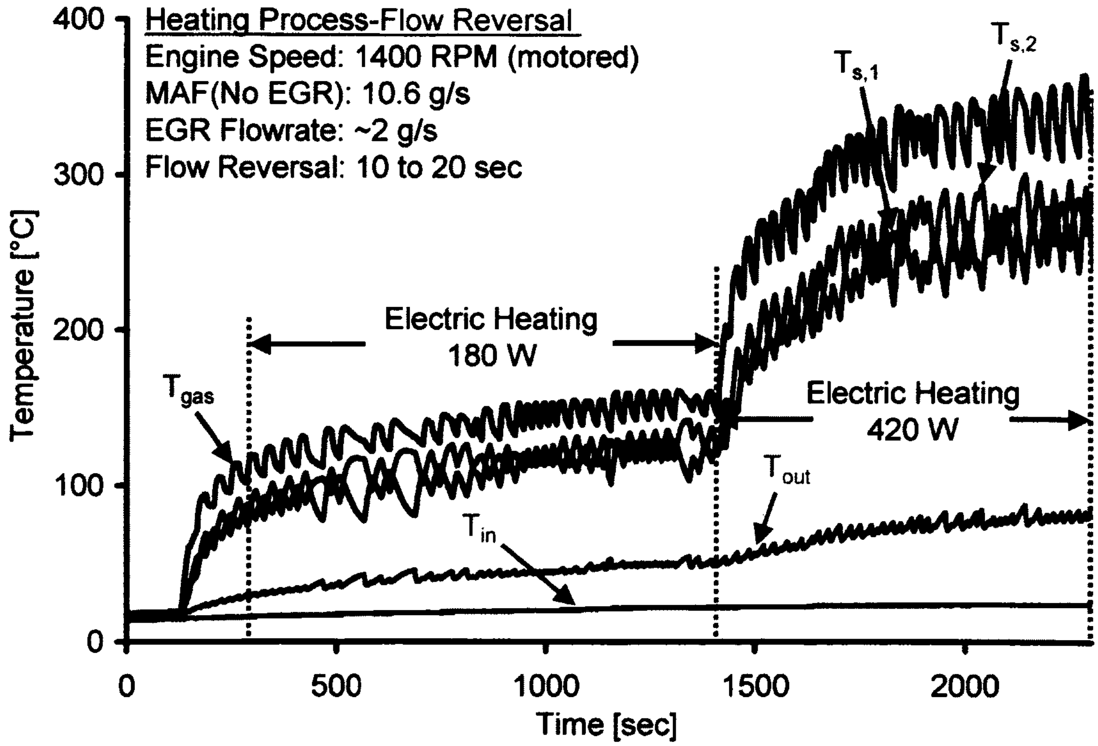

Figure 6.63: Flow Reversal Reformer with Central Heating

Similar test were then conducted at different flow rates and electrical heating input. The results indicated a reduction of up to 50% external heat energy with reversal flow and central fuelling compared to the unidirectional reformer with inlet heating.

The temperature profiles during the CEGR fuel reforming process are shown in Figure 6.64. It was observed that once the central fuel injection was started, the reforming process was generally able to sustain itself (the electric heater switched off in this case). This was not possible with the unidirectional CEGR reformer as the catalytic reforming was not able to sustain the process (the energy migrated out of the reformer). Therefore, a continuous supply of external energy was required with the unidirectional flow. Even without optimizing the setup, a comparison of the two flow modes indicated a reduction of more than 50% external heating requirement with the flow reversal strategy.

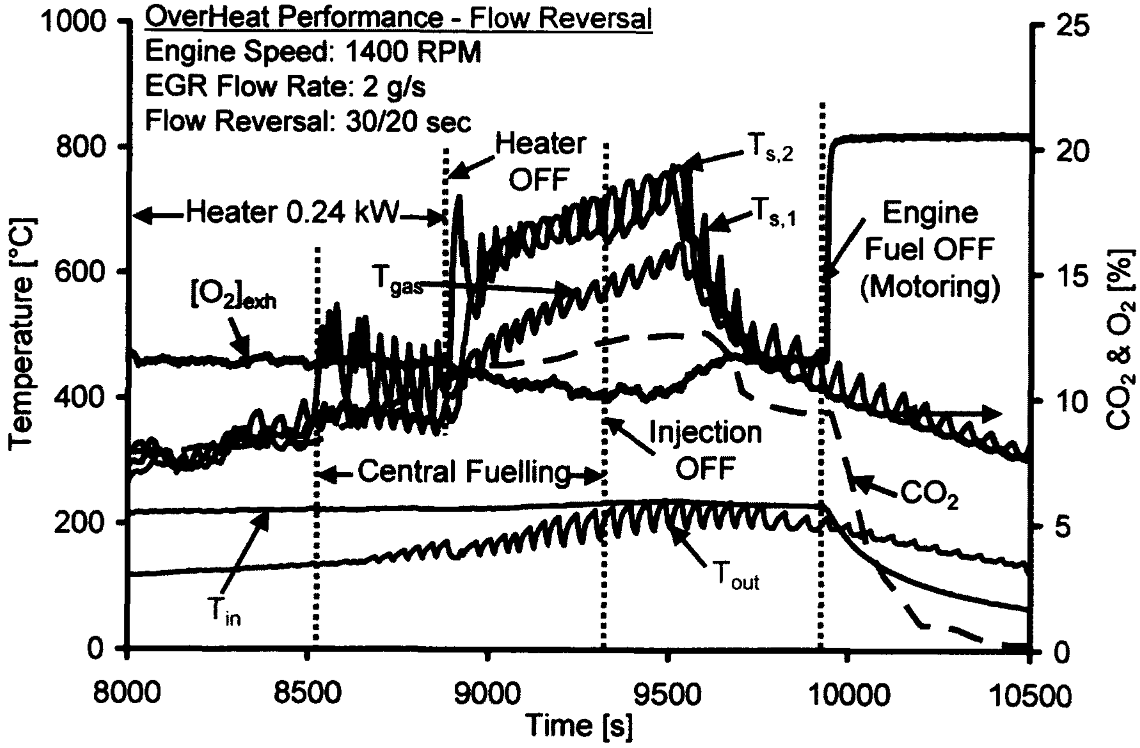

Figure 6.64: Temperature Profiles for Flow Reversal CEGR during Reforming Process

6.14.2. Over Heat Performance

Another important advantage of the flow reversal reforming is its ability to prevent overheating of the reformer monolith once the fuelling is turned off. As the fuel already present inside the reformer is consumed, the process turns highly exothermic (mixture goes from rich-to-stoichiometric-to-lean). The flow reversal operation prevents overheating by distributing the fuel alternately between the two solid sections, thereby allowing the solids to cool down as is evident in Figure 6.64. The results for the unidirectional CEGR reformer are shown in Figure 6.65. Even with reduced exhaust oxygen levels of ~8% (exhaust oxygen was ~10.5% for the flow reversal in Figure 6.64), the fuel accumulated at the entrance of the reformer burned exothermically across the length of the reformer monolith, resulting in a sharp rise in the reformer temperature. Therefore, a large quantity of CO_2 had to be dumped in the CEGR reformer to limit the oxygen supply and prevent overheating which would otherwise result in thermal failure of the reformer.

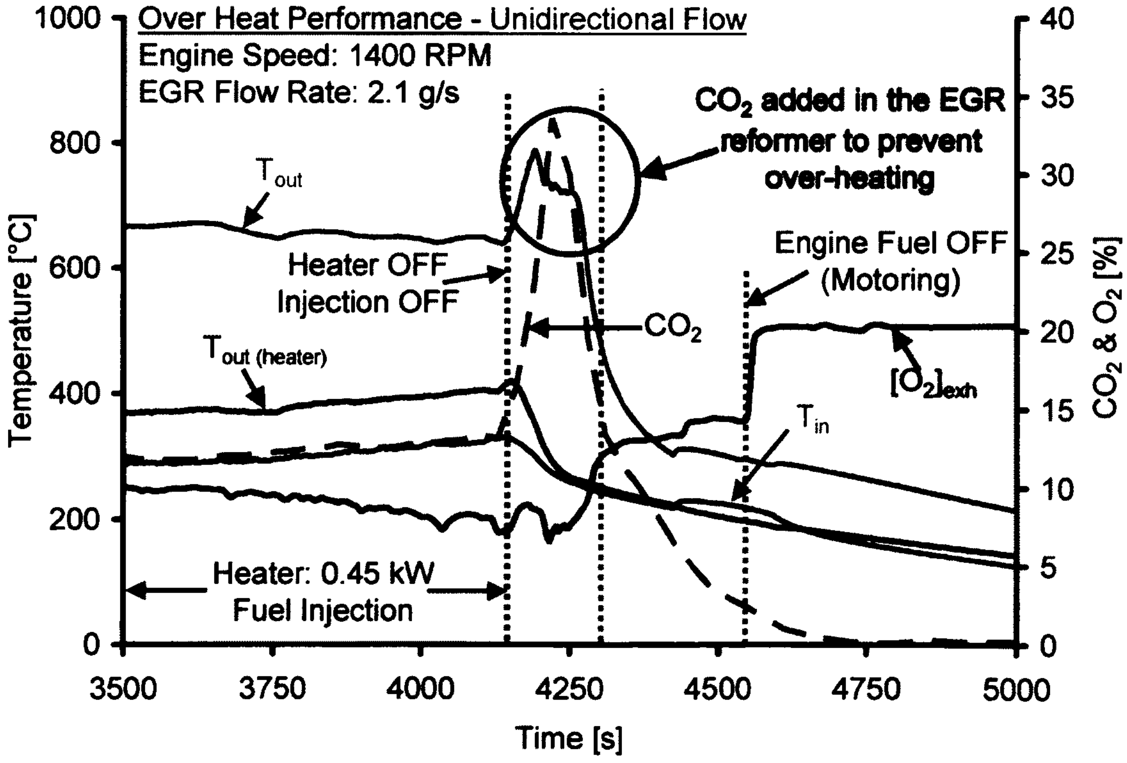

Figure 6.65: Over Heat Performance of the Unidirectional Reformer

6.14.3. EGR Cooling loads

An important consideration with the EGR fuel reforming is the increase in the loading of the EGR cooler. The reforming process generally occurs at elevated temperatures between 500°C to 700°C. The EGR cooler must be able to maintain a consistent EGR stream temperature regardless of the upstream temperature so that the engine efficiency is not adversely affected. In case of the unidirectional flow reformer as shown in Figure 6.66, the reformed gas temperature at the reformer outlet was close to 600°C which is much higher than the temperatures usually associated with raw EGR. Assuming the EGR stream temperature to be 100°C after the EGR cooler (with typical engine coolant temperature of 90°C), it was estimated that the EGR cooler would have to remove approximately 0.9 kW of heat energy from the EGR stream with the unidirectional flow strategy.

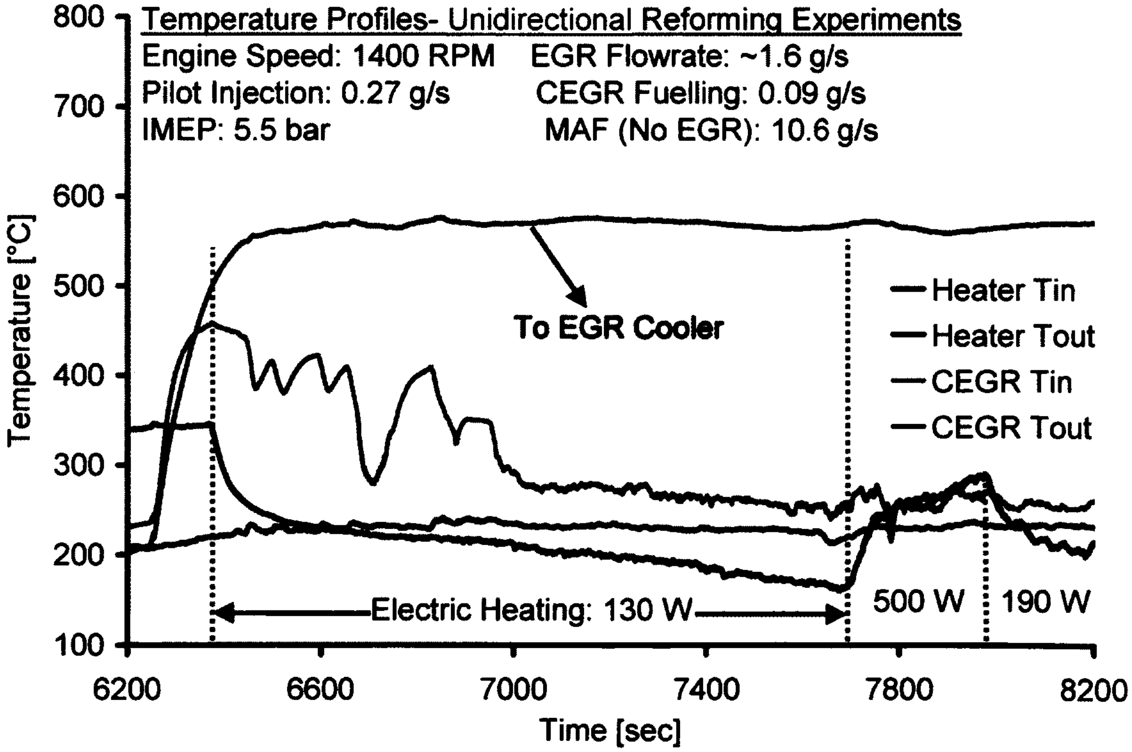

Figure 6.66: EGR Cooling Load – Unidirectional Flow CEGR

The results for the reforming process with flow reversal and central heating/fuelling are shown in Figure 6.67. Although the temperature at the central portion was close to 600°C, the flow reversal operation was able to localize the high temperature within the central region of the reformer. Therefore, the reformer inlet temperature was close to 200°C and the reformer outlet temperature was also much lower (about 170°C). Although the EGR flow rate was slightly higher during the test with the flow reversal strategy, the EGR cooler load was drastically reduced to only 0.14 kW, a reduction by a factor of six.

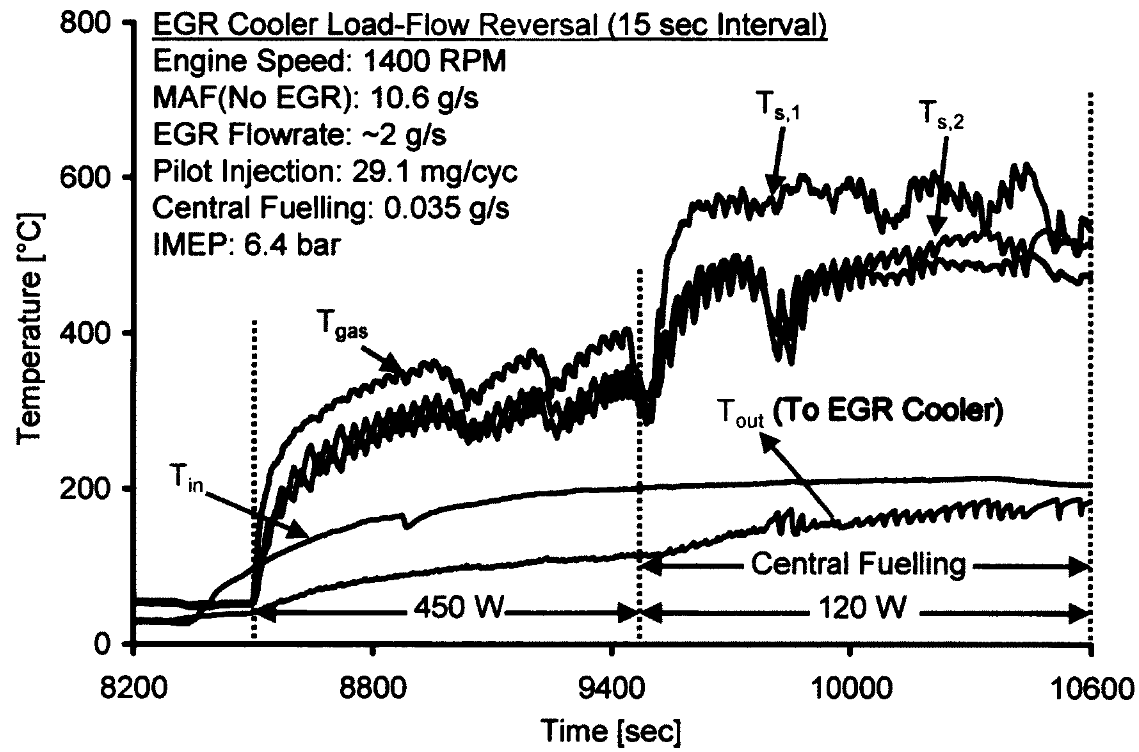

Figure 6.67: EGR Cooling Load – Flow Reversal CEGR

6.15. Other Considerations

Compared with unidirectional EGR reformer, the reversal and central fuelling configuration has the following advantages:

- Save energy during heating up the reformer by trapping the heat in the central section of the reformer;
- Minimize the external heating requirement to sustain endothermic reforming;
- Reduce EGR cooling by maintaining a lower reformer outlet temperature.

Monolith solids have only a moderate heat retention capability (evident as ΔT) when operating with conventional unidirectional flow. The unidirectional flow loses the solid heat relatively fast, even at a reduced gas flow rate. The energy stored in the monolith solid will migrate out of the monolith boundaries if the duration of a unidirectional operation is sufficiently long. Empirical observations in this regard have been reported by Zheng et al. [129,130]. Therefore, the requirement for external heating is higher to ensure sustained reforming operation.

With the integration of a CEGR loop with the engine, the effective path for the EGR flow increases. This can reduce the effect of pressure wave action on the stability of the in-cylinder combustion by reducing the fluctuations in the EGR flow.

The soot in the diesel exhaust adversely affects the durability of the EGR valve. EGR valve fouling is still a challenge for effective implementation of advanced EGR strategies in modern diesel engines. The application of CEGR can help alleviate this problem. The high temperature reformed gases can be used to destroy the soot deposits and clean the EGR valve.

Unlike the reforming process for fuel cell applications, hydrogen is not needed in a pure form in the diesel CEGR, making the system operation simpler. A separate water-gas shift mechanism may not be needed in the EGR reformer since the CO can be combusted again in the diesel engine. In a fuel cell however, the catalyst used in the common polymer-electrolyte-membrane fuel cell, the device most likely to be used in transportation roles, is very sensitive to any leftover carbon monoxide in the gaseous fuel generated in the reformers. The membrane is poisoned by the carbon monoxide and its performance degrades [131].

The reformer fuel delivery is mainly subjected to an exhaust stream of high uncertainties. When the engine operating condition varies, the diesel exhaust is characterized by extensive variations in temperature, pressure, flow rate, oxygen concentration, and combustible contents. The pressure wave action along the exhaust plenums further compounds such complications. For the unidirectional CEGR reformer, all these factors can result in poor mixing of the fuel with the EGR stream, causing over-rich and lean pockets in the catalytic reformer. Hence, fuel slip can occur through the reformer and the reformer temperature can also go very high.

In case of the flow reversal reformer, the central fuelling is not significantly affected by the EGR fluctuation and pressure wave action. Hence, a more uniform thermal loading of the CEGR reformer can be achieved, possibly enhancing the production of gaseous fuel and preventing oxidation and reforming to occur at different regions in the reformer simultaneously.

Another possible application of the CEGR is in the diesel aftertreatment system [132,133]. The decrease in the overall system efficiency with CEGR may be compensated by the reduced fuel penalty for the aftertreatment system. The H_2 generation may also help in diesel aftertreatment system during the regeneration process in a lean NOx trap [134]. The thermal energy of the reformed gas can also be used for decreasing the requirement of attaining the soot regeneration temperature in diesel particulate filters.

The sequence of CEGR operation is characterized by temporally and spatially discrete rich-quench-lean combustion processes. Downstream of the rich combustor, the reformed gases are cooled rapidly before being mixed with the intake air. This quenching process must be regulated so that the temperature of the reformed gases after the EGR cooler is about 80~120°C. Over-quenching can result in condensation of any fuel vapour that has slipped through the catalytic reformer. The thermal management of the fuel injector exposed to a fluctuating high temperature exhaust stream also presents an implementation challenge that must be adequately addressed.

6.16. Conclusions

The work presented in this chapter can be summarized as follows:

- A detailed EGR analysis was carried out to characterize the efficacy of EGR for LTC operation as well as to develop suitable parameters that can provide feedback for the LTC control. The effects of engine load and boost pressure on the EGR were identified and a theoretical operating map for the LTC cycles was proposed.

- A 0-D EGR simulation was setup along with the approximate molar analysis to study the EGR convergence and to estimate the steady-state concentrations after the application of EGR. A single equation was derived that included the effects of the transient build-up of EGR and the eventual convergence of the intake and exhaust concentrations to the steady state values.

- The actual fuel strength of the cylinder charge was quantified in terms of an in-cylinder lambda λ_a and its difference from the fresh air lambda λ was also quantified.

- A 'Charge Dilution Index' was proposed to present a standard measure for the estimation of the EGR independent of the engine operating conditions (load, boost etc). A dimensionless 'Oxygen Utilization' term was also defined to represent the engine load in terms of the intake and exhaust oxygen concentrations.

- A two-lambda sensor technique was proposed and tested to provide fast feedback on the combustion characteristics for the control of LTC cycles.

- The diesel fuel reforming process was tested to generate gaseous fuel on demand in the EGR loop. Novel flow management strategies including flow reversal, partial flow control together with central fuelling and central heating schemes were applied to improve the energy efficiency of the reforming process. The results indicated a reduction of up to 50% supplemental energy with reversal flow and central fuelling compared to the unidirectional reformer with inlet heating.

- The gaseous fuels generated by the diesel fuel reforming process in the EGR loop were shown to enhance the premixed combustion phase and significantly decrease the NOx emission without incurring a soot penalty.

CHAPTER VII

7. TESTING OF DIESEL LOW TEMPERATURE COMBUSTION

The LTC testing phase was divided into two parts. Engine tests were conducted to study the effects of commonly-used techniques that included injection timing retard and EGR on the NOx-soot trade-off for the conventional diesel high temperature combustion. The use of a pilot injection to reduce the combustion noise was also investigated and its effect on the emissions was studied. The tests were done on the Ford engine. The aim of this study was to develop a better understanding of the challenges associated with the emission reduction strategies and to provide useful guidelines for the control of the diesel LTC cycles.

The diesel low temperature combustion was then investigated to realize ultra-low levels of NOx and soot. Three different LTC strategies were experimentally explored to achieve ultra low emissions under independently controlled EGR, intake boost, exhaust backpressure, and multi-event fuel injection events. Empirical comparisons were made between the fuel efficiencies of such LTC cycles. The results were crucial to develop an effective LTC load management strategy as well as to confirm the findings of the EGR analysis.

7.1. Strategies for Reducing NOx and Soot Emissions

Significant improvements in the NOx-soot trade-off can be achieved with injection timing retard, EGR, higher boost and fuel-injection pressures. Therefore, the individual effects of these parameters are presented below.

7.1.1. Injection Timing Retard

The timing of the fuel injection events has a strong influence on the combustion characteristics including the combustion phasing, the peak combustion temperature and pressure. These parameters in turn affect the useful cycle work, emissions, combustion noise and the fuel efficiency.

The effect of injection timing variation was studied by performing a timing sweep at different engine operating conditions. The test results for such a sweep at a baseline engine load of 6.2 bar IMEP are presented. The timing sweep was performed initially by keeping the fuelling rate constant and then the test was repeated by varying the fuelling rate to keep the IMEP constant. The baseline IMEP was achieved with the commanded SOI at 356°CA. The start of injection (SOI) was then varied, by advancing till 340°CA and then by retarding till 365°CA. A single fuel injection was used during these tests.

The NOx and the smoke trends are presented in Figure 7.1. As the injection timing was advanced till 350°CA, the NOx and soot emissions increased, but further advancing the injection timing resulted in reduced smoke levels. This can be explained as follows: The advanced fuel injection timing results in the fuel being injection into a lower temperature environment. Since the ignition delay is exponentially related to the cylinder temperature, a longer ignition delay results in increased premixing of the fuel with the air. Since soot formation primarily occurs during the diffusion-controlled combustion which is significantly reduced because of the enhanced premixing, therefore, the engine-out smoke is reduced.

Retarding the injection timing on the other hand, resulted in simultaneous reduction of NOx and smoke. For the fixed fuelling case, as the timing was retarded to 365°CA, a sharp drop in the NOx was observed. This can be explained by plotting the NOx and smoke emissions against the combustion phasing (represented by the crank angle of 50% heat released) as shown in Figure 7.2.

With the SOI at 364°CA, the combustion was phased well in to the expansion stroke (CA50: 379.6°CA) where the temperature was considerably lower due to the piston progressing into the expansion stroke. A small change of 1°CA in the SOI (365°CA) caused a 6°CA retarding of the CA50. With such late combustion phasing, the combustion was observed to be close to the flame-out condition, with high cycle-to-cycle variations and a significant drop in the IMEP. Therefore, the NOx emission reduced significantly.

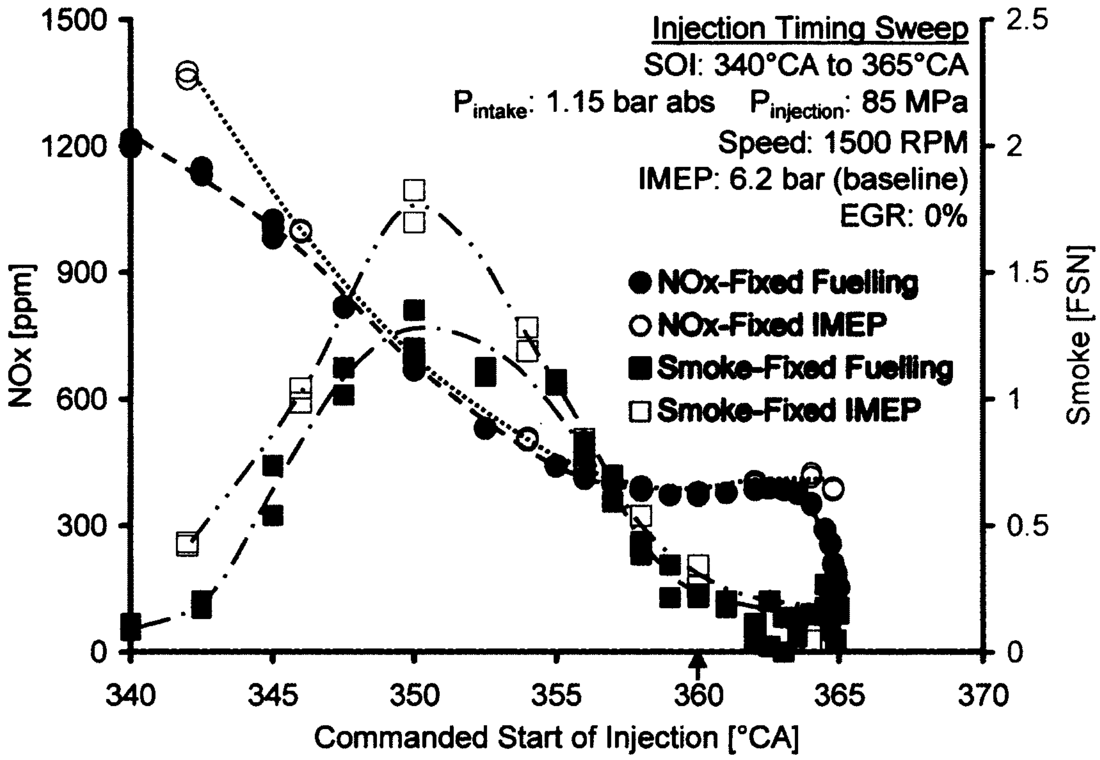

Figure 7.1: NOx & Smoke Trends for SOI Sweep at Fixed Fuelling & Fixed Load

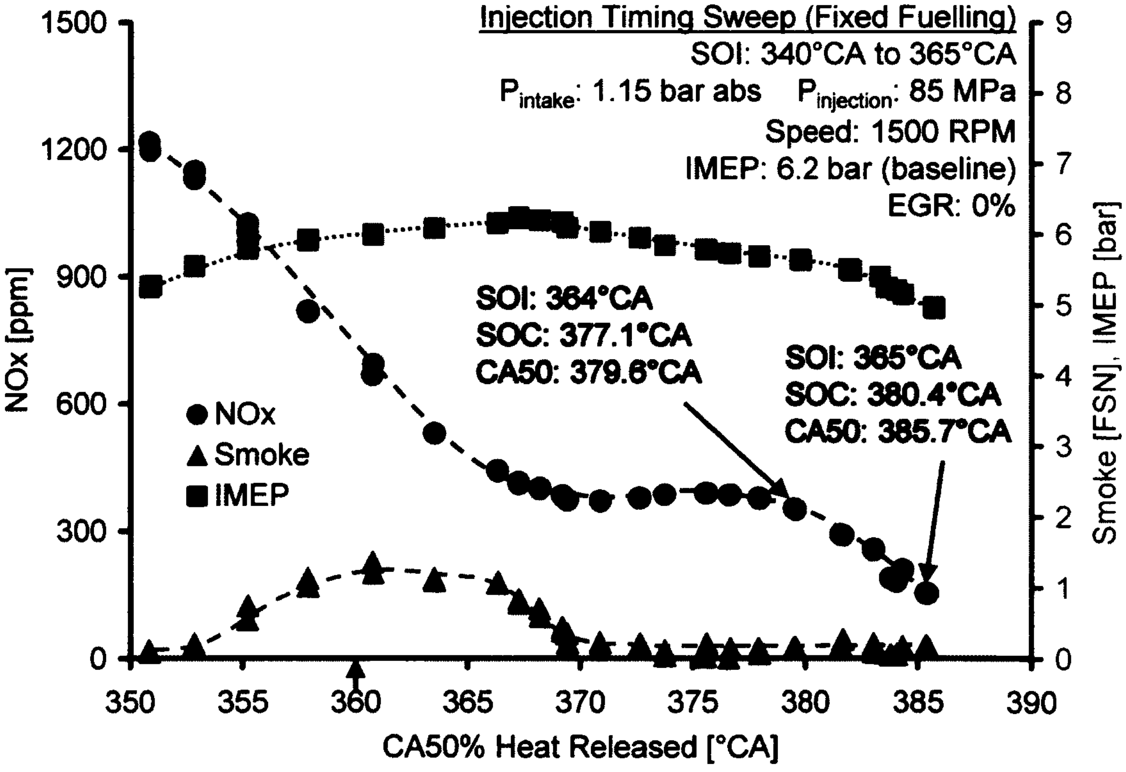

Figure 7.2: NOx and Smoke Trends versus CA50 at Fixed Fuelling

The above reasoning was further supported by analyzing the heat release traces. The heat release rates for the fixed fuelling case are plotted in Figure 7.3. With the SOI at 340°CA, the combustion phasing was much earlier than the TDC and the combustion was comprised primarily of a premixed phase of very short duration (~5°CA). The absence of the diffusion-controlled combustion agreed with the low smoke values while the higher NOx was the result of the short premixed phase. As the SOI was retarded towards TDC (CA50: 360~366°CA), the increasing diffusion controlled combustion coincided with the rising soot values, while the reduction of the premixed phase agreed with the falling NOx emission. Retarding the SOI beyond TDC, the heat release was characterized by a diminishing diffusion-phase (longer ignition delay). The enhanced premixing did not result in an increase in the NOx because of the lower temperatures during the expansion stroke. However, with the SOI at 365°CA, the heat release peak reduced significantly with a marked increase in the combustion duration and was characterized by higher cycle-to-cycle variations, reduced thermal efficiency and a sharp drop in the NOx emission.

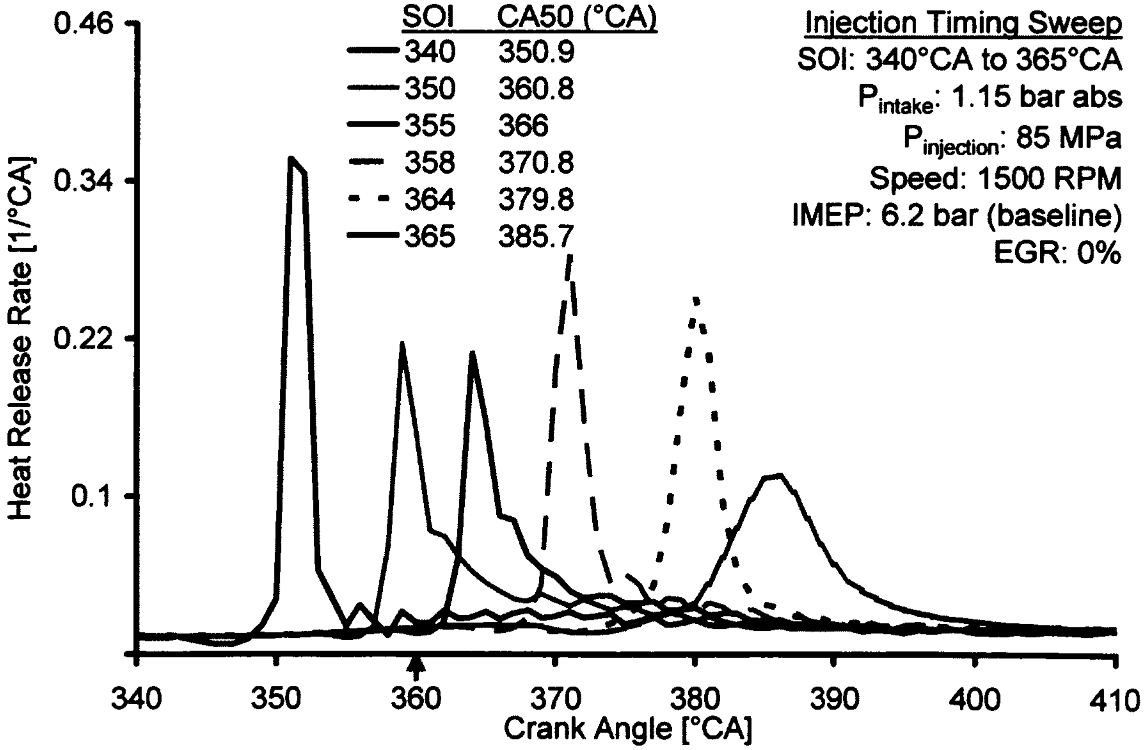

Figure 7.3: Heat Release Rates for the Injection Timing Sweep (Fixed Fuelling)

The pressure traces corresponding to the heat release traces are shown in Figure 7.4. The early combustion phasing was marked with a high maximum rate of pressure rise (20.1 bar/°CA) and a maximum cylinder pressure close to 110 bar. Retarding the SOI progressively reduced the maximum cylinder pressure while the maximum rate of pressure rise was around 12 bar/°CA (CA50: 360~370°CA). For the very late combustion phasing, both the maximum cylinder pressure and the maximum rate of pressure rise were significantly reduced. Similar trends were seen for the fixed IMEP case and therefore have not been plotted.

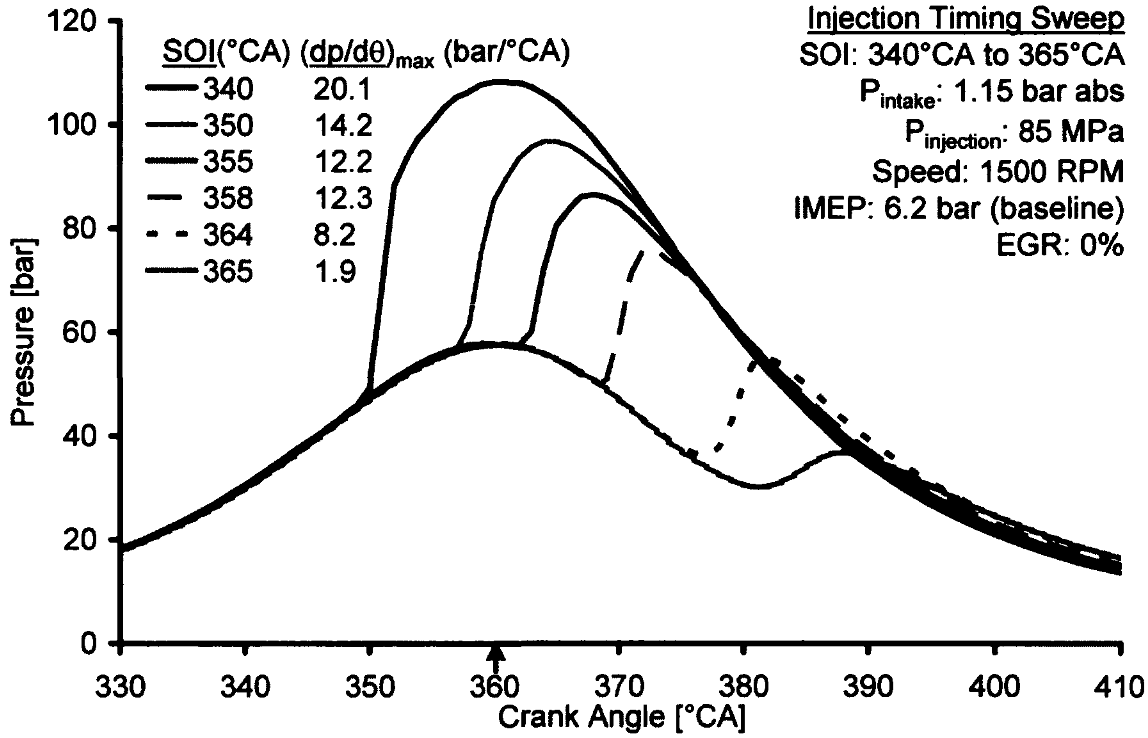

Figure 7.4: Cylinder Pressure Traces for the Injection Timing Sweep (Fixed Fuelling)

To correlate the effect of the injection timing retard with the thermal efficiency, the thermal efficiency and its percentage decrease from the baseline value were plotted against the CA50 in Figure 7.5 for both the fixed fuelling and the fixed IMEP cases. It was observed that the highest efficiency was achieved with the CA50 phased between 365 to 370°CA (5-10°ATDC). Up to 20% reduction in the efficiency was observed by advancing or retarding the combustion phasing (through SOI adjustment). This small window of ~5°CA (marked as A* on the figure) represented the combustion phasing for the best efficiency.

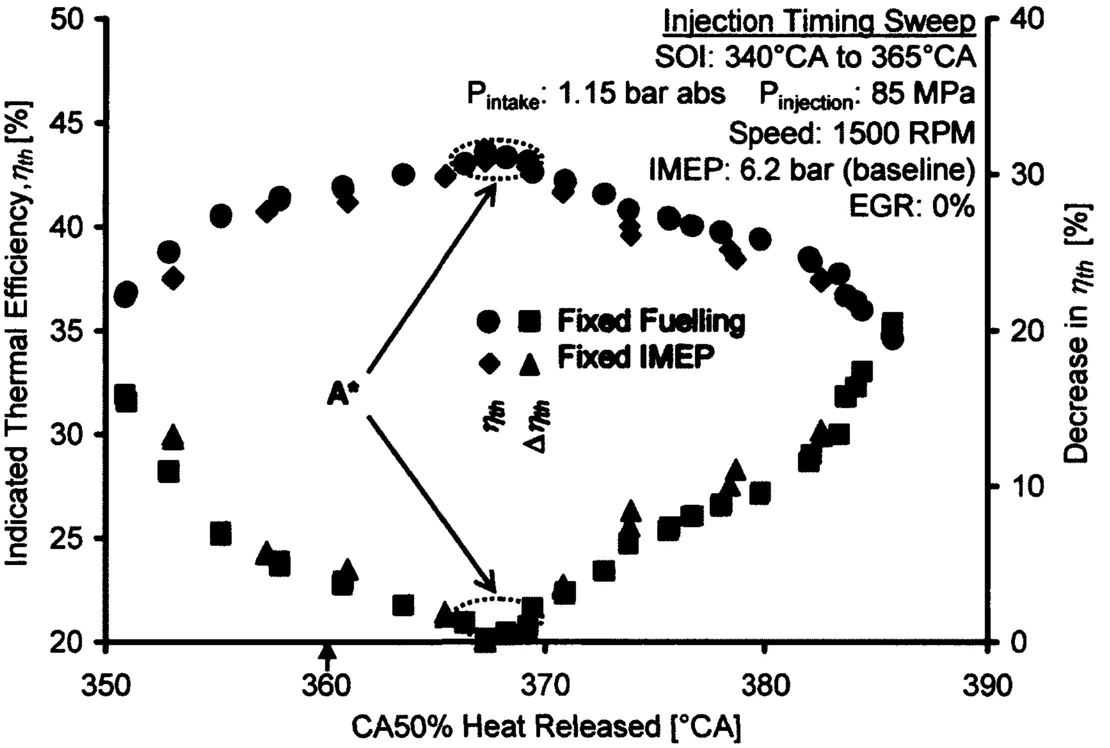

Figure 7.5: Thermal Efficiency Trends versus CA50 for Fixed Fuelling and Fixed Load

The relationship between the SOI and the CA50 is shown in Figure 7.6. The CA50 and the SOI exhibited a linear relationship for SOI ranging from 340 to 358°CA. However, as the SOI was retarded further, the combustion phasing was delayed sharply. The ignition delay curve indicated that the off-phasing (retard) of the combustion from the best efficiency window (A*) was accompanied by a rapid prolonging of the ignition delay. The resulting lowered combustion temperatures reduced the NOx but the CO and HC emissions increased rapidly (Figure 7.7), thereby deteriorating the combustion efficiency.

The results of Figure 7.6 and Figure 7.7 are important for understanding the complexities involved in the control of diesel low temperature combustion. The control system must be able to maintain the combustion at the borderline between

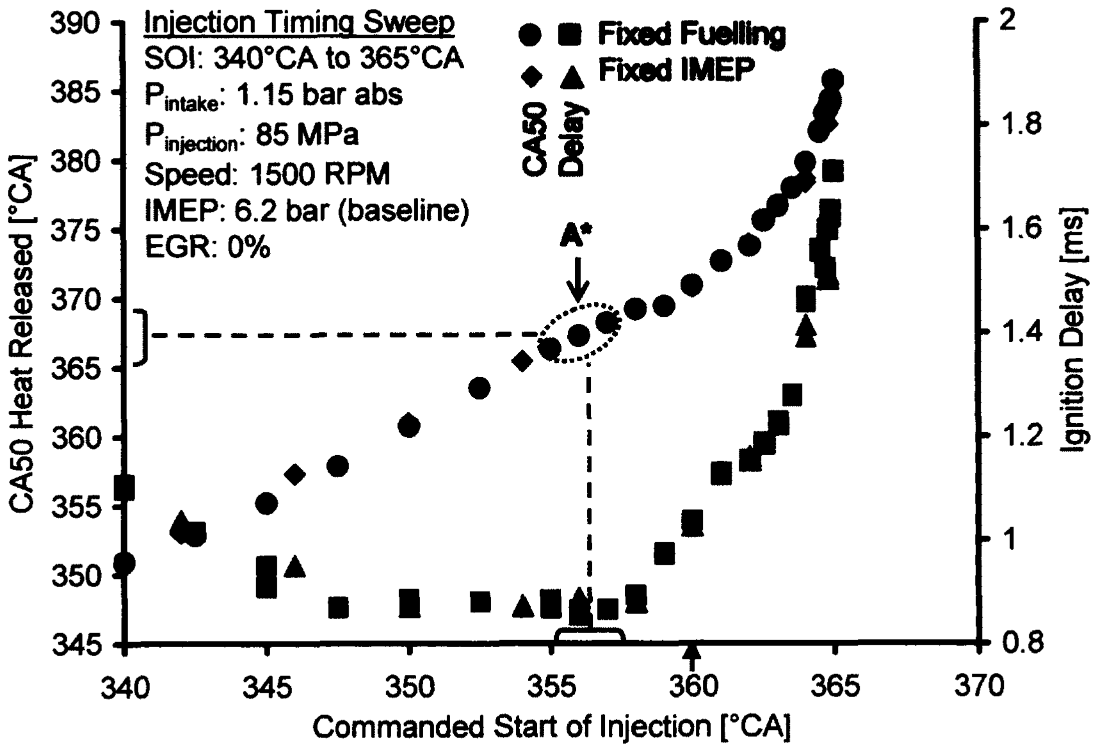

Figure 7.6: CA50 and Ignition Delay versus SOI for Fixed Fuelling and Fixed Load

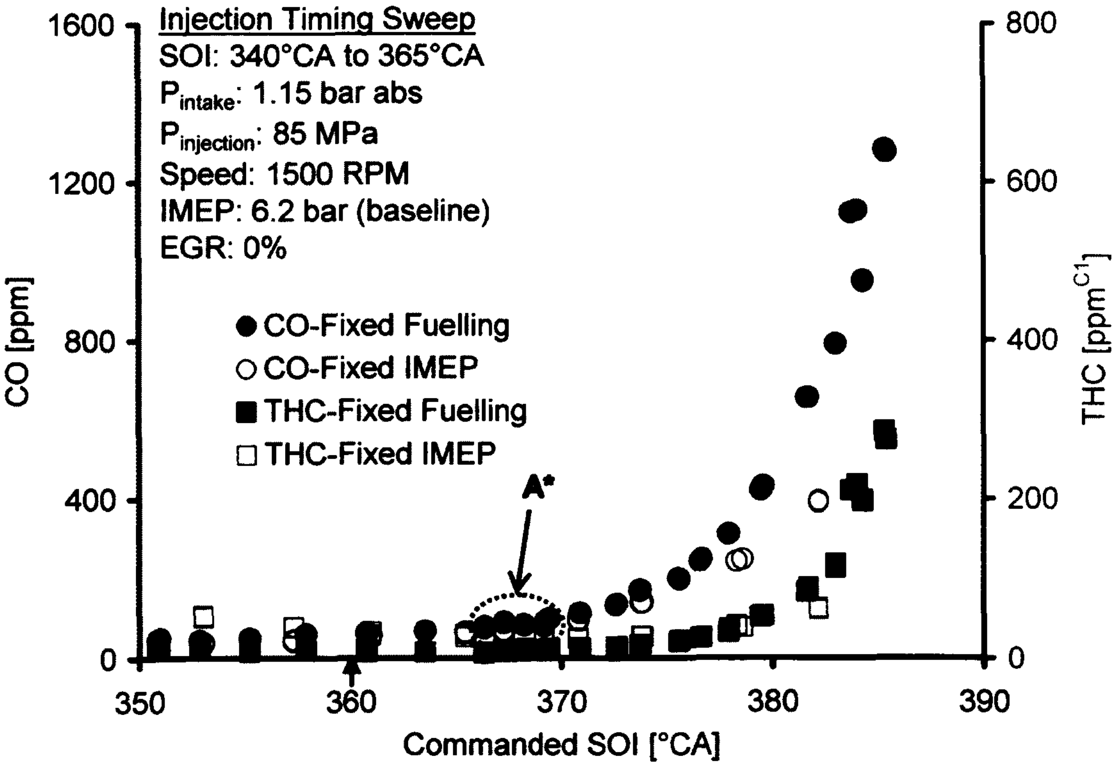

Figure 7.7: CO & THC Emissions versus SOI for Fixed Fuelling and Fixed Load

the stable and unstable regimes to achieve the highest efficiency and the lowest emissions. Any deficiency in the control would result in either an increase in the emissions or high cycle-to-cycle variations, possibly leading to misfire. The near-linear SOI-CA50 relationship was used extensively for the single-shot enabled LTC combustion control, as demonstrated subsequently in Chapter 8.

The efficacy of retarding the injection timing in reducing the NOx emission is shown in Figure 7.8. The NOx emission was reduced significantly without increasing the smoke as the combustion phasing was optimized for the highest efficiency. Further retarding the SOI beyond A* resulted in a sharp increase in the ignition delay at a nearly fixed NOx level. This can be attributed to a trade-off between the increased premixed combustion (with the prolonged ignition delay) and the reducing temperatures during the expansion stroke. The reduction in NOx from this point was accompanied by a sharp rise in the CO and HC emissions. These results also indicated the limitation of the injection timing retard alone to meet the current and future NOx emission levels of ~0.2 g/kWh.

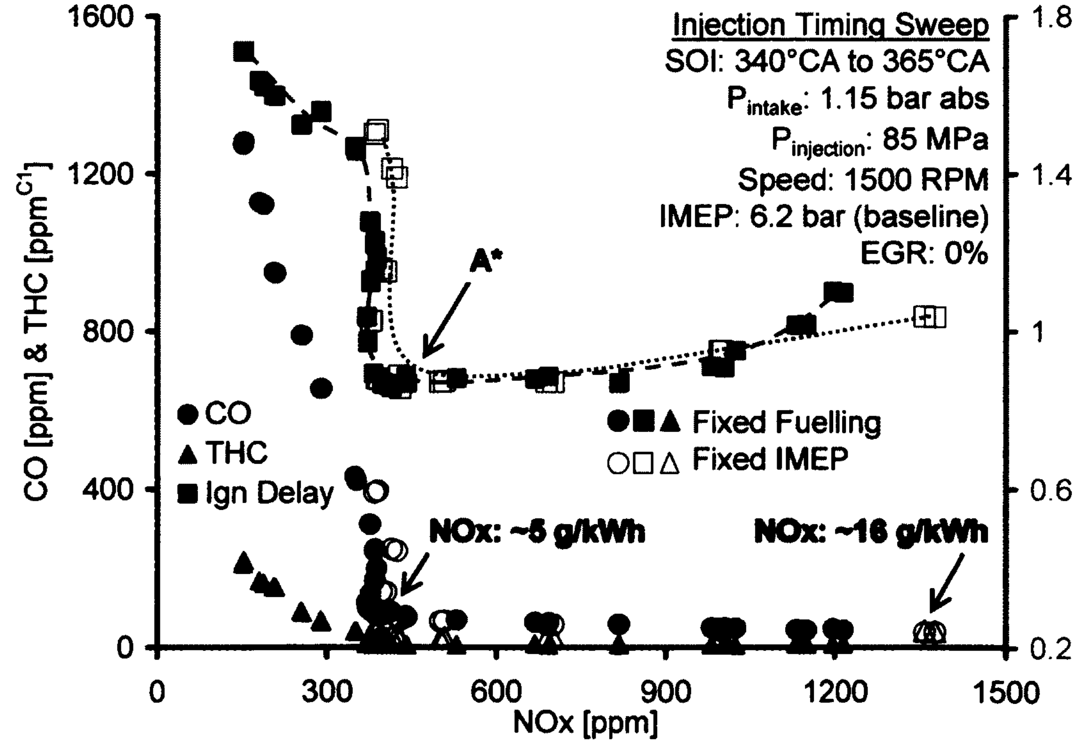

Figure 7.8: CO, THC & Ignition Delay versus NOx for Fixed Fuelling and Fixed Load

To confirm if the observed trends were consistent over a wide load range, the injection timing sweep was repeated at 4.2 and 8.2 bar IMEP (baseline values at the best efficiency) while keeping a fixed fuelling rate. The low load SOI sweep was performed from 330 to 364°CA while the higher load sweep was done from 345 to 367°CA. The NOx and IMEP trends are shown in Figure 7.9.

The NOx increased as a result of advancing the injection timing in both the cases. However, the NOx was seen to decrease for SOI earlier than 340°CA at 4.2 bar IMEP. The CA50 was retained close to 350°CA for SOI around 330°CA so that the long ignition delay allowed for a more thorough mixing of the injected fuel with the cylinder charge. Therefore, a lean charge of high homogeneity existed at the start of combustion that resulted in lower NOx emission. The IMEP trends for the SOI sweep were similar to the results of the 6.2 bar IMEP tests. At 8.2 bar IMEP and retarded injection timing, the NOx was seen to increase. To understand this phenomenon, the cumulative heat release rates were plotted as shown in Figure 7.10.

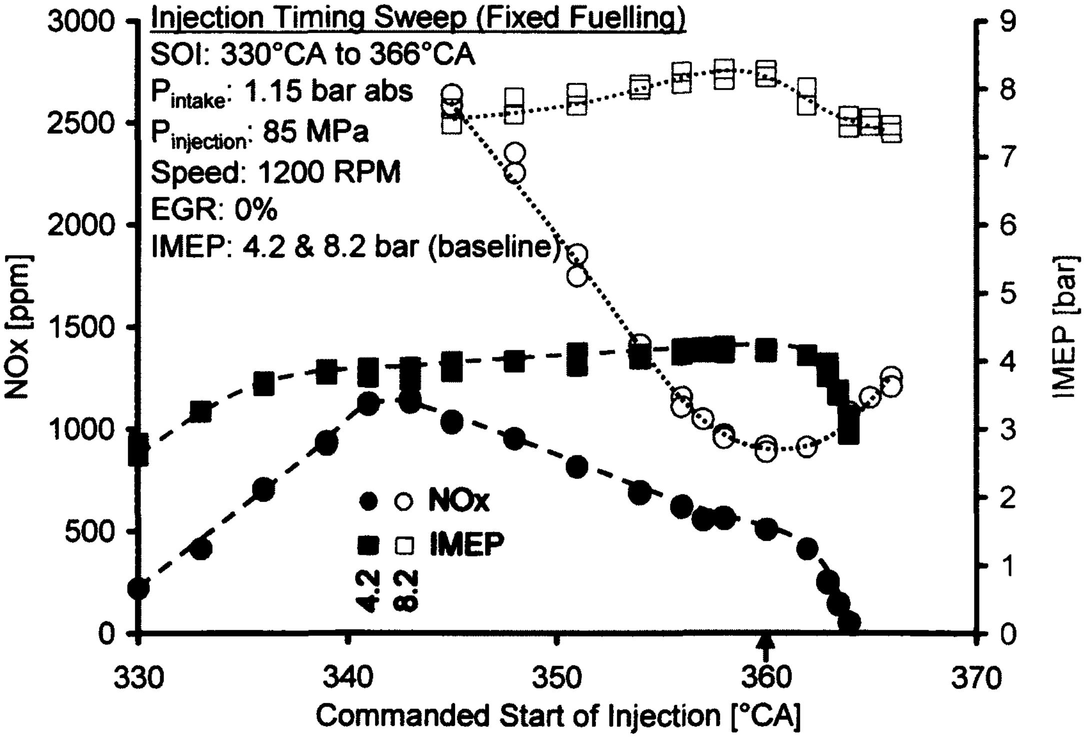

Figure 7.9: NOx and IMEP Trends for SOI Sweep at 4.2 and 8.2 bar IMEP

A sharp increase in the ignition delay (from ~1ms to 1.8 ms) was observed for the late injection timing as the SOI was retarded from 345 to 366°CA. In case of the lower loads (Figure 7.3), the retarded timing after TDC resulted in a long ignition delay and a long combustion duration as well. However, at higher load, it can be seen that despite the significantly longer ignition delay, the combustion duration was reduced from ~34°CA to 14°CA. Therefore, the rapid burning of the cylinder charge was able to overcome the lower temperatures of the expansion stroke. Conversely, at higher loads, the range of the injection timing retard can be increased before deterioration in the combustion occurs.

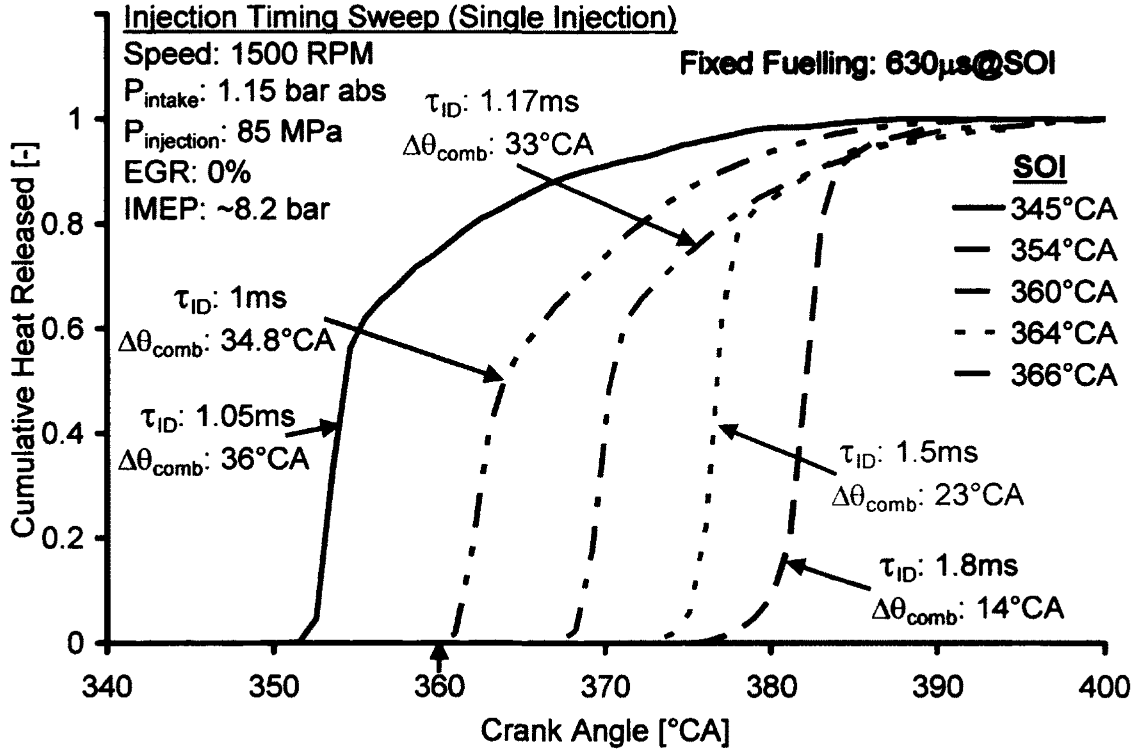

Figure 7.10: Cumulative Heat Release Traces for SOI Sweep at 8.2 bar IMEP

The CO and HC emissions for the 4.2 and 8.2 bar IMEP tests are shown in Figure 7.11. With the very early SOI, the combustion phasing was retained around 350°CA but a sharp rise in the CO emission was observed. For the retarded timing, the onset of the increase in the CO was earlier at 4.2 bar IMEP. A higher engine load, therefore, extends the timing retard range and improves the combustion efficiency for the same SOI.

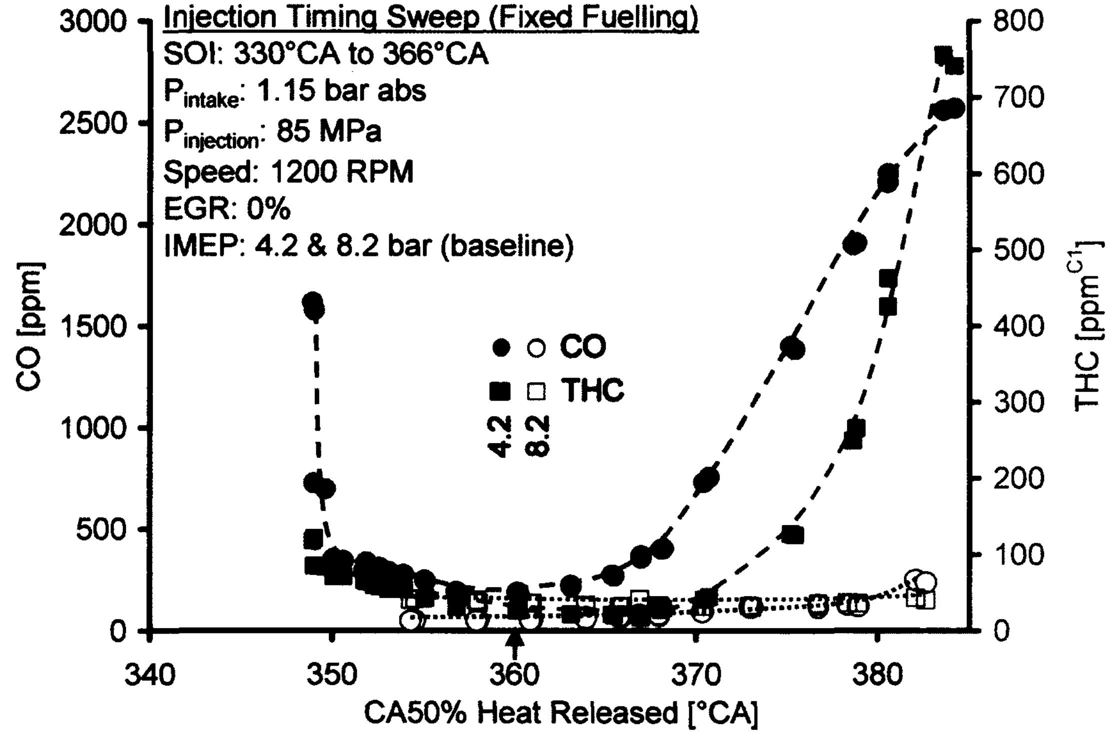

Figure 7.11: CO & THC Emissions versus CA50 at 4.2 and 8.2 bar IMEP

The CA50-SOI relationship for the two loads is shown in Figure 7.12. The results indicated that the CA50-SOI relationship was not affected significantly by the engine load. Furthermore, even though the CA50-SOI trend could be divided into three distinct regions, the relationship could be approximated with linear fits. For retarded phasing, the actual CA50 values were for 4.2 and 8.2 bar IMEP but the slopes were very similar. Therefore, the CA50-SOI relationship should be able to provide a consistent and reliable mechanism for enabling control of the combustion phasing (with a single HR peak) with the injection timing adjustment.

To observe if similar trends could be seen with other pressure-based parameters, the crank angle of the maximum cylinder pressure CA(P_{max}) and the crank angle of the maximum rate of pressure rise CA($(dp/d\theta)_{max}$) were plotted against the SOI as

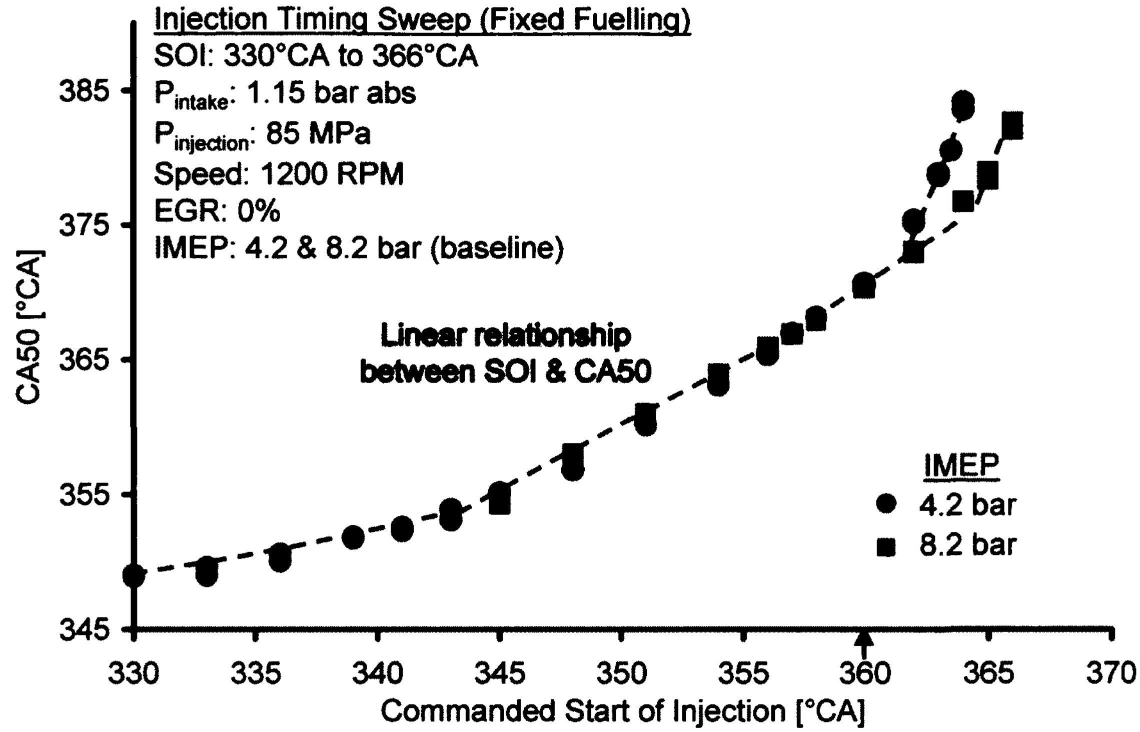

Figure 7.12: CA50 Trends for the SOI Sweeps at 4.2 and 8.2 bar IMEP

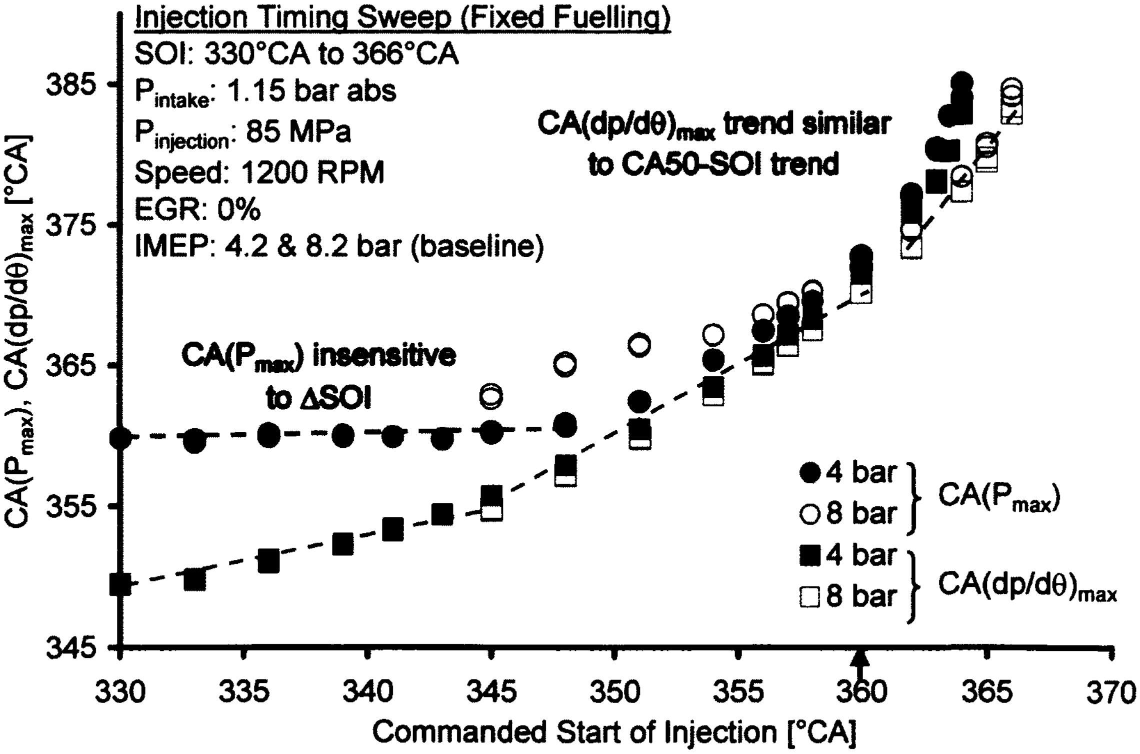

Figure 7.13: $CA(P_{max})$ & $CA(dp/d\theta)_{max}$ for the SOI Sweeps at 4.2 & 8.2 bar IMEP

shown in Figure 7.13. For the early SOIs, the CA(P_{max}) was found to be insensitive to a change in the SOI. Moreover, the effect of load was also found to effect the CA(P_{max}), thereby making it less suitable as a feedback parameter for the combustion phasing control. The CA($dp/d\theta$)$_{max}$ on the other hand, displayed a linear relationship with the SOI, similar to the CA50. Although the absolute values differed slightly from the actual CA50 values, yet the CA($dp/d\theta$)$_{max}$ was found to provide an indirect but a stable measure of the combustion phasing for heat release rates with a single peak. This is important from the point of view of combustion control since the calculation of the CA($dp/d\theta$)$_{max}$ is simpler than that of CA50, and therefore, less computational resources are required (Chapter 5).

The observations and the results of the injection timing sweep were summarized and are given in Table 7.1.

Table 7.1: Summary of the Injection Timing Sweep Tests

Parameter	Observed Effect
NOx	• Generally increases with advanced timing* • Very early timing reduce NOx as combustion approaches a lean homogeneous mixture • Decreases as the timing is retarded† at low loads
Soot	• Decreases as the premixed combustion is enhanced (for both advanced and retarded timings) • Increases as the diffusion-controlled phase increases in proportion to the premixed phase
CO & HC	• Increase for both advanced and retarded timings
CA50	• Displays a linear relationship with the SOI • Largely insensitive to the engine load
Thermal Efficiency	• Decreases on both sides of the CA50 window for best efficiency (5~10°ATDC) • Up to 20% decrease for both advanced and retarded timings
CA(P_{max})	• Insensitive to the advanced timing • Is affected by the engine load
CA($dp/d\theta$)$_{max}$	• Displays a linear relationship with the SOI • Largely insensitive to the engine load

* Before TDC † After TDC

7.1.2. EGR, Boost and Injection Pressure

The application of EGR results in the classical NOx-soot trade-off for the diesel high temperature combustion (Figure 1.8). To alleviate the soot emissions and to shift the NOx-soot trade-off closer to the origin, the effects of boost pressure and injection pressure on the NOx and soot emissions were investigated using a single fuel injection. The combustion phasing was maintained at 366°CA while EGR sweeps were performed at different boost and injection pressures. The results for the NOx emissions are shown in Figure 7.14.

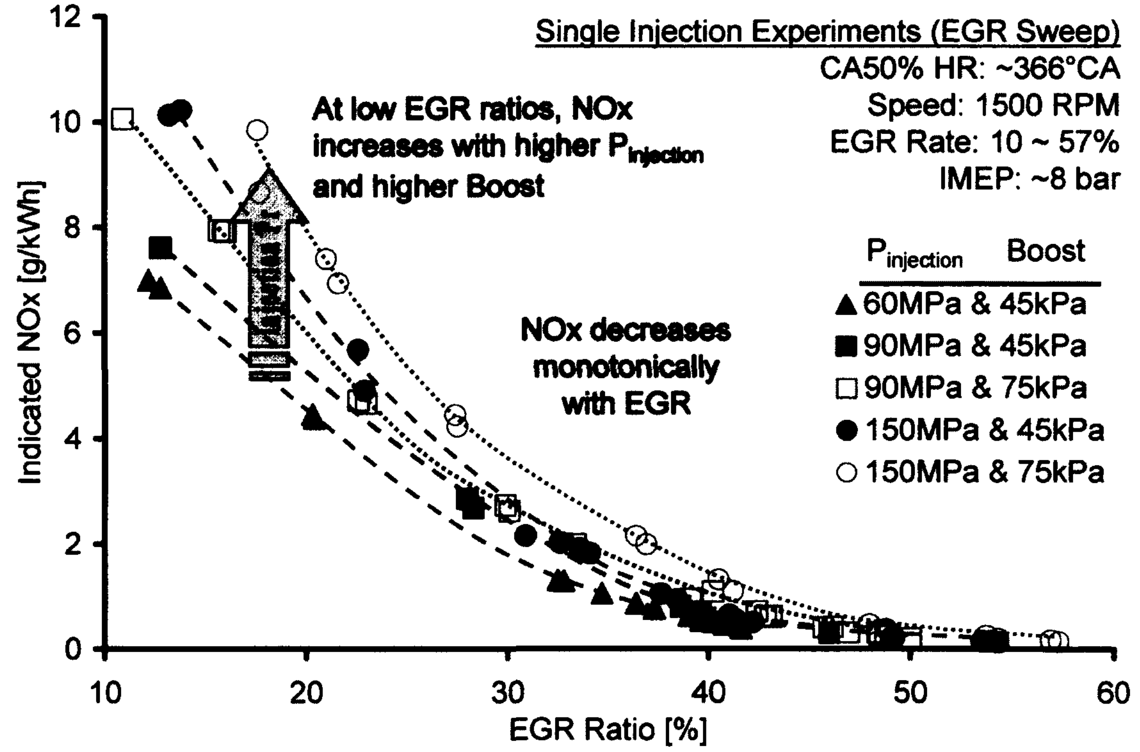

Figure 7.14: Reducing NOx Emission with EGR

The effectiveness of EGR to reduce NOx emission is evident as NOx decreased monotonically with increasing EGR irrespective of the boost level. At low EGR ratios, the NOx emissions exhibited some sensitivity to the boost pressure. On the other hand, a higher fuel injection pressure adds more energy into the mixing process which results in better air utilization. Therefore, at the same EGR level, a slight increase in the NOx emission was observed with a higher injection pressure [135].

At low EGR ratios, the NOx emissions exhibited a higher sensitivity to the injection pressure than to the boost. This is because at low EGR levels, the intake already contains a significant amount of oxygen. Therefore, improvement in the fuel-air mixing due to the higher injection pressure should have a dominant effect as compared to the change in the fuel-charge strength with higher boost.

The soot emission corresponding to the NOx data are shown in Figure 7.15. Increasing the boost helps to lower the fuel strength of the cylinder charge as the availability of the oxygen in the fuel/air charge increases. Therefore, the effect of boost on the soot reduction was significant only at higher soot levels corresponding to lower intake [O_2] (at high EGR rates). Increasing the injection pressure, on the other hand, reduced the soot emissions across the EGR range.

A higher injection pressure allows for increased atomization and penetration of the fuel spray within the cylinder charge, thereby enhancing the premixed part of the diesel combustion. Since soot is believed to be the formed during the diffusion-controlled combustion which is significantly reduced with higher injection pressure, the engine-out soot was curbed even at lower intake [O_2] corresponding to high EGR levels.

These results indicated a significant effect of EGR, boost pressure and fuel injection pressure on the NOx and soot emissions. Therefore, a detailed analysis of these parameters was carried out over a wide range of engine operating conditions and is presented in the single-shot enabled LTC section.

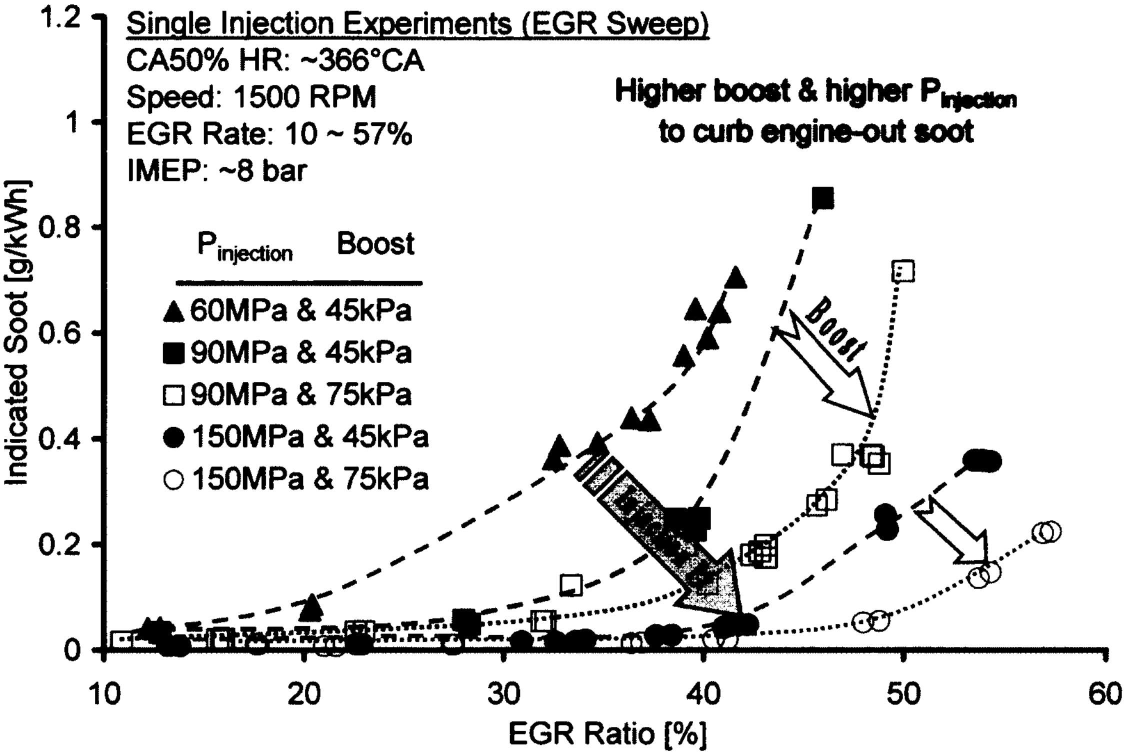

Figure 7.15: Effect of Boost and Injection Pressure on the Soot Emission

7.2. Diesel Combustion Noise

Combustion noise in diesel engines is a consequence of the high rate of pressure rise (pressure gradient or $dp/d\theta$) due to the rapid combustion of the premixed fuel-air mixture. The amount of fuel that takes part in the premixed phase of diesel combustion is strongly related to the time available for mixing and the cylinder temperature history between the SOI and the SOC – the ignition delay period. Therefore, any means to reduce the ignition delay can help to reduce the combustion noise.

The pilot injection can help to reduce the ignition delay duration by elevating the temperature and the pressure before the commencement of the main injection. As a result, the ignition delay of the main injection can be significantly shortened so that the premixed portion of the heat release is reduced, along with a significant decrease in the maximum rate of pressure rise (combustion noise) [136]. Experiments were therefore, conducted to investigate the effect of the two-injection strategy (pilot injection + main injection) on the diesel combustion noise compared to the conventional single-injection strategy.

7.2.1. Single-Shot vs. 2-Shots Strategy

The test matrix for the single and two-injection tests is given in Table 7.2. An EGR sweep was performed to assess the effect of these injection strategies on the noise and NOx and soot emissions. EGR was regulated by changing the opening of the EGR valve while keeping the backpressure constant (~4 kPa). This ensured that the NOx emissions in particular would be minimally affected by the amount of residuals in the cylinder. To maintain the same combustion phasing for both the single- and 2-injection tests during the EGR sweep, the SOI_{Main} (commanded pulse width (PW): 615μs) and SOI_2 (commanded PW: 550μs) were progressively advanced for the single- and 2-injection strategies respectively. The pilot SOI_1 and pulse width (commanded PW: 280μs) were fixed and not changed during the tests.

Table 7.2: Single and 2 Injection Test Matrix

	Number of Injections	
	1	2
SOI_1 [°CA ATDC]	–	-25
SOI_2 [°CA ATDC]	–	-10^*
SOI_{Main} [°CA ATDC]	-11.4^*	–
$P_{injection}$ [MPa]	80	
P_{intake} [bar abs]	1.45	
T_{intake} [°C]	29~32	
IMEP [bar]	7	
EGR	Sweep	
CA50% Heat Released [°CA]	361, 366	

* at baseline EGR of 10%

For the case of combustion phasing (CA50) set at 361°CA, the results are shown from Figure 7.17 to Figure 7.19. The SOC was also fixed at 354°CA.

The commanded SOI for the two strategies is shown in Figure 7.16. During the EGR sweep, the SOI_{Main} and SOI_2 were progressively advanced to maintain the same combustion phasing for both the single- and 2-injection strategies respectively. It was noted that at higher EGR levels (>40%), the ignition delay

(combustion noise) as shown in Figure 7.18.

The application of EGR resulted in the classical NOx-soot trade-off for the high temperature combustion as shown in Figure 7.17. However, the variation of NOx and soot emissions with EGR indicated that there was virtually no difference in the emission performance between the two injection strategies. The use of 2-injection strategy has been reported to reduce NOx emissions and increase soot emissions

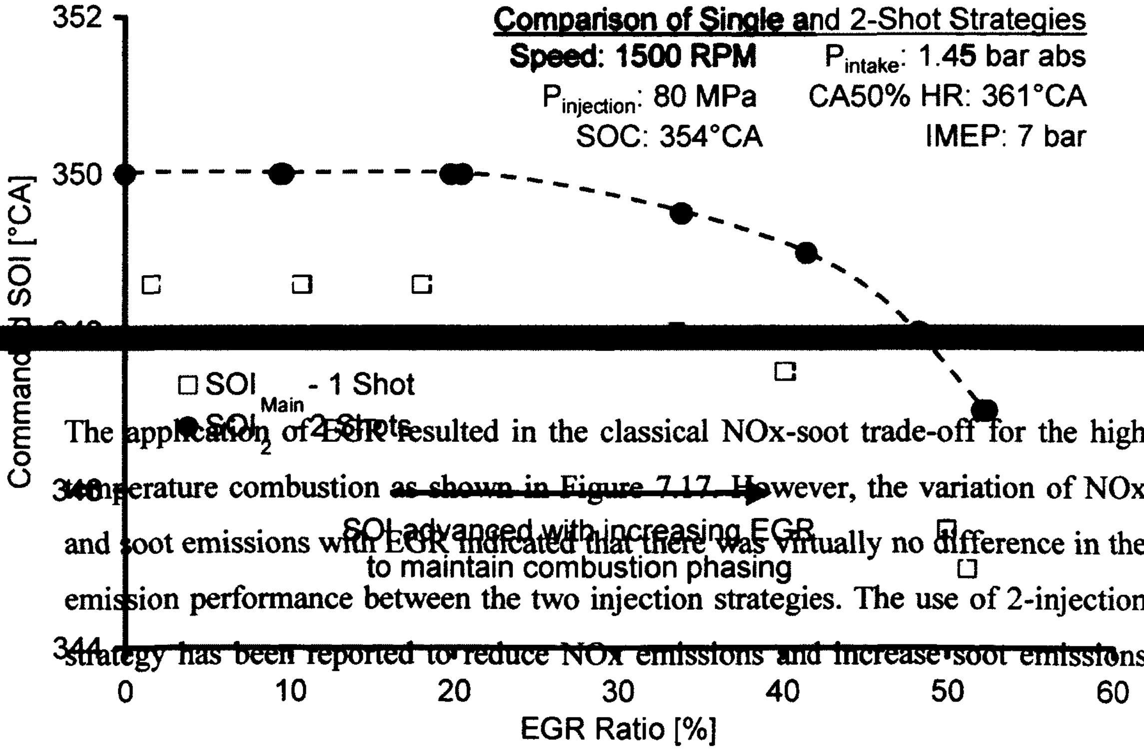

Figure 7.16: Variation of Commanded Start of Injection for Single- and 2-Injection Strategies (CA50 at 361°CA)

compared to the single injection strategy [136,137]. To investigate the reasons for the emissions results of Figure 7.17, the combustion duration was plotted in Figure 7.18. It was observed that although the combustion duration increased with increasing EGR, it was the same for both the injection strategies. However, the 2-injection strategy showed a significant drop in the combustion noise (Figure 7.18) up to 40% EGR.

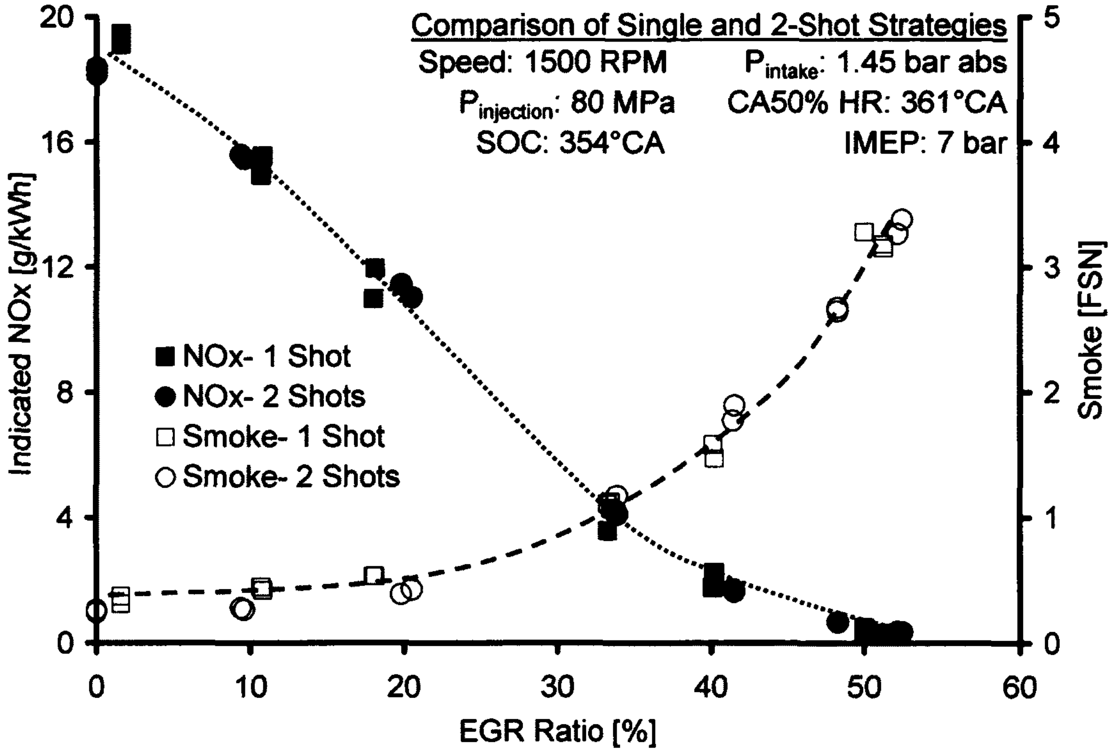

Figure 7.17: NOx and Soot Emissions for Single- and 2-Injection Strategies (CA50 at 361°CA)

To further analyze this aspect, the heat release rates for 3 different levels of EGR are shown in Figure 7.19. For all the 3 cases of 10%, 40% and 51% EGR, the SOC, the CA50 and the combustion duration were the same. The use of the pilot injection reduced the ignition delay of the main injection (indicated in the figures) and suppressed the premixed combustion, thereby resulting in a significant noise reduction. The reduced ignition delay can be attributed to the cool-flame reactions of the pilot fuel and the resulting higher charge temperature during the main injection event. Although reducing the premixed phase may help to reduce NOx

[138,139], the phasing of the combustion is also critical to the production of NOx and soot. Previously published results showed a retarded phasing beyond TDC for the 2-injection strategy [137]. The off-phasing of the combustion after TDC reduces the combustion temperature which may reduce the NOx and increase soot (soot destruction is inhibited). Since the combustion phasing was maintained nearly at TDC during the current work, the diffusion-controlled combustion occurred around TDC. Also, the tail of the combustion matched for both the injection strategies. Therefore, the effect of the 2-injection strategy on the NOx and soot was negligible in this particular case.

As EGR was increased, the dilution effects of EGR increased the ignition delay and the diffusion-controlled combustion was observed to reduce. However, the 2-injection strategy still benefited from lower pressure gradients (combustion noise) compared to the single-injection combustion.

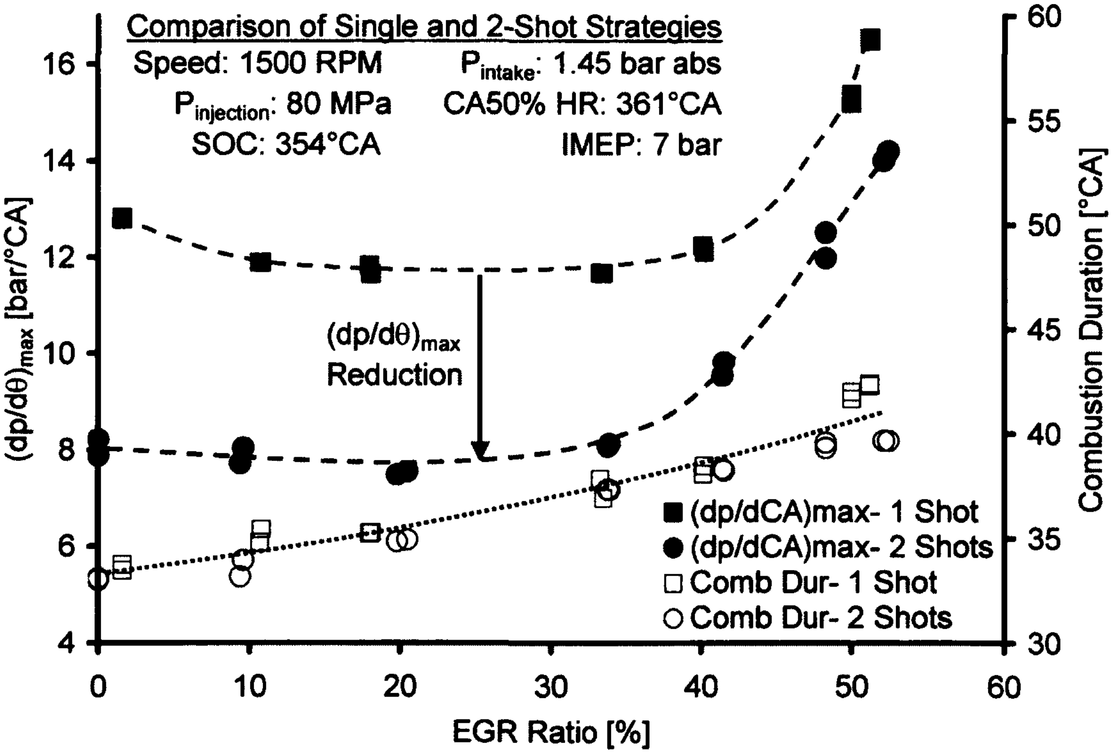

Figure 7.18: $(dp/d\theta)_{max}$ and Combustion Duration for Single- and 2-Injection Strategies (CA50 at 361°CA)

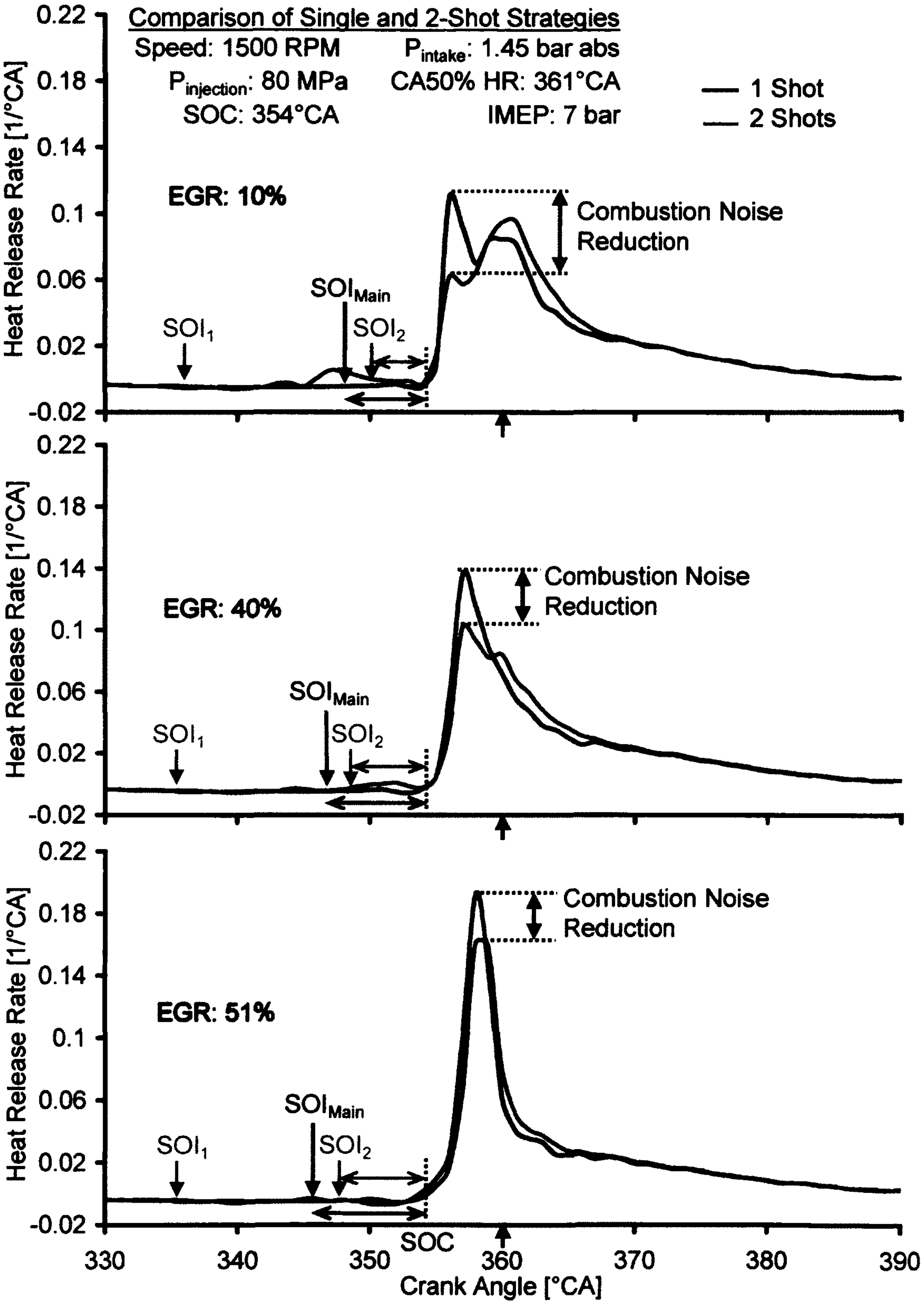

Figure 7.19: Heat Release Rate Comparison between Single- and 2-Injection Strategies (CA50: 361°CA)

The summary of the two injection strategy results with CA50 @ 361°CA along with the fuel efficiency is given in Table 7.3.

Table 7.3: Summary Results for CA50 @ 361°CA

	EGR		
	10%	40%	51%
Single Injection			
$(dp/d\theta)_{max}$ [bar/°CA]	11.9	12.1	16.5
Fuelling Rate [mg/cyc]	20.8		
Indicated Thermal Efficiency [%]	41.3	40.8	40.1
2-Injections			
$(dp/d\theta)_{max}$ [bar/°CA]	8	9.5	14.2
Fuelling Rate [mg/cyc]	21.9		
Indicated Thermal Efficiency [%]	38.5	38.3	36.7

The EGR sweep was performed again with the CA50 fixed at 366°CA but the SOC and the combustion duration were not regulated. The NOx emissions for the two cases were again similar but the soot was observed to increase for the 2-injection strategy with increasing EGR as shown in Figure 7.20.

The reduction in the combustion noise was again observed for the 2-injection strategy (Figure 7.21), consistent with the previous results. The amplitude of the combustion noise was lower in this case as the combustion phasing was away from the TDC. However, the combustion duration for the 2-injection strategy was longer than that for the single injection case and the difference in the combustion duration progressively increased with higher EGR. It was therefore suspected that the longer combustion duration could affect the observed soot increase.

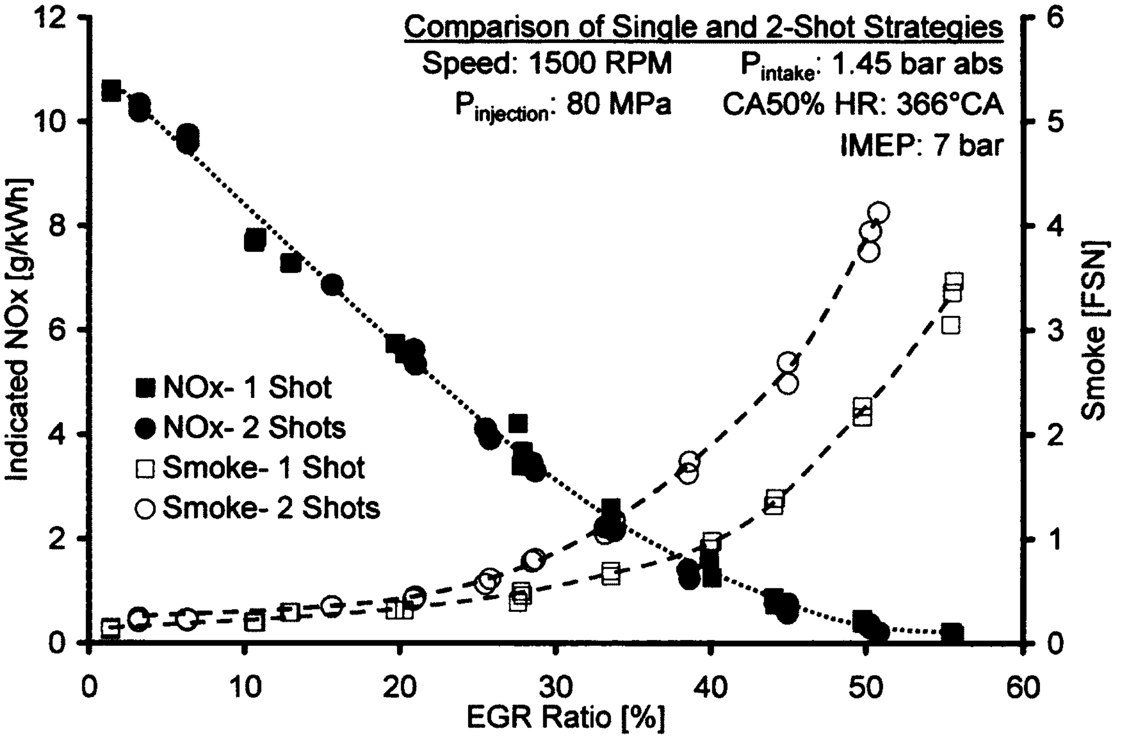

Figure 7.20: NOx & Soot for the Single- and 2-Injection Strategies (CA50 at 366°CA)

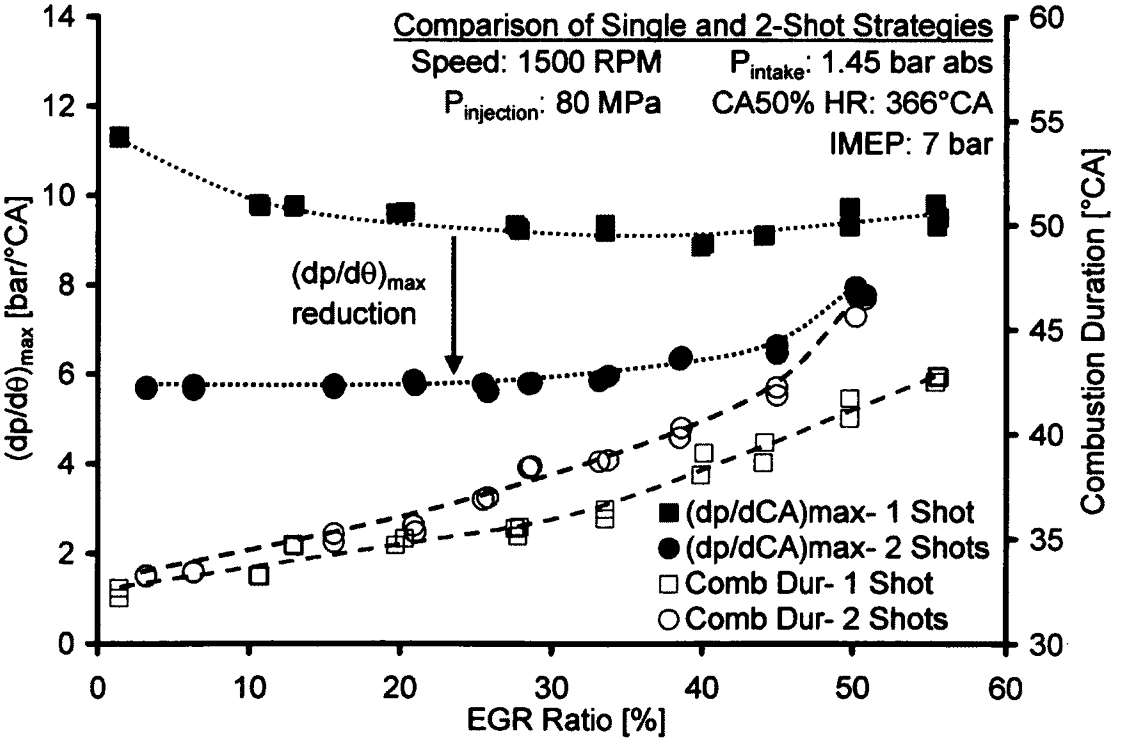

Figure 7.21: $(dp/d\theta)_{max}$ & Combustion Duration for Single- and 2-Injection Strategies (CA50 at 366°CA)

To further investigate the soot increase, the heat release rates were compared and one such comparison for an EGR rate of 33% is shown in Figure 7.22. For the 2-injection strategy, the combustion started earlier, the premixed phase was significantly smaller; however, the diffusion-controlled phase was visibly larger. Moreover, the reduced peak of the premixed phase implied that the prevailing combustion temperatures during the diffusion part were less. Since a lower combustion temperature can reduce the soot oxidation rates during the later part of the combustion, therefore, any increase in the diffusion-controlled phase was prone to negatively affect the engine-out soot emissions.

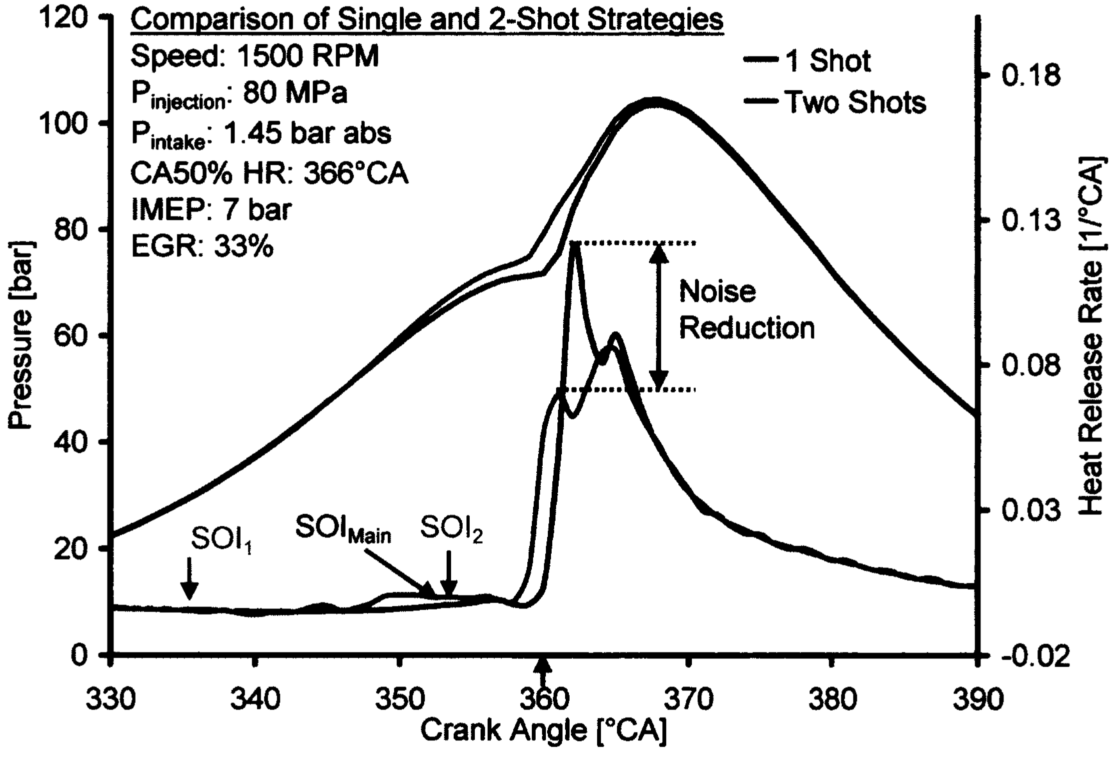

Figure 7.22: Heat Release Rate Comparison between Single- and 2-Injection Strategies (CA50: 366°CA)

The summary of the experiments targeting the diesel combustion noise using the two-injection strategy at 7 bar IMEP is given in Table 7.4.

Table 7.4: Summary of Two-Injection Strategy Tests

Parameter	Observed Effect
NOx	• Decreased with EGR. Trend same as that seen with the single-shot strategy • Value reduced with retarded combustion phasing for both the fuelling strategies.
Soot	• Increased with EGR for both the strategies. • Higher for the two-injection strategy when the combustion duration is more than that for the single-injection strategy
Combustion Noise	• Significantly reduced compared with the single injection strategy across the EGR range
Premixed Combustion	• Reduced significantly and considered the major reason for reducing the combustion noise
Diffusion Combustion	• Contributes to the higher engine-out soot levels. • A higher fraction of the diffusion phase with the two-injection strategy increases soot
Thermal Efficiency	• Slightly lower than the single-injection strategy

7.3. The Necessity of Alternative Combustion Regimes

The results presented above highlight the limitations of the conventional diesel combustion in achieving simultaneous low NOx and low soot emissions. The future emission standards targeting ultra low values of NOx (0.2 g/kWh) and soot (0.01 g/kWh) cannot be met with the strategies presented for the high temperature combustion. Therefore, to ensure compliance with the emission norms, two alternatives exist: the use of diesel exhaust aftertreatment devices or the use of clean combustion technologies.

The aftertreatment device for soot treatment is primarily the diesel particulate filter (DPF) with or without a diesel oxidation catalyst (DOC). Since 2007, DPFs are being increasingly used in production diesel vehicles in North America for meeting the emission standard. However, an aftertreatment device for NOx treatment is still being researched for meeting the 2010 emission standards. The potential NOx treatment technologies include the selective catalytic reduction (SCR) or the lean NOx trap. The functioning and proper functioning of these devices requires a complex system.

The use of clean combustion technologies such as homogeneous charge compression ignition, low temperature combustion etc. is another viable alternative to simultaneously reduce the NOx and soot emissions through in-cylinder combustion optimization and engine hardware improvements. The use of such advanced combustion technologies to meet the emission standards can potentially be more cost effective compared to the diesel aftertreatment devices. Furthermore, any improvement in the combustion process (with the alternate combustion regimes) that reduces the engine-out emissions can potentially reduce or in an ideal scenario, eliminate the necessity of aftertreatment devices.

Therefore, the rest of this chapter describes the testing and control of the diesel low temperature combustion.

7.4. Diesel Low Temperature Combustion

The Diesel low temperature combustion was investigated to realize ultra-low levels of NOx and soot. The implementation challenges for the diesel LTC were quantified and new LTC control strategies were explored experimentally to achieve ultra low emissions under independently controlled EGR, intake boost, exhaust backpressure, and multi-event fuel injection events. The narrow operating regions of LTC cycles which are close to the flame-out limits [140–142] and are generally considered non-viable for continuous engine operation were targeted. Empirical comparisons were made between the fuel efficiencies of such LTC cycles.

7.5. Diesel LTC Challenges

The enhanced premixed burning of lean and/or EGR weakened mixtures in LTC cycles predominantly reduces NOx. A natural consequence of high EGR rates is a substantial increase in the ignition delay period as shown by the test results (Figure 7.23). An increase in the ignition delay above 50% of the baseline value (without EGR) (or greater than 1.5ms) was repeatedly observed during the experimental work, to push the combustion into the LTC regime at different engine operating conditions. The increased ignition delay allows more time for the fuel-air mixing and therefore improves the homogeneity of the cylinder charge. However, the fuel-efficiency of HCCI engines is commonly compromised by the high levels of HC and CO emissions that may drain substantial amount of fuel energy (5~20% for instance) from the engine cycle [30]. The major factors affecting the LTC operation that included the fuel efficiency, load level and the emission trade-off are therefore discussed hereafter.

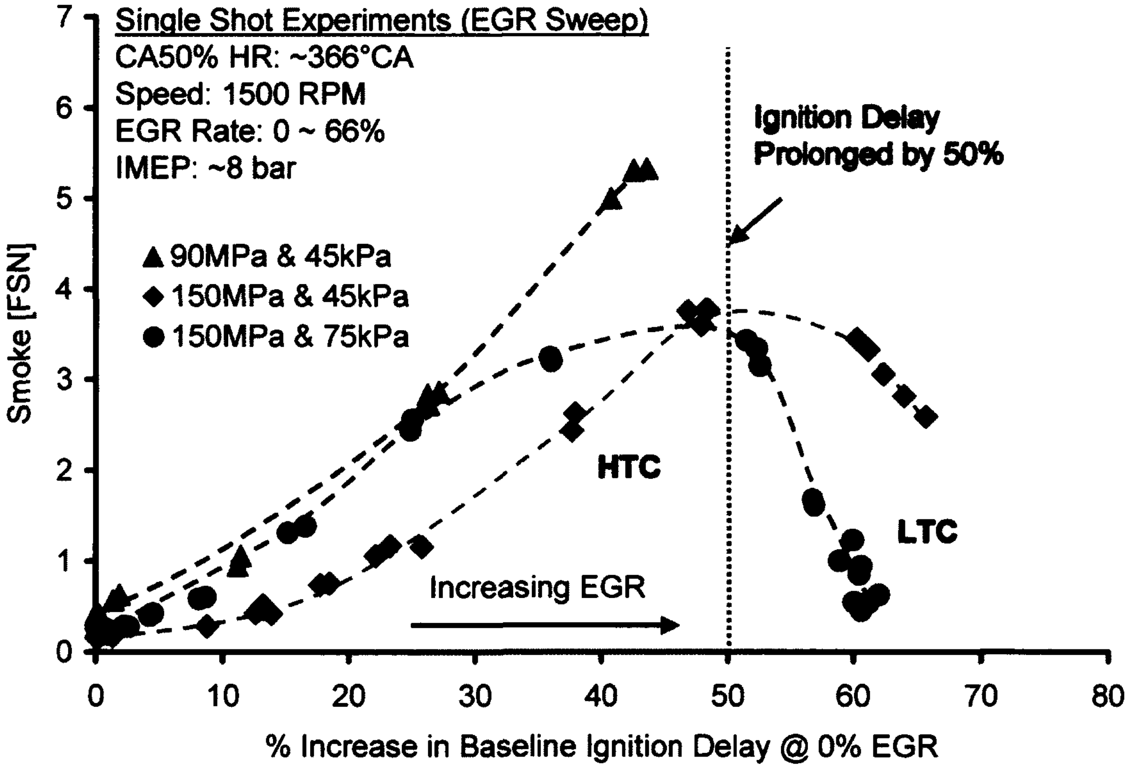

Figure 7.23: Ignition Delay for Enabling LTC

7.5.1. Fuel Efficiency of LTC Cycles

The high HC and CO emissions during LTC cycles can be attributed to the following reasons:

- Off-phasing of the combustion event;
- The lowered combustion temperature of the lean and/or EGR diluted cylinder charge;
- Low volatility of the diesel fuels;

- The flame-out of the locally excessive lean mixture caused by the non-homogeneity of the cylinder charge;
- The fuel condensation and flame quenching on the surfaces of the combustion chamber.

Unlike conventional diesel engines where the phasing of combustion is tightly controllable via fuel injection timing modulation [4,143], the scheduling of fuel delivery in LTC cycles has less leverage on the exact timing of auto-ignition because of the prevailing prolonged ignition delay and compounded cycle-to-cycle variations. In cases of diesel LTC cycles, the crank angle for 50% heat released (CA50) may occur 7~14°CA BTDC, which may result in a substantial fuel-efficiency penalty and combustion roughness [144]. Additionally, any departure from an optimized setting of EGR, intake boost, and charge homogeneity may severely destabilize the combustion process and thus deteriorate the fuel efficiency of the engine cycle [107,145].

Due to the relatively higher boiling temperatures of conventional diesel fuels [146], a cylinder charge of high homogeneity is more difficult to achieve and retain than with gasoline, especially when the temperature level and/or the mixing duration of the cylinder charge is insufficient. In an extreme scenario, attaining homogeneity is more difficult with bio-diesels that commonly have an even higher and narrower boiling range than conventional diesels [106]. Conversely, if such a diesel fuel has been homogenized with the cylinder charge for too long while the charge temperature is insufficiently high for vaporization, the diesel fuel is prone to condense on the surfaces of the combustion chamber as the vaporized diesel fuel would be in prevailing contact, for a few milliseconds or longer, with the surfaces of the piston-cylinder enclosure that significantly departs from a close-to-TDC designated combustion chamber. In comparison, conventional diesel sprays normally only have partial and momentary contacts, typically as fuel impingements with the chamber wall (primarily the bowl of the piston).

An ideal homogeneous charge with diesel fuel should be produced shortly before the cylinder TDC. If the homogeneous charge is produced too early, fuel condensation on the cylinder walls and the piston crown is inevitable. If the charge formation process starts too late or proceeds slowly, a homogeneous charge cannot be produced within the available time window, which may lead to premature ignition, and thus elevated NOx and soot production. Conversely, a large quantity of fuel per injection event may also lead to high HC and CO emissions as demonstrated empirically in Figure 7.24. Therefore, the homogeneity history needs to be controlled to produce the best fuel efficiency, for which multiple fuel injection events of short duration have been found to be effective, a representative case of which is shown in Figure 7.25. A significant improvement in the HC and soot emissions was achieved with the multiple injection strategy. Moreover, the fuel efficiency was also seen to improve as the injected fuel quantity had to be reduced to maintain the load at the same IMEP of 7.3 bar.

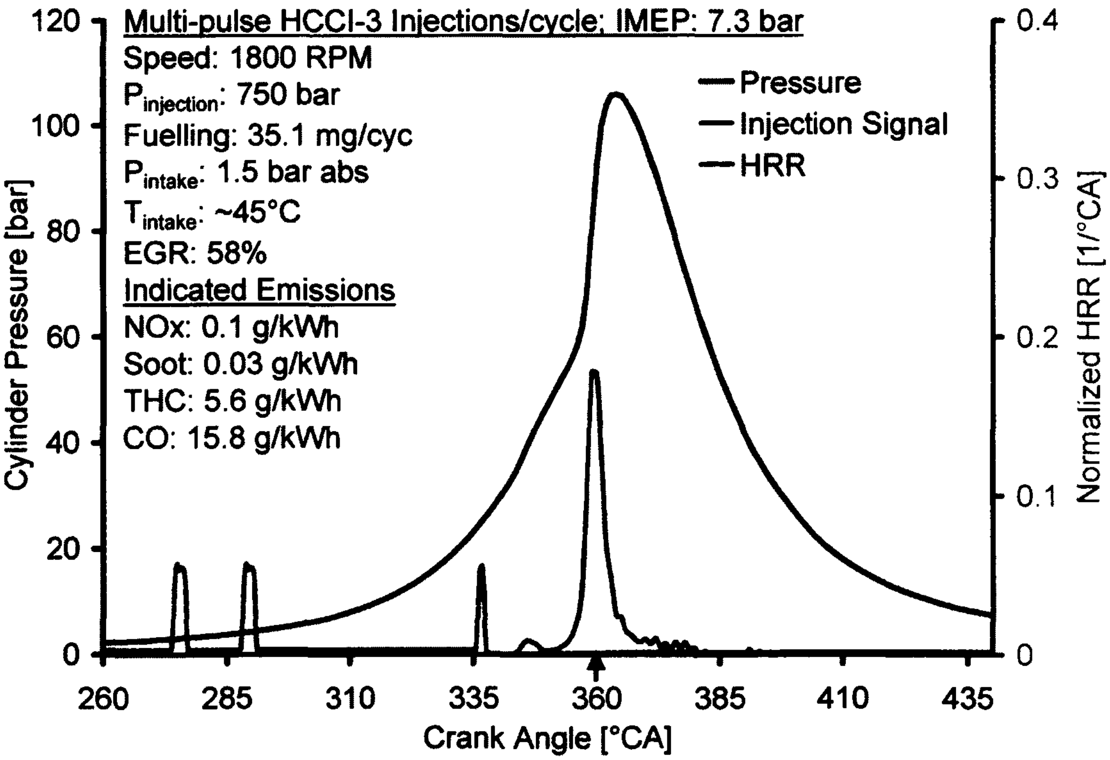

Figure 7.24: Relatively High CO & HC Penalty due to Large Injection Quantity per Shot

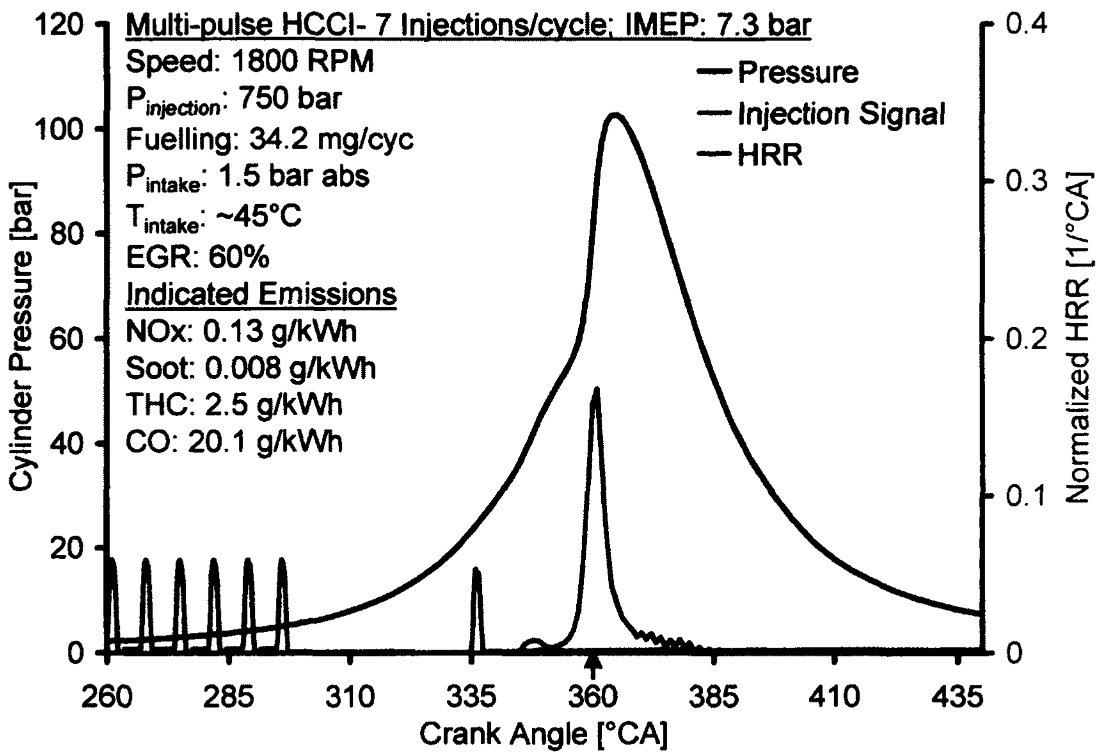

Figure 7.25: Multiple Injections to Improve Charge Homogeneity and Fuel Efficiency

7.5.2. LTC Emission Trade-off

The simultaneous high NOx and soot are inevitable for heterogeneous high temperature combustion (HTC) where a large fraction of the heat is released in a mixing-controlled process and peak combustion temperatures can approach the adiabatic flame temperature for a stoichiometric mixture. EGR is commonly used to dilute the cylinder charge and to lower the combustion temperature; this results in the classical HTC trade-off between NOx and soot formation.

Simultaneous low NOx and low soot are attainable for homogeneous LTC. Low combustion temperatures can be achieved by either premixing to very lean equivalence ratios or by employing EGR to reduce the combustion temperatures of mixtures with high equivalence ratios and thus reduce the NOx formation. The ensuing increase in the ignition delay allows more time for the fuel-air mixing and therefore improves the homogeneity of the cylinder charge that may eventually lead to simultaneous soot and NOx reductions as demonstrated in Figure 7.26.

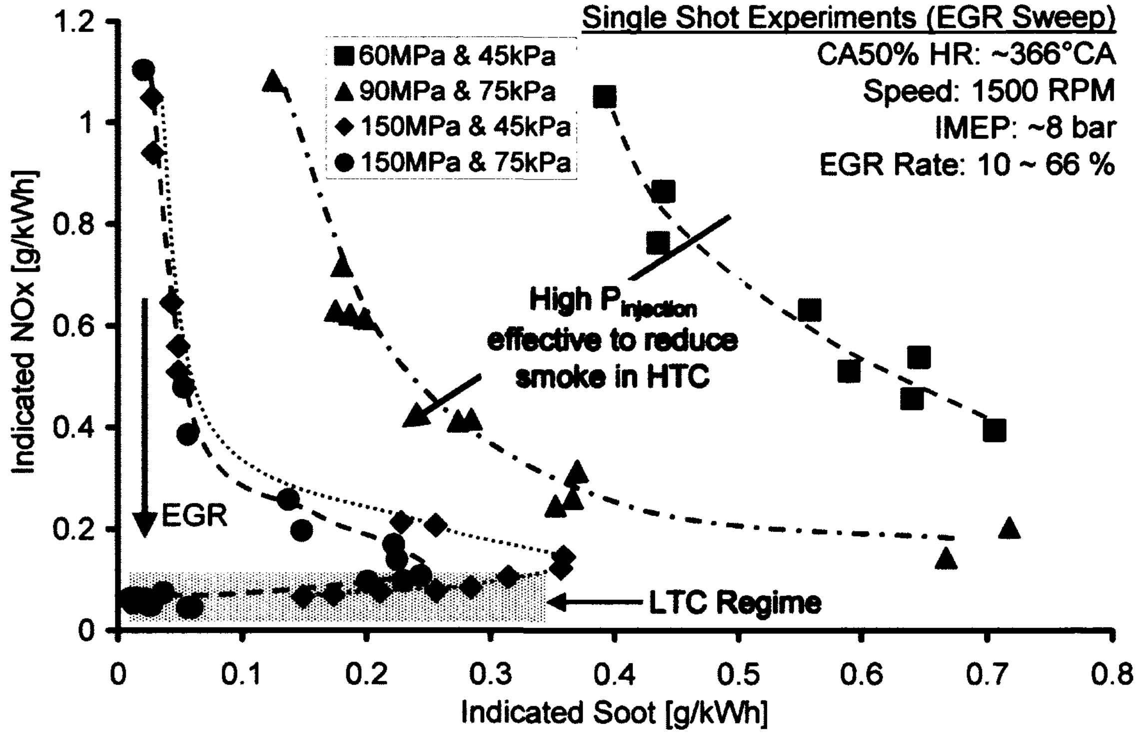

Figure 7.26: NOx-Soot Trade-off in LTC Regime

Thus, the high homogeneity of a cylinder charge, i.e. the parity of local and global air/fuel ratio, is a precursor to simultaneous soot and NOx reductions, which also agrees with the essences of HCCI whose lean and homogeneous cylinder charge typically results in ultra low levels of NOx and soot [35,60,74,147] especially under light loads [35]. The burning of a homogeneous cylinder charge that is lean and/or EGR diluted, i.e. LTC, is closer to non-combustion regions (flameout limits) and therefore, is prone to produce higher CO and HC emissions and to dwell in narrower operating regions. Therefore, a new LTC trade-off, that is, CO and HC vs. NOx and Soot exists, a representative case of which is shown in Figure 7.27. The CO emissions generally tend to follow a similar trend as that for the HC emissions.

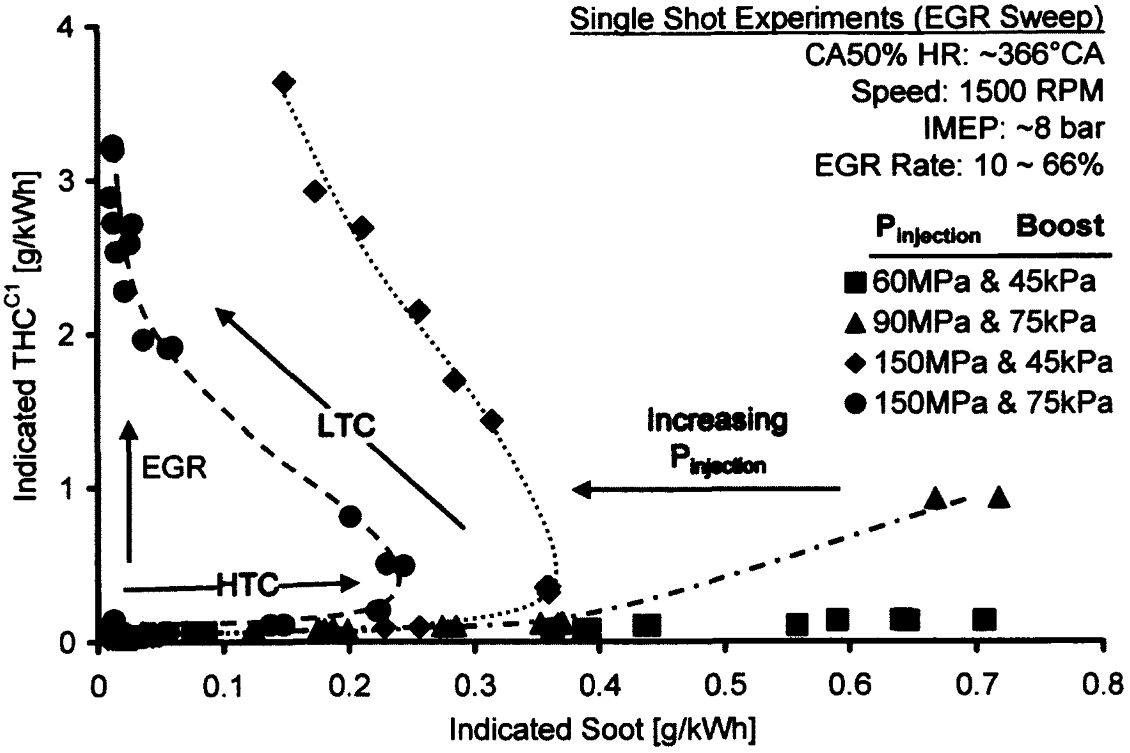

Figure 7.27: LTC Emission Trade-off

7.5.3. Engine Load Level with LTC Cycles

The load level of the LTC cycles is limited by the peak cylinder pressure, the maximum rate of pressure rise and the peak combustion temperature. The low combustion temperature and high homogeneity are more difficult to achieve as the engine load, and thus the fuelling rate, increases. The excess oxygen depletes with higher fuelling rates and the proportion of the premixed fuel reduces within the given ignition delay period. Without employing higher EGR rates to push down the temperature, any non-homogeneity may therefore increase the local flame temperature in regions close to the stoichiometric air/fuel ratio.

The implementation of the LTC cycles is commonly in low compression ratio (CR) engines such as 16:1, 14:1 or even lower [33,66,137]. Engines with a CR of 17:1 or higher are generally considered not suitable or are commonly restricted to low load operation only while operating under LTC cycles. This is so because a higher compression ratio translates into a higher peak compression temperature (assuming

EGR and other conditions to be the same). Therefore, the transition from the high temperature combustion to the LTC cycles requires higher EGR rates to lower the temperature which normally result in very high levels of soot during the transition phase (Figure 7.23).

7.6. LTC Cycle Efficiency Calculations

Automotive diesel engines traditionally produced high burning efficiency especially in high temperature combustion (HTC) cycles. The heat release phasing and shaping were also proximate to the peak cycle efficiency, i.e. the mid heat release CA50 was placed 5~10°CA ATDC, and the duration and the rate of burning were kept short and integrated without splitting. However, new constraints in emission and combustion noise control often compromise the fuel efficiency, i.e. a reduction in the burning efficiency by LTC, off-peak heat release phasing by HCCI, and widened or postponed heat release by heavy EGR application. Additionally, under high loads and high boosts, the combustion process needs to be split or highly delayed to confine the peak cylinder pressure. Furthermore, the technique of post injection has often been applied to incinerate the combustibles after the main combustion or to enable the exhaust aftertreatment, in which the burning energy is released significantly late.

The efficiency of the LTC cycles was evaluated in terms of the indicated thermal efficiency and the combustion efficiency, and all comparisons with the conventional HTC operation were also done based on these two efficiencies. Therefore, it was essential to clearly define the efficiency terms and then compare the efficiency terms for the conventional and the LTC combustion based on these definitions.

7.6.1. Combustion Efficiency

Combustion efficiency is defined as the fraction of the supplied fuel energy that is the released during the combustion process [4]. Mathematically, it is expressed as:

$$\eta_c = \frac{H_R(T_A) - H_P(T_A)}{m_f Q_{HV}} \tag{7.1}$$

and

$$\left[H_R\left(T_A\right)-H_P\left(T_A\right)\right]=m\left(\sum_{i,reactants} n_i\Delta\tilde{h}^o_{f,i}-\sum_{i,products} n_i\Delta\tilde{h}^o_{f,i}\right) \tag{7.2}$$

where

m = mass that passes through the control volume surrounding the engine. It includes both the fuel and the air.

n_i = the number of moles of species i in the reactants or products per unit mass of the working fluid.

$\Delta\tilde{h}^o_{f,i}$ = standard enthalpy of formation of species i at ambient temperature T_A.

$m_f Q_{HV}$ = amount of fuel energy supplied

H = enthalpy at the standard state

The combustion efficiency metric was primarily used to account for the incomplete products of combustion in the exhaust. The typical products of incomplete combustion are CO, HC, soot and very small fraction of hydrogen. For the present research, the CO and HC were only considered. The ultra low levels of soot during the LTC cycles indicated that ignoring the contribution of soot should not have a significant effect on the energy efficiency considerations. In case of hydrogen, previously published results in the literature have shown that the hydrogen becomes a significant contributor to incomplete combustion only when the engine is operated under rich combustion mode [4]. The EGR reforming experiments (Chapter 6) showed that the hydrogen was produced under significantly rich combustion modes. Since all the LTC experiments were done under lean conditions ($\lambda>1$), the contribution of the exhaust hydrogen was excluded from the calculations. An additional source of decrease in the combustion efficiency can be oil dilution if the injection scheduling is very early in the compression stroke. This issue was addressed by setting a criterion for the earliest injection timing that would minimize the oil dilution (explained later in this chapter). However, no attempt was made to quantify the oil dilution.

If the concentration of the exhaust species is known, an alternative expression for combustion efficiency is given by Equation (7.3). In this expression, the chemical energy carried out of the engine by the combustibles is considered as a representative of the combustion inefficiency [4].

$$\eta_c = 1 - \frac{\sum_i x_i Q_{HV_i}}{\left[\dot{m}_f / \left(\dot{m}_a + \dot{m}_f\right)\right] Q_{HV_f}} \tag{7.3}$$

where

x_i = mass fraction of CO or HC

Q_{HV_i} = lower heating value for CO & HC

The lower heating value of CO was taken as 10.1 MJ/kg and the lower heating value of HC was assumed to be the same as that of the diesel fuel (a value of 42.9 MJ/kg was used for the analysis). As mentioned before, only the combustibles in the form of CO and HC were considered while the chemical energy carried by the soot and hydrogen was ignored.

Modern HTC diesel engines may have a burning efficiency exceeding 99.5%. However, as strict in-cylinder NOx control techniques are implemented, the flame temperature reduces, and the exhaust HC and CO rise. The diesel LTC cycles may even downgrade to approach the conventional gasoline engine cycles giving a combustion efficiency of approximately 90~95%.

7.6.2. Indicated Thermal Efficiency

The indicated thermal efficiency is defined as the ratio of the useful work produced per cycle, to the total amount of the fuel energy supplied per cycle that can be released in the combustion process. This efficiency is also called the cycle thermal efficiency or the fuel conversion efficiency. Mathematically, it can be expressed by the following expression:

$$\eta_{th} = \frac{W_c}{m_f Q_{HV}} \tag{7.4}$$

where,

W_c = net useful work produced per cycle and is given by:

$$W_c = \oint p dV \tag{7.5}$$

7.6.3. Effect of Combustion Inefficiency

The amount of the combustibles in the exhaust is not a direct representation of the combustion efficiency. The efficiency is affected by the engine load which is directly related to the fuelling rate for the conventional diesel engine. Therefore, 0-D engine cycle simulations were performed to correlate the exhaust combustibles with the engine load.

For the fuel injected into the engine cylinder $\dot{m}_f$, the burned fuel $\dot{m}_b$ normally completes combustion, while a small portion of fuel, i.e. the fuel loss $\dot{m}_l = \left(\dot{m}_f - \dot{m}_b\right)$, fails to release energy or to release energy fully in the cylinder. The combustion or burning efficiency is thus:

$$\chi_b = \frac{\dot{m}_b}{\dot{m}_f} \tag{7.6}$$

The fuel energy loss was evaluated herein that the exhaust HC was counted to have the same LHV and H:C ratio as diesel fuel; the LHV of CO was counted as ¼ of diesel; however, the soot constituent was ignored. Figure 7.28 shows a calculation for the fraction of exhaust HC ($C_1H_{1.88}$) with respect to the cylinder input fuel. The results indicate that the fuel fraction of exhaust HC is highly dependent on the load level. As highlighted in Figure 12, at high loads for instance, 4000 ppm of exhaust HC would translate to ~4% of fuel energy while the same would equal ~10% at low loads. The same was observed during the testing and control of the diesel LTC cycles (Table 8.3).

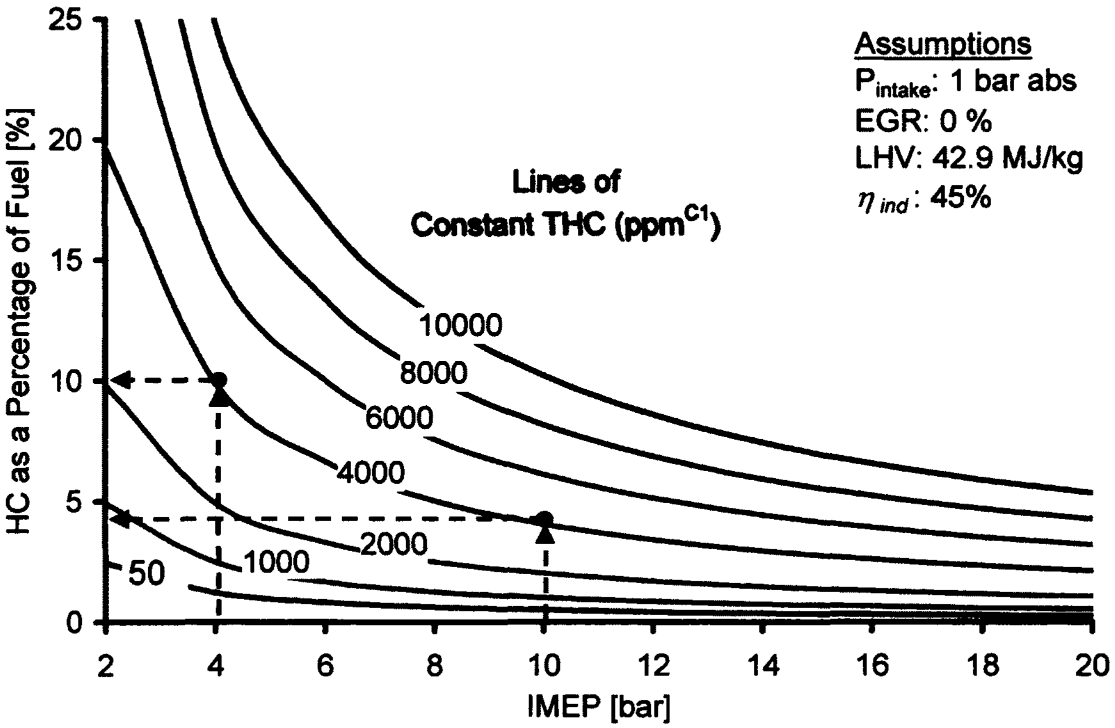

Figure 7.28: Exhaust Energy with respect to Input Fuel at Different Engine Loads

7.6.4. Effect of Combustion Phasing

The effectiveness of the burning efficiency χ_b can be further evaluated in relevance to the impact of the heat release phasing. The heat release phasing efficiency is defined as:

$$\chi_p = \frac{\eta}{\eta_{p\max}} \tag{7.7}$$

In Equation (7.7), η is the actual cycle thermal efficiency when the phase of heat release departs from the timing of maximum thermal efficiency $\eta_{p\max}$, while the heat release rates for both η and $\eta_{p\max}$ are fixed to the actual shape. When the phasing departs from the timing of maximum thermal efficiency, this off-phasing causes an additional efficiency penalty that may be greater than the burning inefficiency, especially at higher loads. If the phasing is early (before TDC), the combustion occurs during the compression stroke. The resulting high pressure and temperature can substantially increase the compression work and therefore, result in a significant decrease in the IMEP (shown in Figure 7.9). A late combustion phasing, on the other hand, effectively results in a shorter expansion stroke so that the amount of useful work is reduced. This can also cause a significant decrease in the IMEP (Figure 7.5, Figure 7.9).

The phasing efficiency penalty was quantified in terms of 'Equivalent Exhaust HC'. Figure 7.29 relates the degree of CA50 off-phasing to the equivalent THC that would result in the exhaust for the same amount of fuel loss. For the LTC types of combustion where the off-phasing of the CA50 can be up to 12°CA BTDC and 20°CA ATDC, the contribution of the CA50 to the fuel-efficiency penalty may be similar or higher than that due to the actual HC and CO emissions in the exhaust. For instance, an off-phasing of -10°CA (advanced) from the best efficiency CA50 at 8 bar IMEP would be equivalent to ~2000ppm THC^{C1} in the exhaust; a similar loss would be encountered when the timing is retarded by ~ 5.5°CA from the best efficiency CA50.

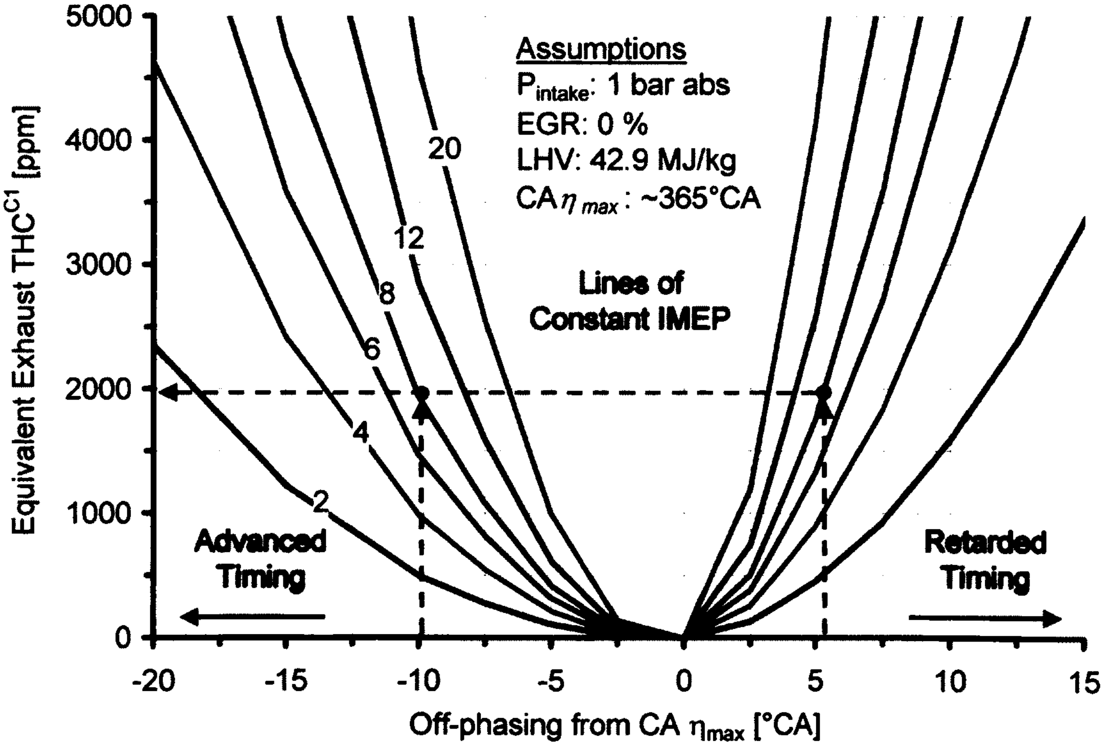

Figure 7.29: Equivalent THC Penalty with CA50 Off-phasing

The equivalent exhaust HC because of the off-phasing of the combustion from the best efficiency window were also related to the decrease in the indicated thermal efficiency through 0-D engine cycle simulations as shown in Figure 7.30. A higher penalty in the combustion efficiency is incurred as the off-phasing of the combustion increases (represented by the HC in this figure). The experimental data for an SOI sweep from 342 to 344.8°CA was performed without EGR. The IMEP was maintained at 6.1 bar by adjusting the fuelling at each SOI. The actual combustion phasing data and the indicated thermal efficiency data was used to estimate the equivalent HC penalty based on Figure 7.29 and the result has also been plotted in Figure 7.30.

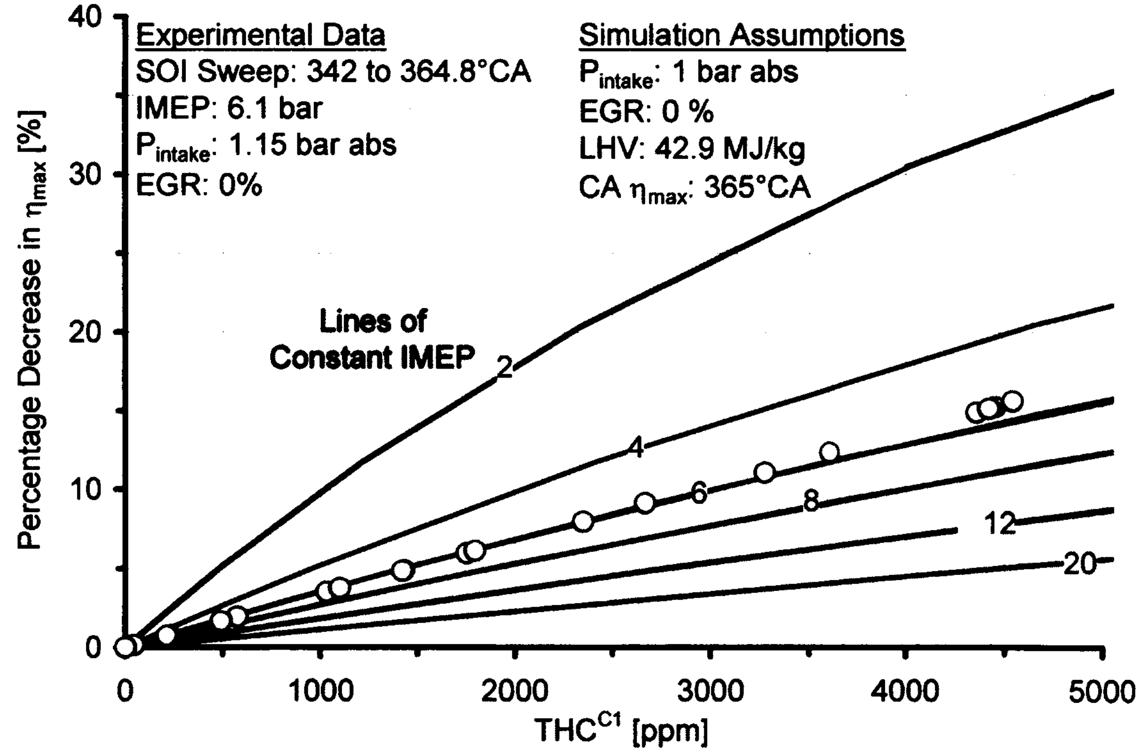

Figure 7.30: Drop in Indicated Thermal Efficiency as a function of the Equivalent Exhaust HC

The actual combustibles for this SOI sweep test (HC + counting CO as ¼ of HC) are shown in Figure 7.31 and were very low (< 200 ppm). Therefore, the decrease in the indicated thermal efficiency observed in the test can be taken as the result of the combustion off-phasing. The effect of the combustion off-phasing has been empirically demonstrated in the multi-shot (early HCCI) LTC tests presented later in this chapter where the earlier-than-TDC burning of the homogeneous cylinder charge resulted in a significant reduction in the efficiency.

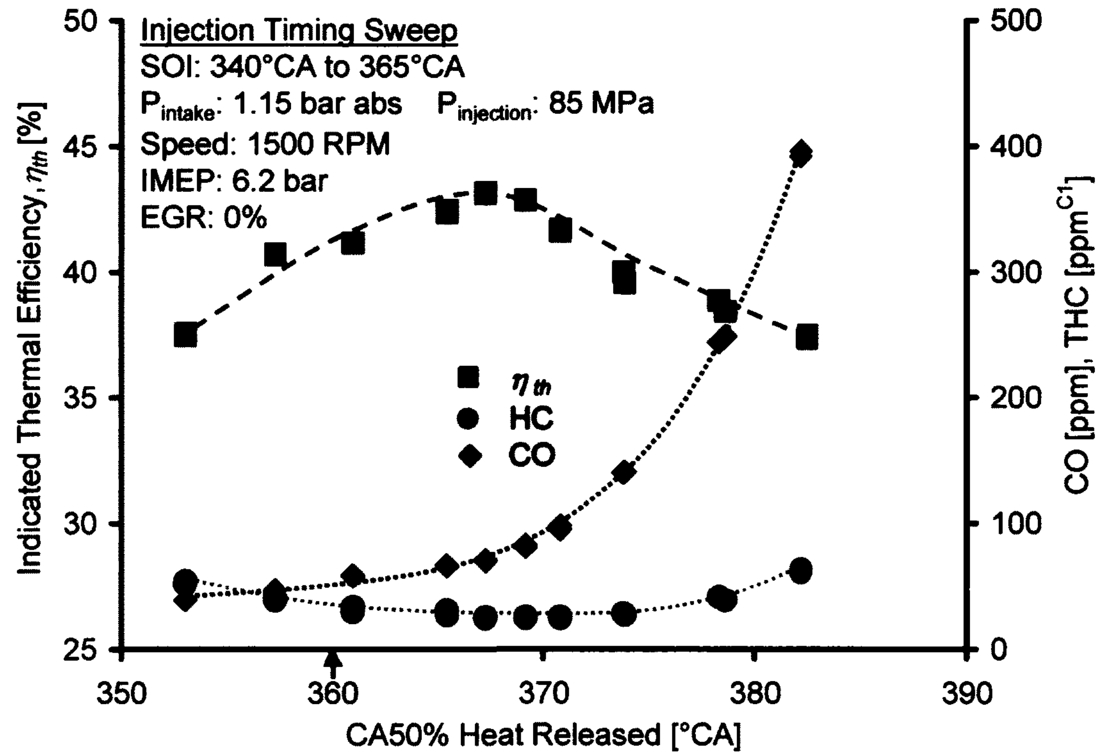

Figure 7.31: Effect of Combustion Phasing on the Indicated Thermal Efficiency and Engine-out Combustibles

7.7. Stability of the LTC Cycles

The burning of a homogeneous cylinder charge that is lean and/or EGR diluted, i.e. LTC, is closer to non-combustion regions (flameout limits). Thus, the LTC cycles are inherently inclined to produce higher unburned combustibles and to dwell in narrower operation regions in stark contrast to the conventional HTC combustion.

The coefficients of variance (COV) of the IMEP and P_{max} have been regarded as suitable measures to quantify the stability of the combustion process [4]. The COV evaluates the data scattering or deviation from the mean value and is mathematically expressed as:

$$COV = \frac{\sigma}{\bar{x}} \tag{7.8}$$

where σ is the standard deviation of the dataset and $\bar{x}$ is the arithmetic mean. The COV of IMEP and P_{max} can therefore be written as:

$$COV_{IMEP} = \frac{1}{IMEP_{mean}}\sqrt{\frac{\sum_{i=1}^{N}\left(IMEP_i - IMEP_{mean}\right)^2}{N-1}} \tag{7.9}$$

and

$$COV_{p_{max}} = \frac{1}{p_{mean}}\sqrt{\frac{\sum_{i=1}^{N}\left(p_i - p_{mean}\right)^2}{N-1}} \tag{7.10}$$

The COV was calculated for each dataset with 200 consecutive cycles of the recorded pressure data and was used as a measure of the stability of the combustion process in this research.

7.8. Implementation of Diesel LTC Cycles

The implementation of the diesel LTC cycles was done on the basis of the fuel injection strategies (Figure 3.4) to prepare a homogeneous cylinder charge (lean or EGR diluted) before the combustion process. The test matrix for the LTC experiments is given in Table 7.5. The single-injection (single-shot) LTC, the multi-shot LTC (early-HCCI) and the split combustion categories were tested under different engine operating conditions and energy efficiency comparisons were made. For the single-shot strategy, the effect of boost and injection pressure on the transition from the HTC to the LTC cycles was investigated and quantified. The minimum levels of boost and fuel injection pressure were identified for both the single-shot LTC and the early HCCI strategies, and efficiency comparisons were also drawn between these two strategies.

Table 7.5: Test Matrix for Diesel LTC Experiments

Test #	LTC Strategy	Implementation	Investigated Parameters
1.	Single-shot LTC	Speed: 1500 RPM Load: 5.2 bar IMEP	EGR
2.	Single-shot LTC	Speed: 1500 RPM Load: 8 to 7.4 bar IMEP	Injection Pressure, Boost, EGR
3.	Multi-shot LTC (Early HCCI)	Speed: 1500 RPM Load: 6.8 & 7.4 bar IMEP	Injection Pressure, Boost, EGR
4.	Single-shot LTC vs. Multi-shot LTC (Performance Comparison)	Speed: 1500 RPM Load: 3.1, 5.2 & 7 bar IMEP	EGR
5.	Single-shot LTC	Speed: 1500/1800 RPM Load: 5.2 bar IMEP	Injection Pressure, Engine Speed
6.	Multi-shot LTC (Early HCCI)	Speed: 1500/1800 RPM Load: 5.2 bar IMEP	Injection Pressure, Engine Speed
7.	Split Combustion LTC	Speed: 1500 RPM Load: 8 & 9.7 bar IMEP	Injection Pressure, Boost, EGR

7.8.1. Single Shot LTC with Heavy EGR – 5.2 bar IMEP (Test # 1)

The first experiment was performed at a baseline IMEP of 5.2 bar (9%EGR). The boost was 1.5 bar abs and the injection pressure was 100MPa. An EGR sweep was performed to push the combustion in to the LTC cycles. The NOx and the soot emissions for the test are shown in Figure 7.32. As EGR was applied, NOx reduced significantly with initially minimal rise in soot. Further increases in EGR led to additional NOx reduction but caused a significant rise in soot (Slope 1-Classical NOx-soot trade-off). However, as heavier EGR was applied, the combustion process resulted in simultaneous reductions of NOx and soot emissions as the combustion essentially entered the LTC regime (Slope 2).

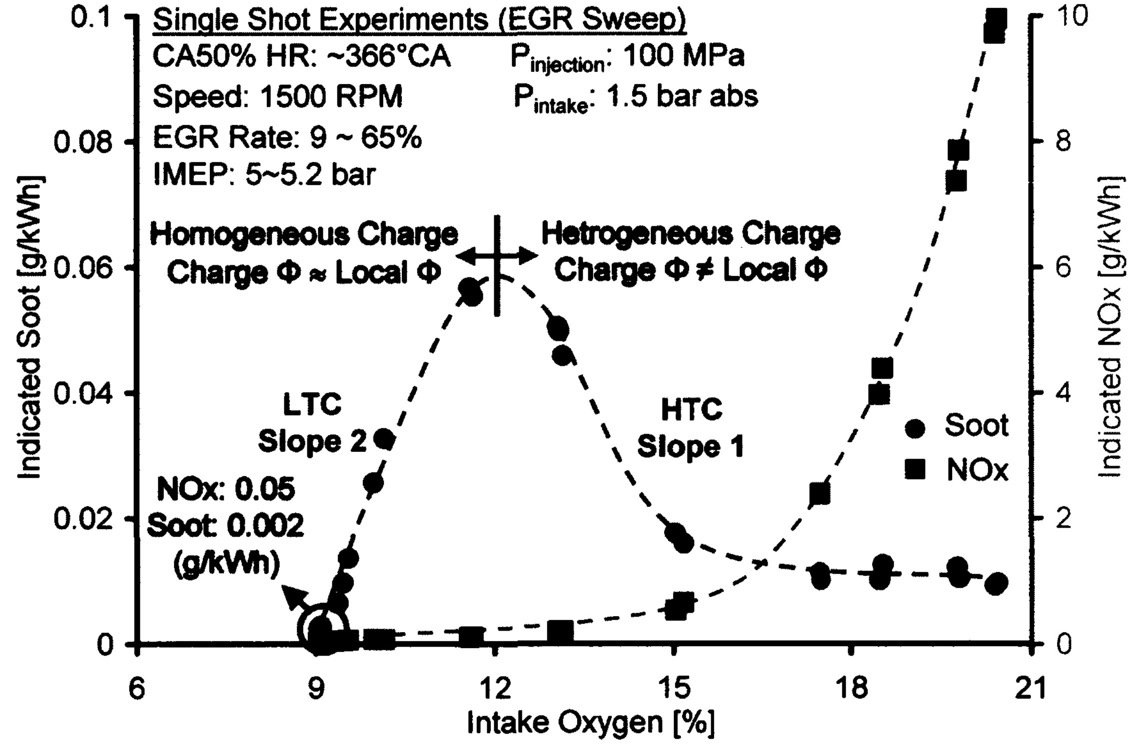

Figure 7.32: NOx & Soot Emissions for EGR-enabled Single Shot LTC (Test # 1)

The heavy use of EGR prolongs the ignition delay and provides more time for the fuel-air mixing. In the HTC combustion, the cylinder charge during combustion is essentially heterogeneous where the global equivalence ratio (decided by the total charge mass and the total injected fuel) is not the same as the local equivalence ratio existing around the fuel spray. However, as the mixing duration is enhanced with EGR, the disparity between the local and the global equivalence ratio is minimized, leading to a more homogeneous cylinder charge.

The terms 'slope 1' and 'slope 2' have been extensively used for the EGR enabled single-shot LTC in this work and are therefore defined as follows:

- Slope 1– the segment of soot climbing but NOx declining curve when EGR increases during HTC combustion. It represents the classical NOx-Soot trade-off.

- Slope 2 – the segment of simultaneous soot and NOx declining curve when EGR increases during LTC combustion. It represents the reduction in NOx and soot enabled with a single injection using heavy EGR.

The CO and THC emissions for the test are shown in Figure 7.33. The HTC combustion was characterized by low CO and HC emissions, an inherent advantage of the conventional diesel combustion process. With Increasing EGR, a rapid rise in the CO emission was observed as the oxygen concentration of the charge and combustion temperatures reduced. With heavier EGR, as the combustion entered the LTC cycles, a sharp rise in the HC emission was also observed, signifying the LTC emission trade-off.

The heat release rates at three EGR levels are shown in Figure 7.34. At 38% EGR, the intake oxygen was still high (17.5%) since the load was low. This is the free NOx reduction region where the enhanced premixing reduced the NOx with minimal soot penalty. At 63% EGR, the combustion had entered slope 2 but the soot was higher than the 2010 target of 0.01 g/kWh. The heat release peak was lower and the premixed combustion phase was wider. At 65% EGR where the soot was below 0.01g/kWh, the heat release was characterized by a much lower rate of rate release and an enhanced premixed combustion compared to the other two heat release traces. This can primarily be attributed to the high intake charge dilution and can be taken as an indicator of a high level of charge homogeneity.

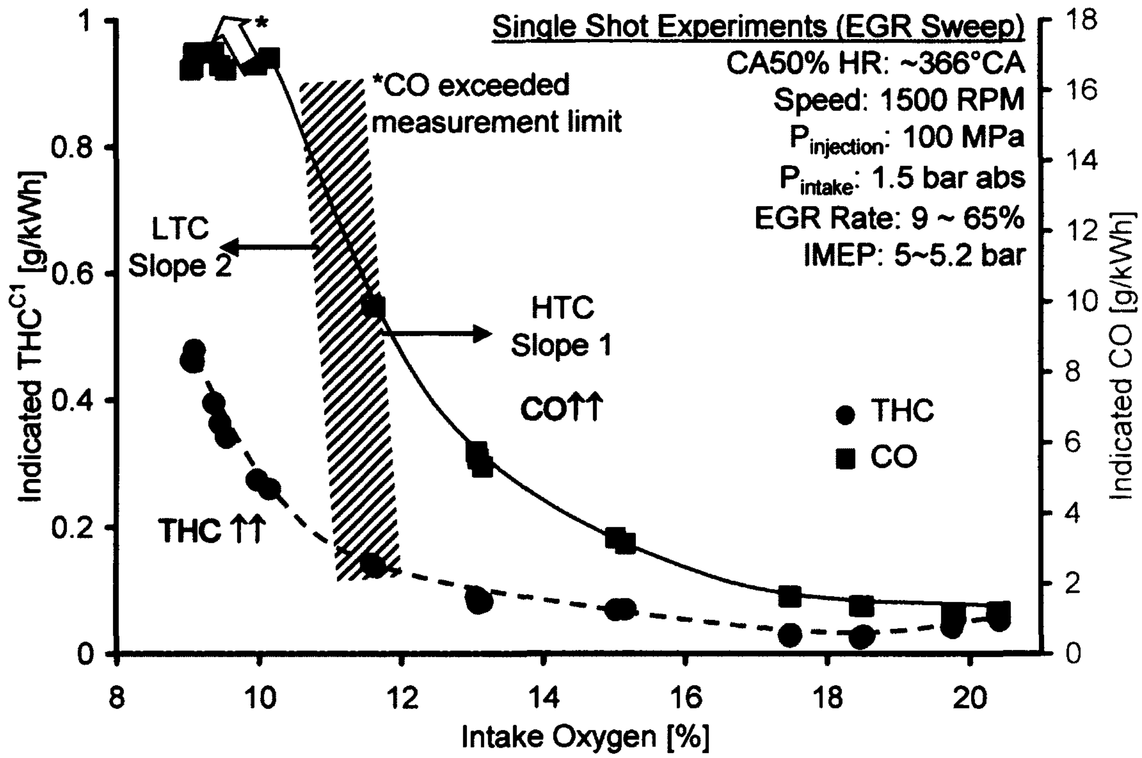

Figure 7.33: HC & CO Emissions for EGR-enabled Single Shot LTC (Test # 1)

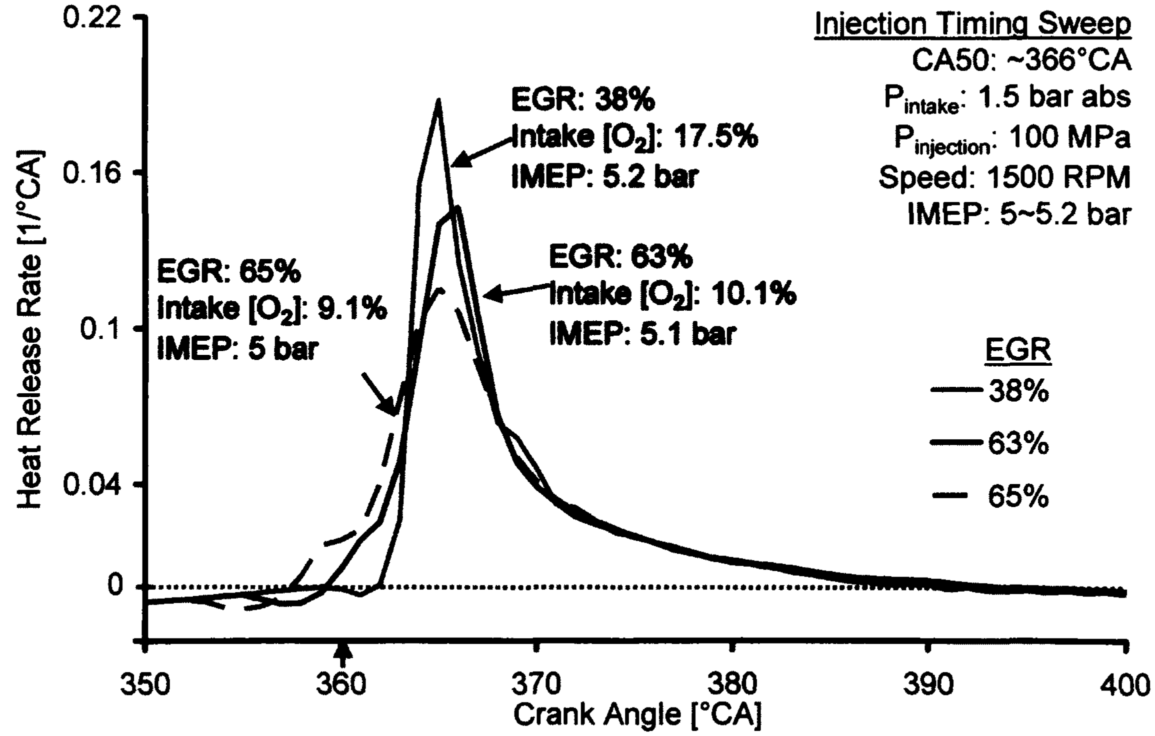

Figure 7.34: Heat Release Rate for EGR-enabled Single-Shot LTC (Test # 1)

The performance of the LTC was compared with the conventional HTC and the results are summarized in Table 7.6. Since the phasing was tightly controlled at 366°CA, only a slight deterioration in the combustion efficiency was observed and the thermal efficiency dropped by 1%. The coefficient of variance (COV) of IMEP is an indicator of the cycle-by-cycle variations. The COV_{IMEP} was 2.9 % which was just at the limit of the generally acceptable threshold of 3%. The combustion noise ($(dp/d\theta)_{max}$) was reduced significantly. A tight control on the engine operating conditions that included EGR and combustion phasing helped to retain the efficiency of the LTC operation, similar to the conventional HTC operation.

Table 7.6: Summary of Single Shot LTC – 5.2 bar IMEP (Test # 1)

Parameter	HTC	LTC
EGR [%]	30	65
IMEP [bar]	5.2	5
Intake O_2 [%]	18.5	9.1
Indicated Thermal Efficiency [%]	40.7	39.7
NOx [g/kWh]	4.38	0.05
Soot [g/kWh]	0.013	0.002
CO [g/kWh]	1.34	>17*
THC [g/kWh]	0.03	0.46
Combustion Efficiency [%]	99.83	97.82
P_{max} [bar]	98.4	93.7
$(dp/d\theta)_{max}$ [bar]	10.7	4.8
CA50 [°CA]	366	366.3
COV P_{max} [%]	0.74	1.98
COV IMEP [%]	2.3	2.9

* Exceeded the measurement limit of 5000 ppm

7.8.2. Single Shot LTC with Heavy EGR – 8 bar IMEP (Test # 2)

The implementation of the single-shot LTC in Test # 1 employed a moderately high injection pressure and a moderate boost pressure as well. To investigate the factors that affect the selection of the boost and injection pressure required for enabling LTC cycles, as well to highlight the implementation challenges (identify the limiting conditions) for the single-shot LTC, an extensive set of tests was run at a relatively high IMEP of 8 bar. Two levels of boost (1.45 bar abs & 1.75 bar abs) and four levels of fuel injection pressure (60 MPa, 90 MPa, 120 MPa & 150 MPa) were used. The baseline IMEP was set at 8 bar with 10% EGR and the fuelling was kept constant for the rest of the tests. A typical SOI adjustment is shown in Figure 7.35. A slight modification in the SOI was required as the EGR was increased up to ~40%. However, as the dilution effect of EGR became stronger at higher EGR levels, the prolonging of the ignition delay resulted in a large change to be made in the SOI to maintain the same combustion phasing. The

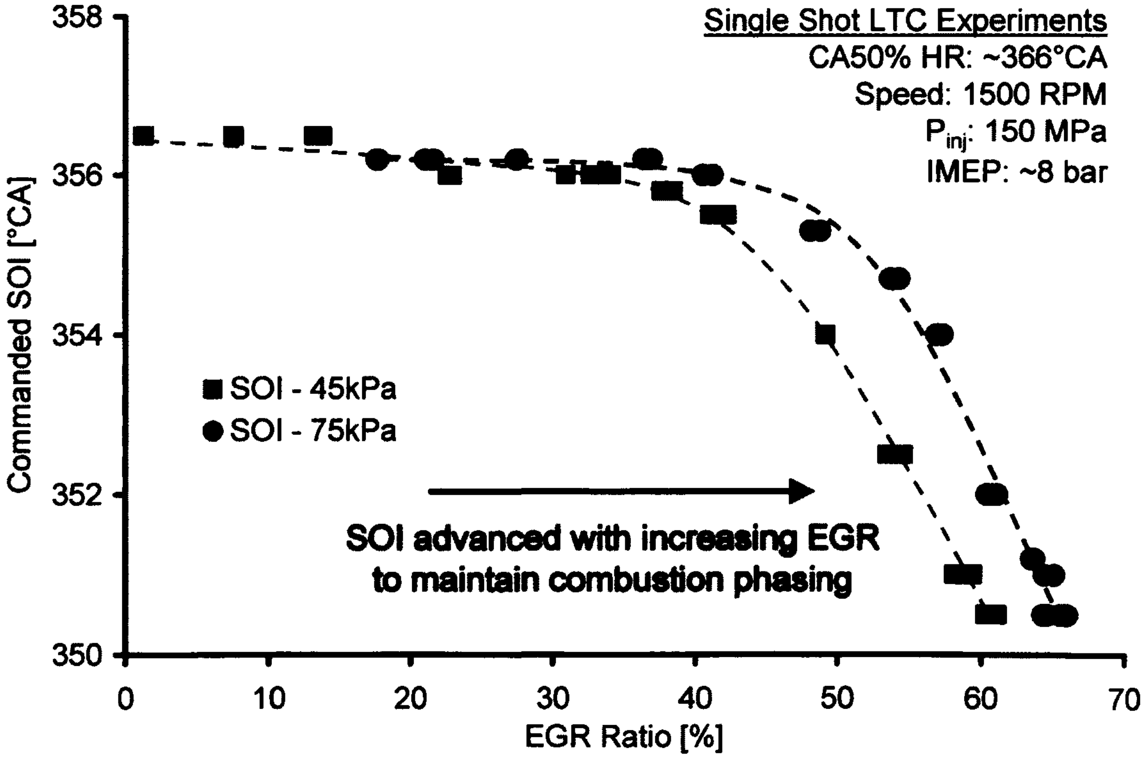

Figure 7.35: SOI Adjustment to maintain Combustion Phasing at 366°CA

effect of boost on the SOI was minor at low EGR levels but was pronounced as the combustion reached the slope 2. Moreover, the higher boost level shifted the deviation of the SOI towards higher EGR values.

In the following sections, an attempt was made to identify the individual effects of EGR, boost and injection pressure on the attainment and the efficiency of the single-shot LTC.

7.8.2.1. Efficacy of EGR in Single-shot LTC

The NOx and soot trends for the injection pressure of 150 MPa and 1.75 bar abs boost are shown in Figure 7.36. The results indicated that the combustion was pushed into the LTC cycles but the soot level was still higher than 0.01 g/kWh. The combustion phasing (CA50) was maintained at 366°CA by adjusting the SOI as the EGR was progressively increased.

The efficacy of EGR in pushing the combustion into the LTC cycles can be attributed primarily to the dilution of the intake charge and the increased charge heat capacity. EGR reduces the intake oxygen concentration by replacing part of the fresh air intake with inert combustion products, namely carbon dioxide (CO_2), water (H_2O) and nitrogen (N_2). The higher heat capacity of the inert gases, together with the reduced oxygen concentration results in reduced local flame temperatures during the combustion process and thus, a reduced rate of NOx formation. Additionally, the lowered compression temperature during the fuel injection events also causes an increase in the ignition delay as the reaction rates are reduced (strongly temperature-dependent) [148]. This effect is similar to that observed with retarding the injection timing. Since the peak combustion temperature is widely believed to the most significant variable affecting NOx production, EGR has proven to be very effective in reducing the engine-out NOx.

However, the soot emissions tend to increase as the EGR is progressively increased during HTC (slope 1) [36]. Soot emissions from diesel engines are the result of the difference between the soot production and soot oxidation processes [28]. The lowered combustion temperature and the charge dilution are thought to reduce the soot oxidation rates associated with the low flame temperatures of diluted mixtures, hereby increasing the soot emissions [34]. However, as the combustion enters the LTC cycles with very high EGR levels (slope 2), the soot emissions decrease sharply. Previous studies suggest that the flame temperature is lowered to levels at which the soot production is inhibited [35].

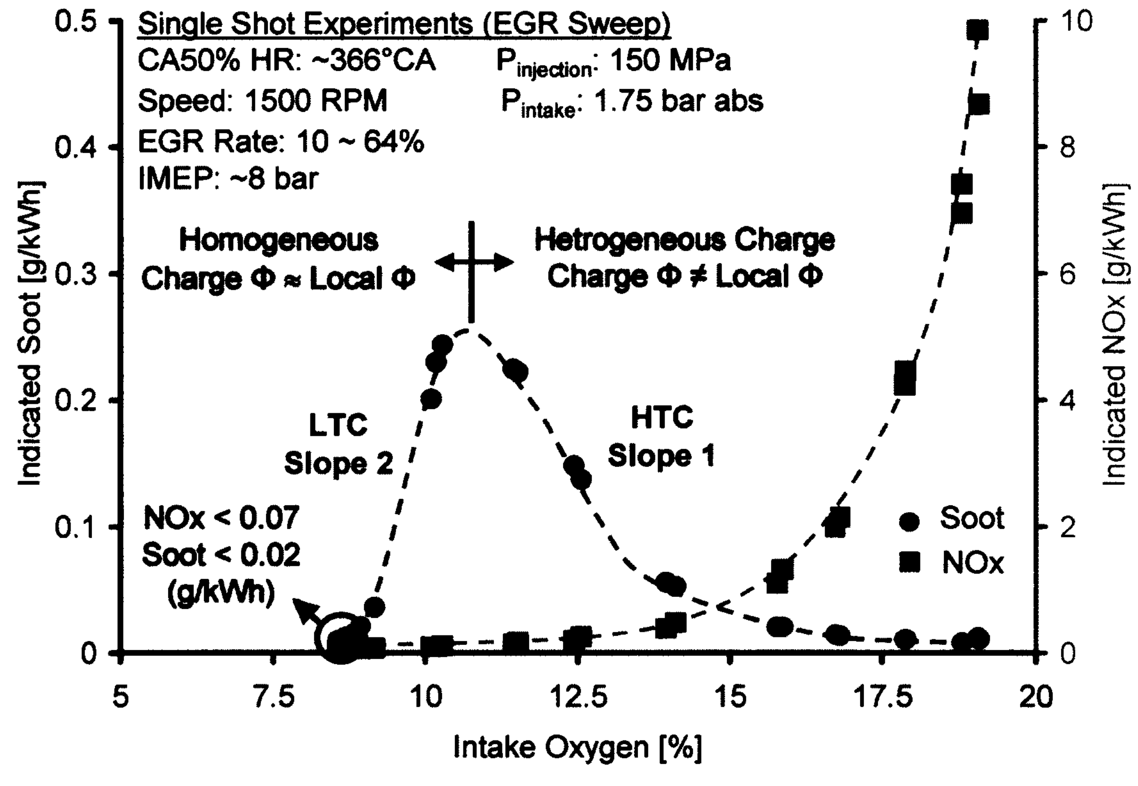

Figure 7.36: NOx & Soot Emissions for EGR-enabled Single Shot LTC (Test # 2)

The lowering of the flame temperature and the EGR-diluted charge produces higher CO and THC emissions as shown in Figure 7.37. The CO emission was generally observed to be a characteristic of Slope 1 (classical NOx-soot trade-off) and was considered to be the result of the reduced oxygen concentration [4,148], while THC increased sharply as the combustion was pushed into the LTC cycles. The indicated thermal efficiency also decreased rapidly (η_{ind}: 42~45% for Slope 1, 36~38% for Slope 2). Compared to the results of test # 1, the CO and HC emissions were observed to be significantly higher, even with the higher injection pressure and the higher boost.

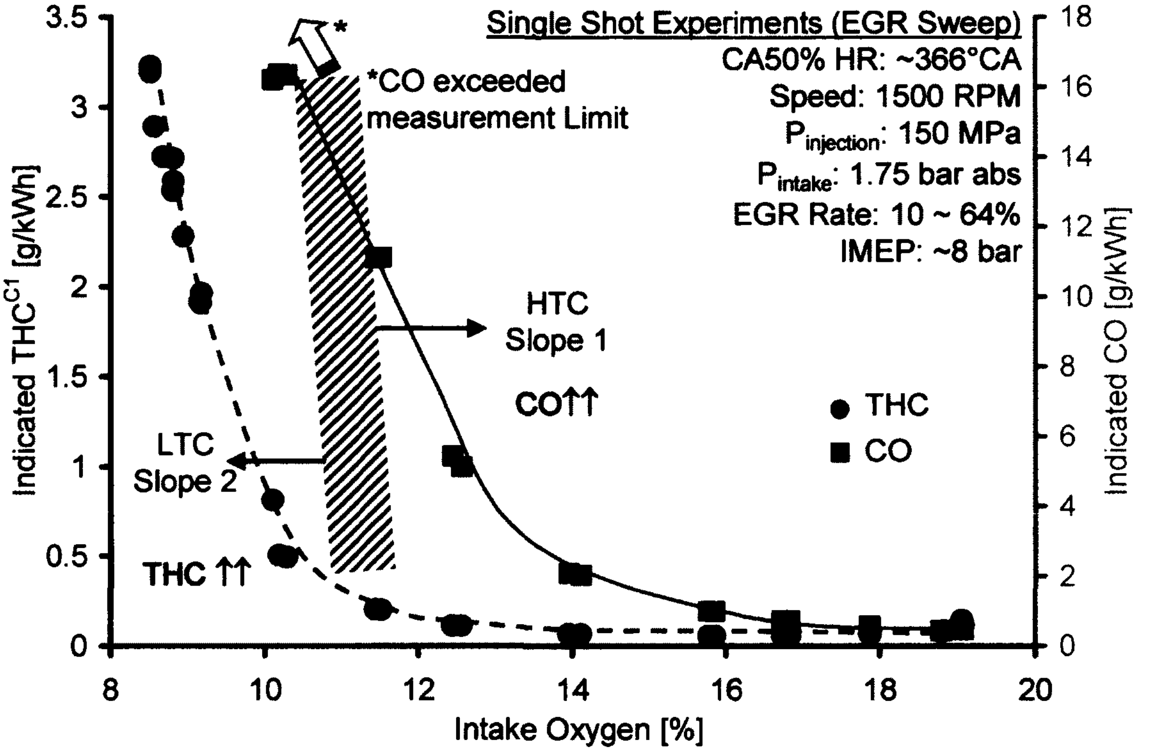

Figure 7.37: High CO and HC Emissions for LTC Cycles

7.8.2.2. Effect of Boost Pressure

The effects of boost pressure on the formation of NOx at a given engine load with the single-shot injection strategy are indicated in Figure 7.38. The effectiveness of EGR to reduce NOx emission was evident as NOx decreased monotonically with increasing EGR irrespective of the boost level. At low EGR ratios, the NOx emissions exhibited some sensitivity to the boost pressure but with heavy use of EGR, it was observed that NOx was virtually grounded and the effect of boost variation became insignificant.

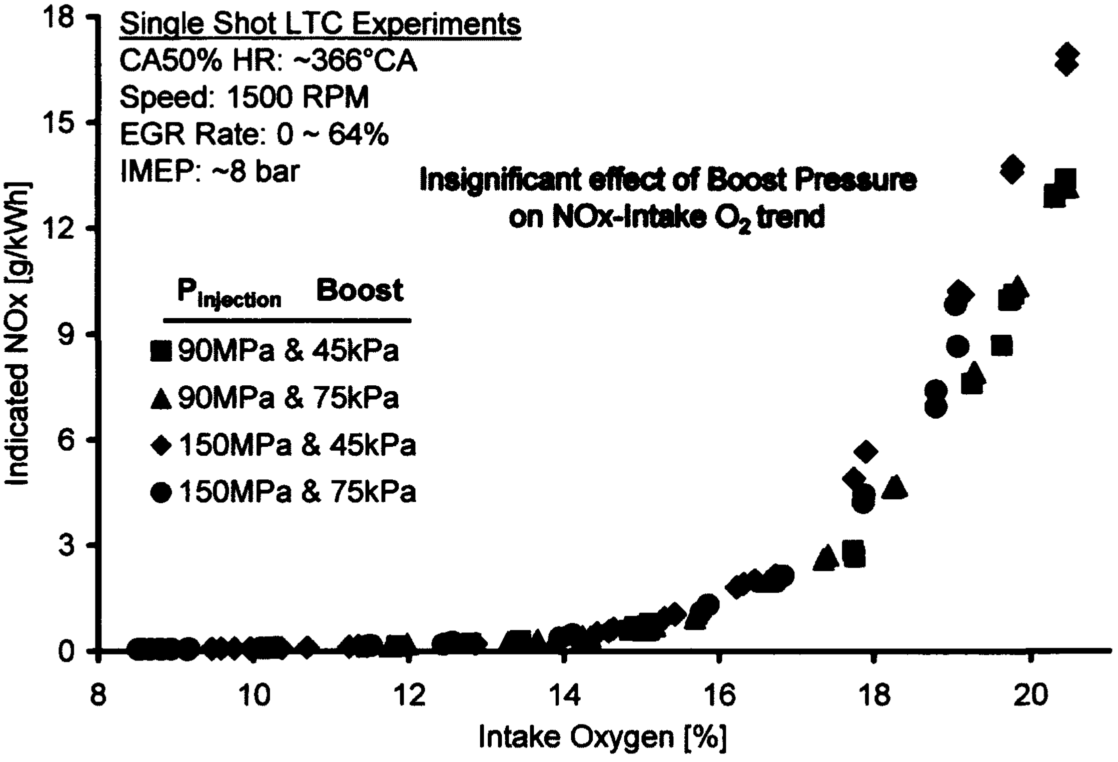

Figure 7.38: Effect of Boost on Engine-out NOx (8 bar IMEP)

The soot emissions corresponding to the NOx data are shown in Figure 7.39. As the boost pressure was increased, the intake [O_2] at which the peak soot occurs was observed to shift towards lower values. A small decrease in the magnitude of the peak was also observed. Increasing the boost helps to lower the fuel strength of the cylinder charge as the availability of the oxygen in the fuel/air charge increases. Therefore, the effect of boost on the soot reduction was significant only at higher soot levels corresponding to lower intake [O_2]. It was also noted that the peak soot levels were suppressed as the combustion proceeded into the LTC regime.

The effect of boost on the soot-NOx trade-off is shown in Figure 7.40. At high intake [O_2], the already low soot levels do not necessitate the use of higher boost as a small penalty in NOx is generally incurred. However, a significant improvement in the soot-NOx trade-off can be achieved at lower intake [O_2] with higher boost pressures as the NOx is essentially grounded. Similar observations have been previously reported in the literature [135].

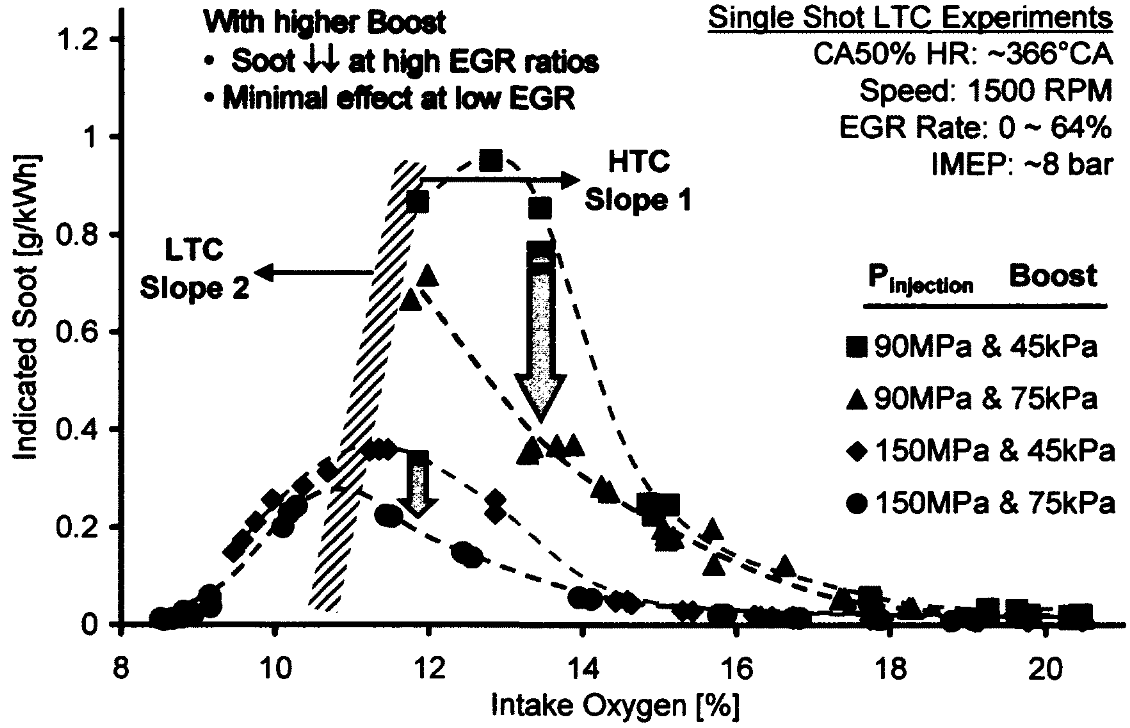

Figure 7.39: Effect of Boost Pressure on Engine-out Soot (8 bar IMEP)

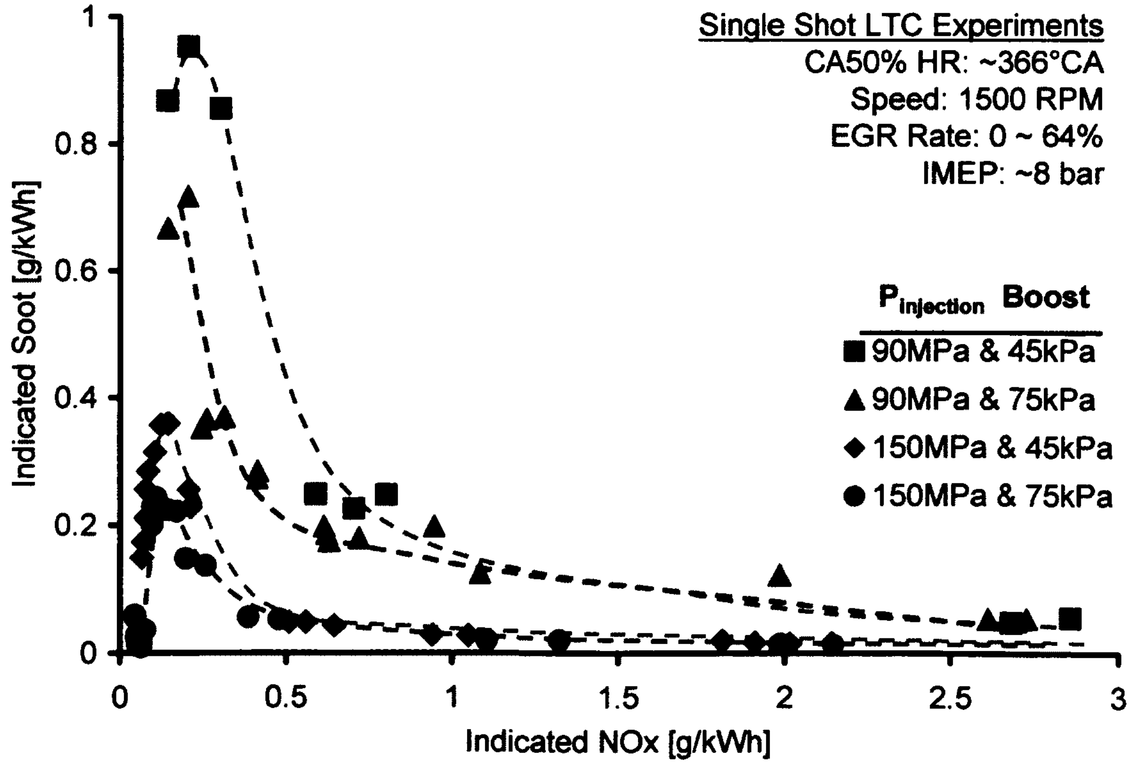

Figure 7.40: Effect of Boost on Soot-NOx Trade-off (8 bar IMEP)

Increasing the boost pressure helps to lower the CO emissions by as much as 50% at low intake [O_2] since CO is the consequence of the reduced oxygen concentration in the combustion chamber as indicated in Figure 7.41. Additionally, a higher boost can also help to delay the onset of CO emissions. A similar trend was observed for the THC emissions as shown in Figure 7.42. The onset of THC emissions was observed to occur later than that of CO and is thought to be the result of both the lowered combustion temperatures and the reduced oxygen concentration.

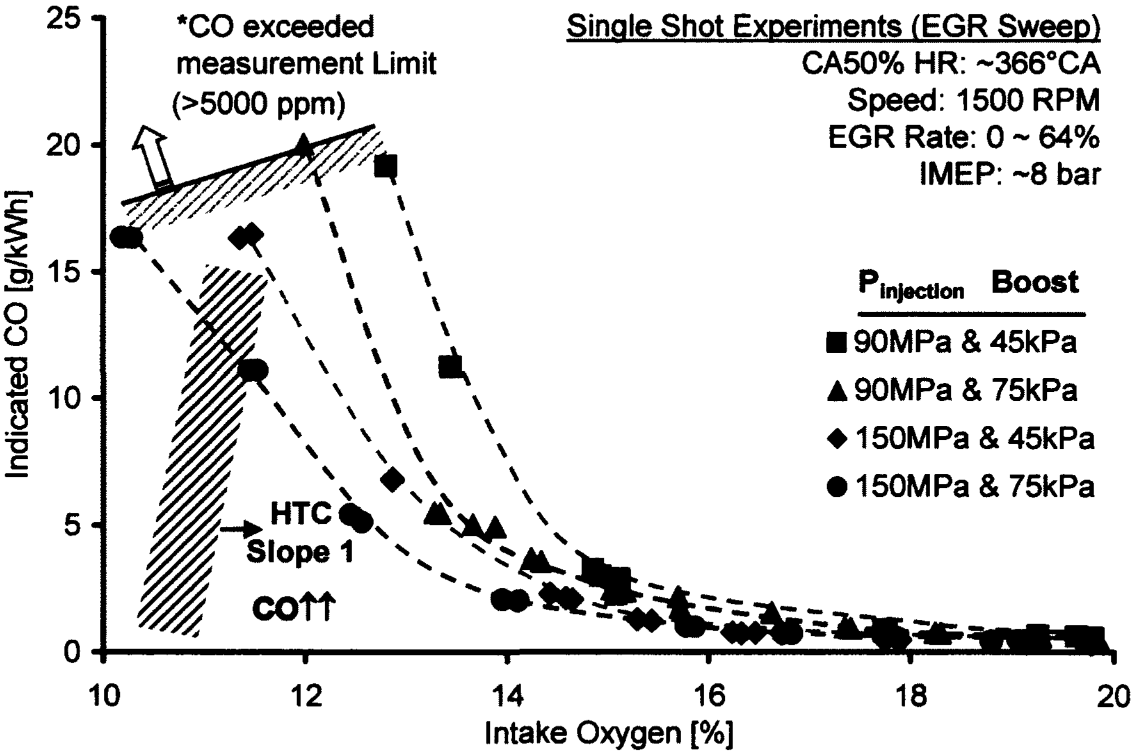

Figure 7.41: Effect of Boost Pressure on Engine-out CO (8 bar IMEP)

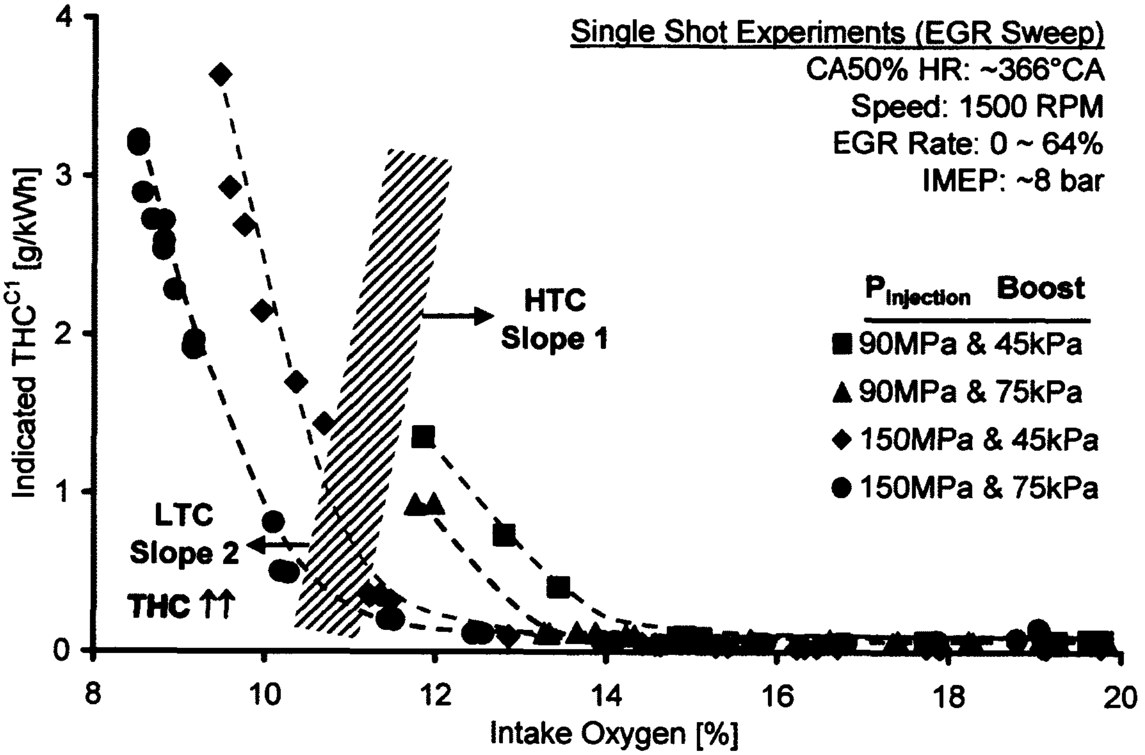

Figure 7.42: Effect of Boost Pressure on Engine-out THC (8 bar IMEP)

The heat release rates for an EGR level of 42% are shown in Figure 7.43. As boost was increased at a constant EGR and constant load level, the effectiveness of the recycled exhaust gases decreased since the combustion became leaner overall. Therefore, the ignition delay was shortened and the premixed part of the combustion was reduced. In other words, increasing the boost serves to lowering the fuel strength of the cylinder charge and can help to extend the EGR application limits. The same trend was shown with 0-D EGR simulations in Chapter 6.

The heat release rates were plotted again for the same intake [O_2] as shown in Figure 7.44. It was observed that the ignition delay was not affected by the change in the boost. Moreover, a higher EGR rate was required at the higher boost to achieve the same oxygen concentration. The decrease in the premixed part of the combustion was observed to be less than that seen for the same EGR results.

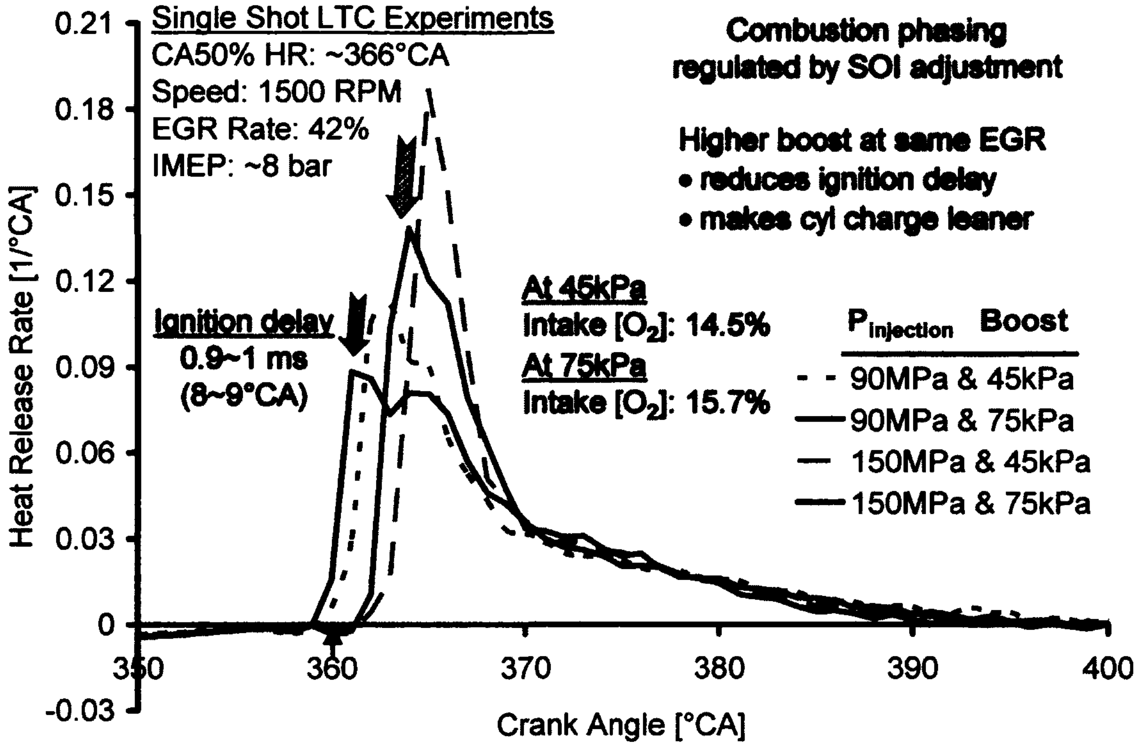

Figure 7.43: Heat Release Rates at different Boost for the Same EGR (8 bar IMEP)

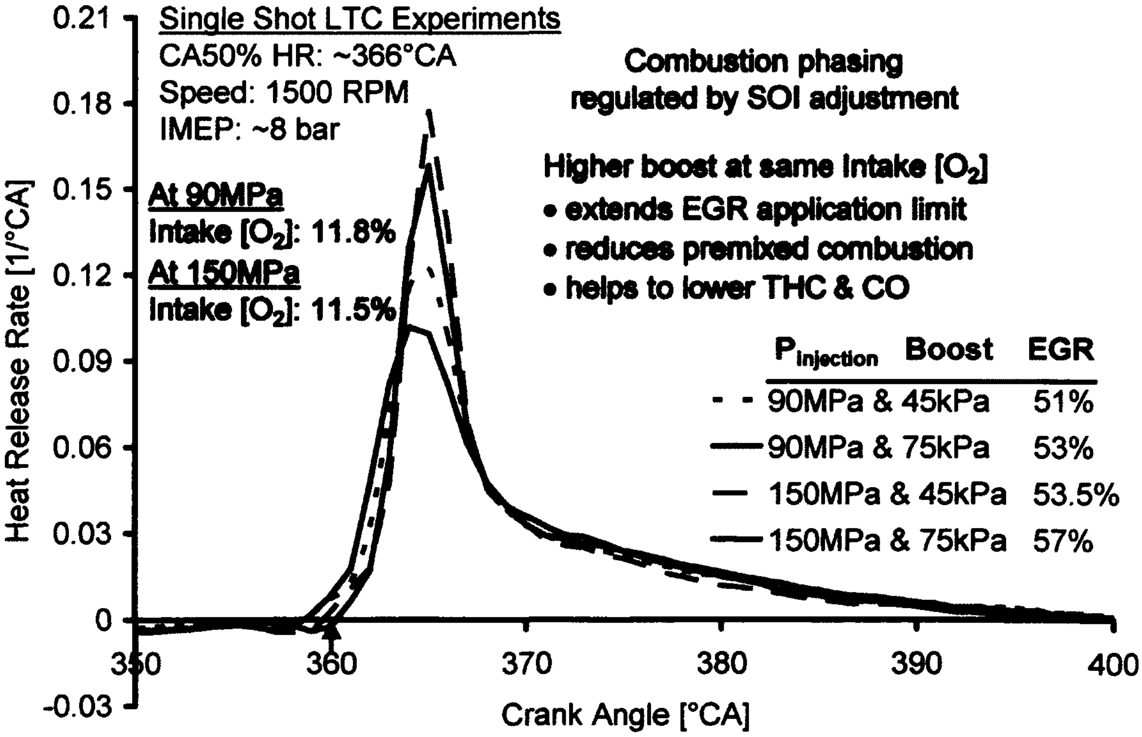

Figure 7.44: Heat Release Rates at different Boost for the same Intake O_2 (8 bar IMEP)

The indicated thermal efficiency and the indicated specific fuel consumption (ISFC) for two boost levels (1.45 bar abs and 1.75 bar abs) at 150MPa injection pressure are shown in Figure 7.45. The fuel efficiency dropped as the combustion entered the LTC cycles in both the cases. However, the efficiency penalty was lower at the higher boost pressure compared to the lower boost operation. Since a higher boost level is effective to reduce the engine-out CO and HC emissions, therefore some of the efficiency penalty can be recovered while achieving simultaneous low NOx and low soot emissions.

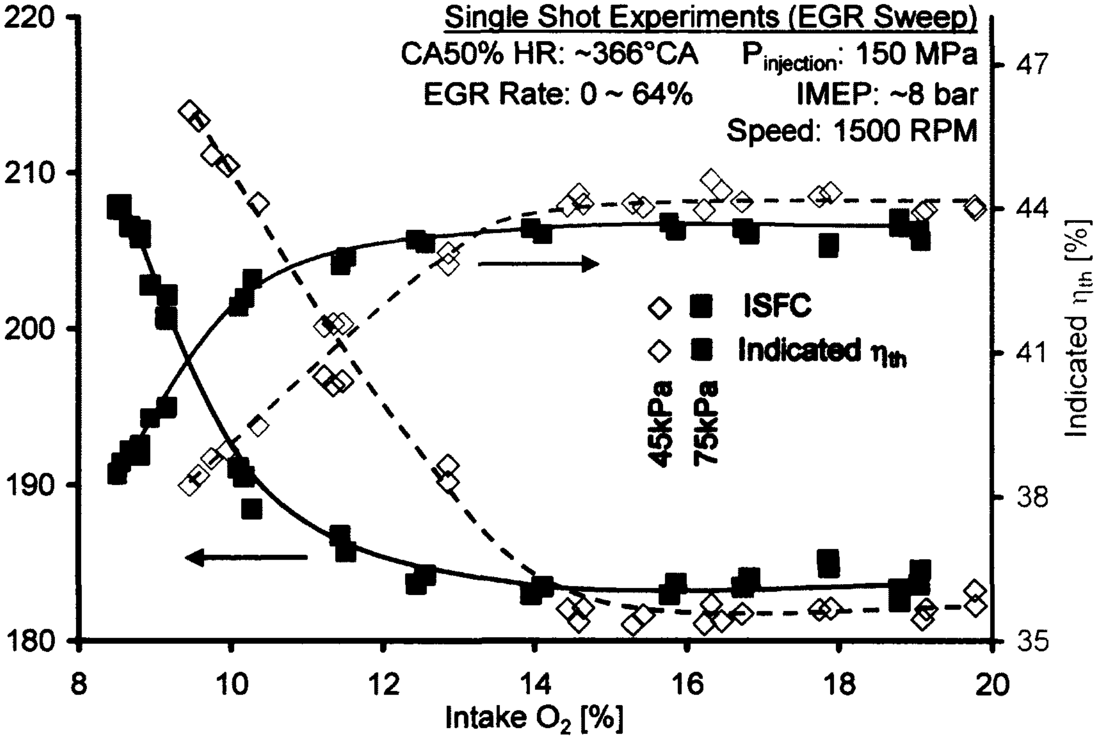

Figure 7.45: LTC Fuel Efficiency Trends (8 bar IMEP)

7.8.2.3. Effect of Injection Pressure

The effects of increasing the injection pressure on the formation of NOx with the single-shot injection strategy are indicated in Figure 7.46. A higher fuel injection pressure adds more energy into the mixing process which results in better air utilization. Therefore, a slight increase in the NOx emission is usually observed for the same EGR [135]. At low EGR ratios, the NOx emissions exhibited a higher sensitivity to the injection pressure than to the boost. This is because at low EGR levels, the intake already contains a significant amount of oxygen. Therefore, improvement in the fuel-air mixing due to the higher injection pressure has a dominant effect as compared to the change in the fuel-charge strength with higher boost. With heavy use of EGR, it was observed that NOx was essentially grounded and the effect of injection pressure was not evident, similar to the boost case.

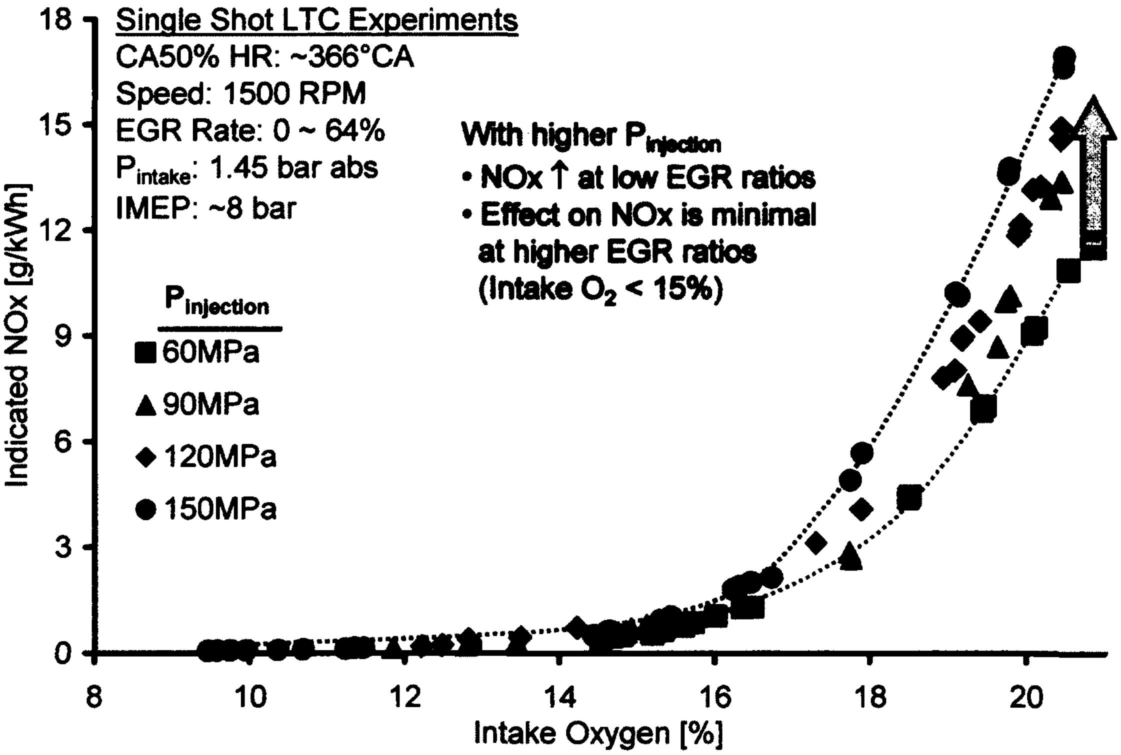

Figure 7.46: Effect of Fuel Injection Pressure on Engine-out NOx (8 bar IMEP)

For the soot emissions, increasing the injection pressure reduced the soot emissions across the EGR range as shown in Figure 7.47. A higher injection pressure allows for increased atomization and penetration of the fuel spray within the cylinder charge, thereby enhancing the premixed part of the diesel combustion. Since soot is believed to be the formed during the diffusion-controlled combustion which is significantly reduced with higher injection pressure, the engine-out soot is curbed even at lower intake [O_2].

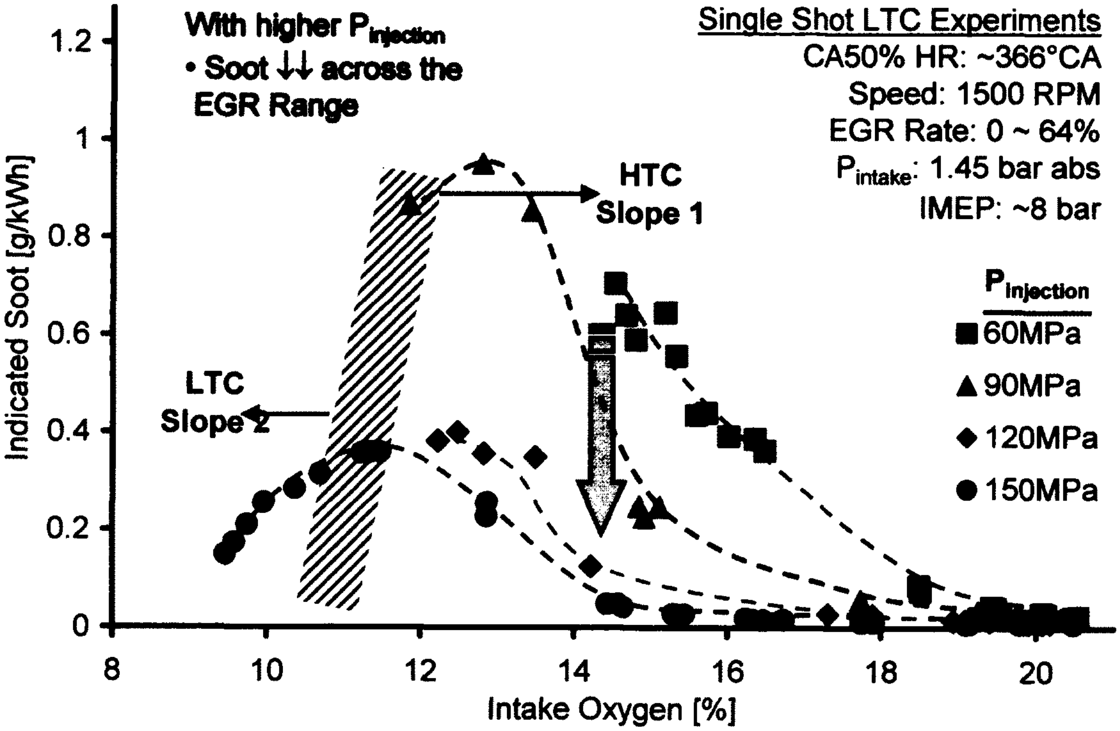

Figure 7.47: Effect of Fuel Injection Pressure on Engine-out Soot (8 bar IMEP)

The effect of injection pressure on the CO and THC emissions is similar to that observed with higher boost as shown in Figure 7.48 and Figure 7.49 respectively. A higher injection pressure not only reduces the CO across the EGR range but also helps to delay the onset of the rapid rise in the CO. In these tests, the CO results for slope 1 are only shown since the CO emission exceeded the analyzer measurement range (indicated on the figure as well). The THC emissions tend to increase rapidly as the simultaneous reduction in NOx and soot is realized (slope 2). A higher injector pressure is effective at curbing the THC at intermediate to low intake [O_2] and can help in attainment of the LTC (slope 2).

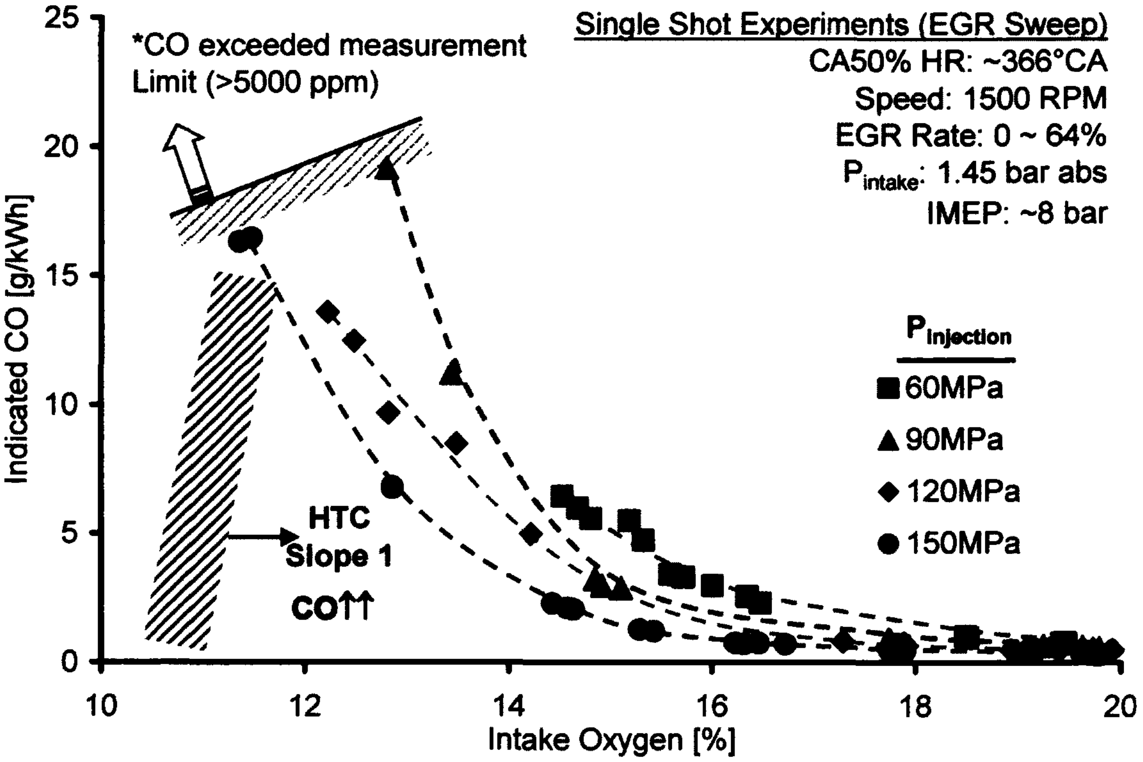

Figure 7.48: Effect of Fuel Injection Pressure on Engine-out CO (8 bar IMEP)

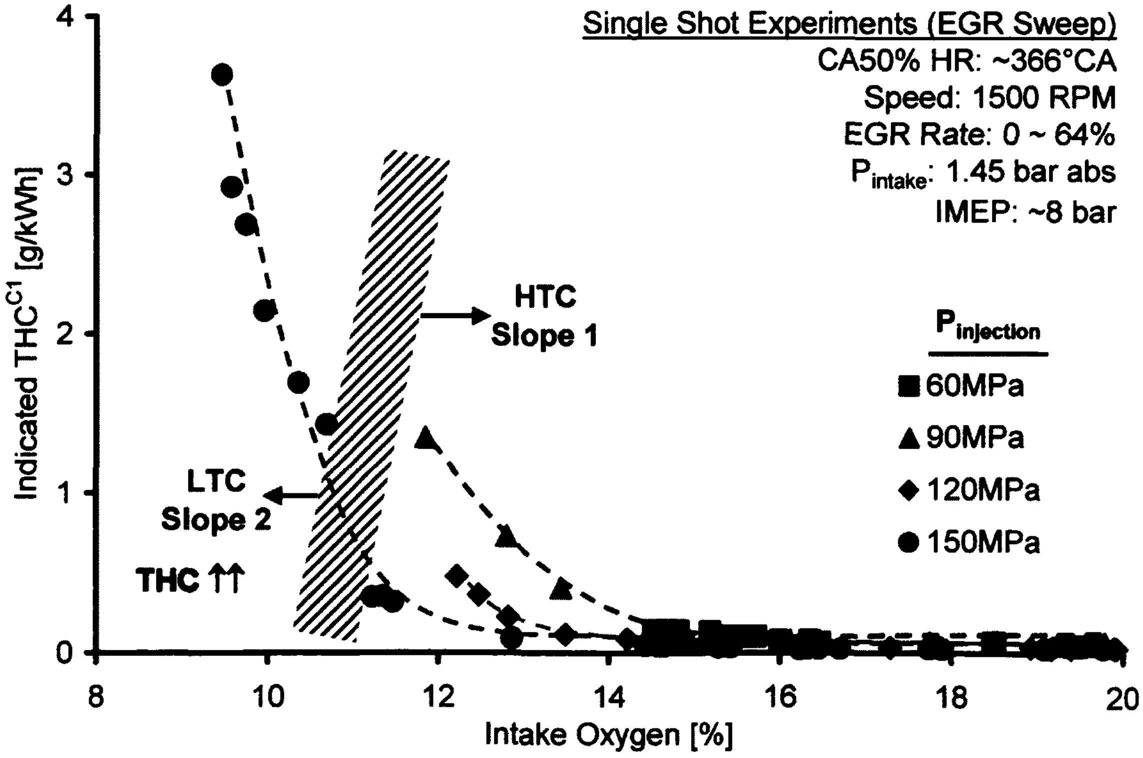

Figure 7.49: Effect of Fuel Injection Pressure on Engine-out THC (8 bar IMEP)

The effect of higher injection pressure on the heat release rates is shown in Figure 7.50. It was observed that the premixed combustion was significantly enhanced with increasing injection pressures. Also, the combustion duration was slightly reduced while maintaining the same combustion phasing (CA50). However, a higher injection pressure had implications on the combustion noise as discussed next.

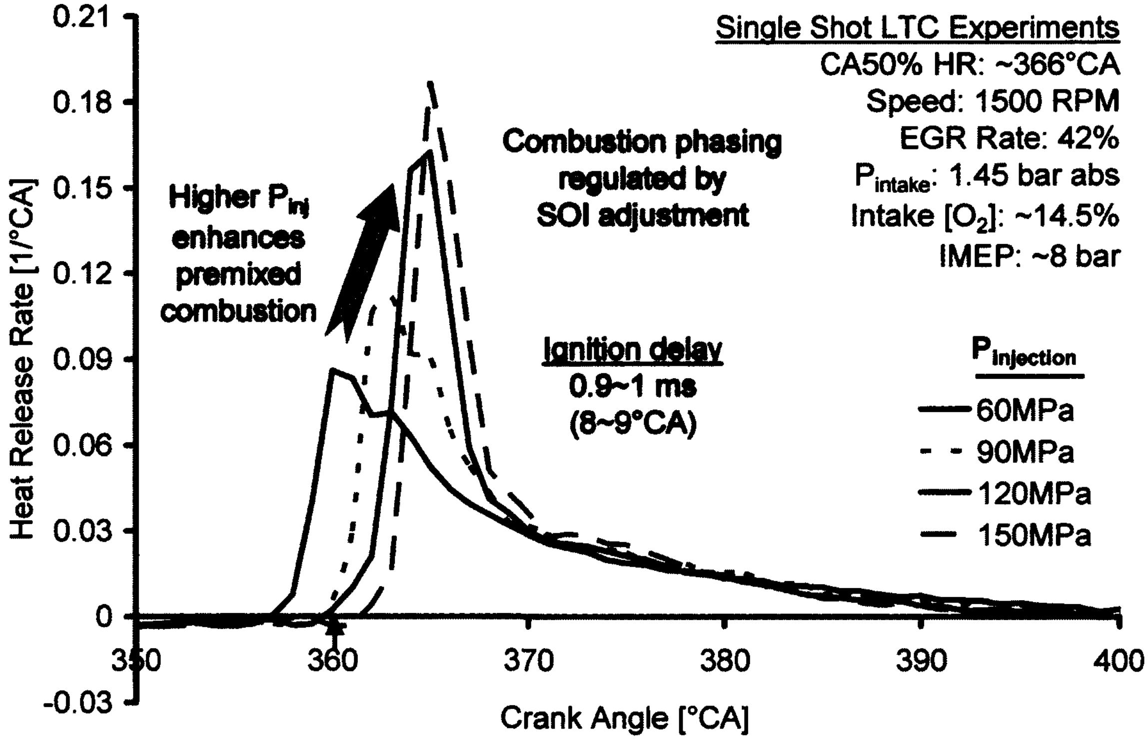

Figure 7.50: Heat Release Rates at different Injection Pressures (8 bar IMEP)

With regards to the maximum rate of pressure rise (a representation of the combustion noise), it was observed that for Slope 1, a higher injection pressure at constant boost and fixed intake [O$_2$] tends to increase the combustion noise (due to enhanced premixed combustion). A higher boost at a fixed injection pressure on the other hand, tends to alleviate the noise levels (since combustion is leaner). The comparison can be made either on the constant EGR or on the constant intake [O$_2$] basis. For example, at 41% EGR, the $(dp/d\theta)_{max}$ was 10.9 bar/°CA for the case of 150 MPa injection pressure and 1.75 bar abs boost (15.8% intake [O$_2$]) while it was

13.1 bar/°CA for 150 MPa & 1.45 bar abs (14.6% intake [O_2]). At the same intake [O_2] of 14.6%, the $(dp/d\theta)_{max}$ increased to 11.8 bar/°CA (150 MPa, 1.75 bar abs). Therefore, the efficacy of boost in alleviating the combustion noise was found to be less at the same intake oxygen as compared to the same EGR level. However, as the combustion entered the LTC regime (Slope 2), the combustion noise levels dropped to ~8 bar/°CA for both the cases (~9.6% intake [O_2]).

The results for the effects of boost and injection pressure on the attainment of slope 2 are summarized in Table 7.7. The values given in the table show the best achievable NOx for each case and all the other parameters have been reported for that engine operating point.

Table 7.7: Summary of Single Shot LTC – 8 bar IMEP (Test # 2)

Parameter	90 MPa		150 MPa	
	1.45 bar abs	1.75 bar abs	1.45 bar abs	1.75 bar abs
NOx [ppm]	26	24	14	11
NOx [g/kWh]	0.142	0.14	0.07	0.05
IMEP [bar]	7.67	7.9	7.1	7.4
EGR [%]	55	60	61	65
Intake O_2 [%]	11.9	11.8	9.5	8.6
Indicated Thermal Efficiency [%]	38.2	38.5	38.1	38.4
Smoke [FSN]	5.3	4.9	2.6	0.46
Soot [g/kWh]	0.86	0.66	0.15	0.012
CO [ppm]	>5200*	>5200*	>5200*	>5200*
THC [g/kWh]	1.35	0.92	3.63	3.22
Combustion Efficiency [%]	97.3	97.1	96.6	97.2
P_{max} [bar]	99.5	115.2	102.1	115.9
$(dp/d\theta)_{max}$ [bar]	8.2	7.4	8	8.1
COV P_{max} [%]	1.7	0.64	1.1	1.01
COV IMEP [%]	2.7	1.4	1.87	1.91

* Exceeded the measurement limit of the analyzer

The use of a higher boost pressure and a higher injection pressure was able to push the combustion into the LTC cycles. A moderate recovery in the combustion efficiency was observed and the penalty in the thermal efficiency was also seen to reduce. However, the HC and CO emissions were very high and indicate the load limit for the single-shot LTC injection strategy. The simultaneous low NOx and low soot are the result of the separation of the fuel injection from the combustion. As more fuel is injected into the cylinder, the prolonging of the ignition delay is limited by the availability of high injection and high boost pressures. Even if higher boost and injection pressures could be achieved, the engine operation would be limited by the physical constraints such as P_{max} and $(dp/d\theta)_{max}$. Therefore, further tests were performed to determine an effective LTC load management strategy as described later on.

7.8.3. Criteria for Timing of Multiple Injection LTC (Early HCCI)

The timing of the multiple injections is critical to maintain the fuel efficiency of the early HCCI cycles as discussed in section 7.5.1. When fuel is injected early in the compression stroke, the major factors affecting the fuel spray are the volatility of the fuel, the prevailing in-cylinder temperature and the density of the charge at the time of injection. The volatility of diesel fuels is much lower than gasoline, making it hard to vaporize the diesel fuel at low temperatures. For a typical diesel fuel, the boiling temperature range is between the initial boiling point (IBP) ~200°C and the final boiling point (FBP) ~340°C. If the injection occurs before the in-cylinder temperature has crossed the IBP threshold, the injection would have a strong propensity to condense on the cylinder walls and the piston crown, resulting in high HC emissions, lower fuel efficiency and even oil dilution. Therefore, to reduce the fuel condensation during early-injection diesel LTC and to form a cylinder charge of high homogeneity, the earliest SOI should be scheduled after the IBP of the fuel has been attained during the compression stroke. The criteria for determining the earliest injection timing that minimizes fuel condensation and also the oil dilution on a crank angle basis is depicted in Figure 7.51.

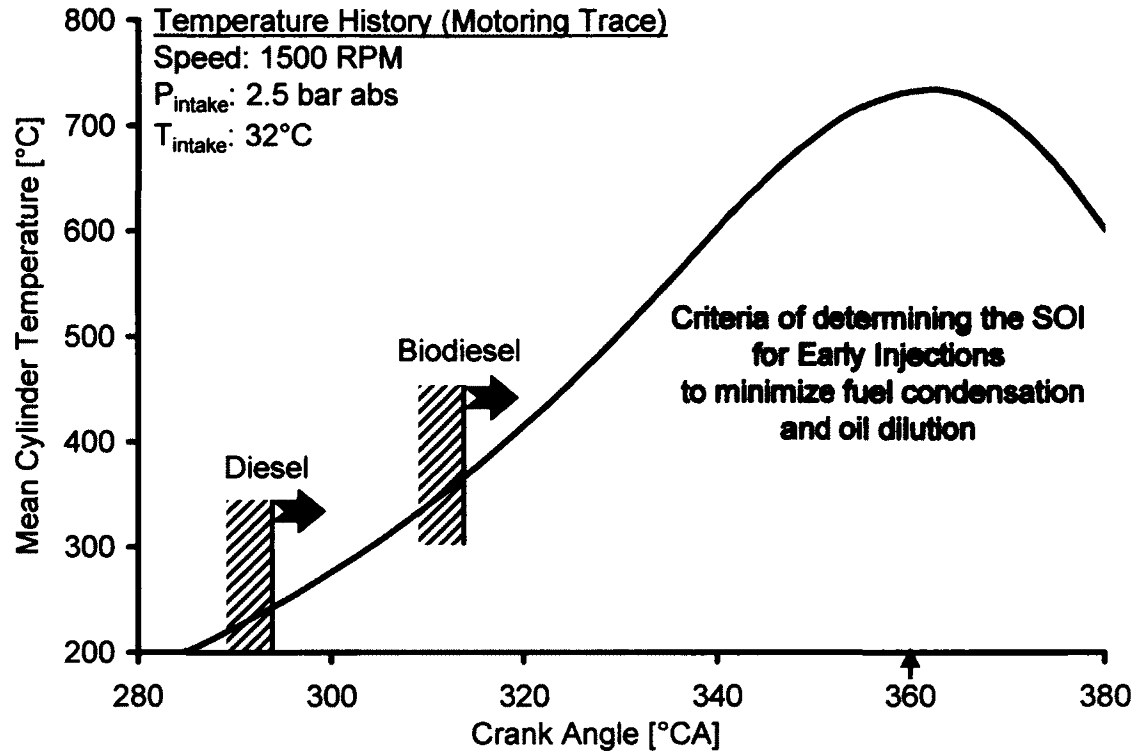

Figure 7.51: Determination of SOI for Early Injection LTC to Minimize Fuel Condensation

The density of the cylinder charge at the time of injection has a direct consequence on the likelihood of the spray impinging on the cylinder walls. A lower charge density at the time of early injection would favour a higher spray penetration. The effect of the injection timing on the wall impingement has been empirically investigated with spray visualization studies by Hiroyasu and Arai [149], Naber and Siebers [150] for non-evaporating sprays. Hiroyasu et al. [149] proposed empirical correlations for spray break-up length, spray-penetration, spray-angle and drop size distribution. Naber et al. [150] investigated the effects of gas density on the penetration and dispersion of diesel sprays and proposed empirical equations for estimating the spray penetration length.

The expressions for the spray penetration length S are divided into two parts: one before the time for spray break-up t_b and the other after the time of spray break-up as follows.

For $0 < t \le t_b$, Hiroyasu et al. [149] proposed the following expressions:

$$S = 0.39 \cdot \sqrt{2\left(\frac{p_f - p_a}{\rho_f}\right)} \cdot t \tag{7.11}$$

$$t_b = 28.65 \frac{\rho_f D_n}{\sqrt{\rho_a}\sqrt{p_f - p_a}} \tag{7.12}$$

and for $t > t_b$, the correlation by Hiroyasu and Naber is of the form [149,150]

$$S = C_1 \frac{(p_f - p_a)^x}{\rho_a^{\,y}} \sqrt{D_n t} \tag{7.13}$$

where

D_n = nozzle diameter, m

p_a = Ambient pressure, Pa

p_f = Injection pressure, Pa

S = Spray penetration length, m

t = Time, seconds

t_b = Break-up time, seconds

ρ_a = Density of cylinder charge, kg/m^3

ρ_f = Density of fuel, kg/m^3

$C_1 = 2.95, x = y = 0.25$ (Hiroyasu – Mechanical fuel-injection system)

$C_1 = 2.25, x = 0.25, y = 0.345$ (Naber –Common–rail fuel injection system)

The effect of injection pressure, start of injection timing and boost pressure on the spray penetration length was numerically investigated using the constants proposed by Naber since these are applicable to common-rail injection systems [151]. Unlike previous studies where a fixed density and ambient pressure are assigned for the calculations, the spray breakup and penetration calculations were integrated into a 0-D diesel engine cycle simulation program. This allowed the variations in the cylinder charge density and the cylinder pressure to be accounted for at each time step. A time step of 11.1μs (corresponding to 0.1°CA resolution at 1500 RPM) was used and the results are shown from Figure 7.52 to Figure 7.54.

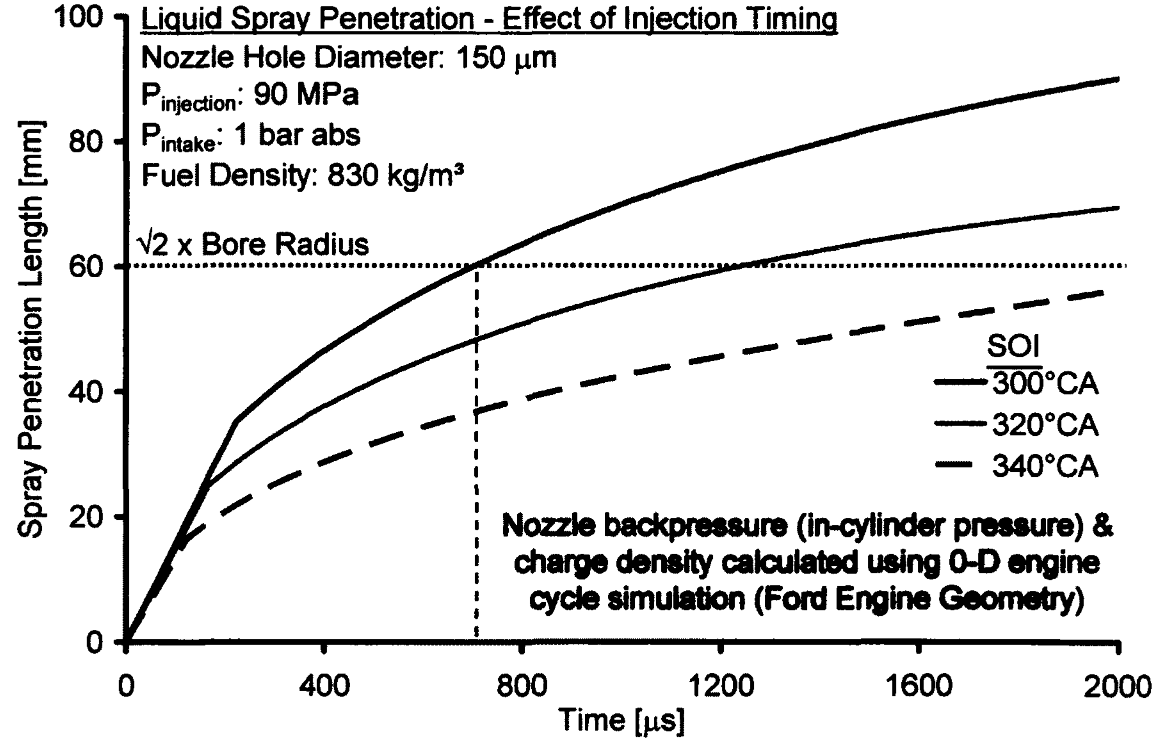

Figure 7.52: Effect of SOI on the Liquid Penetration Length at 90MPa Injection Pressure

The $\sqrt{2}$ x Bore Radius represents the minimum distance from the nozzle tip to the cylinder wall, assuming an injector cone angle of 90°. Among the three analyzed parameters (SOI, Intake Pressure and Injection Pressure), the start of injection had the most significant impact on the liquid spray length followed by the intake pressure and the injection pressure.

It is important to note that the presented numerical analysis does not include the effect of the spray evaporation and predicts the penetration if the spray remains in the liquid phase. Empirical results by Naber et al. [150,151] indicate that the spray penetration length reduces for evaporating sprays and reaches a maximum stable value. In view of this, if an injection of a long duration (for example 1ms at 300°CA) is employed (Figure 7.52), the spray impingement on the wall is almost certain. Reducing the pulse width of the injection and dividing the fuel into multiple injections of short duration (300~400μs) has a higher probability of evaporating before wall impingement can occur. This hypothesis was indirectly confirmed with engine tests and the results presented in Figure 7.25 show that multiple injections of short duration scheduled very early in the compression stroke result in significantly less HC emissions compared to less number of injections of longer duration (Figure 7.24).

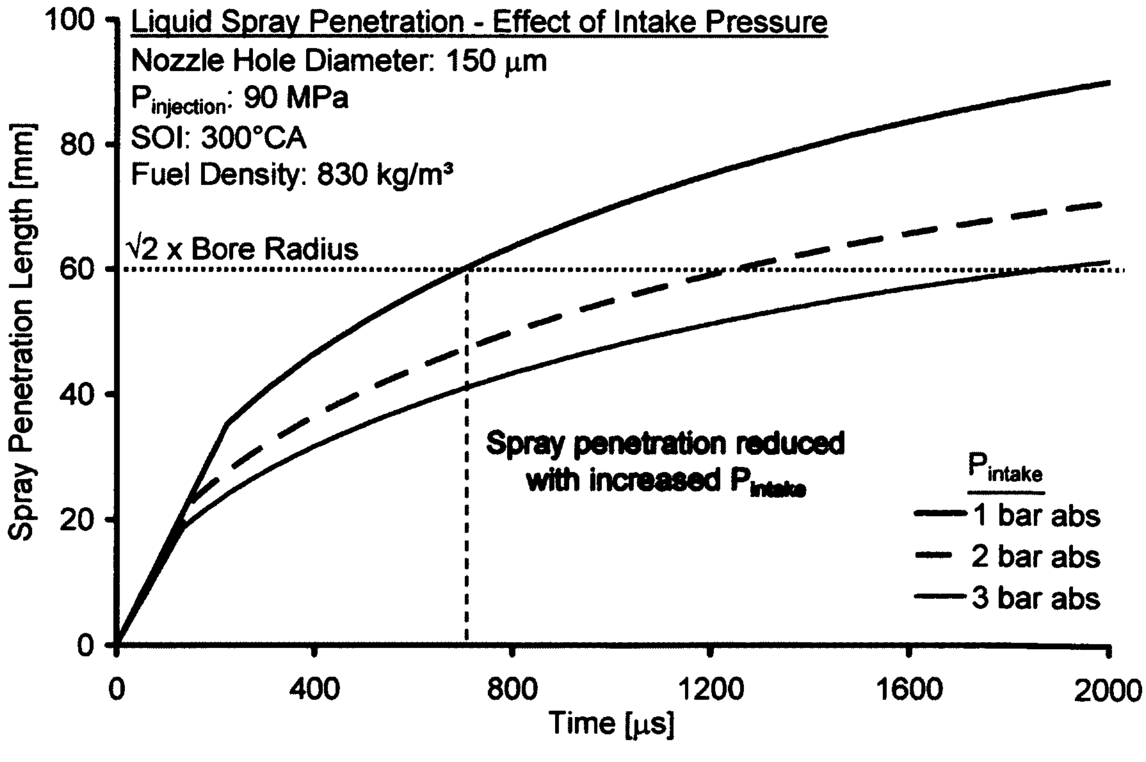

Figure 7.53: Effect of Intake Pressure on the Spray Penetration for SOI@330°CA

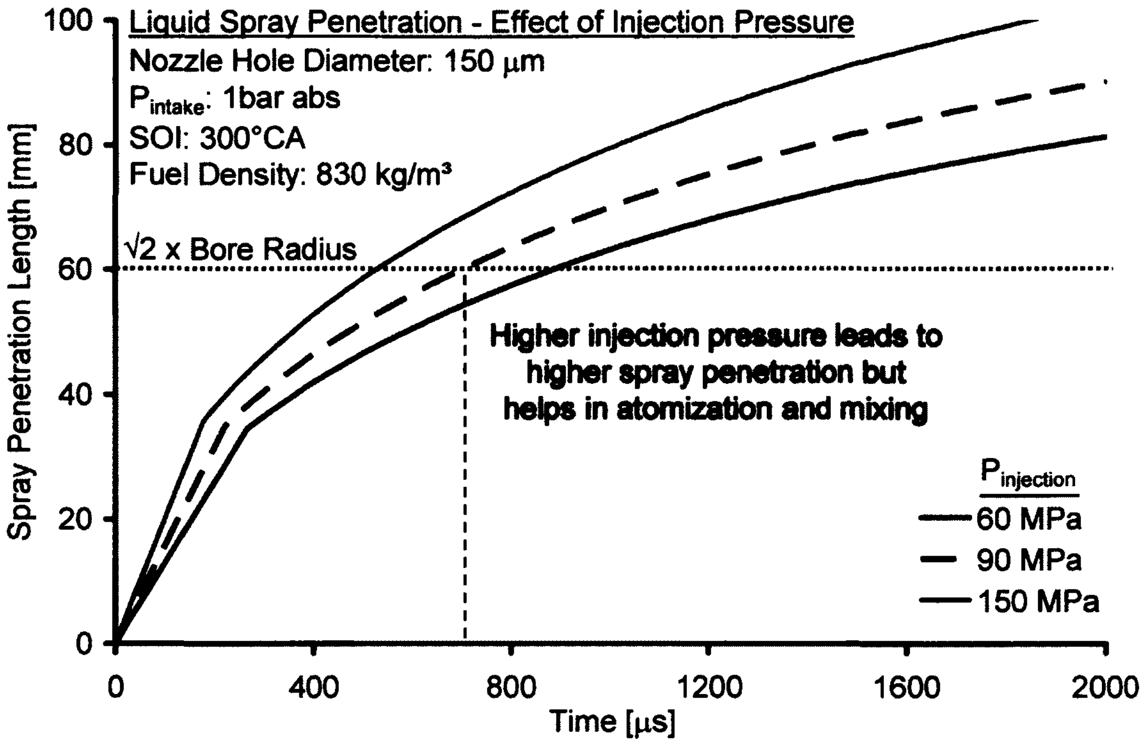

Figure 7.54: Effect of Injection Pressure on the Liquid Spray Penetration Length

The above analysis for the liquid penetration length and the earliest crank angle to avoid condensation helped to decide the injection strategy for the multi-shot LTC experiments. To minimize the chances of wall impingement, the maximum pulse width (injection quantities) for the early injections was always kept less than 400μs.

To determine the latest SOI that would still provide sufficient time for fuel mixing and charge preparation, a timing sweep was performed with 3 injections per cycle at 1500 RPM. The SOI of the 3rd injection was changed from 335°CA to 346°CA while the dwell between the injections was kept constant. Soot was observed to rapidly increase as the SOI of the last injection moved beyond 340°CA. Therefore, the latest SOI timing for the last injection was set at 338°CA during all the tests.

The Ford engine is fitted with solenoid injectors and the minimum dwell between the SOI of any two injections for reliable operation of the injector was observed to be 10°CA or higher. Another sweep was performed by varying the dwell from

11°CA to 18°CA with 3 injections per cycle and the trade-off between CO-THC emissions vs. NOx-soot was mapped. Based on the data, a constant dwell of 12~13°CA was used in the tests at 1500 RPM.

7.8.4. Multi-Shot LTC (Early HCCI) – 6.8 to 7.4 bar (Test # 3)

The first multi-shot LTC tests were done at an engine load of 6.8 bar IMEP. The testing conditions are given in Table 7.8. The load was then slightly increased to 7.4 bar to observe the effect on the performance metrics. Based on the testing results of the single-shot LTC that achieved a load of 7.4 bar IMEP, the same injection pressure was used. The injection duration (pulse width) was kept the same for all the injections.

Table 7.8: Test Conditions for Multi-Shot LTC (Test # 3)

No of Injections	4
SOI_1 [°ATDC]	-58
SOI_2 [°ATDC]	-46
SOI_3 [°ATDC]	-34
SOI_4 [°ATDC]	-22
Dwell [°CA]	12
Injection Pulse Width [μs]	290 (6.8 bar IMEP) 295 (7.5 bar IMEP)
IMEP [bar]	6.8
P_{intake} [bar abs]	2
$P_{injection}$ [MPa]	150
Targeted Indicated NOx	0.15 g/kWh
Targeted Indicated Soot	0.01 g/kWh

The NOx and soot trends at 6.8 bar IMEP are shown in Figure 7.55. The minimum EGR required to meet the targeted NOx was set as the baseline for these tests and was 61% EGR (intake $[O_2]$: 11%). in this case. The combustion phasing at this

EGR was early, about 11°BTDC as shown in Figure 7.56. To improve the combustion phasing, the EGR was increased up to 7%. This further reduced the NOx to ~0.07 g/kWh and improved the combustion phasing by nearly 7°CA to 4°BTDC. It was noted that the soot emission was ultra low throughout the test (<0.0008 g/kWh).

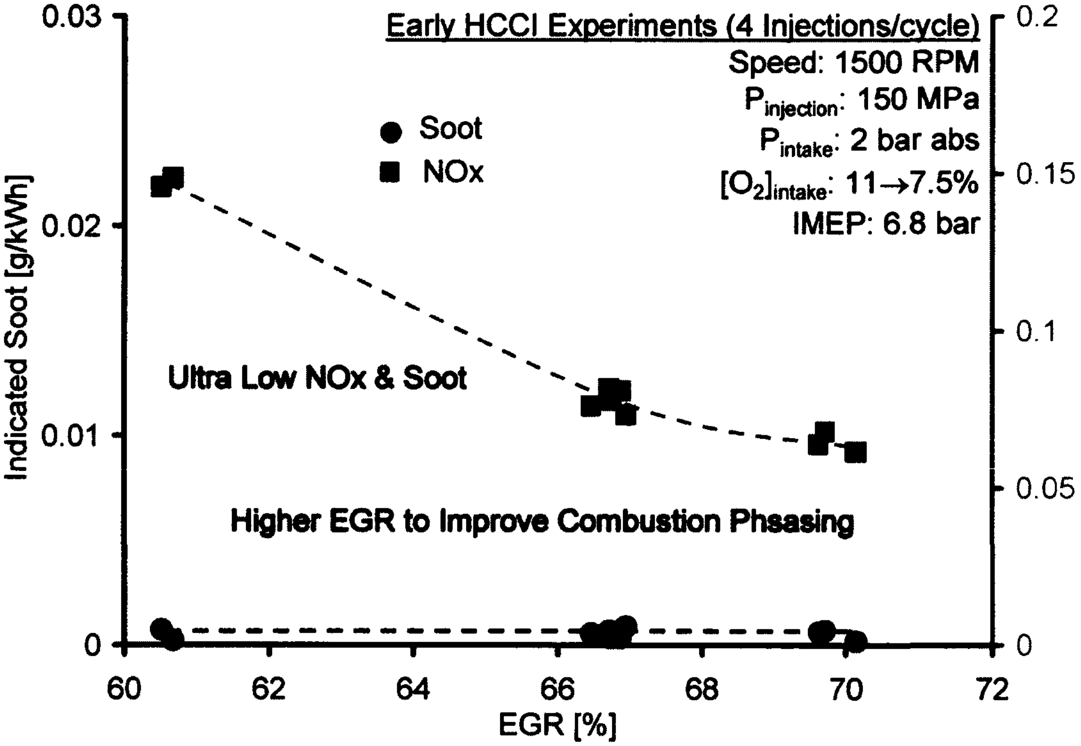

Figure 7.55: NOx and Soot for Early HCCI Experiments - 6.8 bar IMEP (Test # 3)

The improvement in the combustion phasing was also desirable to reduce the peak cylinder pressure. As shown in Figure 7.56, the heat release with 61% EGR was characterized by a mainly premixed combustion of a very short duration. This coupled with the high compression ratio of the Ford engine (18.2:1) resulted in the peak cylinder pressure, reaching the nominal threshold of 160 bar P_{max} for production diesel engines. The use of higher EGR levels diluted the strength of the homogeneous charge, resulting in a delayed as well as a slower heat release rate (the ignition delay was significantly prolonged). This effectively reduced the peak cylinder pressure to ~150 bar.

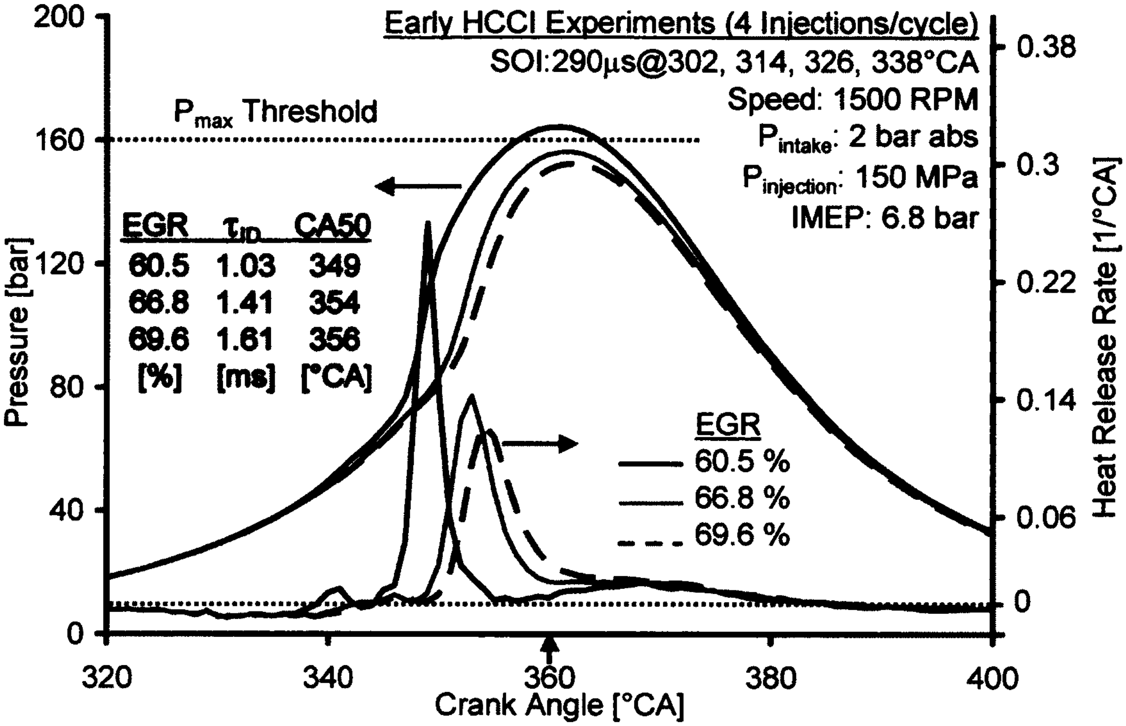

Figure 7.56: Improved Combustion Phasing with EGR (Early HCCI-6.8 bar IMEP) - Test # 3

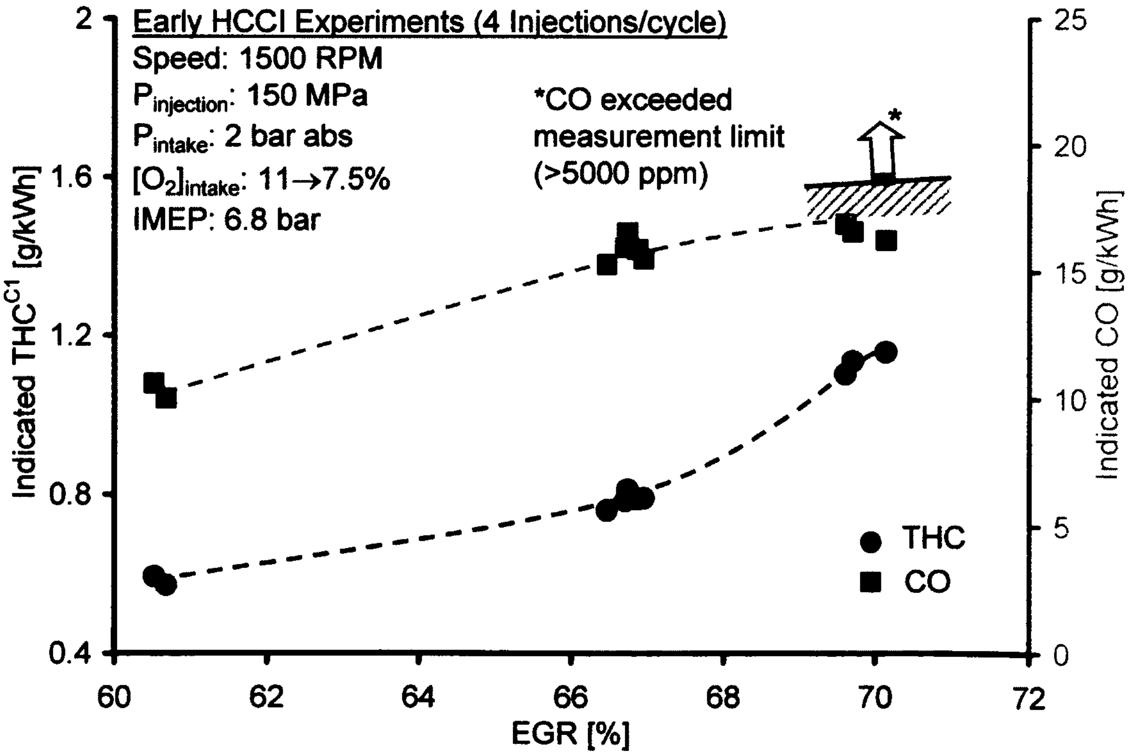

Figure 7.57: CO and THC for Early HCCI Experiments - 6.8 bar IMEP (Test # 3)

The improvement in the combustion phasing with EGR was accompanied by deterioration in the combustion efficiency as shown in Figure 7.57. Both the CO & HC emissions increased significantly with EGR. As already presented with simulation studies (Section 7.6), there exists a trade-off between the gain in the fuel efficiency with the improved combustion phasing versus the increased loss of the fuel through the higher HC and CO emissions.

The summary of the performance metrics for Test # 3 is given in Table 7.9. Although the combustion efficiency was reduced by increasing the EGR, this was more than compensated by the improvement in the combustion phasing (manifested by an increase in the IMEP) at 66.8%. Therefore, the overall indicated thermal efficiency was still higher than that for the lowest EGR value. However, the IMEP reduced with a further increase in the EGR indicating that the optimal trade-off point had been passed.

Table 7.9: Summary of Multi-shot LTC (Test # 3)

Parameter	EGR		
	60.5%	66.8%	69.6%
NOx [ppm]	22	13	13
NOx [g/kWh]	0.15	0.07	0.06
IMEP [bar]	6.75	6.92	6.84
Soot [g/kWh]	0.0002	0.0007	0.0008
CO [ppm]	2437	4289	>5200*
THC [ppm]	281	465	720
P_{max} [bar]	165	157	153
$(dp/d\theta)_{max}$ [bar]	20.6	14.5	12.1
COV P_{max} [%]	1	1.33	1.68
COV IMEP [%]	2.7	2.2	3.2
CA50 [°CA]	348.9	354	356.2
Fuelling [g/s]	0.25	0.25	0.25
Indicated Thermal Efficiency [%]	38.1	39.3	38.7
Combustion Efficiency [%]	98.6	97.8	97.5

* Exceeded the analyzer measurement limit

The load was then increased to 7.4 bar IMEP and the results were compared with the single-shot LTC (7.4 bar) as shown in Figure 7.58. The higher HC with the single shot was compensated by the phasing within the best efficiency window of 5~10°CA ATDC. However, the efficiency was still slightly lower compared to the multi-shot LTC despite the significant off-phasing of the early HCCI combustion. The soot emission was at the borderline (0.01g/kWh) with the single-shot LTC while the multi-shot LTC produced ultra low levels of soot. The CO emission was within the measuring range of the emission analyzer (~4600 ppm) for the multi-shot LTC while the CO emission for the single-shot LTC had exceeded the measurement range close to the start of the slope 2. The main advantage of the single-shot LTC was visible in the much lower peak cylinder pressure compared to the multi-shot strategy.

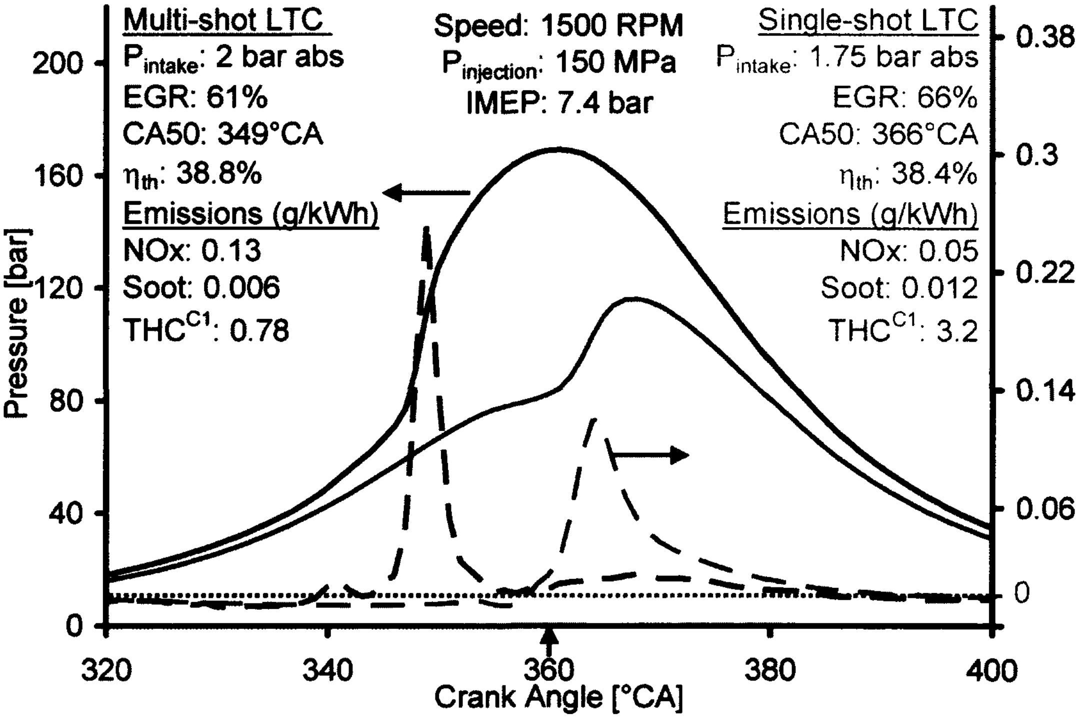

Figure 7.58: Single-Shot vs. Multi-Shot LTC (7.4 bar IMEP)

Based on the above tests and analysis, a detailed performance comparison between the single and multi-shot LTC strategies was carried out in order to help define the boundary limits (engine load, achievable emissions, efficiency, stability) for each strategy.

7.8.5. Performance Comparison of Single- &Multi-shot LTC (Test # 4)

Tests were run to compare the emissions and efficiency of the multi-shot early HCCI (3 or 4 early injections per cycle) against those of the single-shot LTC for three engine load levels. The test matrix is given in Table 7.10. All the injections had the same pulse width for a given IMEP. The boost and injection pressure were kept the same during the comparison process at each load level and are indicated in all the figures. The SOI for the single injection strategy (SOI_{Main}) is also indicated. An EGR sweep was performed to obtain the best LTC emission trade-off between NOx-soot and THC-CO for each of the 3 load levels.

Table 7.10: Test Matrix for the Early HCCI Tests (Test # 4)

	No of Injections	
	3	4
SOI_1 [°ATDC]	-48	-61
SOI_2 [°ATDC]	-35	-48
SOI_3 [°ATDC]	-22	-35
SOI_4 [°ATDC]	-	-22
Dwell [°CA]	13	13
IMEP [bar]	3.1,5.2	7
P_{intake} [bar abs]	1.3,1.5	1.45→2
$P_{injection}$ [MPa]	80,120	100→145
Targeted Indicated NOx	0.15 g/kWh	
Targeted Indicated Soot	0.01 g/kWh	

The emission results for the case of 3.1 bar IMEP are shown in Figure 7.59 and Figure 7.60. Both the injection strategies were observed to meet the set emission targets; however, the soot emissions for the 3 injections were significantly lower (< 0.001 g/kWh) than those achieved with the single injection.

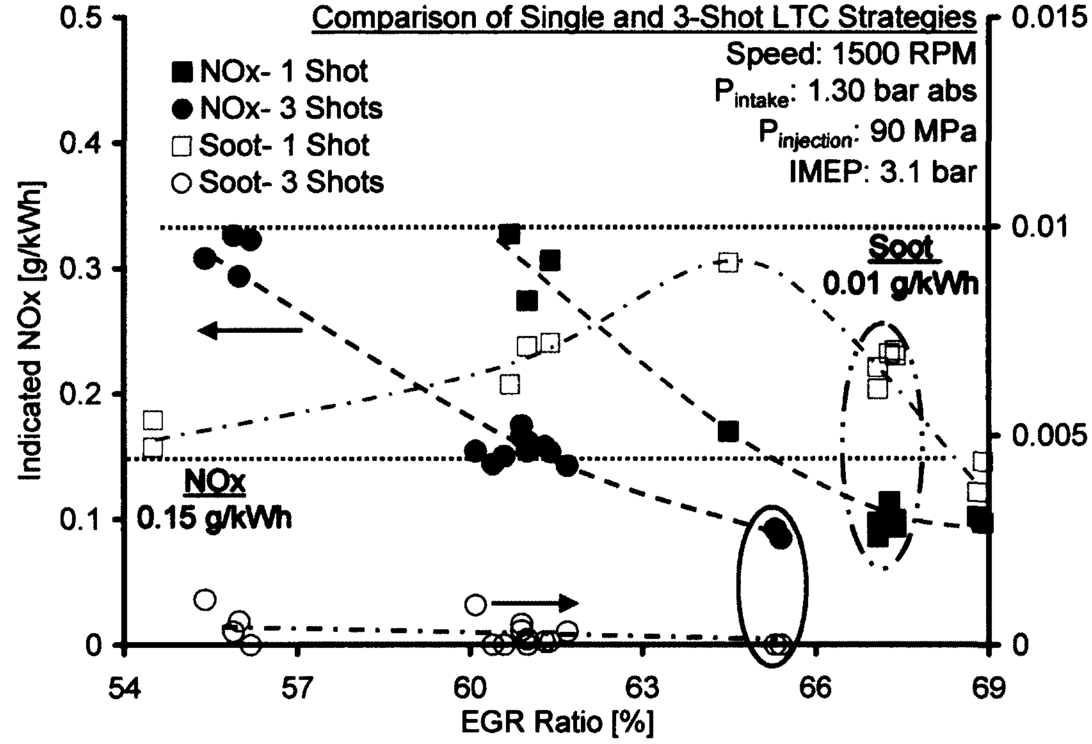

Figure 7.59: NOx & Soot Emissions for Single- & 3-Injection Strategies at 3.1 bar IMEP

For the best NOx and soot emissions as highlighted in Figure 7.59, the THC emissions were slightly lower for the 3 injections. However, the CO emissions were observed to be considerably lower (Figure 7.60). In fact, the CO emission for the single- injection strategy exceeded the measurement limits of the CO analyzer (5000 ppm) and therefore, the results are slightly biased towards the single injection strategy, once the fuel efficiency calculations are compared later on.

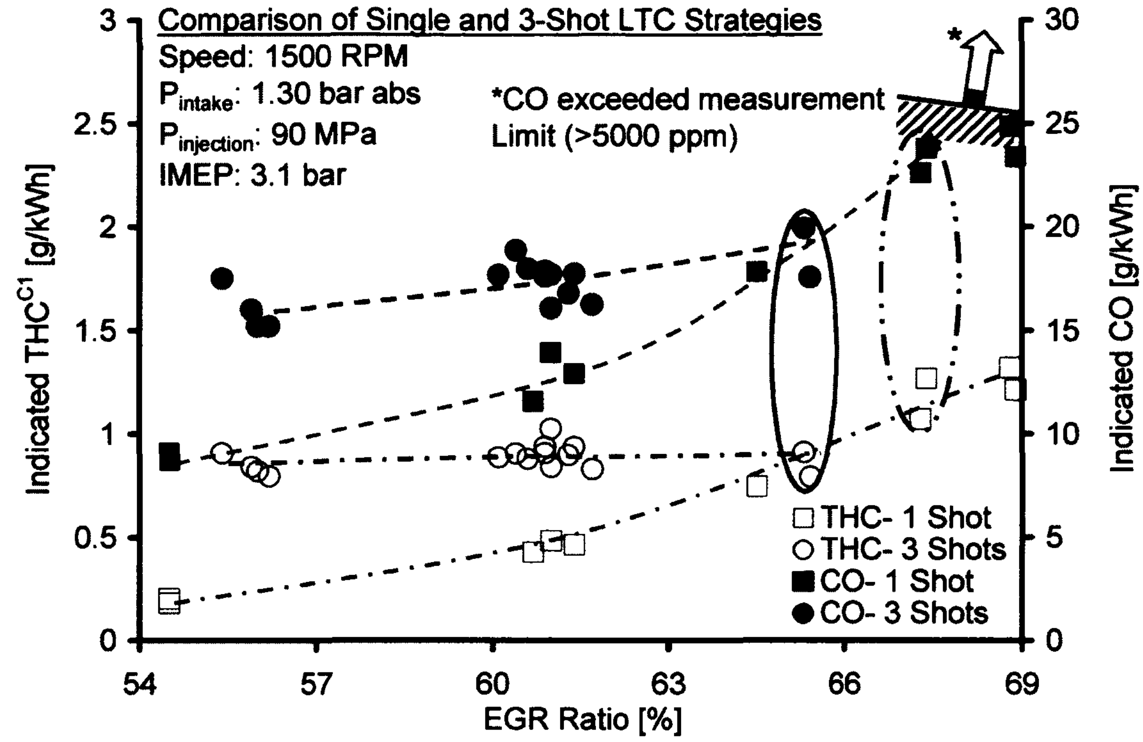

Figure 7.60: THC & CO Emissions for Single- & 3-Injection Strategies at 3.1 bar IMEP

For the case of 5.2 bar IMEP, the NOx and soot emissions are shown in Figure 7.61. Both the injection strategies enabled NOx to be pushed below 0.15 g/kWh. However, the soot was nearly 4 times more than the targeted limit for the single injection case once the best combination with the CO-THC emissions was done (Figure 7.62). The 3 injection strategy again resulted in ultra low levels of soot. It is pertinent to mention here that soot was reduced to around 0.01 g/kWh by increasing the EGR with the single injection but a significantly high CO and THC penalty was incurred. This may have severe implications for the fuel-efficiency as the high levels of THC and CO emissions can drain substantial amount of fuel energy from the LTC cycles.

The 3 injection strategy resulted in considerably lower THC emission and significantly lower CO emission compared to the single injection strategy (CO was more than halved).

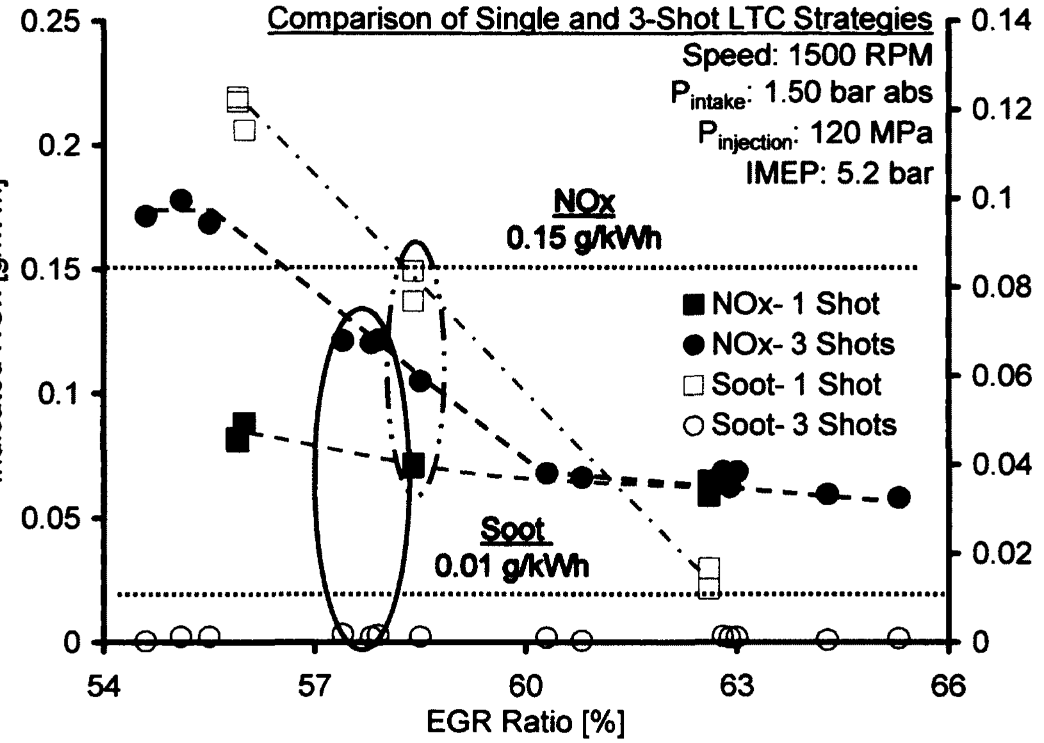

Figure 7.61: NOx & Soot Emissions for Single- & 3-Injection Strategies (5.2 bar IMEP)

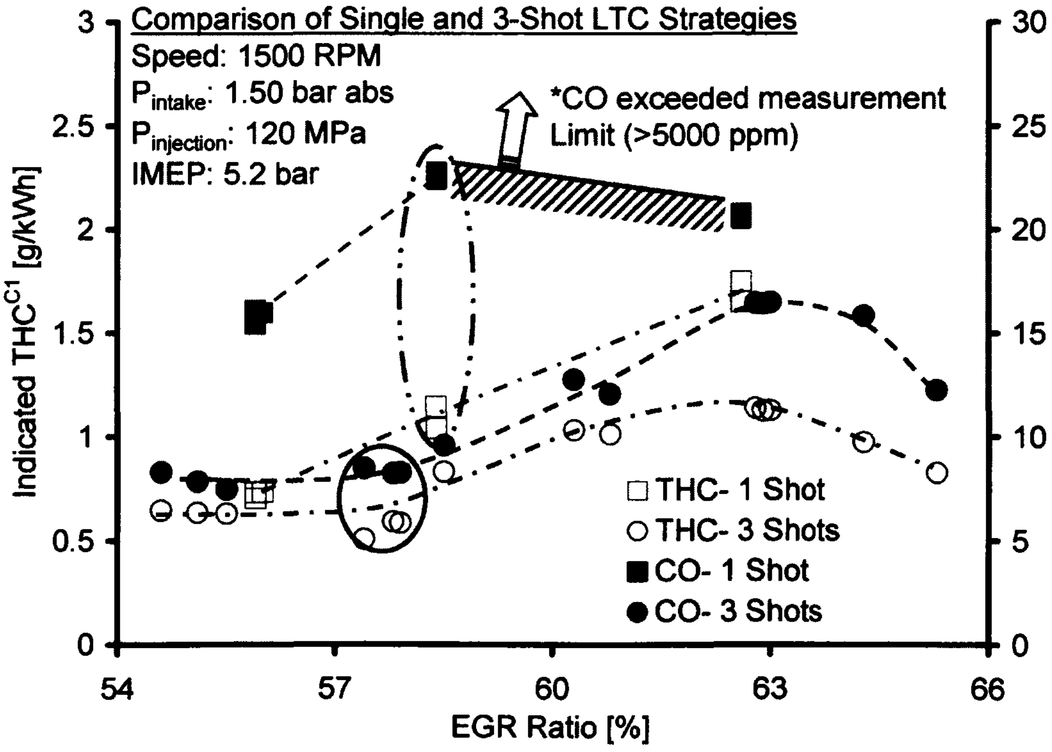

Figure 7.62: THC & CO Emissions for Single- & 3-Injection Strategies (5.2 bar IMEP)

The cylinder pressure traces and the heat release rates for the selected data points in the above figures are shown in Figure 7.63. The pressure gradient for the early LTC was much higher than the single-shot enabled LTC due to the off-phasing of the combustion from TDC. This also has implications on the fuel efficiency of the LTC cycles. As demonstrated for the 7.4 bar IMEP comparison (Figure 7.58), when the phasing departs from the timing of maximum thermal efficiency, this off-phasing causes an additional efficiency penalty that may be greater than the burning inefficiency (due to CO and THC), especially at higher loads. To improve the phasing, higher EGR levels can be employed but this generally deteriorates the combustion efficiency as evident in Figure 7.60 and Figure 7.62. Therefore, any attempts to improve the combustion phasing must be evaluated in terms of the net gain or loss in the thermal efficiency.

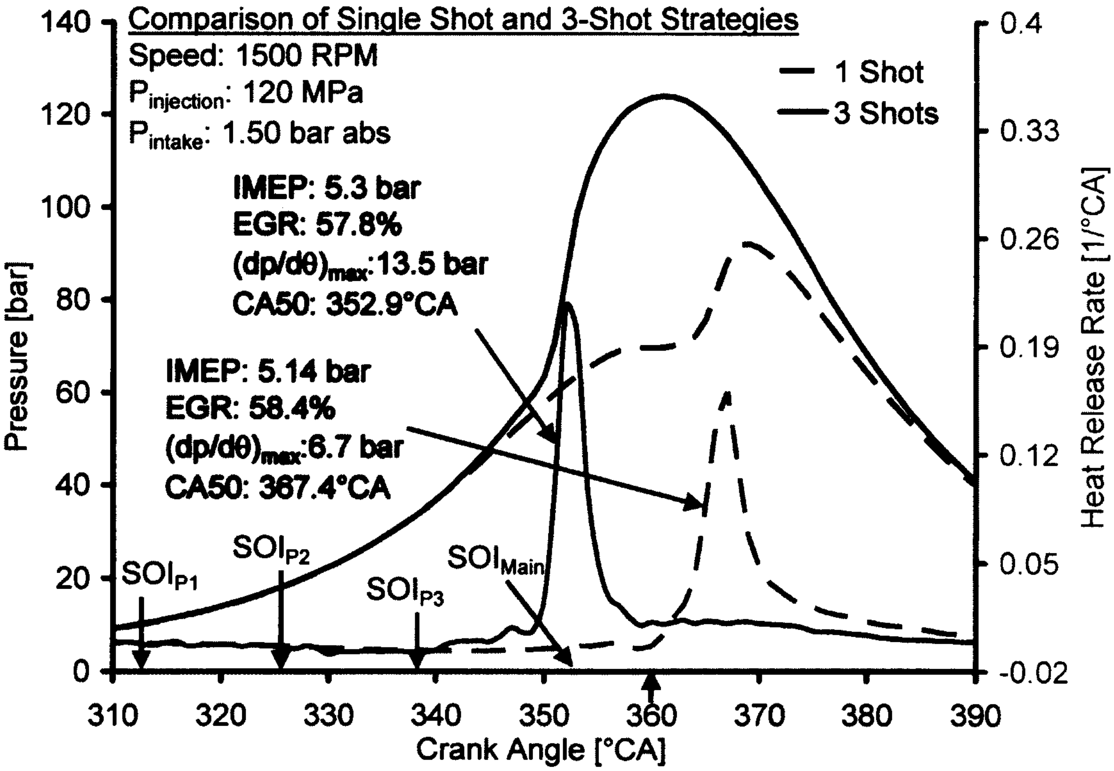

Figure 7.63: Cylinder Pressure Traces and Heat Release Rates for the Best Emissions (5.2 bar IMEP)

A comparison of the log(p)-log(V) traces is presented in Figure 7.64. It was noted that although the CA50 for the 3-shot strategy was much earlier (352.9°CA) which resulted in a larger amount of compression work compared to the single-shot strategy (CA50: 367.4°CA), the early-HCCI diesel LTC operation still produced positive net indicated work output per cylinder swept volume, i.e. IMEP, thus the engine should be able to produce reasonable effective power output when using a multi-cylinder configuration even with combustion occurring before the TDC. Moreover, the identical compression and expansion traces highlight the importance and benefits of exercising independent control on the boost, exhaust backpressure and EGR.

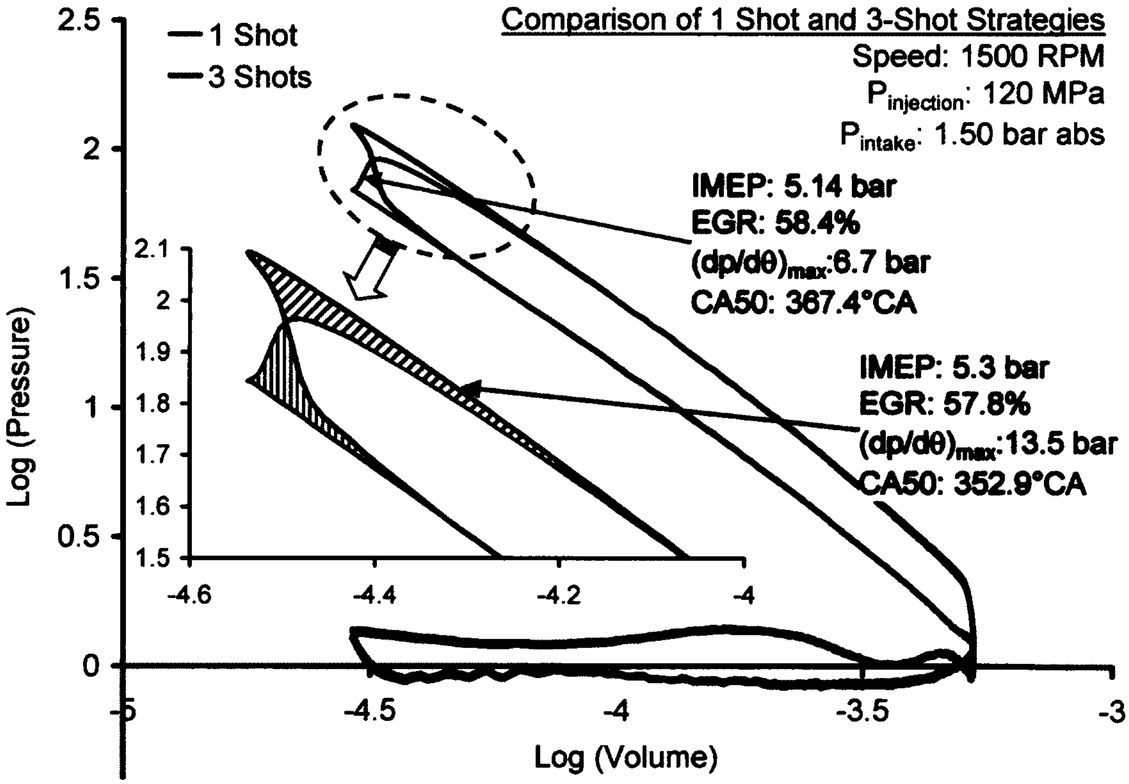

Figure 7.64: Logarithmic Pressure vs. Volume for the Single and Early HCCI Multi-pulse Injections at 5.2 bar IMEP

For the case of 7 bar IMEP, a slightly different approach was used. The tests were first performed at the baseline injection pressure of 100 MPa and intake pressure of 1.45 bar abs. The limiting conditions for EGR application were the CO and THC emissions. As shown in Figure 7.65, the combustion could not be pushed into the LTC cycles for the single-injection strategy. The intake and fuel injection pressures were progressively increased until the combustion entered the LTC regime. Figure 7.65 and Figure 7.66 exclude the emission results at intermediate steps and only show the final results.

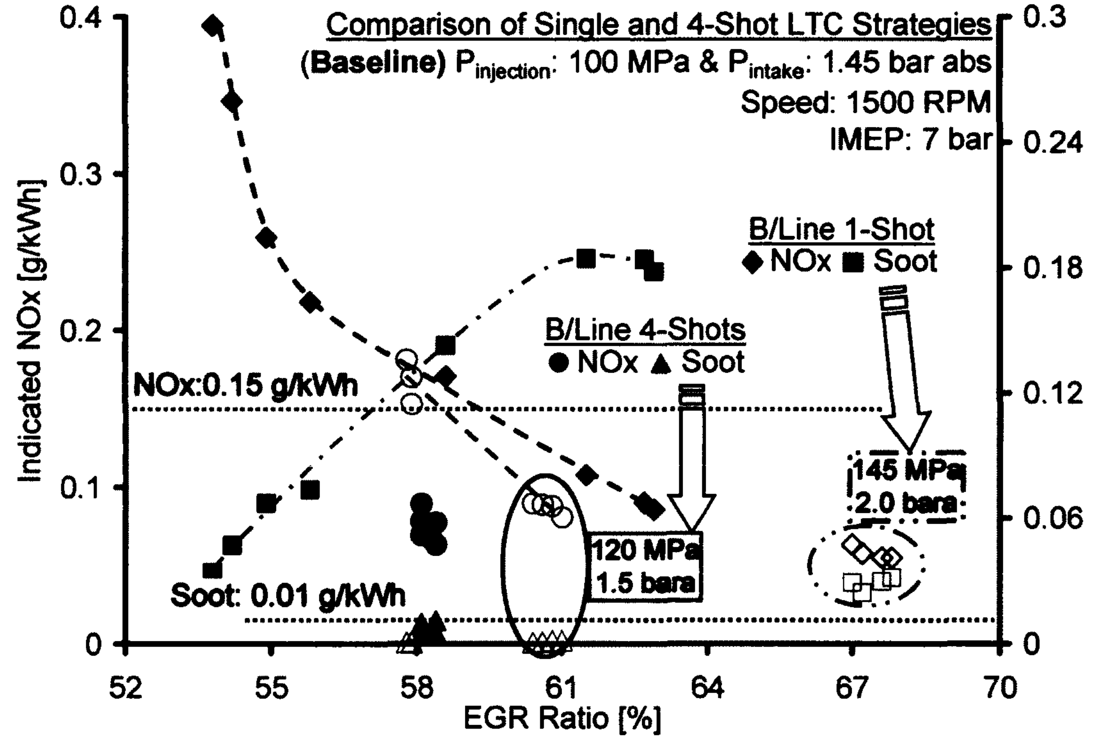

Figure 7.65: NOx & Soot Emissions for Single- and 4-Injection Strategies (7 bar IMEP)

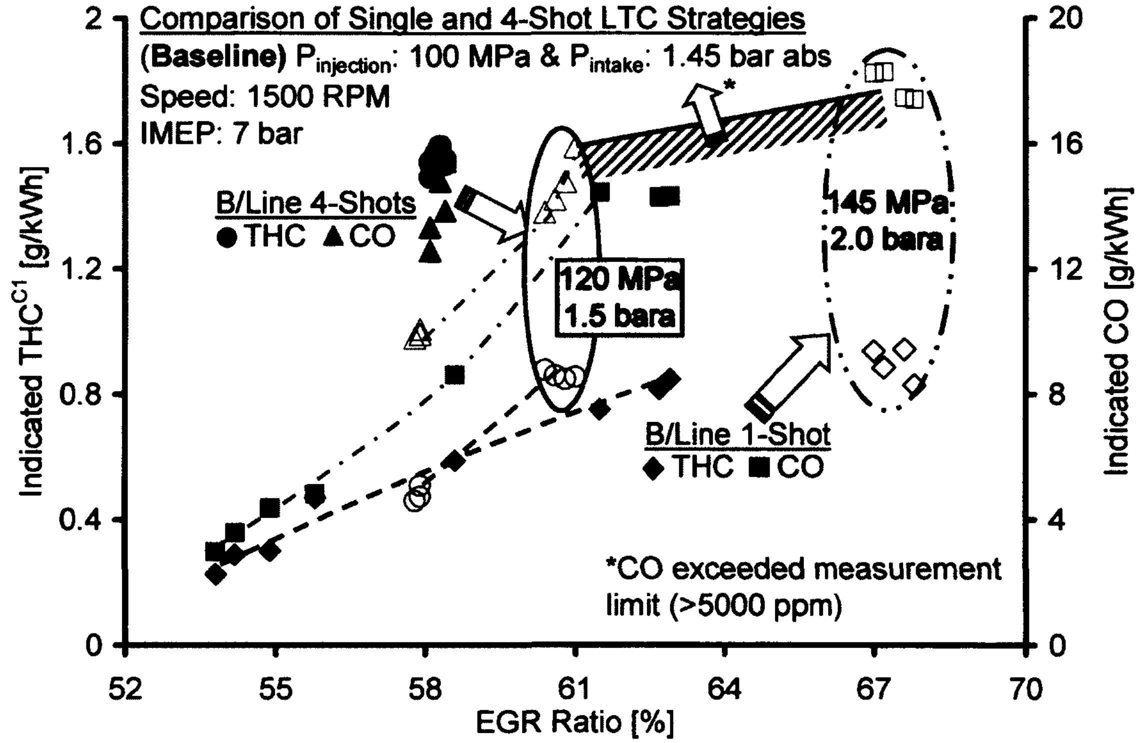

Figure 7.66: THC & CO Emissions for Single- and 4-Injection Strategies (7 bar IMEP)

The single-injection LTC required a much higher boost and injection pressure to enter the LTC regime compared to the multi-injection strategy. This was essential to curb the peak soot levels during the transition and was discussed in detail in context of Figure 7.39. Also, a higher boost and/or injection pressure reduces the brake mean effective pressure (BMEP) and therefore, the fuel efficiency may be significantly affected.

The NOx target was met for both the injection strategies but the soot was nearly 5 times the targeted value of 0.01 g/kWh for the single-injection. The THC and CO emissions were similar for both the cases. However, it must be kept in mind that the 4-injection strategy had considerably lower boost and injection pressures. An increase in boost for the 4-injection strategy was also restricted by the peak cylinder pressure as shown in Figure 7.67.

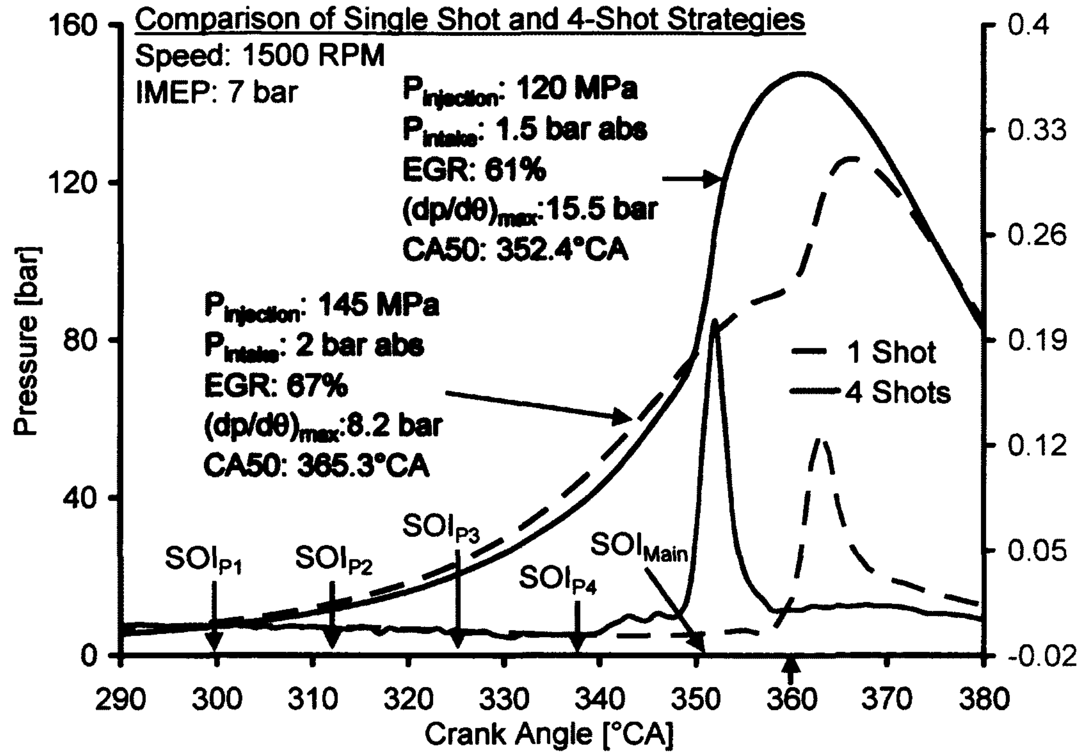

Figure 7.67: Cylinder Pressure Traces and Heat Release Rates for the Best Emissions (7 bar IMEP)

An energy efficiency analysis for the experimental results of 3.1 bar and 5.2 bar IMEP (Figure 7.59 to Figure 7.63) is presented in Table 7.11 [4,9]. For 3.1 bar IMEP, the indicated thermal efficiency of the single injection strategy was higher than that of the 3-injection scheme. For the 5.2 bar IMEP case, the thermal efficiency of the 3-injection strategy slightly improved over that of the single-injection. However, the combustion efficiency of the 3-injection strategy was observed to be higher than that of the single injection strategy at both 5.2 bar IMEP and 3.1 bar IMEP. It should be noted that for the LTC cycles, the combustion inefficiency caused by the excessive HC and CO emissions is not negligible as is generally the case for HTC combustion.

Table 7.11: Energy Efficiency Analysis (Test # 4)

	No of Injections	
	1	3
3.1 bar IMEP		
Indicated NOx [g/kWh]	0.09	0.09
Indicated Soot [g/kWh]	0.006	0.001
Indicated THC^{C1} [g/kWh]	1.1	0.8
Indicated CO [g/kWh]	23*	18
Indicated Power [kW]	2.0	2.0
Fuelling Rate [mg/cyc]	10.2	10.9
Combustion efficiency [%]	97.2	97.9
Ind. Thermal Efficiency [%]	36.7	34
COV IMEP [%]	2.8	3.1
5.1 bar IMEP		
Indicated NOx [g/kWh]	0.07	0.12
Indicated Soot [g/kWh]	0.08	0.001
Indicated THC^{C1} [g/kWh]	1.05	0.6
Indicated CO [g/kWh]	23*	8.5
Indicated Power [kW]	3.3	3.3
Fuelling Rate [mg/cyc]	15.7	15.2
Combustion efficiency [%]	97	98.7
Ind. Thermal Efficiency [%]	38.9	40.1
COV IMEP [%]	3.2	2.5

* Measurement exceeded analyzer range of 5000ppm

Moreover, at higher loads with the single injection strategy, the increased soot levels (above the target value) will require the use of diesel particulate filters (DPF) and hence, supplemental fuel to regenerate the DPF will be required. Therefore, a fuel efficiency penalty to enable DPF operation will further degrade the performance of the single-shot LTC at higher loads.

To compare the engine stability between the two injection strategies, the coefficient of variance (COV) of IMEP was compared. The COV was generally low (~ 3%) with the single injection strategy for both the 3.1 bar and 5.2 bar IMEP cases. However, as the load level increased, the COV of IMEP for the multi-injection strategy was seen to slightly decrease from about 3.1% at 3.1 bar IMEP to 2.5% at 5.2 bar IMEP and 1.96% at 7 bar IMEP.

7.9. Parametric Analyses of LTC Cycles

A higher boost requires a higher EGR rate to push the combustion into the LTC cycles. In production engines with conventional turbochargers, the simultaneous availability of high boost and high EGR presents a significant challenge, especially at low loads. A higher boost requires more of the exhaust to be diverted to the exhaust turbine. However, a high EGR rate requires more of the exhaust gases to be recycled back to the intake. Moreover, the low diesel exhaust temperature at low loads places limits on the practically achievable boost pressure. Therefore, the current trend of the industry has been to employ the lowest possible boost and EGR rates. Another important implication of a higher boost is the necessity of a high exhaust back pressure. To force more exhaust gases back into the high pressure intake, the exhaust pressure needs to be raised. This may significantly increase the pumping work during the exhaust stroke and compromise the engine cycle efficiency. The higher boost also increases the compression work as the piston has to compress a cylinder charge with a high ambient density. Therefore, the mechanical strength of the engine components needs to be substantially enhanced to endure the increased bearing pressures and mechanical stresses.

A similar situation exists for providing a higher injection pressure. The higher the injection pressure, the greater is the engine friction power with the result that the brake power is reduced for the same indicated power output. Therefore, the industrial trend has been to use the minimum necessary injection pressure as warranted to meet the prevalent emission regulations.

Unlike boost pressure whose availability is linked to the amount of EGR required, it is easier to vary the injection pressure since it is largely independent of other engine operating conditions. Moreover, increasing the injection pressure was observed to reduce the soot emissions across the EGR range (Figure 7.47) and was more effective in curbing the soot at a given boost level. In view of the above, it was decided to analyse the effect of injection pressure in the LTC regime only (intake oxygen < 14%) and ascertain the effects on the engine-out emissions and the efficiency of the LTC cycles. The effect of engine speed on the LTC performance was also studied. It is pertinent to mention here that the cost of conducting such parametric analyses can be significant if a number of parameters (for instance boost, intake temperature, engine speed) and their interactions need to be examined. Other analyses techniques such as the 'Design of Experiments' can be employed to reduce the time and the cost associated with such analyses.

7.9.1. Single Shot LTC at 5.2 bar IMEP (Test # 5)

All the test were carried at a load of 5.2 bar IMEP. The combustion phasing was maintained at 366°CA by adjusting the combustion phasing. The boost pressure was fixed at 1.5 bar abs and the engine speed was 1500 RPM during these tests. Four injection pressure levels (60 to 120 MPa) were studied by performing an EGR sweep.

The results for the effect of injection pressure on the NOx emissions are given in Figure 7.68. The results of this test indicated that the injection pressure produced a noticeable change in the NOx trends and the NOx was found to be higher with higher injection pressures even in the LTC regime. Moreover, the decrease in the NOx emissions by half from 30 to 15 ppm (marked in the figure) suggested that the NOx reduction may be the result of LTC-NOx mechanism (Chapter 5) with the generation of a high amount of combustibles with increased EGR.

Regarding the soot emissions (Figure 7.69), the peak soot was significantly curbed by increasing the injection pressure from 60 to 100 MPa. However, a further increase in the injection pressure (120 MPa) did not result in a significant drop in the peak soot levels. Moreover, the higher injection pressure (both 100 and 120 MPa) was able to reduce the minimum soot to within the targeted level of 0.01g/kWh.

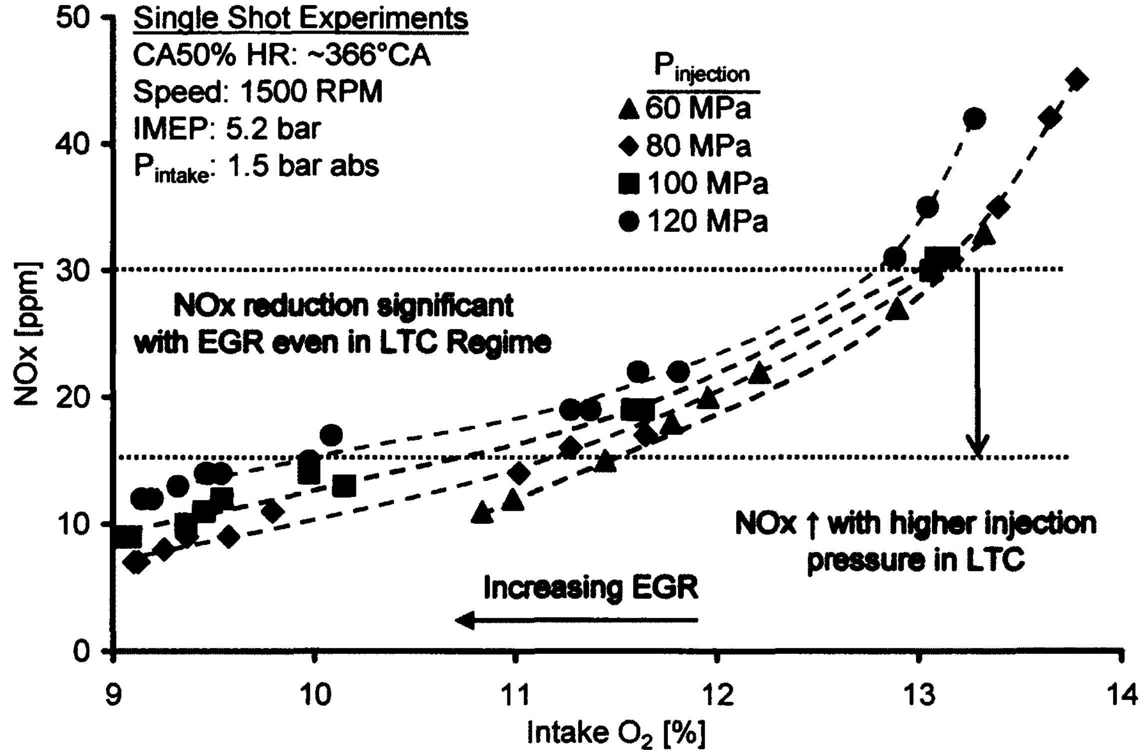

Figure 7.68: Effect of Injection Pressure on NOx (5.2 bar IMEP – Test # 5

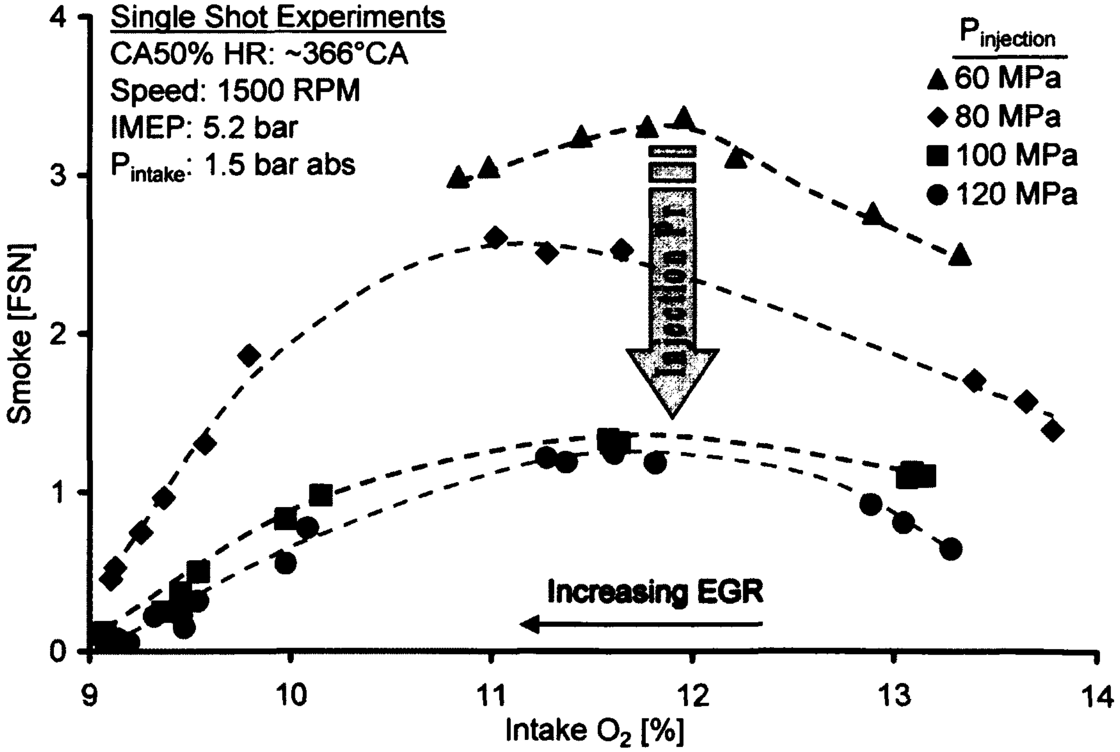

Figure 7.69: Effect of Injection Pressure on Soot (5.2 bar IMEP – Test # 5)

The efficacy of injection pressure for LTC cycles becomes evident when the CO and HC emission trends are observed as shown in Figure 7.70. Increasing the fuel injection pressure from 80 to 100 MPa reduced the HC from 0.8 g/kWh to 0.35 g/kWh at the same intake oxygen. The reduced HC penalty allows higher levels of EGR to be used to push the soot levels to below the desired level. The CO trend was not clearly identified because of the measurement constraints. However, a higher injection pressure delays the onset of the CO emission and may help to reduce CO as well.

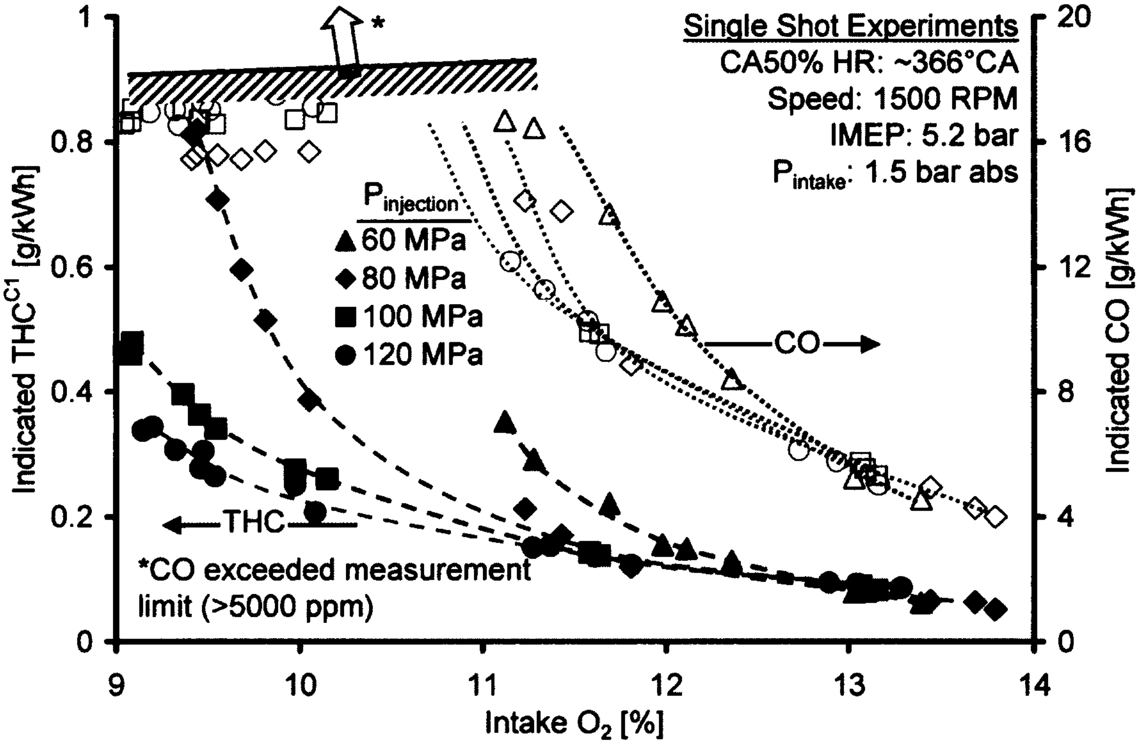

Figure 7.70: Effect of Injection Pressure on THC & CO (5.2 bar IMEP – Test # 5)

The summary of the emissions, LTC efficiency and stability is provided in Table 7.12. The results for the 60 MPa EGR sweep have been shown for reference since the soot levels could not be reduced because of the onset of very high HC and CO. The indicated thermal efficiency improved slightly at a higher injection pressure. A higher injection pressure was also able to limit the deterioration in the combustion efficiency but the COV of IMEP was also found to increase. The recycling of the

CO and HC with heavy EGR and the lowered combustion temperature of the LTC cycles escalate the consecutive cyclic variations of the LTC operation. To improve the cycle-by-cycle performance, either the composition of the recycled gases can be regulated as demonstrated during the CEGR oxidization tests (Chapter 6) or a closed-loop feedback control is required to improve the cycle-by-cycle performance.

Table 7.12: Summary of Injection Pressure Variation Test (Single-Shot LTC, Test # 5)

Parameter	Injection Pressure [MPa]			
	60	80	100	120
NOx [ppm]	11	7	8	12
NOx [g/kWh]	0.06	0.034	0.05	0.07
Intake O_2 [%]	10.8	9.1	9.1	9.2
Indicated Thermal Efficiency [%]	40.9	39.2	39.7	40.5
Smoke [FSN]	3	0.45	0.11	0.06
Soot [g/kWh]	0.22	0.01	0.002	0.0014
CO [ppm]	>5200*	>5200*	>5200*	>5200*
THC [g/kWh]	0.35	0.81	0.47	0.36
Combustion Efficiency [%]	97.8	97.9	97.9	98
P_{max} [bar]	96.4	91.9	93.7	94.6
$(dp/d\theta)_{max}$ [bar]	6.8	4.2	4.8	3.4
COV P_{max} [%]	1.03	1.99	1.98	1.5
COV IMEP [%]	1.9	2.7	2.9	4.2

* Exceeded the analyzer measurement limit

To study the effect of engine speed on the attainment of LTC combustion, the single-shot enabled LTC was tested at a higher speed of 1800 RPM. The injection pressure was 80 MPa and the CA50 was fixed at 366°CA by adjusting the SOI. All the other parameters were also retained within close limits. A comparison of the performance metrics with those at 1500 RPM is shown from Figure 7.71 to Figure 7.73.

The cylinder pressure and the heat release rates at the two engine speeds indicate a precise control on the combustion. At 1800 RPM, the premixed phase of the combustion was decreased and the combustion duration was slightly increased. To maintain the combustion phasing, the SOI at 1800 RPM was advanced. While the ignition delay did not change in terms of crank angle degrees, it was reduced once seen in the time domain. This had severe implications on all the emissions as presented below.

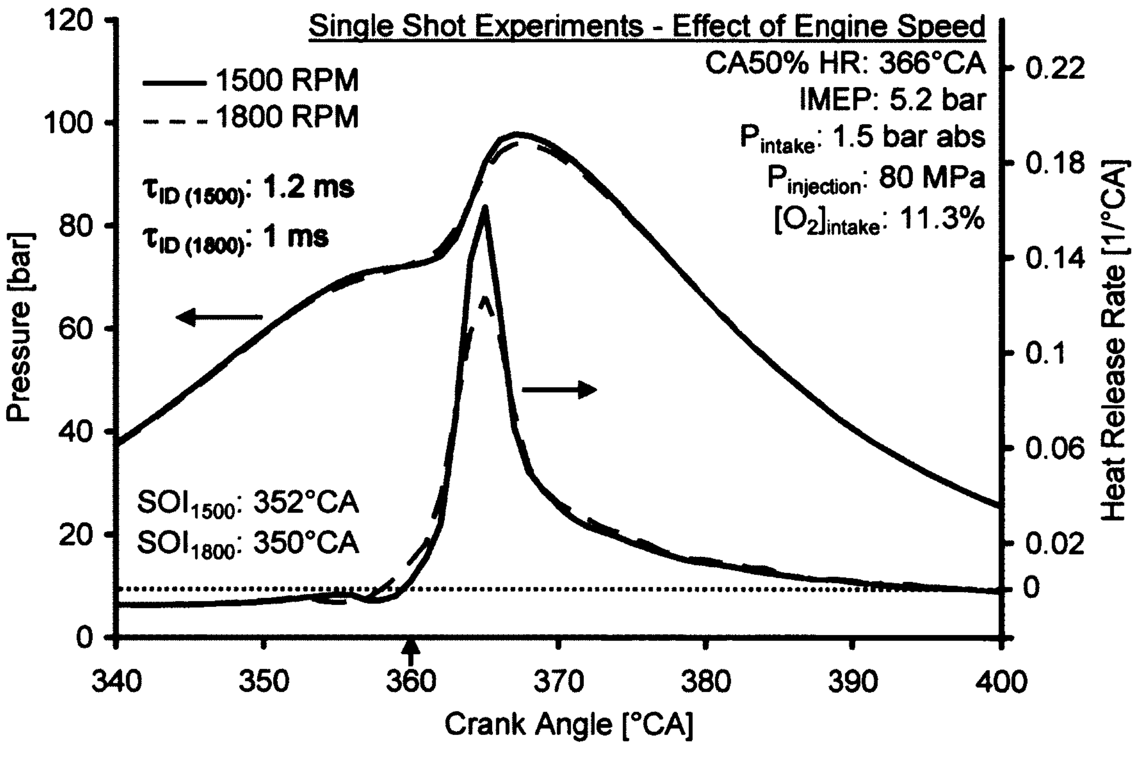

Figure 7.71: Cylinder Pressure & Heat Release Rate at Different Speeds (5.2 bar IMEP – Test # 5)

NOx was found to reduce at higher speeds but a large increase in the soot was observed. This was the result of the reduced ignition delay and the corresponding increase in the diffusion controlled combustion. The CO and HC emissions were

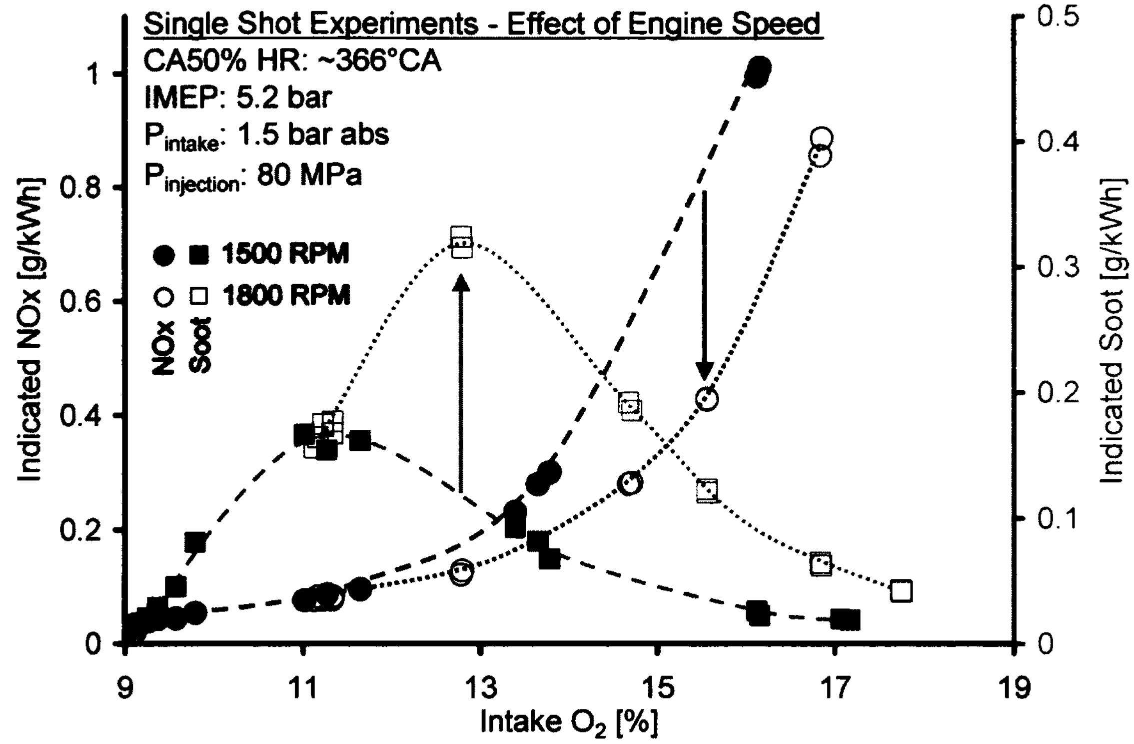

Figure 7.72: Effect of Engine Speed on NOx & Soot (5.2 bar IMEP – Test # 5)

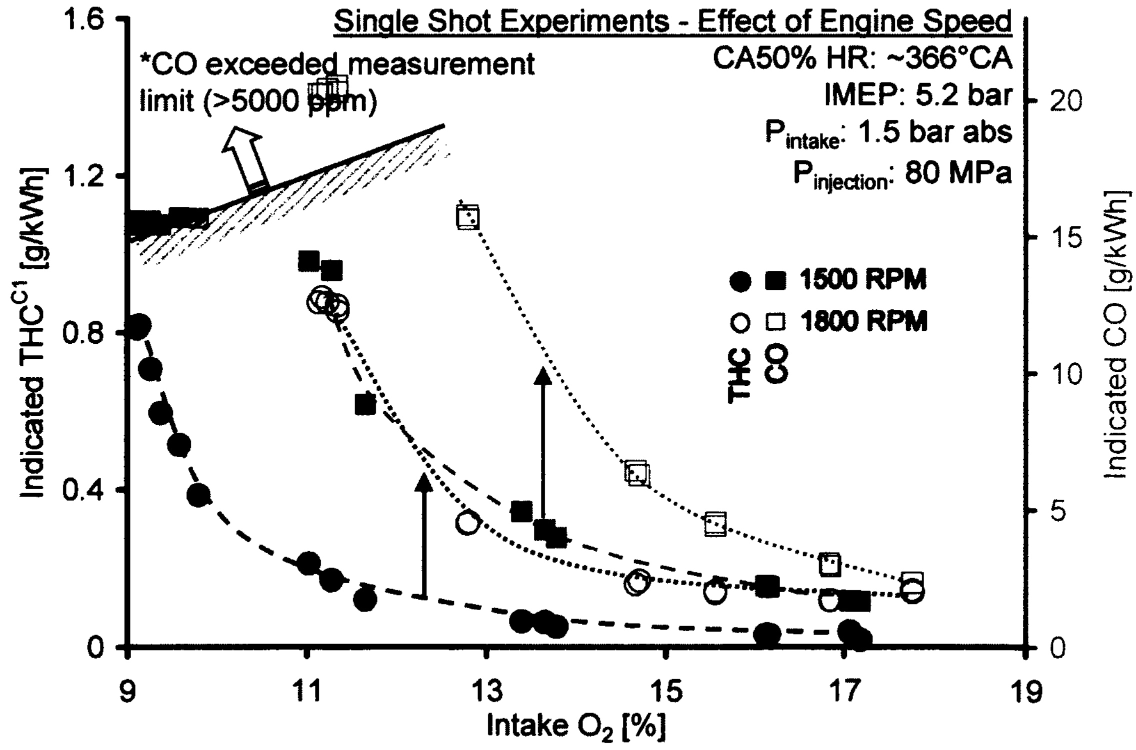

Figure 7.73: Effect of Engine Speed on THC & CO (5.2 bar IMEP – Test # 5)

also observed to be significantly higher (Figure 7.73) and the onset of the rapid deterioration in the emissions was at a much higher intake oxygen (lower EGR rate). The soot could therefore not be reduced to ultra low values.

A brief discussion on the effect of speed is presented here. At higher engine speeds, the time available between the fuel injection and the start of combustion, that is, the ignition delay (in ms) is reduced. Since the underlying enabler for the LTC is the separation of the fuel injection event from the combustion, a higher injection pressure in combination with advanced injection timing are necessary to ensure the separation of the two events. However as the speed is increased further, it is not physically possible to further increase the ignition delay and therefore, the load level has to be reduced to maintain the combustion in the LTC regime, with ultra low levels of NOx and soot emissions. Similar trends have been reported in the literature for high compression ratio diesel engines [74–76]. A lower compression ratio decreases the propensity for premature ignition with the fuel injection advanced further into the compression stroke, provides for an inherently longer ignition delay because of the lower temperatures during the compression process, and therefore, the speed range of the single-shot LTC should be higher for lower compression ration engines. Alternately, the load level of the LTC cycles can be increased at low engine speeds with low compression ratio engines [152].

7.9.2. Multi Shot LTC (Early-HCCI) at 5.2 bar IMEP (Test # 6)

The injection pressure variation was repeated for the multi-shot LTC at 5.2 bar IMEP. The injections were scheduled at 312, 325 and 338°CA, and the pulse width of each injection was the same for a given injection pressure. Since the early injections have a higher propensity for cylinder wall impingement and are affected by the fuel injection pressure, therefore, an effort was made to correlate the injection pressure with the fuel efficiency deterioration. The results for the effect of injection pressure on the engine performance metrics are shown from Figure 7.74 to Figure 7.78. It is noted that the maximum possible error in the reported results is about 5% and this aspect should be given due consideration while analyzing the minor variations within the reported results.

The NOx emission displayed an increasing trend with the injection pressure (Figure 7.74), similar to the single-shot LTC tests. Ultra low NOx levels were achieved at all the injection pressures.

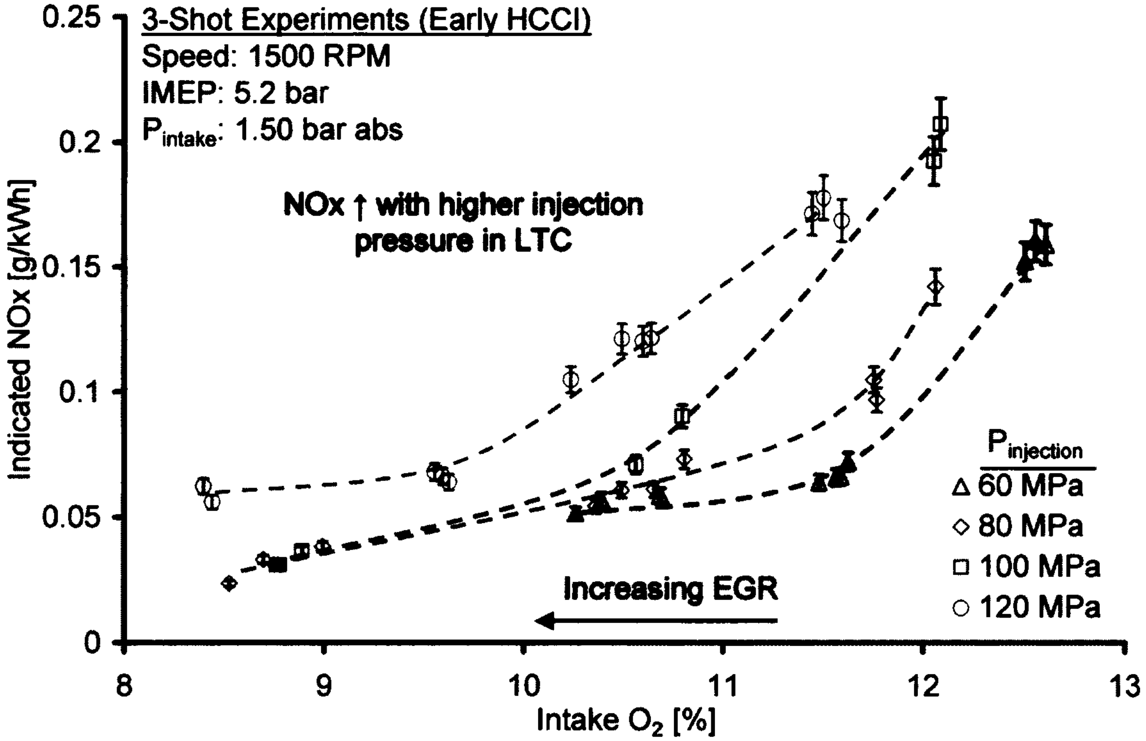

Figure 7.74: Effect of Injection Pressure on NOx (5.2 bar IMEP – Test # 6)

The CO and HC results are shown in Figure 7.75 and Figure 7.76 respectively. The CO emission was the lowest at 80 MPa and showed an increasing trend with higher injection pressure. However, the CO trend at 60MPa was inconsistent and displayed a higher level for the same charge dilution. A similar observation was made for the HC emissions at 60MPa where the HC emission was found to be insensitive to the EGR. Moreover, the HC results provided an insight in to the effect of the injection pressure on the combustion efficiency deterioration. The HC values were very similar for both 80 & 100 MPa pressures. However, a significant increase in the HC emissions was observed for the 120MPa test results. As shown with the spray penetration calculations (Section 7.8.3), a higher injection pressure

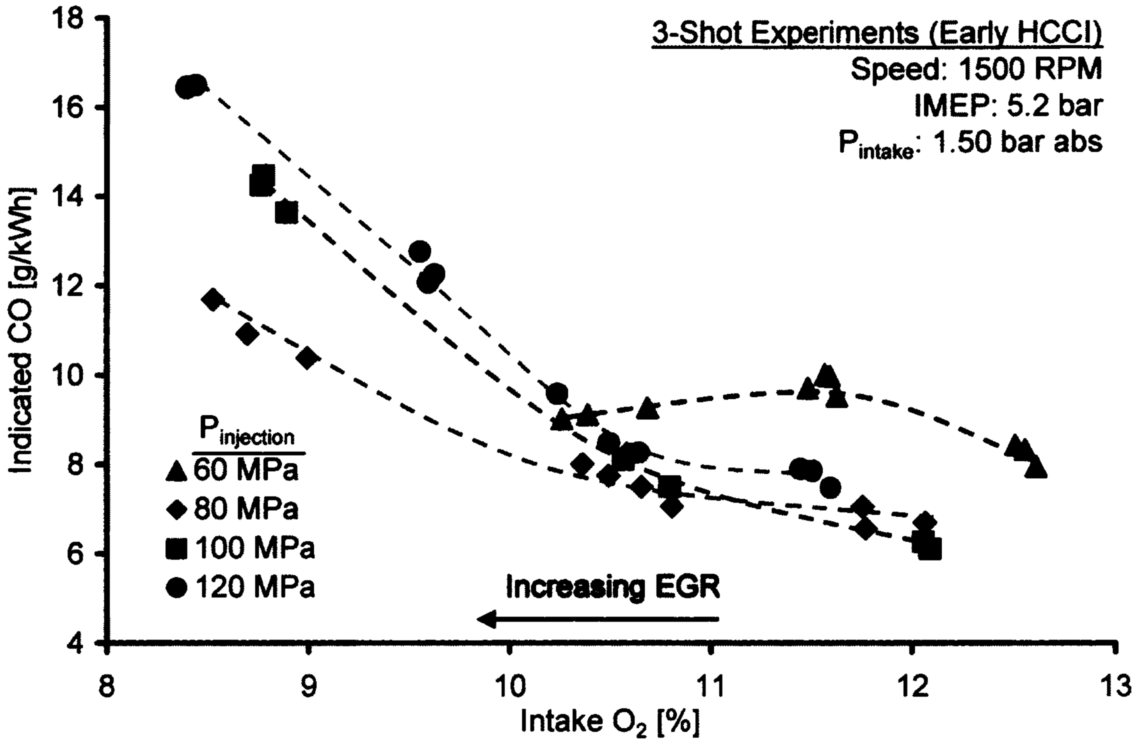

Figure 7.75: Effect of Injection Pressure on CO (5.2 bar IMEP – Test # 6)

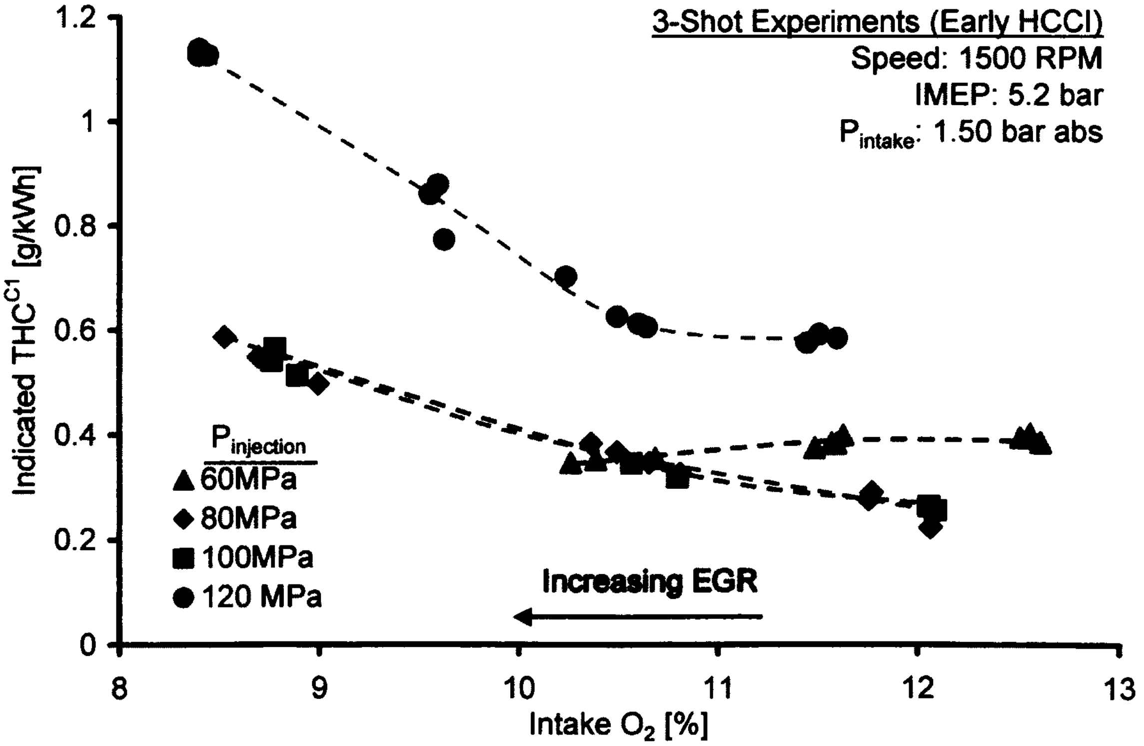

Figure 7.76: Effect of Injection Pressure on THC (5.2 bar IMEP – Test # 6)

increases the spray penetration length and therefore, the spray has a higher chance of impinging on the cylinder walls, given all the other parameters (charge density, temperature, composition) are the same.

To understand the different behaviour observed at 60MPa, the soot emissions were plotted as shown in Figure 7.77. Ultra low soot values were achieved for all the four injection pressures. However, the soot levels still showed a distinct increase at 60MPa as the EGR was increased. The increase in soot can be attributed to the reduced homogeneity of the cylinder charge as a result of the low injection pressures. The reduced penetration of the fuel spray may result in locally richer pockets of the cylinder charge, despite the combustion being overall lean and highly diluted. This also agrees with the slight reduction seen in the CO and HC levels at 60MPa.

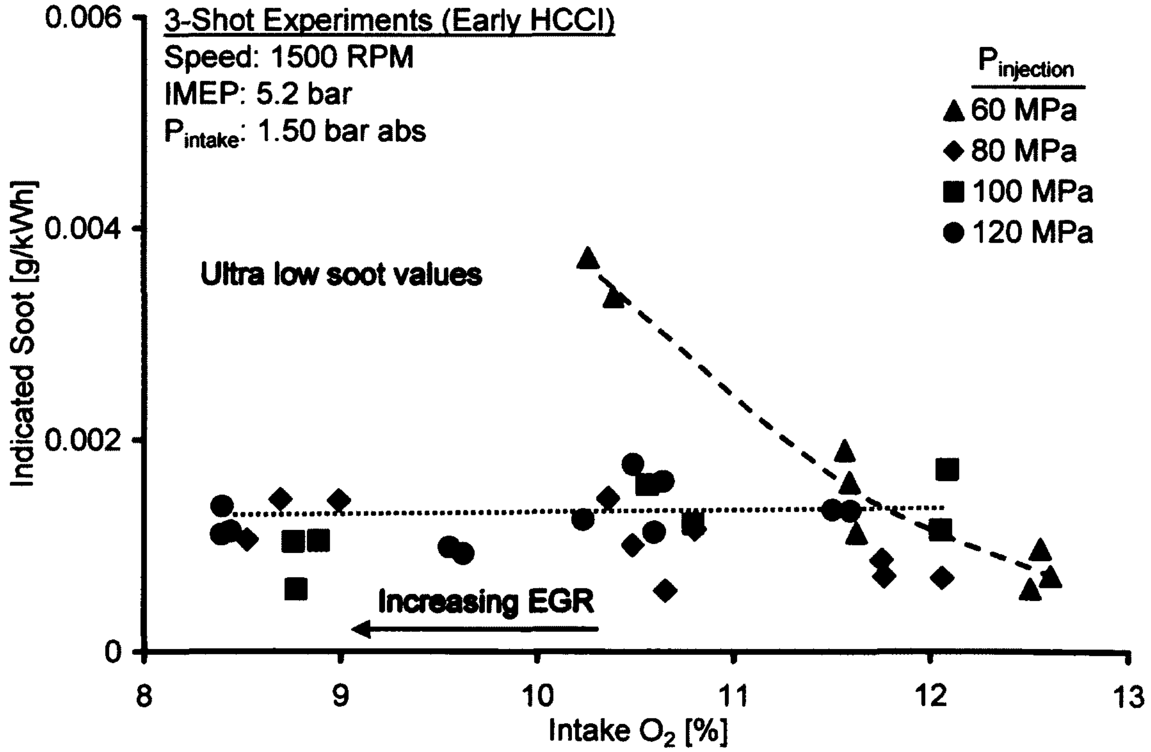

Figure 7.77: Effect of Injection Pressure on Soot (5.2 bar IMEP – Test # 6)

Based on these observations and results, the CO and HC were plotted as a function of the injection pressure at the same intake oxygen (~11.5%) and the results are shown in Figure 7.78. It was found that the CO and HC emissions were the lowest at 80 and 100 MPa. A lower injection pressure resulted in an HC and CO rise, with the CO rising more rapidly than HC (reduced homogeneity). A higher injection pressure, on the other hand, caused a higher rise in the HC compared to the CO (higher propensity for wall wetting). These observations had synergy with the spray penetration length calculations which provided indicators for the selection of the boost and injection pressure to minimize the spray impingement on the cylinder walls.

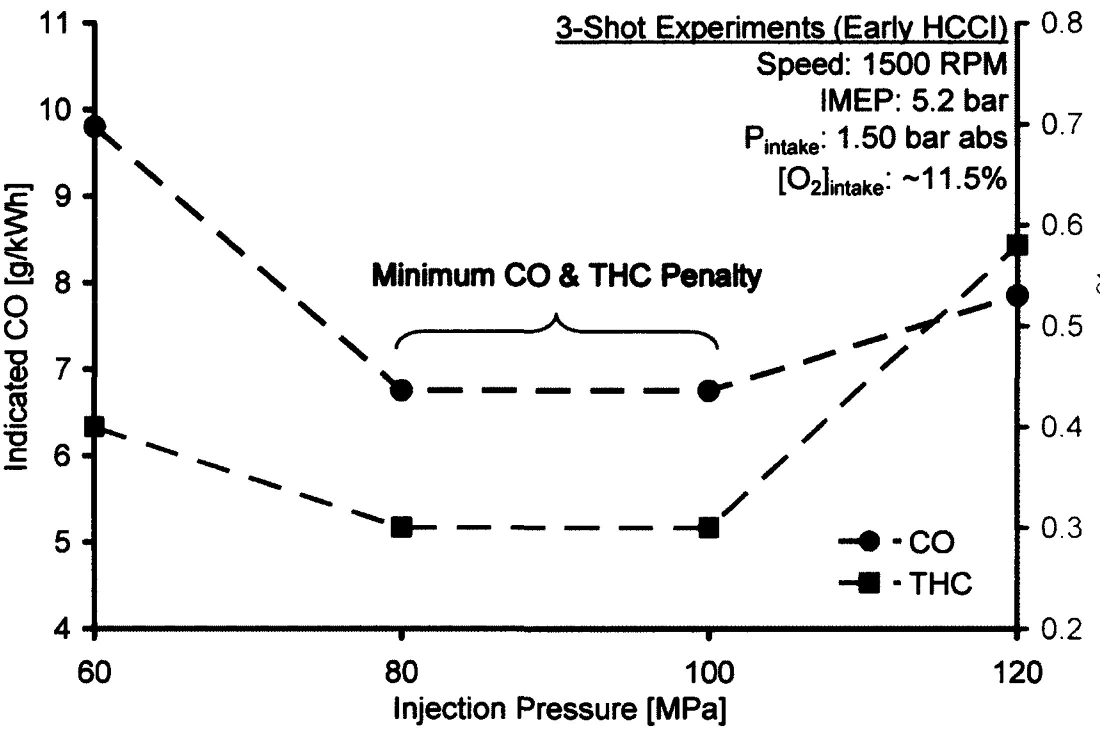

Figure 7.78: Injection Pressure for Minimum CO & THC Penalty

The summary of the results at the same intake oxygen of ~11.5% is given in Table 7.13. A slight improvement in the combustion efficiency at 80 and 100 MPa was seen, as a result of the lower CO and HC emissions. Between the results for 80 and 100 MPa, the NOx, P_{max} and $(dp/d\theta)_{max}$ were lower for 80MPa. The COVs of P_{max} and IMEP also indicated that the overall performance in terms of stability of the combustion process was slightly improved at 80MPa.

Table 7.13: Summary of Injection Pressure Variation Test (Multi-Shot LTC, Test # 6)

Parameter	Injection Pressure [MPa]			
	60	80	100	120
NOx [ppm]	11	13	19	21
NOx [g/kWh]	0.07	0.08	0.14	0.16
Intake O_2 [%]	~11.5			
Indicated Thermal Efficiency [%]	39.6	39.9	39.8	39.3
Soot [g/kWh]	< 0.002			
CO [g/kWh]	9.8	6.7	6.8	7.9
THC [g/kWh]	0.38	0.29	0.29	0.59
Combustion Efficiency [%]	98.7	99	99	98.6
P_{max} [bar]	122.5	121.4	122.9	124.6
$(dp/d\theta)_{max}$ [bar]	12.9	12.6	14.3	16.5
COV P_{max} [%]	1.06	0.65	0.66	0.91
COV IMEP [%]	3.4	2.1	2.3	2.5

The effect of higher engine speed (1800 RPM) on the multi-shot LTC was also investigated at 5.2 bar IMEP. The injection pressure was chosen as 80MPa, based on the results of the injection pressure variation test. The SOIs for the multiple injections were 312, 325 and 338°CA at 1500 RPM. To maintain the same dwell between the injections (in ms), the timing of the injection pulses at 1800 RPM was modified to 305, 320.5 and 336°CA.

The results for the NOx and soot emissions are shown from in Figure 7.79. No clear trend was observed in the NOx emissions between the two speeds although the values were very low. The soot emission at both the speeds was ultra low and no difference could be detected. The corresponding CO & HC emissions shown in Figure 7.80 indicate an increase in both the CO and HC at higher speed, similar to the single-shot LTC. However, the CO emission was much lower than the single-shot LTC at high speed and within the measuring range of the emission analyzer.

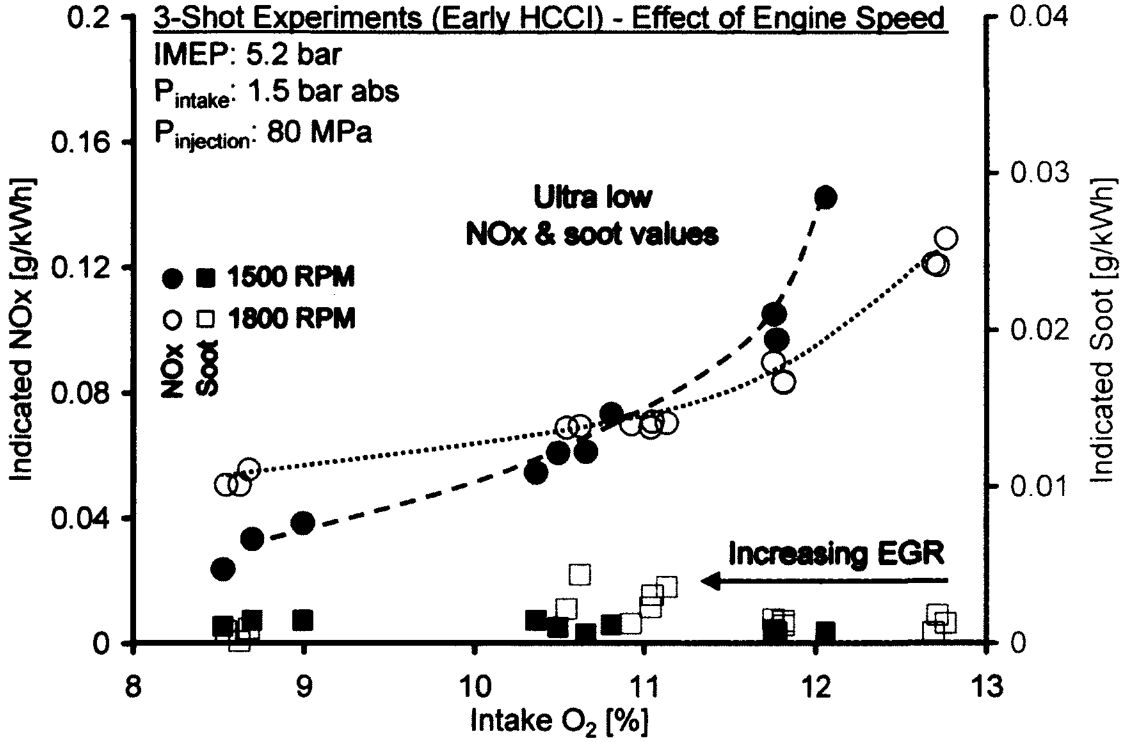

Figure 7.79: Effect of Engine Speed on NOx & Soot (5.2 bar IMEP – Test # 6)

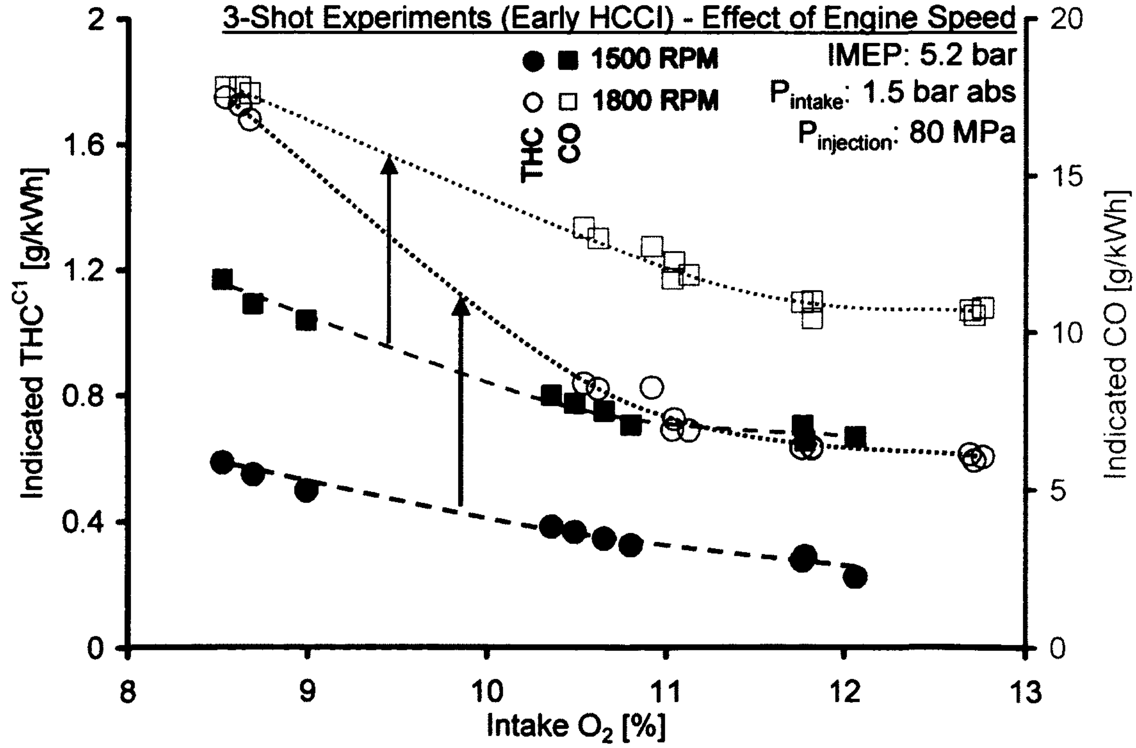

Figure 7.80: Effect of Engine Speed on THC & CO (5.2 bar IMEP – Test # 6)

The cylinder pressure and the heat release traces for the two speeds are plotted in Figure 7.81. The phasing of the combustion was slightly delayed at the higher speed. The advanced timing of the first injection and the improved combustion phasing could partly explain the rise in the CO and the HC emissions. It was also noted that the peak cylinder pressure was almost the same.

At higher speeds, it was possible to enable the multi-shot LTC and achieve ultra low NOx and soot levels. This was an improvement over the single-shot LTC where the low soot emissions could not be achieved at 1800 RPM. These tests provided the necessary foundation to ascertain an effective LTC load management strategy, explained later in this chapter.

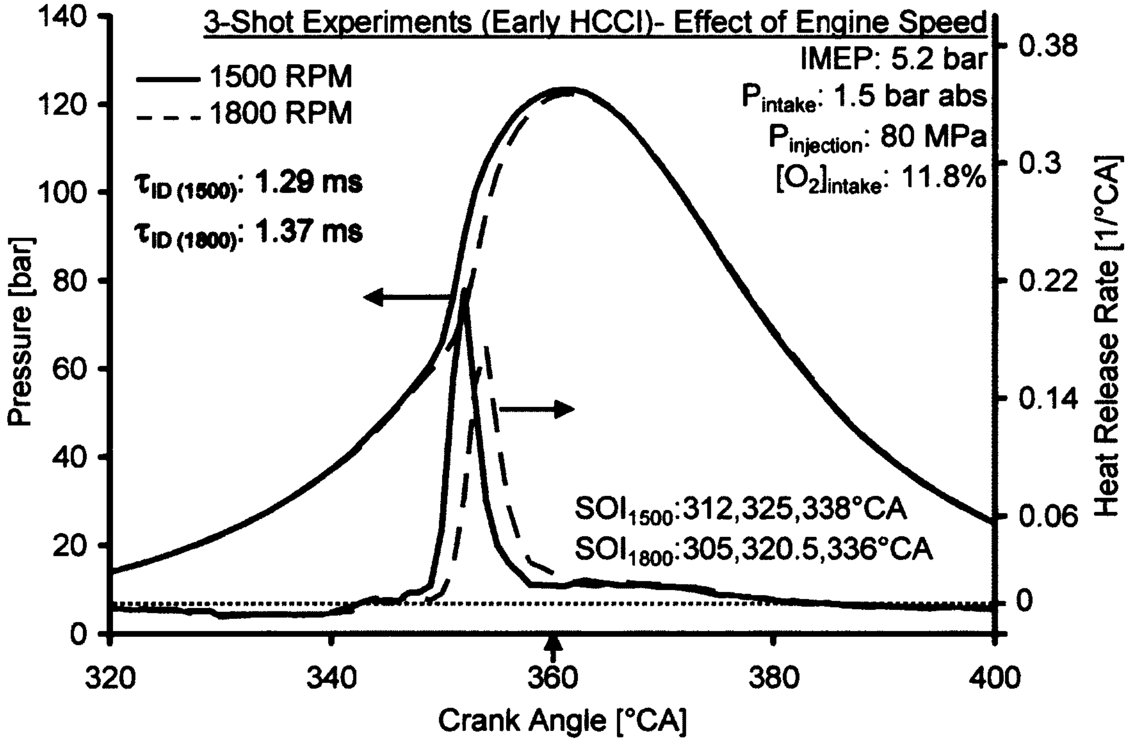

Figure 7.81: Cylinder Pressure & Heat Release Rate at Different Speeds (5.2 bar IMEP – Test # 6)

7.10. Strategy for Extending the LTC Load Level

Raising the load level for LTC cycles requires the use of higher boost. However, with the multi-shot LTC, the early phasing of the combustion results in higher maximums for the cylinder pressure and the rate of pressure rise. This places a restriction on the load level that can be attained with the multi-shot strategy as demonstrated in Figure 7.82. To highlight the restrictions on the achievable LTC load levels imposed by the high CR, the boost was set at 2.5 bar abs and 3 early injections (SOI_1: 299°CA, SOI_2: 312°CA, SOI_3: 325°CA) were enabled. The maximum cylinder pressure reached the 160 bar threshold at an IMEP of only 2.2 bar and 58% EGR (Figure 7.83).

Therefore, an alternate strategy for high load operations can be the mode of split burning LTC, in which a partial amount of fuel is delivered to produce HCCI combustion before the TDC and the remaining for post-TDC late combustion. The latter may benefit from the virtual EGR produced by the HCCI burning and timed to eliminate combustibles and raise power output.

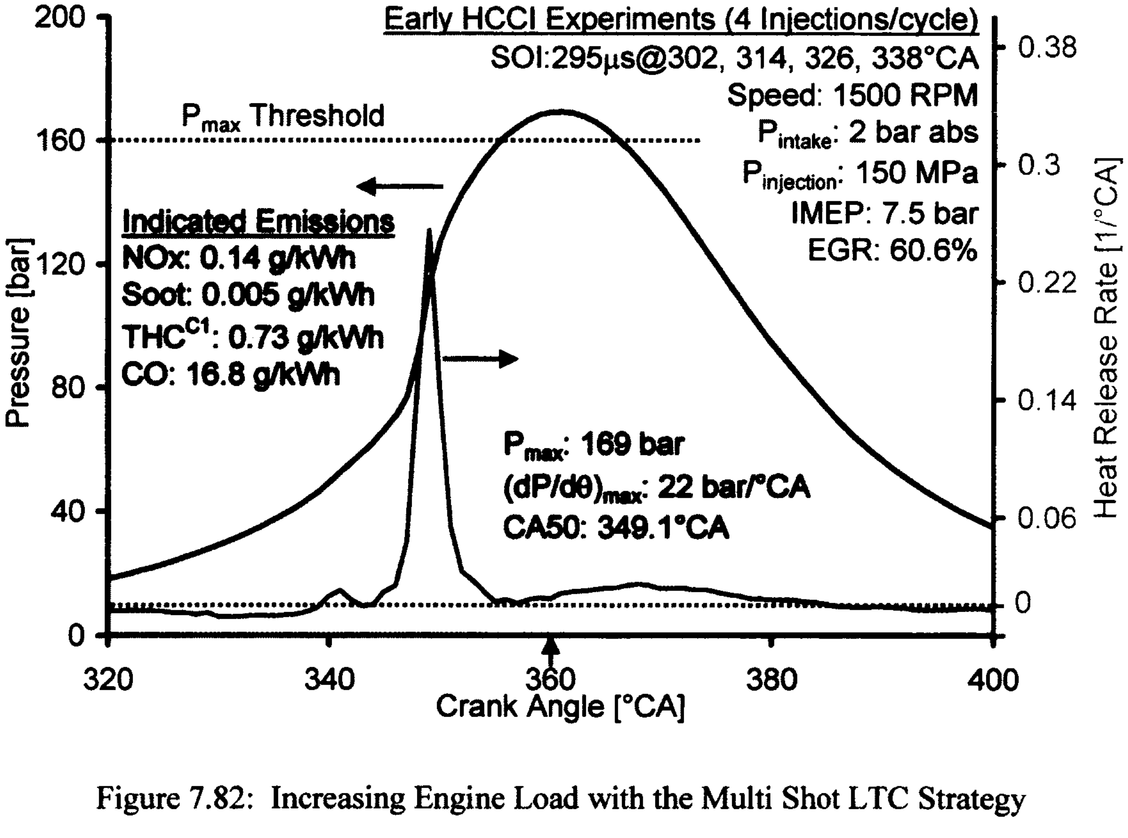

Figure 7.82: Increasing Engine Load with the Multi Shot LTC Strategy

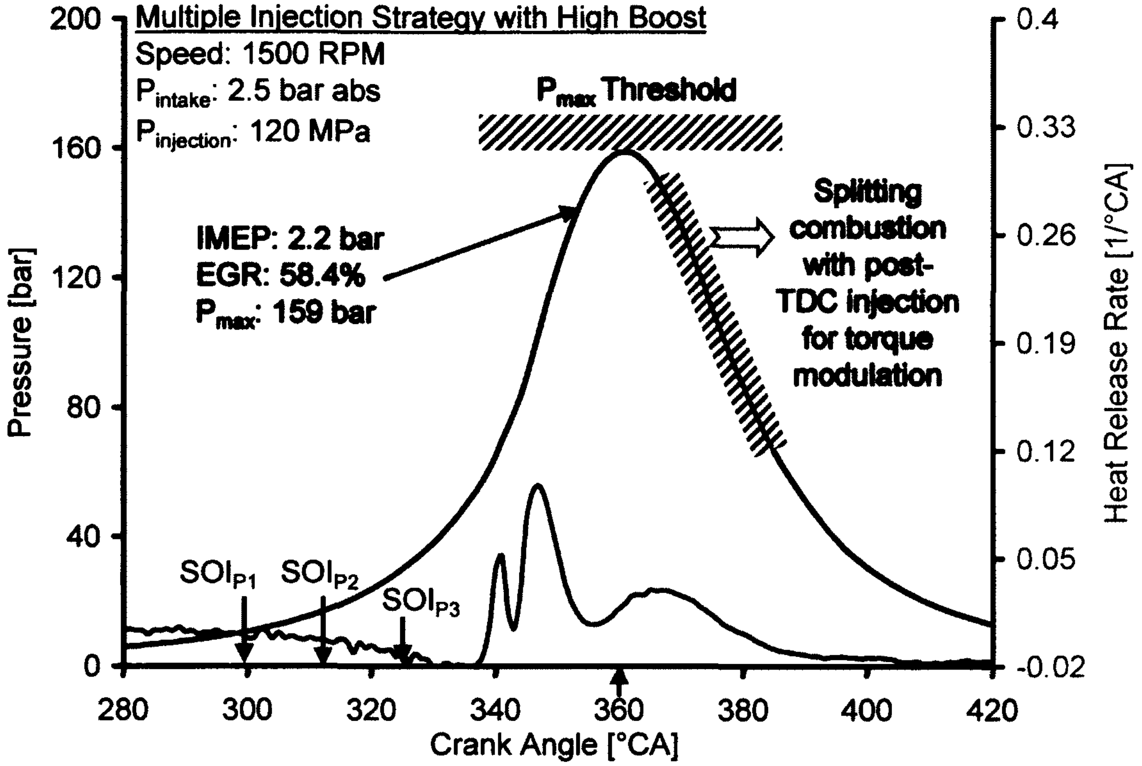

Figure 7.83: Strategy to Increase the LTC Load Level for High CR Diesel Engines

7.11. Implementation of Split Burning LTC (Test # 7)

Engine tests were conducted for the split burning LTC. A comparison of the early-HCCI and split burning strategy was first performed at a relatively moderate baseline load of 5 bar IMEP. The split burning LTC was then enabled to exceed the early-HCCI load and the impact on the emissions and the combustion characteristics was analyzed. The timing and the injection durations for all the tests are marked on the figures. The results for the comparison are shown in Figure 7.84.

The contribution of the early HCCI combustion phase of the split burning LTC produced an IMEP of 3.8 Bar. The post-TDC injection was the enabled to increase the engine load to 5.9 bar IMEP. It was observed that the peak cylinder pressure was significantly reduced even at a higher engine load because of the leaner HCCI phase of the split burning. LTC and also resulted in an improvement in the CA50 from 350.1°CA to 352.1°CA. With the post burning enabled, the overall combustion phasing was moved towards TDC, as a result of the late combustion phase (Figure 7.85).

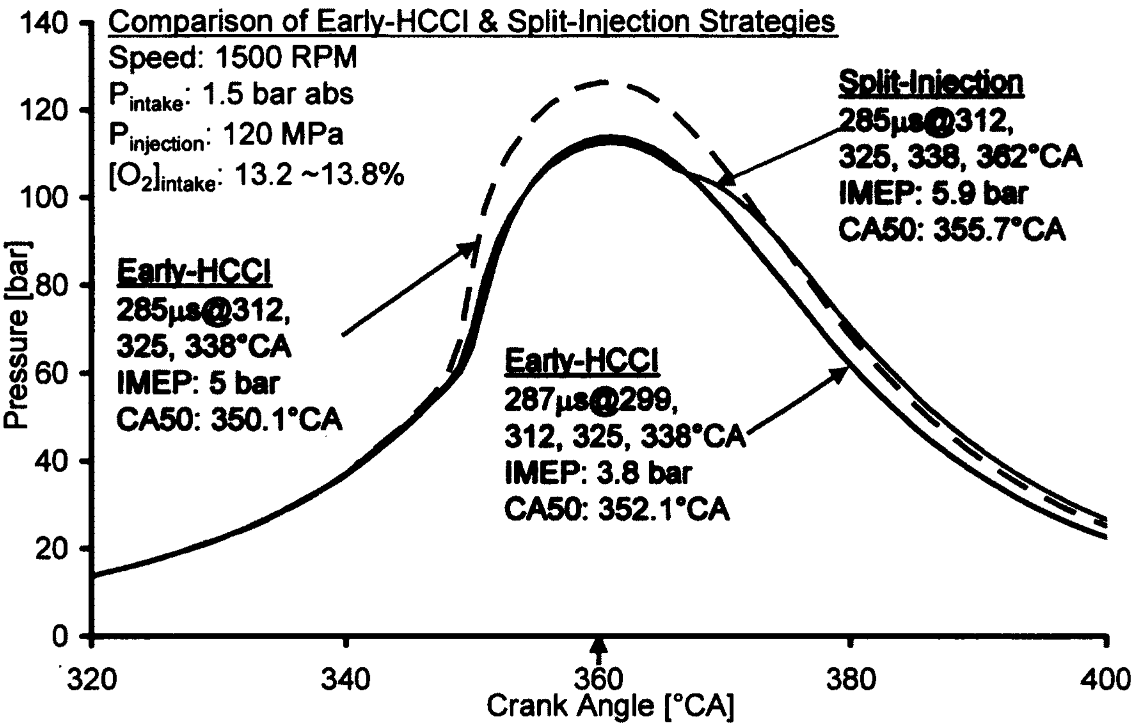

Figure 7.84: Implementation of Split Burning LTC (5.9 bar IMEP – Test # 7)

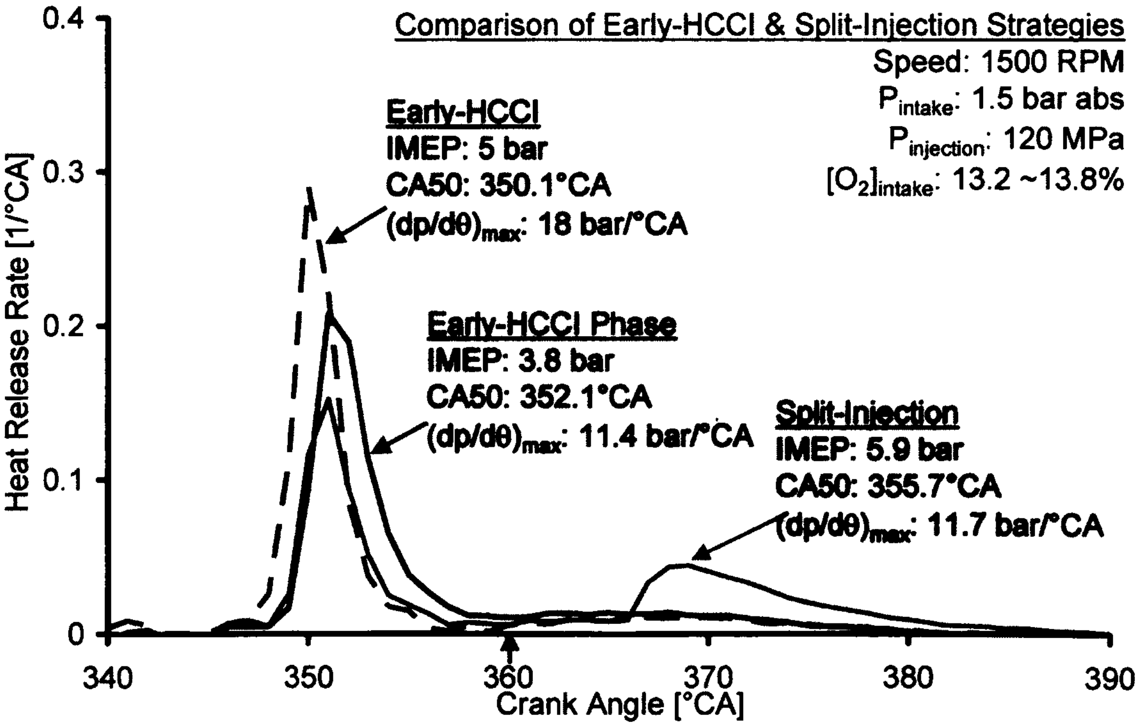

Figure 7.85: Heat Release Rates for the Split Burning LTC (5.9 bar IMEP- Test # 7)

The performance comparison between the early HCCI and the split burning LTC is given in Table 7.14. It must be mentioned here that the split burning LTC had a higher load compared to the early HCCI test. The split burning LTC had higher combustion efficiency (lower HC & CO) despite the higher load. It was observed that the post-TDC combustion helped to oxidize the CO & HC and therefore improve the efficiency. However, the late burning during the expansion stroke also resulted in a significant rise in the soot. The smoke number corresponding to 0.16 g/kWh for the split combustion was 1.9. Although this is much higher than the targeted soot limit of 0.01g/kWh, nonetheless, it was still below the DPF-tolerant soot level of ~2.5 FSN [153]. The DPF-tolerant soot is a new terminology being used in the industry to allow for more aggressive combustion technologies to reduce the NOx below the regulated level since the aftertreatment of NOx is considered more challenging than the soot aftertreatment. Therefore, for the split burning strategy, the DPF-tolerant soot level of 2.5 FSN was taken as an alternate target as long as the NOx target was being met.

Table 7.14: Performance Comparison for Split Burning LTC (Test # 7)

Parameter	Early HCCI LTC	Split Burning LTC
IMEP [bar]	5	5.9
NOx [g/kWh]	0.3	0.18
Intake O_2 [%]	13.2	13.8
Indicated Thermal Efficiency [%]	38.9	39.6
Soot [g/kWh]	0.001	0.16
CO [ppm]	2240	1849
THC [g/kWh]	1.11	0.63
Combustion Efficiency [%]	98.4	98.8
P_{max} [bar]	125.7	112.6
$(dp/d\theta)_{max}$ [bar]	18	11.7
COV P_{max} [%]	1.21	1.82
COV IMEP [%]	3.5	4.6

The split injection LTC was then tested to extend the load limit of the LTC cycles. The results of one such test is shown in Figure 7.86. The target IMEP was 8 bar IMEP and the injection scheduling comprised of 4 early injections to produce an HCCI-type early combustion while a single injection at TDC was configured for the post-TDC combustion. The other engine operating conditions are given in the figure. The use of a higher boost (1.95 bar abs) with a moderate injection pressure (120 MPa) allowed the NOx target (0.15 g/kWh) to be easily exceeded. The soot was also 1.49 FSN, within the DPF-tolerant soot range. The CO and HC were low, compared to the single-shot LTC results (Figure 7.37 & Table 7.7). The maximum cylinder pressure and the maximum rate of pressure rise were also lower than the results obtained with the early HCCI combustion tests (Table 7.9). The combustion efficiency was 98% and the indicated thermal efficiency was 40.9%. Although the combustion efficiency was low, the combustion phasing was nearly at TDC; therefore the gain due to the combustion phasing versus the HC & CO emissions resulted in an indicated thermal efficiency above 40%.

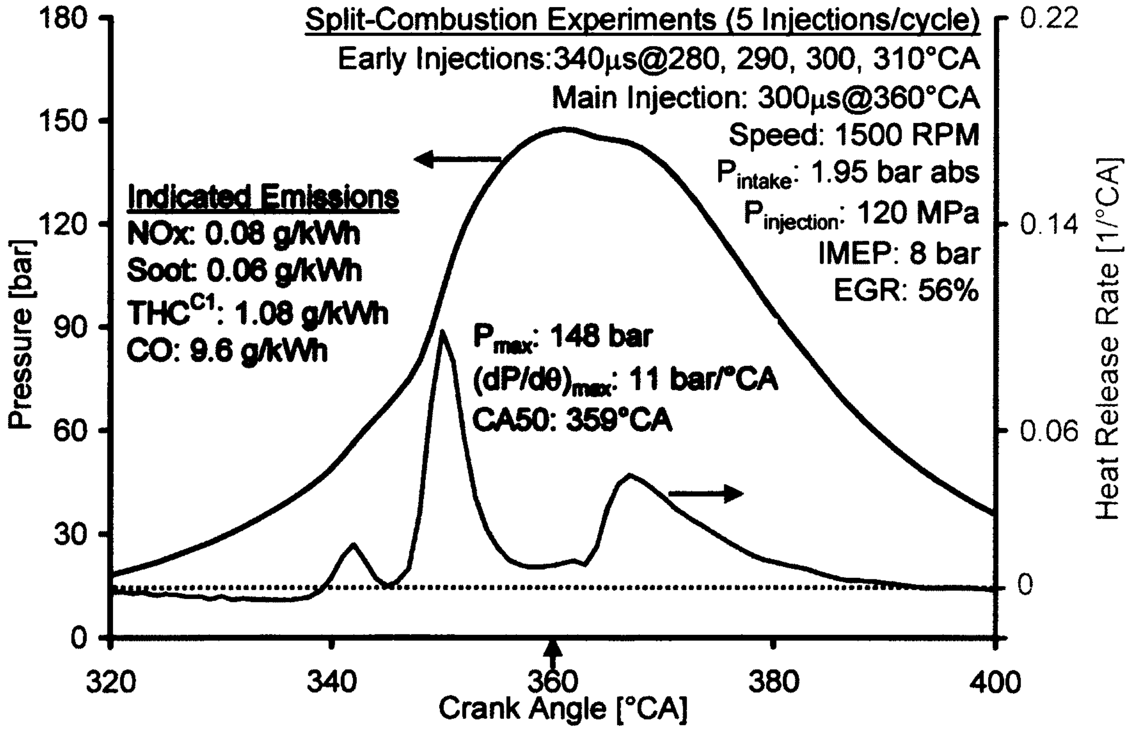

Figure 7.86: Split Burning LTC (8 bar IMEP – Test # 7)

It was then attempted to increase the load level to ~10 bar IMEP with the same engine operating conditions as for the 8 bar IMEP test. The NOx emission was pushed below the limit but the smoke was very high (~4 FSN) and the HC emission also exceeded 4 g/kWh). Therefore, the boost pressure was increased slightly to 2 bar abs and the injection pressure was increased to 150 MPa compared to the 8 bar IMEP test. The fuel injection scheduling and the injection pulse widths are marked in the figure. The results of the test are shown in Figure 7.87.

An IMEP was 9.7 bar was attained for this test. The NOx was 0.06 g/KWh and satisfied the target limit of 0.15 g/kWh. The smoke was 2.8 FSN, close to the DPF-tolerant soot limit. The HC and the CO were high which resulted in a combustion efficiency of 96.1 %. Since the load was high, an indicated thermal efficiency of 38.6% was still achieved. A higher boost could have helped to reduce the CO & HC penalty while reducing the soot as well, but was limited by the peak cylinder pressure which was close to 170 bar.

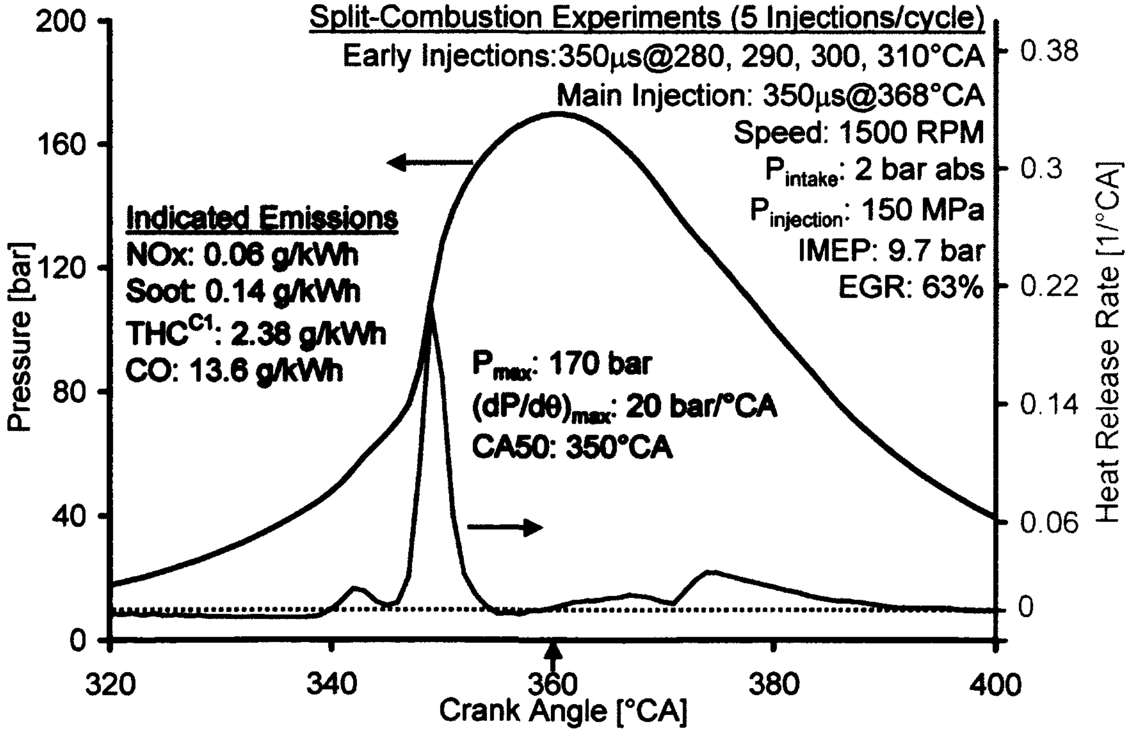

Figure 7.87: Split Burning LTC (9.7 bar IMEP –Test # 7)

7.12. Diesel LTC Load Management

Based upon the above results and analysis, the load management of the LTC cycles was devised as follows:

7.12.1. EGR Enabled Single-Shot LTC

The mode of EGR enabled LTC is suitable for low load operations, in which a single shot of fuel is delivered close to the end of cylinder compression, i.e. TDC. The heat release phasing is fully controllable via injection timing and thus high energy efficiency is attainable. The implementation of the single shot LTC mode with heavy EGR is straight forward and can be achieved as long as sufficient boost pressure and high injection pressure can be attained. The test results indicated that for high compression ratio diesel engines like the Ford engine used in this work, the single-injection LTC should be limited to ~4 bar IMEP.

7.12.2. Multi-Shot LTC (Early HCCI)

The mode of early injection HCCI is suitable for mid load operations (4 to 7 bar IMEP), in which the fuel is delivered in multiple events and by milliseconds prior to TDC, and thus the heat release phasing is not directly controllable. The combustion phasing is largely decoupled from the injection timing and is controlled by chemical kinetics and modulation of the charge temperature history. EGR is usually applied to suppress premature ignition and combustion noise.

7.12.3. Split Burning LTC

The mode of split burning LTC is suitable for high load operations (greater than 7 bar IMEP), in which a partial amount of fuel is delivered to produce HCCI combustion and the remaining for post-TDC late combustion. The latter may benefit from the virtual EGR produced by the prior HCCI burning and timed to best eliminate combustibles and raise power output.

This strategy can further be integrated to account for the full range of engine load as summarized in Figure 7.88. As the load requirements change, there is a need to switch between diesel and LTC combustion modes for maintaining emissions below the desired levels which can be implemented with different EGR strategies. For example, idle and full load operations can be enabled with conventional diesel operation and high amounts of EGR. For low to high loads, LTC cycles can be employed using the strategies outlined above.

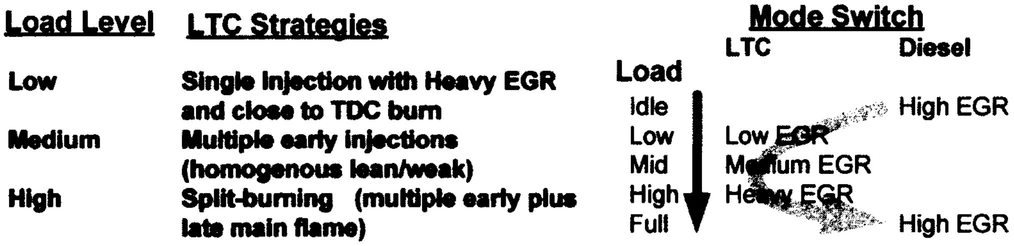

Figure 7.88: Diesel LTC Load Management

7.13. Conclusions

For high compression ratio diesel engines such as the Ford engine used in this work, the attainment of ~10 bar IMEP during the LTC cycles has not been previously demonstrated in the literature without the use of advanced engines technologies. Such advanced technologies include the variable valve timing (VVT), variable compression ratio (VCR) and dual-loop EGR with DOC, to name a few. One of the objectives of this research was to extend the LTC load level for the high compression diesel engines which was successfully demonstrated.

The fundamental criteria for achieving the low temperature combustion is the separation of the fuel injection events from the combustion to provide sufficient time for fuel-air mixing and the preparation of a cylinder charge of high homogeneity. Three strategies to improve the charge homogeneity were investigated. The empirical and analytical work presented in this chapter can be summarized as follows:

- Single-shot LTC: The single-shot LTC was enabled with heavy EGR to realize ultra low NOx and soot emissions at low loads (3~5 bar).

- The efficacy of boost, EGR and injection pressure was demonstrated in enabling this mode of combustion and also to reduce the CO and HC emissions that otherwise deteriorate the combustion efficiency.

- A higher injection pressure reduces soot emissions across the EGR range but the effect of boost on the soot reduction is significant only at higher soot levels. Moreover, the peak soot values are observed to shift towards lower intake [O_2] values.

- NOx reduces monotonically with increasing EGR. NOx shows a higher sensitivity to the injection pressure than the boost at low EGR ratios. Moreover, at high EGR levels, although the NOx appears to be virtually grounded, the effect of injection pressure is still discernible.

- An intake oxygen concentration less than 14% was generally found to reduce NOx to very low levels and an intake oxygen of 8~11% was found necessary for achieving simultaneous low-NOx and low-soot combustion.

- The onset of the simultaneous low-NOx and low-soot combustion is preceded by a significant increase in the un-burnt hydrocarbons and carbon monoxide. In general, CO rises with heavy EGR because of reduced oxygen availability (11~14%) and is largely attributed to the NOx-Soot trade-off. THC is more sensitive to the lowered combustion temperature and the further reduced oxygen concentration (8~12%) with heavy EGR.

- The effect of higher injection pressure or boost in combination with higher EGR was shown to be capable of reducing the HC and CO emissions, and therefore mitigate the efficiency loss.

- The single-shot LTC at moderate engine loads (up to 8 bar IMEP) incurs a very high CO and HC penalty and the ultra low soot levels are difficulty to attain.

- At higher engine speeds, the HC and CO penalty tends to rise rapidly and therefore, the attainable load level would reduce significantly.

- Multi-shot (early HCCI) LTC: For this strategy a diluted homogeneous cylinder of high homogeneity charge was prepared prior to the combustion with the implementation of precisely timed multi-pulse fuel-injection events early during the compression stroke and a heavy use of EGR.
    - A criterion for the earliest injection timing was presented based on the fuel boiling characteristics and the phenomenological spray penetration model to minimize spray wall-impingement and therefore reduce the HC emissions.
    - The effect of the injection on the combustion efficiency was empirically demonstrated to emphasize the correct selection of the injection pressure. A lower injection pressure resulted in an HC and CO rise, with the CO rising more rapidly than HC (reduced homogeneity). A higher injection pressure, on the other hand, caused a higher rise in the HC compared to the CO (higher propensity for wall wetting).
    - The effect of the combustion off-phasing from the best efficiency crank-angle window was quantified in terms of equivalent exhaust HC. A trade-off between the contribution of the off-phasing and the exhaust combustibles to the cycle efficiency penalty was analytically calculated and empirically demonstrated.
    - This combustion mode was largely applicable to mid-load engine operating conditions and was realized up to 7.5 bar IMEP with ultra low NOx and soot emissions with a low HC penalty.
    - The load range of this strategy was primarily limited by the high compression ratio that resulted in very high peak cylinder pressures, exceeding 160 bar and also very high maximum rate of pressure rise (>20 bar).
    - At higher engine speed, the multi-shot strategy was demonstrated to achieve ultra low NOx and soot, with a moderate CO and HC penalty.

- Split Burning LTC: This strategy consisted of delivering a part of the fuel early in the compression stroke to prepare a cylinder charge of high homogeneity that underwent an HCCI type of combustion earlier than TDC. The remaining fuel was delivered close to the top-dead-centre (usually after the end of the first heat-release) to produce a post-TDC combustion that was primarily used to increase the engine load. This part of fuel had a short ignition delay and had combustion characteristics similar to the conventional combustion.
    - The splitting of the heat release helped to reduce the peak cylinder pressure and the maximum rate of pressure rise associated with the multi-shot LTC. The containment of the pressure levels enabled the load level to be increased up to 9.7 bar IMEP.
    - The post-TDC part of the combustion helps to destroy the carbon-monoxide and hydrocarbons produced earlier in the cycle, thereby improving the combustion efficiency. The late combustion also tends to benefit from the virtual EGR produced during the first part of the combustion, thus maintaining the low NOx without significant EGR addition.
    - Ultra low soot is not attainable at high loads because of the conventional burn of the near-TDC injection. The smoke readings were >2 FSN An alternate DPF-tolerant soot limit of 2.5 FSN was used as the criteria.

Based on the efficiency comparisons, analyses and test results, the major characteristics of the LTC strategies and the applicable load ranges are summarized in Table 7.15.

Table 7.15: Major Characteristics of LTC Strategies

	Strategy		
	Single-Shot LTC	Early HCCI LTC	Split Burning LTC
Demonstrated Load Range	3.1 to 7.2 bar IMEP	3.1 to 7.5 bar IMEP	5.9 to 9.7 bar IMEP
Suitable Load Range	Up to 4 bar IMEP	4 to 7 bar IMEP	> 7 bar IMEP
CO & HC Penalty	Moderate to high	Low to moderate	Moderate to high
Phasing Penalty	No	High	Low
EGR	Heavy	High	Moderate
Phasing Control	Direct SOI Control	No	Yes, for Post-TDC Combustion only
Limiting Conditions	High CO & HC, Peak Soot Level	P_{max} (>160 bar), $(dp/d\theta)_{max}$ (> 20 bar/°CA)	P_{max} (>160 bar), High Soot, CO & HC
NOx	<0.15 g/kWh	<0.15 g/kWh	<0.15 g/kWh
Soot	Low (<0.01 g/kWh), Boost & injection pressure to suppress peak soot levels	Ultra Low <0.005 g/kWh	DPF-tolerant < 2.5 FSN

CHAPTER VIII

8. CONTROL OF DIESEL LOW TEMPERATURE COMBUSTION

The implementation of LTC modes is challenged by the higher cycle-to-cycle variation of heavy EGR operation and the narrower combustion mode corridors. The EGR-induced prolonged ignition delay is largely associated with the cyclic variations that deteriorate the combustion efficiency which, in turn, causes fluctuations in the combustion products. While the transition from the HTC to the LTC regime is relatively easier to implement, maintaining of stable engine operation for LTC is generally less feasible. The LTC combustion is sensitive to small variations (or drift) in the EGR (Figure 6.1) with the result that a tight control on the various operating parameters is essentially required. For the single-injection test results, the LTC cycles were prevented from entering the zones of high instability by manually adjusting the combustion phasing through SOI modification to keep the phasing within the crank angle window (5~10°CA) for best efficiency. It was therefore desirable to devise and implement an automatic LTC combustion control strategy using a suitable feedback for cycle-by-cycle or if possible, within-the-same-cycle control. The details of the control methodology and the system development are first presented, followed by the actual control test results.

8.1. Prerequisites for the Combustion Control System

This section describes the work done to realize the implementation of the control strategies.

8.1.1. Pressure-Data Smoothing Techniques

The filtering or smoothing of the pressure data is essential for a stable and robust feedback. A disturbance in the pressure signal can be due to the pressure sensor not flush-mounted with the cylinder head or electrical noise interfering with the signal. Any extraneous noise in the pressure signal must not affect the stability of the control system. The preferred way to prevent such a scenario is to remove or reduce any noise from the pressure signal before it reaches the controller. Therefore, a data smoothing algorithm which was simple enough to be implemented in the FPGA but effective enough to remove sharp spikes in the data was devised and implemented as explained below.

8.1.1.1. Smart Smoothing Algorithms

A sharp spike in the pressure data can be mistaken for the maximum rate of pressure rise which would render the control system susceptible to over- or under-compensate the control action, thereby resulting in unstable behaviour. To identify and remove such a sharp spike, a smart algorithm was devised.

The sequence of events in a 4-point window for detection of a spike is shown in Figure 8.1. As indicated in the left window, points 2 and 3 are both above the set threshold. The algorithm checks the second last point (Point # 3) against both Points # 1 & # 4 to see if it is above a certain threshold value. If so, it is replaced by the average of the two end points (i.e. 1 and 4). As the data passes through this 4-point window, it is corrected if the value lies outside the limits set due to the noise.

A major advantage of this algorithm is that it introduces a fixed delay in the pressure data, 0.2°CA in the case of a 4-point window. As long as the delay is fixed and known, the control action can be suitably adjusted to account for such a delay.

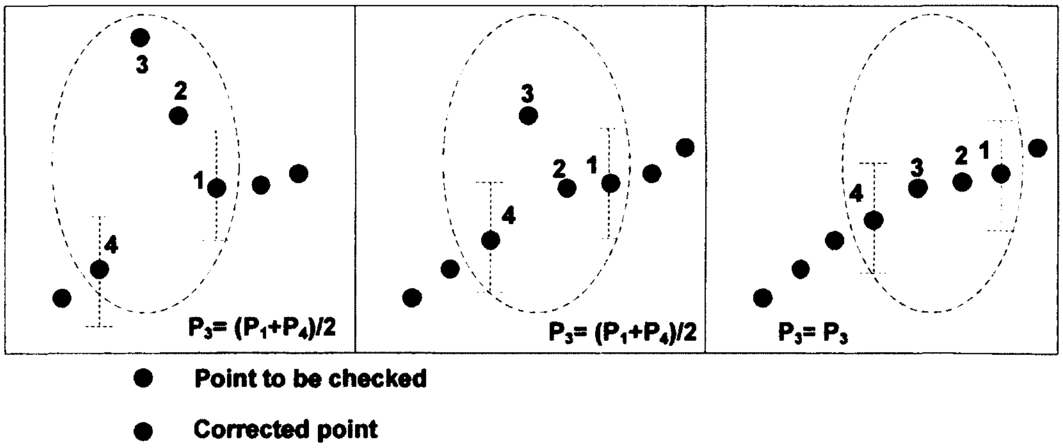

Figure 8.1: Smart Smoothing Algorithm

The size of the window can be selected based on the maximum width of the spike that is anticipated. An example of the algorithm application is shown in Figure 8.2. With a 4-point window, a spike up to 2 points wide is detected and removed. However, a 3-point wide spike is reduced in amplitude but is not totally eliminated. Therefore, the size of the analysis window must be 2-point greater than the maximum width of the anticipated noise. In this work, a 5-point window was used to filter the pressure data.

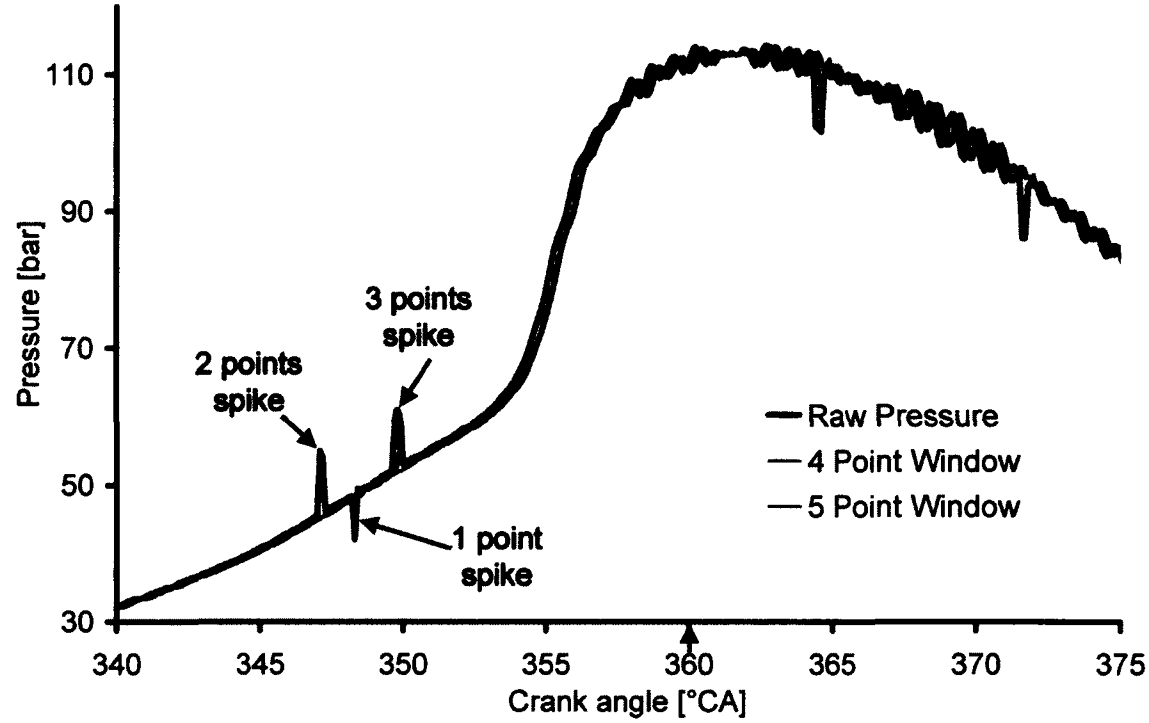

Figure 8.2: Application of Smart Smoothing Algorithm

8.1.1.2. Crank Angle Resolution

The LTC cycles for diesel engines are bounded within narrow operating pathways where the excursions are sharply punished by the deteriorations in exhaust emissions, fuel efficiency, combustion noise, and operational stability. To enable accurate control on the LTC cycles, the feedback on the combustion phasing must be accurate and be able to account for small changes. The crank angle resolution of the cylinder pressure data is therefore critical for improving the quality of the control system. To high light this aspect, the cylinder pressure for an engine test with 0.1°CA resolution is shown in Figure 8.3. The data was also reduced to 1°CA resolution by extracting every 10 data point to simulate a 1°CA resolution encoder. The heat release rates were calculated and have also been plotted in the figure.

It can be observed that the heat release is defined by 6 data points for the 1°CA resolution compared to the 60 data points for the heat release calculated from the 0.1°CA resolved pressure. The 1°CA resolution data assumes a linear fit between the points which can introduce errors in the calculation of the combustion phasing as shown in Figure 8.4.

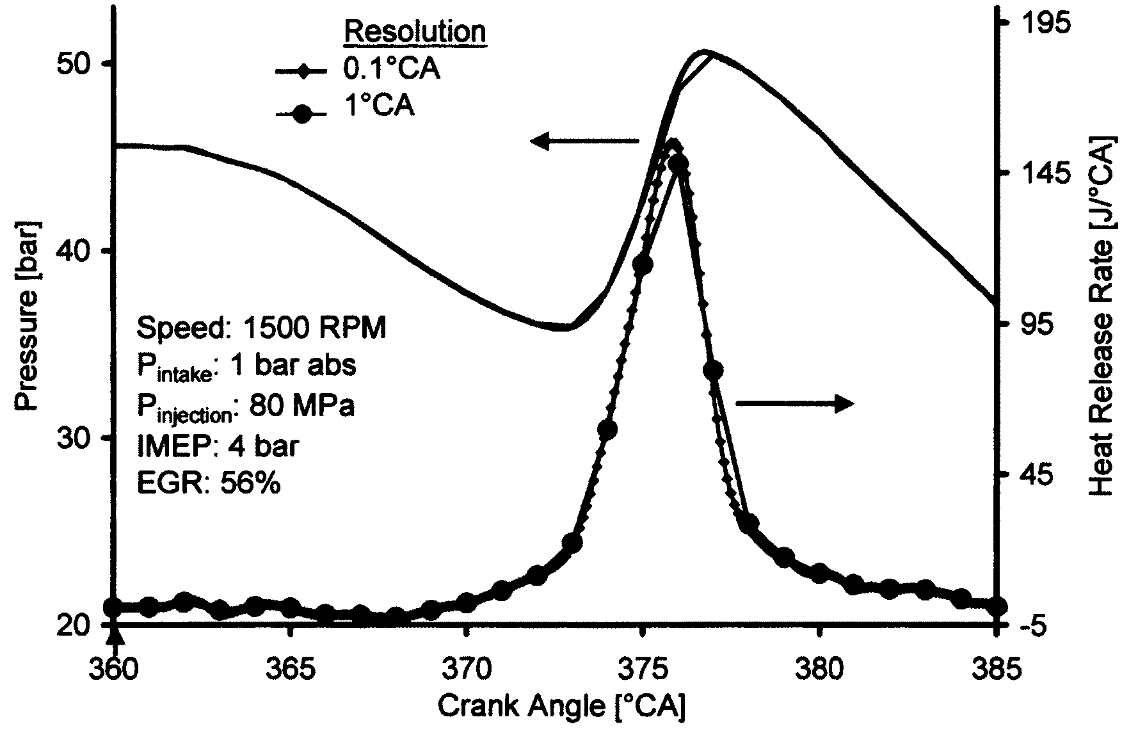

Figure 8.3: Effect of Crank Angle Resolution on Cylinder Pressure based Feedback

The reduced resolution of the cylinder pressure data resulted in an error of 0.5°CA in the prediction of the CA50. Although this might seem trivial in the normal analysis of the data, but for LTC control, half a degree crank angle error in the SOI adjustment can result in mis-fire since the LTC cycles are inherently close to the flame-out limits. Therefore, for all the control work, a resolution of 0.1°CA for the pressure data was employed and the estimation of the combustion parameters (explained in the next section) was done in the FPGA-RT systems with 0.1°CA resolved data. It is also noted that the results shown in these figures highlight the possibility of getting an erroneous estimate under certain engine operating conditions and the effect of the crank angle resolution may not be significant otherwise.

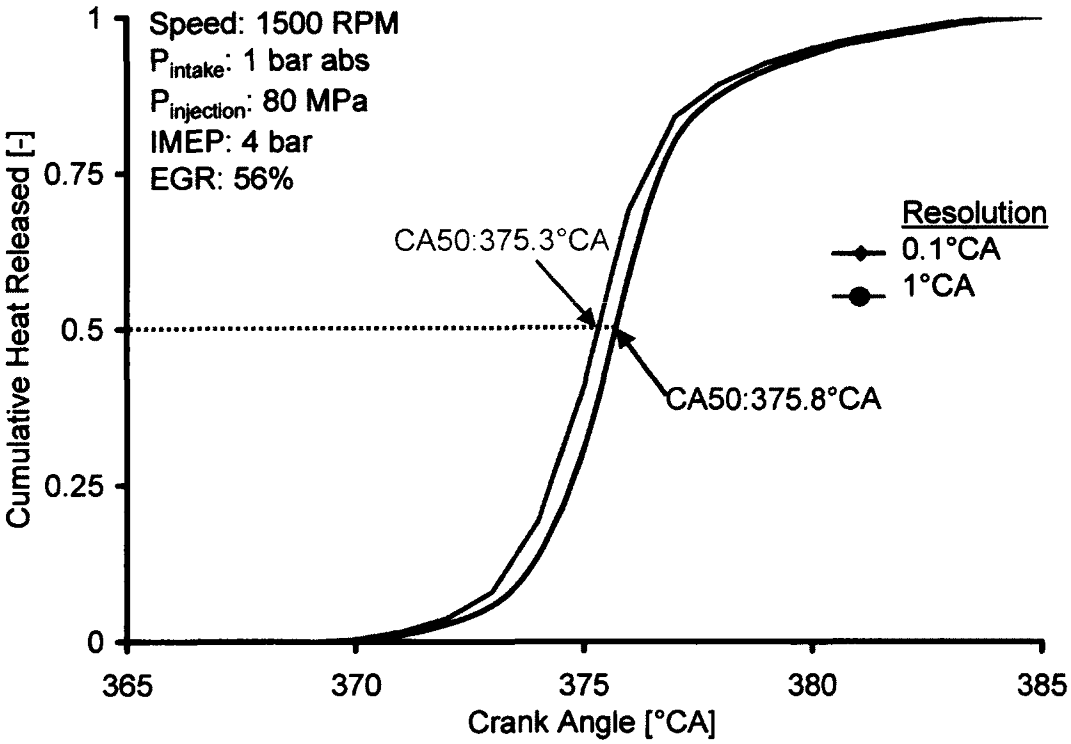

Figure 8.4: Error in CA50 caused by Crank Angle Resolution

8.1.2. Estimation of Combustion Parameters

With a retarded combustion phasing, the peak of the maximum combustion pressure can be lower than the peak motoring pressure. An algorithm programmed to simply detect the amplitude and crank angle of the peak cylinder pressure would detect the peak motoring pressure. If such a parameter is being used as feedback, then this would render the feedback useless for control. As discussed in Chapter 5, if the motoring pressure could be estimated and subtracted from the actual (or fired) pressure, then the resulting trace could be conveniently used to find the desired parameter's amplitude as well as the position. The actual motoring pressure trace estimated in the FPGA according to the procedure detailed in Chapter 5 is shown in Figure 8.5.

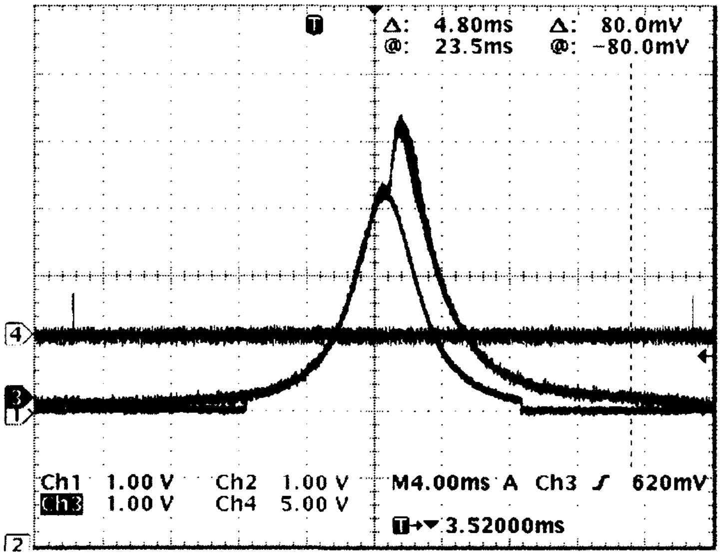

Figure 8.5: Motoring Pressure Estimation in the FPGA

If the peak combustion pressure is lower than the motoring pressure, the detection of the peak combustion pressure is not possible since the peak compression pressure is higher than the actual combustion pressure. The cylinder pressure for a delayed combustion phasing obtained during an injection timing sweep experiment is shown in Figure 8.6. The estimated motoring pressure is also plotted in the figure. The maximum rate of pressure rise for the pressure data is shown in the top part of Figure 8.7. It can be seen that the maximum rate of pressure rise for the combustion is masked by the compression part of the curve.

Since the maximum rate of pressure rise was shown to provide a reasonable estimate of the combustion phasing in Chapter 7, the procedure to determine the location and the amplitude of the maximum rate of pressure rise was programmed in the FPGA (shown in Figure 8.7) as follows:

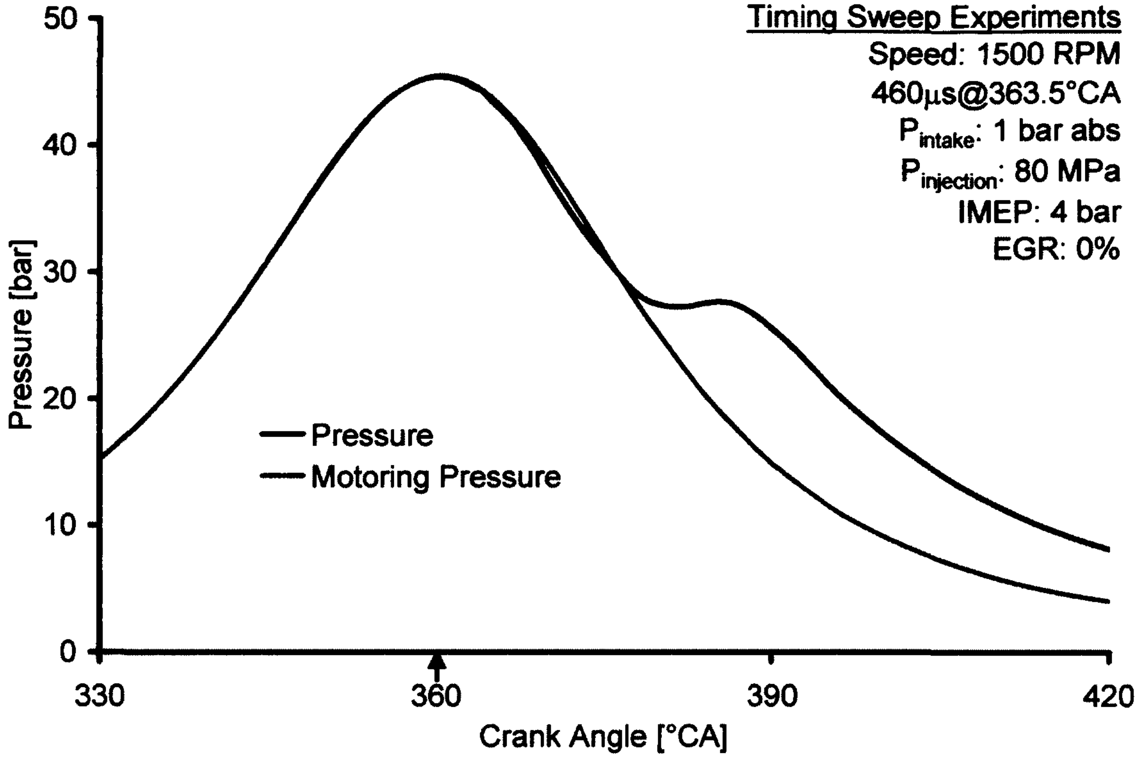

Figure 8.6: Cylinder Pressure for Delayed Combustion Phasing

- The combustion pressure is first obtained by subtracting the motoring pressure from the fired pressure.

$$p_{comb}(\theta) = p(\theta) - p_{mot}(\theta) \tag{8.1}$$

- Next, the rate of change of the generated motoring pressure is calculated:

$$\left(\frac{dp}{d\theta}\right)_{mot} = p_{mot}(\theta) - p_{mot}(\theta - 1) \tag{8.2}$$

- The rate of change of the combustion pressure is calculated in a similar manner. The resulting trace allows the location (or the crank angle) of the maximum rate of pressure rise to be determined as indicated in Figure 8.7.

$$\left(\frac{dp}{d\theta}\right)_{comb} = p_{comb}(\theta) - p_{comb}(\theta - 1) \tag{8.3}$$

- The actual rate of pressure rise is then obtained by adding the motoring rate-of-pressure-rise to the combustion rate-of-pressure-rise. The resulting trace is the actual rate-of-pressure-rise and the amplitude is determined by reading the data corresponding to the identified location of the combustion peak.

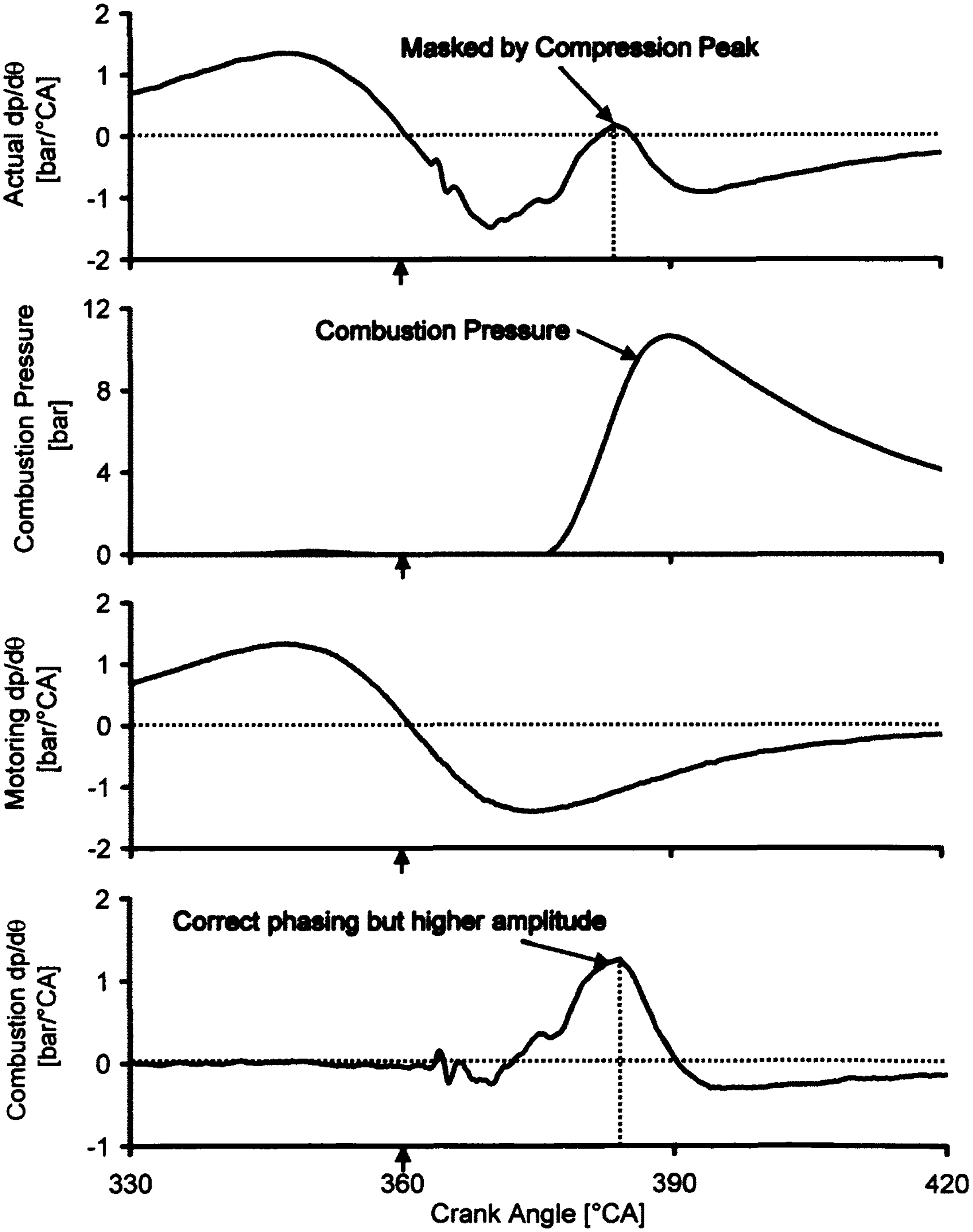

Figure 8.7: Calculation Steps for Estimating the Combustion Parameters

The combustion rate of pressure rise calculated using this procedure in the FPGA during an actual test is shown in Figure 8.8. The value of the maximum rate of pressure rise was only 3.2 bar/°CA in this case which would not be detectable if only the original pressure trace was used.

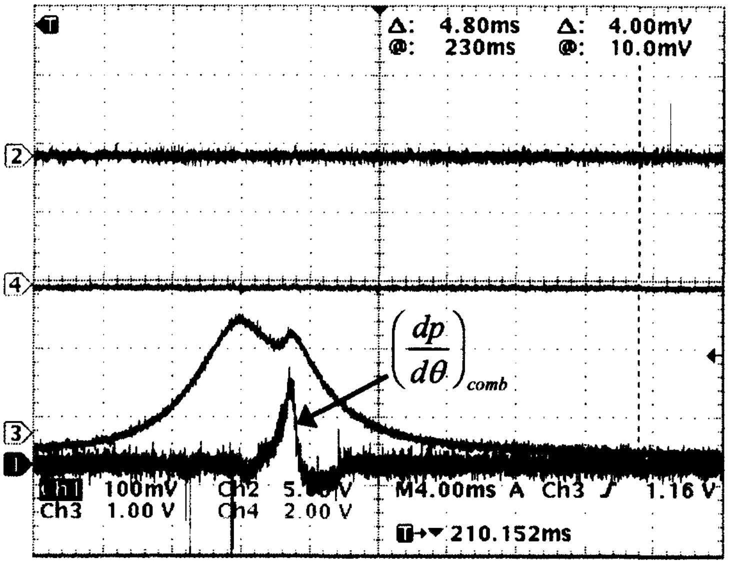

Figure 8.8: Estimation of Fired (Combustion) Parameters in the FPGA

8.1.3. Within Same Cycle IMEP Estimation

To reduce the cycle-to-cycle variations in the combustion that may occur due to either a transient change in the intake boost or the EGR, it was thought necessary to be able to detect that change before the completion of the combustion cycle. To enable adaptive combustion control within the same engine cycle, an IMEP estimation methodology was proposed and devised as follows:

The partial history of IMEP for the previous cycle is tracked along that of the intake and compression strokes for the current cycle as schematically shown in Figure 8.9. The contributions of the previous and the current cycles are further weighted as given by Equations (8.4) and (8.5).

$$IMEP = \left[\frac{\int_{previous} p_{avg} dV}{V_d}\right]_{W_1} + \left[\frac{\int_{current} p_{avg} dV}{V_d}\right]_{W_2} \tag{8.4}$$

and

$$W_1 + W_2 = 1 \quad \& \quad 0.7 \le \frac{W_1}{W_2} \le 1.3 \tag{8.5}$$

where p_{avg} is the average pressure over the crank angle interval (0.1°CA), V_d is the displacement volume (499 cm³ for the single cylinder), W_1 is the weighting factor applied to the previous cycle's contribution to the IMEP, W_2 is the weighting factor applied to the current cycle's contribution to the IMEP, and dV is the rate of change of cylinder volume over the crank angle interval. The dV data for a complete engine cycle was mapped as a function of the crank angle in the distributed RAM of the FPGA.

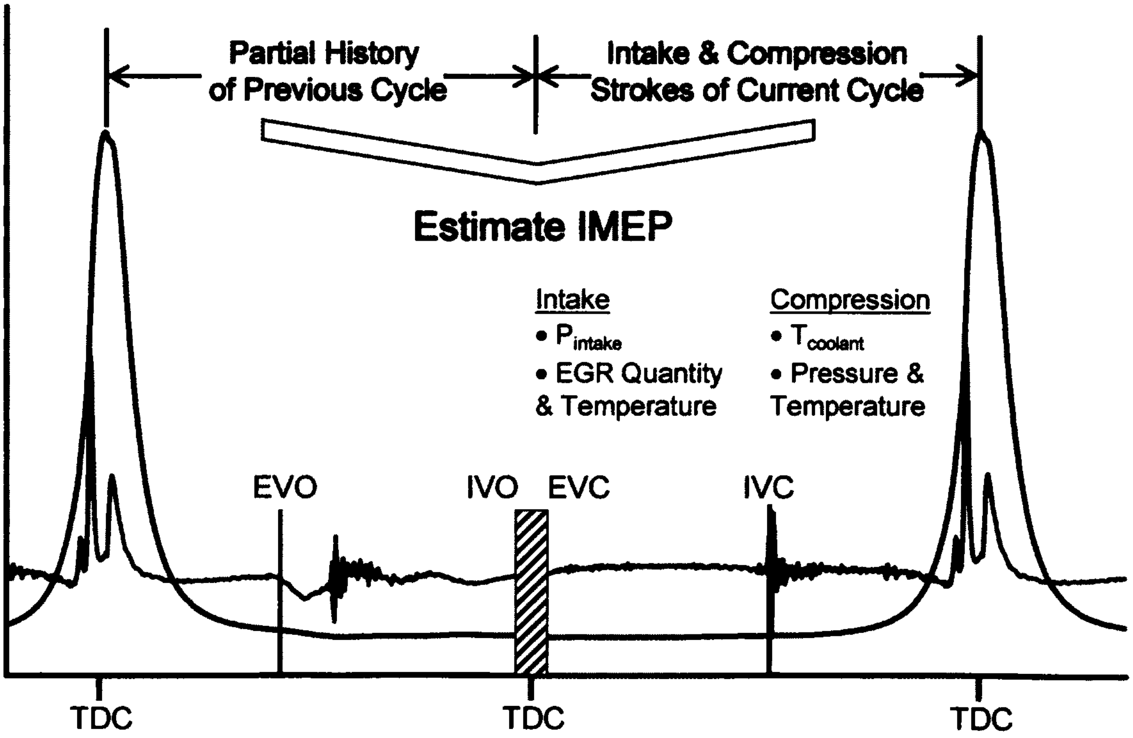

Figure 8.9: IMEP Estimation for Within-Same-Cycle Estimation

The weighting factors decide the crank angle window for which the IMEP estimate is done. The selection of the weighting factors is done by the controller on-the-fly as follows:

- Based on the CA50 of the previous cycle, the starting point of the estimation window is adaptively modified by the controller and the weighting factors are calculated. Two possible scenarios exist:

  a) If the CA50 feedback of the previous cycle occurred before the TDC, a weighting factor proportional to the off-phasing of the CA50 from the TDC is calculated and an IMEP estimation is done promptly near the TDC of the current cycle to check if the targeted IMEP is being met. Therefore, $W_1 \geq W_2$ in this case.

  b) If the CA50 occurred after the TDC of the previous cycle, the controller reduces the weighting factor of the previous cycle such that the IMEP estimation includes the effect of the main combustion event. The crank angle window is therefore shifted after the TDC and $W_1 \leq W_2$ in this case.

- The final IMEP estimate is calculated over the crank angle window (representing one complete cycle) decided by the controller and can be represented by the conventional definition given in Equation (8.6).

$$IMEP = \frac{\oint p_{avg} dV}{V_d} \tag{8.6}$$

If a shortfall in the IMEP estimate exists (due to either a transient change in the intake boost, EGR or the fuelling), a decision to meet the deficiency with post-TDC torque modulation within the same cycle is communicated to the fuel injection controller. The timing of the post-injection is decided by the fuel injection controller based on relevant cylinder pressure characteristics (CA50, P_{max}) and the SOI of the last injection (to ensure separation from the main combustion event) while the pulse-width of the post-injection is decided by a standard PI controller implemented on the FPGA of the combustion characterization system (described in the next section). The corrective action generated by the PI controller is then executed by the fuel injection control system. The tuning of the PI controller was performed along with gain scheduling for different engine operating conditions. A simplified schematic of this process for the case of CA50 occurring before the TDC is shown in Figure 8.10.

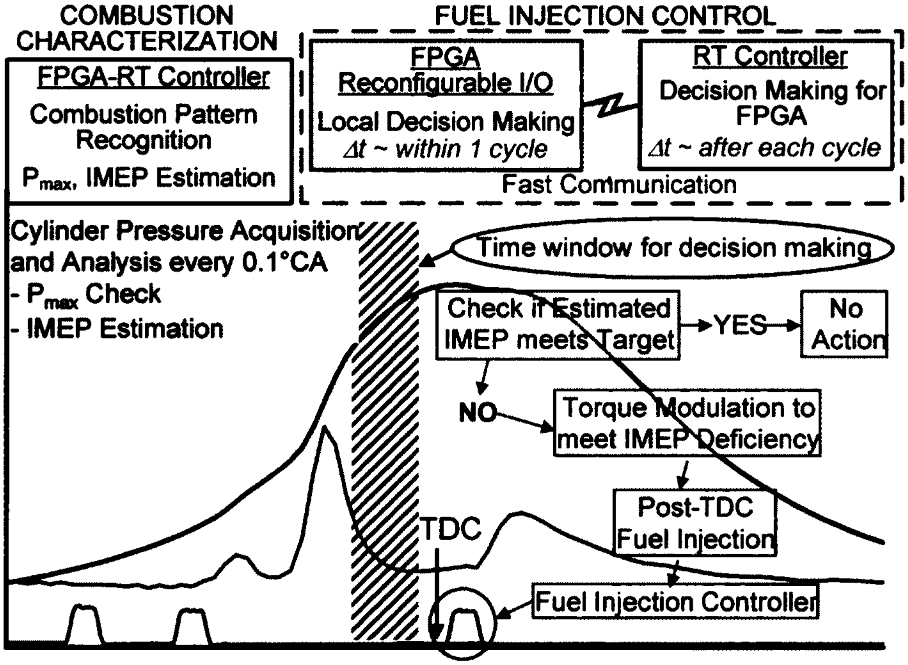

Figure 8.10: Scheme for Adaptive Control within Same Cycle

8.2. Combustion control Platform

Three sets of real-time controllers embedded with FPGA devices were used concurrently to analyze the cylinder pressure data and to generate the necessary control signals for dynamically and precisely commanding the fuel injection strategies as shown in Figure 8.11. The functioning of each of the FPGA/RT system is as follows:

- The 'Fuel Injection' controller can configure up to 6 independent injections/cycle (injection timing, pulse width) and generates a TTL pulse train that serves as the input for the injector power drives. The controller can perform prompt combustion pattern recognition using the maximum cylinder pressure p_{max} or the maximum rate of pressure rise, $(dp/d\theta)_{max}$ as the feedback parameters.

- The 'Combustion Characterization' controller is programmed to provide an estimate of the IMEP for within same-cycle control. The controller also calculates the combustion phasing represented by the CA50 either by using the apparent heat release analysis or the 'Pressure Departure Ratio (PDR)' algorithm for cycle-by-cycle combustion control. The programming and integration of this controller (FPGA #1) was done as a part of this research work.
- The 'System Pre-control' maintains the rail pressure using a PID controller for the Pressure control valve (PCV) and the volume control valve (VCV) of the fuel injection pump. The controller can operate either independently or in collaboration with the fuel injection controller.

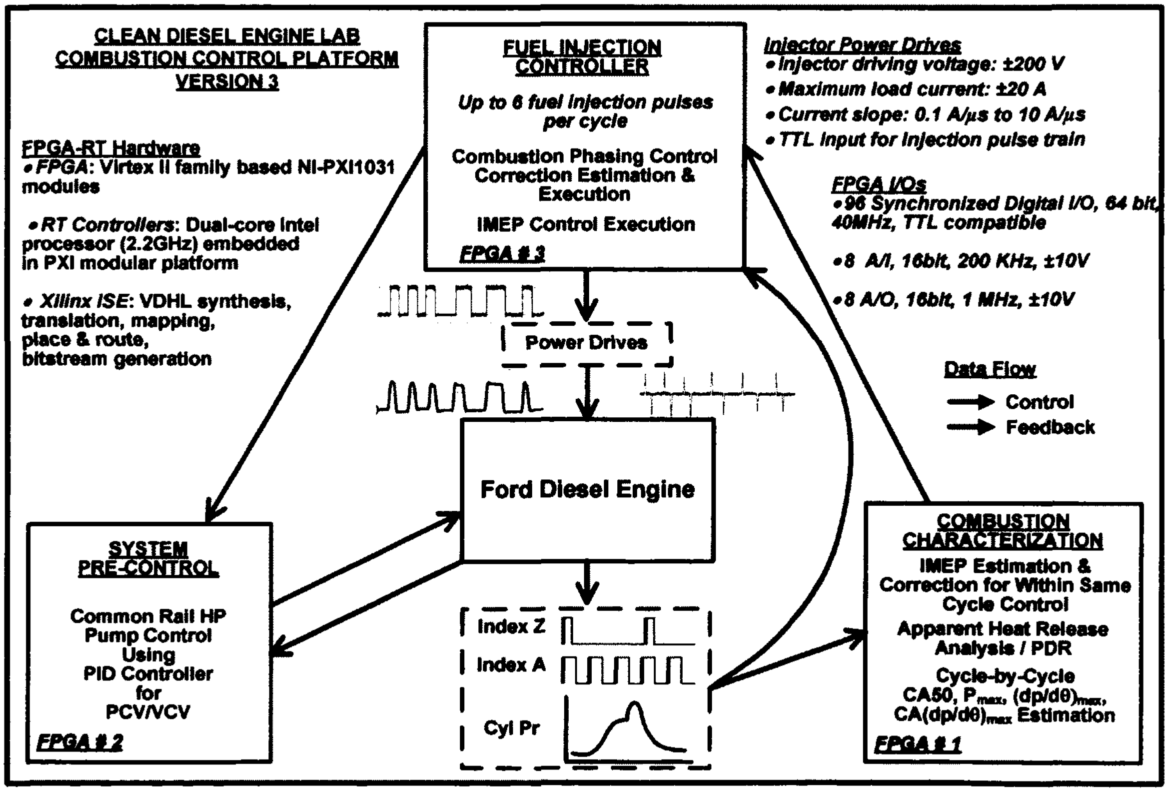

Figure 8.11: CDEL Combustion Control Platform

The data transfer between the FPGA devices is done using the high speed digital/analog channels. The FPGA devices are based on the Virtex-II FPGAs (28,672 LUTs per device) with each slice containing two 4-input LUTs, two flip-flops, wide-function multiplexers, and carry logic.

The injector power drives enable the injector opening/ closing voltages to be adjusted between ±200 V and the current between ±20 A. An RS-485 link is used to program the power drives.

8.3. Adaptive Control Tests

To test and validate the developed adaptive control methodologies, engine tests were done for the single-shot LTC and the results are presented in the following sections.

8.3.1. Within-same-cycle Adaptive Control

Validation tests for within-same-cycle control were conducted at an IMEP setpoint of 4.5 bar. The proportional gain of the controller was set at 8 and the correction generated for the pulse width quantity was limited to ±10μs. This was done to safeguard the engine in case of a sudden change in the injection quantity. The nominal post injection quantity was 250μs. To study the transient response of the control system, the engine speed and boost pressure were rapidly changed from 1000 RPM/1.5 bar abs to 1500/2 and then again to 100/1.5. The results for the adaptive control within the same cycle are shown in Figure 8.12.

It can be seen that a stable IMEP was maintained during the transients. A small spike in the IMEP was noted. It was because of the limited change allowed in the injection pulse-width per cycle. Once the control was switched off and the procedure was repeated, a large deficit (~1 bar) in the IMEP was observed as the engine speed increased to 1500 RPM and the boost increased to 2 bar abs. The variation of the post-injection quantity was calculated by the RT-FPGA controller processing the pressure data and provided to the fuel injection controller for modifying the injection quantities.

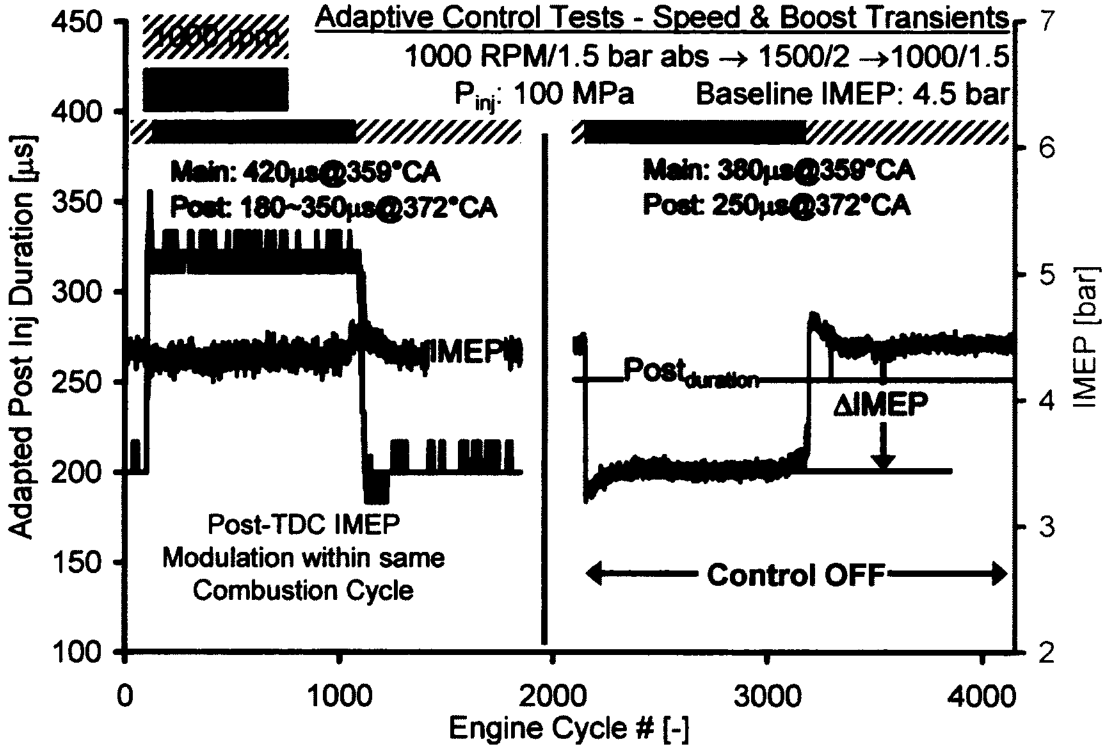

Figure 8.12: Torque Modulation with Post-TDC Injection

Another set of the test data is shown in Figure 8.13. The proportional gain of the controller was increased to 14 and the rate limiter set to ±15μs. The crank angle of the maximum rate of pressure rise was fixed at 365°CA through the combustion characterization controller. The IMEP setpoint was fixed at 6 bar such that the main injection initially produced an IMEP of 3.5 bar and the post injection produced the remaining 2.5 bar IMEP. The EGR was then rapidly increased to push the combustion into the LTC cycles.

Once the combustion had entered the LTC regime, a large change in the setpoint was introduced by suddenly reducing the quantity (commanded pulse width) of the main injection from 400μs to 375μs to observe the response of the post-TDC load modulation. From the results, it is clear that the post-injection quantity was modified by the control system to compensate for the sudden drop in the load. The procedure was repeated again by further decreasing the main injection quantity to 330μs and the control system was able to adequately respond to the load transient.

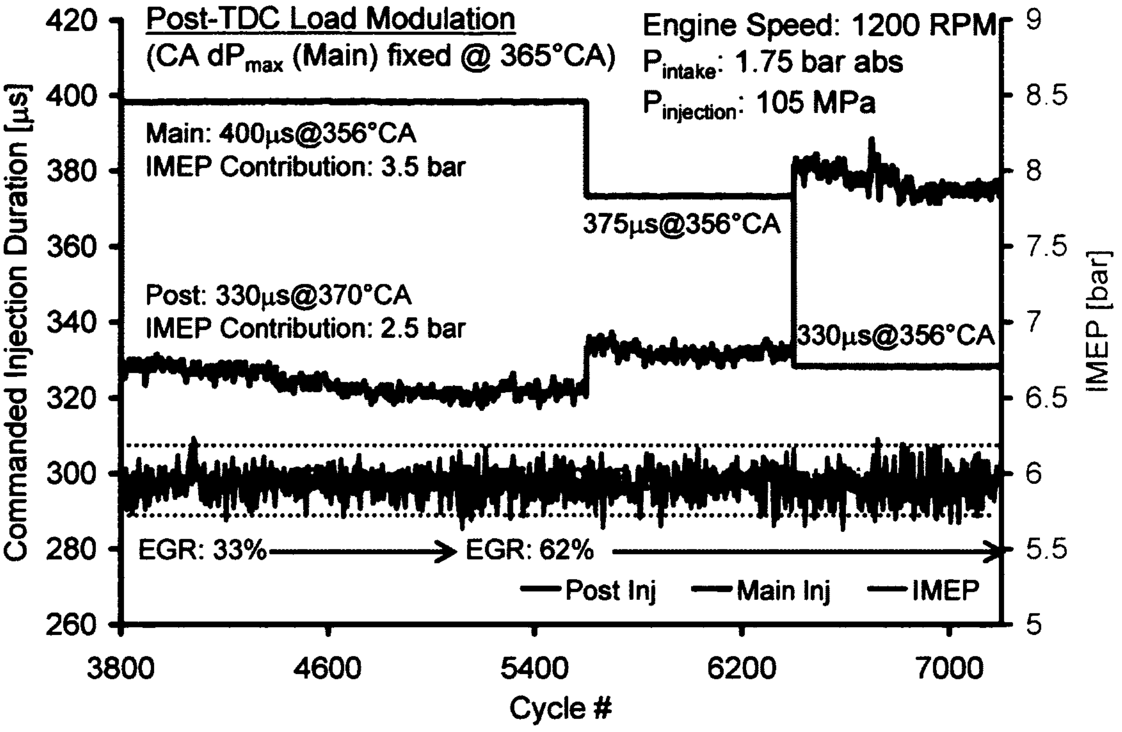

Figure 8.13: Post-TDC Load Modulation with $CA(dP/d\theta)_{\max}$ Control

To confirm if the error (reduction in the main injection quantity) and the control action (increase in the post-TDC injection quantity) were performed within the same cycle, a small section of the data from Figure 8.13 has been plotted in Figure 8.14. It was seen that the control action and the corrective action by the controller were carried out in the same cycle (Cycle # 5601). Moreover, the increased gain of the controller and the relaxation of the injection quantity change within one cycle permitted the control system to compensate for the disturbance with one cycle. The IMEP was retained within ±0.25 bar in this test.

The cylinder pressure and the heat release traces for the data in Figure 8.13 are shown in Figure 8.15. It is evident that the controller effectively locked the phasing of the main heat release event at 365°CA during the transients.

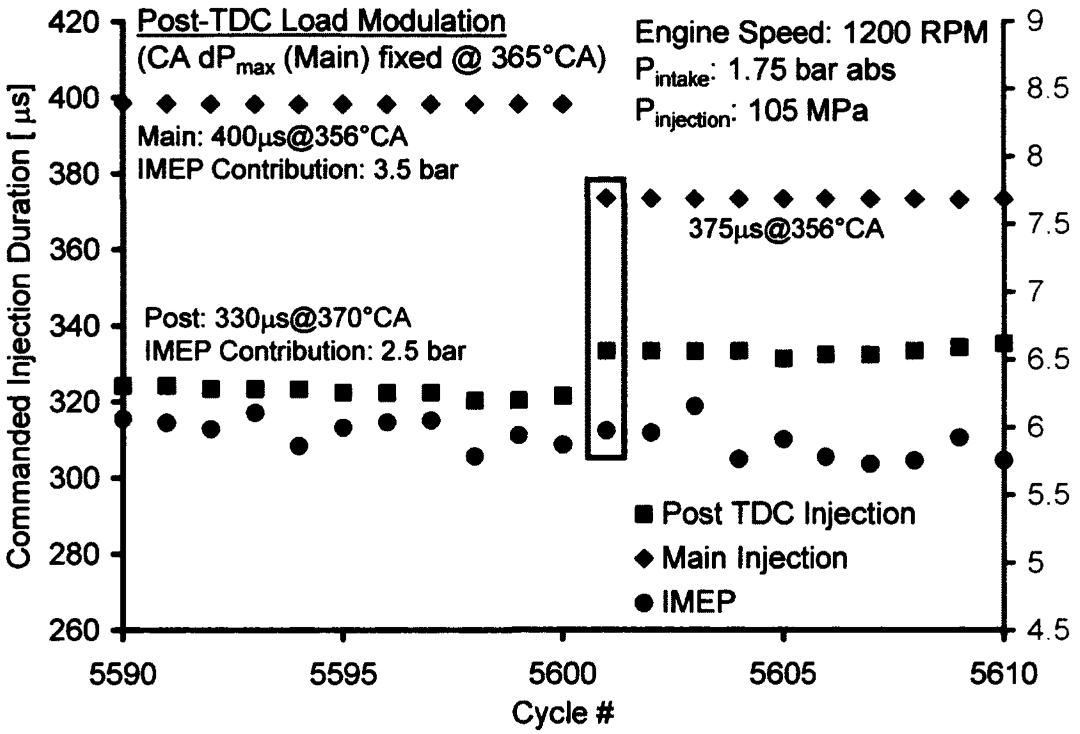

Figure 8.14: Within Same Cycle Control – System Response

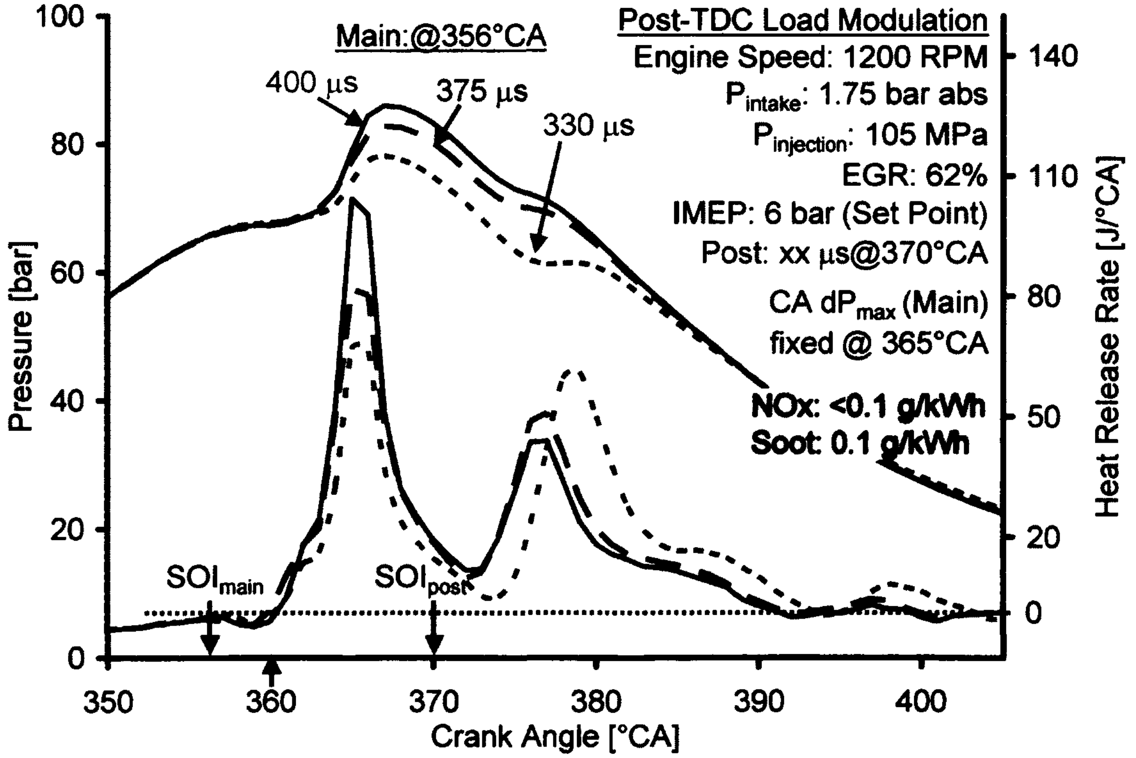

Figure 8.15: Cylinder Pressure and Heat Release Traces for Transients in LTC Mode

The cumulative heat release traces are shown in Figure 8.16. The contribution of the main injection was reduced from 60 to 40% and the post-injection was adjusted on-the-fly by the control system to maintain a constant IMEP. It is pertinent to mention here that the load (IMEP) transients tested during these tests are much larger than those normally encountered during normal engine operation. This was done to test the robustness and the response of the control system. As such, the control system should be able to correct and adjust any minor fluctuation in the load during the normal operation.

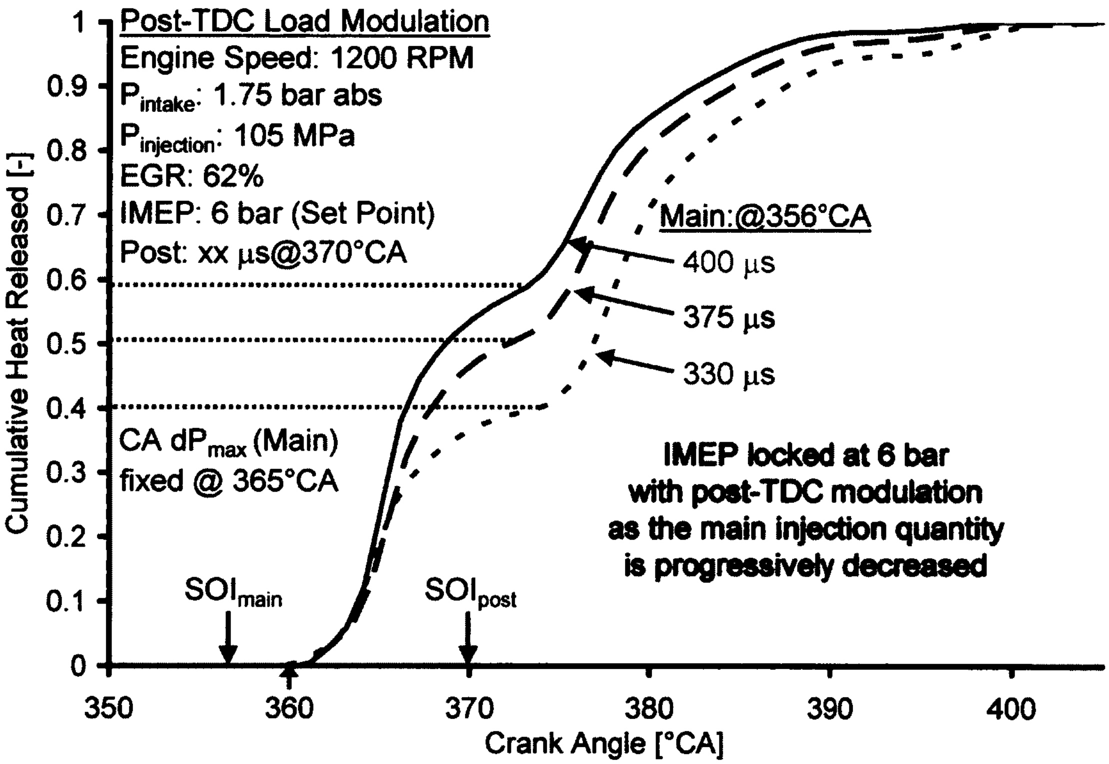

Figure 8.16: Cumulative Heat Release Traces

The summary of the results is given in Table 8.1. As the contribution of the main injection towards power production decreased, the combustion noise also reduced significantly. However, the thermal efficiency decreased primarily due to the off-phasing of the post-combustion event from the phasing window for best efficiency. The NOx and soot emissions were maintained while the HC and CO emissions also showed an insignificant increase. Moreover, the prompt adaptation of the post-

TDC fuel injection to maintain the IMEP during LTC mode also partially eliminated the cycle-to-cycle variations compared to LTC engine operation without control. To quantify the cyclic variations, the COV of IMEP was calculated for both the cases. For LTC operation without adaptive control (main injection only), the COV of IMEP was 2.8 % while with post-TDC IMEP modulation, the COV of IMEP ranged from 1.6~2.2%, corresponding to the reduction in the main injection from 400μs to 330μs.

Table 8.1: Summary of Results for IMEP Transients in LTC Mode

Heat Release [%]		$(dp/d\theta)_{max}$	Indicated η_{th}	Indicated Emissions [g/kWh]			
Main	Post	[bar]	[%]	NOx	Soot	THC^{C1}	CO
100	-	7.3	47.1	0.08	0.06	0.52	10.6
60	40	5.7	44.6	0.08	0.07	0.53	10.1
50	50	5.3	42.8	0.07	0.1	0.58	10.6
40	60	3.8	42.8	0.07	0.1	0.7	11.9

8.3.2. Cycle-by-cycle Adaptive Control

The second phase of the adaptive tests included the cycle-by-cycle control of the single-shot LTC. The control tests were performed by using a number of different parameters as feedback for the control system and the results are presented in the following sections.

8.3.2.1. CA $(dp/d\theta)_{max}$ as the Feedback

The transition into LTC mode of operation and maintaining stable operation in the LTC regime for conventional diesel is demonstrated in Figure 8.17. A high load of ~7 bar was selected to test the robustness of the control system. The setpoint of the CA $(dp/d\theta)_{max}$ was 365°CA. The phasing was estimated by the 'combustion characterization' controller and communicated to the 'fuel injection' controller which modified the timing (SOI) of the injection proportional to the phasing error. The adaptive fuel-injection control was able to successfully anchor the combustion phasing within a narrow band with heavy EGR (up to 65%). The soot measurements unlike other emission measurements were performed at discrete points and therefore show a step-wise pattern.

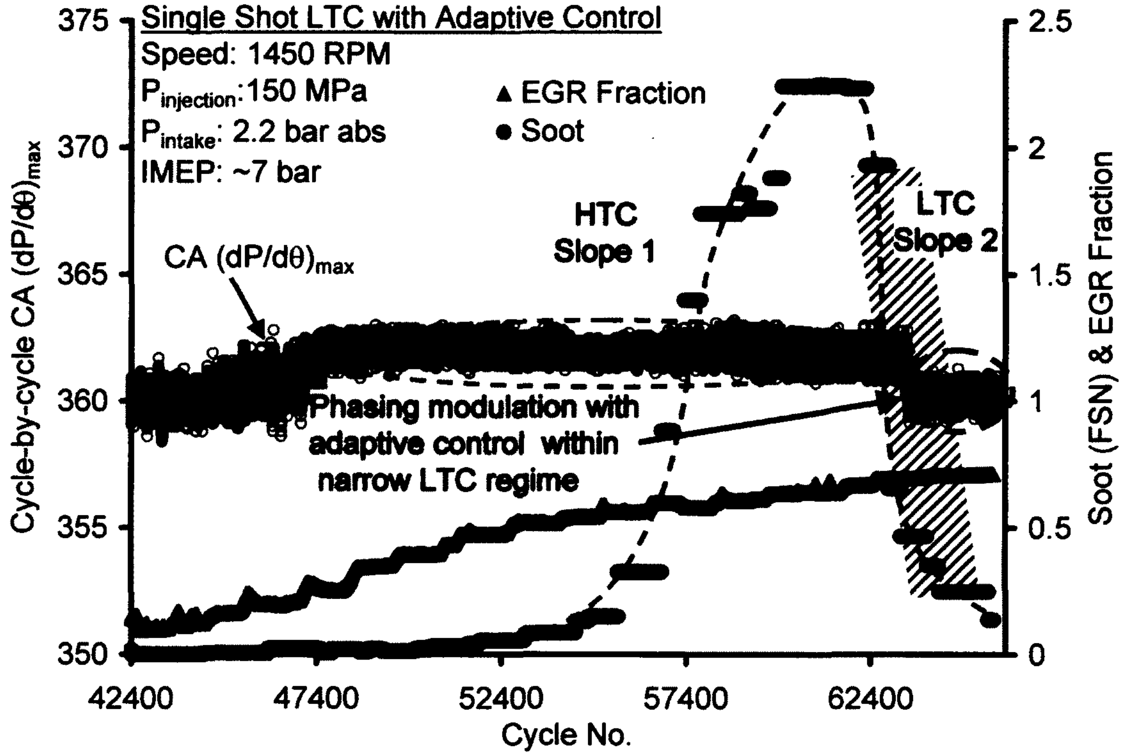

Figure 8.17: LTC Cycles Stabilized with Adaptive Control

8.3.2.2. CA$(dp/d\theta)_{max}$ & $(dp/d\theta)_{max}$ as the Feedback Parameters

It was shown in Chapter 7 that the combustion noise (maximum rate of pressure rise) was effectively reduced with the use of a two-injection (pilot+main) strategy. To enable the control system to regulate the combustion noise in addition to the combustion phasing, engine tests were configured to regulate both the amplitude and the crank angle of the maximum rate of pressure rise. An overview of the test results is shown in Figure 8.18. The engine load was 4.5 bar IMEP and a two-injection strategy was applied, with the pilot injection primarily for combustion noise control. The control action was performed as follows:

- To maintain the CA$(dp/d\theta)_{max}$ at the desired setpoint, the timing of the main injection was adjusted by the controller. Since a minimum dwell time was essential between the two injections, the timing of the pilot and the main was advanced simultaneously so that the dwell between the two injections was kept constant.
- For maintaining the amplitude below the desired setpoint level, the $(dp/d\theta)_{max}$ was controlled by increasing the pilot injection quantity while simultaneously decreasing the main injection quantity to maintain the same load level.

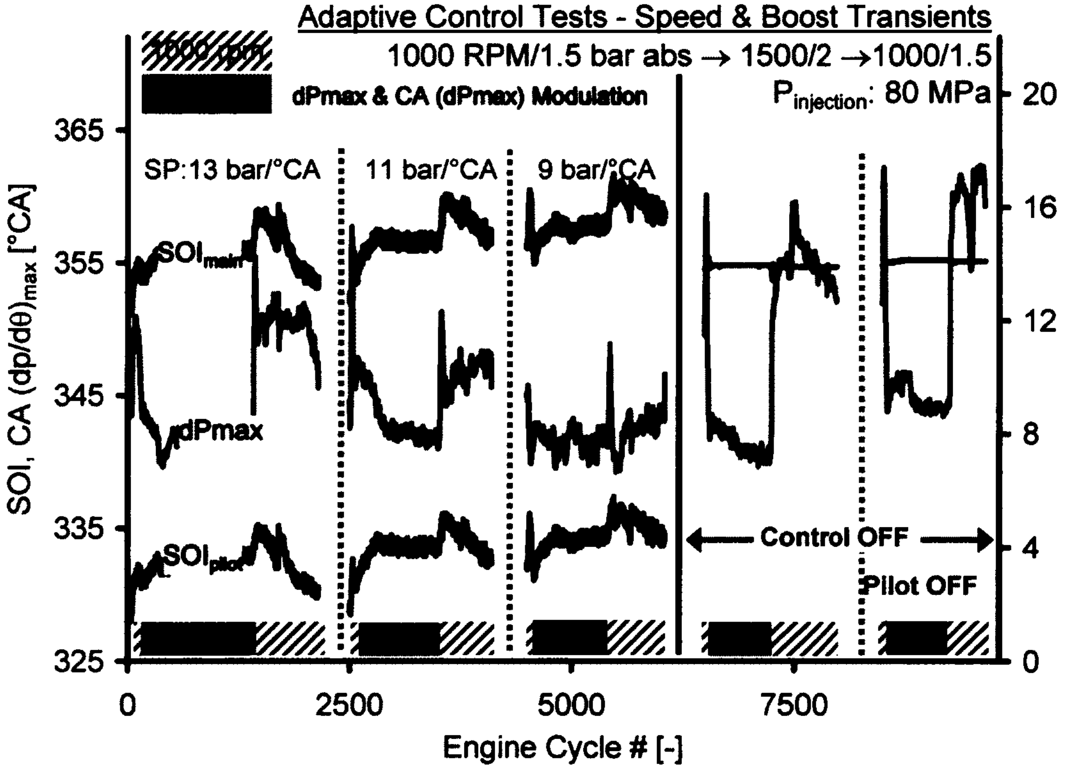

Figure 8.18: Adaptive Control tests with CA $(dp/d\theta)_{max}$ & $(dp/d\theta)_{max}$ Modulation

Speed and boost transients were applied to check the response of the control system at three levels of $(dp/d\theta)_{max}$ while maintaining the CA$(dp/d\theta)_{max}$ (a representation of the combustion phasing) at 363°CA. With the engine operating at 1500 RPM and 2 bar abs boost pressure, the

$(dp/d\theta)_{max}$ was low (~8 bar/°CA) because the combustion was overall lean. When the transition was made to the 1000 RPM/1.5 bar abs condition, the control system was able to restrict the $(dp/d\theta)_{max}$ below the setpoint value of 13bar/°CA. The tests were repeated by successively setting the setpoint at 11 and 9 bar/°CA and the desired control action was realized. It is noted that with the control switched off, the $(dp/d\theta)_{max}$ value increased up to 16 bar/°CA. However, with the adaptive control applied, the system was able to effectively maintain the desired noise level during the transients. The $CA(dp/d\theta)_{max}$ was also maintained within a narrow band.

8.3.2.3. CA50 as the Feedback

It was shown in Chapter 5 that the CA50 provides a robust and accurate estimation of the combustion phasing over a wide range of engine operating conditions. Engine tests were therefore conducted using CA50 as the feedback parameter for enabling the single-shot LTC strategy and to stabilize the LTC cycles during heavy EGR use. The CA50 was calculated using the *PDR* algorithm (Chapter 5.10.3) programmed with an FPGA/RT controller. An EGR sweep was performed at an engine load of 6 bar IMEP to push the combustion into the LTC cycles while maintaining the combustion phasing at 367°CA. The fuelling was also kept constant at 500μs. The emission results are shown in Figure 8.19 and Figure 8.20.

As EGR was progressively increased, the NOx and soot displayed the classical trade-off during the high temperature combustion. Increasing the EGR further pushed the combustion into the LTC regime where simultaneous reduction in NOx and soot was realized. The THC and CO emissions in Figure 8.20 increased with the higher dilution and lowered combustion temperature during LTC. A comparison with the LTC results at 5.2 bar IMEP (Figure 7.33) showed that the HC and CO emissions were comparable, although the load was higher in this case.

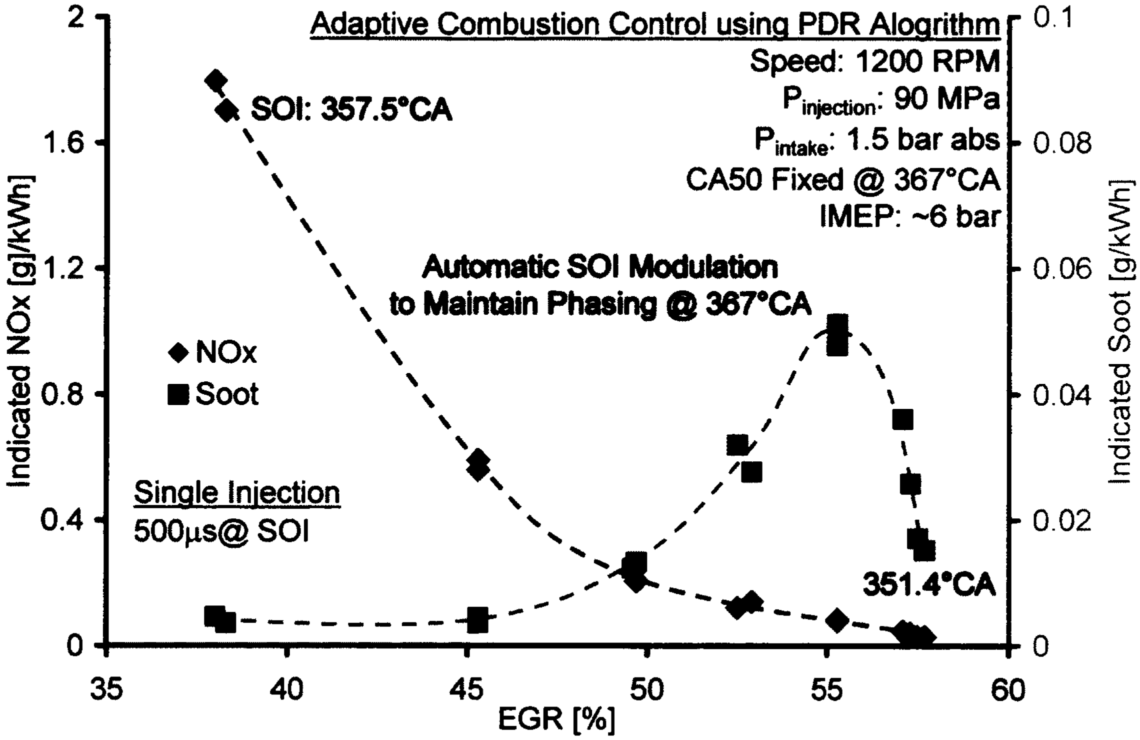

Figure 8.19: NOx & Soot Trends (Adaptive control using CA50)

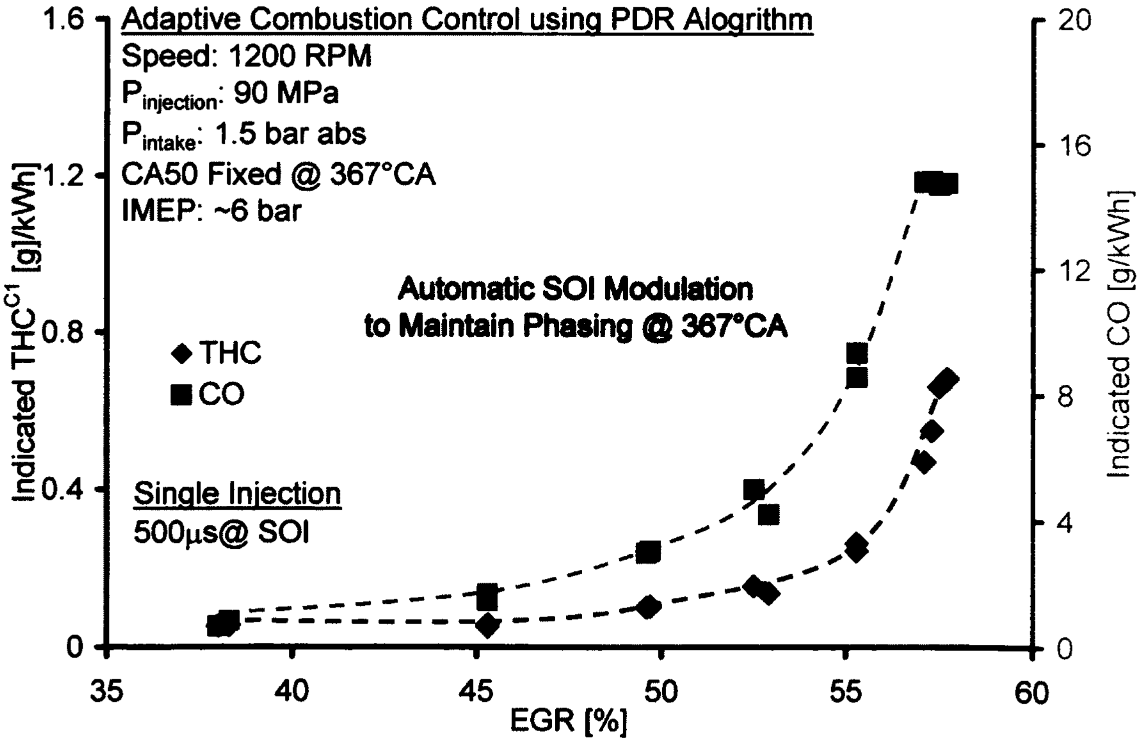

Figure 8.20: THC & CO Trends (Adaptive Control using CA50)

The cylinder pressure and the heat release rate at two different EGR levels (slope 1 and slope 2) are shown in Figure 8.21. The control system was able to maintain the phasing at 367°CA by cycle-by-cycle adapting the SOI.

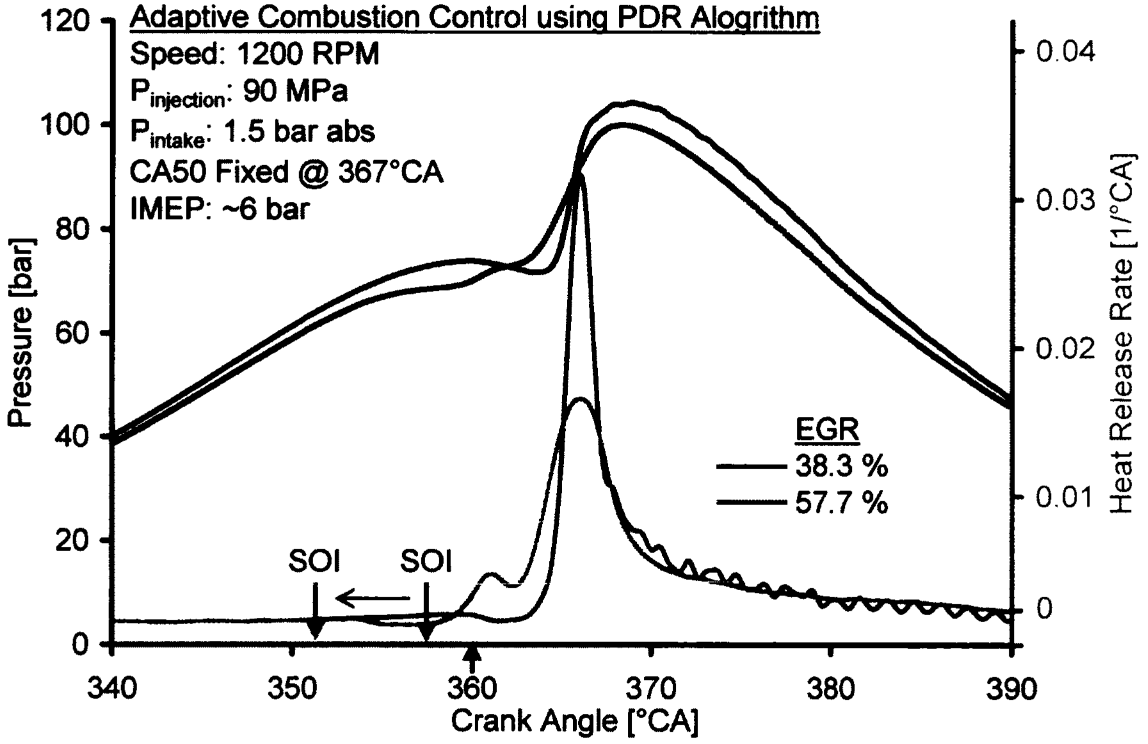

Figure 8.21: Enabling LTC Cycles with CA50 as the Feedback Parameter

A comparison of the crank angle of maximum rate of pressure rise ($CA(dP/d\theta)_{max}$) and the crank angle of 50% heat released ($CA50$) is shown in Figure 8.22. It can be seen that the $CA(dP/d\theta)_{max}$ is an indirect approximation of the combustion phasing and can provide reasonable accuracy for combustions characterized by a single peak of the heat release. However, the $CA50$ is a direct and more accurate representation of the combustion phasing and therefore, provides for more robust operation. Furthermore, with the split burning LTC or a complex heat release pattern (2 or more than two peaks with the phasing away from the TDC), the $CA(dP/d\theta)_{max}$ becomes ineffective in providing an accurate feedback.

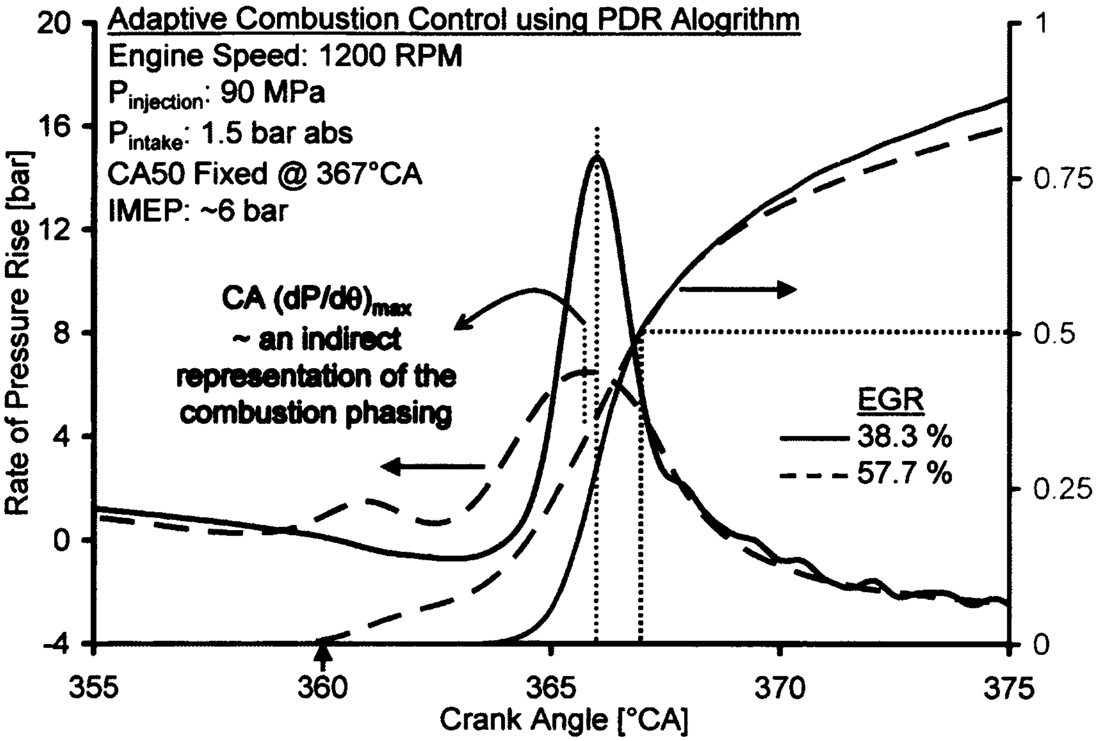

Figure 8.22: Comparison between $CA(dP/d\theta)_{\max}$ & $CA50$ as Feedback Parameters

To observe the performance of the control system on a cycle-by-cycle basis, the $CA50$ and the $CA(dP/d\theta)_{\max}$ for 200 consecutive pressure cycles have been plotted in Figure 8.23. The $CA50$ was controlled within ±1°CA of the setpoint during the LTC cycles. The data for the $CA(dP/d\theta)_{\max}$ has been shown for reference purpose only to indicate that it is an indirect representation of the combustion phasing.

The summary of the test is given in Table 8.2 . The combustion efficiency penalty was slightly higher compared to the test without the control (Table 7.6 and Table 7.11). However the major benefit of the automatic control was the improvement in the stability of the LTC operation, quantified in terms of the coefficient of variance of IMEP and $P_{\max}$. There was a negligible increase in the COVs, thereby indicating the ability of the control system to stabilize the combustion process.

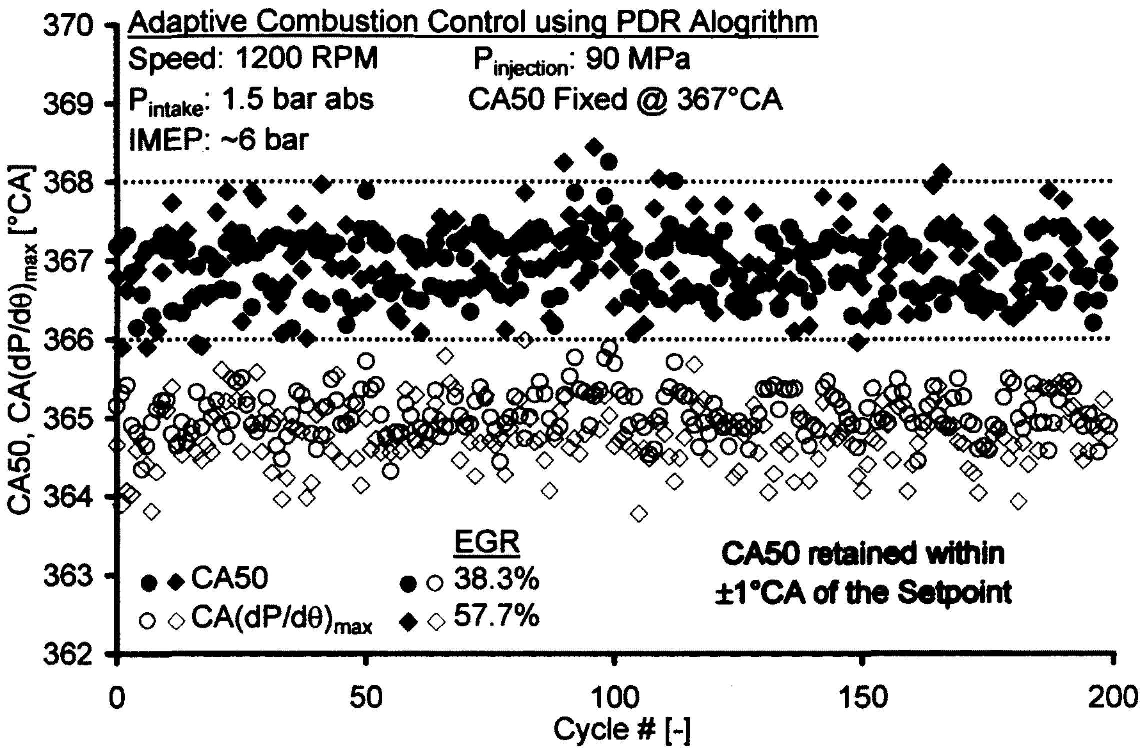

Figure 8.23: Cycle-by-cycle Control with CA50 as Feedback

Table 8.2: Single-shot LTC Control using CA50 as Feedback

Parameter	EGR [%]	
	38.3	57.7
IMEP [bar]	6.13	5.98
NOx [g/kWh]	1.2	0.05
Intake O_2 [%]	13.1	10
Indicated Thermal Efficiency [%]	42.3	41.1
Soot [g/kWh]	0.003	0.015
CO [g/kWh]	0.84	14.8
THC [g/kWh]	0.05	0.68
Combustion Efficiency [%]	99.7	97.9
P_{max} [bar]	104.2	99.8
$(dp/d\theta)_{max}$ [bar]	14.8	6.4
COV P_{max} [%]	1.1	1.3
COV IMEP [%]	1.81	1.86

8.3.2.4. CA50 & IMEP Modulation

A decrease in the engine load is generally observed as the combustion is pushed into the LTC cycles – a result of the combustion off-phasing and the deterioration in the combustion efficiency. The last test indicated that maintaining the combustion phasing within a narrow band helped to improve the combustion efficiency and the IMEP penalty was also reduced. To maintain the same engine load in the LTC regime, the last test was configured by enabling a post-TDC injection to make up for any decrease in the IMEP. The engine operating conditions are marked in the figures. The IMEP in this case was estimated after each cycle and the corrective action was performed in the next cycle. The phasing was maintained by modulating the timing of the main injection. A constant dwell of ~13.6°CA was maintained between the two injections.

The main injection was first enabled and its contribution to the IMEP was set at 4.5 bar IMEP. The post injection was configured to increase the engine load to 6.1 bar IMEP, the setpoint for this test. The combustion phasing setpoint was 367°CA. An EGR sweep was performed to move the combustion into the LTC regime.

The cylinder pressure and the heat release rates for the test are shown in Figure 8.24. The main injection has been shown for comparison purpose. As the combustion was split into two phases, a significant drop in the heat release peak was observed. Moreover, with higher EGR, the timing of the main and post were advanced to correct of for the combustion phasing while the post injection duration was modified by the controller to maintain the IMEP. The cylinder pressure and heat release traces are an indicator of the quality of the control action.

This aspect was further examined with the cumulative heat release traces shown in Figure 8.25. The CA50 was maintained at 376°CA while both EGR and the fuelling quantities changed. The figure also indicated that the main injection contributed about 75% of the total heat released.

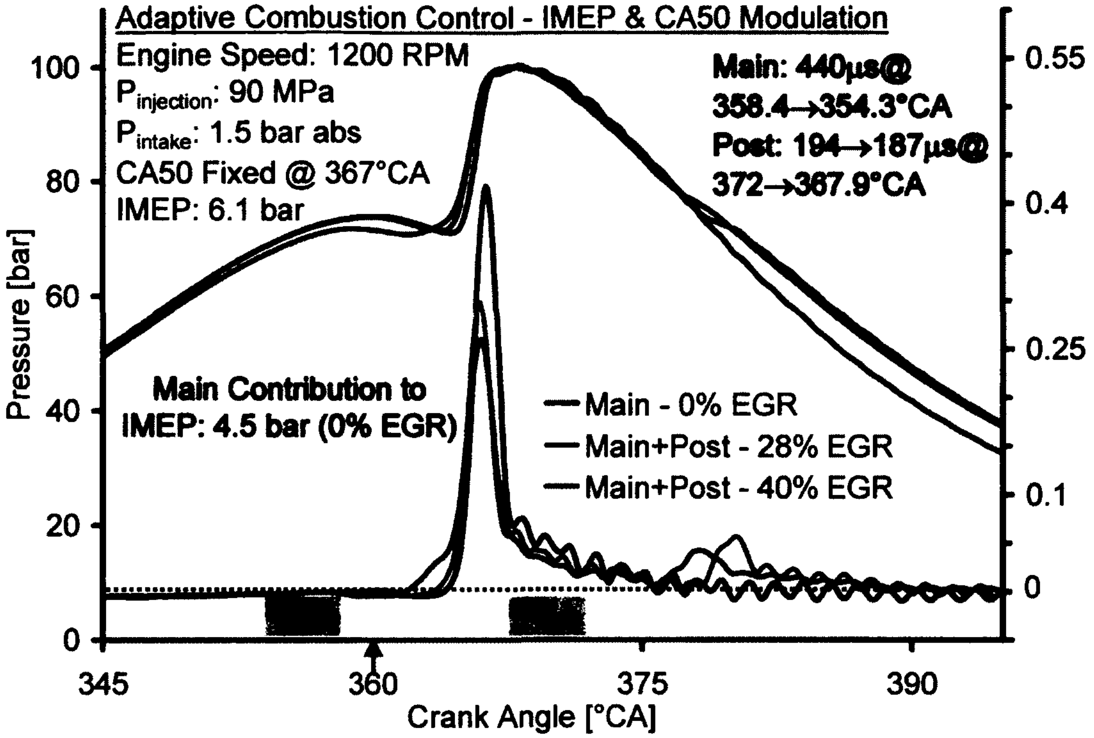

Figure 8.24: LTC Operation with CA50 & IMEP based Feedback Control

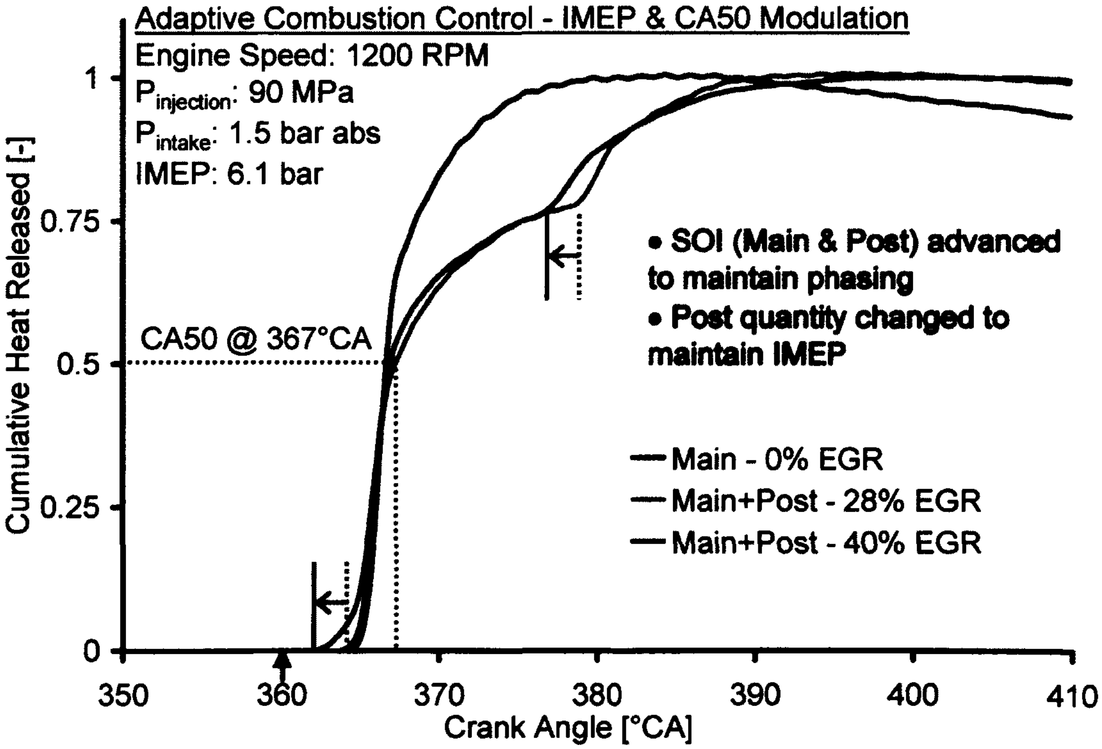

Figure 8.25: Cumulative Heat Release Traces for CA50 & IMEP based Feedback Control

The NOx and soot emissions for the test are shown in Figure 8.26. The NOx levels were very low; however the soot was within the DPF-tolerant level. The CO and THC emissions were also low. It is pertinent to mention here that the use of the post-injection with the single-shot injection is not an effective combination to enable LTC cycles. However, the aim was to gauge the performance of the control system. Tests were performed (shown later in this chapter) where both the IMEP and the combustion phasing were adjusted with the main injection timing and the pulse width to achieve the LTC cycles (consistent with the definition of the single-shot LTC).

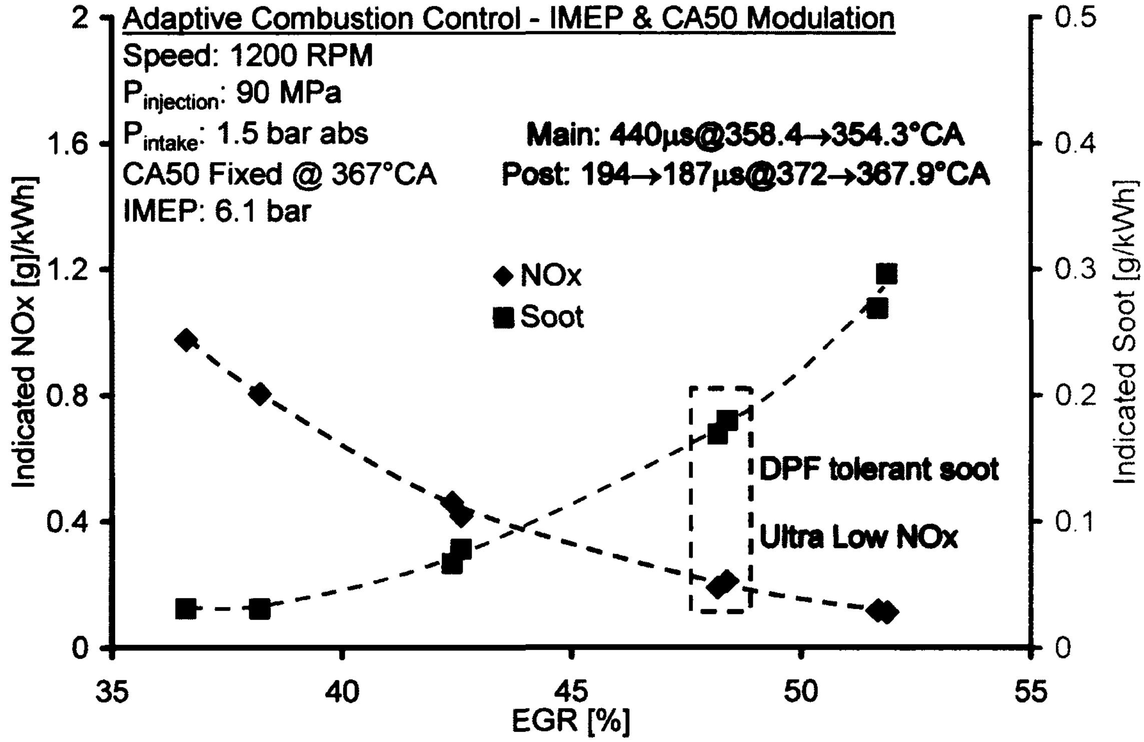

Figure 8.26: NOx and Soot for the CA50 & IMEP based Feedback Control

To analyze the response of the control system to transients in the engine operation, a large change in the commanded pulse width (quantity) was introduced by suddenly reducing the commanded pulse width of the main injection from 440µs to 410µs and again from 410µs to 390µs at a fixed EGR rate of 41%. The cylinder pressure and the heat release results are shown in Figure 8.27. The reduction in the main injection quantity was compensated by the controller by increasing the post injection quantity by the controller. The timing of both the injections was also modified to maintain the phasing at 367°CA.

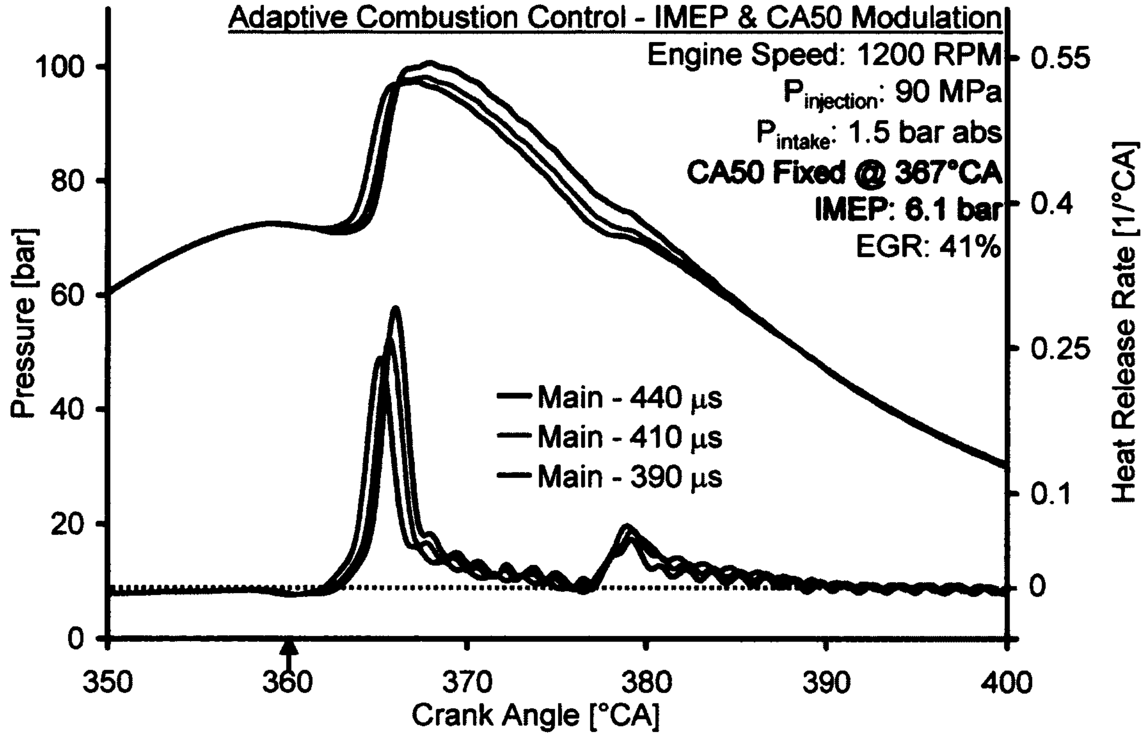

Figure 8.27: Cylinder Pressure and Heat Release after Load Transients

The injection pulse widths and the timing for both the main and the post injections are given in Figure 8.28. The change in the main injection quantity reduced its contribution to about 60% of the total heat released. This reduction was compensated by the post injection as its quantity was increased from 185μs to 236μs. The cycle-by-cycle response of the controller during the transients is shown in Figure 8.29. The CA50 was retained with the desired limits. The IMEP setpoint was also followed except for a few cycles during the transient which was because of the

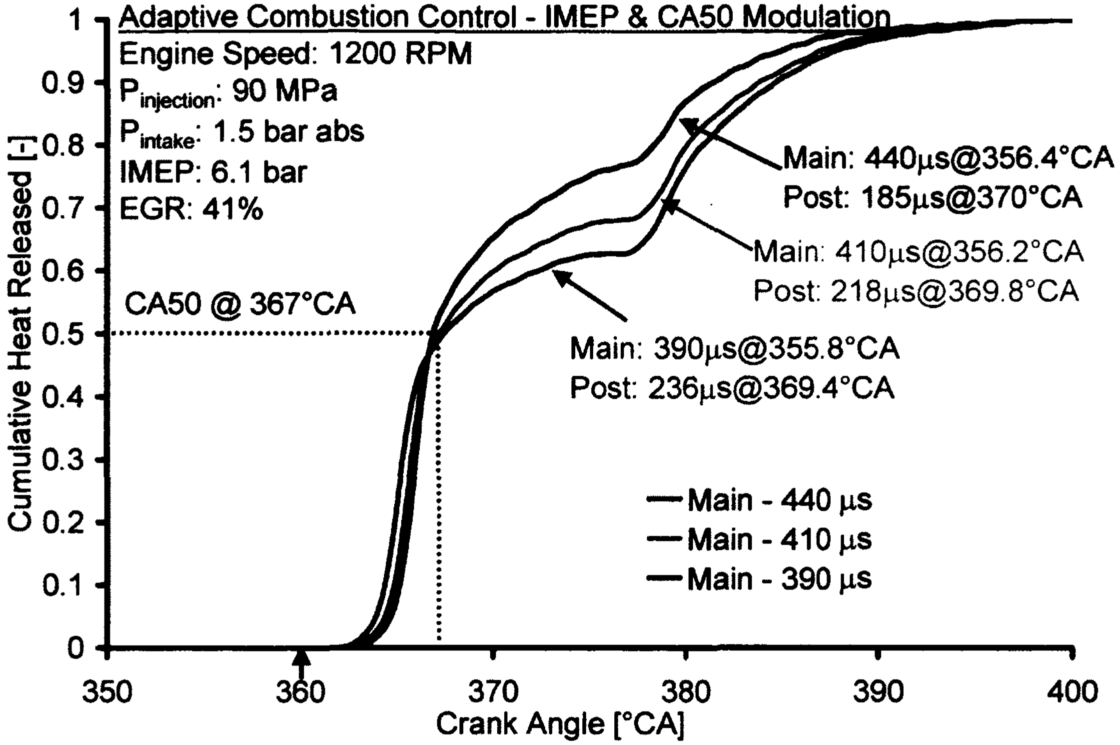

Figure 8.28: Cumulative Heat release Traces after Load Transients

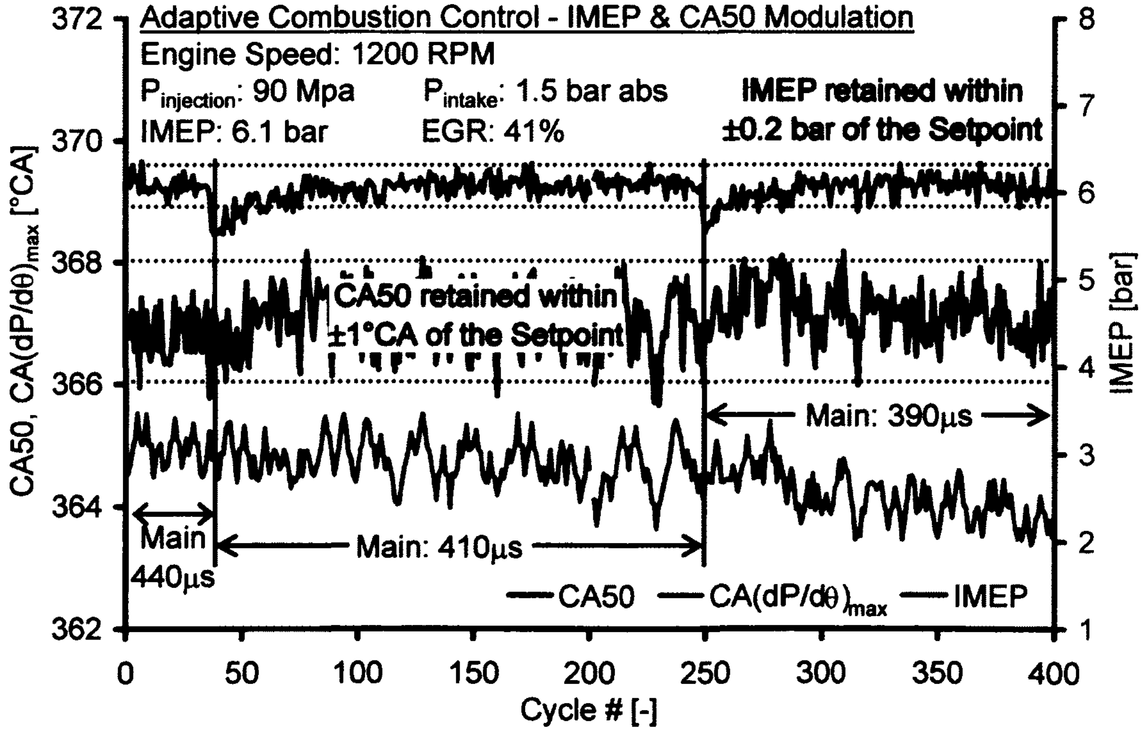

Figure 8.29: Transient Response of the Control System

post injection quantity correction limited to ±10 μs per cycle. The $CA(dP/d\theta)_{\max}$ has also been plotted to highlight the fact that as the post injection contribution to the heat release increased, the $CA(dP/d\theta)_{\max}$ started to change for the same combustion phasing, determined by the CA50.

8.4. Integrating the Systematic and Adaptive Control

The control results presented till now indicated that the adaptive control of the combustion based on the cylinder pressure-based feedback can improve the stability and combustion efficiency of the LTC cycles. In all these tests, the selection and application of the EGR and boost parameters was done manually to attain the ultra low NOx levels. An effort was therefore made to integrate the systematic control of EGR and boost pressure with the adaptive combustion control system and the overall structure of the proposed control strategy is presented in Figure 8.30. The fast feedback estimator (FFE) will condition the cylinder pressure signal, process the data and provide the necessary feedback to the fuel-injection control system (FCS) on either a cycle-by-cycle basis or within-same-cycle basis.

The SFE will provide feedback on the exhaust and intake conditions that include the oxygen concentrations, fresh-air lambda and the in-cylinder lambda to help optimize the boost and EGR for improving combustion stability and emissions, based on the output of the intake and exhaust lambda sensors. The NFE (smart NOx sensor, being the slowest element, will provide feedback on the engine-out NOx using the smart NOx sensor that will be used to ensure the emission level conformity while navigating the narrow operating corridors of LTC. Moreover, the NFE could also be used to provide an overall verification feedback on the control strategy.

The parametric analysis and correction (PAC) will be a look-up table (LUT) oriented approach, based on the theoretical operating maps for LTC operation (from the EGR analysis – Chapter 6) that will provide the approximate boundary conditions for the desired LTC operation. The boost-EGR controller will adjust the boost and EGR based on the feedback from the SFE and the corrective actions generated by the PAC.

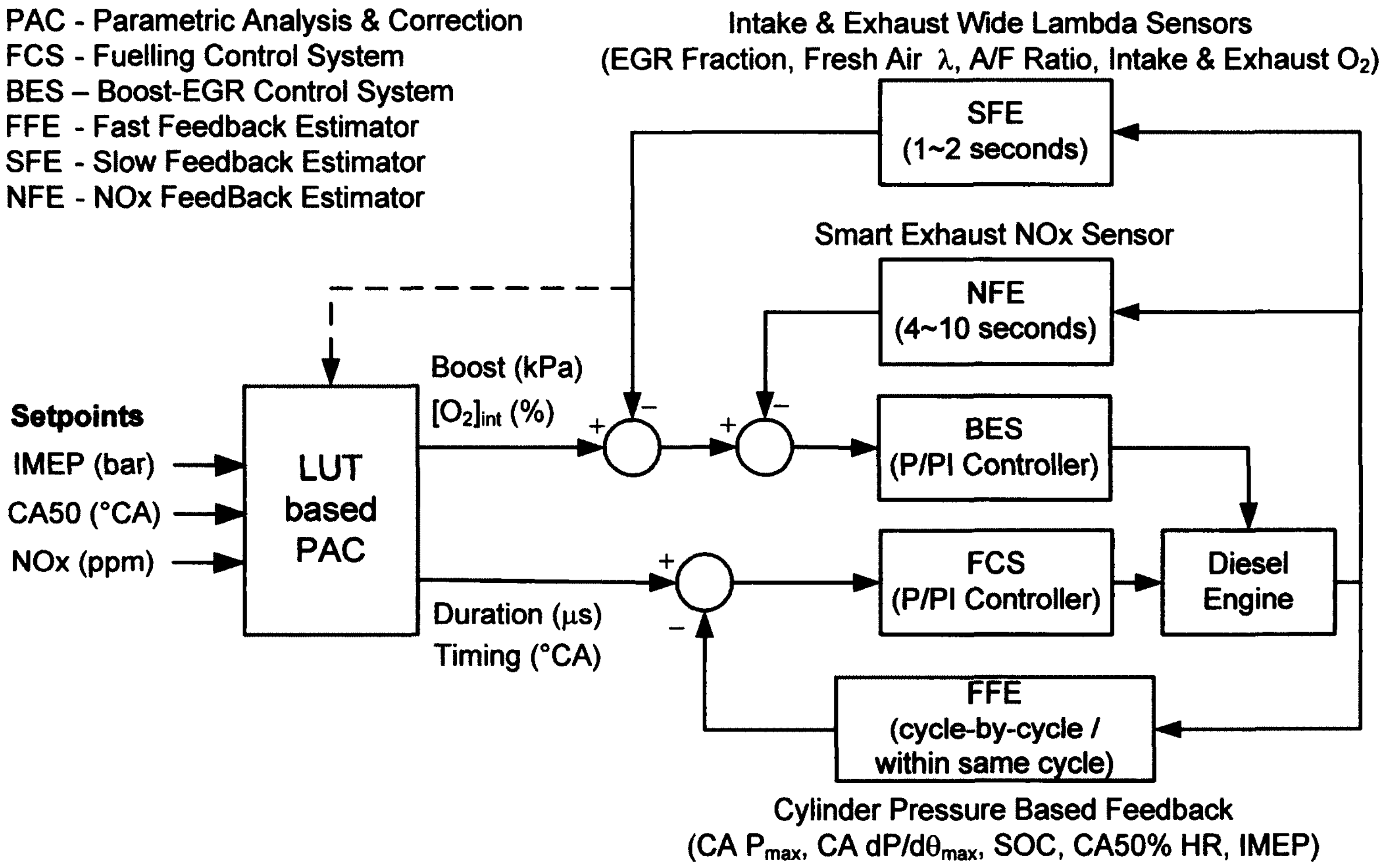

Figure 8.30: Structure of the Proposed Adaptive Control System

The overall control strategy was partially implemented in this work. The details are as follows:

- The existing 'combustion characterization' FPGA-RT controller was used as the FFE. The FFE ran the *PDR* heat release estimation algorithm in real-time for fast cycle-by-cycle feedback. The IMEP calculation for within-same-cycle control using the methodology described earlier was also run concurrently on the FFE, including the P/PI controller for the injection quantity correction.

- The existing 'fuel-injection' controller running on another RT-FPGA controller was designated as the FCS. The FCS implemented the SOI modulation based on the feedback from the FFE.

- The smart NOx sensor was controlled using the CAN Bus with LabVIEW running on a Windows based PC.

- The Wide band lambda sensors were run though their own dedicated controller that was configured using the RS-232 link. The output of the controller was processed using LabVIEW running on a Windows based PC.

- The Boost-EGR control (BES) system was also a LabVIEW based PC system that built upon the boost-back pressure controller already configured as a part of this work. The LUT based PAC was also programmed on the same PC. However, the full automatic execution of the BES and the PAC was not realized in this work and during the engine tests, the control action was performed manually based on the feedback from the other sub-systems.

- The communication between the various elements of the PC based control system was done using the DataSocket technology built into LabVIEW. The DataSocket uses the Ethernet TCP/IP protocol and efficiently transferred data over the laboratory local area network.

8.5. Control Strategy for Navigating LTC Corridors

A strategy for attaining low temperature combustion with the minimum of penalty was devised as shown in Figure 8.31. At low loads with moderate injection pressures and low boost, the soot emission is low regardless of the intake charge dilution as already demonstrated during the testing of the single-shot LTC (Figure 7.59). Therefore, the combustion can be pushed into the LTC cycles at low load levels and the engine load can then be increased inside the narrow LTC operating corridors while managing the injection pressure, boost and EGR to minimize the associated penalties.

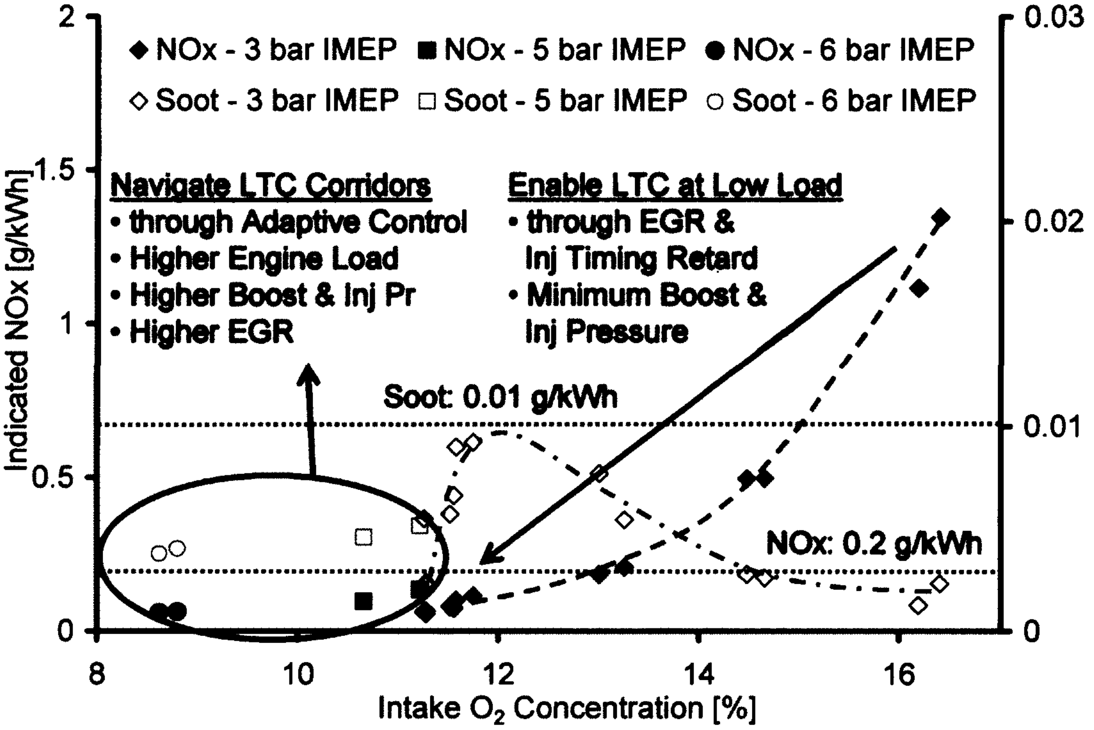

Figure 8.31: Strategy for Attaining LTC and Navigating Narrow LTC Corridors

The implementation of the strategy is empirically demonstrated from Figure 8.32 to Figure 8.34. The setpoint of the combustion phasing was fixed at 374°CA, quite late into the expansion process. This was intentionally done to increase the instability in the combustion and move the combustion close to the flame-out region. The combustion phasing of the single-injection enabled LTC was based on the crank angle of the maximum rate of pressure rise. The engine speed was 1500 RPM and the injection pressure was 90MPa. The intake pressure was set at 2 bar abs, relatively high to ensure that sufficient oxygen was available to the combustion process during the load transitions. The targeted IMEP was 6 bar and the test was started at a low IMEP of 2 bar (Initial Setpoint).

Heavy EGR was manually applied based on the feedback from the NOx sensor and the wide-band lambda sensors to push the combustion into the LTC cycles with ultra low NOx and soot. The IMEP setpoint was then increased to 3.9 bar while managing the EGR to maintain the NOx below 20 ppm. The engine was run for a few minutes at this load to ensure stable operation and to obtain steady-state emission values. The IMEP setpoint was then increased to 6.5 bar and the procedure repeated. The emission history during the test is shown in Figure 8.32. The load increase from 2 bar to 3.9 bar IMEP did not cause any change in the CO and HC emissions. The NOx dropped slightly as the effectiveness of EGR was enhanced with the load. The next increase to 6.5 bar IMEP reduced NOx further, caused a minor change in the HC emission but the CO levels rose sharply and reached the measurement limits of the emission analyzer. Although CO increased, its contribution to the combustion inefficiency was much lower than HC (LHV of CO ~ one-fourth of HC) and therefore, the stability of the combustion was not compromised as later. Moreover, the increase in CO indicated the need for a higher injection pressure or boost since the load can be considered high for the single-shot LTC.

The cylinder pressure traces for the three IMEP setpoints at the same EGR level of 63% are shown in Figure 8.33. The results showed that the control system was able to effectively stabilize the combustion at such a late phasing. The smoke level was also ultra low and below 0.001 g/kWh during the test.

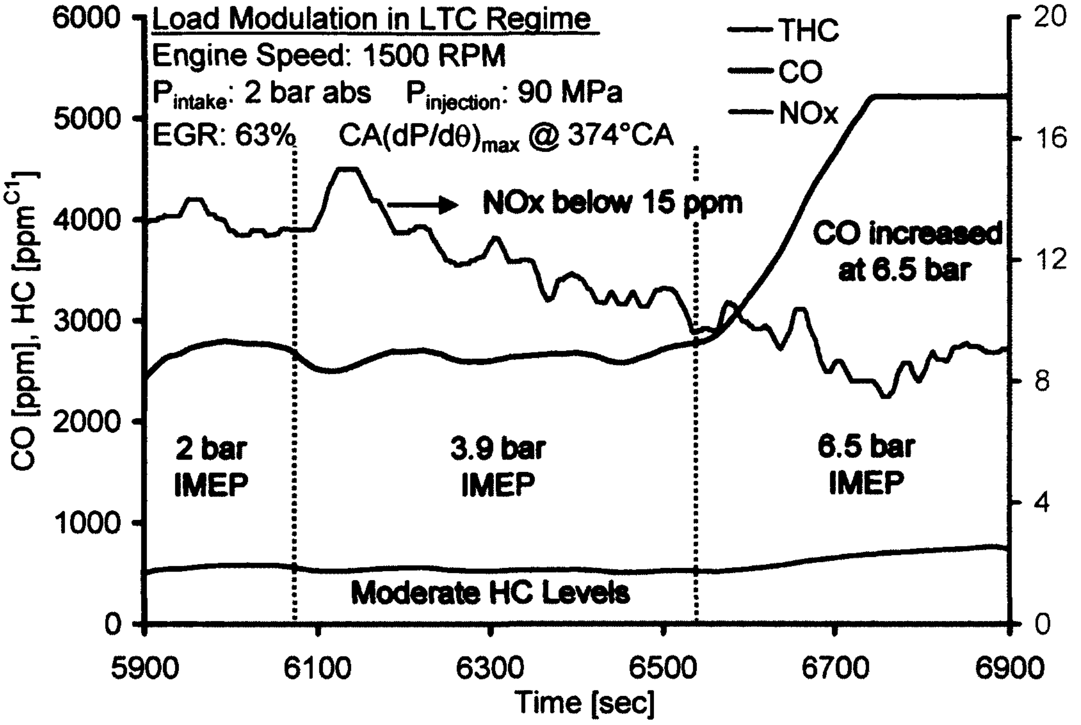

Figure 8.32: Emission History during LTC Load Management

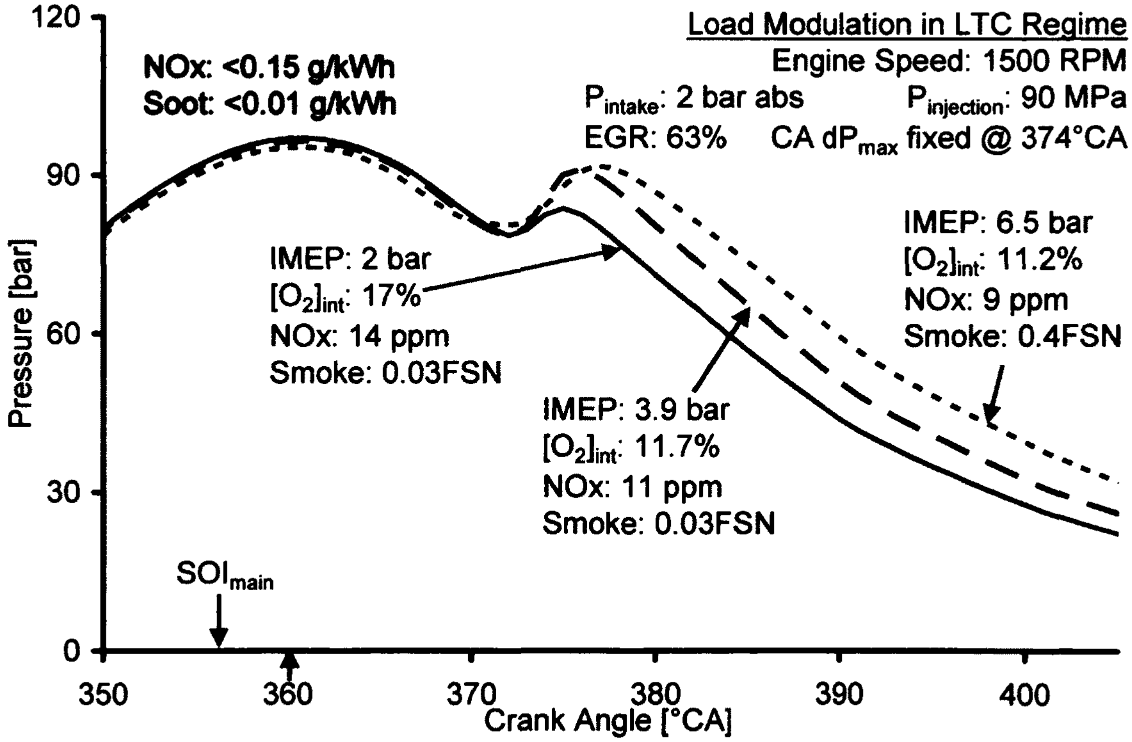

Figure 8.33: LTC Load Management with Overall Control Strategy

The heat release rates corresponding to the cylinder pressure traces are shown in Figure 8.34. The control system was able to maintain the phasing even when the combustion was highly diluted for the case of 6.5 bar IMEP. The heat release trace for the 6.5 bar IMEP indicates that the heavy EGR reduced burning rate significantly, thereby pronging the combustion duration. The late burning of the cylinder charge also suggests an increase in the CO where the oxidation of CO into CO_2 may freeze because of the lowered combustion temperatures.

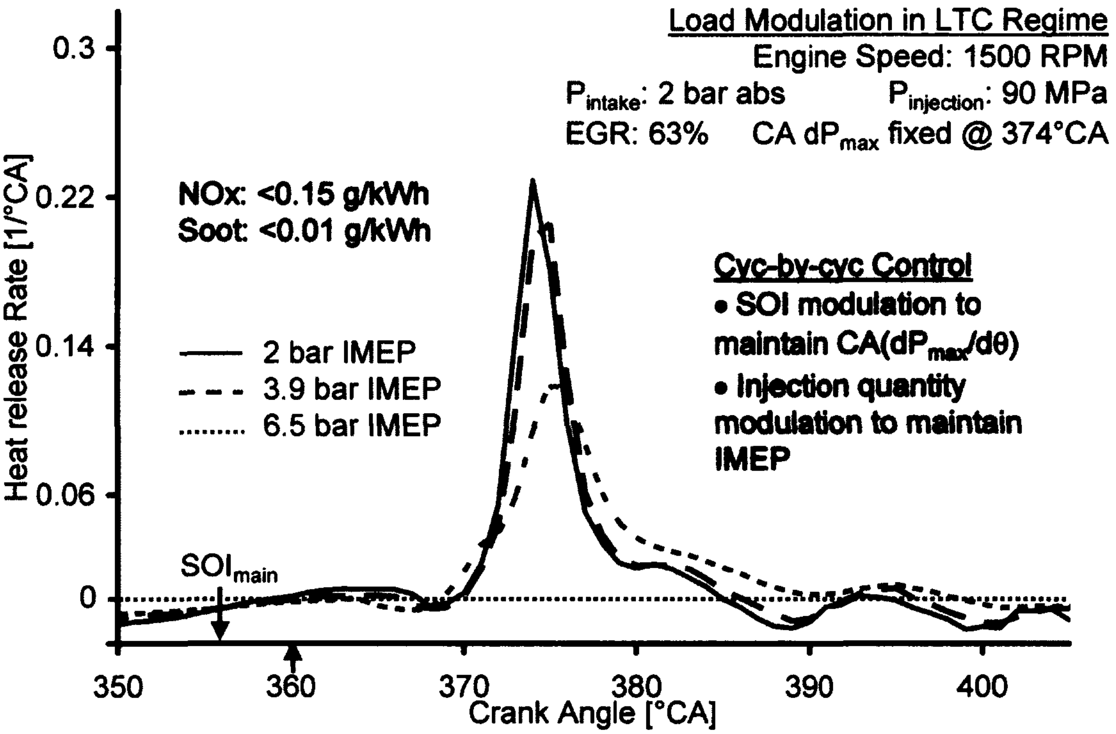

Figure 8.34: Heat Release Rates for Overall Control Strategy

The results for the test are summarized in Table 8.3. Once the emissions are examined on a g/kWh basis, the performance at 2 bar IMEP was inferior to the 3.9 bar IMEP. The COV of IMEP was also higher than that for the 3.9 and 6.5 bar IMEP. From the results, the load of 3.9 bar IMEP was found to have the highest indicated thermal efficiency along with the lowest CO and HC emissions compared to the other two loads. The COV of IMEP, an indicator of the process stability was also low (~1.8%) at 3.9 bar IMEP.

These results provided further evidence to support the LTC load management strategy that proposed the use of the single shot LTC at low loads. The results of the testing and control phases suggest that for the Ford Engine (CR 18.2:1), the single-shot LTC strategy should be employed up to an IMEP of 4 bar and then the combustion mode should be switched to the multiple-shot (early HCCI) LTC strategy. The results also indicate that the integration of the systematic and adaptive combustion control can help to stabilize the combustion process while navigating the LTC pathways with ultra low emissions of NOx and soot.

Table 8.3: Summary of LTC Load Management

Parameter	IMEP [bar]		
	2	3.9	6.5
NOx [ppm]	14	11	19
NOx [g/kWh]	0.18	0.09	0.04
Intake O_2 [%]	17	11.7	11.2
Indicated Thermal Efficiency [%]	37.9	39.9	38.6
Smoke [FSN]	0.03	0.03	0.4
Soot [g/kWh]	0.001	0.0006	0.009
CO [ppm]	2736	2653	>5200*
CO [g/kWh]	24	12.8	>15.9*
THC [ppm]	559	532	712
THC [g/kWh]	2.5	1.28	1.01
Combustion Efficiency [%]	98.9	99.5	99.5†
$(dp/d\theta)_{max}$ [bar]	3.1	5.6	3.2
COV P_{max} [%]	0.14	0.14	0.29
COV IMEP [%]	3.51	1.82	1.91

* Exceeded the measurement limit

† Actually lower because of the higher CO

8.6. Conclusions

LTC control strategies based on cylinder pressure characteristics were formulated based on the diagnostics and testing of diesel LTC cycles. The LTC control strategies were explored experimentally to enable and stabilize the LTC when heavy EGR is applied.

- An IMEP estimation methodology for within-same cycle control was proposed and shown to stabilize the LTC load level with post-TDC torque modulation.
- A methodology for recognizing the pressure characteristics of retarded combustion events was detailed and shown to be effective for closed loop feedback control.
- Application tests were conducted to assess the performance of various cylinder pressure based feedback parameters in improving the stability of single-shot LTC cycles while maintaining ultra low NOx and soot emissions.
- An overall strategy for integrating the systematic and adaptive combustion control was proposed and partially implemented.
- A LTC control strategy for navigating the narrow LTC corridors was devised and implemented with the combined systematic (in manual mode) and closed loop combustion control.
- The control system was demonstrated to maintain the stability of the LTC cycles during load, boost and speed transients

CHAPTER IX

9. CONCLUSIONS AND FUTURE WORK

Extensive experimental research was carried out to investigate and improve the diesel low temperature combustion through diagnostics, testing and control work. The conclusions and the recommendations from the research are presented below.

9.1. LTC Efficiency and Load Range Improvements

Based on the empirical and analytical analyses, the load management and efficiency improvements of the LTC cycles were demonstrated with three fuelling strategies.

Single-shot LTC: The single-shot LTC was enabled with heavy EGR to realize ultra low NOx and soot emissions at low loads (3~5 bar). The significant findings for this combustion mode were:

- An intake oxygen concentration of less than 14% was generally found to reduce NOx to very low levels and an intake oxygen of 8~11% was found necessary for achieving simultaneous low-NOx and low-soot combustion.
- In general, the CO rises with heavy EGR because of reduced O_2 availability (11~14%). The THC is more sensitive to the lowered combustion temperature and the further reduced oxygen concentration (8~12%) with heavy EGR.

Multi-shot (early HCCI) LTC: This combustion mode was largely applicable to mid-load engine operating conditions and was realized up to 7.5 bar IMEP with a low HC penalty. The significant contributions were:

- An injection timing scheduling criterion to minimize the HC emissions based on the fuel boiling characteristics and the phenomenological spray penetration model.
- Quantification of combustion off-phasing with equivalent-exhaust HC and the demonstration of a trade-off between the off-phasing and the exhaust combustibles.

Split Burning LTC: The splitting of the heat release helped to reduce the peak cylinder pressure and the maximum rate of pressure rise. The containment of the pressure levels enabled the load to be increased up to 9.7 bar IMEP. The significant contributions were:

- The post-TDC part of the combustion helps to destroy the CO and HC produced earlier in the cycle, thereby improving the combustion efficiency.
- Ultra low soot was not attainable because of the conventional burn of the post-TDC combustion. An alternate DPF-tolerant soot limit of ~2.5 FSN was satisfied for this mode.

The demonstrated LTC load range without engine hardware modifications for the compression ratio of 18.2:1 is plotted in Figure 9.1.

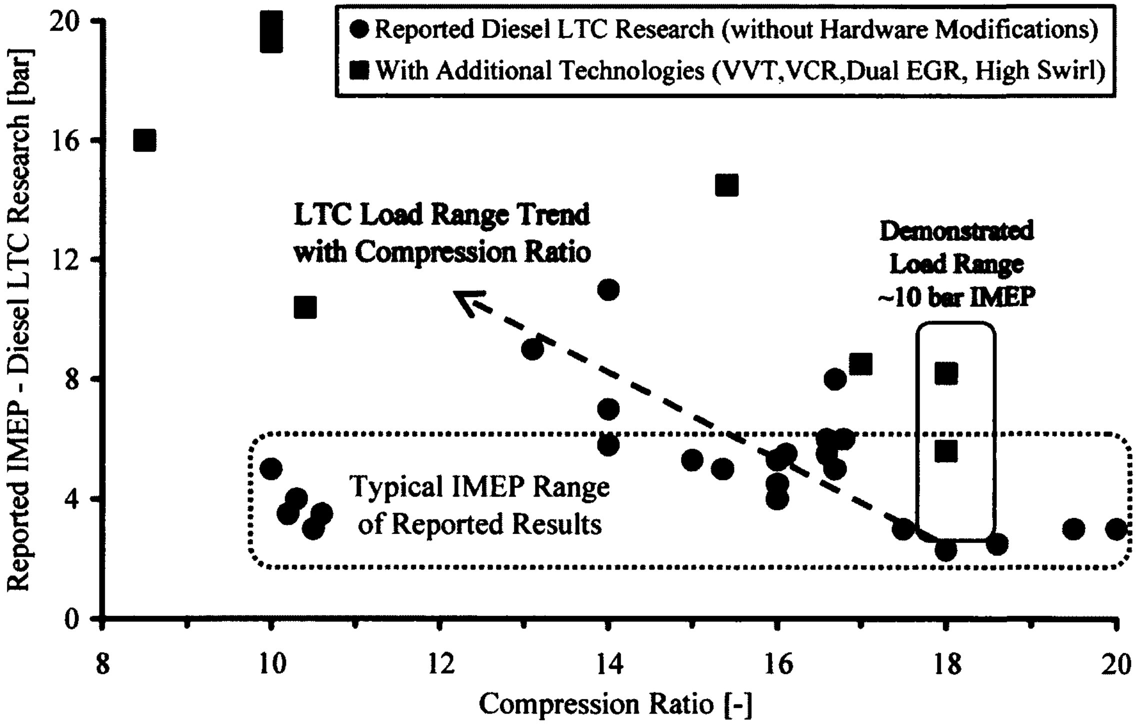

Figure 9.1: LTC Load Range Reported in this Research Work

9.2. Control of Diesel Low Temperature Combustion

LTC control strategies based on the cylinder pressure characteristics were formulated in accordance with the results obtained from the diagnostics and testing of diesel LTC cycles. The significant contributions of the control work are as follows:

- An IMEP estimation methodology for within-same-cycle control was proposed and shown to stabilize the LTC load level with post-TDC torque modulation.
- A methodology for recognizing the pressure characteristics of retarded combustion events was detailed and shown to be effective for closed-loop feedback control.
- An overall strategy for integrating the systematic and adaptive combustion control was proposed and partially implemented.
- A LTC control strategy for navigating the narrow LTC corridors was devised and implemented with the combined systematic (in manual mode) and closed-loop combustion control.
- The control system was demonstrated to maintain the stability of the LTC cycles during load, boost and speed transients.

9.3. LTC Combustion Diagnostics

The diagnostics work was crucial to develop the research methodology employed for investigating the diesel LTC and provided essential guidelines for the testing and control work. The significant contributions resulting from the diagnostics work are as follows:

- The in-cylinder gas sampling studies established the efficacy of this research methodology for the homogeneous charge type of combustion where the local charge characteristics are in parity with those of the global cylinder charge.
- With the in-cylinder sampling tests, a LTC NOx reduction mechanism was identified for nitric oxide (NO) levels up to 300 ppm in the engine intake stream. The low NOx levels in the exhaust were confirmed to be the result of the NO-HC interaction. A minimum HC/NO ratio of 10~15:1 was quantified for the significant

oxidation of NO. A lower ratio considerably decreased the NO conversion while a high ratio indicated an insignificant or a small increase in the conversion.

- In-cylinder sampling studies for lean homogeneous charge combustion fuelled with DME confirmed the in-cylinder production (up to 20 ppm) and the subsequent oxidation/destruction of NO within the combustion regime. The engine-out NOx was only 1~2 ppm.
- A computationally efficient 'Diesel Pressure Departure Ratio' algorithm for accurately estimating the combustion phasing for a multitude of combustion strategies in real-time was proposed and validated with engine tests. The algorithm was demonstrated to provide a reliable and accurate feedback in real-time during the LTC control tests with less demand on the hardware resources.
- A theoretical operating map for the LTC cycles was proposed based on the detailed EGR analysis. The actual fuel strength of the cylinder charge was quantified in terms of an in-cylinder lambda λ_a and its difference from the fresh air lambda λ was quantified.
- The transient build-up of EGR and the concentration convergence was described with a single mathematical expression. A 'Charge Dilution Index' was proposed to present a standard measure for the estimation of the EGR independent of the engine operating conditions (load, boost etc).

9.4. Catalytic EGR Treatment

The diesel fuel reforming process was tested to generate gaseous fuel on demand in the actual EGR system of a diesel engine at the Clean Diesel Engine Laboratory. This was among the first empirical demonstrations of the diesel fuel reforming process in the EGR loop, based on a review of the published literature. A sophisticated setup for enabling the EGR reforming process and maintaining control over the critical process parameters was established. Novel flow management strategies including flow reversal, partial flow control together with central fuelling and central heating schemes were applied to the EGR reforming process for the first time to improve the energy efficiency of the reforming process. The results indicated a reduction of up to 50% supplemental energy with reversal flow and central fuelling compared to the unidirectional reformer with inlet heating. The gaseous fuels (H_2 +CO) generated by the diesel fuel reforming process in the EGR loop were shown to enhance the premixed combustion phase and significantly decrease the NOx emission without incurring a soot penalty.

9.5. Advanced Research Platform

The preliminary testing of the diesel LTC cycles highlighted the sensitivity of the LTC cycles to small variations in the engine operating conditions such as EGR (0.5%), injection timing (0.2°CA) and pulse-width (5μs). Therefore, to enable the evaluation of the different LTC fuelling/control strategies, an advanced emission sampling and measurement, data acquisition, and a high performance combustion-control platform was developed during the course of this research.

The test engines' sub-system development included the setting up of the automatic boost and back-pressure control system, fuel and intake flow measurements, CAN Bus-based EGR control system, and an online data processing and synchronization system. The installation of a NOx transient sensor was devised and successfully implemented to provide fast feedback (~750ms) and the validation of the control strategies. A two-lambda sensor technique was devised and implemented to provide fast feedback (~500ms) on the intake dilution and exhaust parameters prevalent during the LTC cycles. The in-cylinder gas sampling system was setup by integrating a number of sub-systems and through extensive hardware modifications to gain access to the combustion chamber.

The resulting combustion research platform enabled the detailed testing and precise control of the LTC fuelling strategies. Furthermore, the implementation challenges for the LTC cycles were identified and quantified, thereby making it possible to devise and evaluate the systematic control of the LTC cycles. In addition, this setup provides a high quality, advanced platform for future engine research and development work at the Clean Diesel Engine Laboratory.

In conclusion, the objectives of the research work and the achieved results are summarized in Table 9.1.

Table 9.1: Stated Objectives and Achieved Results

Objective	Based on Literature Review	Results of Current Work
Extend LTC Load Range (18.2 Compression Ratio)	< 4 bar IMEP	Demonstrated up to 9.7 bar IMEP
Indicated Thermal Efficiency	10 to 20% Penalty	Reduced up to 6% penalty
Combustion Inefficiency	Up to 5 %	< 3%
Stability	Unstable, high cyclic variability	Stable engine operation with Adaptive Control ($COV_{IMEP} < 3\%$)
Navigation (Load Transients) within LTC regime	Not available	Enabled with Adaptive & Systematic Control System

9.6. Significant Contributions of the Dissertation

Low temperature combustion strategies are being actively considered as part of the solution for achieving simultaneous reduction of the NOx and soot emissions from diesel engines – a requisite proviso for conforming to the future emission regulations. The author has successfully conducted a systematic investigation, with refereed (peer-reviewed) publications, of the testing, diagnostics and control of LTC cycles in modern diesel engines. The contributions of the dissertation include the following:

- The theoretical operating map for the diesel LTC cycles (Section 6.2.5) presents the basic framework for enabling this combustion mode. It also provides the essential guidelines for the development of the control strategies, including the identification of the boundary conditions for navigating the narrow LTC corridors. The map incorporates the effects of the boost pressure-EGR interaction on the fuel strength of the cylinder charge and is applicable to any modern direct-injection diesel engine.

- The 'Diesel Pressure Departure Ratio' algorithm (Section 5.10.3) provides a robust and efficient means of estimating the combustion phasing for a multitude of combustion strategies. The calibration of the algorithm for a given diesel engine is a trail and error process, requiring a set of cylinder pressure traces corresponding to different combustion strategies. The nominal time for the calibration procedure is a few hours and may typically involve 2~3 iterations. Once the model is calibrated to a specific engine configuration, it is largely not affected by the operating conditions. The reduced numerical complexity compared to the apparent heat release model may enable the use of this algorithm with production engine control units.

- The LTC NOx mechanism (Section 5.4) provides a new analytical pathway towards quantifying the combustion efficiency associated with the LTC operation. The generation of a significant amount of NO_2 (a much strong oxidizer than oxygen) can be utilized in the exhaust aftertreatment, for instance, during the DPF regeneration. This may not only reduce the supplemental energy requirements of the aftertreatment systems, but may also favour the use of mix-mode combustion systems where the LTC operation can be utilized for supplying the combustibles and NO_2 to the aftertreatment systems while maintaining simultaneous low NOx and low soot as well.

- The IMEP estimation algorithm (Section 8.1.3) for enabling control within-the-same-cycle offers a new approach to improve the stability of the LTC cycles. Since the LTC cycles are close to the flame-out limits, the application of this algorithm can aid in the engine load management while navigating through the narrow LTC corridors. The algorithm is also able to adapt the estimation to the different combustion modes within-the-same-cycle basis, thus improving the robustness of the estimation.

- The quantification of the combustion phasing efficiency in terms of the 'Equivalent Exhaust HC' (Section 7.6.4) allows the possibility of optimizing the thermal efficiency of the early HCCI cycles. The trade-off between the phasing and the combustion efficiency can also be utilized to offset the disadvantages of the HCCI cycles, such as the high maximum cylinder pressure and the maximum rate of pressure rise.

9.7. Future Work

The following are the recommendations for the future work:

- The in-cylinder gas sampling studies of LTC cycles with DME should be extended to higher engine loads and the crank angle-resolved evolution of hydrocarbons correlated with the NO oxidation/destruction. The HC speciation under both HTC and LTC conditions should be quantified (Chapter 5).

- The Yanmar engine should be converted to a common-rail configuration with independent control of the SOI, rail pressure and boost for enabling in-cylinder gas sampling studies for direct injection diesel LTC cycles (Chapter 5).

- The in-cylinder sampling studies should be extended to include the pollutant evolution for both high-temperature and low-temperature biodiesel combustion (Chapter 5).

- The *PDR* algorithm should be extended to include the effects of heat transfer and specific heat ratio variations (Chapter 5). The algorithm should be implemented using a standard engine control unit to make it viable for use in production diesel engines.

- The EGR analyses should be extended to include the effect of the EGR stream temperature and the combustion inefficiency (Chapter 6).

- The generation of gaseous fuels with EGR reforming should be tested for its potential benefits in the aftertreatment systems to improve the regeneration efficiency while reducing the supplemental energy requirements (Chapter 6).

- The effect of temperature modulation on the LTC cycles should be examined with variable-valve timing or variable compression ratio systems to extend the load range for high-compression ratio diesel engines (Chapter 7).

- The effect of engine speed on the LTC cycles should be investigated. At higher speeds, the time available for the preparation of a homogeneous mixture is considerably reduced. Therefore, the speed range for the three LTC strategies needs to be identified (Chapter 7).

- The systematic control should be fully implemented to include the automatic estimation and control of the boost pressure and EGR. This would help in the model-based control of the LTC cycles (Chapter 8).

- A theoretical investigation of the IMEP control methodology within-the-same-cycle should be carried out to develop a mathematical formulation for model-based control (Chapter 8).

REFERENCES

1. Schindler K.P., 1997, "Why Do We Need the Diesel", SAE Paper 972684.

2. Majewski W.A. and Khair, M.K., 2006, "Diesel Emissions and Their Control", R-303, SAE International, Warrendale.

3. Zheng M., 2004, "Fundamentals of Clean Diesel Engine Technology", Lecture Notes, University of Windsor.

4. Heywood J.B., 1988, "Internal Combustion Engine Fundamentals", McGraw-Hill Inc.

5. Zheng M., 2008, "Biodiesel Low Temperature Combustion", International Biofuels Symposium, SAE International Powertrain, Fuels and Lubricants Meeting, Tongji University, China.

6. Gillespie G., Martin R. and Vader S., 2007, "Development of a Lightweight Electric Urban Delivery Truck", Publication No. TP14757E, Transport Canada.

7. Harding Energy Inc., 2004, "Harding Battery Handbook for Quest® Rechargeable Cells and Battery Packs".

8. Benson R.S. and Whitehouse N.D., 1979, "Internal Combustion Engines", Pergamon Press.

9. Stone R, 1999, "Introduction to Internal Combustion Engines", 3rd Edition, Macmillan.

10. Bosch R. GmbH, 2007, "Automotive Handbook", 7th Edition, SAE International, Warrendale, USA.

11. Hiroyasu H., Nishida K., Suzuki M., Oda H., Yoshikawa S. and Arai M., 1992, "Total In-Cylinder Sampling Experiment on Emission Formation Processes in a D.I. Diesel Engine", SAE Paper 902062.

12. Aoyagi Y., Kamimoto T., Matsui Y. and Matsuoka S., 1980, "A Gas Sampling Study on the Formation Processes of Soot and NO in a DI Diesel Engine," SAE Paper 800254.

13. Donahue R.J., Borman G.L. and Bower G.R., 1996, "Cylinder-Averaged Histories of Nitrogen Oxide in a D.I. Diesel with Simulated Turbocharging", SAE Paper 942046.

14. Zhao H., Lowry G. and Ladommatos N., 1996, "Time-Resolved Measurements and Analysis of In-Cylinder Gases and Particulates in Compression-Ignition Engines", SAE Paper 961168.

15. Duggal V.K., Priede T. and Khan I.M., 1978, "A Study of Pollutant Formation within the Combustion Space of a Diesel Engine", SAE Paper 780227.

16. Voiculescu I.A., and Borman G.L., 1978, "An Experimental Study of Diesel Engine Cylinder-Averaged NOx Histories", SAE Paper 780228.

17. Kamimoto T. and Bae M-H., 1988, "High Combustion Temperature for Reduction of Particulate in Diesel Engines', SAE Paper 880423.

18. Shimazaki N., Hatanaka H., Yokota, K. and Nakahira T., 1996, "A Study of Diesel Combustion Process under the Condition of EGR and High-Pressure Fuel Injection with Gas Sampling Method", SAE Paper 960030.

19. Epsey C. and Dec J., 1993, "Diesel Engine Combustion Studies in a Newly Designed Optical-Access Engine Using High-Speed Visualization and 2-D Laser Imaging", SAE Paper 930971.

20. Uyehara O.A., 1980, "Diesel Combustion Temperature on Soot", SAE Paper 800969.

21. Mellor A.M., Mello J.P., Duffy K.P., Easley W.L. and Faulkner J.C., 1998, "Skeletal Mechanism for NOx Chemistry in Diesel Engines", SAE Paper 981450.

22. Teng H. and Regner G., 2006, "Fuel Injection Strategy for Reducing NOx Emissions From Heavy-Duty Diesel Engines Fuelled With DME", SAE Paper 2006-01-3324.

23. Turns S.R., 2000, "An Introduction to Combustion - Concepts and Applications", 2nd Edition, McGraw-Hill.

24. United States Environmental Protection Agency, 1999, "Nitrogen Oxides (NOx), Why and How They Are Controlled", Technical Bulletin, EPA-456/F-99-006R.

25. Ramos J.I., 1989, "Internal Combustion Engine Modelling", Taylor & Francis.

26. Majewski W.A., 2002, "Diesel Particulate Matter", DieselNet Technology Guide, www.dieselnet.com – Accessed on December 12, 2008.

27. Kook S., Bae C., Miles P.C., Choi D. and Pickett L.M., 2005, "The Influence of Charge Dilution and Injection Timing on Low-Temperature Diesel Combustion and Emissions", SAE Paper 2005-01-3837.

28. Miyamoto N., Ogawa H., Goto N. and Sasaki H., 1990, "Analysis of Diesel Soot Formation under varied Ignition Lag with a Laser Light Extinction Method", SAE Paper 900640.

29. Sjöberg M. and Dec J.E., 2005, "An Investigation into Lowest Acceptable Combustion Temperature for Hydrocarbon Fuels in HCCI Engines", Proceedings of the Combustion Institute, (30), pp. 2719-2726.

30. Zheng M., Reader G.T. and Hawley J.G., 2004, "Diesel Engine Exhaust Gas Recirculation – A Review on Advanced and Novel Concepts", Energy Conversion and Management, (45)-6, pp. 883-900.

31. Dec J.E., 1997, "A Conceptual Model of DI Diesel Combustion Based on Laser-Sheet Imaging", SAE Paper 970873.

32. US Environmental Protection Agency (EPA), March 2004, "Highway Diesel Progress Review-Report 2", Office of Transportation and Air Quality, EPA 420-R-04-004.

33. Dronniou N., Lejeune M. and Balloul I., 2005, "Combination of High EGR Rates and Multiple Injection Strategies to Reduce Pollutant Emissions", SAE Paper 2005-01-3726.

34. Ladomatos N., Abdelhalim S. and Zhao H., 1998, "Control of Oxides of Nitrogen from Diesel Engines using Diluents while minimizing the Impact on Particulate Pollutants", Applied Thermal Engineering, (18), pp. 963-980.

35. Akihama K., Takatori Y., Inagaki K., Sasaki S. and Dean A.M., 2001, "Mechanism of the Smokeless Rich Diesel Combustion by Reducing Temperature", SAE Paper 2001-01-0655.

36. Satoh K., Zhang L., Hatanaka H., Takatsuki T. and Yokota K., 1997, "Relationship between NOx and PM emissions from DI diesel engine with EGR", JSAE Review, (18)-4, pp. 369-375.

37. Jacobs T.J., Bohac S.V., Assanis D.N. and Szymkowicz P.G., 2005, "Lean and Rich Premixed Compression Ignition Combustion in a Light-Duty Diesel Engine", SAE Paper 2005-01-0166.

38. Idicheria C.A. and Pickett L.M., 2005, "Soot Formation in Diesel Combustion under High-EGR Conditions", SAE Paper 2005-01-3834.

39. Kweon C., Okada S., Stetter J.C., Christenson C.G., Shafer M.M., Schauer J.J. and Foster D.E., 2003, "Effect of Injection Timing on Detailed Chemical Composition and Particulate Size Distributions of Diesel Exhaust", SAE Paper 2003-01-1794.

40. Bessonette P.W., Schleyer C.H., Duffy K.P., Hardy W.L. and Liechty M.P., 2007, "Effects of Fuel Property Changes on Heavy-Duty HCCI Combustion", SAE Paper 2007-01-0191.

41. Alleman T.L. and McCormick R.L., 2003, "Fischer-Tropsch Diesel Fuels - Properties and Exhaust Emissions: a Literature Review", SAE Paper 2003-01-0763.

42. Forest C.A. and Muzzell P.A., 2005, "Fischer Tropsch Fuels: Why Are They of Interest to the U.S. Military?", SAE Paper 2005-01-1807.

43. Gjirja S., Olsson E. and Eklund A., 2000, "Fischer-Tropsch Fuels Impact on a Diesel Engine Performance" SAE Paper 2000-25-0006.

44. Schubert P.F., Russel B.J., Freerks R.L., DeVore J. and Fanick E.R., 2002, "Impact of Ultra-Clean Fischer-Tropsch Diesel Fuel on Emissions in a Light-Duty Passenger Car Diesel Engine", SAE Paper 2002-01-2725.

45. Natural Resources Canada, 2008, "What is Biodiesel?", Retrieved from http://oee.nrcan-rncan.gc.ca/transportation/fuels/biodiesel/biodiesel.cfm?attr=8 – December 13, 2008.

46. Choi C.Y. and Reitz R.D., 1999, "An Experimental Study on the Effects of Oxygenated Fuel Blends and Multiple Injection Strategies on DI Diesel Engine Emissions", Fuel, (78), pp. 1303-1317.

47. Lin C-Y. and Lin H-A., 2006, "Diesel Engine Performance and Emission Characteristics of Biodiesel Produced by the Peroxidation Process", Fuel, (85), pp. 298- 305.

48. Patterson J., Hassan M.G., Clarke A., Shama G., Hellgardt K. and Chen R., 2006, "Experimental Study of DI Engine Performance Using Three Different Biodiesel Fuels", SAE Paper 2006-01-0234.

49. Rosca R., Rakosi E., Manolache G. and Niculaua M., 2005, "Fuel and Injection Characteristics for Biodiesel Type Fuel from Waste Cooking Oil", SAE Paper 2005-01-3674.

50. Murayama T., Zheng M., Chikahisa T., Oh Y-T., Fujiwara Y., Tosaka S., Yamashita M. and Yoshitake H., 1995, "Simultaneous Reductions of Smoke and NOx from a

DI Diesel Engine with EGR and Dimethyl Carbonate", SAE Transactions, Paper 952518.

51. Monyem A., van Gerpen J.H., and Canakci M., 2001, "The Effect of Timing and Oxidation on Emissions from Biodiesel-fuelled Engines", Transaction of the American Society of Agricultural Engineers, (44)-1, pp. 35-42.

52. Zheng M., Mulenga M.C., Reader G.T., Tan Y., Wang M. and Tjong J, 2007, "Neat Biodiesel Fuel Engine Tests and Preliminary Modelling", SAE Paper 2007-01-0616.

53. Opdal O.A., December 2006, "Production of Synthetic Biodiesel via Fischer-Tropsch Synthesis", Norwegian University of Science and Technology.

54. Miers S.A., Ng H., Ciatti S.A. and Stork K., 2005, "Emissions, Performance, and In-Cylinder Combustion Analysis in a Light-Duty Diesel Engine Operating on a Fischer-Tropsch, Biomass-to-Liquid Fuel", SAE Paper 2005-01-3670.

55. Brusstar M.J. Hamady F.J. and Schaefer R.M., 2007, "Low Engine-Out NOx Emissions with DME Using High Pressure Injection", SAE Paper 2007-01-4093.

56. Chapman E.M., Boehman A., Wain K., Lloyd W., Perez J.M., Stiver D. and Conway J., 2003, "Impact of DME-Diesel Fuel Blend Properties on Diesel Fuel Injection Systems", Annual Technical Progress Report DE-FC26-01NT41115, Pennsylvania State University.

57. Kamimoto T., Yokota H., Kobayashi H., 1987, "Effect of High Pressure Injection on Soot Formation Processes in a Rapid Compression Machine to Simulate Diesel Flames", SAE 871610.

58. Frenklach M., Taki S., and Matula R.A., 1983, "A Conceptual Model for Soot Formation in Pyrolysis of Aromatic Hydrocarbons." Combustion and Flame, (49), pp. 275-282.

59. Kitamura T., Ito T., Senda J., and Fujimoto H., 2002, "Mechanism of Smokeless Diesel Combustion with Oxygenated Fuels Based on the Dependence of the

Equivalence Ratio and Temperature on Soot Particle Formation", Internal Journal of Engine Research, (3), pp. 223-248.

60. Zheng M., **Asad U.**, Reader G.T., Tan Y. and Wang M., 2008, "Energy Efficiency Improvements for a Diesel Engine in Low Temperature Combustion", International Journal of Energy Research, International Journal of Energy Research, (33), pp. 8-28.

61. Zhao F., Asumus T., Assanis D., Dec J., Eng J. and Najt P., 2003, "Homogeneous Charge Compression Ignition (HCCI) Engines, Key Research and Development Issues", SAE SP-94.

62. **Asad U.** and Zheng M., 2008, "EGR Oxidation and Catalytic Fuel Reforming for Diesel Engines", ASME Internal Combustion Engine Division Paper ICES 2008-01-1684.

63. Zheng M. and **Asad U.**, 2007, "Preliminary Energy Efficiency Analyses of Diesel EGR Fuel Reforming with Flow Reversal and Central Fuelling", SAE 2007 Transactions-Journal of Fuels and Lubricants, (116)-4, pp. 896-908, 2007-01-4035.

64. Stanglmaier R.H. and Roberts C.E., 1999, "Homogeneous Charge Compression Ignition, HCCI: Benefits, Compromises and Future Engine Applications", SAE Paper 1999-01-3682.

65. Helmantel A. and Denbratt I., 2004, "HCCI Operation of a Passenger Car Common-Rail DI Diesel Engine with Early Injection of Conventional Diesel Fuel", SAE Paper 2004-01-0935.

66. Kodama Y., Nishizawa I., Sugihara T., Sato N., Iijima T. and Yoshida T., 2007, "Full-load HCCI Operation with Variable Valve Actuation System in a Heavy-Duty Diesel Engine", SAE Paper 2007-01-0215.

67. Shimazaki N., Minato A. and Nishimura T., 2007, "Premixed Diesel Combustion using Direct Injection near Top Dead Centre", International Journal of Engine Research, (8), pp. 259-270.

68. Zheng M., Mulenga M.C., Reader G.T., Wang M. and Ting D.S-K., 2006, "Influence of Biodiesel Fuel on Diesel Engine Performance and Emissions in Low Temperature Combustion", SAE Paper 2006-01-3281.

69. Takeda Y. and Keiichi N., 1996, "Emission Characteristics of Premixed Lean Diesel Combustion with Extremely Early Staged Fuel Injection", SAE Paper 961163.

70. Shimazaki N., Akagawa H. and Tsujimura K., 1999, "An Experimental Study of Premixed Lean Diesel Combustion", SAE Paper 1999-01-0181.

71. Iwabuchi Y., Kawai K., Shoji T. and Takeda Y., 1999. "Trial of New Concept Diesel Combustion System - Premixed Compression-Ignition Combustion", SAE Paper 1999-01-0185.

72. Yanagihara H., 2001, "Ignition Timing Control at Toyota 'UNIBUS' Combustion System", A new Generation of Engine Combustion Processes for the Future, pp. 35-42, Editions Technip, Paris.

73. Hasegawa R. and Yanagihara H., 2003, "HCCI Combustion in DI Diesel Engine", SAE Paper 2003-01-0745.

74. Kimura S., Aoki O., Ogawa H., Muranaka S. and Enomoto Y., 1999, "New Combustion Concept for Ultra-Clean and High-Efficiency Small DI Diesel Engines", SAE Paper 1999-01-3681.

75. Kimura S., Ogawa H., Matusi M. and Enomoto Y., 2002, "An Experimental Analysis of Low Temperature and Premixed Combustion for Simultaneous Reduction of NOx and Particulate Emissions in Direct Injection Diesel Engines", Int Journal of Engine Research, (3)-4, pp. 249-259.

76. Kimura S., Aoki O., Kitahara Y. and Aiyoshizawa E., 2001, "Ultra-Clean Combustion Technology Combining a Low-Temperature and Premixed Combustion Concept for Meeting Future Emission Standards", SAE Paper 2001-01-0200.

77. Zheng M., **Asad U.**, Kumar R., Reader G.T., Mulenga M.C., Bombardier W., Wang M and Tjong J., 2007, "An Investigation of EGR Treatment on the Emission and Operating Characteristics of Modern Diesel Engines", SAE Paper 2007-01-1083.

78. Zheng M., Reader G.T., **Asad U.**, Tan Y. and Wang M., 2008, "Adaptive Control to Improve Low Temperature Diesel Engine Combustion", Paper No. DE1-2, Proceedings of the 7th COMODIA International Conference on Modelling and Diagnostics for Advanced Engine Systems, Japan.

79. Colban W.F., Miles P.C. and Oh S., 2007, "Effect of Intake Pressure on Performance and Emissions in an Automotive Diesel Engine Operating in low Temperature Combustion Regimes", SAE Paper 2007-01-4063.

80. Mariani F. and Postrioti L., 1996, "Modelling Diesel Engine Using KIVA II 3D-Code: Validation of a New Global Combustion Model and its Sensitivity to the Spatial Discretization", SAE Paper 960872.

81. Zheng M., 1993, "Thermodynamic Modelling and Experimental Investigation of a Synthetic Atmosphere Diesel Engine System", PhD Thesis, University of Calgary, Canada.

82. Han X., **Asad U.**, Kumar R., Mulenga M.C., Banerjee S., Wang M., Reader G.T. and Zheng M., 2007, "Empirical Studies of the Diesel Low Temperature Combustion on a Modern Diesel Engine", Combustion Institute/Canadian Section, 2007 Spring Technical Meeting.

83. Bowen, C.E., 1998, "An Experimental Investigation into the Use of Exhaust Gas Recirculation for Diesel Engine NOx Control", PhD Thesis, University of Calgary, Canada.

84. National Instruments Corporation, 2004, "**Lab**oratory **V**irtual **I**nstrumentation **E**ngineering **W**orkbench (LabVIEW)", Version 7.1.

85. Cambustion Limited, 2004, "HFR 500 Fast Response FID Hydrocarbon Measurement System – User Manual", Version 2.6.

86. Cambustion Limited, 2004, “fNOx400 Fast Response Nitric Oxide Measurement System – User Manual”, Version 1.17.

87. Lancaster D.R., Krieger R.B. and Lienesch J.H., 1975, “Measurement and Analysis of Engine Pressure Data”, SAE Paper 750026.

88. Hori M., Matsunaga N., Marinov N., Pitz W. and Westbrook C., 1998, “"An Experimental and Kinetic Calculation of the Promotion Effect of Hydrocarbons on the NO-NO_2 Conversion in a Flow Reactor," Proceedings of the Combustion Institute, Volume 27, pp. 389-396.

89. Sandia National Laboratories, 2006, “A Detailed Molecular-beam Mass-spectrometric Study and Modelling of a Low-pressure Dimethyl Ether Flame”, CRF News, Volume 28, No.3, pp. 4-5.

90. Shudo T., Ono Y. and Takahashi T., 2002, “Influence of Hydrogen and Carbon Monoxide on HCCI Combustion of Dimethyl Ether”, SAE Paper 2002-01-2828.

91. Iida N. and Sato S., 2003, “Analysis of DME Homogeneous Charge Compression Ignition Combustion”, SAE Paper 2003-01-1825.

92. Khalil S.K., Wallace F.J. and Hawley J.G., 2002, “Further Developments of a Computational Model for HSDI Diesel Engines with High-pressure Common Rail Fuel Injection”, Proceedings of Thermo- and Fluid Dynamic Processes in Diesel Engines (Thiesel), Valencia, Spain, pp. 471–485.

93. Lyn W.T., 1962, “Study of Burning Rate and Nature of Combustion in a Diesel Engine”, Proceedings of Ninth International Symposium on Combustion, The Combustion Institute, pp. 1069-1082.

94. Grimm B.M. and Johnson R.T., 1990, “Review of Simple Heat Release Computations”, SAE Paper 900445.

95. Krieger R.B. and Borman G.L., 1966, “The Computation of Apparent Heat Release for Internal Combustion Engines”, Proc. Diesel Gas Power, ASME 66-WA/DGP-4.

96. Gatowski J.A., Balles E.N., Chun K.M., Nelson F.E., Ekchian J.A. and Heywood, J.B., 1984, "Heat Release Analysis of Engine Pressure Data", SAE Paper 841359.

97. Brunt M.F.J., Rai H. and Emtage A.L., 1998, "The Calculation of Heat Release Energy from Engine Cylinder Pressure Data", SAE Paper 981052.

98. Brunt M.F.J. and Platts K.C., 1999, "Calculation of Heat Release in Direct Injection Diesel Engines", SAE Paper 1999-01-0187.

99. Lakshminarayanan P.A., Aghav Y.V., Dani A.D. and Mehta P.S., 2002, "Accurate Prediction of the Heat Release in a Modern Direct Injection Diesel Engine", Proceedings of the Institute of Mechanical Engineers, (216), pp. 663–675.

100. **Asad U.**, Zheng M., Ting D.S-K, Kumar R., Banerjee S., Reader G.T. and Tjong J., 2006, "Real-time Heat Release Analysis towards On-fly Combustion Control for Diesel Engines", Proceedings of the Combustion Institute/Canadian Section, Spring Technical Meeting, Waterloo, Canada.

101. Reitz R.D. and Hardy W.L., 2006, "An Experimental Investigation of Partially Premixed Combustion Strategies Using Multiple Injections in a Heavy-Duty Diesel Engine", SAE Paper 2006-01-0917.

102. Maiboom A., Tauzia X. and Hétet J-F., 2008, "Experimental Study of Various Effects of Exhaust Gas Recirculation (EGR) on Combustion and Emissions of an Automotive Direct Injection Diesel Engine", Energy, (33)-1, pp. 22-34.

103. Zheng M., Reader G.T., Kumar R., Mulenga C., **Asad U.**, Tan Y. and Wang M., 2006, "Adaptive Control to Improve Low Temperature Diesel Engine Combustion", 12th Diesel Engine-Efficiency and Emission Reduction (DEER) Conference, Michigan, USA.

104. Kim M.Y. and Lee C.S., 2007, "Effect of a Narrow Fuel Spray Angle and a Dual Injection Configuration on the Improvement of Exhaust Emissions in a HCCI Diesel Engine", Fuel, (86), pp. 2871-2880.

105. Chryssakis C.A. and Assanis D.N., 2005, "Effect of Multiple Injections on Fuel-Air Mixing and Soot Formation in Diesel Combustion using Direct Flame Visualization and CFD Techniques", ASME ICES 2005-1016.

106. Zheng M., Mulenga M.C., Reader G.T., Wang M., Ting D.S–K. and Tjong J., 2008, "Biodiesel Engine Performance and Emissions in Low Temperature Combustion", Fuel (87), pp. 714-722.

107. Kumar R., Zheng M., **Asad U.** and Reader G.T., 2007, "Heat Release based Adaptive Control to Improve Low Temperature Diesel Engine Combustion", SAE Paper 2007-01-0771.

108. Zheng M., Kumar R. and Reader G.T., 2006, "Adaptive Fuel Injection Tests to Extend EGR Limits on Diesel Engines", SAE Paper 2006-01-3426.

109. Bengtsson J., Strandh P., Johansson R., Tunestål P. and Johansson B., 2004, "Control of Homogeneous Charge Compression Ignition (HCCI) Engine Dynamics", Journal of Adaptive Control and Signal Processing, (18)-2, pp. 167-179.

110. Amann C., 1985, "Cylinder Pressure Measurement and its Use in Engine Research", SAE Paper 852067.

111. Rassweiler G.M. and Withrow L., 1938, "Motion Pictures of Engine Flames Correlated with Pressure Cards", SAE Journal (Trans), (42), pp. 185-204 (Reprinted SAE Paper 800131, 1980).

112. Telborn K., 2002, "A Real-Time Platform for Closed-Loop Control and Crank Angle based Measurement", Masters Thesis, Linköping University, Sweden.

113. Klein M., 2004, "A Specific Heat Ratio Model and Compression Ratio Estimation", Linköping University, Sweden.

114. Sellnau M.C., Matekunas F.A., Battiston P.A., Chen-Fang C. and Lancaster D.R., 2000, "Cylinder-Pressure-Based Engine Control Using Pressure-Ratio-Management and Low-Cost Non-Intrusive Cylinder Pressure Sensors", SAE Paper 2000-01-0932.

115. Matekunas F., November 1986, "Engine Combustion Control with Ignition Timing by Pressure Management Ratio", US Patent No 4622939.

116. Timnoey D.J., 1987, "Problems with Heat Release Analysis in D.I. Diesel", SAE Paper 870270.

117. Timoney D.J., 1987, "Effects of Important Variables on Measured Heat Release Rates in a D.I. Diesel", SAE Paper 870271.

118. Karim G.A. and Khan M.O., 1971 "An Examination of Some of the Errors Normally Associated with the Calculation of Apparent Rates of Combustion Heat Release in Engines", SAE Paper 710135.

119. Rocco V., 1993, "D.I. Diesel Engine In-Cylinder Pressure Data Analysis under TDC. Setting Error", SAE Paper 930595.

120. Bosch R. GmbH, 2005, "Planar Wide Band Lambda Sensor-LSU4.9", Technical Product Information # Y258E00015e, June 2005.

121. Tsolakis A., Hernandez J.J., Megaritis A. and Crampton M., 2005, "Dual Fuel Diesel Engine Operation Using H_2 Effect on Particulate Emissions", Energy & Fuels (19), pp. 418-425.

122. Tsolakis A., Megaritis A. and Wyszynski M.L., 2003, "Application of Exhaust Gas Fuel Reforming in Compression Ignition Engines Fuelled by Diesel and Biodiesel Fuel Mixtures", Energy & Fuels, (17), pp. 1464-1473.

123. Nagaki H., Furutani H., and Takahashi S., 1999, "Acceptability of Premixed Hydrogen in Hydrogen Diesel Engine", SAE 1999-01-2521.

124. Kirwan J.E., Quader A.A. and Grieve M.J., 2002, "Fast Start-Up On-Board Gasoline Reformer for Near Zero Emissions in Spark-Ignition Engines", SAE 2002-01-1011.

125. Tsolakis A., Megaritis A. and Wyszynski M.L., 2004, "Low Temperature Exhaust Gas Fuel Reforming of Diesel Fuel", Fuel, (83), pp. 1837–1845.

126. Kumar R., Zheng M., Reader G. T., Ko S. J. and Ting D. S-K., 2004, "Preliminary Energy Efficiency Analysis of an EGR Fuel-Reformer", SAE Transactions, 2004-01-2918.

127. Zheng M. and Reader G.T., 2004, "Energy Efficiency Analyses of Active Flow Aftertreatment Systems for Lean Burn Internal Combustion Engines", Energy Conversion and Management, (45), pp. 2473–2493.

128. **Asad U.**, Banerjee S., Reader G.T., Wang M. and Zheng M., 2007, "Energy Efficiency Analysis between In-cylinder and External Supplemental Fuel Strategies", SAE Paper 2007-01-1125.

129. Zheng M., Mirosh E.A., Klopp W.E., Ulan D.A. , Pardell M.E., Newman P.E. and Matros Y.S., 1999, "Development of a Compact Reverse-Flow Catalytic Converter for Diesel Dual-Fuel LEV", SAE Paper 1999-01-3558.

130. Liu B., Hayes R.E., Checkel M.D., Zheng M. and Mirosh E., 2001, "Reverse Flow Catalytic Converter for a Natural Gas/Diesel Dual Fuel Engine", J Chem Eng Sci, (56), pp. 2641–58.

131. Crabtree G.W., Dresselhaus M.S. and Buchanan M.V., 2004, "The Hydrogen Economy", Physics Today, (57)-12, pp. 39-45.

132. Delphi Corporation, 2006, "Delphi Diesel Fuel Reformer System", retrieved from http://ppd.delphi.com/pdf/ppd/pwrtrn/dsl_fuel_ref_sys.pdf – Accessed on December 12, 2008.

133. Cohn D.R., 2006, "Onboard-Plasmatron Hydrogen Production", 2006 U.S. Department of Energy Heavy Vehicle Systems Review, Argonne National Laboratory, Illinois, USA.

134. Kong Y., Crane S., Patel P. and Taylor B., 2004, "NOx Trap Regeneration with an On-Board Hydrogen Generation Device", SAE 2004-01-0582.

135. Alriksson M., Gjirja S. and Denbratt I., 2007, "The Effect of Charge Air and Fuel Injection Parameters on Combustion with High Levels of EGR in a HDDI Single Cylinder Diesel Engine", SAE Paper 2007-01-0914.

136. Vanegas A., Won H., Felsch C., Gauding M. and Peters N., 2008, "Experimental Investigation of the Effect of Multiple Injections on Pollutant Formation in a Common-Rail DI Diesel Engine: SAE Paper 2008-01-1191.

137. Mendez S. and Thirouard B., 2008, "Using Multiple Injection Strategies in Diesel Combustion: Potential to Improve emissions, Noise and Fuel Economy Trade-off in Low CR Engines", SAE Paper 2008-01-1329.

138. Satoh K., Zhang L., Hatanaka H., Takatsuki T. and Yokota K., 1997, "Relationship between NOx and PM emissions from DI diesel engine with EGR", JSAE Review, (18)-4, pp. 369-375.

139. Yun H., Sellnau M., Milovanovic N. and Zuelch S., 2008, "Development of Premixed Low-Temperature Diesel Combustion in a HSDI Diesel Engine", SAE Paper 2008-01-0639.

140. Huang Y., Sung C.J. and Eng J.A., 2004, "Dilution limits of n-Butane/Air Mixtures under Conditions Relevant to HCCI Combustion", Combustion and Flame (136), pp. 457–466.

141. Liao S.Y., Jiang D.M., Huang Z.H., Cheng Q., Gao J. and Hu Y., 2005, "Approximation of Flammability Region for Natural Gas–Air–Diluent Mixture", Journal of Hazardous Materials (A125), pp. 23–28.

142. Shebeko Y.N., Fan W., Bolodian I.A. and Navzenya V.Y., 2002, "An analytical Evaluation of Flammability Limits of Gaseous Mixtures of Combustible–Oxidizer–Diluent", Fire Safety Journal, (37), pp. 549–568.

143. Borman G.L. and Gagland K.W., 1998, "Combustion Engineering", WCB/McGraw-Hill, USA.

144. Zheng M., Tan Y., Mulenga M.C. and Wang M., 2007, "Preliminary Thermal Efficiency Analyses of Diesel Low Temperature Combustion Cycles", SAE Transactions, (116)-4, 2007-01-4019.

145. Shaver G.M., Roelle M.J. and Gerdes J.C., 2006, "Modelling Cycle-to-Cycle Dynamics and Mode Transition in HCCI Engines with Variable Valve Actuation", Journal of Control Engineering Practice, (14), pp. 213–222.

146. Abdel-Rahman A., 1998, "On the Emissions from Internal Combustion Engines: a Review", International Journal of Energy Research, (22), pp. 483–513.

147. **Asad U.**, Zheng M., Han X., Reader G.T. and Wang M., 2008, "Fuel Injection Strategies to Improve Emissions and Efficiency of High Compression Ratio Diesel Engines", SAE Transactions, (117)-4, 2008-01-2472.

148. Helmantel A., 2008, "Reduction of NOx Emissions from a Light Duty DI Diesel Engine in Medium Load Conditions with High EGR Rates", SAE Paper 2008-01-0643.

149. Hiroyasu H. and Arai M., 1990, "Structure of Fuel Sprays in Diesel Engines", SAE Transactions, (99)-2, pp. 1050-1061, 900475.

150. Naber J.D. and Siebers D.L., 1996, "Effects of Gas Density and Vaporization on Penetration and Dispersion of Diesel Sprays", SAE Paper 960034.

151. Kennaird D., Crua C., La Coste J., Heikal M., Gold M. and Jackson N., 2002, "In-Cylinder Penetration and Break-Up of Diesel Sprays Using a Common-Rail Injection System", SAE Paper 2001-01-1626.

152. Noehre C., Andersson M., Johansson B. and Hultqvist A., 2006, "Characterization of Partially Premixed Combustion", SAE Paper 2006-01-3412.

153. Kuhn M., 2007, "Challenges of Meeting Tier 2 Bin 2 Tailpipe Emissions", 13th Diesel Engine-Efficiency and Emissions Research (DEER) Conference, Michigan, USA.

154. Annand W.J.D., 1963, "Heat transfer in the Cylinders of Reciprocating Internal Combustion Engines", Proc. Instn. Mechanical Engineers, (177)-36, pp 973-990.

155. Woschni G., 1967, "A Universally Applicable Equation for the Instantaneous Heat Transfer Coefficient in the Internal Combustion Engine", SAE Paper 670931.

156. Silvis W.M., 1997, "An Algorithm for Calculating the Air/Fuel Ratio from Exhaust Emissions", SAE Paper 970514.

APPENDIX A: SIGNIFICANT SAE PAPERS ON DIESEL LTC & HTC STRATEGIES

Table A.1 lists some of the important SAE publications during the last 2 decades describing the LTC strategies for simultaneous reduction of NOx and soot in diesel engines.

Table A.1: Significant Publications on LTC

Publication	Major Engine Specifications	Tested Fuels
Early-HCCI		
SAE 830264 (Port Injection)	CR 7.5:1	Iso-octane ,n-heptane, isopropyl-benzene
SAE-961160 (Port Injection)	CR 7.5:1 to 17:1, SR 2.7, Mexican hat re-entrant bowl	Diesel
SAE 2003-01-2293 (Port Injection)	CR 14:1 to 18:1, ω bowl	Diesel fuels and blends
SAE 2006-01-3281 (Port Injection)	CR 17.8: 1, Mexican hat bowl	Diesel, Bio-diesel
SAE 2005-01-2127 (Port Injection)	CR 11.4:1, shallow bowl	n-heptane
SAE 1999-01-3679 (Port Injection)	CR 9.6:1 to 22.5:1	Diesel, Gasoline, Iso-octane, n-heptane
SAE 961163, 970898 (PREDIC)	CR 16.5:1, Shallow dish bowl	Diesel
SAE 980533, 1999-01-0181 1999-01-0183 (PREDIC)	CR 16.5:1, Shallow dish bowl	Diesel, DME, Propane
SAE 2003-01-0745, 2003-01-1817 (UNIBUS)	CR 18.4:1, Squish lip type bowl	Diesel, n-heptane
SAE 1999-01-0185 (PCI)	CR 12:1	Diesel
SAE 2004-01-1907 (PCI)	CR 14.5:1, Shallow dish toroidal bowl	Diesel
SAE 2007-01-3614 (PCI)	CR 12.5, 14, 16.5 and 20:1, SR 2.1, Re-entrant bowl	Diesel
SAE 2007-01-0215 (Early HCCI)	10 to 16.8:1, Variable valve timing, Re-entrant, shallow dish and deep-bowl	Diesel

Single-Injection LTC with Heavy EGR		
SAE 2001-01-0655 (Smokeless Rich Combustion)	CR18.6:1	Diesel
SAE 2006-01-3386 (Smokeless Rich Combustion)	CR 16:1, Swirl Ratio 2.2	Diesel
SAE 1999-01-3681 (MK Combustion)	CR 18:1, SR 3 ~5, Toroidal	Diesel
SAE 2001-01-0200 (MK Combustion)	CR 16 to 17.5:1, SR 3.6 ~10, Toroidal bowl	Diesel
Catalytic EGR Fuel Reforming		
SAE 2007-01-1083	CR 17.8:1, Mexican hat bowl	Diesel
SAE 2007-01-2044	NA	Diesel
SAE 2007-01-4035	CR 17.8:1, Mexican hat bowl	Diesel

Some important SAE publications during the last 2 decades that describe the improvements made in the NOx-soot trade-off and the technologies involved are presented in Table A.2.

Table A.2: Publications detailing the NOx-Soot Trade-off Improvements

Publication	Improvement Technique
SAE 930592	Boost, Injection Timing, Pressure &Rate Shaping, Swirl Ratio
SAE 941926	2-valve to 4-valve per cylinder, Swirl Ratio
SAE 950604	Injection Pressure, Nozzle Geometry
SAE 960633	Multiple-Injection Schemes
SAE 960840	EGR Cooling
SAE 981931	Air Path Optimization, Common-rail Injection
SAE 1999-01-1502	Combustion Chamber Design, Swirl Ratio
SAE 2000-01-0510 SAE 2000-01-0946	Combustion Chamber Design

SAE 2001-01-0197	Injection Pressure, Swirl Ratio
SAE 2001-01-3260	Advanced Turbocharging Technologies
SAE 2002-01-0502	Post Injection Patterns
SAE 2003-01-1793	Boost, Combustion Chamber & Nozzle Designs
SAE 2003-01-1783	Nozzle Hole Size
SAE 2005-01-0907	Fuel Injection Rate Shaping
SAE 2008-01-0641	Post Injection

APPENDIX B: FIRST LAW HEAT RELEASE MODEL

The basis for the modelling of the heat release is the first law of thermodynamics for an open system and is stated as:

$$\delta Q_{gr} = dU + \delta W + \sum h_i dm_i + \delta Q_{ht} \qquad \text{(B.1)}$$

where δQ_{gr} is the chemical energy released during combustion, dU is the change in the sensible energy of the charge, δW represents the piston work, equal to pdV. The mass flux term is the flow across the system boundary due to the fuel injection and flows into and out of crevice regions and piston ring blow-by.

The cylinder charge is treated as a single zone with the following assumptions:

- Uniform thermodynamic properties and gas composition throughout the combustion chamber; Heterogeneity of the charge is neglected.
- The heat release process is based on the averaged properties in a single zone.
- Equilibrium thermo-chemistry is assumed (chemical dissociation is ignored).
- Piston blow-by is neglected.
- The gas mixture follows the ideal gas law.

The change in the sensible energy can therefore be written as:

$$dU = m_c c_v(T)dT + u(T)dm_c \qquad \text{(B.2)}$$

where m_c is the mass of the cylinder charge (kg), c_v is the specific heat at constant volume (J/kg K) and u is the specific internal energy (J/kg K).

From the ideal gas law, neglecting the change in the specific gas constant, R, the following equation can be written:

$$dT = \frac{1}{m_c R}\left(pdV + Vdp - RTdm_c\right) \tag{B.3}$$

$$c_v = \frac{R}{\gamma - 1} \tag{B.4}$$

where T is the mean charge temperature (K), p is the cylinder pressure (Pa), V is the cylinder volume (m^3), $\gamma = c_p / c_v$ (gamma) is the ratio of the specific heats.

Inserting Equations (B.2), (B.3), (B.4) in Equation (B.1), the heat released during combustion is:

$$\delta Q_{gr} = \frac{1}{\gamma - 1}\left[\gamma pdV + Vdp + \left(u - c_v T\right)dm_c\right] - \sum h_i dm_i + \delta Q_{ht} \tag{B.5}$$

or on a crank angle basis,

$$\frac{dQ_{gr}}{d\theta} = \frac{1}{\gamma - 1}\left[\gamma p\frac{dV}{d\theta} + V\frac{dp}{d\theta} + \left(u - c_v T\right)\frac{dm_c}{d\theta}\right] - \sum h_i \frac{dm_i}{d\theta} + \frac{dQ_{ht}}{d\theta} \tag{B.6}$$

Equation (B.6) gives the gross heat release rate during the period from intake valve closure (IVC) to exhaust valve closure (EVC) for the crank angle interval, $d\theta$. The cumulative heat release Q_{cum} is obtained by summing the incremental values from equation (B.6) over the combustion period, from the start of combustion (SOC) to the estimated end of combustion (EOC) so that

$$Q_{cum,gross} = \sum_{i=SOC}^{EOC} dQ_{gr,i} \tag{B.7}$$

The in-cylinder heat transfer rate in Equation (B.6) can be estimated from empirical heat transfer correlations by Annand [154] or Woschni [155].

Annand's Heat Transfer Correlation:

$$\begin{gathered}\frac{dQ_{ht}}{dt}=A_c\left[a\frac{k}{D}(\mathrm{Re})^b\left(T-T_w\right)+c\left(T^4-T_w^4\right)\right]\\ \mathrm{Re}=\frac{\rho v_p D}{\mu}\end{gathered}\tag{B.8}$$

where A_c is the combustion chamber surface area (m^2), T_w is the mean wall temperature (K), t is the time (s), k is the thermal conductivity (Wm^{-2}K^{-1}), ρ is the density (kg/m^3), μ is the dynamic viscosity of the cylinder charge (Pa.s), Re is the Reynolds number, a,b,c are Annand's empirical coefficients, D is the cylinder bore (m) and $v_p=2NS$ is the mean piston speed (m/s) with S as the piston stroke (m) and N as the engine speed in revolutions per second.

For direct injection diesel engines, the typical values of the constants are $a=0.26\sim0.375$, $b=0.75\pm0.15$ and $c=3.88\pm1.39\times10^{-8}$ $(Wm^{-2}K^{-4})$.

Woschni's Correlation:

$$\begin{gathered}\frac{dQ_{ht}}{dt}=A_c\left[C_3D^{-0.2}p^{0.8}T^{-0.53}v_c^{\ 0.8}\right]\left(T-T_w\right)\\ v_c=C_1v_p+C_2\frac{VT_r}{p_rV_r}\left(p-p_{mot}\right)\end{gathered}\tag{B.9}$$

where C_1,C_2,C_3 are Woschni's empirical coefficients, v_c is the characteristics velocity (m/s), p_r,V_r,T_r are the pressure (Pa), volume (m^3) and temperature (K) at a convenient reference state and p_{mot} is the motored cylinder pressure at the same crank angle as p (Pa). For the closed cycle calculations, $C_1=2.28+0.308\left(v_s/v_p\right)$ where $v_s=\pi DNS_R$ is the swirl velocity (m/s) and S_R is the swirl ratio. $C_3=0.0128$, $C_2=0$ before combustion and $C_2=3.24\times10^{-3}\left(ms^{-1}K^{-1}\right)$ during combustion. The reference state is usually chosen as the crank angle of the intake valve closing.

Ratio of Specific Heats:

The ratio of specific heats or gamma varies with the charge temperature and composition, and has a significant effect on the rate of heat release. Variation in the EGR, air excess ratio (λ), the charge pressure and temperature affect the gamma value to varying degrees but generally, it is found sufficient to vary gamma as a function of temperature only [98]. A number of correlations exist in the literature for estimating the temperature dependence of the ratio of specific heats [81,119]. Most are of the form:

$$\gamma = a_0 + a_1 T + a_2 T^2 + a_3 T^3 + a_4 T^4 \tag{B.10}$$

where a_0, a_1, a_2, a_3, a_4 are coefficients from curve fitting the empirical data. A good estimation can be made by taking $a_0 = 1.439$, $a_1 = -1.295 \times 10^{-4}$, $a_2 = 2.138 \times 10^{-8}$, $a_3 = 7.047 \times 10^{-12}$, $a_4 = -1.877 \times 10^{-15}$.

APPENDIX C: CARBON BALANCE METHOD FOR ESTIMATING COMBUSTION METRICS

The calculation of the air/fuel ratio from the composition of the exhaust gases is based on the general equation for the complete combustion of a hydrocarbon fuel with air, suitably modified to account for the actual combustion conditions. It is often assumed that air is a simple mixture of oxygen and nitrogen. Actually, air contains a number of other gases, notably about 1.8% argon and 0.035% CO_2. The inert gases do not take part in the combustion and can be lumped together with the nitrogen. The CO_2 quantity is small and ignoring it causes a 0.2% error in the calculated results [156]. The following equation represents the combustion of a hydrocarbon fuel with air:

$$\begin{aligned}&C_\alpha H_\beta O_\gamma + \lambda\left(\alpha+\frac{\beta}{4}-\frac{\gamma}{2}\right)(O_2+3.76N_2)\rightarrow\\&\alpha CO_2+\frac{\beta}{2}H_2O+\lambda\left(\alpha+\frac{\beta}{4}-\frac{\gamma}{2}\right)3.76N_2+(\lambda-1)\left(\alpha+\frac{\beta}{4}-\frac{\gamma}{2}\right)O_2\end{aligned} \tag{C.1}$$

However, the actual exhaust composition also contains the incomplete products of combustion namely CO and HC. Therefore, Equation (C.1) can be rewritten as follows:

$$\begin{aligned}&C_\alpha H_\beta O_\gamma + \lambda\left(\alpha+\frac{\beta}{4}-\frac{\gamma}{2}\right)(O_2+3.76N_2)\rightarrow CO_2+H_2O\\&+\left(CO+H_\beta C_\alpha\right)+\lambda\left(\alpha+\frac{\beta}{4}-\frac{\gamma}{2}\right)3.76N_2+O_2\end{aligned} \tag{C.2}$$

Note that the mole quantities of carbon, hydrogen and oxygen are not balanced in Equation (C.2).

The carbon contained in the fuel that is added to the system should be quantitatively equal to the carbon that is contained in the engine exhaust. Therefore, by measuring the actual concentrations of the CO_2, CO and HC in the exhaust, a number of combustion metrics can be determined. It is important to note that the application of EGR results in the recirculation of the exhaust gas back into the intake stream and the composition of the

EGR is the same as that of the exhaust gases. Therefore, the application of EGR does not affect the calculations using the carbon balance method.

$$\text{Reactants: Fuel } \left(\dot{m}_f\right) + \text{Fresh Air } \left(\dot{m}_a\right) + \text{EGR } \left(\dot{m}_{EGR}\right)$$

$$\text{Products: Exhaust } \left(\dot{m}_f + \dot{m}_a + \dot{m}_{EGR}\right)$$

The measurement of the exhaust species is done on a dry basis at standard temperature and pressure. Therefore, the amount of water removed during the conditioning of the exhaust gas needs to be accounted for. Moreover, the molecular weight of the exhaust gas can be calculated or can be assumed to be equal to that of the air (28.97 g/mol) without incurring a significant error in the calculation [156].

The following calculations are shown for a hydrocarbon fuel with no oxygen ($\gamma = 0$), i.e. $C_\alpha H_\beta$. It is assumed that all the carbon in the reactants comes from the fuel and therefore, the mass of carbon in the fuel can be written as:

$$\text{Mass of Carbon in Fuel} = \dot{m}_f \frac{12.011\alpha}{MW_f}$$

The mass of carbon in the exhaust can be written as follows:

$$\text{Mass of Carbon in Exhaust} = \frac{12.011\left(\dot{m}_f + \dot{m}_a - \dot{m}_{H_2O}\right)\cdot\left(y_{CO_2} + y_{CO} + \alpha y_{HC}\right)}{MW_{exh}}$$

Combining these expressions, the carbon mass balance for the combustion is given by the following equation:

$$\frac{\alpha \dot{m}_f}{MW_f} = \frac{\left(\dot{m}_f + \dot{m}_a - \dot{m}_{H_2O}\right)\cdot\left(y_{CO_2} + y_{CO} + \alpha y_{HC}\right)}{MW_{exh}} \tag{C.3}$$

where

$\dot{m}_f$ is the mass flow rate of fuel (g/s)

$\dot{m}_a$ is the mass flow rate of fresh air (g/s)

$\dot{m}_{H_2O}$ is the mass flow rate of water removed from the exhaust sample (g/s)

y_i is mole fraction of the exhaust species $(i = CO_2, CO, HC)$

MW_f is the molecular weight of the fuel and equal to $12.011\alpha + 1.008\beta$ g/mol

MW_{exh} is the molecular weight of the exhaust gas and equal to 28.97 g/mol.

Similarly, the hydrogen balance can be written as:

$$\frac{\beta \dot{m}_f}{MW_f} = \frac{\left(\dot{m}_f + \dot{m}_a - \dot{m}_{H_2O}\right) \cdot \beta \left(y_{HC}\right)}{MW_{exh}} + \frac{2m_{H_2O}}{18.016} \tag{C.4}$$

Equations (C.3) and (C.4) are two equations with two unknowns, $\dot{m}_f$ and $\dot{m}_{H_2O}$. Equation (C.3) can be rewritten in terms of $\dot{m}_{H_2O}$ as follows:

$$\dot{m}_{H_2O} = \left[\frac{\dfrac{\left(\dot{m}_f + \dot{m}_a\right) \cdot \left(y_{CO_2} + y_{CO} + \alpha y_{HC}\right)}{MW_{exh}} - \dfrac{\alpha \dot{m}_f}{MW_f}}{y_{CO_2} + y_{CO} + \alpha y_{HC}} \right] \tag{C.5}$$

Substituting Equation (C.5) in Equation (C.4) and solving for the air/fuel ratio (AFR), we get:

$$AFR = \frac{\dot{m}_a}{\dot{m}_f} = \frac{9.008\beta \cdot \left(y_{CO_2} + y_{CO}\right) + \alpha \cdot MW_{exh} - MW_f \cdot \left(y_{CO_2} + y_{CO} + \alpha y_{HC}\right)}{MW_f \cdot \left(y_{CO_2} + y_{CO} + \alpha y_{HC}\right)} \tag{C.6}$$

Using the measured mass flow rate of the fresh air intake, the fuel flow rate, $\dot{m}_f$ can be determined as:

$$\dot{m}_f = \frac{MW_f \cdot \dot{m}_a \cdot \left(y_{CO_2} + y_{CO} + \alpha y_{HC}\right)}{9.008\beta \cdot \left(y_{CO_2} + y_{CO}\right) + \alpha \cdot MW_{exh} - MW_f \cdot \left(y_{CO_2} + y_{CO} + \alpha y_{HC}\right)} \tag{C.7}$$

The value of α and β are fixed for a given fuel $C_\alpha H_\beta$ and the $\dot{m}_a$ is the measured mass flow rate of the fresh air. In this research work, the fuel had a $\left(H/_C\right)$ ratio of 1.88 (Table 4.6). Therefore, Equation (C.7) becomes

$$\dot{m}_f = \frac{13.906 \cdot \dot{m}_a \cdot \left(y_{CO_2} + y_{CO} + y_{HC}\right)}{16.935 \cdot \left(y_{CO_2} + y_{CO}\right) + 28.97 - 13.906 \cdot \left(y_{CO_2} + y_{CO} + y_{HC}\right)} \tag{C.8}$$

The air excess ratio, λ can also be calculated from Equation (C.6) by:

$$\lambda = \frac{\dot{m}_a / \dot{m}_f}{\left(\dot{m}_a / \dot{m}_f\right)_s} \tag{C.9}$$

where the stoichiometric AFR, $\left(\dot{m}_a / \dot{m}_f\right)_s$ is calculated from Equation (C.1) for λ=1.

A comparison of the AFR calculated using the above method with the measured AFR is shown in Figure C.1.

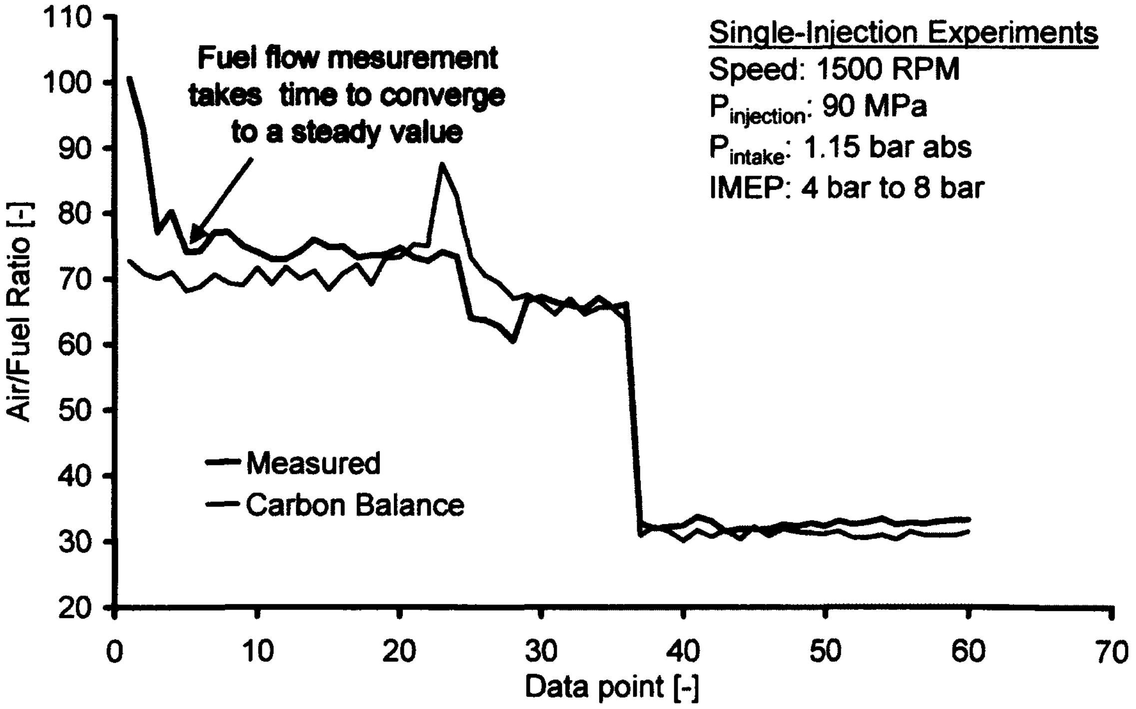

Figure C.1: AFR calculated using the Carbon Balance Method

APPENDIX D: MATHEMATICAL DEFINITIONS OF EGR

Table D.1: Some Common Mathematical Expressions for EGR found in the Literature

EGR Definition	Explanation of Term	Operating Conditions	Reference
$d=\frac{(CO_2)_c}{(CO_2)_e}$	d= charge dilution fraction $(CO_2)_c$= volumetric % of CO_2 before combustion $(CO_2)_e$= volumetric % of CO_2 in the exhaust	SI engine	Benson , 1971
$\% EGR=\frac{CO_{2,intake}}{CO_{2,exhaust}}\cdot 100$		Single cylinder, DI diesel engine 0~20% Cooled EGR	Yu, 1981
$\% EGR=\frac{V_o-V_{air}}{V_o}\cdot 100$	V_o = flow rate of intake fresh air without EGR V_{air} = flow rate of intake fresh air with EGR	DI diesel engine 0~70% EGR (cooled and un-cooled)	Narusawa, 1990 Sato, 1993 Yoshikawa, 1993
$EGR=\frac{m_{EGR}}{m_{int}}$ $m_a=m_{int}(1-EGR)$	m_{EGR}= mass of recirculated exhaust gas m_{int} = total mass of intake m_a = mass of intake fresh air	DI diesel engine, 0~40% un-cooled EGR	Lapuerta, 1995
$\%EGR=\frac{\%CO_{2(int)}-\%CO_{2(amb)}}{\%CO_{2(exh)}-\%CO_{2(amb)}}$		DI diesel engine, 0~10% un-cooled EGR, high engine load	Pierpont, 1995

EGR Definition	Explanation of Term	Operating Conditions	Reference
$\text{EGR}(\%) = \frac{m_{\text{EGR}}}{m_{\text{a}} + m_{\text{f}} + m_{\text{EGR}}} \cdot 100$	m_{EGR} = mass of recirculated exhaust gas m_a = mass of intake fresh air m_f = mass of injected fuel	IDI diesel engine, 10~25% cooled and un-cooled filtered EGR	Abd-Alla, 2002
$\text{EGR}(\%) = \frac{[m_{\text{a}}]_{without\ EGR} - [m_{\text{a}}]_{with\ EGR}}{[m_{\text{a}}]_{without\ EGR}} \cdot 100$	$[m_{\text{a}}]_{withoutEGR}$ = mass flow rate without EGR $[m_{\text{a}}]_{with\ EGR}$ = mass flow rate with EGR	DI diesel engine, 5~20% EGR	Jothi, 2008

APPENDIX E: CONTROLLER AREA NETWORK

The Controller Area Network (CAN) is an International Standardization Organization (ISO) defined serial communication bus originally developed for the automotive industry to replace the complex wiring harness with a two-wire bus. The specification calls for high immunity to electrical interference and the ability to self-diagnose and repair data errors. The CAN bus was developed by BOSCH as a multi-master, message broadcast system that specifies a maximum signalling rate of 1 megabit per second (Mbps). Unlike a traditional network such as USB or Ethernet, CAN does not send large blocks of data point-to-point from node 1 to node 2 under the supervision of a central bus master. In a CAN network, many short messages like temperature or RPM are broadcast to the entire network, which provides for data consistency in every node of the system. The CAN network topology is shown in Figure E.1.

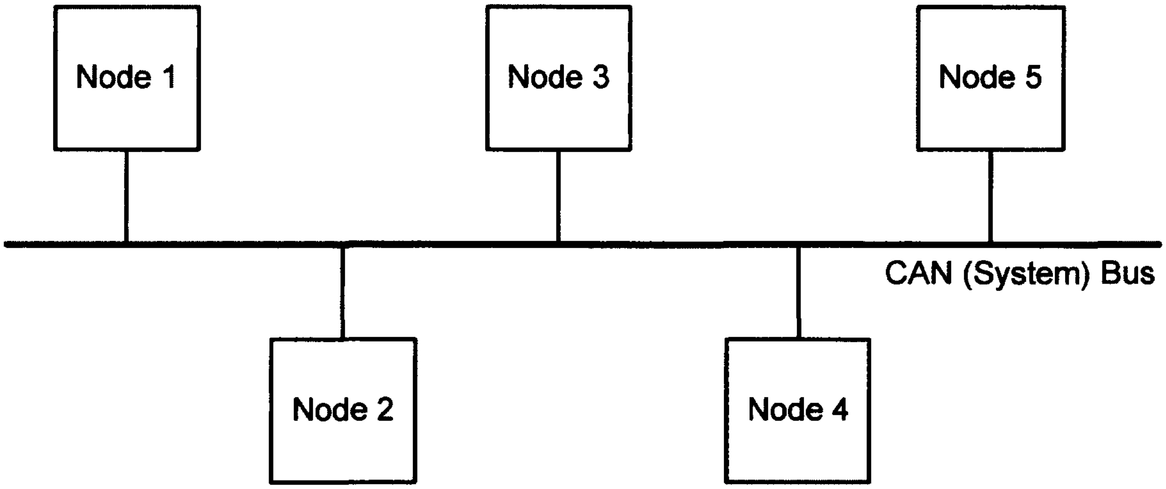

Figure E.1: CAN Bus Topology

The CAN Bus consists of two wires (usually a twisted pair that can be shielded or unshielded) as shown in Figure E.2. The pair of signal wires (CAN_H and CAN_L) constitutes a transmission line. The transmission line needs to be electrically terminated so that each signal change on the line is prevented from being reflected back from the end, causing interference. Because communication flows both ways on the CAN bus, the CAN bus requires both ends of the cable be terminated. However, this requirement does not mean that every device should have a termination resistor. If multiple devices are placed along the cable, only the ends of the cable should have the termination resistors. The termination resistors on a cable should match the nominal impedance of the cable. ISO 11898 requires a cable with a nominal impedance of 120 Ω, so a 120 Ω resistor should be used at each end of the cable. Each termination resistor should be capable of dissipating 0.25 W of power.

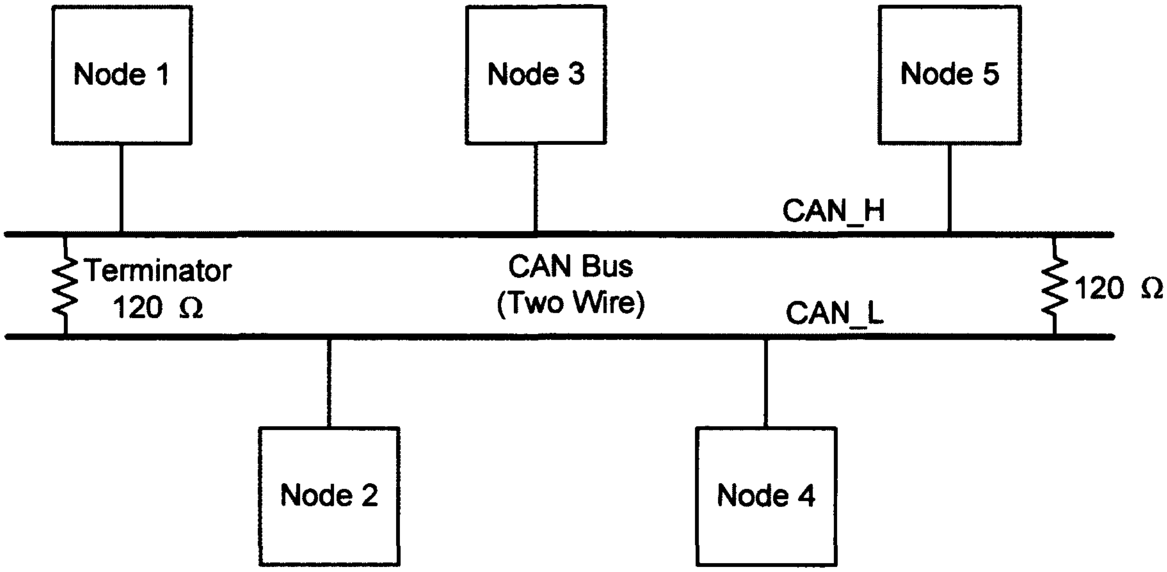

Figure E.2: Bus Termination

Bit Encoding

CAN uses the Non-Return-to-Zero (NRZ) encoding for data communication on a differential two wire bus as shown in Figure E.3. Unlike the Return-to-Zero (RZ) encoding in which the signal returns to zero between each pulse, the NRZ encoding uses two different voltage levels for the two binary digits with no other neutral or rest condition. Therefore, the NRZ code requires only half the bandwidth to achieve the same data-rate as compared to the RZ format. However, the NRZ is not inherently a self-synchronization code so some additional means to ensure synchronization is required to prevent bit slip.

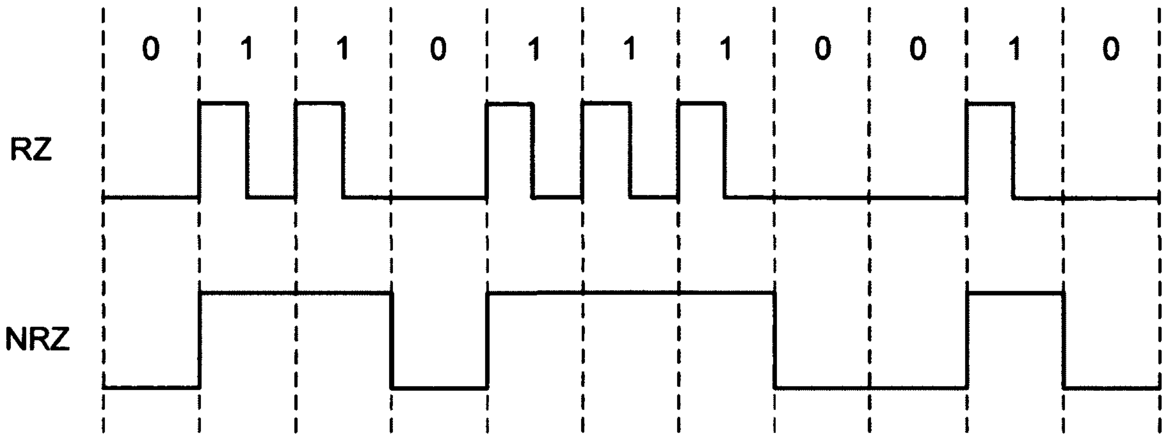

Figure E.3: Bit Encoding

A fundamental CAN characteristic (Figure E.4) is the opposite logic state between the bus, and the controller input/output. Normally, a logic-high is associated with a one, and a logic-low is associated with a zero - but not so on a CAN bus. The two signal lines of the bus, CAN_H and CAN_L, in the recessive state (1), are passively biased to ~2.5 V (~0V Differential Signal). The dominant state (0) on the bus takes CAN_H ~1V higher to ~3.5V, and takes CAN_L ~1V lower to ~1.5V, creating a typical 2V differential signal.

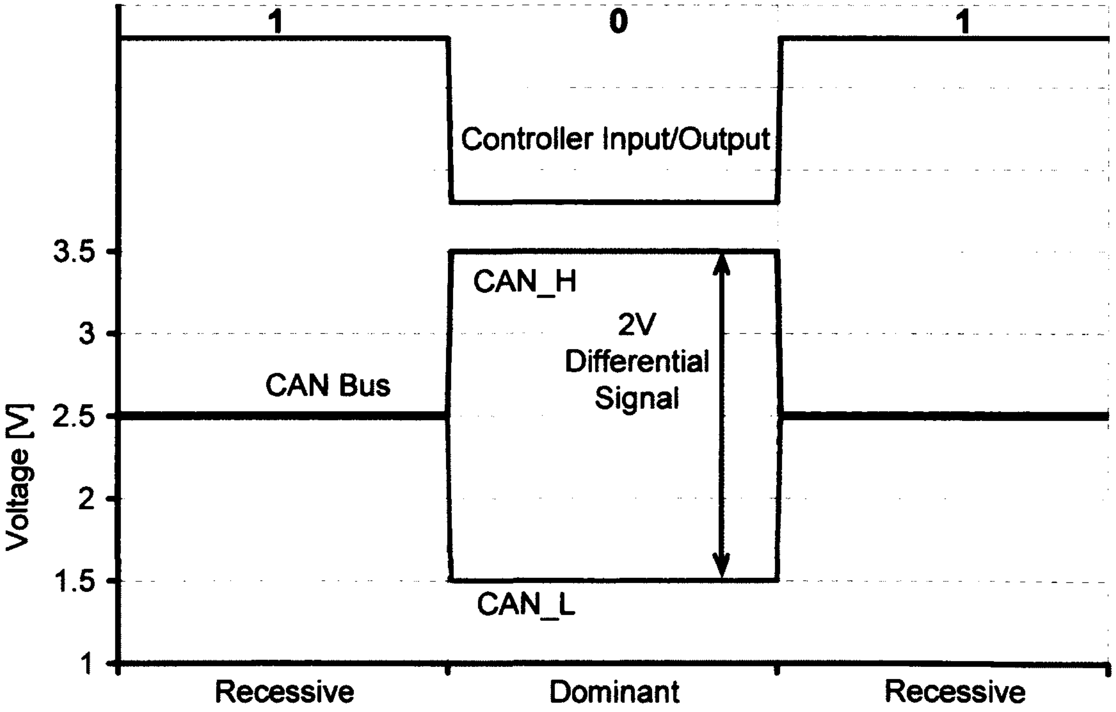

Figure E.4: CAN Dominant and Recessive Bus States

Bit Stuffing

Bit stuffing is the insertion of non-information bits into the data stream to limit the number of consecutive bits of the same value in the data to be transmitted. A bit of the opposite value is inserted after the maximum allowed number of consecutive bits to ensure reliable transmission. With the NRZ encoding, the receiver must count the time between transitions to determine the number of bits, and if that time is too long, the receiver can lose count. In case of the CAN, when 5 bits of the same logic level occur in succession during normal operation, a bit of the opposite logic level is stuffed into the data as shown in Figure E.5.

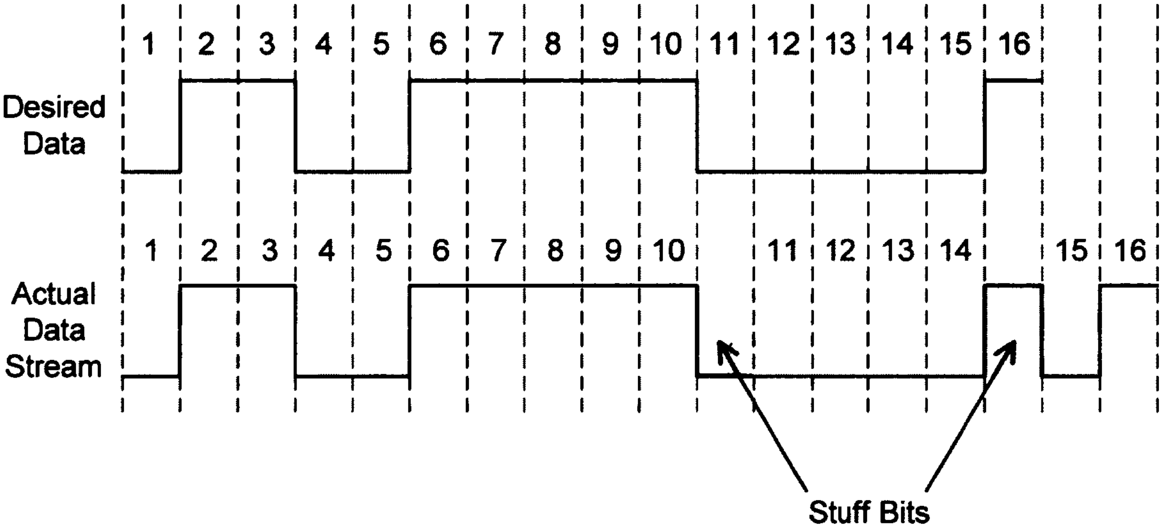

Figure E.5: Bit Stuffing

Non-Destructive Bitwise Arbitration

To determine the priority of messages, CAN uses the established method known as Carrier Sense, Multiple Access protocol with Collision Detection and Arbitration on Message Priority (CSMA/CD+AMP) to provide collision resolution with the enhanced capability of bitwise arbitration, and to deliver maximum use of the available capacity of the bus. CSMA means that each node on a bus must wait for a prescribed period of inactivity before attempting to send a message. CD+AMP means that collisions are resolved through a non-destructive bitwise arbitration, based on a preprogrammed priority of each message in the identifier field of a message. Bus access is event-driven and takes place randomly. If two nodes try to occupy the bus simultaneously, access is implemented with a nondestructive, bit-wise arbitration. Nondestructive means that the node winning arbitration just continues on with the message, without the message being destroyed or corrupted by another node. The higher priority identifier always wins bus access. That is, the last logic-high in the identifier keeps on transmitting because it is the highest priority. The CAN communication protocol is summarized in Table E.1.

Table E.1: CAN Communication Protocol

Carrier Sense	Listen until network is idle, must wait if another node is transmitting
Multiple Access	Many nodes can access an idle network at any time
Collision Detection + Arbitration on Message Priority	Method of resolving collisions through a non-destructive bitwise arbitration based on the message priority

The allocation of priority to messages in the identifier is a feature of CAN that makes it particularly attractive for use within a real-time control environment. The lower the binary message identifier number, the higher its priority. An identifier consisting entirely of zeros is the highest priority message on a network because it holds the bus dominant the longest. Therefore, if two nodes begin to transmit simultaneously, the node that sends a last identifier bit as a zero (dominant) while the other nodes send a one (recessive) retains control of the CAN bus and goes on to complete its message. A dominant bit always overwrites a recessive bit on a CAN bus.

Note that a transmitting node constantly monitors each bit of its own transmission. The CAN arbitration process that is handled automatically by a CAN controller is shown in Figure E.6. Because each node continuously monitors its own transmissions, as node 2's recessive bit is overwritten by node 1's higher priority dominant bit, node 2 detects that the bus state does not match the bit that it transmitted. Therefore, node 2 halts transmission while node 1 continues on with its message. Another attempt to transmit the message is made by node 2 once the bus is released by node 1.

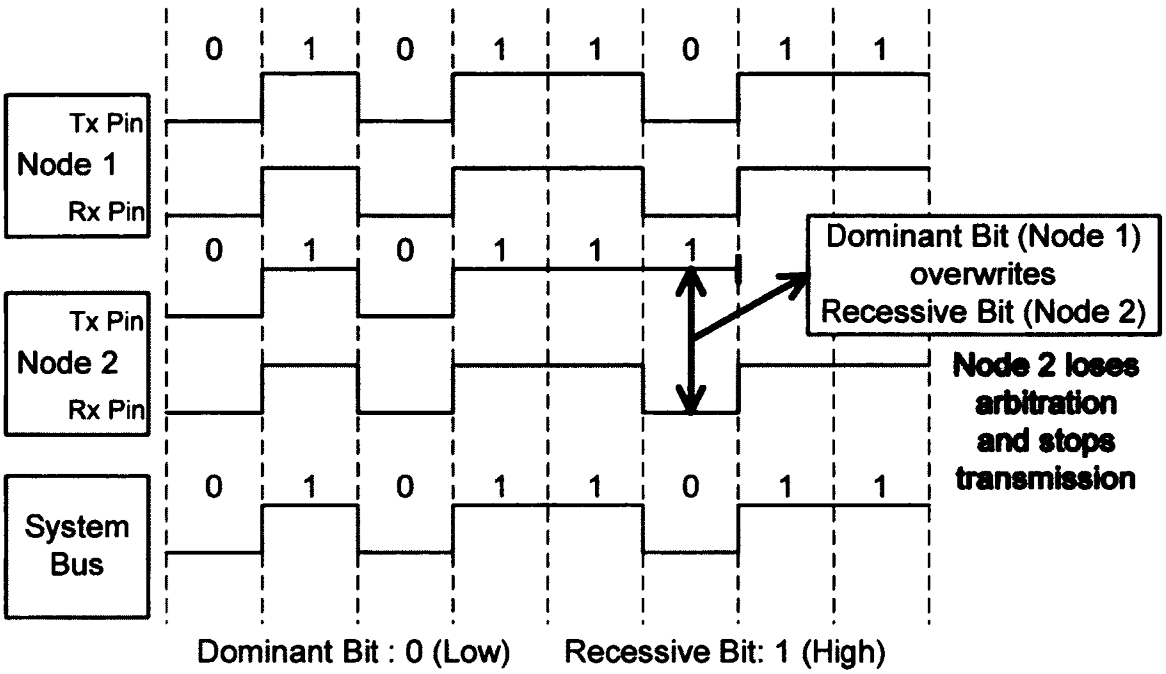

Figure E.6: Bitwise Arbitration

Message Based Communication

CAN protocol is a message-based protocol, not an address based protocol. This means that messages are not transmitted from one node to another node based on addresses. Embedded in the CAN message itself is the priority and the contents of the data being transmitted. All nodes in the system receive every message transmitted on the bus (and will acknowledge if the message was properly received). It is up to each node in the system to decide whether the message received should be immediately discarded or kept to be processed. A single message can be destined for one particular node to receive, or many nodes based on the way the network and system are designed.

Another useful feature built into the CAN protocol is the ability for a node to request information from other nodes. This is called a Remote Transmit Request (RTR). Instead of waiting for information to be sent by a particular node, a node specifically requests data to be sent to it.

One additional benefit of this message-based protocol is that additional nodes can be added to the system without the necessity to reprogram all other nodes to recognize this addition. This new node will start receiving messages from the network and, based on the message ID, decide whether to process or discard the received information.

CAN Message Frame Description

The CAN protocol defines four different types of messages (or frames). The first and most common type of frame is a Data Frame. This is used when a node transmits information to any or all other nodes in the system. Second is a Remote Frame, which is basically a Data Frame with the RTR bit set to signify that it is a Remote Transmit Request. The other two frame types are for handling errors. One is called an Error Frame and the other is called an Overload Frame. Error Frames are generated by nodes that detect any one of the many protocol errors defined by CAN. Overload errors are generated by nodes that require more time to process messages already received.

The most common frame utilized is the data frame and is described in detail below.

CAN Data Frame

The ISO-11898:2003 Standard, with the standard 11-bit identifier, provides for signaling rates from 125 kbps to 1 Mbps. The standard was later amended with the "extended" 29-bit identifier. The standard 11-bit identifier field in Figure E.7 provides for 2^{11}, or 2048 different message identifiers, whereas the extended 29-bit identifier in Figure E.8 provides for 2^{29}, or 537 million identifiers.

Data Frames consist of fields that provide additional information about the message as defined by the CAN specification. The meaning of each bit field of the standard data frame (Figure E.7) is given in Table E.2.

CAN 2.0: Standard Data Frame

SOF	11-bit Identifier	RTR	IDE	r0	DLC	0...8 Bytes Data	CRC	ACK	EOF	IFS

Figure E.7: Standard CAN Data Frame

Table E.2: Explanation of Bit Fields in the Standard Data Frame

Field Name	Length (bits)	Purpose
Start of Frame (SOF)	1	The single dominant SOF bit marks the start of a message and is used to synchronize the nodes on a bus after being idle.
Identifier	11	The Standard 11-bit identifier establishes the priority of the message. The lower the binary value, the higher its priority.
Remote Transmission Request (RTR)	1	The RTR is dominant when information is required from another node. All nodes receive the request, but the identifier determines the specified node. The responding data is also received by all nodes and used by any node interested.
Identifier Extension Bit (IDE)	1	A dominant IDE means that a standard CAN identifier with no extension is being transmitted.
Reserved Bit (r0)	1	Reserved bit (for possible use by future standard amendment) – should be set to dominant.
Data Length Code (DLC)	4	The DLC indicates the number of bytes of data being transmitted.
Data Field	0-64 bits	Up to 64 bits (0-8 Bytes) of data to be transmitted.
Cyclic Redundancy Check (CRC)	15+1	The 16-bit (15 bits plus recessive delimiter bit) CRC contains the checksum (number of bits transmitted) of the preceding application data for error detection.
Acknowledge (ACK)	1+1	Every node receiving an accurate message overwrites this recessive bit in the original message with a dominant bit, indicating an error-free message has been sent. Should a receiving node detect an error and leave this bit recessive, it discards the message and the sending node repeats the message after rearbitration. In this way, each node acknowledges (ACK) the integrity of its data. ACK is 2 bits, the second being a delimiter (always recessive)
End of Frame (EOF)	7	The EOF field (normally recessive) marks the end of a CAN frame (message) and disables bit-stuffing. It indicates a stuffing error when dominant.
Interframe Space (IFS)	3	Indicates the time required by the controller to move a correctly received frame to its proper position in a message buffer area.

The Extended CAN data frame shown in Figure E.8 is the same as the Standard data frame with the addition of 3 new bit fields as explained in Table E.3.

CAN 2.0: Extended Data Frame

SOF	11-bit Identifier	SRR	IDE	18-bit Identifier	RTR	r1	r0	DLC	0...8 Bytes Data	CRC	ACK	EOF	IFS

Figure E.8: Extended CAN Data Frame

Table E.3: Additional Bit Fields in the Extended Data Frame

Field Name	Length (bits)	Purpose
Substitute Remote Request (SRR)	1	The SRR bit replaces the RTR bit in the standard message location as a placeholder in the extended format. Must be recessive (1).
Identifier Extension Bit (IDE)	18	A recessive bit in the IDE indicates that more identifier bits follow. The 18-bit identifier extension follows the IDE.
Reserve Bit (r1)	1	Following the RTR and r0 bits, an additional reserve bit is included ahead of the DLC bit and should be set to dominant

The last two message types are Error Frames and Overload Frames. When a node detects one of the many types of errors defined by the CAN protocol, an Error Frame occurs. Overload Frames tell the network that the node sending the Overload Frame is not ready to receive additional messages at this time, or that intermission has been violated. These errors will be discussed in more detail in the next section.

Fast, Robust Communication

Because CAN was initially designed for use in automobiles, a protocol that efficiently handled errors was critical if it was to gain market acceptance. The initial version 1.0 of the CAN specifications was updated to version 2.0B and specified a maximum communication rate 1 Mbit/sec. At this rate, even the most time-critical parameters can be transmitted serially without latency concerns. In addition to this, the CAN protocol has a comprehensive list of errors it can detect that ensures the integrity of messages.

CAN nodes have the ability to determine fault conditions and transition to different modes based on the severity of problems being encountered. They also have the ability to detect short disturbances from permanent failures and modify their functionality accordingly. CAN nodes can transition from functioning like a normal node (being able to transmit and receive messages normally), to shutting down completely (bus-off) based on the severity of the errors detected. This feature is called Fault Confinement. No faulty CAN node or nodes will be able to monopolize all of the bandwidth on the network because faults will be confined to the faulty nodes and these faulty nodes will shut off before bringing the network down. This is very powerful because Fault Confinement guarantees bandwidth for critical system information.

There are five error conditions that are defined in the CAN protocol and three error states that a node can be in, based upon the type and number of error conditions detected. The following section describes each one in more detail.

Detected Errors

CRC Error. A 15-bit Cyclic Redundancy Check (CRC) value is calculated by the transmitting node and this 15-bit value is transmitted in the CRC field. All nodes on the network receive this message, calculate a CRC and verify that the CRC values match. If the values do not match, a CRC error occurs and an Error Frame is generated. Since at least one node did not properly receive the message, it is then resent after a proper intermission time.

Acknowledge Error. In the Acknowledge Field of a message, the transmitting node checks if the Acknowledge Slot (which it has sent as a recessive bit) contains a dominant bit. This dominant bit would acknowledge that at least one node correctly received the message. If this bit is recessive, then no node received the message properly. An Acknowledge Error has occurred. An Error Frame is then generated and the original message will be repeated after a proper intermission time.

Form Error. If any node detects a dominant bit in one of the following four segments of the message: End of Frame, Interframe Space, Acknowledge Delimiter or CRC Delimiter

(Figures E.7 & E.8), the CAN protocol defines this to be a form violation and a Form Error is generated. The original message is then resent after a proper intermission time.

Bit Error. A Bit Error occurs if a transmitter sends a dominant bit and detects a recessive bit, or if it sends a recessive bit and detects a dominant bit when monitoring the actual bus level and comparing it to the bit that it has just sent. In the case where the transmitter sends a recessive bit and a dominant bit is detected during the Arbitration Field or Acknowledge Slot, no Bit Error is generated because normal arbitration or acknowledgment is occurring. If a Bit Error is detected, an Error Frame is generated and the original message is resent after a proper intermission time.

Stuff Error. As explained earlier, the CAN protocol uses the NRZ bit encoding method. This means that the bit level is placed on the bus for the entire bit time. CAN is also asynchronous, and bit stuffing is used to allow receiving nodes to synchronize by recovering clock information from the data stream. Receiving nodes synchronize on recessive to dominant transitions. If there are more than five bits of the same polarity in a row, CAN will automatically stuff an opposite polarity bit in the data stream. The receiving node(s) will use it for synchronization, but will ignore the stuff bit for data purposes. If, between the Start of Frame and the CRC Delimiter, six consecutive bits with the same polarity are detected, then the bit stuffing rule has been violated. A Stuff Error then occurs, an Error Frame is sent, and the message is repeated.

Error States

Error-Active. An Error-Active node can actively take part in bus communication, including sending an active error flag, which consists of six consecutive dominant bits. The Error Flag actively violates the bit stuffing rule and causes all other nodes to send an Error Flag, called the Error Echo Flag, in response. An Active Error Flag, and the subsequent Error Echo Flag may cause as many as twelve consecutive dominant bits on the bus; six from the Active Error Flag, and zero up to six more from the Error Echo Flag. A node is Error-Active when both the Transmit Error Counter (TEC) and the Receive Error Counter (REC) are below 128. Error-Active is the normal operational mode, allowing the node to transmit and receive without restrictions.

Error-Passive. A node becomes Error-Passive when either the TEC or the REC exceeds 127. Error-Passive nodes are not permitted to transmit Active Error Flags on the bus, but instead, transmit Passive Error Flags which consist of six recessive bits. If the Error-Passive node is currently the only transmitter on the bus then the passive error flag will violate the bit stuffing rule and the receiving node(s) will respond with Error Flags of their own (either active or passive depending upon their own error state). If the Error-Passive node in question is not the only transmitter (i.e. during arbitration) or is a receiver, then the Passive Error Flag will have no effect on the bus due to the recessive nature of the error flag. When an Error-Passive node transmits a Passive Error Flag and detects a dominant bit, it must see the bus as being idle for eight additional bit times after an intermission before recognizing the bus as available. After this time, it will attempt to retransmit.

Bus-Off. A node goes into the Bus-Off state when the Transmit Error Counter is greater than 255 (receive errors can not cause a node to go Bus-Off). In this mode, the node can not send or receive messages, acknowledge messages, or transmit Error Frames of any kind. This is how Fault Confinement is achieved. There is a bus recovery sequence that is defined by the CAN protocol that allows a node that is Bus-Off to recover, return to Error-Active, and begin transmitting again if the fault condition is removed.

The fault confinement states are summarized in Figure E.9.

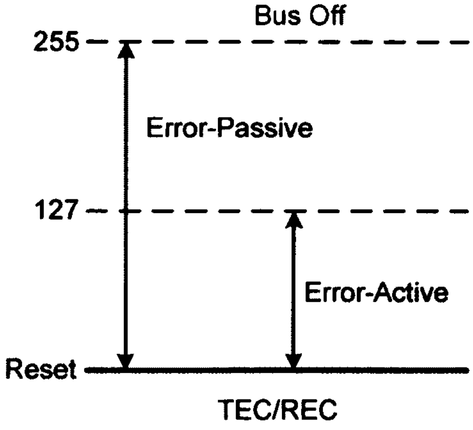

Each node on the network may be in one of the three states:

Error-Active	• Node transmits/receives messages • Upon detecting an error, an active error frame (6 dominant bits) is sent • TEC & REC <=127
Error-Passive	• Node Transmits/receives messages • Upon detecting an error, a recessive error frame (6 recessive bits) is sent • TEC and/or REC >=128 & TEC<=255
Bus-Off	• Node does not transmit/receive messages until reset from host microcontroller

Figure E.9: Fault Confinement States – CAN Protocol

The error counters are incremented/decremented based on successful/unsuccessful messages as shown in Table E.4.

Table E.4: Error Counters

Receive Error Counter (REC)	
If receiver sends an error frame	REC=REC+1
If receiver was first to start an error frame	REC=REC+8
If receiver monitors a Bit Error while sending an error frame	REC=REC+8
After successfully receiving a message	REC=REC-1
Transmit Error Counter (TEC)	
If transmitter sends an error frame	TEC=TEC+8
If transmitter monitors a Bit Error while sending an error frame	TEC=TEC+8
After successfully transmitting a message	TEC=TEC+1

CAN Documents

A number of standards have been published for the CAN protocol depending on the automotive application and are given in Table E.5.

Table E.5: CAN Documents

Passenger Car	
SAE J2411	Single Wire CAN
ISO 11898	High Speed CAN
ISO 11519-2	Low Speed CAN
ISO 15765	Diagnostics on CAN
Heavy Truck and Bus/Agriculture	
SAE J1939	Truck and Bus
ISO 11783	Agriculture and Forestry

The CAN Bus

The CAN data and physical layers, which are normally transparent to a system operator, are included in any controller that implements the CAN protocol. Connection to the physical medium is then implemented through a line transceiver, to form a system node as shown in Figure E.10.

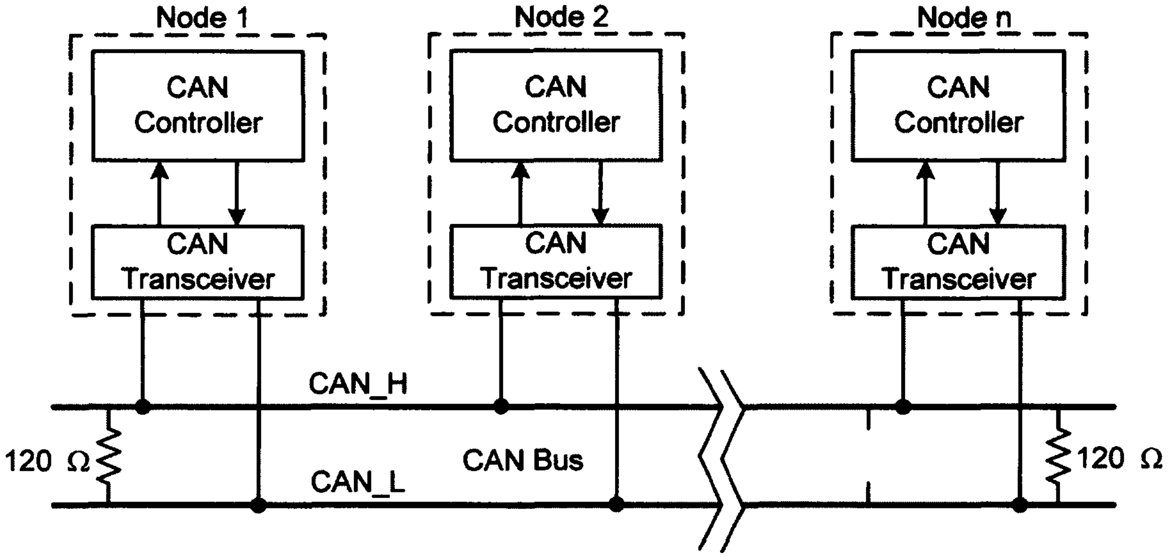

Figure E.10: Details of a CAN Bus

Signalling is differential which is where CAN derives its robust noise immunity and fault tolerance. Balanced differential signalling reduces noise coupling and allows for high signalling rates over twisted-pair cable. Balanced means that the current flowing in each signal line is equal but opposite in direction, resulting in a field-cancelling effect that is a key to low electrical noise. The use of balanced differential receivers and twisted-pair cabling enhance the common-mode rejection and high electrical noise immunity of a CAN bus.

The High-Speed ISO 11898 Standard specifications are given for a maximum signalling rate of 1 Mbps with a bus length of 40 m and a maximum of 30 nodes. It also recommends a maximum un-terminated stub length of 0.3 m.

Conclusion

The CAN protocol was optimized for systems that need to transmit and receive relatively small amounts of information (as compared to Ethernet or USB, which are designed to move much larger blocks of data) reliably to any or all other nodes on the network. CSMA/CD+AMP allows every node to have an equal chance to gain access to the bus, and allows for smooth handling of collisions. Since the protocol is message-based and not address based, all nodes on the bus receive every message and acknowledge every message, regardless of whether they need the data or not. This allows the bus to operate in node-to-node or multicast messaging formats without having to send different types of messages.

Fast, robust message transmission with fault confinement is also a significant advantage of the CAN because faulty nodes will automatically drop off the bus, thereby preventing any one node from bringing down the complete network. This effectively guarantees that bandwidth will always be available for critical messages to be transmitted.

APPENDIX F: DETAILS OF SELECTED REFERENCES

Ref #	Publication	Research Area	Tested Parameters	Significant Results
1	SAE 972684	Summary advantages of diesel engines		Up to 30% higher fuel-economy for diesel powered vehicles on US FTP cycle. A comparison of exhaust emissions over a period of 160,000 km showed that diesel engines produced lower CO and HC compared to the gasoline engine, but at the same time had a higher NOx and particulate emission.
11	SAE 902062	Crank-angle resolved pollutant formation studies	Fuel: Diesel 4-Cylinder, CR: 16.5:1 Load: 10 bar IMEP Emissions NOx: 600~800 ppm PM: 0.05~0.1 mg/mg of fuel	NOx and particulate form rapidly, reaching peak values before a late stage of the diffusion burning period. The NOx concentration froze during the expansion stroke and showed an almost constant value after the end of the diffusion combustion. The particulate concentration showed a decrease from their peak values due to oxidation
13	SAE 942046	Crank-angle resolved pollutant formation studies	Fuel: Diesel, CN=48/62.5 Single Cylinder, CR: 16.0:1 Load: 6, 10 bar IMEP Emissions NOx= 700~1600 ppm PM: Not reported	For the turbo-charged engine with no EGR the NO formation took place throughout the burn duration. This was contrary to the other reported results that NOx was primarily formed during the premixed combustion.

14	SAE 961168	Crank-angle resolved pollutant formation studies	Fuel: Diesel Load: 3, 5 bar BMEP Emissions NOx <100 ppm with EGR PM: ~ 0.05 mg/Liter of Free gas.	The NOx concentrations rose rapidly after SOC, and reached peak concentration within a ms from the SOC. NOx declined slightly after reaching its peak and the chemistry effectively froze after 90°ATDC. Tests with EGR showed its effectiveness in reducing the NOx through out the combustion process. The peak particulate concentration in the cylinder was up to 20 times greater than the exhaust concentration. The use of even a moderate amount of EGR resulted in almost three times increase in the maximum particulate concentration.
15	SAE 780227	In-cylinder sampling studies for emission formation	Fuel: Diesel, CN=48/62.5 Single Cylinder, IDI CR: 16.0:1 Load: 5.5 bar BMEP Emissions NOx= 700~1600 ppm Smoke: 0~0.5 g/m^3	Maximum concentrations of the unburnt HC, CO and soot occurred near the combustion chamber wall whereas most of the NO was formed in the central region of the chamber. This was attributed to the formation of mixtures with a high equivalence-ratio towards the periphery of the combustion chamber and more homogeneous-stoichiometric mixture at the center of the chamber. The combustion was divided into three phases: a) In the first phase, a small amount of heat is released by the combustion of a rich air-fuel mixture. The soot and the CO were mainly formed in this stage of the combustion. b) In the second phase, approximately half of the heat was released by combustion of a slightly lean-mixture. The availability of excess oxygen and high-temperature led to the formation of NOx & this stage was also characterized by the oxidation of the soot and CO formed in the first stage of the combustion. c) In the last phase, the CO to CO_2 conversion took place and released the remainder of the heat.

17	SAE 880423	Constant volume combustion bomb		Based on the soot formation studies in the flame studies, constant volume chamber experiments and the NOx simulation results, an equivalence ratio and temperature map was prepared that depicts the regions of soot and NOx formation. Based on this map, pathway for simultaneous low-NOx and soot was formulated
18	SAE 960030	Crank-angle resolved pollutant formation and combustion visualization study	Fuel: JIS No.2 Single Cylinder Diesel, CR: 18.5:1, ϕ=0.69 without EGR. Emissions NOx: 200 ppm Smoke at 200ppm = 8 Smoke number (Bosch)	The pollutant formation was investigated in the presence of EGR and high injection pressure. The soot emission decreased at higher injection pressure due to accelerated soot-oxidation. The NOx formation was lowered with EGR due to reduction in oxygen concentration and slower combustion.
19	SAE 930971	Diesel combustion studies in optical engine	Reference Fuel: 67.6% heptamethylnonane and 32.4% n-hexadecane with cetane no. 42.5) 2) Low-sooting fuel: 80% 2-ethoxyethyl ether and 20% heptamethylnonane Single Cylinder Optical Engine, CR: 11: 1 Load: ϕ: 0.21 and 0.43 without EGR	The soot was distributed throughout the cross section of the combusting fuel jet. For the time period from the initiation of the luminous combustion to the end of the fuel-injection the soot concentration was higher in the head-vortex region compared to the upstream region. However, at the end of the injection the soot concentration and the soot particle size increased significantly
22	SAE 2006-01-3324	Diesel low-temperature combustion with DME		A 3-injection strategy with timing for the main injection determined by the cylinder temperature has been proposed to realize the LTC cycle.

25	SAE 2006-01-0053	Diesel low-temperature combustion with DME		Miller cycle for the low load operations and the multiple injection strategy with high rates of EGR for high load operations proposed as a solution to meet US 2010 emission standards with DME engine.
27	SAE 2005-01-3837	Diesel low-temperature combustion	Conventional Diesel Fuel, Single Cylinder Optical Engine CR: 18.7:1 Load: 3.3 bar IMEP Emissions NOx: 8ppm Soot luminosity: 0.0001 to 1 [a.u]	The ignition delay was prolonged as the charge was increasingly diluted with EGR. ϕ at ignition not reduced with dilution. Therefore, a greater quantity of ambient fluid was mixed with the fuel to achieve the same fuel/O_2 ratio. Consequently, the mixing process remained important under dilute operating conditions as well. The NOx, CO emissions and the soot luminosity correlated with the peak adiabatic flame temperature. The NOx emission and soot luminosity were lowered as the flame temperature decreased while CO emissions increased due to the decline in the oxidation rates. At the highest dilution levels and most retarded injection timing, the NOx-temperature correlation exhibited lower activation energy or a reduced sensitivity to peak flame temperature.
28	SAE 900640	Soot formation for diesel fuel with laser extinction methods.	Conventional Diesel fuel, Single Cylinder Optical Engine CR: 17:1 Load: $\lambda = 1.8$ Emissions NOx: Not reported Soot concentration: $<5g/m^3$	Soot formation initiated at ignition and reaches its peak value immediately after ignition. During the later part of the combustion, soot oxidized. This sequence of soot formation & oxidation was observed for ignition-delays up to 2ms. The maximum and the final soot concentrations decreased with increasing ignition delay. The increased soot formation with shorter ignition delay was due to formation of rich-mixture and increased fuel amounts injected directly into the flame. At shorter ignition delays the soot formation also shifted to hotter regions of the flame.

29	Proceedings of the Combustion Institute, (30), pp. 2719-2726.	HCCI combustion for hydrocarbon fuels	Fuel: Iso-octane, primary reference fuel 80, Single Cylinder CR: 18.0:1 Load: ϕ=0.08 to 0.28 Emissions NOx: Not reported Soot: Not reported	At 1200RPM,, the model predicted a peak charge temperature of 1500 K for complete CO oxidation. The lowest acceptable peak charge temperature did not change with fuel type and auto-ignition characteristics. The lowest acceptable peak charge temperature was also independent of the combustion phasing relative to TDC. The onset of CO was more gradual for the experiment compared to the single-zone model, attributed to a thermal distribution caused by crevices & thermal boundary layer. Engine speed affects the lowest acceptable peak charge temperature since it directly affects the time available at the peak temperature. The effect is relatively modest since the OH level is highly sensitive to peak temperature.
31	SAE 970873	Diesel combustion study using laser sheet studies	Reference Fuel: 67.6% heptamethylnonane and 32.4% n-hexadecane with cetane no. 42.5) 2) Low-sooting fuel: 80% 2,ethoxyethyl ether and 20% heptamethylnonane Single Cylinder Optical Engine, CR: 10:1, 11:1 Load: ϕ= 0.21 and 0.43 without EGR Quantitative NOx values not reported.	The chemiluminescence imaging showed ignition occurred progressively at multiple points across the downstream regions of all the fuel jets, beginning well before the start of the premixed burn spike. The imaging data also suggested that the premixed burn spike occurred under fuel-rich conditions (equivalence ratios of 2-4), and that the initial soot formation took place during the premixed combustion. In contrast to the classical calculations a short liquid-fuel penetration was observed and all the fuel in the main combustion zone was observed to be in vapour phase. Soot was formed throughout the jet cross-section, instead of the jet-periphery as assumed earlier. The NOx formation was noticed in the mixing controlled burn

33	SAE 2005-01-3726	Diesel low-temperature combustion	European diesel fuel, CN = 54, C/H = 1.96 Single Cylinder Engine CR: 14:1, 10bar BMEP Emissions Lowest NOx reported: <0.5 g/kWh Smoke at lowest NOx < 0.04 g/kWh	The soot emissions were reduced by a factor of 5 with an early pilot-injection strategy. The implementation early pilot-injection strategy also led to oil-dilution. The implementation of the post-injection enhanced the oxidation of soot and CO.
34	Applied Thermal Engineering, (18), pp. 963-980.	Diesel engine combustion		The dilution of intake charge with EGR had the strongest effect on emissions. The higher specific heat capacity of the CO_2 or H_2O in comparison to that of the O_2 it replaced, had little effect on NOx and particulate emissions. The chemical effects, resulting from the dissociation of the CO_2 or H_2O, also had little effect on emissions. Adding EGR to the engine air flow rate, rather than displacing some of the inlet air, allowed to reduce NOx with little penalty of increased particulate emissions.
35	SAE 2001-01-0655	Diesel low-temperature combustion	Fuel: Diesel 4-Cylinder, CR: 18.6:1 Load: 2 bar BMEP Emissions NOx: ~0.0 g/kW-hr Smoke: ~0.0 g/kW-hr	The smokeless combustion was obtained by significant reduction in the combustion flame temperature by application of large of EGR. At such low temperatures the soot formation the soot formation was suppressed by suppression of soot formation from PAH mixture.

37	SAE 2005-01-0166	Diesel premixed combustion	Fuel: LSD CN=52 4-Cylinder, CR: 16:1 Load: 4 bar BMEP Emissions: Lean PCI NOx: 1.2 g/kWh Smoke: ~0.3 g/kWh Emissions: Rich PCI NOx: 0.16 g/kWh Smoke: 0.03 g/kWh	Low-temperature combustion strategy was demonstrated with higher rates of exhaust gas recirculation, high fuel injection pressures, and injection timings near TDC
38	SAE 2005-01-3834	Diesel low temperature combustion	Fuel n-heptane No.2 Diesel (70% tetraethoxy-propane + 30% heptamethyl-nonane) Configuration: Constant volume combustion vessel	The planar laser-induced incandescence (PLII) imaging & soot measurements showed that the peak soot volume fraction (fv) decreased & the width of sooting region grew with increasing EGR. ϕ computed at the flame lift-off length location was same at different ambient O_2 values implying that there was equal amount of fuel-oxygen mixing prior to combustion in the diesel fuel jet irrespective of the ambient oxygen concentration. The PLII imaging showed there was a reduction in soot formation rate with decreasing O_2 concentration because of the lower combustion temperature. However, there was an increase in the residence time for soot formation, allowing more time for accumulation of soot. Therefore, with EGR, the trend in soot formation was determined by a competition between decreased soot formation rates and increased residence time considerations. An increase in the ambient temperature when employing EGR led to an increase in the soot formation. This was consistent with modelling studies which predicted that both the soot-formation and the residence time increase with increasing ambient temperature

39	SAE 2003-01-1794	Diesel combustion	Fuel No.2 diesel, CN=39 Ultra-low sulphur, CN=53 Single Cylinder, CR: 13.1:1 Load: 25% and 75% Emissions (25% load) NOx: ~30 g/kg of fuel PM: 0.55 g/kg of fuel Emissions (75% load) NOx: ~20 g/kg of fuel PM: ~4.5 g/kg of fuel	The advanced injection timing decreased both elemental carbon and organic carbon at high loads. The fuel composition did not have a significant impact on organic carbon emissions
41	SAE 2003-01-0763	Fischer-Tropsch diesel review	Daimler Chrysler 1.9L I4, Ford 1.2L Diata I4, GM 1.26L I-3, Dodge Ram 2500, VW Golf TDi, Navistar T444E, Cummins 5.9B Engine, DDC Series 60, Peugeot 405	Most FT diesel fuels had a near zero sulphur content, high cetane number, and low aromatic content which made them an attractive alternative to conventional diesel. Average PM reduction was 26% compared to conventional diesel fuel, the NOx emissions however increased due to higher cetane number.
44	SAE 2002-01-2725	Fischer-Tropsch diesel	1.9 L, 1999 VW Golf GL TDI. Tests procedure: Federal Test Procedure driving cycle, Highway fuel-economy test, US-06 driving cycle	The fischer-tropsch's diesel produced lower particulate emission on all the three test-cycle. The PM reduction was up to 90% on the US06 driving cycle. However, the NOx emissions increased up to 4% with the use of fischer-tropsch diesel

46	Fuel, (78), pp. 1303-1317	Experimental studies with oxygenated fuel (biodiesel) with multiple injection	Fuels a) No.2 diesel, CN=54 b) 20% & 40% biodiesel blend c. 7.8% and 15.6% TGME blend Single Cyl, CR: 16.1:1 Load: ϕ: 0.5 and 0.25 with no EGR Emissions (High-load) NOx: 3.0~6.0 g/kWh PM: 0.2~0.6 g/kWh Emissions (Low-load) NOx: 4~9 g/kWh PM: 0.15~0.5 g/kWh	The experiments showed that it was possible to reduce soot emissions with little or no penalty on NOx emissions with oxygenated fuels at high engine load. The greatest benefits in emissions were observed with single injection strategy at retarded SOI timings. With the split-injection strategies the soot reducing influence of oxygenates was less significant than the injection strategy itself. For the tests at low engine loads, the oxygenated fuel blends had a little effect on particulate emissions due to the excess oxygen under these conditions TGME: tripropylene glycol monomethyl ether
47	Fuel, (85), pp. 298- 305	Experimental studies with biodiesel	No.2 diesel, CN=51 Commercial biodiesel Four-Cylinder CR: Not provided Load: Up to 4 bar BMEP Emissions (Biodiesel) NOx: ~50 ppm/[g/hr] Emissions (Diesel) NOx: ~50 ppm/[g/hr]	In comparison with ASTM No. 2D diesel, the three kinds of biodiesels showed higher fuel consumption rate. The biodiesel with the additional peroxidation process showed the lower NOx emission index.

48	SAE 2006-01-0234	Experimental studies with biodiesel	No.2 diesel, CN=54 5, 50 and 100 (% v/v) blends of Soya, Rapeseed & Waste biodiesel Four-Cyl, CR: 18.5:1 Load: < 7 bar BMEP Emissions (100% load, Rapeseed) NOx: ~10 g/kWh Smoke: ~1.5 FSN Emissions (100% load, Diesel) NOx: ~10 g/kWh Smoke: ~3.5 FSN	It was possible to use 5% biodiesel without any deterioration in the performance or the emission characteristics. At the full-load condition, with 100% biodiesel there was a smoke reduction of up to 1.5 FSN for a similar NOx. However, there was a decrease in power production as well. For instance, at 2000 rpm, a ten percent reduction in maximum power was observed with the rapeseed and soy derivative fuels. For the fuels considered, in the unmodified engine, rapeseed based biodiesel gave significant advantage with respect to the combustion and emissions characteristics.
49	SAE 2005-01-3674	Injection characteristics studies with biodiesel	No.2 diesel, CN=54 Used cooking-oil Injection-test rig	A biodiesel type fuel was produced from waste vegetable oil using the base catalyzed method. The important physical properties of the biodiesel were close to or within the requirements of the international standards concerning biodiesel fuels. The cyclic fuel delivery, pressure wave propagation time, average injection rate and maximum pressure during injection were significantly affected when pure biodiesel was used as fuel.

50	SAE 952518	Experimental studies with dimethyl carbonate addition	No.2 diesel, CN~45 Blends of diesel and dimethyl carbonate (DMC) up to 12% Single-Cylinder/ Optically accessible combustion bomb. CR: Not available Load: < 5.3 bar BMEP Emissions (5.3 bar BMEP, Diesel) NOx: ~200 ppm Smoke: ~4.7 BSU Emissions (5.3 bar BMEP, Diesel with 10% DMC) NOx: ~200 ppm Smoke: ~4.1 BSU	For the test with no EGR, the smoke reduced almost linearly with DMC concentration. With 10% of DMC contained in fuel, a smoke reduction of 35~50% was attainable. In addition noticeable reductions of HC and CO were observed. However, the increasing oxygen content of fuel led to a small increase in NOx. The combined test of EGR and DMC also showed a simultaneous reduction in both NOx and smoke. The combustion bomb studies showed that the particulate formation was reduced and its oxidation speed increased in the presence of DMC. The thermal cracking test confirmed that most particulate formation prone species were reduced when DMC was blended with diesel fuel. For addition of small amounts of DMC, even though the thermal efficiency of DMC engine was maintained at the diesel fuel level, there was a slight increase in the specific fuel consumption
54	SAE 2005-01-3670	Experiments with diesel and bio-fuel	No.2 diesel, CN=47 Bio-fuel, CN = 80 Four-Cylinder, with optical access from cyl#4, CR: 19.0:1 Load: 7 bar BMEP Emissions (No.2 diesel) NOx: 3~7 g/kWh Emissions (Bio-fuel) NOx: 3~7 g/kWh	The lower sulphur and aromatic content reduced the number of nucleation sites for soot, thus promoting improved late-cycle oxidation for the bio-fuel. The improvements in soot-oxidation rates were able to overcome the effect of higher soot production rates due to shorter ignition delays with the bio-fuel.

55	SAE 2007-01-4093	Experimental tests with DME at high-injection pressure	No.2 diesel, CN=40~45 DME, CN = 65~68 V-6 engine in single-cylinder mode. Spray chamber studies. CR: 18.0:1 Load: <16 bar IMEP Emissions (DME) NOx: < 0.27 g/kWh Smoke: < 0.2 FSN	A hydraulically intensified fuel injection system for DME was developed that was capable of nearly 1500 bar peak injection pressure. It was possible to achieve NOx<0.27 g/kWh and smoke < 0.5FSN with the application of EGR and high-injection pressure system.
57	SAE 871610	Soot formation studies in a rapid compression machine		Both the Sauter Mean Diameter and the air-entrainment rate increased at higher injection pressures. For an evaporating spray, the length of the liquid-phase of the spray was not influenced by the injection pressure. The soot-concentration and the combustion duration decreased as the injection pressure was increased
63	SAE 2007-01-4035	Diesel EGR Fuel Reforming	Flow control strategies (straight flow vs flow reversal, full-flow vs partial flow) Inlet vs central heating and fuelling	First application of active flow management in EGR loop. Compared to the straight flow, an energy saving of more than 50% is possible with flow reversal. Overheat protection. Reduced EGR cooling requirement. Recycled reformate enhances premixed combustion
65	SAE 2004-01-0935	Diesel HCCI	Fuel: Diesel, CN=53 Single cylinder. CR: 17.0, 13.4, 11.1 Load: Up to 9bar IMEP Emissions Ind NOx: < 0.2 g/kWh Ind soot: ~ 0.01 g/kWh	With a combination of low-compression ratio, cooled intake-temperature and large amounts of EGR it was possible to achieve HCCI combustion up to a load of 9bar IMEP with close to TDC combustion phasing. The increased CO and HC lead to decrease in fuel-efficiency by 10~20% for most of the operating points

66	SAE 2007-01-0215	Diesel HCCI	Conventional Diesel Single Cylinder CR of 16.8, 13, 10 and VVT, Load: up to 18.3 bar BMEP Emissions NOx: 0.01 g/kWh Smoke: 0.1 BSN BSFC: 224 g/kWh	Highest HCCI shown with details. Main enablers: CR10+AFR 15.1 + VVT
69	SAE 961163	Premixed lean diesel combustion	Diesel, CN=19, 40, 62 Single cylinder. CR: 16.5, Load: λ~2.5 with no EGR Emissions NOx: 10~20 ppm Soot: ~ 0.0 FSN	It was possible to prepare a lean air-fuel mixture with an extremely early injection. The combustion of the lean-premixed mixture produced simultaneous low-NOx and soot combustion. This combustion was accompanied by an increase in THC and CO levels that occurred to the fuel-air mixture becoming over-lean and entering quench areas.
70	SAE 1999-01-0181	Premixed lean diesel combustion	Diesel, CN=62 Dimethyl ether, Propane n-pentane Single cyl, CR: 16.5 λ~2.0 with no EGR Emissions NOx: ~ 0 ppm Soot: ~ 0.0 FSN	Gaseous fuel was used to prepare a homogeneous lean mixture before the combustion process. The mixture heterogeneity had an impact on the start of combustion/combustion phasing. The operation limit of high load condition was restricted to an equivalence ratio of 2.0 ~ 2.4. This limit was decided by knock limit or the increase in the NOx emission.

71	SAE 1999-01-0185	Premixed diesel combustion	Diesel, CN=58 Single cylinder CR: 18, 13.5, 12 Load: λ ~2.3 with no EGR. ~1.23 with EGR Emissions NOx: ~ 0 ppm Soot: ~ 0.0 FSN	Premixed combustion was achieved with an early injection. This combustion was characterized by lack for luminous flame. “Impinged-spray” was implemented to lower the spray penetration. The modified spray led to improved fuel-economy and better smoke emission. The use of supercharging enabled to expand the operating range of premixed combustion.
73	SAE 2003-01-0745	Diesel HCCI combustion	Diesel, CN=53 Single cylinder CR: 18.4 Load: 6 bar BMEP Emissions NOx: ~ 10 ppm Soot: ~ 0.2 FSN	2-injection strategy was adopted for the ignition control in HCCI combustion. The first fuel was injected at early injection timing. Injection timing and quantity, intake gas temperature and boost pressure are controlled precisely so that the first fuel undergoes only low-temperature reaction. The high temperature reaction of all fuel is controlled by the second injection.
74	SAE 1999-01-3681	Diesel low-temperature combustion	Conventional Diesel Both Single & Multi-Cylinder, CR: 18:1, 17.5:1, 16:1 Load: 7 bar BMEP Emissions NOx: 95% reduction Smoke: < 1 BSU BSFC: Up to 10% penalty	Introduction of the concept of Modulated-Kinetics for simultaneous low-NOx and low-soot Implementation of low-temperature combustion with premixed combustion

79	SAE 2007-01-4063	Diesel low-temperature combustion	No.2 Diesel Single Cylinder CR: 16.7:1 Load: 3, 6 and 8 bar IMEP Emissions NOx: ~5 ppm Smoke: ~0 FSN	Two different LTC strategies were examined: a) dilution-controlled regime characterized by high rates of exhaust gas recirculation (EGR) with early-injection (roughly 30° BTDC), b) a late-injection (near TDC) regime employing moderate EGR levels. -For both LTC strategies, increased intake pressure reduces emissions of HC and CO. Increased intake pressure also reduces peak soot emissions at high load and shifted the "Slope-2" region of the soot-EGR curve towards lower oxygen concentrations
87	SAE 750026	Measurement and analysis of cylinder pressure data	Fuel: Gasoline Eng Configuration: Single Cylinder CR: Not provided Load: 5 bar IMEP Emissions NOx: ~ Not provided Smoke: ~ Not provided	Earliest paper to discuss the digital data-processing of cylinder pressure. Detailed procedure provided for the scaling of the pressure data, averaging of the raw-data and analysis of the fired pressure traces.
94	SAE 900445	Review of heat-release computations	Diesel, CN=53, 50.1, 36, 34 Eng Configuration, CR, load: Not provided Emissions NOx: ~ Not provided Smoke: ~ Not provided	A 2-cylinder pressure transducer based heat-release rate computation was compared to a 1 pressure transducer based computation. 1 pressure transducer based method was comparable to the dual-pressure transducer based method for both direct and in-direct injection diesel engine. The heat-release rate based on the combustion pressure (1 transducer method) was able to detect the variations in fuel-property and engine operating characteristics such as engine speed.

97	SAE 981052	Heat-release analysis	Simulated pressure used Fuel: Gasoline CR: 10.0:1 Load: 7~8 bar IMEP Emissions NOx: Not provided Smoke: Not provided	The most significant errors in the computation of the gross-heat release rate were due to incorrectly assigned ratio of specific heats and charge to wall heat transfer rates. The use of a heat transfer multiplier in conjunction with a First Law equation provided improvements to the gross-release rate computation
98	SAE 1999-01-0187	Heat-release analysis	Fuel: Diesel Multi-cylinder engine CR: Not provided Load: up to 10 bar BMEP Emissions NOx: Not provided Smoke: Not provided	The most significant errors in the computation of gross heat-release analysis were observed to be due to are due to incorrectly assigned ratio of specific heats and charge to wall heat transfer rates. An alternative heat release model, called the polytropic index first law model, was developed. This model uses a variable polytropic index to approximately cater for the charge to wall heat transfer.
101	SAE 2006-01-0917	Partially premixed combustion with multiple injections	Fuel: Diesel Single-cyl, CR: 16.1:1 Load: up to 11 bar BMEP Emissions NOx + HC: < 2.7 g/kWh Soot: <0.0134 g/kWh	Early premixed injections produced simultaneous lowering of NOx and PM through better mixing It was possible to optimize injection timings to obtain better spray targeting emissions. Use of a close-coupled post injection increases in-cylinder mixing and decreases PM emissions. Splitting the pilot injection into two premixed injections reduced fuel spray wall impingement, which helped to lower the PM emissions

103	12th DEER Conference	Diesel HCCI combustion	Conventional Diesel Single Cylinder CR: 18.2:1 Load: 7 bar IMEP Emissions NOx: <10 ppm Smoke: <0.1 FSN	Diesel HCCI combustion provided an cycle thermal efficiency that was comparable to the diesel engines with heavy-emission control but was lower than the efficiency of the conventional diesel cycle due to phasing and un-burnt CO and HC considerations. It was possible to obtain a better combustion-phasing with very early injection strategy but this method this method was limited by high HC emissions. Close to TDC injection strategy had lower HC emissions but this method was associated with higher rates of pressure rise.
104	Fuel, (86), pp. 2871-2880	Diesel HCCI	Conventional Diesel Single Cylinder CR: 15:1 Load: Up to 6 bar IMEP Emissions NOx: <10 ppm Smoke: <0.1 FSN	The fuel injection cone angle was modified from 156° to 60° to reduce the wall wetting problem & avoid an out of bowl injection for early timing required for HCCI cycles. The narrow angle concept was effective in maintaining a high IMEP when the fuel was injected at an early timing for HCCI combustion. This was primarily due to higher combustion efficiency with the narrow-cone angle. NOx emissions were greatly reduced as the injection timing was advanced ahead of 30°BTDC. For the dual injection strategy, the pilot injection at 50°BTDC and the second injection close to TDC provided an adequate compromise between the emission and the efficiency considerations.

108	SAE 2006-01-3426	Cylinder pressure based control to extend the limits of EGR application	Conventional Diesel Single Cylinder CR: 18.2:1 Load: Up to 5.7 bar BMEP Emissions NOx: <10 ppm Smoke: <0.1 FSN	A simplified approach based on crank-angle for maximum rate-of-pressure rise was demonstrated for the cylinder pressure based control. The use of cylinder pressure based control extended the EGR application range and showed simultaneous low-NOx and soot combustion. The cylinder pressure based control allowed to keep the combustion phasing locked during the transients of major LTC enablers such as boost and EGR.
110	SAE 852067	Cylinder-pressure measurement and its use	Review paper	Reviews of cylinder pressure measurement techniques have been provided. Techniques of phasing for the pressure signal and determining the cylinder volume have been discussed. Procedure for calculating mass-fraction burnt has also been discussed
114	SAE 2000-01-0932	Cylinder pressure based control	Fuel: Gasoline 4-cylinder engine CR: Not provided Load: up to 4 bar IMEP Emissions NOx : Not provided Smoke: Not provided	The ratio of fired-to-motored pressure was established as a means to efficiently estimate combustion phasing and mixture dilution for each cycle. The system adaptively optimizes combustion for every cycle in each cylinder. Precise engine control was demonstrated for a variety of functions such as spark timing control, misfire detection, and knock detection.
116	SAE 870270	Heat-release analysis	Diesel, CN = 48.9 Single-cylinder CR: 15.9, 15.5: 1 Load: up to 9bar IMEP Emissions NOx : Not provided Smoke: Up to 7 BSU	High frequency oscillations introduced in the cylinder pressure after the beginning of combustion effected the computation of heat-release rate analysis. This was overcome by using averaged cylinder pressure over 100 non-consecutive cycles and smoothing the cylinder pressure data using a cubic spline curve-fitting technique.

117	SAE 870271	Heat-release analysis	Diesel, CN = 48.9 Single-cylinder CR: 15.9, 15.5: 1 Load: Not provided Emissions NOx : Not provided Smoke: Up to 6 BSU	Effect of swirl-ratio, injection-rate, bowl-size and engine speed on heat-release rate.
118	SAE 710135	Heat-release analysis	Review paper	The sources of errors associated with the derivation of heat-release rate equation have been identified as the use of mass-averaged property, heat-transfer approximations, and resolution of pressure measurement
119	SAE 930595	Heat-release analysis	Diesel Single-cylinder CR: 18:1 Load: Not provided Emissions NOx : Not provided Smoke: Not provided	The effect of TDC error was evaluated on the heat-release rate after compensating the error due to heat-transfer. In some cases, an error of 1°CA resulted in up to 10% variation in estimating the net heat released. Similarly the TDC phasing error had a significant impact on the estimation of the cycle-work.
121	Energy & Fuels (19), pp. 418-425.	Diesel combustion with EGR-reformer	Diesel, CN=53.9 Single cyl, CR: 15.5:1 Load: 4.5 and 6.1 bar IMEP Emissions NOx : 300~700 ppm Smoke: 1~5 BSU	The use of reformed EGR instead of the conventional EGR was able to reduce smoke for a similar NOx value. The smoke reduction with the use of reformed-EGR was attributed to increased premixed combustion-phase and use of hydrogen as a fuel.
122	Energy & Fuels, (17), pp. 1464-1473	CI combustion of diesel and bio-diesel in the presence of reformed EGR	Diesel, CN=53.9 Single cyl, CR: 15.5:1 4 and 5.5 bar IMEP NOx : 200~800 ppm Smoke: 1~4 BSU	The use of EGR produced the traditional NOx-smoke trade-off. However, when reformed EGR was used (up to 2% hydrogen in the intake) it was possible to reduce NOx and smoke simultaneously. For a similar value of NOx reformed EGR reduced smoke by up to 0.5BSU

126	SAE 2004-01-2918	EGR Reformer	Simulation study with propane as the fuel for EGR-reformer	Energy efficiency analysis for the EGR reformer system using CHEMKIN and engine-simulation software SAES showed that a small amount of gaseous fuel can be generated with marginal decrease in the overall system efficiency
134	SAE 2004-01-0582	NOx trap with reformed hydrogen as the reducing agent	Diesel, CN= 51.2 Multi-cylinder engine CR: Not provided Load: Up to 8.2 bar BMEP Emissions NOx : ~100 ppm Smoke: Not-provided	The hydrogen-rich reformate was able to regenerate NOx traps and achieve a conversion efficiency of 90% with a fuel-penalty of 4.7%. For a similar NOx conversion efficiency the fuel-penalty with diesel fuel was close to 8%. The reformate was able to perform regenerations at temperatures of 150°C, whereas the minimum regeneration temperature with the diesel fuel was close to 450°C.
135	SAE 2007-01-0914	Diesel experiments	Diesel, CN= 51.2 Single-cylinder CR: 14:1 Load: 8.8 bar BMEP Emissions NOx : 0.8 g/kWh Smoke: 0.0134 g/kWh	Higher charge air pressure and higher EGR levels gave a simultaneously low-NOx and low-soot combustion. Increasing the needle opening pressure results in lower soot emissions, lower HC and CO emissions and a slight increase in NOx emissions. Increased EGR cooling helped to lower the soot emissions for a constant NOx. For a given EGR level, no soot-reduction was obtained with the use of the post-injection strategy
136	SAE 2008-01-1191	Experiments with multiple-injection strategy	Diesel, CN= 53.6 4-cylinder CR: 18.3:1 Load: up to 6.4 IMEP Emissions NOx : ~ 200 ppm Smoke: < 0.3 FSN	The use of pilot-injection strategy helped to lower the NOx at a slight smoke penalty. The use of a late main injection strategy with as short dwell helped to reduce CO and HC emissions compared to the single injection strategy. The use of post injection strategy helped in the simultaneous reduction of NOx and soot.

137	SAE 2008-01-1329	Experiments with multiple-injection strategy	Diesel, European Norm EN 590 (minimum CN= 51) 4-cylinder and single-cylinder, CR: 14, 15 and 16:1, Load: 4, 7 and 13 bar IMEP Emissions (13 bar IMEP) NOx : 3.3 g/kWh Smoke: 1.5 FSN	At low load, the split injection strategy reduced the EGR requirements to maintain the similar NOx level as the single injection strategy. The split injection strategy also had the advantage of lower CO, HC and combustion noise. Multi injection strategy was particularly helpful for smoke reduction at high-loads. Pressure waves had an impact on the fuelling quantity of the secondary and later injections. The multiple-injection strategy with very small pilot injections was not considered challenging from the point of view of repeatability.
139	SAE 2008-01-0639	Diesel low-temperature experiments	Diesel, CN= 43 Single cyl, CR: 15:1 Load: 3 & 6 bar IMEP Emissions (6bar IMEP) NOx : ~20 ppm Smoke: ~ 0.25 FSN	Single injection strategy was developed to 3 bar IMEP condition; triple injection strategy was developed at 6 bar IMEP condition. Small pre-injection and post-injection of 1 mg/cycle was implemented at 6 bar IMEP to reduce combustion and noise and soot emissions
148	SAE 2008-01-0643	Diesel low-temperature combustion	Diesel, CN= 53 Single-cylinder CR: 15.8:1 Load: 13bar IMEP Emissions (13 bar IMEP) NOx : <0.4 g/kWh Smoke: ~ 0.2 g/kWh	- By combining higher swirl, injection pressure and higher boost-pressure it was possible to reduce the NOx to 0.34 g/kWh at 13bar IMEP without a significant penalty on fuel-economy. At this condition the soot was observed to be 0.2 g/kWh.

APPENDIX G: GLOSSARY OF TERMS

SOC – refers to the 'Start of Combustion' and is defined as the crank angle at which the value of the normalized cumulative heat release curve is 0.05.

CA50 – is the crank angle at which the value of the normalized cumulative heat release curve is 0.5. This is taken as a measure of the combustion phasing.

EOC – refers to the 'End of Combustion' and is defined as the crank angle corresponding to the first zero crossing of the heat release rate curve after its maximum.

Combustion Duration – is the duration from the SOC to the crank angle at which the value of the normalized cumulative heat release curve becomes 1.

Slope 1– the segment of soot climbing but NOx declining curve when EGR increases during HTC combustion. It represents the classical NOx-Soot trade-off.

Slope 2 – the segment of simultaneous soot and NOx declining curve when EGR increases (during LTC combustion). It represents the reduction in NOx and soot enabled with a single injection using heavy EGR.

Heavy EGR – refers to large amounts of recycled exhaust gases that result in nearly halved oxygen and high carbon dioxide contents in the engine intake. This indicates EGR levels (typically 50~70%) beyond those commonly applied in production diesel engines.

LTC – refers to any combustion mode that results in ultra low emissions of in-cylinder NOx and PM in conventional diesel engines.

Ignition delay – The time duration between the start of injection (the last injection in case of multiple-shots) and the start of combustion.

SOS – The start of sampling crank angle at which the direct gas sampling valve is commanded to be opened.

SRF –The number of engine cycles after which the valve operation is repeated is the sampling repetition frequency.

SD – The opening time of the direct gas sampling valve (sampling duration) at each opening event.

Index Z – The TTL signal from the encoder corresponding to the physical TDC of the engine (commonly called the trigger).

Index A – The TTL signal from the encoder used as an external clock to provide information on the position of the crank angle with respect to the TDC.

Combustion Noise – The audible noise associated with the premixed or uncontrolled combustion phase and generally represented by the maximum rate of pressure rise.

APPENDIX H: HARDWARE SPECIFICATIONS

The major specifications of the hardware components (engine sensors, data acquisition devices, emission analyzers, control actuators and sensors) that were used to develop the engine testing and control platform for this research are given below:

Table H.1: Data Acquisition Devices

Device Model		SCXI 1102	PCI-6023E	PCI-6024E	PCI-6070E	PCI-6221	PCI-6229	PCI-6122
Analog Input	Number of Channels	32 DI	16 SE / 8 DI	16 SE / 8 DI	16 SE / 8 DI	16 SE / 8 DI	32 SE / 16 DI	4 SE / 4 DI
	Maximum Range	±100 mV	±10 V	±10 V	±10 V	±10 V	±10 V	±10 V
	Sampling Rate	333 kS/s	200 kS/s	200 kS/s	1.25 MS/s	250 kS/s	250 kS/s	500 kS/s/ch
	Resolution		12 bits	12 bits	12 bits	16 bits	16 bits	16 bits
Analog Output	Number of Channels	–	–	2	2	2	4	–
	Maximum Range			±10 V	±10 V	±10 V	±10 V	
	Update Rate			10 kS/s	1 MS/s	833 kS/s	833 kS/s	
	Resolution			12 bits	12 bits	16 bits	16 bits	
Digital Input / Output	Number of Channels	–	8	8	8	24	48	8
	Logic Level		TTL	TTL	TTL	TTL	TTL	TTL
	Maximum Range		0 – 5 V	0 – 5 V	0 – 5 V	0 – 5 V	0 – 5 V	0 – 5 V
	Clock Rate		1 MHz	1 MHz	1 MHz	1 MHz	1 MHz	10 MHz
Counters	Number of Channels	–	2	2	2	2	2	2
	Logic Level		TTL	TTL	TTL	TTL	TTL	TTL
	Maximum Range		0 – 5 V	0 – 5 V	0 – 5 V	0 – 5 V	0 – 5 V	0 – 5 V
	Resolution		24 bits	24 bits	24 bits	32 bits	32 bits	24 bits
	Source Frequency		20 MHz	20 MHz	20 MHz	80 MHz	80 MHz	20 MHz

Table H.2: Hardware for Cylinder Pressure Measurement

Hardware	Piezo-electric Cylinder Pressure Transducer		Charge Amplifier
Model	Kistler 6043A60 (Yanmar)	AVL GU13P (Ford)	Kistler 5010B
Range	0–250 bar	0–200 bar	10–999000 pC
Sensitivity	20 pC/bar	15 pC/bar	0.01–9990 pC/bar
Output	–	–	±10 V
Accuracy	< ±0.5 %	< ±0.6 bar	< ±0.5 %

Table H.3: Air Flow and Fuel Flow Measurement

Hardware	Air Flow		Fuel Flow		
Model	BOSCH HFM5-3.5	Dresser Roots Meter 5M175	FP-213 Flow Detector	FP-2140H Flow Detector	DF-210A Flow Meter
Measurement Range	1.6–102 g/s	2.36 m^3/min 175 psig maximum	1–1000 ml/min	5-2000 ml/min	–
Resolution	0.02 g	2.622 x 10^{-4} m^3	0.01 ml	0.1 ml	–
Output	0–5 V	Pulse Output	0.01 ml/pulse	0.1 ml/pulse	0–10V TTL Pulse
Accuracy	< ±3 %	< 0.3 %	< ±0.5 %	< ±0.2 %	–

Table H.4: Boost & Exhaust Backpressure Control

Hardware	Electro-pneumatic Pressure Regulator		Pressure Sensor
Model	ITV 3051-31N4N4	ITV 1031-21N4N4	BOSCH DS-K-TF
Range	0.005 to 0.9 MPa Programmable	0.005 to 0.5 MPa Programmable	0-5 bar Differential
Control Signal (Input)	0-10 VDC	0-5 VDC	–
Output Signal	1-5 VDC	1-5 VDC	0.5–5 VDC
Sensitivity	< 0.2 %	< 0.2 %	–
Accuracy	< ±0.5 %	< ±0.5 %	< ±2 %

Table H.5: CAN Hardware for EGR Valve Control

Model	NI USB-8473
Number of Ports	1
Termination	External
Data Transfer	High Speed (up to 1 Mbit/s)
CAN API	Full Frame API
Transceiver	Philips TJA1041
Time Stamping	Hardware 1 μs Resolution
CAN Compliance	CAN 2.0A (11-bit) and CAN 2.0B (29-bit) Arbitration ID

Table H.6: Emission Analyzers

Manufacturer & Model	Species	Working Principle	Range	Resolution	Output	Miscellaneous
CAI 602P	CO_2	Non-Dispersive Infra-Red (NDIR)	0–2 % 0–10 %	0.001 %	0-10 VDC	Programmable output
CAI 602P	O_2	Paramagnetic	0–25 %	0.01 %	0-10 VDC	Programmable output
CAI 600 HCLD	$NO/NO_2/NOx$	Chemiluminescence	0–3,000 ppm	0.01 ppm	0-10 VDC	4 programmable ranges, Programmable output
CAI 300M-HFID	THC	Heated Flame Ionization Detector	0–3,000 ppm	0.01 ppm	0-10 VDC	8 selectable ranges
CAI 300	CO	NDIR	0–2,000 ppm 0–5,000 ppm	0.01 ppm	0-10 VDC	–
CAI 300	O_2	Paramagnetic	0–25 %	0.01 %	0-10 VDC	–
CAI 200	CO_2	NDIR	0–8 % 0–40 %	0.01 %	0-10 VDC	–
AVL 415S	Smoke / Dry Soot	Variable Sampling Smoke Meter	0–10 FSN (0–32) g/m³	0.001 FSN / 0.01 mg/m³	0-10 VDC	Programmable output
Cambustion *f*NOx400	$NO/NO_2/NOx$	Chemiluminescence	0-10,000 ppm	0.1-50 mV/ppm	0-10 VDC	9 programmable ranges
Cambustion HFR-500	THC	Heated Flame Ionization Detector	0-1,000 to 200,000 ppm	0.05-10 mV/ppm	0-10 VDC	8 selectable ranges

VITA AUCTORIS

NAME: Usman Asad

PLACE OF BIRTH: Rawalpindi, Pakistan

YEAR OF BIRTH: 1974

EDUCATION: Senior Cambridge/GCE 'O' Levels
St. Mary's Academy, Rawalpindi, Pakistan
1978-1989

Higher Secondary School Certificate
F.G. Sir Syed College, Rawalpindi, Pakistan
1989-1991

BSc Mechanical Engineering with Honours
University of Engineering & Technology, Lahore, Pakistan
1992-1995

MASc Mechanical Engineering
University of Windsor, Ontario, Canada
2004-2006

PhD Candidate
University of Windsor, Ontario, Canada
2006-2009

LIST OF PUBLICATIONS

Refereed Journal Publications

1. **Usman Asad**, Ming Zheng, "*Efficacy of EGR and Boost in Single-shot Enabled Low Temperature Combustion*", SAE 2009 Transactions, Journal of Engines, pp. 1-13, 2009-01-1126.
2. **Usman Asad**, Ming Zheng, Xiaoye Han, Graham T. Reader, Meiping Wang, "*Fuel Injection Strategies to Improve Emissions and Efficiency of High Compression Ratio Diesel Engines*", SAE 2008 Transactions, Journal of Engines, V117-3, pp. 1220-1233, 2008-01-2472.
3. Ming Zheng, **Usman Asad**, Graham T. Reader, Yuyu Tan, Meiping Wang, "*Energy Efficiency Improvements for a Diesel Engine in Low Temperature Combustion*", International Journal of Energy Research, 33 (2009), pp. 8-28.
4. **Usman Asad**, Ming Zheng, "*Fast Heat Release Characterization of Modern Diesel Engines*", International Journal of Thermal Sciences, 47 (2008), pp. 1688-1700.
5. Ming Zheng, **Usman Asad**, "*Preliminary Energy Efficiency Analyses of Diesel EGR Fuel Reforming with Flow Reversal and Central Fuelling*", SAE 2007 Transactions, Journal of Fuels and Lubricants, V116-4, pp. 896-908, 2007-01-4035.
6. Ming Zheng, Graham T. Reader, Dong Wang, Jun Zuo, Raj Kumar, Mwila C. Mulenga, **Usman Asad**, David S-K Ting, Meiping Wang, "*A Thermal Response Analysis on the Transient Performance of Active Diesel Aftertreatment*", SAE 2005 Transactions, Journal of Fuels and Lubricants, V114-4, pp. 1804-1815, 2005-01-3885.

Refereed Conference Publications

7. Ming Zheng, **Usman Asad**, Xiaoye Han, Meiping Wang, Graham T Reader, "*Hydrocarbon Impacts on Diesel HCCI Cycles*", Submitted to the ASME Internal Combustion Engine Division, 2009 Fall Technical Conference, Sept 27-30, Switzerland.

8. Ming Zheng, Yuyu Tan, Graham T. Reader, **Usman Asad**, Xiaoye Han, Meiping Wang, "Prompt Heat Release Analysis to Improve Diesel Low Temperature Combustion:, 2009 SAE International Powertrain, Lubricants and Fuels Conference, Florence, Italy, SAE Paper 2009-01-1883.
9. Ming Zheng, Graham T. Reader, **Usman Asad**, Yuyu Tan, Meiping Wang, "*Adaptive Control to Improve Low Temperature Diesel Engine Combustion*", 7th COMODIA International Conference on Modelling and Diagnostics for Advanced Engine Systems, Hokkaido University, Sapporo, Japan, Paper No. DE1-2.
10. Ming Zheng, **Usman Asad**, Graham T Reader, Xiaoye Han, Mohammad Pournazeri, David S-K Ting, Meiping Wang, "*Diesel EGR Fuel Reformer Improvement with Flow Reversal and Central Fuelling*", SAE Powertrain and Fuels and Lubricants Congress, China, SAE Paper No. 2008-01-1607.
11. **Usman Asad**, Ming Zheng, "*EGR Oxidation and Catalytic Fuel Reforming for Diesel Engines*", ASME Internal Combustion Engine Division, 2008 Spring Technical Conference, Chicago, USA, ICES 2008-1684.
12. **Usman Asad**, Ming Zheng, "*Real-time Heat Release Analysis for Model-based Control of Diesel Combustion*", SAE 2008 World Congress, Detroit, USA, SP-2159, SAE Paper No. 2008-01-1000.
13. Ming Zheng, Siddhartha Banerjee, Xiaohong Xu, Graham T Reader, **Usman Asad,** Xiaoye Han, "*Energy Efficiency Improvement of Diesel Aftertreatment with Flow Reversal and Central Fuelling*", ASME Internal Combustion Engine Division, 2007 Fall Technical Conference, USA, ICEF 2007-1631.
14. **Usman Asad**, Siddhartha Banerjee, Graham T. Reader, Meiping Wang, Ming Zheng, "*Energy Efficiency Analysis between In-cylinder and External Supplemental Fuel Strategies*", SAE 2007 World Congress, Detroit, USA, SP-2140, SAE Paper 2007-01-1125.
15. Ming Zheng, **Usman Asad**, Raj Kumar, Graham T. Reader, Mwila C. Mulenga, William Bombardier, Meiping Wang, Jimi Tjong, "*An Investigation of EGR Treatment on the Emission and Operating Characteristics of Modern Diesel*

Engines", SAE 2007 World Congress, Detroit, USA, SP-2090, SAE Paper 2007-01-1083.

16. Raj Kumar, Ming Zheng, **Usman Asad**, Graham T. Reader, "*Heat Release Based Adaptive Control to Improve Low Temperature Diesel Engine Combustion*", SAE World Congress, Detroit, USA, SP-2087, SAE Paper 2007-01-0771.

17. Ming Zheng, **Usman Asad**, Graham T. Reader, David S-K. Ting, "*A Preliminary Thermal Response Analysis of Exhaust Pipe Plenums for Diesel Aftertreatment Improvement*", SAE 2006 Powertrain and Fluid Systems Conference, Toronto, Canada, SAE Paper 2006-01-3310.

18. **Usman Asad**, Ming Zheng, David S-K Ting, Graham T. Reader, "*Effect of Internal Exhaust Gas Recycling on n-Heptane HCCI Combustion*", ASME Internal Combustion Engine Division, 2005 Fall Technical Conference, ICEF 2005-1245.

Other Conference Publications

19. Ming Zheng, Graham T Reader, **Usman Asad**, Yuyu Tan, Kelvin Xie, Meiping Wang, "*An Enabling Study of Diesel Low-Temperature Combustion via Adaptive Control*", US DOE 2008 Diesel Engine Emission Reduction Conference, Detroit, USA.

20. Mohammad Pournazeri, **Usman Asad**, Xiaoye Han, Meiping Wang, Ming Zheng, "*Preliminary Analysis to Improve the Diesel EGR Reformer Efficiency with Periodic Flow Reversal and Supplemental Water and Fuel injections*", Combustion Institute–Canadian Section, 2008 Spring Technical Meeting, University of Toronto, Canada.

21. Xiaoye Han, **Usman Asad**, Raj Kumar, Mwila C. Mulenga, Siddhartha Banerjee, Meiping Wang, Graham T. Reader, Ming Zheng, "*Empirical Studies of Diesel Low Temperature Combustion on a Modern Diesel Engine*", Combustion Institute–Canadian Section, 2007 Spring Technical Meeting, University of Alberta, Canada.

22. Yuyu Tan, Mwila C. Mulenga, **Usman Asad**, Meiping Wang, G. T. Reader and M. Zheng, "*Preliminary Analysis of Fuel Efficiency of Diesel HCCI Cycles*",

Combustion Institute–Canadian Section, 2007 Spring Technical Meeting, University of Alberta, Canada.

23. Ming Zheng, Graham T Reader, Raj Kumar, Mwila C Mulenga, **Usman Asad**, Yuyu Tan, Meiping Wang, "*Adaptive Control to Improve Low Temperature Diesel Engine Combustion*", US DOE 2006 Diesel Engine Emission Reduction Conference, Detroit, USA.

24. **Usman Asad**, Ming Zheng, David S-K. Ting, Raj Kumar, Siddhartha Banerjee, Graham T. Reader, Jimi Tjong, "*Real-time Heat Release Analysis towards On-fly Combustion Control for Diesel Engines*", Combustion Institute–Canadian Section, 2006 Spring Technical Meeting, University of Waterloo, Canada.

25. Mwila C. Mulenga, Ming Zheng, Graham T. Reader, David S-K. Ting, Yuyu Tan, **Usman Asad**, Meiping Wang, "*Investigating EGR on Low-temperature Combustion NOx and PM in Diesel Engines*", Combustion Institute–Canadian Section, 2006 Spring Technical Meeting, University of Waterloo, Canada.

Poster Presentations

26. Mwila C. Mulenga, **Usman Asad**, Raj Kumar, Yuyu Tan, Xiaoye Han, Meiping Wang, "*Compatibility of Bio-diesel Fuels in Modern Common-rail Diesel Engines*", AUTO21 SAE Network Colloquium at Windsor, Canada, April 2008.

27. Mwila C. Mulenga, **Usman Asad**, Raj Kumar, Yuyu Tan, Xiaoye Han, Meiping Wang, "*Low Temperature Combustion and Adaptive Control*", 2007 Automotive Parts Manufacturers Association Annual Conference & Scientific Exhibition, and AUTO21 2007 Scientific Conference, Hamilton, Canada, May, 2007.

28. Mwila C. Mulenga, **Usman Asad**, Raj Kumar, Yuyu Tan, Xiaoye Han, Meiping Wang, "*Low Temperature Combustion & Adaptive Control*" AUTO21 HQP Network Colloquium, Windsor, Canada, April 2007.

29. Raj Kumar, Meiping Wang, **Usman Asad**, Dong Wang, Siddhartha Banerjee, "*Active-flow Aftertreatment & Model-based Combustion Control for HCCI Engine*", 2006 AUTO21 Network HQP Meeting, Barrie, Canada, May 2006.

30. Raj Kumar, Meiping Wang, **Usman Asad**, Dong Wang, Siddhartha Banerjee, "*Active-flow Aftertreatment & Model-based Combustion Control for HCCI Engine*", 2006 Automotive Parts Manufacturers Association Annual Conference & Exhibition, Hamilton, Canada, May 2006.